

SYNTHESIS AND PROPERTIES OF NON-HEME IRON-NO_x COMPLEXES FOR THE
GENERATION OF NITROXYL DONORS AND NITRITE REDUCTION CATALYSTS

by

BRIAN CLARK SANDERS

(Under the Direction of Todd C. Harrop)

ABSTRACT

The biological interplay between Fe and N_yO_x is significant to both human physiology and the remediation of global pollution. The interconversion of N_yO_x species is primarily mediated by metalloenzymes, in which Fe plays a critical role. Due to their critical role in biology and the environment, the study of Fe-N_yO_x interactions is of fundamental interest in coordination chemistry. Additionally, thiol-containing biomolecules have direct interaction with Fe-N_yO_x. For example, Fe(III)-NO₂ complexes react with thiols to NO or HNO and the corresponding sulfenic acids. Given the complex interplay between N_yO_x, Fe, and thiols, there is a need to rationalize this intricate chemistry through model complexes. Our approach involves the design and synthesis of modular non-heme complexes in which donor strength, flexibility, and secondary-sphere interactions are readily tuned. This methodology has facilitated the isolation and characterization of the first non-heme {FeNO}⁸ and Fe(II)(NO₂)₂ complexes, and allowed for the first study of their reactivity with Fe(III)-porphyrins, Fe(III)-myoglobin, thiols, and protons. From these reactivity studies we have demonstrated nitroxyl-transfer to metMb to give MbNO, thus outlining the proof-of-principle for the rational design of metal-based HNO donors. Moreover, we have demonstrated that reactions of non-heme {FeNO}^{7/8} complexes with

thiols ultimately leads to various dinitrosyl iron complexes (DNICs) in an oxidation state dependent manner. These results suggest a possible route to DNIC formation from non-heme {FeNO}^{7/8} complexes in biology. Lastly, the development of non-heme NO₂⁻ reduction catalysts is discussed. In the presence of H⁺/thiols the selective and catalytic conversion of NO₂⁻ to NO(g) is observed. However, in the presence of only thiols, a net three-electron reduction of Fe(II)(NO₂)₂ to the Fe(I)(NO)₂ DNIC is observed, and suggests a possible role for Fe-NO₂ and thiols in the formation of biological DNICs. Described in this dissertation is the synthesis, characterization, and reactivity of a series of non-heme Fe-NO_x complexes, which provides the basis for the development of non-heme NO₂⁻ reduction catalysts and Fe-based HNO donor molecules for the purpose of cardiovascular therapies and environmental remediation.

INDEX WORDS: Nitroxyl, Nitrite, Iron, Non-heme, Nitric Oxide

SYNTHESIS AND PROPERTIES OF NON-HEME IRON-NO_x COMPLEXES FOR THE
GENERATION OF NITROXYL DONORS AND NITRITE REDUCTION CATALYSTS

by

BRIAN CLARK SANDERS

B.S., University of Tennessee, 2008

A Dissertation Submitted to the Graduate Faculty of The University of Georgia in Partial

Fulfillment of the Requirements for the Degree

DOCTOR OF PHILOSOPHY

ATHENS, GEORGIA

2015

© 2015

Brian Clark Sanders

All Rights Reserved

SYNTHESIS AND PROPERTIES OF NON-HEME IRON-NO_x COMPLEXES FOR THE
GENERATION OF NITROXYL DONORS AND NITRITE REDUCTION CATALYSTS

by

BRIAN CLARK SANDERS

Major Professor:	Todd C. Harrop
Committee:	Michael K. Johnson
	Jeffrey L. Urbauer

Electronic Version Approved:

Julie Coffield
Interim Dean of the Graduate School
The University of Georgia
May 2015

ACKNOWLEDGEMENTS

I would like to thank my advisor, Professor Todd C. Harrop, for his support and willingness to take a chance on a me. I also thank Todd for introducing me to the field of bioinorganic chemistry, an area that I expect to always be of interest and pursuit in my future research. Todd's willingness to guide students and teach them the proper way to traverse an academic/research landscape is, and will be, exceptionally valuable to me in my future career. I look forward to watching the Harrop laboratory continue to grow and thrive.

I would also like to thank Prof. Michael K. Johnson and Prof. Jeffrey L. Urbauer and their labs for support and assistance with EPR and NMR, respectively. Moreover, I would like to thank MKJ and JLU for their guidance and genuine support as members of my graduate committee. Thank you for your letters of recommendation and continued support. I would also like to thank Dr. Phillips for assistance with MS experiments, Dr. Wei for assistance with X-ray diffraction, Dr. Wylie, Dr. Cui, and Henry Niedermaier for assistance with NMR, Brian Vaccaro for assistance with EPR, and Dr. Hassan for assistance with GC-MS. I would also like to thank Dr. Jay Agarwal for his collaborative nature and scientific curiosity.

I would like to thank my group members past and present. Thank you Dr. Ashis K. Patra and Koustubh Dube for your seminal work in the Harrop lab from which I was able to expand upon with my own research projects. Thank you Dr. Eric Gale for your mentality and creative chemical mind, you are an inspiration and excellent researcher. I look forward to future science and discussions with you. Thank you to Dr. Vivian Ezeh for your wonderful attitude and

persistence as a researcher, you taught me many things and importantly served as an excellent role model in the pursuit of both teaching and researching chemistry. I look forward to following your career and future achievements. Thank you for your support. Thank you to my current lab members: Ellen Broering, Melody Rhine, Ramsey Steiner, and Phan Truong for your support, collaboration, and teamwork. It has truly been a pleasure working with all of you and I thank you for your selflessness and your ever-present willingness to help one another. I can only hope I helped you all equal to that in which you helped me. I truly could not have done it without you.

I would like to thank my wonderful family: my parents George and Cheryl Sanders, brother John, sister-in-law Ali, nephew Eli, aunt Kila, Uncle Michael, cousins Meghan and Laura, and Grandmother Ina Lima for their love and support. I love you all very much and would not be where I am today without you. Thank you all!

TABLE OF CONTENTS

CHAPTER	Page
1 INTRODUCTION AND LITERATURE REVIEW	1
1.1 An Overview: Nitrogen Oxides and the Nitrogen Cycle	1
1.2 An Overview: Nitrogen Oxides and Mammals	5
1.3 An Overview: Nitrogen Oxides and the Environment.....	9
1.4 The Coordination Chemistry of HNO, NO, and NO ₂ ⁻ with Iron.....	11
1.5 The {FeNO} ⁿ (<i>n</i> = 6, 7, 8) Formulation in Biology.....	18
1.6 Nitroxyl (NO ⁻ /HNO) Chemistry and Pharmacology.....	31
1.7 {FeNO} ⁸ Heme Coordination Complexes.....	41
1.8 {FeNO} ⁸ Non-heme Coordination Complexes.....	62
1.9 Nitrite in Biology	75
1.10 Heme Fe(NO ₂) Model Complexes.....	89
1.11 Reactivity of Heme Fe(II/III) Complexes.....	108
1.12 Non-heme Fe(NO ₂) Model Complexes	120
1.13 Research Objective and Purpose.....	131
1.14 References.....	133

2	SYNTHESIS, PROPERTIES, AND REACTIVITY OF A SERIES OF NON-HEME {FeNO} ^{7/8} COMPLEXES: IMPLICATIONS FOR Fe-NITROXYL COORDINATION	156
2.1	Abstract	157
2.2	Introduction	158
2.3	Results and Discussion	163
2.4	Spectroscopic and Electrochemical Properties of {FeNO} ⁷ Complexes	169
2.5	Synthesis and Spectroscopic Properties of {FeNO} ⁸ Complexes	173
2.6	Reactivity of {FeNO} ⁷ and {FeNO} ⁸ Complexes	177
2.7	Conclusions	197
2.8	Materials and Methods	199
2.9	Supporting Information	217
2.10	References	244
3	NO ₂ ⁻ ACTIVATION AND REDUCTION TO NO BY A NON-HEME Fe-(NO ₂) ₂ COMPLEX	250
3.1	Abstract	251
3.2	Introduction	252
3.3	Spectroscopic and Reactive Studies of Complex 1 ^{MeCN} and 2	253
3.4	Reactive Studies of 2	256
3.5	Conclusions	261
3.6	Materials and Methods	261
3.7	Supporting Information	273
3.8	References	288

4	PROGRESS TOWARD CONTROLLING SECONDARY-SPHERE INTERACTIONS IN A Fe-(NO ₂) ₂ COMPLEX.....	293
4.1	Abstract.....	293
4.2	Introduction.....	294
4.3	Synthesis, Spectroscopic, and Reactive Studies of Complexes 3 and 4	298
4.4	Reactivity Studies of 2 , 4 , and 5	306
4.5	Conclusions and Future Outlook.....	312
4.6	Materials and Methods.....	313
4.7	Supporting Information.....	327
4.8	References.....	345
5	CONCLUSIONS.....	349

APPENDICES

A	NON-HEME NO _x COMPLEXES WITH FIVE-COORDINATE LIGANDS.....	352
---	----------------------------------------------------------------------	-----

CHAPTER 1

INTRODUCTION AND LITERATURE REVIEW

1.1 An Overview: Nitrogen Oxides and the Nitrogen Cycle

Nitrogen oxides of the formula N_yO_x (where $y = 1, 2$ and $x = 1, 2, 3$) are critically functioning inorganic components of life processes. Because these molecules exist with varying degrees of oxygenation, protonation, structure, and redox state, N_yO_x species comprise a complex molecular network of signaling and function through interconversion and chemical reactivity. In biology, the root of these molecular transformations are metalloenzymes that are capable of both N-N and N-O bond cleavage and bond formation. Thus, the intricate biological interplay of N_yO_x is in large part mediated by metals.¹ For example, N-containing biomolecules (e.g. amino and nucleic acids) that allow for life to exist on Earth are derived primarily from atmospheric N_2 converted to NH_3 by nitrogen-fixing bacteria. Certain microorganisms, such as green sulfur and cyanobacteria contain the metalloenzyme nitrogenase and are able to reduce N_2 into NH_3 , a process called nitrogen fixation.²⁻⁵ At the molecular heart of this enzyme is an elegant Fe-Mo cofactor capable of breaking the N_2 triple bond, a unique characteristic of this complex enzyme (Fig. 1.1).^{6,7} Alongside N_2 fixation are additional pathways that transform N_yO_x species and constitute the global nitrogen cycle (Fig. 1.2).⁴ For example, nitrifying bacteria perform the oxidative conversion of NH_4^+ into NO_3^- (nitrification), an essential nutrient for plants. Moreover, NO_3^- can be reduced back to N_2 or NH_4^+ (denitrification) by denitrifying bacteria, with the use of heme-cofactors, under two separate pathways (*vide infra*, Fig. 1.1).

Overall, the metalloenzyme-dependent transformations of N_yO_x comprise much of the terrestrial and aquatic contributors to the diverse nitrogen species on the planet.⁴

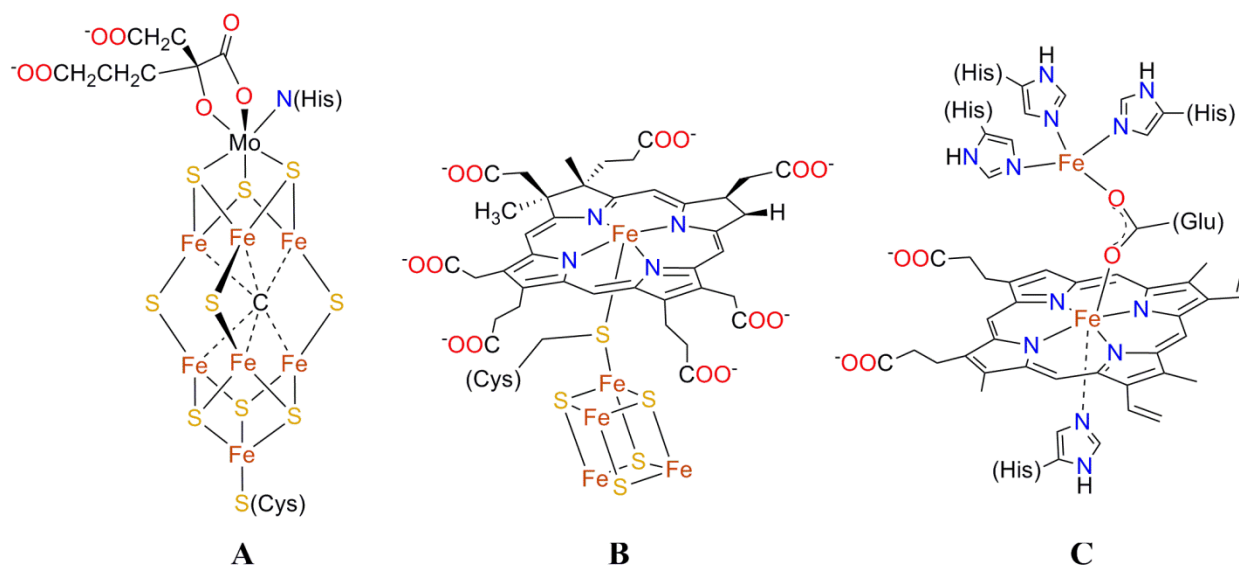


Figure 1.1. Prototypical examples of Fe-containing cofactors for N_yO_x transformations. A) FeMo-cofactor/active site from nitrogenase enzyme with coordinated homocitrate. B) Siroheme cofactor (SC) from SC nitrite reductase (SCNiR) with Cys-bridged [4Fe-4S] cluster. C) Nitric oxide reductase (NorBC) active site from *Paracoccus denitrificans* with *b* heme and Fe_B non-heme active site bridged by a glutamate residue.

The nitrogen cycle is comprised of four major N_yO_x conversion pathways: fixation ($N_2 \rightarrow NH_3$); nitrification ($NH_3 \rightarrow NO_x$); denitrification ($NO_x \rightarrow N_2$); and ammonium oxidation ($NH_4^+ \rightarrow N_2$) as detailed in Fig. 1.2.⁸ Microbes perform N_yO_x transformations through metalloenzymes primarily for the exchange/production/storage of energy, although in some cases N_yO_x are thought to act as signaling molecules.^{9,10} The reduction of N_2 is energetically very costly and requires a consumption of 16 equiv of ATP throughout the process, thus N_2 fixation in

photoautotrophs (e.g. green-sulfur bacteria and cyanobacteria) is a light-driven process, alternatively, some proteobacteria (e.g. Rhizobium) live in symbiosis with plants to exchange fixed-N for carbon compounds produced by the plants.⁸ Alternatively, the oxidation of $\text{NH}_3/\text{NH}_4^+$ to NO_3^- by nitrifying bacteria results in electron equivalents to drive ATP-dependent metabolism.⁸ Equally important, and most relevant to this dissertation are the denitrifying bacteria that utilize NO_3^- (in the absence of O_2) as the terminal electron acceptor in their respiration process. Denitrifying bacteria reduce NO_3^- for two biological purposes. First, the reduction of NO_3^- all the way to NH_4^+ for *assimilation* or incorporation into organisms, and second, the *dissimilation* path where coupled reduction of NO_3^- and oxidation of organic molecules provides energy for the organism. Denitrifiers contain a series of metalloenzymes that contain Fe, Cu, and Mo which make up the molecular machinery to perform the reduction of either O_2 to H_2O or, in the absence of O_2 reduce NO_3^- to N_2 .⁸ The overall cycle of fixation, nitrification, and denitrification are the most powerful natural process affecting the amount and type of N-containing molecules on Earth. Although this chemistry is almost exclusively unique to microorganisms, the reliance of higher-order species on N_yO_x transformations is evident. Accordingly, the chemistry of N_yO_x is truly global and affects all living organisms.

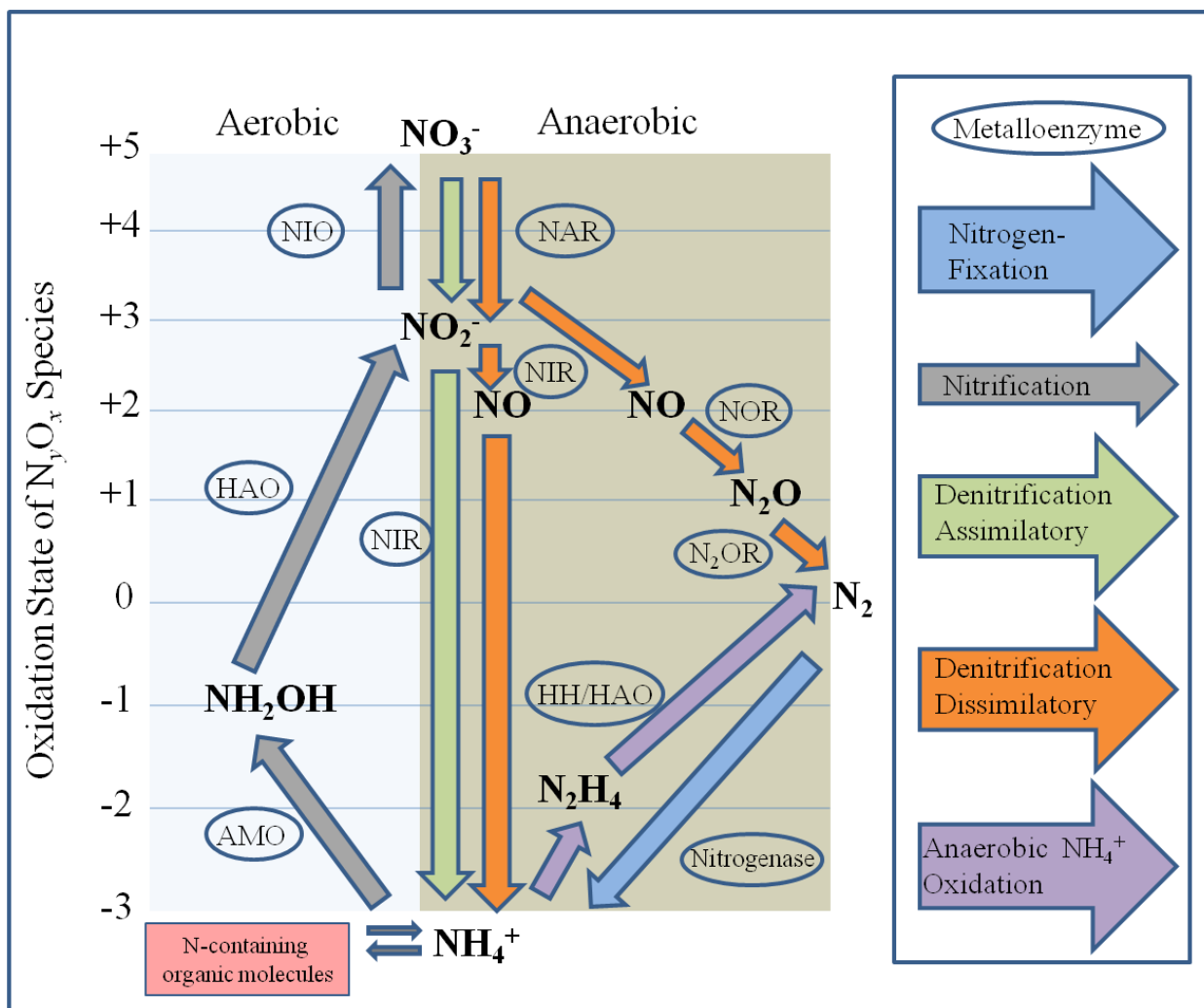


Figure 1.2. Diagram representing the metalloenzyme dependent chemical transformations of N_yO_x species within the global nitrogen cycle. This figure was modeled from reference 10. Enzyme abbreviations and encoding genes: nitrate reductases (NAR) (genes: nas, euk-nr, narG, napA), nitrite reductases (NiR) (genes: nir, nrf), nitric oxide reductase (NOR) (gene: norB), nitrous oxide reductase (N₂OR) (gene: nosZ), nitrogenase (gene: nif), ammonium monooxygenase (AMO) (gene: amo), hydroxylamine oxidoreductase (HAO) (gene: hao), nitrite oxidoreductase (NIO) (gene: nxr), and hydrazine hydrolase (HH) (gene: hh).

1.2 An Overview: Nitrogen Oxides and Mammals

Mammalian species do not need the N_yO_x -dependent energy exchange that denitrifying bacteria require. Yet, N_yO_x species are prevalent in aerobic organisms and are required in humans for immune response, neurotransmission, and cardiovascular action.⁸ For example, mammalian biological signaling pathways are known to involve NO and proposed to involve HNO, both of which have experimental evidence supporting NO_2^- as a precursor for these gaseous signalers.¹¹⁻¹⁴ These studies were performed with either water-soluble Fe-porphyrins (Fe(por)) or through heme protein-dependent reduction of NO_2^- to NO (*vide infra*). Importantly, heme is present in many enzymes of the global nitrogen cycle, notably those involving NO_2^- , NO, and NH_2OH , as well as proposed HNO intermediates.⁸ Also, non-heme species such as dinitrosyl iron complexes (DNICs) are known to transport NO throughout the mammalian cardiovascular system.¹⁵ Both heme and non-heme centers are responsible for the generation and receiving of N_yO_x molecules in biology. Therefore, the interactions of NO_2^- , NO and HNO at Fe centers stand as a critical common feature of many life forms.

The reduction of NO_2^- to NO is one of great importance. The transformation of a water-soluble anion to a neutral gaseous molecule is the first committed step in the series of denitrification transformations (Figure 1.2).¹⁶ Moreover, the production of NO from NO_2^- has biological significance distinct from that of the nitrogen cycle. For example, NO has been widely studied under the context of mammalian physiology. The discovery of NO as an indispensable signaling molecule within cardiac physiology was worthy of the 1998 Noble prize in Medicine or Physiology, awarded to Furchgott, Ignarro, and Murad.¹⁷⁻¹⁹ Due to the integral relationship between NO and metal centers, this discovery expanded the fields of coordination chemistry and bioinorganic chemistry as well as biochemistry, medicine, and drug discovery. In humans, NO

has three distinct roles: (i) cardiovascular maintenance, (ii) neuronal signaling, and (iii) immune response. Accordingly, there are nitric oxide synthases (NOS, heme, Fe) corresponding to each of these functions that produce NO through oxidation of L-arginine with O₂ and its bipterin cofactor, (*vide infra*).²⁰⁻²²

More recently though (2000's - present), an alternative physiological source of NO has been uncovered. For some time, NO₃⁻ and NO₂⁻ were thought of as non-critical or even harmful components of mammalian diets. On the contrary, the NO₃⁻/NO₂⁻ reduction pathway has been implicated as a critical source for NO production and subsequent signaling with particular interest in cardiovascular response.^{9,14,23-25} An interesting point is that NiR genes extend from bacteria to archaea and fungi, but not further to higher order species. For instance, mammalian species do not contain the genetic prerequisites for specific NiR enzymes. However, this chemistry is proposed to occur at a multitude of heme-containing enzymes, (*vide infra*). This recent discovery highlights an entirely new branch of N_yO_x chemistry that supports mammalian life function and warrants further study and development.

Among NO₂⁻ and NO, the enigmatic HNO molecule proffers unique interaction with mammalian cardiovascular systems.²⁶⁻³³ The one-electron reduction of a metal-nitrosyl (M-NO) can provide a metal-stabilized nitroxyl complex M-NO⁻ or M-HNO species if protonated. These species are typically very transient when M = Fe, yet have been implicated in the catalytic cycles of multiple Fe-containing metalloenzymes. For example, a nitroxyl intermediate is proposed in the denitrifying Fe-containing enzyme nitric oxide reductase (P450nor), a heme-dependent enzyme that catalyzes the net reduction of 2 NO to N₂O and H₂O.³⁴⁻³⁶ In addition, experimental evidence suggests that HNO, instead of NO, can be generated from the oxidation of L-Arginine by heme-containing NOS under certain *in vitro* conditions in absence of its bipterin cofactor,

highlighting a possible endogenous pathway for HNO formation.³⁷ These enzymes and others exemplify the relevance of HNO as both an intermediate in enzymatic cycles as well as a possible biological signaling molecule. Furthermore, the *in vivo* studies comparing NO and HNO outline divergent signaling pathways for the redox relatives. This important bifurcation of the downstream cascades between NO and HNO stresses the subtlety (1 e⁻/1 H⁺ difference) of N_yO_x function and signaling in physiology.²⁶⁻³³

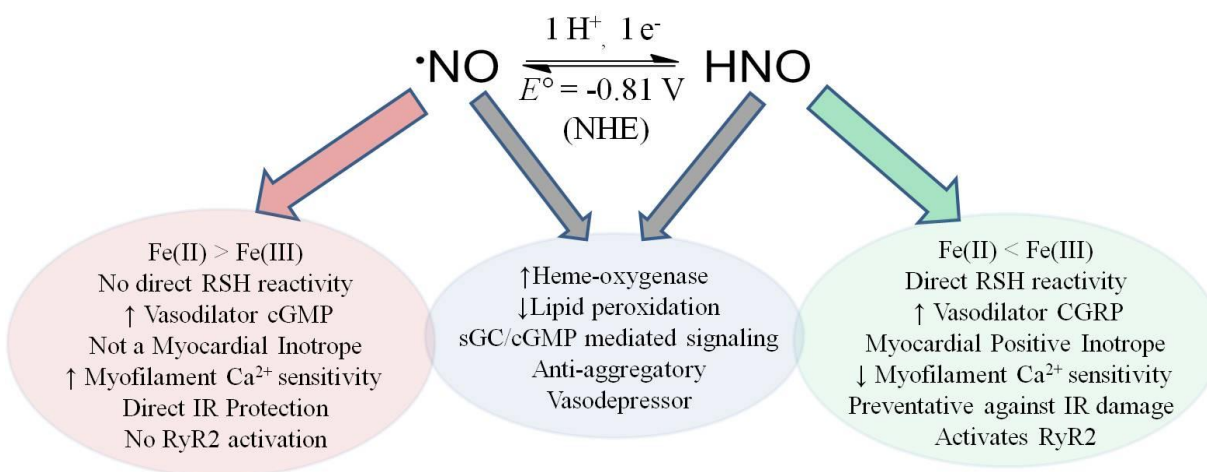


Figure 1.3. NO and HNO redox potential³⁸ and their pharmacological targets and subsequent effects.³³ Abbreviations: RSH = thiol, IR = ischemic reperfusion, RyR2 = ryanodine receptor 2, sGC = soluble guanylate cyclase, cGMP = cyclic guanosine monophosphate, CGRP = calcitonin gene-related peptide.

The promising pharmacology of HNO and its distinction from NO signaling has prompted the detailed study of HNO as biological regulator. HNO and NO are distinct effectors in their *in vivo* and *in vitro* chemistry (Fig. 1.3). First, HNO has a greater affinity for thiols (RSH) to form N-hydroxysulfonamides (RS(O)NH₂); while NO is less reactive with RSH, though

can produce S-nitrosothiols (RSNO), in the presence of an oxidant.³³ Second, HNO reacts with O₂ to form peroxyxynitrite (ONOO⁻), a potent reactive nitrogen species (ROS); conversely, NO reacts with superoxide (O₂⁻) to promote antioxidant activity. Additionally, there is some discrepancy regarding the affinity of HNO for Fe(II) vs. Fe(III) hemes; though, NO has a higher affinity than HNO for Fe(II) hemes.^{27,39}

The *in vivo* or *ex vivo* effects of NO and HNO with respect to ischemic reperfusion (IR) models have been studied.^{40,41} These studies model the tissue conditions when blood supply returns to an oxygen-starved area that has implications to heart-attack, tissue injury, and organ transplants. Interestingly, HNO acts under a protective mechanism if administered prior to loss of blood-flow, whereas NO can be administered during stopped flow and helps to minimize tissue damage due to reperfusion injury. These experiments clearly support divergent roles for NO and HNO and exemplifies their condition dependence. Other biological studies support the orthogonal nature of HNO and NO in pharmacology (Fig. 1.3).²⁶⁻³³ For instance, the HNO pro-drug cyanamide (H₂NCN) is used clinically for the treatment of alcoholism, in which released HNO inhibits aldehyde dehydrogenase (ALDH) through reaction with an active site thiol, an effect not observed with NO.⁴²⁻⁴⁶

The study of HNO and NO and their potential generation/interaction with metals is one of great interest to cardiovascular diseases. This is due to the vasodilation (opening of blood vessels) properties of NO and the combined vasodilation and heart muscle contractility properties of HNO. In order to understand the production and interaction of NO and HNO at metal centers, particularly Fe, a detailed study of the fundamental coordination chemistry with Fe is required. Thus, the future development of NO and HNO based therapies and technologies

largely depends on modeling the chemistry of heme and non-heme biological complexes and their interactions with NO_2^- , NO , and NO^-/HNO .

1.3 An Overview: Nitrogen Oxides and the Environment

The advent of the Haber-Bosch process ultimately led to the development of synthetic chemical fertilizers, allowing for increased agricultural production and *sustainable* population increase.⁴⁷ In fact, it is estimated that 33-50% of Earth's NH_4^+ is generated through the Haber-Bosch process comparable to the two natural contributors, lightning and N-fixation.⁸ The production and subsequent saturation of agricultural lands with NH_4NO_3 certainly facilitated an agricultural boom, but as with many anthropogenic developments has resulted in some unwanted side-effects.^{3,4,48,49} For example, NO_3^- and NH_4^+ have excellent water solubility and thus wide-mobility from soil to aquatic streams, rivers, and reservoirs. In fact, much of the NO_3^- and NH_4^+ implemented in agricultural production is lost in water run-off, or volatilisation of gaseous products like NH_3 or N_2O .⁵⁰ The latter process is of major concern due to increased loss of N_2O from farmlands due to the potency of this greenhouse gas.⁸ Moreover, the mobility of NH_4^+ and NO_3^- has lead to the saturation of aquatic ecosystems such as lakes and oceans as well as drinking water reservoirs with N_yO_x species, thus creating an ecological imbalance. Other anthropogenic sources such as mining and industry also contribute to this imbalance.^{3,4,10} An over-saturation of N_yO_x in an ecosystem has major implications. For example, an ecological zone with too much N_yO_x will suffer from eutrophication, the over-stimulated growth of phytoplankton and algae, ultimately leading to low O_2 concentration in aquatic environments and the death of higher order species.³ With respect to human health, excess NO_3^- and NO_2^- are implicated either directly, or through formation of N-nitrosamines in several pathologies

including methemoglobinemia, cancer, thyroid atrophy, and birth defects.⁵¹ Due to negative anthropogenic influence, there is an over-saturation of N_yO_x in the environment and thus a need for positive human impact to develop new technologies to regain N_yO_x balance in the environment in a non-destructive fashion.

It is clear that N_yO_x and Fe are connected in ways that affect all organisms on Earth. Therefore advances in the field of Fe-mediated N_yO_x transformations can be very impactful. The chemistry of NO_2^- , NO, and NO^-/HNO pertain closely to that of cardiovascular physiology in which NO_2^- is thought to serve as a potential reservoir for NO and HNO. Moreover, the same redox sequence of reducing NO_2^- to NO and further to N_2O with the intermediacy of an NO^-/HNO species is known to occur in the heme-containing metalloenzymes nitrite reductase (NiR) and nitric oxide reductase (NOR), on the dissimilatory pathway of denitrifying bacteria. The dissimilatory enzymes and their transformations offer an apparent avenue to design and develop bioinspired molecular catalysts for the reduction NO_2^- to NO and further NO to HNO. What becomes clear is that the chemistry of N_yO_x and Fe is a deeply rooted evolutionary trait that sustains organisms from bacteria to humans. The critical functions of N_yO_x in biology certainly warrants their detailed study. Considering that the roles of NO_2^- , NO, and HNO have only recently (within 30 years) been realized in humans, and given the vast network of N_yO_x transformations, it is likely that other N_yO_x species will be shown to have critically functioning roles yet to be understood. Due to the diversity and function of N_yO_x and the direct interconversion and interaction with metal centers, the study of metalloproteins and model complexes is important.

Accordingly, the ability to design low-molecular weight platforms that (i) catalyze controlled N_yO_x transformations, (ii) stabilize enzymatically-relevant intermediates or unique complexes, and/or (iii) deliver the N_yO_x species NO_2^- , NO and HNO will certainly impact the areas of research regarding cardiovascular signaling/therapy as well as environmental remediation.

1.4 The Coordination Chemistry of HNO, NO, and NO_2^- with Iron

1.4.1 NO and HNO with Iron

The fundamental chemistry of the gaseous free-radical NO is well-defined.⁵²⁻⁵⁴ The molecular orbital diagram for NO depicts the π^* HOMO as singly-occupied, thus making the formal N-O bond order 2.5 (Fig. 1.4). The redox activity of NO can traverse different oxidation states i.e. NO^+ (nitrosonium), NO, and NO^- (nitroxyl anion), having E° values of +1.2 V, -0.8 V, and -1.7 V vs. NHE, respectively. The redox isomers of NO involve the removal or addition of electrons to the π^* orbital. As such, the N-O bond length and vibrations frequency (ν_{NO}) are dependent on the redox state. For example, the N-O bond lengthens and its bond energy decreases from NO^+ (1.06 Å, 2377 cm^{-1}) to NO (1.154 Å, 1875 cm^{-1}) to $^3NO^-$ (1.26 Å, 1470 cm^{-1}) (Figs. 1.5, 1.6, and 1.7).⁵⁴

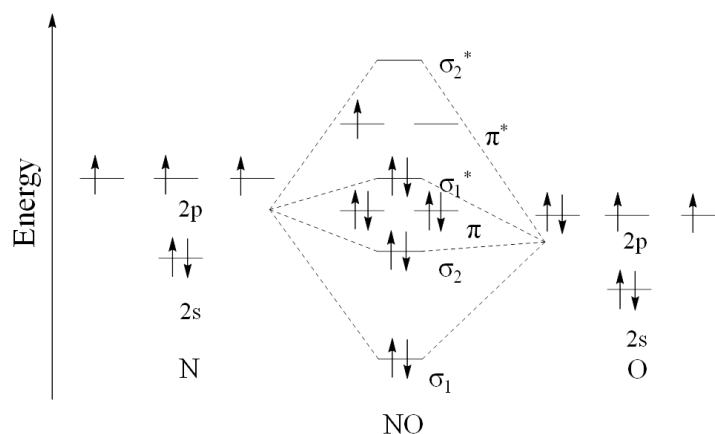


Figure 1.4. Molecular orbital diagram for nitric oxide (NO).

Protonation of the NO^- ligand to form free ${}^1\text{HNO}$ slightly decreases the N-O bond length to 1.211 Å and increases ν_{NO} to 1565 cm^{-1} . Moreover, the HNO molecule is bent, sp^2 -hybridized, having a H-N-O bond angle of 108.5° .^{55,56} The NO^-/HNO has an accessible triplet state and can exist in a singlet or triplet state depending on the protonation state; this drastically effects its acid-base equilibrium (Fig. 1.5). For example, free ${}^1\text{HNO}$ is more stable by 20 kcal/mol than the triplet state, accordingly, the ground-state ${}^1\text{HNO}$ has an estimated $\text{p}K_{\text{a}}$ of 11.6.^{38,57} In contrast, the NO^- anion is a ground state triplet and is stabilized by ~16-21 kcal/mol versus its singlet state; however, ${}^3\text{NO}^-$ is 16 kcal/mol less stable than ${}^1\text{HNO}$ (Fig. 1.5). This discontinuity in the spin-state of nitroxyl and its anion complicates their interconversion in solution; however it suggests that (i) it is unlikely that free HNO is formed directly from free NO under physiological conditions with biological reductants, and (ii) if HNO were to form endogenously, a metal center seems to be a probable mediator of the spin-state dilemma. However, additional questions of M-HNO bonding, spin-state, redox potential, $\text{p}K_{\text{a}}$, and vibrational data remain only partially understood.

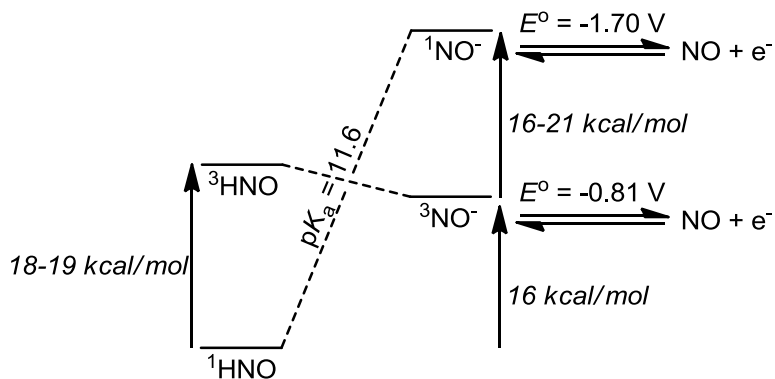


Figure 1.5. Thermochemical scheme of the acid-base and redox properties of free nitroxyl. Fig. 1.5 is a modified version from reference 58 and compiles values from references 38,56,59,60. Figure reused from reference 66 with permission.

The primary bonding interactions of NO with a metal center include a σ -bond from the N lone-pair to the metal center and π -backbonding from the metal to the π^* orbitals of the NO ligand. Calculations demonstrate that it is possible for the $\eta^1\text{-N}$ complex to isomerize to either the $\eta^1\text{-O}$ species or a side-on $\eta^2\text{-NO}$, though experimentally these observations are sparse for first-row transition metals and are only obtained by low-temperature photolysis experiments. Some relevant examples include $[\text{Fe}(\text{CN})_5(\text{NO})]^{2-}$ and $[\text{Fe}(\text{por})\text{NO}]$ (where por = porphyrin).^{54,61-63} Nonetheless, the vast majority of M-NO species in biology and in first-row transition metal models are N-bound. The metric parameters of many metal nitrosyls (N-bound) have been determined experimentally.^{54,64} When bound to a metal center, the NO^n species (where $n = +1, 0, \text{ or } -1$) can still exhibit various formal oxidation states which can now be coupled with the metal center. For instance, if considering Fe(II), d^6 , then the Fe-NO unit can exist in the following states: Fe(I)- NO^+ , Fe(II)-NO, Fe(III)- NO^- . This resonance between the Fe-NO unit is termed redox non-innocence and is in part due to the high degree of covalency in the Fe-NO bond.⁶⁵ Because of the non-innocent nature of nitrosyls, it can be difficult to assign accurate

oxidation states for both the metal and the nitrosyl. Thus, a formulation was developed by Enemark and Feltham in 1974 to describe the overall electronic nature of the M-NO unit.⁶⁶ This formulation, termed the Enemark-Feltham (E-F) notation sums the total number of *d*-electrons of the metal with the total number of π^* electrons in the NO ligand to give the formula of $\{\text{MNO}\}^n$ (where *n* represents the *d* + π^* electrons). If considering the examples provided above, then Fe(I)-NO⁺ ($d^7 + 0\pi^* = 7$), Fe(II)-NO ($d^6 + 1\pi^* = 7$), Fe(III)-NO⁻ ($d^5 + 2\pi^* = 7$), then all of these redox isomers are formally $\{\text{FeNO}\}^7$ meaning the total number of electrons stays the same and thus no redox chemistry is occurring outside the resonance of the FeNO unit. However, if one looks at a series of redox events within one species, for example Fe(III)-NO an $\{\text{FeNO}\}^6$ species, then addition of electrons to this system could occur at either the metal center or the NO ligand or in essence both. For convention, one can consider just metal-centered reduction holding the nitrosyl in its neutral free radical state. Therefore, a one-electron reduction of Fe(III)-NO $\{\text{FeNO}\}^6$ gives Fe(II)-NO $\{\text{FeNO}\}^7$ where an additional one-electron reduction would afford Fe(I)-NO $\{\text{FeNO}\}^8$ (Fig. 1.6). Each of these redox isomers could potentially resonate to change the formal redox state on the metal and nitrosyl, thus the E-F notation is an important caveat of M-NO chemistry.

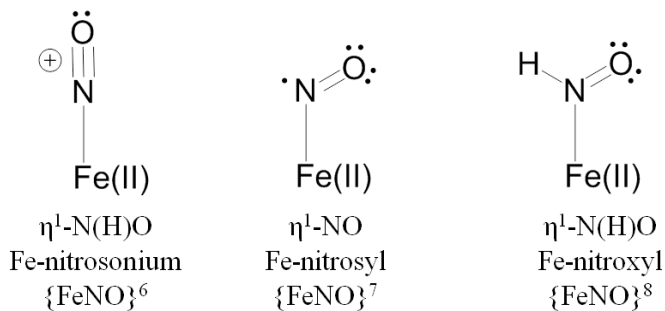


Figure 1.6. Examples of Enemark-Feltham notation for Fe-NO.

As observed in NO species, the overall redox state of the Fe-NO unit drastically changes the physical and chemical properties of the complex. For instance, the M-N-O bond angle decreases upon reduction while the N-O bond length increases. Both of these phenomenon highlight the greater electron occupancy of the N-O π^* orbital that decreases the bonding character in the NO bond and rehybridizes the NO ligand from sp ($\sim 180^\circ$) to sp^2 ($\sim 120^\circ$). For example, NO^+ (isoelectronic to CO and CN^-) binds in a linear fashion to metal centers, comparably, NO^- (isoelectronic to O_2) binds in a bent geometry.⁵⁴ Given the wide range of redox states available to metal-nitrosyls one may expect a diverse set of spectroscopic parameters for each state. Accordingly, the N-O bond lengths of coordinated NO can range from ~ 1.0 - 1.8 \AA and M-NO bond lengths can vary from 1.62 - 1.9 \AA . Similarly, ν_{NO} ranges from 1200 to 1900 cm^{-1} and the Fe-N-O bond angle can vary from $\sim 120^\circ$ to 180° . Taken together, identifying the spectroscopic signatures of a particular metal-nitrosyl complex can provide information about the overall oxidation state of the M-NO unit.^{54,67}

1.4.2 NO_2^- with Fe

The interactions of NO_2^- with metal ions is of primary importance to the global nitrogen cycle and human physiology. Accordingly, the fundamental physical parameters of such complexes have been pursued. Crystallographic parameters for NaNO_2 show an N-O bond length of 1.23 - 1.25 \AA and O-N-O angle of 110 - 116° .⁶⁸⁻⁷⁰ Moreover, NO_2^- has a straightforward acid-base equilibrium with nitrous acid (HNO_2 pK_a of 3.35).⁷¹ IR-spectroscopy of NO_2^- in KBr at 8 K show N-O bands at 1316 , 12755 , and 798 cm^{-1} and represent the ν_{symm} , ν_{asymm} , and δ_{symm} , respectively.⁷² A comparison of the physical parameters for NO_2^- , NO, and HNO are shown in Figure 1.7.

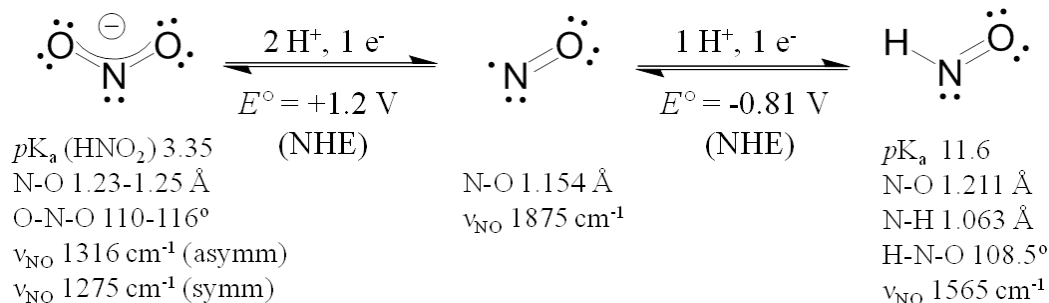


Figure 1.7. Physical parameters of NO_2^- , NO, and HNO. Values taken from multiple references and cited in the text.

The redox chemistry of NO_2^- shows a one electron oxidation ($E^\circ = +1.04 \text{ V}$ vs. NHE) characterized as the $\text{NO}_2^\bullet/\text{NO}_2^-$ redox couple.⁷¹ The reduction of NO_2^- under standard conditions, where HNO₂ is the predominate species, spontaneously affords NO. However, such conditions do not exist physiologically and the thermodynamically favored reduction becomes less favorable. For example, at pH 7 the $E^\circ = 0.268 \text{ V}$ and at pH = 14 the $E^\circ = -0.460 \text{ V}$.⁷³

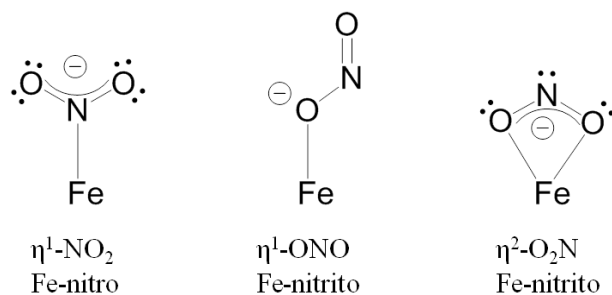


Figure 1.8. Proposed coordination of NO_2^- to an Fe center.

The bonding properties of Fe with NO_2^- display a variety of geometries, however, unlike M-NO species, these different isomers are more common and energetically accessible (Fig. 1.8). For example, NO_2^- can readily isomerize from N-bound (nitro) to O-bound (nitrito), calculated as ~ 5 kcal/mol less stable in a truncated porphyrin model for both Fe(II) and Fe(III).⁷⁴ Additionally, the bidentate $\eta^2\text{-O}_2\text{N}$ bonding mode has been structurally characterized in a non-heme model.⁷⁵ Because isomerization energy is low, nitro-to-nitrito conversions can be initiated by irradiation, hydrogen-bonding (H-bonding), or a trans-influence from an ligand axial to the NO_2^- ligand.⁷⁶ The more common form, and that which is formed in the Fe-NiR systems is the N-bound or nitro form. The general bonding profile of NO_2^- places it at the strong-field end of the spectrochemical series. When N-bound, NO_2^- provides σ -donation through the lone-pair on N, which positions the N-O bonds for π -backbonding and acceptance of $d\pi$ electron density from the metal center into N-O π^* orbitals. Unlike NO, the NO_2^- unit is typically considered redox innocent and formal oxidation states are readily assigned. Nonetheless, the N-bound NO_2^- is an excellent π -acceptor and can receive significant electron density from the metal center (Fig. 1.9). The most common oxidation states for Fe- NO_2^- species is Fe(II) and Fe(III).⁶⁴ The ν_{NO} for Fe(II/III)-nitro (N-bound) complexes are in the range of 1285-1390 cm^{-1} , in comparison to the Fe(II/III)-nitrito (O-bound) complexes typically have two distinct bands at ~ 1500 and 930 cm^{-1} .⁷⁷ The latter can be rationalized as the distinct N-O single bond and N=O double bond of the Fe-nitrito ligand, as compared to the resonance (bond order of 1.5) for the Fe-nitro species (Fig. 1.8). Correspondingly, the typical bond lengths for Fe(II/III)-porphyrin models and heme-proteins are Fe-N = 1.85-2.10 Å and N-O 1.2-1.4 Å as compared to NaNO_2 having N-O = 1.23-1.25 Å. A more detailed analysis of Fe(por) models and heme-proteins is discussed below.

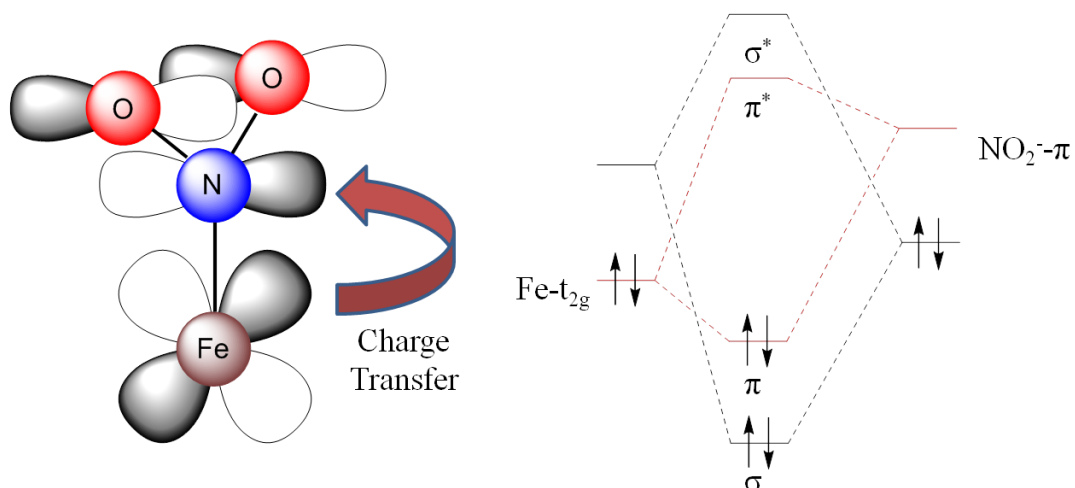


Figure 1.9. *Left:* Orbital representation of $d\pi \rightarrow \text{NO}\pi^*$ backbonding of N-bound NO_2^- ligand. *Right:* Simplified MO diagram of the $\text{Fe-}t_{2g}$ orbital interaction with the NO_2^- vacant π -orbital to give $\text{Fe-NO}_2^- \pi$ -bond.⁷⁸

1.5 The $\{\text{FeNO}\}^n$ ($n = 6, 7,$ and 8) Formulation in Biology

1.5.1 $\{\text{FeNO}\}^6$ Examples

In order to provide a context for the $\{\text{FeNO}\}^n$ notation within biology, the chemistry and physiology of $\{\text{FeNO}\}^6$, $\{\text{FeNO}\}^7$, and $\{\text{FeNO}\}^8$ complexes in proteins will be discussed. The $\{\text{FeNO}\}^6$ formulation can be obtained experimentally through reaction of a Fe(III)-heme with NO(g). While the $\{\text{FeNO}\}^6$ notation is rare in biology, several heme proteins have been observed to traverse this state. Additionally, the use of NO as a vibrational probe to bind Fe(III) heme proteins can be useful.^{79,80} With respect to biology, blood-feeding insects such as *Rhodnius prolixus* (kissing bug) and *Cimex lectularius* (bed bug) utilize small proteins known as nitrophorins (NPs) to delivery and release NO in the blood stream of their victims.^{81,82} The protein contains a heme in the ferric state bound to NO, or $\{\text{FeNO}\}^6$. Upon introduction to the bloodstream, the local NO concentration is much lower and the NO diffuses away from the NP

heme and into the host's NO signaling pathway. This increases local blood flow and also serves as an anticoagulant. Thus, the insect is uninhibited in its feeding.

Nitrile hydratase (NHase) is a non-heme Fe(III) enzyme found in bacteria that catalyzes the conversion of nitriles to amides. There has been extensive efforts to develop functional NHase analogues due to the interest in industrial production of amides.^{83,84} The N_2S_3Fe active site consists of two deprotonated carboxamido-N donors, and three Cys sulfurs; two of the basal plane Cys groups are post-translationally oxidized to sulfenato (RSO^-) and sulfinato (RSO_2^-).^{85,86} The active form of the enzyme, NHase, contains a LS Fe(III) center that can bind endogenous NO to form an inactive $\{FeNO\}^6$ complex, that is photolabile and termed the 'dark form' or $NHase_{dark}$. The inactive $NHase_{dark}$ is activated by photolysis of the Fe-NO bond with visible light.⁸⁷ Although, the exact reasoning behind the NO-dependent modulation of NHase activity is not known, these observations suggest a regulatory function of NO that can be affected by light. Thus, it is possible that other Fe-containing enzymes may operate under a regulatory mechanism involving NO and light.

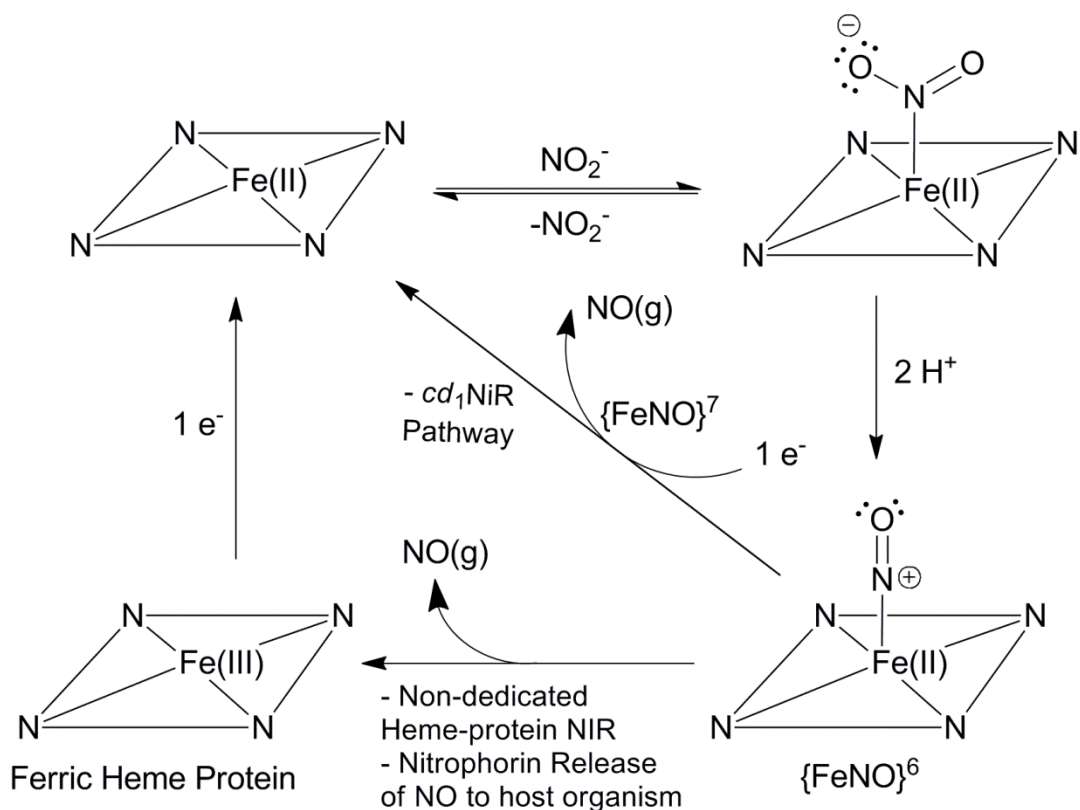


Figure 1.10. Scheme showing the $\{\text{FeNO}\}^6$ intermediate in NiR enzymes.

The chemistry of $cd_1\text{NiR}$ ⁸⁸ and cytochrome *c* NiR ($cc\text{NiR}$)^{78,89} also traverses an $\{\text{FeNO}\}^6$ species in their catalytic reduction of NO_2^- to NO and NH_3 , respectively.⁹⁰ This intermediate occurs after NO_2^- binds the Fe(II)-heme followed by two protonation events and homolytic N-O bond cleavage to afford H_2O and $\{\text{FeNO}\}^6$. This metal-nitrosyl can then either dissociate under an oxidative denitrosylation mechanism to give NO, be reduced by one-electron to promote release of NO ($cd_1\text{NiR}$), or can remain bound to the Fe center and receive $6e^-/5\text{H}^+$ to produce NH_3 ($cc\text{NiR}$). Similarly, the $\{\text{FeNO}\}^6$ species is implicated as an intermediate in the reduction of NO_2^- by globin proteins and other non-dedicated heme-containing NiR proteins. The activity of these non-dedicated NiR proteins is proposed to be, in part, responsible for the physiological

effects of NO_2^- with respect to the cardiovascular system. This intermediate serves as a critical point to the possible reactivity with RSH to give RSNO, NO_2^- to give N_2O_3 , or release of free NO. Mechanistic proposals regarding the reduction of NO_2^- by heme proteins and model complexes is discussed more thoroughly in later sections.

In addition to its biological significance, many other Fe-proteins stabilize the $\{\text{FeNO}\}^6$ complex including: myoglobin (Mb),^{79,80,91,92} hemoglobin (Hb),⁹³ and horseradish peroxidase (HRP).^{79,88,94} These examples underscore the utility of NO as a spectroscopic probe for investigating the structural and electronic properties of metalloenzymes. In addition, the use of NO as a substrate analogue and spectroscopic probe for O_2 can be helpful in the study of what would otherwise be a transient species with respect to O_2 activation chemistry.

1.5.2 $\{\text{FeNO}\}^7$ Examples

The $\{\text{FeNO}\}^7$ notation in heme proteins, porphyrin models, and non-heme models have been well studied, and are thermodynamically quite stable and readily isolable. Moreover, the remarkable stability of this state often leads to omission of this species in enzymatic cycles. Counter to this fact is the observation that *cd*₁NiR actually releases NO from the $\{\text{FeNO}\}^7$ state (Fig. 1.10). Though unusual, this catalytically relevant $\{\text{FeNO}\}^7$ complex highlights the subtlety of H-bonding networks and differing porphyrin electronic contributions on heme-protein active sites. The mechanism of *cd*₁NiR will be discussed in more detail in a forthcoming section.

Understanding the chemistry of Fe- O_2 enzymes has been facilitated by the use of NO as a spectroscopic probe. Similar to NO, O_2 is a non-innocent or redox-active ligand, i.e. the bonding of O_2 to Fe(II) can be more accurately described as Fe(III)(O_2^-), not Fe(II)(O_2). Accordingly, the E-F notation can be applied to give both species as $\{\text{FeO}_2\}^8$. In this light, Fe-NO can serve as

relatively stable analogue for Fe-O₂, which aids in studying reactive {FeO₂}^{8/9} intermediates in oxygenase enzymes.⁹⁵⁻⁹⁸ Primarily, the use of NO to study Fe-O₂ activation is applied to non-heme enzymes which afford an $S = 3/2$ ground state derived from $S = 5/2$ Fe(III) antiferromagnetically coupled to an $S = 1$ NO⁻ ligand. Specific examples include the {FeNO}⁷ analogues of isopenicillin *N* synthase (2His/1Carboxylate),^{97,99} α -keto acid-dependent enzymes,⁹⁸ dinuclear Fe hemerythrin protein ((His)₃Fe(Glu/Asp)₂Fe(His)₂),¹⁰⁰ and superoxide reductase (4His, 1Cys).¹⁰¹ Cysteine dioxygenase (CDO) is another example where O₂ activation has been studied through an {FeNO}⁷ enzyme analog, but in this case an unusual (for non-heme enzymes) $S = 1/2$ ground state is observed and assigned as $S = 0$ LS Fe and $S = 1/2$ NO. This difference from other non-heme {FeNO}⁷ enzymes is thought to arise from the interaction of the cysteine substrate with the active site Fe, where the amide-N and thiolate donors form a strong-field coordination-sphere promoting LS configuration at Fe prior to substrate oxygenation.¹⁰²

A critical physiological example of {FeNO}⁷ species can be seen in soluble guanylate cyclase (sGC), the one known receptor for NO in biology. The sGC enzyme is a Mg²⁺-dependent, *b* heme-containing enzyme activated by NO. Upon activation, sGC converts guanosine 5'-triphosphate (GTP) in cyclic guanosine monophosphate (cGMP). Targets in the cGMP signaling pathway include phosphodiesterases, ion-gated channels, and cGMP-dependent protein kinases that regulate physiological functions such as vasodilation, platelet aggregation, and neurotransmission.¹⁰³ From a molecular perspective, activation of the enzyme occurs when NO binds to the Fe(II)-heme center of the enzyme. The strong trans-influence of NO causes the weakly bound axial His ligand to dissociate from the Fe center that allows for a several hundred-fold increase in activity (Fig. 1.11).

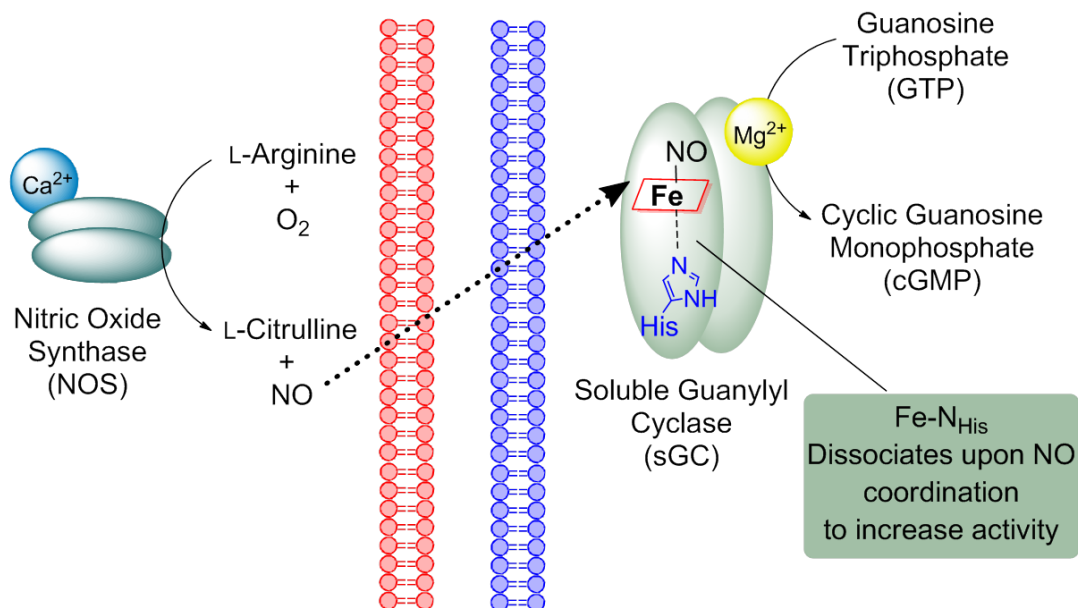


Figure 1.11. Schematic representing the Ca^{2+} dependent oxidation of L-Arginine to L-Citrulline and NO by NOS. The subsequent interaction of NO with sGC weakens the His-Fe bond to cause a conformational change and activation of the enzyme to convert GTP to cGMP.¹⁰³

There is currently some controversy as to the influence of excess NO on the sGC system. For instance, some proposals suggest that two molecules of NO can interact with sGC. One proposal details that a dinitrosyl species is formed at the heme center where two NO molecules bind axial to one another to give a very unusual $\{\text{Fe}(\text{NO})_2\}^8$ species.¹⁰⁴ Alternatively, another proposal infers that a second molecule of NO can bind to a cysteine rich non-heme site on the enzyme. Lastly, others still find that sGC only binds one NO and is unchanged in the presence of excess NO.¹⁰⁵⁻¹⁰⁷ The debate remains unresolved and is a point of active research with relevance to cGMP related disorders and signaling.

1.5.3 {FeNO}⁸ Examples

Until recently, the primary activator of sGC was thought to be NO. However, HNO has been shown to have a vasorelaxant response in mammals. The pK_a of HNO is 11.6, and is thus predominantly protonated at physiological pH. Through the use of HNO donors in animal studies, it was shown that HNO relaxes the vasculature with a concomitant increase in cGMP, and when sGC inhibitors were used, this response was significantly depressed.¹⁰⁸ This observation supports the direct activation of sGC by HNO, and can explain the similarities in the response of NO and HNO with respect to vasodilation (Fig. 1.3). Interestingly, HNO does not activate Fe(III)sGC though one can imagine the reaction of HNO + Fe(III) to give Fe(II)NO + H⁺ as a means to turn on the sGC enzyme; however this does not occur *in vitro*.³⁹

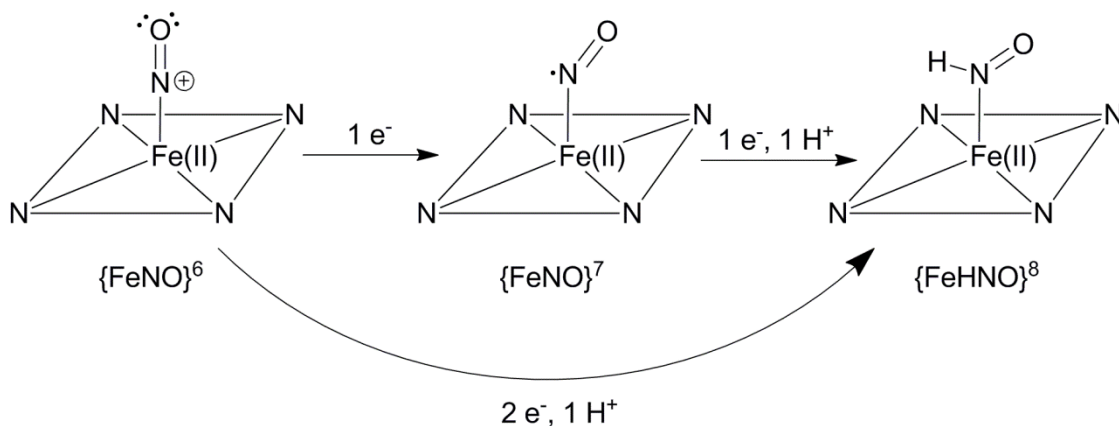


Figure 1.12. Scheme representing possible conversion of $\{FeNO\}^6$ to $\{FeNO\}^8$. One option is the two-electron reduction that avoids the stable $\{FeNO\}^7$ species. Alternatively, the single electron steps would traverse $\{FeNO\}^7$.

Direct evidence for the endogenous formation of HNO remains elusive; however, the likelihood that NO and HNO are in direct equilibrium is low, *vide supra* (Fig. 1.5). Therefore,

mediation of this process through a metal center is likely. The $\{\text{FeNO}\}^8$ formulation represents a highly-reduced Fe-NO unit and may serve as an endogenous source of HNO. Commonly, the formal oxidation state is considered as a resonance structure between Fe(I)-NO and Fe(II)-NO⁻; further protonation/reduction of such species is relevant to enzymatic cycles. Several enzymes are thought to cycle through an $\{\text{FeNO}\}^8$ state. For instance, after reduction of NO₂⁻, the *ccNiR* enzyme would contain a transient $\{\text{FeNO}\}^6$ state, a one-electron transfer to the active site would afford a $\{\text{FeNO}\}^7$ species. Counter to the $\{\text{FeNO}\}^6$ and $\{\text{FeNO}\}^8$ states, the $\{\text{FeNO}\}^7$ state is often catalytically irrelevant due to its high-stability and strong affinity for NO (Fig. 1.12). Thus, the *ccNiR* enzyme is expected to rapidly transfer two electrons to the active site and afford a transient $\{\text{FeNO}\}^8$ intermediate that is subsequently protonated and further reduced to ammonia.^{78,89} This mechanistic proposal is similar to what is proposed for the siroheme-containing nitrite reductase enzyme (SCNiR, Fig. 1.1B).¹⁰⁹⁻¹¹¹

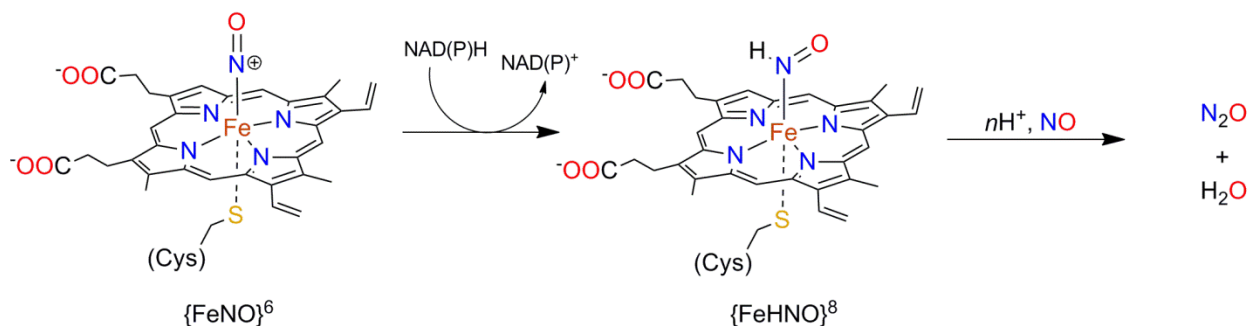


Figure 1.13. Active site representation of P450_{nor} enzyme and the putative $\{\text{FeHNO}\}^8$ intermediate to produce N₂O from a total of two NO molecules.

Fungal denitrification processes have also been discovered.¹¹² The nitric oxide reductase (NOR) enzyme, containing the P450_{nor} cofactor, also traverses a proposed heme $\{\text{FeNO}\}^8$

species in its reduction of NO to N₂O and H₂O. The active site of P450nor contains a heme *b* with proximal cysteinate ligand.³⁶ Although direct experimental evidence for the intermediates of these reactions is lacking, there are several hypotheses that support the requisite formation of an {FeHNO}⁸ species for N₂O production.^{34,35} Interestingly, P450nor receives electrons directly from NAD(P)H for the conversion of the {FeNO}⁶ to the {FeHNO}⁸ species (Fig. 1.13). This conversion is proposed to occur through direct hydride (H⁻) transfer to the Fe(III)NO.³⁶ In the conversion of NO to N₂O by P450nor, it is proposed that the nitroxyl ligand could exist in a protonation state of zero to two protons. Each additional proton would require formal oxidation of the Fe center and formal reduction of the NO⁻ ligand. Because the mechanism is speculative at this point, this proposal is primarily supported by DFT.³⁵ These computations show that [Fe(IV)NHOH]⁻ (still formally {Fe(H)₂NO}⁸) or the resonance form [Fe(III)NHOH][•] is a probable intermediate prior to the coupling of the second NO[•] molecule. The radical pathway is likely to provide appropriate energy and kinetics to facilitate N-N bond coupling and loss of water.³⁵

An alternative mechanism for NO reduction occurs through the dinuclear Fe enzymes NorBC (Fig. 1.1C) and flavodiiron proteins (FDPs, Fig. 1.14). NorBCs are a respiratory denitrification enzymes, whereas FDPs scavenge NO in pathogenic bacteria, archaea, and some protozoan parasites, that are involved in microbial resistance to the host's immune response of NO release.¹¹³ The active sites of NorBC and FDP are quite different, the FDP protein contains a dinuclear non-heme active site that is bridged by a carboxylate ligand proximal to a flavin mononucleotide cofactor.^{114,115} The NorBC enzyme, on the other hand, contains a mixed *b* heme that is oxo-bridged to a non-heme Fe(His)₃ site.¹¹⁶ Although the active sites of these enzymes differ, most proposals support that both iron centers bind one NO in the reduction process; i.e.

two separate Fe(II)-NO or ($\{\text{FeNO}\}^7$)₂. At this point, there are three possibilities toward formation of N₂O (Fig. 1.14). One pathway involves the two proton and two electron reduction of the FeNO units to afford an ($\{\text{FeHNO}\}^8$)₂ species (Pathway A, Fig. 1.14).¹¹⁴ This intermediate could effectively dimerize and release N₂O and H₂O. An alternative proposal for the FDP family is formation of the ($\{\text{FeNO}\}^7$)₂ followed by oxidative denitroxylation to give Fe(III)Fe(III), N₂O and H₂O (Pathway B, Fig. 1.14).^{114,117} The exact N-N bond formation mechanism remains elusive but may proceed through a diferric hyponitrite intermediate, $[\text{Fe(III)-(ONNO)}^{2-}\text{-Fe(III)}]$ (Pathway C, Fig. 1.14).¹¹⁸ Even with the lack of direct evidence for an $\{\text{FeNO}\}^8$ species in FDP and NorBC, the ($\{\text{FeNO}\}^7$)₂ unit is thought to have a reduced nitrosyl ligand, thus favoring an Fe(III)-NO⁻ (formally nitroxyl ligand) assignment.

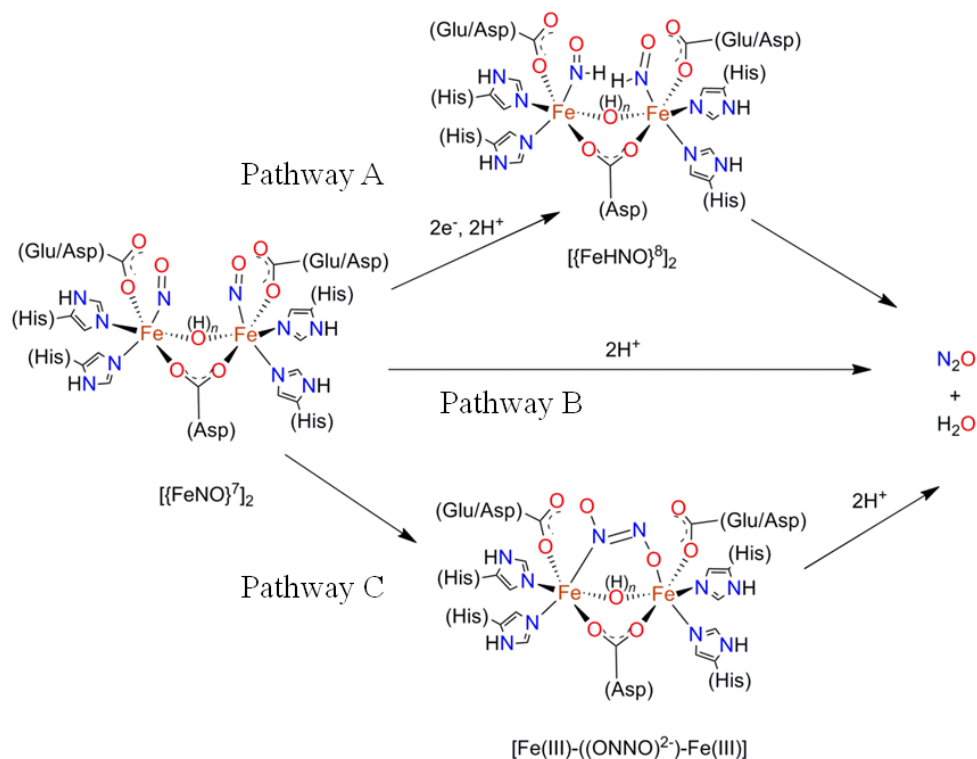


Figure 1.14. Possible routes to nitric oxide reduction by FDP enzymes, flavin mononucleotide cofactor not shown for clarity. Similar mechanistic proposals can be made for the NorBC (*b* heme/non-heme Fe_B site) enzymes active site shown in Figure 1.1C.

Given the fleeting nature of $\{FeO_2\}^8$ adducts in non-heme oxygenase enzymes, the $\{FeNO\}^8$ analogue of the taurine/ α -ketoglutarate dioxygenase (α KG)-dependent enzyme, TauD has been pursued.¹¹⁹ The α -ketoglutarate (α KG)-dependent family of enzymes are mononuclear non-heme-Fe proteins that produce succinate and CO_2 from decarboxylation of α KG to form an $Fe(IV)=O$ species for aliphatic C-H bond activation of substrate. The basal plane of the octahedral active site consists of one His, one Asp, and two carbonyl oxygen donors when α KG is bound. An axial His ligand is situated *trans* to the site of O_2 binding and activation.¹²⁰ The initial O_2 adduct, an $\{FeO_2\}^8$ species, has been spectroscopically studied with NO to form $\{FeNO\}^7$ and $\{Fe(H)NO\}^8$ analogues of the TauD enzyme.¹¹⁹ Contrary to most heme $\{FeNO\}^8$

species that are $S = 0$, this non-heme $\{\text{FeNO}\}^8$ complex has a triplet ground-state. Because the Fe center is octahedral and has a His donor axial to NO, comparable to many heme systems, the spin-state change is likely due to the four ligands in the basal plane, three of which are O-donors. The presence of O-donors is known to effect the spin-state of Fe complexes, and favors a high-spin species ($S_{\text{Fe}} = 1, 2, \text{ or } 3$), correspondingly, the NO^- ligand, can either be $S = 0$ or $S = 1$. The resulting analysis could only determine that the $\{\text{FeNO}\}^8$ species was paramagnetic and limited the possible spin-state as either ($S_{\text{Fe}} = 1, 2, \text{ or } 3$).¹¹⁹ Moreover, this study was performed at cryogenic temperatures due to the instability of the $\{\text{FeNO}\}^8$ species. Although not necessarily biologically relevant, the TauD $\{\text{FeNO}\}^8$ complex is an interesting study into the effect of ligand field on spin-state $\{\text{FeNO}\}^8$ complexes, and furthermore distinguishes non-heme $\{\text{FeNO}\}^8$ complexes as having an accessible HS state, not observed in heme complexes.

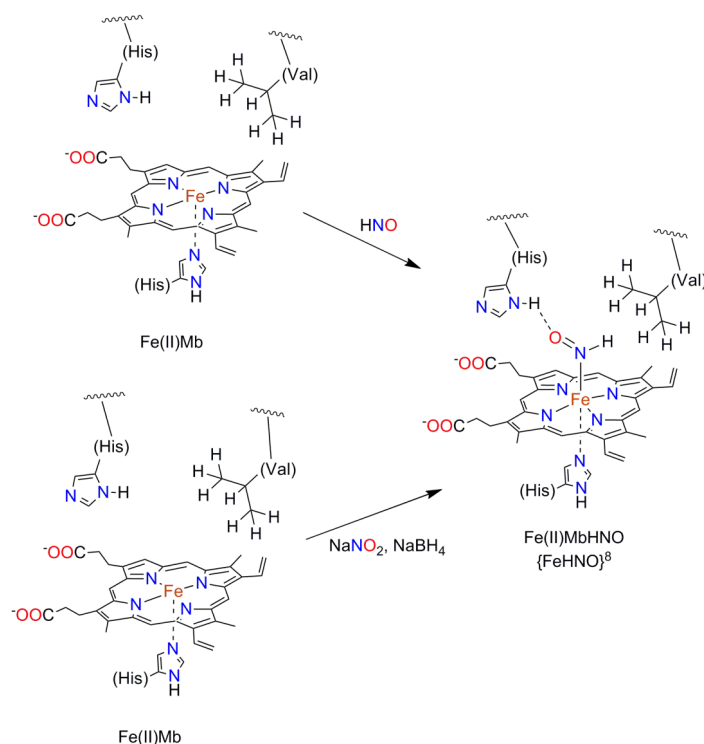


Figure 1.15. Synthesis and proposed stabilization of HNO with Mb protein.

As exemplified in the prior examples, the stability of $\{\text{Fe}(\text{H})\text{NO}\}^8$ is typically low and such species are often fleeting. One outlier to this trend is found in Mb. The species in Mb is remarkably stable in deoxygenated, buffered solutions for months.¹²¹⁻¹²⁵ The stability is due to favorable secondary-sphere interactions that place the H of HNO in proximity to a hydrophobic Val residue while the O-atom is stabilized through H-bonding to a His residue. This interaction is similar to the stabilization of O_2 in the same binding site (Fig. 1.15). The $E_{1/2}$ for the Fe(III/II) couple of the Mb-HNO complex is -0.87 V vs. SCE (-0.63 V vs. NHE), making it an unlikely candidate for the generation of HNO directly from $\{\text{FeNO}\}^7$ Mb under physiological conditions.¹²⁶ *In vitro* studies demonstrate that deoxyMb can trap free HNO generated by an HNO-donor with $k_{\text{on}} = 2.2 \times 10^5 \text{ M}^{-1}\text{s}^{-1}$, which is comparable to $k_{\text{on}} = \sim 1 \times 10^6 \text{ M}^{-1}\text{s}^{-1}$ for the MbCO complex.^{122,127,128} The affinity of deoxyMb for O_2 and the potential reactivity of HNO and MbO₂ to afford NO and H₂O₂ requires oxygen-free conditions.¹²⁹ Accordingly, the existence of MbHNO in physiology would require binding of free NO to deoxyMb under anaerobic and strongly reducing conditions or binding of free HNO under anaerobic conditions. The latter is more likely, assuming HNO is formed endogenously, making Mb a candidate for the stabilization and deliver HNO in biology. The low dissociation rate of MbHNO may necessitate cooperative binding and/or conformational changes to induce release of HNO; regardless, the study of MbHNO has provided an excellent spectroscopic vantage point (*vide infra*) into heme-HNO interactions.

1.6 Nitroxyl (NO⁻/HNO) Chemistry and Pharmacology

1.6.1 Sources of HNO

The generation of endogenous HNO in biology is controversial and direct experimental evidence/detection of free HNO through *in vivo* studies does not exist; however, strong *in vitro* evidence suggests that it is possible to produce HNO through several mechanisms (Fig. 1.16). A likely source of HNO is NOS.¹³⁰ The NOS active site contains a heme bound by a cysteinate ligand. At this active site both O₂ activation and substrate oxidation are performed, similar to cytochrome P450. The enzyme requires multiple cofactors for production of NO including FAD, FMN, NADPH, and tetrahydrobiopterin (BH₄). The substrate for NOS is L-Arg, which is oxidized to L-citrulline through a *N*-hydroxy-L-Arginine intermediate that is dependent on the presence of O₂. The NOS enzyme consists of three domains, a reductase domain, an oxidase domain (heme) and a calmodulin binding domain (Fig. 1.17).^{22,131} The reductase domain binds the flavins FAD and FMN as well as NADPH, while the oxidase domain houses the active site and facilitates substrate proximity to the Fe(IV)=O oxidant as well as the BH₄ cofactor. There are currently three known human isoforms of NOS, inducible NOS (iNOS, immune response), endothelial NOS (eNOS, vaso-regulator), and neuronal NOS (nNOS, neurotransmitter).

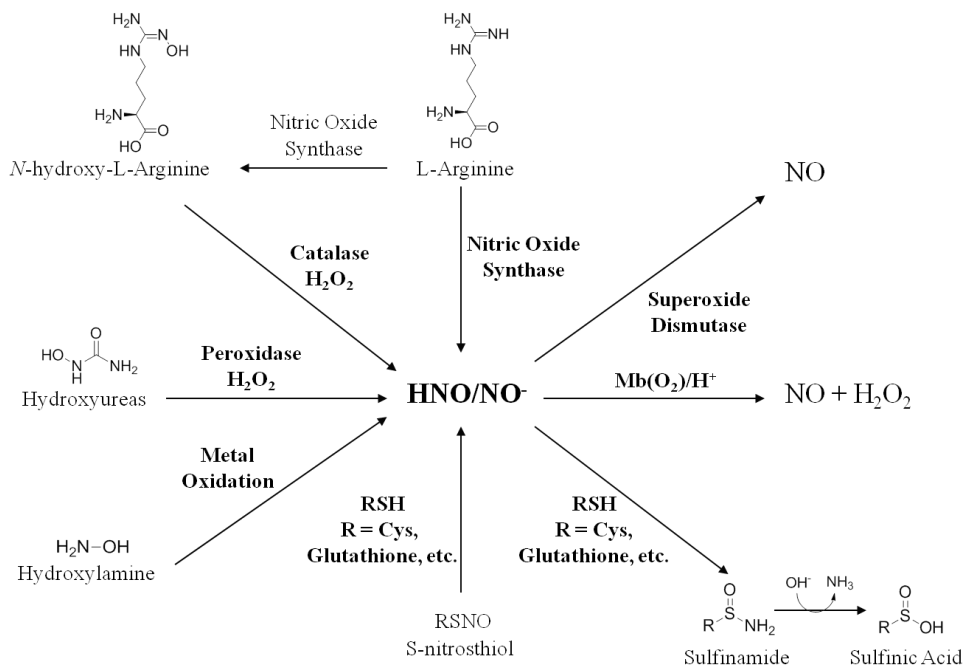


Figure 1.16. Proposed biological routes to the possible formation of HNO and some reactive pathways of HNO.¹³⁰

Experimental *in vitro* evidence shows that NOS can produce HNO through oxidative degradation of the intermediate *N*^G-hydroxy-L-Arg (NHA).¹³²⁻¹³⁴ Additionally, when the NOS enzyme is depleted of its BH₄ cofactor, HNO may also be produced.¹³⁵⁻¹³⁷ The production of NO by NOS is enhanced when in the presence of SOD.¹³⁸ This may suggest that HNO is produced from NOS and then oxidized to NO by SOD (Fig. 1.16). It appears that NOS can produce both NO and HNO. Thus, the molecular machinery may already be in place for the endogenous production of HNO. The ability for NOS to produce HNO, *in vitro* at least begs the question as to the condition-dependent synthesis of NO vs. HNO, and whether or not the enzyme is acting as an (H)NOS.¹³⁰

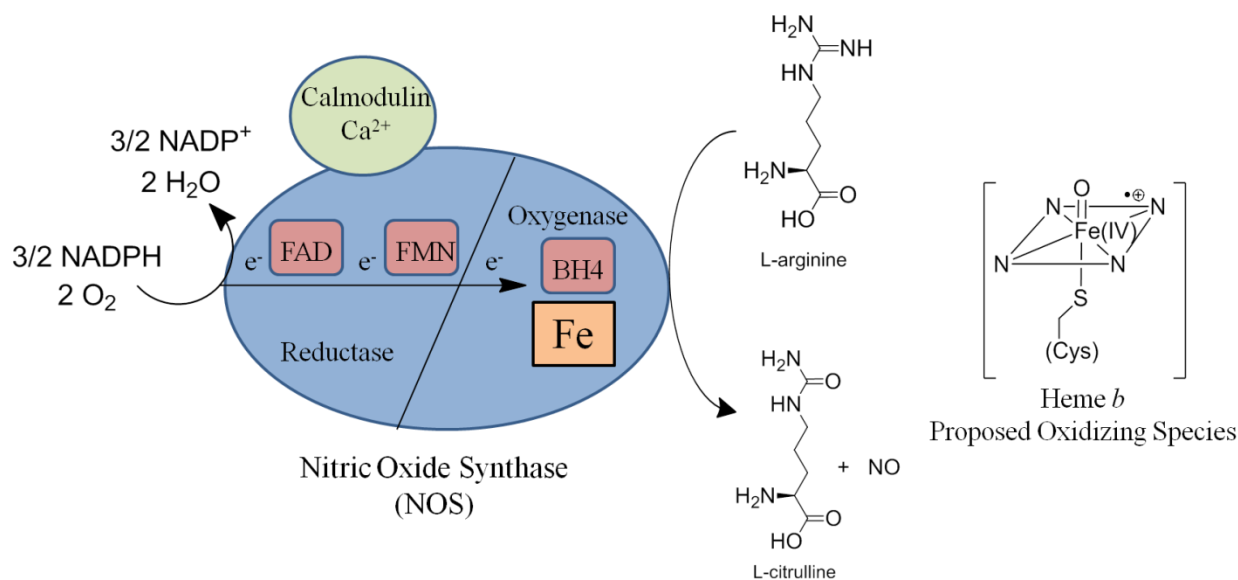


Figure 1.17. Representation of the nitric oxide synthase (NOS) enzyme, cofactors and substrate oxidation.¹³⁹

Provided NOS utilizes oxidative degradation of a NHA to form NO or HNO, allows for the possible heme-mediated conversion of other N-containing species by a similar pathway.¹⁴⁰ For example, HRP-mediated oxidation of hydroxylamine (H₂NOH) in the presence of H₂O₂ yields HNO (Fig. 1.16). This reaction was demonstrated through *in vitro* trapping experiments with glutathione (GSH) and highlights a probable mechanism of HNO formation from a simple bio-molecule at a common enzyme active site (Heme *b*/proximal His).¹⁴¹ This also supports current theories on the biological interplay between HNO and H₂O₂.^{133,142} Interestingly, HRP does not form HNO from NHA.¹³⁰ In addition to hydroxylamine, the commonly used therapeutic N-hydroxyurea (treatment for sickle-cell anemia) can be oxidatively transformed into NO and HNO.^{143,144} This reaction is also shown to occur at H₂O₂-dependent HRP. Overall, several other molecules have been implicated as precursors to HNO. Examples include, hydroxamic acids (RC=ONHOH), NaN₃, and H₂NCN; the latter of which has been used as an anti-alcoholism drug

for many years in Europe and Japan. A general mechanism for these reactions is shown in Figure 1.18. Other proposals exist for the production of HNO. One pathway includes the metal-mediated reduction of NO by superoxide dismutase (SOD) or xanthine oxidase.¹³⁰ Also, the reaction of S-nitrosothiols (RSNO), a known biological species, and RSH can liberate HNO upon formation of disulfide (Fig. 1.16).¹³⁰

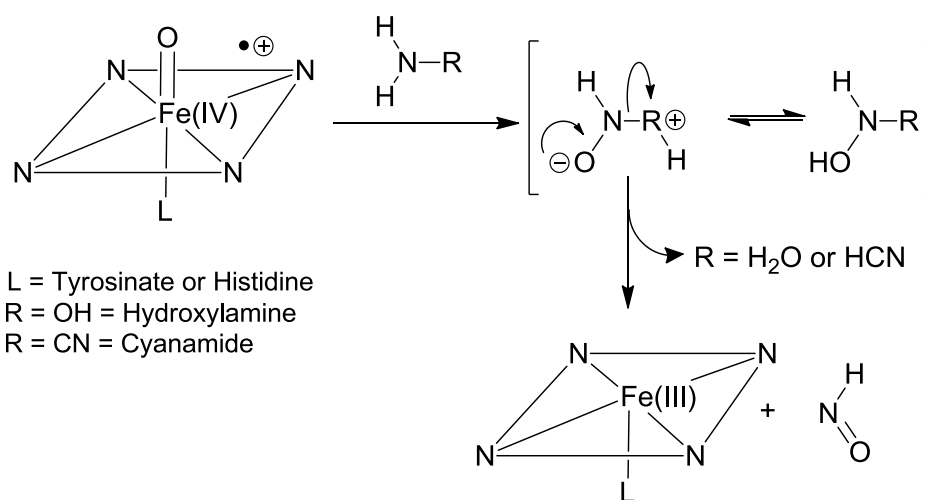
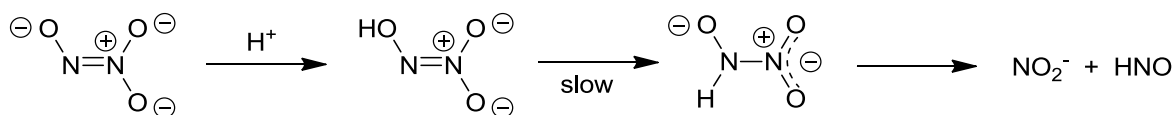


Figure 1.18. A potential mechanism for oxidative degradation of hydroxylamine (H_2NOH) and cyanamide (H_2NCN) by a $[\text{por}(\bullet+)\text{Fe}(\text{IV})=\text{O}]$ such as horseradish peroxidase (HRP) and catalase.

The prodrug cyanamide acts as an HNO donor only after its reaction with catalase.¹⁴⁵ This is another example of heme-mediated oxidative degradation to release HNO, the mechanism of which can be seen in Figure 1.18. Cyanamide bioactivation to give HNO is known to react with thiol residues in the active site of aldehyde dehydrogenase (ALDH).⁴⁵ This efficiently disrupts EtOH metabolism and warrants its use as an anti-alcoholism agent. The ALDH inhibition is an excellent example of HNO and thiol interactions in biology. With respect

to AIDH, the enzyme contains two thiols in the active site and can be either reversibly inhibited or irreversibly inhibited with HNO depending on pH.^{45,145} For instance, the reaction of HNO with a thiol produces an N-hydroxysulfenamide (RSNHOH) which rearranges to RS(O)NH₂. In the presence of another thiol, N-hydroxysulfenamide can react with RSH to give disulfide (RSSR) or react with OH⁻ to give sulfinic acid (Fig. 1.16).¹⁴⁶ Since AIDH has two thiols, it can either form RSSR (reversible, pH > 8.5) or RS(O)NH₂ (irreversible inhibition, pH < 7.5). It is notable that the presence of glutathione (GSH) or dithiothreitol (DTT) circumvents AIDH inhibition, likely due to interception of HNO and formation of the sulfenamide or disulfide of GSH or DTT.⁴⁵ Notably, AIDH inhibition does not occur through interaction of HNO at a metal center and implicates thiols as an important biological target for HNO (*vide infra*).

Angeli's Salt



Piloly's Acid

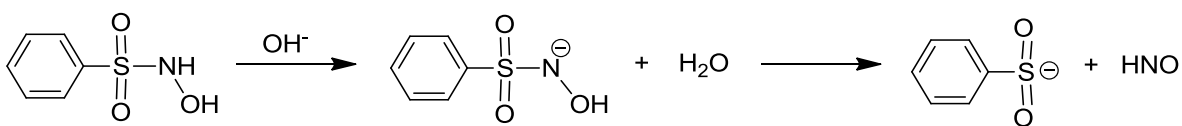
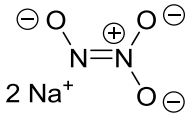
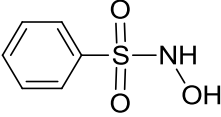
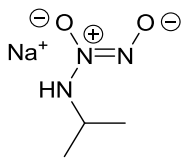
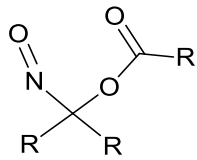
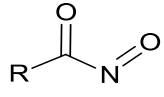
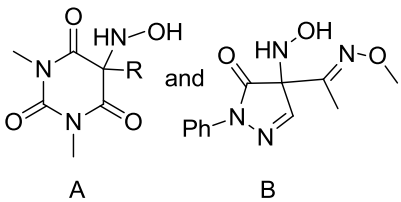


Figure 1.19. Proposed mechanisms for the acid-dependent decomposition of Angeli's salt and the base-decomposition of Piloly's acid to form HNO.

Due to the rapid dimerization rate of the HNO molecule ($8 \times 10^6 \text{ M}^{-1}\text{s}^{-1}$) to form N₂O and H₂O, the potential for direct treatment or study of a system with free HNO is nearly impossible.^{134,147,148} Thus, the use of molecules that either spontaneously decompose or react

with another species to form HNO is required for therapy or experimental work. The therapeutic use of HNO prodrugs like cyanamide and *N*-hydroxy urea are no exception and require the enzymes catalase and horseradish peroxidase for HNO release, respectively.^{45,143,144} These current therapies follow nearly a century of HNO formation through decomposition of organic and inorganic N-containing molecules.¹³⁰ The two oldest known HNO donors, Angeli's salt (AS, Na₂N₂O₃) and Piloty's acid (PA, C₆H₅SO₂NHOH), were first published in 1896 (Fig. 1.19, Table 1.1).^{149,150} The rate of HNO release from AS or PA is pH dependent, with rates increasing under more acidic conditions for AS and rates increasing under more basic conditions for PA. This can readily be rationalized through the proposed decomposition mechanisms (Fig. 1.19). Correspondingly, AS is the most commonly used HNO donor for biological assays and has a decomposition rate of $k = 4-5 \times 10^{-3} \text{ s}^{-1}$.¹⁵¹ The decomposition is spontaneous and does not require bioactivation, however the rates of AS decomposition have been shown to increase in the presence of metal complexes such as Fe and Mn porphyrins by up to 100-fold. HNO formation is proposed to occur through a M-N₂O₃ complex followed by decomposition and liberation of HNO.¹⁵²

Table 1.1. HNO Donors and their properties.³³

HNO Donor	Properties	Limitations	References
 <p>Angeli's Salt</p>	<ul style="list-style-type: none"> • Spontaneously dissociates to release HNO and NO₂⁻ • $t_{1/2} \sim 2.5$ min ($4 < \text{pH} < 8$) • NO release at $\text{pH} < 4$ 	<ul style="list-style-type: none"> • Co-release of NO₂⁻ • NO can be released at high concentrations • Short half-life 	31,37,147,153
 <p>Piloty's Acid</p>	<ul style="list-style-type: none"> • Base-dependent release of HNO 	<ul style="list-style-type: none"> • $\text{pH} > 7.4$ required • Releases NO at physiological pH 	153
<p>H₂N—C≡N</p> <p>Cyanamide</p>	<ul style="list-style-type: none"> • Requires oxidation by catalase to become an HNO donor • Currently used therapeutic for anti-alcoholism 	<ul style="list-style-type: none"> • Requires H₂O₂ and catalase for HNO release • Co-release of HCN 	153
 <p>Isopropyl Amines/NONOate</p>	<ul style="list-style-type: none"> • Dissociates to release HNO at physiological pH • $t_{1/2} \sim 2.3$ min • HNO donor <i>in vivo</i> 	<ul style="list-style-type: none"> • At $\text{pH} < 7$, NO can be released • Mixed NO/HNO donor • Short half-life • Co-releases cytotoxic R₂NNO 	27,153
 <p>Acyloxy Nitroso</p>	<ul style="list-style-type: none"> • Activated by nucleophilic attack • Modular R-groups can affect HNO release kinetics 	<ul style="list-style-type: none"> • Lower potency than Angeli's salt 	147,153,154
 <p>Acyl Nitroso</p>	<ul style="list-style-type: none"> • Produced by laser photolysis from 3,5-diphenyl-1,2,4-oxadiazole-4-oxide • Then requires base for HNO release 	<ul style="list-style-type: none"> • Complicated release of HNO • Acyl nitroso species are very unstable • $t_{1/2} < 1$ ms 	155
 <p>A and B</p> <p>N-substituted Hydroxylamines</p>	<ul style="list-style-type: none"> • Various half-lives: <ul style="list-style-type: none"> A. $t_{1/2} = 0.7$ min B. $t_{1/2} = 9.5$ min • HNO released at physiological pH 	<ul style="list-style-type: none"> • Newer compounds that require more rigorous testing for <i>in vivo</i> application 	156

In addition to AS and PA, other HNO-donors have been developed such as NONOates (IPA/NO)¹⁵⁷ and acyloxynitroso compounds.¹⁵⁴ Each donor has unique properties and limitations that are summarized in Table 1.1. Nonetheless, limitations such as co-release of cyanide, NO, or NO₂⁻ from current donors can complicate experimental observations or even lead to formation of toxic nitrosamines. Taken together, AS is still the most used and most reliable HNO donor for experimental study. Due to limitations of each donor, the development of novel organic and inorganic platforms having diverse half-lives, kinetics, and *in vivo* properties for donation of HNO in biological media is a current area of research. However, the use of AS and PA have enabled the current level of understanding of HNO in a biological setting.¹⁴⁷

1.6.2 Targets and Pharmacology of HNO

The use of HNO donors has detailed the pharmacological properties of this reactive nitrogen species (RNS). Generally, the properties of HNO are compared and contrasted to those of NO due to the chemical similarity and well understood physiology of NO. The major biological targets of HNO are metal centers and thiols, thus there are numerous potential targets in the biological milieu. The properties of HNO are typically reducing with respect to metals and are known to reduce Cu, Fe, and Mn centers.^{27,28,158} This mechanism could potentially form NO from the one electron oxidation of HNO and is proposed to occur at SOD, thus implicating SOD as a possible player in NO and HNO pharmacology (Fig. 1.16).¹⁵⁹ It has been proposed that HNO preferentially targets Fe(III) vs. Fe(II) proteins, yet this point is not always the case due to the fact that HNO does not activate Fe(III) sGC.³⁹ Small molecule studies certainly support Fe(III) and Mn(III) porphyrins as traps for HNO to give the corresponding {FeNO}⁷ and {MnNO}⁶ complexes, more favorably to reaction with NO.¹⁶⁰ Therefore, it is safe to say that

HNO is more reactive with Fe(III) than NO, but HNO can interact with Fe(II) proteins as seen with sGC and trapping of HNO by Mb.¹²⁵ The preferential reactivity of Fe(II)-heme with NO and Fe(III)-heme with HNO is a viable distinction to the signaling of these nitrogen oxides. Moreover, the reaction of HNO with cysteine thiol residues of attenuates sGC activity.³⁹ Thus, sGC is an excellent example of an enzyme that HNO activates through interaction with Fe, and attenuates through reaction with thiol residues of the same protein.

The clearest distinction between HNO and NO reactivity and biological targeting is that HNO is thiophilic.⁵⁷ Accordingly, reaction with thiols encompasses much of the known bioactivity for HNO.^{58,161} This distinction became clear after the development of the HNO pro-drug cyanamide that inhibits ALDH through thiol modification (*vide supra*). The thiol-dependent inhibition of several other proteins has been reported, for instance glyceraldehyde 3-phosphate dehydrogenase (GADPH) and mitochondrial respiratory complexes I and II are inhibited by HNO.¹⁵³ In addition, HNO can target thiols on ion-channels. This process opens voltage-dependent K⁺ channels as well as Ca²⁺ channels on non-adrenergic/non-cholinergic nerves through interaction of HNO with a thiol residue or possibly a metal ion.^{37,153} The Ca²⁺ channel interaction is proposed as the mechanism to which these nerves release calcitonin gene-related peptide (CGRP), a vasodilatory neuropeptide, and the most common biomarker for HNO in plasma.¹⁶² This peptide stimulates endothelial release of NO, increases cAMP in vascular smooth muscle tissue, and activates K⁺ ion-channels to evoke vasodilation.¹⁶³⁻¹⁶⁵ However, studies using an antagonist (CGRP₈₋₃₇) demonstrated that the vasodilation produced through injection of AS was uninhibited by the antagonist.

This *in vivo* result implies that HNO stimulation of CGRP levels is not a significant contributor to the vasodilatory properties of AS (HNO); the true molecular mechanism behind the vasodilation observed with AS is still not fully understood, and may imply interaction of HNO with sGC to obtain vasodilation.¹⁶²

Another distinct property of HNO is its ability to elicit myocardial contractility or heart muscle contraction, a phenomenon which is not observed with NO donors.^{162,163,166,167} This unique effect occurs within the cardiomyocyte through a cGMP-independent interaction of HNO with ryanodine receptors (RyR2) to trigger Ca^{2+} release into the sarcoplasmic reticulum. The interaction is a direct result of HNO interacting with thiols of the RyR2 receptor.^{167,168} In addition, HNO has been shown to play a protective role for heart tissue in the setting of heart failure. Taken together, the ability to protect against tissue injury after stopped blood-flow, contract heart-muscle cells, dilate vasculature, and its potential cytoprotective role as an antioxidant clearly details the therapeutic potential of HNO. The vast potential of HNO as a therapeutic is clear; unfortunately, the direct administration of HNO to a patient is not possible. Thus, the use of molecules capable of delivering HNO is a necessity for HNO-based therapies and experimental studies. Currently, HNO donors (Table 1.1) release through pH-dependent or enzymatic decomposition pathways. Provided that HNO interacts with Fe(II)-heme proteins (sGC) and can further be stabilized at Fe(II)-hemes (MbHNO), might suggest an alternative to the inorganic-based (AS, $\text{Na}_2\text{N}_2\text{O}_3$) or the more predominant organic-based HNO donors. Moreover, the relationship between Fe proteins and HNO highlights metal nitrosyls as a possible means to stabilize and release HNO under controlled conditions. In this light, the study of small molecule $\{\text{FeNO}\}^n$ complexes has been of paramount significance to the interactions of NO with numerous heme or non-heme proteins either for endogenous activity or as a spectroscopic probe

into the active site of a Fe-protein (*vide supra*). However, a burgeoning area of research is the study of reduced iron nitrosyls or $\{\text{FeNO}\}^8$ systems. These species offer insight into intermediates formed in many Fe-proteins, but also provide a new avenue for the development of HNO donors. Due to the relevance of these species to enzymatic cycles and the interaction of Fe proposed in HNO pharmacology, a review of the current small-molecule $\{\text{FeNO}\}^8$ heme and non-heme literature is presented below.

1.7 $\{\text{FeNO}\}^8$ Heme Coordination Complexes⁶⁷

The interaction of small gaseous molecules, such as NO, CO, and O₂ with the prototypical heme proteins Hb and Mb have long been of fundamental interest given their imperative role in aerobic physiology.¹⁶⁹ Even in 2011, new insight into reactions mediated by Hb have implicated these finely tuned reaction centers as being involved in more than just oxygen transport, such as the hypoxic generation of NO and nitrite anhydrase activity.¹⁷⁰⁻¹⁷² Collectively, discrete Fe-por complexes have provided valuable insight into the role of heme iron in a variety of small molecule activation pathways.¹⁷³ Motivated by the numerous examples of heme-NO interactions, synthetic chemists have focused their efforts on constructing heme models utilizing a variety of porphyrin derivatives. Analogous to the variations in the heme cofactor of proteins, synthetic porphyrins also provide suitable ancillary ligand platforms that can be systematically varied with regards to peripheral C-H bond saturation (sp^3 vs. sp^2 hybrids) and functional group modification. Indeed, nature has employed such variations on the peripheral carbon backbone of hemes to impart subtle differences in electronic properties.

Understanding the fundamental properties and the reaction chemistry of heme proteins has in part been made possible through the synthesis and characterization of specific low molecular weight or small molecule Fe-por complexes.¹⁷⁴

1.7.1 Synthesis and Experimental Properties of Heme {FeNO}⁸ Complexes⁶⁷

Due to their roles in mammalian physiology, Hb and Mb have been studied for more than 140 years.^{170,175} In light of the similar structural and electronic properties of the heme ligand in these proteins, Fe-por complexes have long been used as models. The first reported work (1973) of a Fe-porphyrin nitrosyl (Fe(por)NO) involved the binding of NO to Fe(II)(por) in order to extrapolate kinetic and thermodynamic parameters of Fe-O₂ interactions using NO as an analogue due to its rich spectroscopy.¹⁷⁶ Shortly thereafter spectroscopic¹⁷⁷ and structural¹⁷⁸ characterization of the first Fe(por)NO complex was reported in 1974 with the tetraphenylporphyrin (TPP) ligand, which has been used widely as a platform in numerous metal constructs (Fig. 1.20). The report of the very stable complex [Fe(TPP)(NO)] (**1**), an {FeNO}⁷ species as defined by the E-F notation,⁶⁶ involved its synthesis, and structural/spectroscopic characterization.¹⁷⁷ These early investigations suggested the nitrosyl to be a neutral NO• ligand coordinated to a LS Fe(II) center ($S_{tot} = 1/2$) when six-coordinate (6C), which has been further verified recently (2005-2006) by detailed DFT computational work from Lehnert and coworkers.^{179,180} However, 5C {FeNO}⁷ complexes such as **1** display a strong mixing between Fe d_z^2 and NO π^* orbitals in their frontier MOs and suggest more LS Fe(I)-NO⁺ character in these systems.¹⁸¹

Establishment of the electronic structure of this $\{\text{FeNO}\}^7$ system is crucial since it is the principal entry point for nearly all of the $\{\text{FeNO}\}^8$ -por systems that are described in the discussion below. This assignment and its corresponding spectroscopic benchmarks therefore set the stage in addressing the fate of the electron in the $\{\text{FeNO}\}^7$ -to- $\{\text{FeNO}\}^8$ reduction (i.e. localized on Fe or NO).

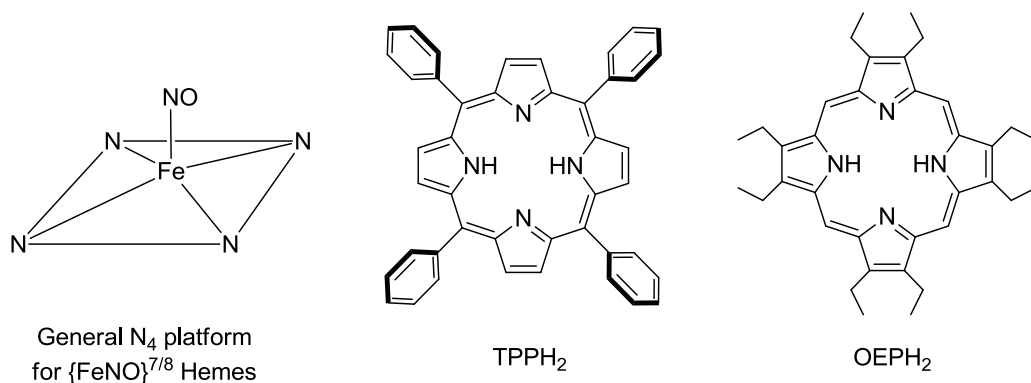


Figure 1.20. The N_4 platform (*left*) represents the general coordination of the FeNO unit in porphyrin-based ligand systems that are also described in Figs. 1.21-1.23. The porphyrin ligands (*center, right*, H represents dissociable ligand protons) support the $\{\text{FeNO}\}^n$ complexes in $[\text{Fe}(\text{TPP})(\text{NO})]$ (**1**), $[\text{Fe}(\text{TPP})(\text{NO})]^-$ (**2**), and $[\text{Fe}(\text{OEP})(\text{NO})]^-$ (**3**) (abbreviations defined in the text).

The first account of an $\{\text{FeNO}\}^8$ -por complex was communicated in early 1982 by Kadish and Olson, which described the electrochemical properties of $[\text{Fe}(\text{TPP})(\text{NO})]^-$ (**2**) and $[\text{Fe}(\text{OEP})(\text{NO})]^-$ (**3**) (where OEP = dianion of octaethylporphyrin) (Fig. 1.20).¹⁸² Both complexes displayed reversible diffusion-controlled cyclic voltammograms (CVs), which afforded $E_{1/2}$ values of -0.93 and -1.10 V (vs. SCE, CH_2Cl_2) for the $\{\text{FeNO}\}^7 \leftrightarrow \{\text{FeNO}\}^8$ redox couple of **1** and **2**, respectively (Table 1.2). Similar electrochemical experiments were performed in neat pyridine with little change to $E_{1/2}$, inferring minor (if any) influence of a second axial N-

donor or on solvent polarity. Additional redox waves were found in the CV that were assigned to other processes demonstrating the rich redox chemistry associated with the Fe-por unit. Unfortunately, attempts to isolate the $\{\text{FeNO}\}^8$ complexes **2** and **3** after exhaustive electrolysis at -1.20 V only resulted in the corresponding $\{\text{FeNO}\}^7$ derivatives. At the time, the unstable nature of the $\{\text{FeNO}\}^8$ species was proposed to be due to disproportionation or decomposition in the electrochemical cell even at the highly reducing potentials used. However, it appears that the non-isolability of **2** and **3** could be due to the reaction $\{\text{FeNO}\}^8 + \text{H}^+ \rightarrow \{\text{FeNO}\}^7 + \frac{1}{2} \text{H}_2(\text{g})$ via a transient Fe-HNO that results from the presence of trace water as a proton source in the solvent (*vide infra*). Although not suggested at the time, this initial report was indicative of the difficult nature in isolating this elusive species and only limited spectroscopic and theoretical analyses have been the norm in terms of characterization (*vide infra*).

Table 1.2. Electrochemical and Spectroscopic Data of {FeNO}^{7/8} Heme Systems

Molecule	$E_{1/2}$ (V) ^a	ν_{NO} (cm ⁻¹)	$\Delta\nu_{\text{NO}}$ (cm ⁻¹) ^b	ν_{FeN} (cm ⁻¹) ^c	Ref
{FeNO}⁷					
[Fe(TPP)(NO)] (1)	-0.93 ^d	1681 ^e	-	525 ^e	182,183
MbNO (12)	-0.87 ^f	1612 ^f	-	552 ^f	80,126
{FeNO}⁸					
[Fe(TPP)(NO)] ⁻ (2)	-	1496 ^e	-185	549 ^e	182,183
[Fe(OEP)(NO)] ⁻ (3)	-1.08 ^g	1441 ^h	-229	-	184,185
[Fe(OEC)(NO)] ⁻ (4)	-1.08 ^g	-	-	-	184
[Fe(OEiBC)(NO)] ⁻ (5)	-1.11 ^g	-	-	-	184
[Fe(OEPone)(NO)] ⁻ (6)	-0.71 ^e	1442 ^h	-220	-	185,186
[Fe(2,4-OEPdione)(NO)] ⁻ (7)	-0.65 ^e	1442 ^h	-223	-	185,186
[Fe(TFPPBr ₈)(NO)] ⁻ (9)	-0.19 ^d	1547 ⁱ	-	-	187
[Fe(TPPS)(NO)] ⁵⁻ (11)	-0.63 ^f	-	-	-	188
[Fe(TMPyP)(NO)] ³⁺	-0.57 ^f	-	-	-	189
MbHNO (13)	-	1385 ^f	-227	649 ^f	121,126

^a Data represents the $E_{1/2}$ value for the {FeNO}^{7/8} redox couple normalized to the saturated calomel reference electrode (SCE) based on information found in ¹⁹⁰. ^b Denotes the change in stretching frequency upon reduction from {FeNO}⁷-to-{FeNO}⁸. ^c Possible coupling of ν_{FeN} with the Fe-N-O bend can also occur. ^d CH₂Cl₂. ^e THF. ^f H₂O. ^g ⁿBuCN ^h THF-d₈ ⁱ solid-film on NaCl.

The electrochemical observation of the {FeNO}⁷ ↔ {FeNO}⁸ redox couple in the TPP and OEP systems inspired further modes of characterization, including the spectroelectrochemistry of the complexes in numerous organic solvents with various donor properties.¹⁹¹ It was hypothesized that these measurements would shed light into the role solvents play in stabilizing and ultimately in isolating the {FeNO}⁸ complex. Similar to the initial CVs

for **2** and **3** in CH₂Cl₂, CVs in various polarity/donorability solvents revealed two reversible, diffusion-controlled, redox events that were assigned to the {FeNO}^{6/7/8} redox couples. The $E_{1/2}$ values for the {FeNO}^{7/8} couple for **2** and **3** were in the -0.75 to -0.95 V range (vs. SCE) depending on the solvent (Table 1.2). In general, the {FeNO}⁸-por complex was stabilized (shifted to more positive potentials) in higher dielectric solvents like DMF. This stabilization is presumably due to efficient solvation of the anionic species although solvent coordination at the vacant axial position of these 5C complexes is possible but has not been suggested.

The electrochemical properties of {FeNO}⁸-por complexes do not appear to change significantly with modifications to the porphyrin unit. For example, the $E_{1/2}$ for the {FeNO}⁷ ↔ {FeNO}⁸ redox couple is ~ -1 V (vs. SCE) for many derivatized porphyrins (Table 1.2). Such values include: -1.08 (OEP) (**3**), -1.08 (OEC = dianion of octaethylchlorin) (**4**), -1.11 V (OEiBC = dianion of octaethylisobacteriochlorin) (**5**) (vs. SCE, THF) (Fig. 1.21, Table 1.2).¹⁸⁴ It has been suggested that the invariance of $E_{1/2}$ supports an FeNO-centered reduction that is nearly independent of the macrocycle and may actually be more localized on NO-based MOs rather than Fe AOs.¹⁹¹ Though seemingly accurate, this proposal should be modified to incorporate the non-innocent nature of the NO ligand i.e. the similarity in $E_{1/2}$ suggests primarily {FeNO} unit reduction as opposed to exclusive Fe- or NO-based reduction. As suggested in this work and now verified by the numerous studies on both heme and non-heme Fe-NO complexes (*vide infra*), these results support a unique bonding behavior of the Fe-NO subunit and conclude no distinct advantage of one porphyrin macrocycle over the other in terms of NO binding and electrochemical reduction potentials.¹⁸⁴

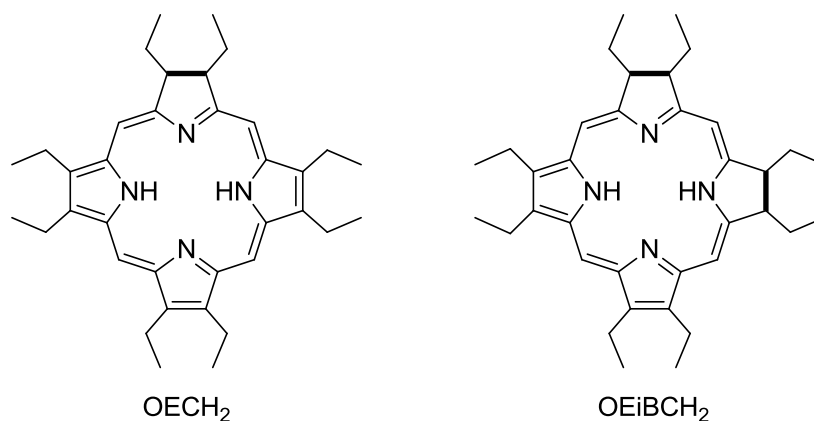


Figure 1.21. Porphyrin ligand platforms (H represents dissociable ligand protons) with varying degrees of peripheral C-H saturation that support the $\{\text{FeNO}\}^n$ complexes, $[\text{Fe}(\text{OEC})(\text{NO})]^-$ (**4**) and $[\text{Fe}(\text{OEiBC})(\text{NO})]^-$ (**5**) (abbreviations defined in the text). The general coordination of the FeNO subunit is as described in Fig. 1.20.

At this point (early 1990s) the existence of $\{\text{FeNO}\}^8$ nitrosyls was proposed based on primarily electrochemical evidence;^{182-184,188,189,191} however, other standard measurements were clearly needed. Indeed, vibrational spectroscopy (infrared: IR or resonance Raman: rR) would be the most useful due to the nature of the frontier MOs in these systems i.e. π^* NO. IR and/or rR analysis could confirm reduction and provide vibrational expectation values by establishing the relative and absolute changes in the N-O and Fe-N stretching frequencies (ν_{NO} and ν_{FeN} , respectively). Thus, Ryan and coworkers expanded the work on **2** and **3** utilizing spectroelectrochemical techniques coupled with vibrational analysis. The use of UV-vis and rR measurements provided the first vibrational spectroscopic benchmarks for the $\{\text{FeNO}\}^8$ heme platform.¹⁸³

Complex **2** was generated by electrochemical reduction of $\{\text{FeNO}\}^7$ **1** in THF and its rR spectrum (Soret excitation) was recorded. Comparison of the rR of **1** and **2** revealed complete disappearance of the ν_{NO} band of $[\text{Fe}(\text{TPP})(\text{NO})]$ (**1**) at 1681 cm^{-1} with the appearance of a very

weak but reproducible ν_{NO} at 1496 cm^{-1} ($\Delta \nu_{\text{NO}} = 185 \text{ cm}^{-1}$ from $\{\text{FeNO}\}^7$), which was confirmed by ^{15}NO labeling ($\nu_{^{15}\text{NO}} = 1475 \text{ cm}^{-1}$; $\Delta \nu_{\text{NO}} = 21 \text{ cm}^{-1}$). The low-energy region of the rR spectrum also contained a second isotope-sensitive peak, assigned as the Fe-N(O) (ν_{FeN}) stretch. Interestingly, the ν_{FeN} band blue-shifted by 24 cm^{-1} upon reduction to 549 cm^{-1} in the $\{\text{FeNO}\}^8$ complex **2** (525 cm^{-1} in **1**) (Table 1.2). The 185 cm^{-1} red-shift in ν_{NO} points toward a dramatic decrease in the N-O bond order, which is consistent with additional occupation of an NO π^* -like MO in the $\{\text{FeNO}\}^8$ complex. However, there is a significant blue-shift in ν_{FeN} implying an increase in the order of this bond. Based on a low-level computed MO diagram^{177,192} of Fe(por)NO complexes, the singly occupied MO (SOMO) of the $\{\text{FeNO}\}^7$ precursor contains both N-O π^* and Fe(d_z^2)-N(O) σ -based orbital contributions. Thus, according to this MO analysis, reduction to **2** should theoretically decrease ν_{NO} and increase ν_{FeN} . Indeed, the weakening of the N-O bond and strengthening of the Fe-N bond is what is observed experimentally; however, other effects such as coupling to the Fe-N-O bend may be a more suitable explanation (*vide infra*). Collectively, **2** was proposed to be 5C and contain a LS Fe(II) coordinated to NO^- (the spin-state of the nitroxyl anion i.e. singlet or triplet was not assigned).

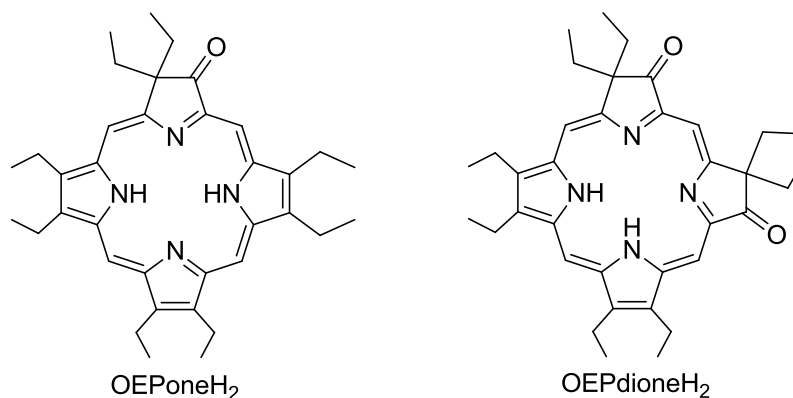


Figure 1.22. Porphinone ligand platforms (H represents dissociable ligand protons) that support the $\{\text{FeNO}\}^n$ complexes, $[\text{Fe}(\text{OEPone})(\text{NO})]^-$ (**6**) and $[\text{Fe}(\text{OEPdione})(\text{NO})]^-$ (**7**) (abbreviations defined in the text). The general coordination of the FeNO subunit is as described in Fig. 1.20.

The vibrational analysis of $\{\text{FeNO}\}^8$ -por systems was further expanded by Ryan's group in 2010 to include more significant modifications on the porphyrin ligand than described previously. These included the $[\text{Fe}(\text{por})(\text{NO})]^-$ complexes where por = OEP (**3**), OEPone (dianion of octaethylporphinone) (**6**), and OEPdione (dianion of octaethylporphinedione) (**7**) (Fig. 1.22).¹⁸⁵ The por ligands in **6** and **7** were used since they mimic the peripheral features in heme d_1 that contain C=O groups commonly referred to as porphyrines. Furthermore, heme d_1 is present at the active site of one of the key microbial enzymes involved in denitrification, NiRs, which goes through a proposed $\{\text{FeNO}\}^8$ transition state in the catalytic reduction of nitrite-to-nitric oxide or ammonia at the heme center.^{78,89,193} The electro/spectroelectrochemistry of the FeNO porphyrines were first reported in 1997¹⁸⁶ and the corresponding $E_{1/2}$ values were similar to previous Fe(por)NO systems: -0.71 (**6**) and -0.65 V (**7**) (vs. SCE, THF) (Table 1.2). The overall shift of ~ 0.4 V toward more positive potentials from the OEP derivative **3** was attributed to the greater electron withdrawing nature of the corresponding macrocyclic ligands in the following order: OEP < OEPone < OEPdione. Interestingly, although $E_{1/2}$ changed, the

vibrational frequencies are unaffected by the respective oxidized macrocycles with ν_{NO} at ~ 1665 cm^{-1} for $\{\text{FeNO}\}^7$ and ~ 1442 cm^{-1} ($\Delta\nu_{\text{NO}} \sim 220$ cm^{-1}) for $\{\text{FeNO}\}^8$ (**3**, **6**, **7**) in all three OEP derivatives (Table 1.2). It appears that the C=O groups on the porphyrin have little influence on the degree of bonding/anti-bonding character in the FeNO unit, which was further supported by DFT calculations (*vide infra*).

Table 1.3. Geometric Parameters of 5C and 6C Heme {FeNO}^{7/8} Systems

Molecule	Geometric Parameters ^a				Ref
	Fe-N (Å)	N-O (Å)	∠Fe-N-O (°)	Fe-N _{trans} (Å)	
{FeNO}⁷					
[Fe(TPP)(NO)] ^b (1)	1.739	1.163	144.4	-	194
[Fe(TPP)(NO)(MI)]	1.750	1.182	138	2.173	195
[Fe(P)(NO)]-calc.	1.705	1.179	146	-	179
[Fe(P)(NO)(MI)] (14) -calc.	1.734	1.186	140	2.179	179
[Fe(P)(NO)(CH ₃ S)] ⁻ -calc.	1.788	1.198	138	2.416	35
MbNO ^{c,d} (12)	1.76	1.12	150	2.05	196
[Fe(TFPBr ₈)(NO)] (8)-calc.	1.711	1.182	144.4	-	187
{FeNO}⁸					
MbHNO (13)	1.82	1.24	131	2.09	121
[Fe(P)(NO)(MI)] ⁻ (15) -calc.	1.795	1.211	124	2.439	35
[Fe(P)(HNO)(MI)]-calc.	1.789	1.236	132	2.082	181
[Fe(P)(NO)(CH ₃ S)] ²⁻ (16)-calc.	1.776	1.215	131	2.587	35
[Fe(P)(HNO)(CH ₃ S)] ⁻ -calc.	1.824	1.252	133	2.354	35
[Fe(P)(NO)(ImH)] ⁻ (17)-calc.	1.814	1.215	120.3	2.419	197
[Fe(P)(HNO)(ImH)] -calc.	1.811	1.217	132	2.098	197
[Fe(P)(NO)(NH ₃)] ⁻ -calc.	1.790	1.21	126	2.271	78
[Fe(P)(HNO)(NH ₃)] -calc.	1.782	1.23	131	2.090	78
[Fe(TFPBr ₈)(NO)] ⁻ (9)-calc.	1.790	1.201	122.7	-	187
[Fe(P)(NO)] ⁻ -calc.	1.778	1.211	123.1	-	187

^a Data consists of experimental and DFT calculated parameters (denoted by calc.). ^b Crystal structure obtained at 33 K in order to reduce disorder in FeNO unit. ^c Data obtained from EXAFS.^{121,196} ^d Additional crystallographic data from sperm whale Mb has been obtained: Fe-N(O) 1.89 Å; N-O 1.15 Å; Fe-N-O 112°; Fe-N_{trans} 2.18 Å¹⁹⁸ and from horse heart Mb in which two distinct structures are observed dependent on preparation method: Fe-N(O) 1.87 Å (2.13 Å); N-O 1.20 Å (1.17 Å); Fe-N-O 144° (120°); Fe-N_{trans} 2.08 Å (2.15 Å).^{199,200}

As of 2010, knowledge of synthetic $\{\text{FeNO}\}^8$ heme complexes were at the same level as in the 1990s i.e. non-isolable and synthesized *in situ* with electrochemical and vibrational information in terms of overall characterization. Stabilization of $\{\text{FeNO}\}^8$ had only been modest with electron-withdrawing peripheral groups providing, at best, a ~ 0.30 V cathodic shift in $E_{1/2}$.¹⁸⁵ In hopes of stabilizing *and* isolating the elusive $\{\text{FeNO}\}^8$ species, Doctorovich utilized a fully halogenated TPP-derivative (Fig. 1.23) in expectation of a more stable $\{\text{FeNO}\}^8$ system due to the electron withdrawing nature of the halogen substitution.^{187,201} This work was an extension of earlier work done with halogenated Fe porphyrins.²⁰² The $\{\text{FeNO}\}^7$ complex, namely $[\text{Fe}(\text{TFPPBr}_8)(\text{NO})]$ (**8**) (where $\text{TFPPBr}_8 = 2,3,7,8,12,13,17,18$ -octabromo-5,10,15,20-[tetrakis-(pentafluorophenyl)]porphyrin), was obtained through reductive nitrosylation of $[\text{Fe}^{\text{III}}(\text{TFPPBr}_8)\text{Cl}]$ in a 2:1 $\text{CH}_2\text{Cl}_2/\text{MeOH}$ solvent mixture with $\text{NO}(\text{g})$. Chemical reduction of **8** with cobaltocene ($[\text{Co}(\text{Cp})_2]$; $E_{1/2} \sim -1.00$ V vs. SCE)¹⁹⁰ in CH_2Cl_2 afforded the $\{\text{FeNO}\}^8$ complex $[\text{Co}(\text{Cp})_2][\text{Fe}(\text{TFPPBr}_8)(\text{NO})]$ (**9**) as a solid in 90% yield (Fig. 1.23). This report in 2010 marked the first account of an isolable and thermally stable heme $\{\text{FeNO}\}^8$ complex. As expected, the CV of **8** in CH_2Cl_2 revealed two positively shifted (with respect to TPP analogue **1**) reversible reduction waves with the $\{\text{FeNO}\}^{7/8}$ couple at $E_{1/2} = -0.19$ V (vs. SCE, CH_2Cl_2). Notably, this value is the most positive of all the $\{\text{FeNO}\}^8$ complexes reported to date. The effectiveness of the redox modulation is most distinct when compared to the $\{\text{FeNO}\}^{7/8}$ $E_{1/2}$ of the non-halogenated TPP in **1** (-0.93 V vs. SCE in CH_2Cl_2), that is cathodically shifted by nearly 1 V ($\Delta E_{1/2} = 0.74$ V) in **8**.

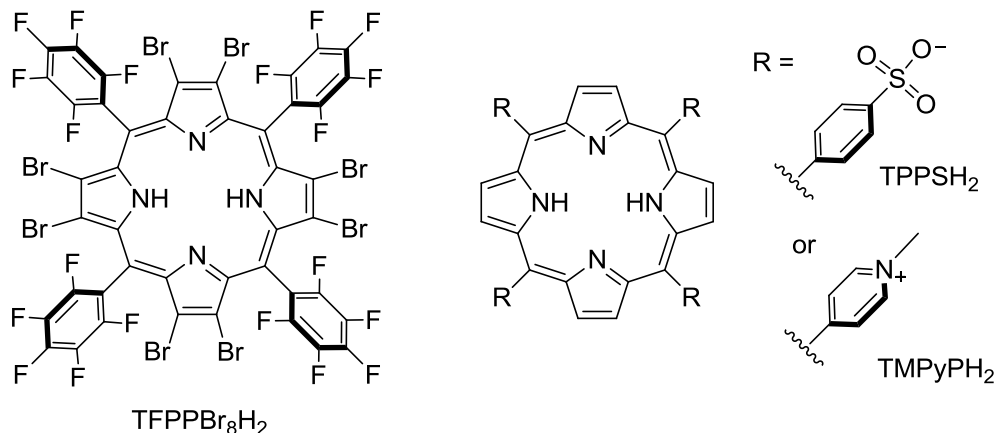


Figure 1.23. Porphyrin ligand platforms (H represents dissociable ligand protons) that support the $\{\text{FeNO}\}^n$ complexes, $[\text{Fe}(\text{TFPPBr}_8)(\text{NO})]$ (**8**), $[\text{Fe}(\text{TFPPBr}_8)(\text{NO})]^-$ (**9**), $[\text{Fe}(\text{TPPS})(\text{NO})]^{4-}$ (**10**), $[\text{Fe}(\text{TPPS})(\text{NO})]^{5-}$ (**11**), and $[\text{Fe}(\text{TMPy})(\text{NO})]^{3+}$ (abbreviations defined in the text). The general coordination of the FeNO subunit is as described in Fig. 1.20.

The additional stabilization of the $\{\text{FeNO}\}^8$ complex **9** allowed for more detailed spectral characterization than in previous reports. The ^1H NMR spectrum of **9** showed only one signal corresponding to the $[\text{Co}(\text{Cp})_2]^+$ protons of the counteranion. Furthermore, ^{15}N NMR measurements of **9**- ^{15}NO displayed a single peak at +790 ppm (vs. CH_3NO_2 in CD_2Cl_2), a value at the upper limit of previously characterized and severely bent $\{\text{CoNO}\}^8$ nitrosyls having M-N-O angles of $\sim 130^\circ$.^{203,204} It is well established that the ^{15}N NMR signal is quite sensitive to the redox state and angle of the MNO unit, supporting the assignment of a severely bent Fe-N-O angle and $S = 0$ ground state for **9**. Solution-state FTIR data for **9** proved difficult to interpret since the ν_{NO} of **9** was masked by intense vibrational bands between $1450\text{-}1550\text{ cm}^{-1}$ from the por ligand. However, solid-state FTIR (solid-film NaCl) revealed a weak shoulder at 1550 cm^{-1} , which was assigned to the ν_{NO} of **9**. Notably, even in the solid-state, the 1550 cm^{-1} band slowly decreased within minutes of data collection, with reappearance (although not quantitative) of the 1715 cm^{-1} ν_{NO} band of the $\{\text{FeNO}\}^7$ species **8**. In support of the presence of an intact Fe-NO

bond in **9**, chemical oxidation with ferrocenium quantitatively regenerated the $\{\text{FeNO}\}^7$ complex **8**. Additional reactivity of the complex with biologically relevant targets was not discussed; however, protonation of **9** with strong acids such as trifluoroacetic acid (TFA) afforded the $\{\text{FeNO}\}^7$ along with $\text{H}_2(\text{g})$ evolution via a proposed $\{\text{FeHNO}\}^8$ intermediate, similar to the probable side-reaction in the electrochemical synthesis of **2** and **3**.¹⁸³ Only strong acids such as TFA facilitated this reaction indicating the coordinated NO^- to be a relatively weak base. Although this unique $\{\text{FeNO}\}^8$ -por complex was isolable and relatively stable under anaerobic conditions, the absence of crystallographic data highlights the instability of this species in solution. DFT calculations have served an integral part of rationalizing the bonding description of the unique $\{\text{FeNO}\}^8$ E-F notation, which is highlighted in a forthcoming section.

Meyer and coworkers investigated the electrocatalytic reduction of NO_2^- to NH_3 in neutral to acidic solutions, using a water-soluble Fe(III)-por complex, $[\text{Fe}(\text{TPPS})(\text{H}_2\text{O})]^{3-}$ (TPPS = hexaanion of *meso*-tetrakis(*p*-sulfonatophenyl)porphyrin) as an NiR model (Fig. 1.23, Table 1.2).¹⁸⁸ Chemical reduction of the $\{\text{FeNO}\}^6$ complex $[\text{Fe}(\text{TPPS})(\text{NO})]^{3-}$ was achieved with a large excess of NaNO_2 and $\text{NO}(\text{g})$, resulting in the clean generation of $[\text{Fe}(\text{TPPS})(\text{NO})]^{4-}$ (**10**), the $\{\text{FeNO}\}^7$ species. Differential pulse polarography revealed a well-defined, pH-dependent peak at -0.63 V ($\text{pH} > 2.6$ vs. SCE, H_2O) indicating that rapid reduction occurs at this potential and is consistent with formation of the putative $\{\text{FeNO}\}^8$ species, $[\text{Fe}(\text{TPPS})(\text{NO})]^{5-}$ (**11**). The first reduction associated with the FeNO unit, $\{\text{FeNO}\}^6$ -to- $\{\text{FeNO}\}^7$, is independent of pH whereas the second reduction has a complex pH dependence, similar to that seen in polypyridine Ru- and Os-NO complexes.²⁰⁵ The second reduction is pH-independent at $\text{pH} > 2.6$; however, in the range $2.6 > \text{pH} > 1.4$, the electrochemical reaction assumes pH dependence. The authors note that there is no pH-dependence seen in this range for the solvato species, $[\text{Fe}(\text{TPPS})(\text{H}_2\text{O})]^{3-}$,

which supports protonation at NO and not the sulfonate groups of TPPS. The mechanism of nitrite reduction to ammonia mediated by NiR has been postulated to go through a series of proton coupled electron transfer reactions at the coordinated nitrogen oxide substrate.^{78,89,193} Support for this mechanism was also provided by a series of Ru-NO and Os-NO polypyridine complexes that are not structurally related to NiR.^{205,206} Furthermore, analogous chemistry with Os nitrosyls inferred the assignment of this species to be the coordinated HNO complex, $[\text{Fe}(\text{TPPS})(\text{HNO})]^{4+}$.²⁰⁷ Mechanistically speaking, the Os and Ru systems do offer insight into the mechanism for reduction of nitrite via an $\{\text{FeNO}\}^8$ species; however, a major difference is the apparent lability of the axial NO ligand in **11** with subsequent loss of HNO. This chemistry is in contrast to the continuously coordinated NO in the Os or Ru systems. This deligation process appears to be the reason why the reduction of **10** to **11** is not reported as reversible. Further reductions, past the $\{\text{FeNO}\}^8$ $[\text{Fe}(\text{TPPS})(\text{NO})]^{5-}$ (**11**) species, are consistent with the production of ammonia (NH_3), nitrous oxide (N_2O) and hydroxylamine (H_2NOH) depending on the $[\text{NO}_2^-]/[\text{Fe}(\text{III})]$ ratio, as well as the electrons added per NO_2^- and the electrolysis time.¹⁸⁸ Complimentary results were obtained with an additional water-soluble cationic porphyrin, $[\text{Fe}(\text{TMPyP})(\text{NO})]^{4+}$ (where TMPyP = dication of *meso*-tetrakis(*N*-methyl-4-pyridyl)porphine) (Fig. 1.23, Table 1.2), under similar conditions described above.¹⁸⁹

While synthetic efforts on Fe(por)NO complexes have provided many of the spectroscopic benchmarks for $\{\text{FeNO}\}^8$, the challenge still remains to isolate discrete molecules and understand their underlying reactivity. Much work has been done involving protein-heme adducts of the $\{\text{FeNO}\}^7$ notation, in particular MbNO (**12**), though the surprising stability ($t_{1/2} >$ weeks) of the $\{\text{FeHNO}\}^8$ adduct of Mb, namely MbHNO (**13**), has allowed for the first experimental parameters of this unique E-F notation in a metalloprotein. Reported in 2000 by

Farmer and coworkers,¹³⁶ **13** can be synthesized by a variety of different routes. For example, **13** can be prepared by the traditional biochemical procedure in which metMb (Fe(III)Mb), nitrite (NO_2^-), and dithionite ($\text{S}_2\text{O}_4^{2-}$) are mixed with the formation of **13** monitored by UV-vis although caution should be noted as the spectrum of **13** is similar to the $\{\text{FeNO}\}^7$ MbNO (**12**).²⁰⁸ Furthermore, **13** can be produced efficiently through trapping of free HNO from a donor molecule like Angeli's salt with deoxyMb.^{125,136,209,210} Another report demonstrated that the $\{\text{FeNO}\}^6$ MbNO species could be reduced by two electrons with hydride sources such as NaBH_4 to also generate **13**.²¹¹ Regardless of the route employed, all afford **13** as the predominant isolable material.

Due to its inherent stability, $\{\text{FeHNO}\}^8$ **13** has been characterized by numerous techniques including ^1H NMR,²¹² rR, and even structural methods such as X-ray absorption spectroscopy (XAS).¹²¹ The protonated state of the NO ligand in **13** was confirmed from ^1H NMR where the HNO proton displays a broad but relatively well-defined resonance at 14.8 ppm (20% D_2O /80% pH 10 carbonate buffer).¹²⁵ Other advanced NMR techniques including $^1\text{H}/^{15}\text{N}$ -coupled experiments lend further validity to this peak assignment. The rR spectrum of **13** ($\lambda_{\text{ex}} = 413$ nm; pH 10 carbonate buffer) showed the expected shift of the ν_{NO} band at 1612 cm^{-1} from MbNO²¹³ to 1385 cm^{-1} for **13** ($\Delta\nu_{\text{NO}} = 227\text{ cm}^{-1}$). This was further confirmed by ^{15}N isotopes as ν_{NO} of **13**- ^{15}NO shifted to 1355 cm^{-1} ($\Delta\nu_{\text{NO}} = 30\text{ cm}^{-1}$). Another isotope-sensitive band also appeared at 649 cm^{-1} (**13**- $^{15}\text{NO} = 636\text{ cm}^{-1}$; $\Delta\nu_{\text{NO}} = 13\text{ cm}^{-1}$) that has been traditionally assigned as the ν_{FeN} band¹²¹. Interestingly, this band is blue-shifted by $\sim 100\text{ cm}^{-1}$ compared to $\{\text{FeNO}\}^7$ MbNO (**12**) at 552 cm^{-1} ,²¹³ which is comparable to the shift found in the $\{\text{FeNO}\}^8$ TPP complex **2**.¹⁸³ As stated previously, the blue-shift does not necessarily imply a stronger force constant for the Fe-N bond in MbHNO **13** compared to that in MbNO **12**. Possible explanations to this

significant change could be (i) coupling of the Fe-N stretch with the Fe-N-O bend and (ii) the reduced Fe-N-O angle in **13** compared to **12**, which lowers the effective reduced mass in the harmonic oscillator equation due to the proton-N bond. Either scenario could result in an increase in the low-energy frequency, an effect that is completely independent of a change in the bond order.⁸⁰

The heme site in **13** also provided the first insight into the structure of a biological {FeNO}⁸ species (Table 1.3)¹²¹. This work was compared to earlier research pertaining to MbNO (**12**) in which EXAFS was used in determination of the primary coordination sphere structure.¹⁹⁶ Therefore upon reduction of **12** to **13**, both the N-O and Fe-N(O) bond lengths increase from 1.12 Å to 1.24 Å and 1.76 Å to 1.82 Å, respectively. The Fe-N(O) bond in **13** is quite long, but subsequent theoretical calculations provide support for the elongated bond.¹⁹⁷ The Fe-N-O bond angle of 132° is notably decreased in **13** from 150° in **12**.¹²¹ To date (2012), these parameters are *the only experimental structural parameters of an {FeNO}⁸-por system* (small molecule or macromolecule) and are quite complementary with what has been determined theoretically at the heme site in Mb and the aforementioned synthetic analogues (*vide infra*). Formal oxidation state assignments for Fe and NO in **13** have not been made; however, XANES data suggest considerable reduction at Fe implying an Fe(I) oxidation state, which is further corroborated by the long Fe-NO bond of MbHNO. As suggested below, a formal resonance structure that highlights the extent of metal-ligand covalency in the FeNO unit of heme {FeNO}⁸ systems seems viable.

1.7.2 Theoretical Descriptions of Heme {FeNO}⁸ Complexes⁶⁷

DFT calculations have provided a critical perspective into the rich bonding of M-N-O complexes.¹⁸¹ This is particularly the case for {FeNO}⁸-por complexes since an X-ray crystal structure of this species has yet to be reported. Furthermore, only minimal experimental parameters for these systems have been obtained.¹²¹ The ability to probe the electronic structure of heme active sites *in silico* certainly proves valuable in this particular area of metal-nitrosyl chemistry. Undoubtedly the work of many researchers involving theoretical studies pertaining to {FeNO}⁷ porphyrins has been paramount to the understanding of the reduced {FeNO}⁸ congeners, which are the focus of this review. More detailed analysis on the {FeNO}⁷ E-F notation is the subject of other articles^{179,214} and will only be discussed here in reference to {FeNO}⁸ systems.

In an effort to generate structural and electronic information on possible nitroxyl intermediates involved in biological NO_x processing, theoretical accounts of the heme {FeNO}⁷ [Fe(P)(MI)(NO)] (**14**) and {FeNO}⁸ complexes [Fe(P)(MI)(NO)]⁻ (**15**) (where P = porphine²⁻ and MI = 1-methylimidazole) have been performed. The computations by Lehnert³⁵ were performed with BP86/TZVP to elucidate the mechanism and potential intermediates involved in NO reduction in the fungal NOR (P450nor) enzymes with the model [Fe(P)(CH₃S)(NO)]²⁻ (**16**) where comparisons with **15** were made. Both 6C models generate similar structural properties and MO assignments; therefore, we will limit the majority of our discussion to **15** since {FeNO}⁸ heme complexes involving thiolate ligation have yet to be synthesized. Additional DFT studies on a similar 6C [Fe(P)(ImH)(NO)]⁻ (**17**) (where P = porphine²⁻ and ImH = Imidazole) have also been performed with the B3LYP and BLYP functionals, which yielded similar results to **15**. For simplicity we will focus the majority of our theoretical descriptions with the BP86 results of **15**.

The optimized structure of the $\{\text{FeNO}\}^7$ complex $[\text{Fe}(\text{P})(\text{MI})(\text{NO})]$ (**14**) was described as a LS Fe(II)-NO• species ($S_{\text{tot}} = 1/2$) with distinct radical character on the N of NO.¹⁸⁰ Evaluation of the electronic ground state revealed 88% Fe(II)-NO• character with a 12% contribution from a ligand field excited state. The single electron is found in a mixed SOMO consisting primarily of Fe d_z^2/d_{xz} and NO π^*_h (horizontal to the plane formed by Fe-N-O). In fact, the Fe and NO of **14** contribute equally to this orbital accounting for 42% and 43% contributions, respectively. This large degree of Fe and NO character is demonstrative of large covalent character in the Fe-NO bond of **14**. Reduction of **14** to $[\text{Fe}(\text{P})(\text{MI})(\text{NO})]^-$ (**15**) resulted in few changes to the nature of the frontier MOs from **14** viz. the incoming electron spin-pairs and resides with the lone electron in the former Fe-N σ -bonding SOMO of $\{\text{FeNO}\}^7$ resulting in a singlet ($S_{\text{tot}} = 0$) ground state. While the triplet state of both **15**, **16**, and **17** were shown to be nearly isoenergetic to their respective singlet states, no experimental evidence of this electronic species exists. Thus, in terms of orbital character, the HOMO in **15** consists of nearly equal Fe and NO contributions, which supports reduction occurring across the FeNO entity as a whole. Separate DFT studies (BP86/TZVP) on the derivatized porphyrins $[\text{Fe}(\text{OMPone})(\text{NO})]^-$ and $[\text{Fe}(\text{OMPdione})(\text{NO})]^-$ (where OMP = the dianion of octamethylporphinone/dione) also draw similar conclusions.¹⁸⁵ Therefore, considering only the existence of the singlet ground state for these $\{\text{FeNO}\}^8$ heme complexes, the oxidation state designation can be described as intermediate between LS Fe(II)-NO⁻ ↔ LS Fe(I)-NO•.

As expected, the reduction of $[\text{Fe}(\text{P})(\text{MI})(\text{NO})]$ (**14**) and $[\text{Fe}(\text{P})(\text{ImH})(\text{NO})]$ (**17**) has a pronounced effect on the structural and spectroscopic parameters of the DFT-generated $\{\text{FeNO}\}^8$ complexes (Table 1.3).^{35,197} For example, upon reduction of **14** to **15**, the Fe-N(O) and N-O bonds increased in length (Fe-N(O): 1.734 Å to 1.795 Å; N-O: 1.186 Å to 1.211 Å) and showed

lower calculated force constants (3.26 to 2.50, 12.22 to 10.29, and 0.61 to 0.21 mdyn/Å for the Fe-N(O), N-O, and Fe-N_{trans}, respectively).³⁵ This decrease in bond order correlated with a calculated ν_{NO} of 1511 cm⁻¹ (BP86) for **15** and 1578 cm⁻¹ (B3LYP) for **17**. Additionally, the Fe-N-O angle decreased from 140° to ~120° for both **15** and **17**, and the axial imidazole Fe-N_{trans} distance increased from 2.179 Å to 2.439 Å in **15**.^{35,197} This dramatic bond elongation is not a manifestation of improper functional choice as analogous results were obtained for **17** using B3LYP and BLYP.¹⁹⁷ Accordingly, the *trans* influence of NO⁻ is large. However, this particular result does not correlate with the experimental Fe-N_{trans} of histidine from MbHNO **13**, which was observed to be ~2 Å (EXAFS).¹²¹ This difference appears to be a question of the *trans* labilizing ability of NO⁻ versus HNO, which one would expect to be larger for the anionic ligand. Indeed, analysis of the HNO version of **17** (BLYP)¹⁹⁷ revealed a calculated Fe-N_{trans} = 2.144 Å and ν_{NO} = 1416 cm⁻¹ comparable to the same experimental parameters found for MbHNO **13** (Fe-N_{trans} = 2.09 Å; ν_{NO} = 1385 cm⁻¹).¹²¹ Collectively, the calculated bond distances, angles, and vibrational properties of **17** (when discriminating HNO and NO coordination) are remarkably similar to those obtained experimentally from the EXAFS of MbHNO, thus lending some validity to the accuracy and overall predictive power of these methods.

Analogous structural and electronic parameters were obtained for the halogenated 5C FeNO complexes **8** and **9**.¹⁸⁷ The computed geometry for the 5C {FeNO}⁷ complex [Fe(TFPPBr₈)(NO)] (**8**) (LANDL2DZ/PBE exchange-correlation) compared favorably to experiment aside from the determined atypical N-O bond length of 1.42 Å likely due to the dramatic ruffling of this highly substituted porphyrin; whereas theory provides a more reasonable N-O bond length of 1.182 Å. Moreover, the Fe-N(O) bond of 1.711 Å and Fe-N-O angle of 144.4° for [Fe(TFPPBr₈)(NO)] serves as a point of reference prior to reduction.¹⁸⁷ Subsequent

addition of an electron to form the $\{\text{FeNO}\}^8$ complex $[\text{Fe}(\text{TFPPBr}_8)(\text{NO})]^-$ (**9**) revealed an N-O and Fe-N(O) bond increase to 1.201 and 1.790 Å, respectively. The decreased Fe-N-O angle (122.7°) is indicative of FeNO unit reduction and double occupation of an Fe- d_z^2 σ/NO π^* orbital analogous to the simple 6C porphyrin complex **15**. The HOMO of **9** consisted of more Fe (44%) than NO (27%) character with some ligand contributions symptomatic of a decrease in covalency of the Fe-NO bond. This contrasts with the near equivalent contributions of Fe and NO to the HOMO of **15** likely attributed to the strong electron withdrawing character of the porphyrin ligand in **9**. In further support of the nature of reduction, a natural population analysis was performed and the atomic charges were computed for the $\{\text{FeNO}\}^7$ species **1** and **8** and the $\{\text{FeNO}\}^8$ species **2** and **9**. This analysis showed strong similarity in both cases revealing a net reduced charge on Fe and NO when comparing the $\{\text{FeNO}\}^7$ and $\{\text{FeNO}\}^8$ species. Importantly, the computed charges for **1** and **(2)** are as follows: Fe, 0.69 (0.56); NO, -0.02 (-0.21); for **8** and **(9)** are: Fe, 0.66 (0.55); NO, 0.01 (-0.13).¹⁸⁷

There are relatively fewer examples of non-heme compared to heme $\{\text{FeNO}\}^8$ systems and only one non-heme metalloenzyme has been found in this particular E-F notation.¹¹⁹ Although these species are not defined explicitly in biology, they do offer promise as potential HNO therapeutics and offer key insight into how one treats the $\{\text{FeNO}\}^n$ unit in such platforms. Formation of $\{\text{FeNO}\}^8$ complexes has been primarily limited to ligands with N_4 tetradentate or N_4O pentadentate constructs as well as a derivative of the nitroprusside (NP) anion. The synthesis, spectroscopy and theoretical description are reported in the forthcoming sections along with a brief account of the reactivity of such reduced iron-nitrosyl units. Additional 5C trigonal bipyramidal phosphine-ligated $\{\text{FeNO}\}^8$ complexes have been also reported, but these species will not be discussed in this review.²¹⁵⁻²¹⁷

1.8 {FeNO}⁸ Non-heme Coordination Complexes⁶⁷

1.8.1 Synthesis and Experimental Properties of Non-Heme {FeNO}⁸ Complexes⁶⁷

Inspired by earlier work involving electrochemical²¹⁸ and DFT²¹⁹ characterization of 6C mononuclear non-heme {FeNO}⁷ iron-nitrosyls, Wieghardt and coworkers reported a detailed study of an {FeNO}^{6/7/8} series supported by one common N₄O platform, namely *trans*-[Fe(NO)(cyclam-ac)]^{2+/1+/0} (where cyclam-ac = monoanion of 1,4,8,11-tetraazacyclotetradecane-1-acetic acid) (Fig. 1.24).²²⁰ Previous studies involving the related 5C {FeNO}⁷ complex, *trans*-[Fe(NO)(Cl)(cyclam)]⁺ (*S*_{tot} = 1/2), displayed a reversible {FeNO}^{7/8} couple at -0.90 V (vs. SCE, MeCN, 298 K).²²¹ It is likely that the cyclam-ac ligand would provide more stability to the corresponding NO complexes since it only contains one vacant coordination site thus limiting reaction chemistry to one axial position. The {FeNO}⁷ species [Fe(NO)(cyclam-ac)]⁺ (**18**), was synthesized via reductive nitrosylation of the Fe(III) complex, [FeCl(cyclam-ac)]⁺, with LiBEt₃H and NO(g). Complex **18** was then reduced using [Co(Cp)₂] at ambient temperature in MeCN to furnish the {FeNO}⁸ complex, *trans*-[Fe(NO)(cyclam-ac)] (**19**), which was not stable in solution and difficult to isolate. In spite of the inherent lack of stability of **19**, a multitude of spectroscopic studies were performed at low temperature and, combined with DFT, provided the initial insight of a non-heme {FeNO}⁸ system. While the cyclam-ac ligand nicely supports the {FeNO}^{6/7/8} series, our discussion below will focus on the implications derived from the {FeNO}^{7/8} complexes.

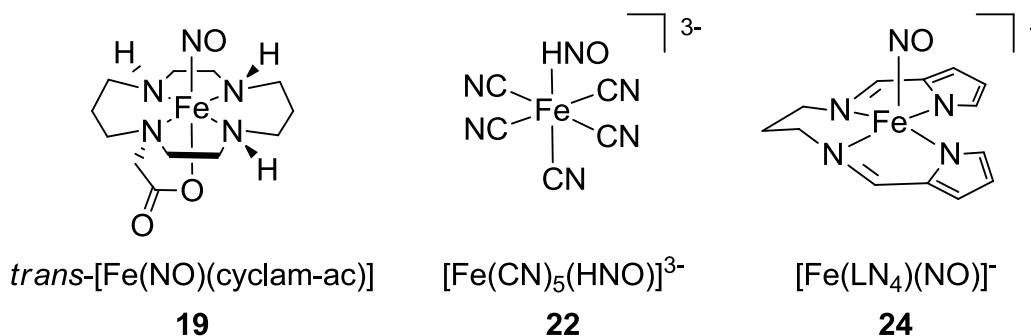


Figure 1.24. Non-heme iron {FeNO}⁸ complexes.

A series of *in situ* measurements (primarily at low temperature) combined with DFT computations were performed to obtain the spectroscopic, electrochemical, and structural parameters of **19**. The CV displayed a reversible {FeNO}⁷ ↔ {FeNO}⁸ redox couple at $E_{1/2} = -0.99$ V (vs. SCE, MeCN, 293 K). Low-temperature spectroelectrochemical experiments were obtained using an OTTLE cell to monitor the *in situ* changes upon reduction of **18**-to-**19** with UV-vis (MeCN, 273 K) and FTIR (MeCN, 253 K) spectroscopies.²²⁰ The UV-vis of the **18**-to-**19** conversion revealed several isosbestic points with the disappearance of peaks at 395 nm and 540 nm and the generation of new broad absorbance features at 440 nm and 590 nm. As expected, the strong ν_{NO} for **18** (1607 cm⁻¹) significantly red-shifted to a less intense band centered at 1271 cm⁻¹ ($\Delta\nu_{\text{NO}} = 336$ cm⁻¹) in the {FeNO}⁸ complex **19**. This assignment was further confirmed utilizing ¹⁵N¹⁸O to afford ν_{NO} at 1228 cm⁻¹ ($\Delta\nu_{\text{NO}} = 43$ cm⁻¹, a value in close agreement with that calculated for a classic harmonic oscillator = 1214 cm⁻¹). Additional insight was obtained from evaluation of the ν_{CO} stretching frequencies of the ligand, which trended toward larger values. This change is consistent with a weakening of the Fe-O_{carboxylate} bond *trans* to NO upon reduction of the nitrosyl ligand, which supports our previous discussion on the *trans*-influence of nitroxyl anion in heme systems (*vide supra*). For example, ν_{CO} bands in {FeNO}⁷ **18** were observed at 1657 and 1355 cm⁻¹ whereas {FeNO}⁸ **19** were at 1619 and 1380 cm⁻¹ for the C=O and C-O,

respectively (*in situ* IR measurements in MeCN). Another interesting feature in the IR spectrum of **19** is the disappearance of the ν_{NH} of cyclam-ac (3223 cm^{-1} for **18**) that is supportive of an H•••O-N H-bonding interaction between the cyclam-ac NH group with the coordinated NO^- . Further support for this assignment was provided by the appearance of a broadened ν_{ND} at 2400 cm^{-1} when using deuterated cyclam-ac to form **19**. The broadening is rationalized based on the reduced Fe-N-O bond angle (122.4° from DFT, *vide infra*) along with the anionic nature of the formal NO^- ligand in **19**. It is also noted that this H-bond could factor into stabilization of the $\{\text{FeNO}\}^8$.²²⁰

Table 1.4. Electrochemical and Spectroscopic Data of $\{\text{FeNO}\}^{7/8}$ Non-Heme Systems

Molecule	$E_{1/2}$ (V) ^a	ν_{NO} (cm^{-1})	$\Delta\nu_{\text{NO}}$ (cm^{-1}) ^b	Ref
$\{\text{FeNO}\}^7$				
<i>trans</i> -[Fe(NO)(cyclam-ac)] ⁺ (18)	-0.99 ^c	1607 ^c	-	220
[Fe(CN) ₅ (NO)] ³⁻ (20)	-1.00 ^d	1648 ^e	-	218,222
[Fe(LN ₄)(NO)] (23)	-0.98 ^c	1704 ^f	-	223
$\{\text{FeNO}\}^8$				
<i>trans</i> -[Fe(NO)(cyclam-ac)] (19)	-	1271 ^c	-336	220
[Fe(CN) ₅ (HNO)] ³⁻ (22)	-	1380, 1304 ^d	-268	224
[Fe(LN ₄)(NO)] ⁻ (24)	-	1604 ^f	-100	223

^aData represents the $E_{1/2}$ value for the $\{\text{FeNO}\}^{7/8}$ redox couple; normalized to the saturated calomel reference electrode (SCE) based on information found in ¹⁹⁰. ^b Denotes the change in stretching frequency upon reduction from $\{\text{FeNO}\}^7$ -to- $\{\text{FeNO}\}^8$. ^c MeCN. ^d H₂O. ^e D₂O. ^f KBr.

To propose a possible oxidation state assignment of the Fe center in **18** and **19**, zero-field Mössbauer (MB) experiments at 80 K were also performed. The MB spectrum of solid **18**

displayed an isomer shift value (δ) of 0.26 mm s^{-1} and a quadrupole splitting (ΔE_Q) of $+0.74 \text{ mm s}^{-1}$ consistent with other $\{\text{FeNO}\}^7$ complexes.⁵⁴ In comparison, the MB spectrum of a frozen MeCN solution of **19** (prepared *in situ* from chemical reduction of **18**) displayed $\delta = 0.41 \text{ mm s}^{-1}$ and $\Delta E_Q = +1.69 \text{ mm s}^{-1}$. Importantly, the signal due to **19** only accounted for 40% of the total spectrum with the remaining 60% from reformed **18** highlighting the relative instability of this non-heme $\{\text{FeNO}\}^8$ species. The small difference in the isomer shift value ($\Delta\delta = 0.15 \text{ mm s}^{-1}$) upon reduction of **18**-to-**19** implies more of an NO-based reduction in **19**. Collectively, the spectroscopic and theoretical analyses (*vide infra*) point to a LS Fe(II) center coordinated to $^1\text{NO}^-$ ($S_{\text{tot}} = 0$) as the oxidation state assignments for the non-heme complex **19**.

Another 6C non-heme Fe-nitrosyl that has furnished the $\{\text{FeNO}\}^8$ notation is the hypotensive agent $[\text{Fe}(\text{CN})_5(\text{NO})]^{2-}$, commonly referred to as nitroprusside (NP). It is well-established that the Fe center in NP stabilizes the nitrosyl ligand as an NO^+ cation bound to LS Fe(II). Upon introduction to biological fluids, NP can release NO and cause vasorelaxation; thus, the utility of NP can be found in its therapeutic potential. However, the exact mechanism of *in vivo* reduction of NP, an $\{\text{FeNO}\}^6$ complex, to $\{\text{FeNO}\}^7$ $[\text{Fe}(\text{CN})_5(\text{NO})]^{3-}$ (**20**) has yet to be clarified. It has been shown that further reduction to the formal $\{\text{FeNO}\}^8$ state, $[\text{Fe}(\text{CN})_5(\text{NO})]^{4-}$ (**21**) or the protonated version $[\text{Fe}(\text{CN})_5(\text{HNO})]^{3-}$ (**22**), could be achieved at a Hg electrode held at $\sim -1.0 \text{ V}$ (vs. SCE, H_2O).²¹⁸ Computational²¹⁹ and more recent (2009) spectroscopic²²⁴ studies of **21** and **22** set out to fully characterize the Fe-bound nitroxyl species in aqueous solution. These studies provided the first insight into the bonding/stability and subsequent fate of this non-heme nitroxyl species under biologically relevant conditions.

Initial spectroscopic proof for the formation of **21** came from *in situ* UV-vis monitoring of the sequential reduction of NP with dithionite.^{218,224} The intense band of the $\{\text{FeNO}\}^7$ NP

complex **20** at 348 nm disappeared with the appearance of a new band at 445 nm, which was assigned as a metal-to-ligand charge transfer (MLCT) band in the $[\text{Fe}(\text{CN})_5(\text{NO})]^{4-}$ complex **21** (pH 10, 25 °C) and was supported by earlier theoretical studies.^{219,224} Additional equiv of dithionite caused these bands to decay, presumably due to further reduction and loss of the NO ligand. The stability of **21** has an apparent pH dependence and solution pHs ≥ 10 lead to immediate decomposition. The re-oxidation back to the $\{\text{FeNO}\}^7$ complex **20** is the bulk product in basic media where **21** has a half-life of ~50 min. The solution stability of the $\{\text{FeNO}\}^8$ complex is better at slightly acidic to neutral pHs of 6-7 presumably due to protonation of the NO^- in **21**, thus forming the HNO complex **22**. In this pH range, complex **22** is the primary species and is stable even in the presence of potential oxidants such as ferricyanide ($[\text{Fe}(\text{CN})_6]^{3-}$), $[\text{Fe}(\text{H}_2\text{O})_6]^{3+}$, or methyl viologen. In contrast to the stability at near neutral pH, sequential addition of the same oxidants at basic pH to **21** resulted in stoichiometric regeneration of the $\{\text{FeNO}\}^7$ and $\{\text{FeNO}\}^6$ species. It was suggested that the difference in the pH-dependent decomposition pathways support complex **21** as a strong reducing agent at basic pH providing its electron to an oxidant and regenerating the $\{\text{FeNO}\}^7$ species, $[\text{Fe}(\text{CN})_5(\text{NO})]^{3-}$ (**20**). Whereas **22**, the conjugate acid of **21**, decomposes to $[\text{Fe}(\text{CN})_6]^{4-}$ and N_2O at pH 6-7 through loss of HNO via the known dehydrative dimerization to N_2O and H_2O .²²⁴

Additional solution-state FTIR spectroscopic studies of the $\{\text{FeNO}\}^8$ species **22** formed in phosphate buffer at pH 6 revealed a ν_{NO} band at 1384 cm^{-1} , which shifted to 1352 cm^{-1} ($\Delta\nu_{\text{NO}} = 32\text{ cm}^{-1}$) using ^{15}NO -labeled NP. This value is significantly lower than the ν_{NO} of NP (1938 cm^{-1}) and the $\{\text{FeNO}\}^7$ analogue of NP **20** (1648 cm^{-1} ; $\Delta\nu_{\text{NO}}$ from $\{\text{FeNO}\}^8$ **22** = 268 cm^{-1}). These values are consistent with primary reduction occurring at the nitrosyl ligand and are assigned to the Fe-HNO derivative **22** based on the pH used and the increased stability of the

protonated species. The dramatic red-shift in ν_{NO} upon reduction supports principal electron occupation in NO π^* MOs. Further vibrational analysis from rR studies ($\lambda_{\text{ex}} = 457.9$ nm) corroborated the IR assignments as seen in the two ν_{NO} bands at 1380 cm^{-1} ($\nu_{15\text{NO}} = 1350\text{ cm}^{-1}$) and 1304 cm^{-1} ($\nu_{15\text{NO}} = 1286\text{ cm}^{-1}$) corresponding to symmetric and asymmetric stretches of the HNO of **22**, respectively (pH 6 buffer). An additional isotope-sensitive band occurred at 662 cm^{-1} ($^{15}\text{NO} = 649\text{ cm}^{-1}$), which has been assigned as a mixed $\nu_{\text{FeN}}/\delta_{\text{FeNO}}$ mode. Interestingly, the ν_{FeN} stretch shifted to lower energy, in contrast to the heme models discussed previously (*vide supra*). Typically for heme systems, ν_{FeN} shifts to higher energies in $\{\text{FeNO}\}^7 \rightarrow \{\text{FeNO}\}^8$ reductions due to a combination of π -backbonding and electron occupation in a MO that has Fe-N(O) σ -bonding character although other reasons for the heme blue-shifts have been postulated (see above). Therefore, it seems that protonation has an effect on the nature and strength of this backbonding interaction and additional electron density is now involved in the H-N(O) bond and is thus less available for constructive NO π^* -Fe d_z^2 overlap.²²⁴

Additional support of the HNO ligand in **22** comes from ^1H NMR, which revealed a downfield singlet at $\delta = 20.02$ ppm (pH 6 phosphate buffer, 25% D_2O) that is split into a doublet ($J_{\text{NH}} = 71.14$ Hz) in the ^{15}NO labeled isotopomer. This measurement strongly supports the assignment of the HNO-bound adduct and a diamagnetic ($S_{\text{tot}} = 0$) ground state for **22**. Importantly, the solution stability of **22** allowed for the determination of the $\text{p}K_{\text{a}}$ for an Fe-bound HNO by an ^1H NMR pH titration. This result provided the first experimentally determined $\text{p}K_{\text{a}}$ for an Fe-bound HNO molecule and is critical to the mechanistic proposals for the proton-dependent enzymatic cycles involving reduction of Fe-coordinated NO, e.g. NOR, NOS, and NiR. Based on the titration experiment, a $\text{p}K_{\text{a}}$ value of 7.7 was determined²²⁴ and, as expected, is lower than that of free ^1HNO ($\text{p}K_{\text{a}} = 11.6$).³⁸

In an effort to bridge heme and non-heme nitrosyl chemistry, Harrop and coworkers synthesized the $\{\text{FeNO}\}^7$ and $\{\text{FeNO}\}^8$ complexes $[\text{Fe}(\text{LN}_4)(\text{NO})]$ (**23**) and $[\text{Co}(\text{Cp}^*)_2][\text{Fe}(\text{LN}_4)(\text{NO})]$ (**24**), respectively (where LN_4 represents the dianionic-di-imine-di-pyrrolide planar tetradentate ligand of a hybrid heme ligand, see Fig. 1.24).²²³ The $\{\text{FeNO}\}^7$ complex **23** is very stable and does not react with excess O_2 or NO and is not photolabile. Spectroscopic studies of **23** are typical of 5C sq-py $\{\text{FeNO}\}^7$ species ($\nu_{\text{NO}} = 1704 \text{ cm}^{-1}$ (KBr); $S_{\text{tot}} = 1/2$). X-ray analysis revealed that the Fe center is in a distorted sq-py geometry derived from the four basal N-donors of $[\text{LN}_4]^{2-}$ that are coordinated in an asymmetric fashion. Complex **23** is unique from most 5C $\{\text{FeNO}\}^7$ systems as noted in the quasi-linear nature of its Fe-N-O angle of $\sim 160^\circ$, while the N-O and Fe-N distances of 1.171 and 1.700 Å, respectively, are more typical for $\{\text{FeNO}\}^7$ species.²²⁵ The unexpected linearity in the Fe-N-O bond has been ascribed to considerable d_z^2 - p_z mixing in the HOMO of **23**, which minimizes repulsion between the Fe d_z^2 and the σ lone-pair of NO.²²⁵ Lastly, analogous to the porphyrin models, the CV of **23** displayed a reversible redox wave at $E_{1/2} = -0.98 \text{ V}$ (vs. SCE, MeCN), which has been assigned to the $\{\text{FeNO}\}^{7/8}$ redox couple. This demonstrated that on the CV timescale, the LN_4 imine/pyrrolide platform can support a reduced nitrogen oxide ligand and the $\{\text{FeNO}\}^8$ unit.²²³

As suggested from the electrochemistry of **23**, the corresponding $\{\text{FeNO}\}^8$ complex was isolable. The $\{\text{FeNO}\}^8$ complex **24** was thus obtained by reduction of **23** with $[\text{Co}(\text{Cp}^*)_2]$ ($E_{1/2} \sim -1.50 \text{ V}$ vs. SCE)¹⁹⁰ in toluene at RT under N_2 to produce the violet solid $[\text{Co}(\text{Cp}^*)_2][\text{Fe}(\text{LN}_4)(\text{NO})]$ (**24**) in quantitative yield. In contrast to other $\{\text{FeNO}\}^8$ complexes that have been synthesized and studied *in situ*, complex **24** was isolated as an air-sensitive solid at RT. Additionally, **24** could be chemically oxidized with FcPF_6 in MeCN to quantitatively regenerate **23**. Thus, the NO ligand remains bound throughout the $\{\text{FeNO}\}^7 \leftrightarrow \{\text{FeNO}\}^8$ redox

process. Complex **24** exhibited modest stability in solvents such as MeCN ($t_{1/2} = 4.25$ h), which allowed for extensive spectroscopic characterization of this $\{\text{FeNO}\}^8$ complex utilizing UV-vis, FTIR, FTMS, ^{15}N NMR, and MB.²²³ The electronic absorption spectrum of **24** displayed bands at 560 nm ($\epsilon = 1800 \text{ M}^{-1} \text{ cm}^{-1}$) and 781 nm ($\epsilon = 450 \text{ M}^{-1} \text{ cm}^{-1}$), differing from **23** with λ_{max} at 661 nm ($\epsilon = 640 \text{ M}^{-1} \text{ cm}^{-1}$) and 720 nm ($\epsilon = 510 \text{ M}^{-1} \text{ cm}^{-1}$) both reported in MeCN. The low-energy band appears to be *d-d* in nature while the 560 nm band is of CT character. The FTIR spectrum of **23** displays a very strong ν_{NO} at 1704 cm^{-1} , which shifted to 1673 cm^{-1} ($\Delta\nu_{\text{NO}} = 31 \text{ cm}^{-1}$) in the ^{15}NO isotopomer (KBr). Upon reduction, the intense ν_{NO} of **23** disappeared with the appearance of a new isotope-sensitive ν_{NO} stretch at 1604 cm^{-1} (1570 cm^{-1} for ^{15}NO ; $\Delta\nu_{\text{NO}} = 34 \text{ cm}^{-1}$ in KBr). This would be more in-line with an overall $S_{\text{tot}} = 0$ LS Fe(II)-NO⁻ ↔ LS Fe(I)-NO• resonance structure in contrast to the LS Fe(II)-NO⁻ assignment for Wieghardt's complex **19**.²²⁰ Furthermore, ^1H and ^{15}N NMR in CD₃CN confirmed the diamagnetism of **24** implying an overall $S = 0$ ground state. The ^{15}N NMR displayed one signal at 743 ppm²²³ consistent with a severely bent Fe-N-O angle and similar to the reported ^{15}N NMR data for $\{\text{FeNO}\}^8$ complex **9** ($\delta = 790$ ppm in CD₂Cl₂).¹⁸⁷

The zero-field MB of $\{\text{FeNO}\}^8$ **24** revealed a mixture with the predominant species (75%) being the $\{\text{FeNO}\}^8$ exhibiting $\delta = 0.51 \text{ mm s}^{-1}$ and $\Delta E_{\text{Q}} = +1.41 \text{ mm s}^{-1}$, analogous to complex **19**.^{220,223} These values are similar to **19** ($\delta = 0.41 \text{ mm s}^{-1}$, $\Delta E_{\text{Q}} = +1.69 \text{ mm s}^{-1}$; generated at 253 K in MeCN), which has been formally assigned as containing a LS Fe(II) center. The most logical comparison of **24** is with its oxidized congener $\{\text{FeNO}\}^7$ **23**, which displayed $\delta = 0.11 \text{ mm s}^{-1}$ and $\Delta E_{\text{Q}} = 1.41 \text{ mm s}^{-1}$. Interestingly, the δ value for **23** is similar to 5C $\{\text{FeNO}\}^6$ complexes⁵⁴ that display more NO⁺ character for the coordinated nitrosyl. Accordingly, the best way to interpret the resulting MB parameters is as a change in the overall

π -accepting ability of the NO ligand. The MB δ value appears to *increase* with a *decrease* in the π -accepting ability in a series of related Fe-L-NO complexes²²⁰ and this seems to be the trend when comparing **23** and **24**. Thus, the stark difference in δ upon reduction of **23** to **24** indicates a change in the overall π -accepting ability of the ligand, as is seen in reduction of complex **18** to **19**. This analysis is suggestive of NO⁻/NO[•] character of the bound nitrosyl in **24**. As a whole, complex **24** is the first example of a relatively stable and isolable non-heme {FeNO}⁸ complex.

Complex **24** was also shown to engage in reaction chemistry typical of HNO-forming molecules such as Angeli's salt and Piloty's acid (Fig. 1.19). For example, **24** demonstrated its HNO-donor characteristics in its reaction with Fe(III)-Mb (metMb) under physiological conditions (phosphate-buffered saline, pH 7.2). Reaction of **24** with equine skeletal metMb efficiently formed MbNO via a reductive nitrosylation mechanism where NO⁻/HNO serves as both the reductant and NO source. This reaction was shown to be quantitative by UV-vis spectroscopy where the corresponding heme Soret (422 nm) and Q-bands (540, 575 nm) of MbNO appear almost instantaneously (~2 min) upon addition of the {FeNO}⁸ complex. This reaction is comparable to the reaction of other Mb species such as sperm whale metMb with Angeli's salt (Na₂N₂O₃), which takes 15.5 min for the production of MbNO to go to completion.²¹⁰ Additional reactivity with thiols such as GSH were also tested since thiols are known biological targets for HNO.²²⁶⁻²²⁸ Indeed, reductive nitrosylation of metMb was completely inhibited when GSH was present. In contrast to the known reaction of thiols with HNO to form sulfinamides, it appeared that the main product of **24** with GSH was the formation of the dinitrosyl compound [Fe₂(μ -GS)₂(NO)₄]⁻ (or reduced Roussin's red ester = rRRE by UV-vis and ESI-MS). While the exact nature of the NO ligand in complex **24** cannot be completely verified, preliminary reactivity of this {FeNO}⁸ complex is somewhat consistent with classic

HNO donor molecules. In fact, complexes like **24** offer new avenues for HNO therapeutics that have yet to be explored with other {FeNO}⁸ systems.

1.8.2 Theoretical Descriptions of Non-Heme {FeNO}⁸ Complexes⁶⁷

Prior to the informative characterization of the nitroxyl species [Fe(CN)₅(HNO)]³⁻ (**22**), Olabe²¹⁹ reported theoretical efforts to elucidate the electronic structures of the FeNO unit in NP analogues of various E-F notations.^{229,230} The computed and synthesized (*vide supra*) results revealed a sizeable stability imparted on the Fe-HNO complex **22** relative to the nitroxyl anion Fe-NO⁻ complex **21**. The HNO complex was found to be more stable as a ground state singlet ($S_{tot} = 0$). Furthermore, protonation at N of NO⁻ was favored over other sites, e.g. NO-H or H-CN, by ~24 kcal/mol.²¹⁹ The considerable energy differences suggested significant charge density residing primarily on the N of NO thus facilitating protonation. This analysis is further supported by the computed structural parameters of the {FeNO}⁷ **20** and {FeNO}⁸ **22** NP species. The major structural changes upon reduction/protonation include a decrease in the Fe-N-O angle from 146.6° to 137.5° ($\Delta_{\text{FeNO}} = 9.1^\circ$) with a subsequent increase in Fe-N (1.737 Å to 1.783 Å), as well as an increase in N-O (1.199 Å to 1.249 Å) (Table 1.5).²¹⁹ These results infer occupation of an orbital primarily centered on NO upon formation of **22**. The calculated ν_{NO} vibrational modes of 1394 and 1338 cm⁻¹ are in good agreement with the experimental rR bands, $\nu_{\text{NO}} = 1380, 1304$ cm⁻¹ for the symmetric and asymmetric stretch, respectively.^{219,224} The large decrease in the N-O bond strength of **22** associated with the reduced N-O stretching frequency and increased bond length, supports mainly NO π^* MO occupation by the reducing electron. Collectively, the experimental and theoretical results firmly support a LS Fe(II) coordinated to ¹HNO (formally an NO⁻ ligand) oxidation state.

Table 1.5. Geometric Parameters of 5C and 6C Non-Heme {FeNO}^{7/8} Systems

Molecule	Geometric Parameters ^a				Ref
	Fe-N (Å)	N-O (Å)	∠Fe-N-O (deg)	Fe-N _{trans} (Å)	
{FeNO}⁷					
<i>trans</i> -[Fe(NO)(cyclam-ac)] ⁺ (18)	1.722	1.167	148.7	2.012	220
[Fe(CN) ₅ (NO)] ³⁻ (20)-calc.	1.737	1.199	146.6	-	219
[Fe(LN ₄)(NO)] (23)-calc.	1.690	1.183	149.9	-	223
{FeNO}⁸					
<i>trans</i> -[Fe(NO)(cyclam-ac)] (19)-calc.	1.752	1.261	122.4	2.127	220
[Fe(CN) ₅ (HNO)] ³⁻ (22)-calc.	1.783	1.249	137.5	-	219
[Fe(LN ₄)(NO)] ⁻ (24)-calc.	1.681	1.219	142.0	-	223

^aData consists of experimental and DFT calculated parameters (denoted by calc.).

Similar computational results were obtained for the non-heme {FeNO}⁸ complex **19** containing the cyclam-ac ligand (BP86/TZVP).²²⁰ A qualitative bonding description of **19** is, much like **22**, suggestive of a LS Fe(II) coordinated to ¹NO⁻ (*S*_{tot} = 0), but further insight into the bonding profile of this non-heme complex advocates the notion of a more localized NO unit reduction. Given the multiple oxidation state assignments possible for {FeNO}⁸ and other E-F notations, the relative energies of all possible {FeNO}⁸ derivatives, i.e. singlet vs. triplet, protonated vs. non-protonated, N vs. O protonation among others were considered. Of these possibilities, the singlet, non-protonated {FeNO}⁸ version of **19** was the electronic ground state. The structural parameters of the {FeNO}⁷ species **18** serves as a comparison to the theoretically established {FeNO}⁸ **19**. Therefore, upon reduction (see Table 1.5) to form **19**, the Fe-N bond was shown to elongate from 1.723 (exptl: 1.722) Å to 1.752 Å in **19**. Correspondingly, the N-O

bond increases a considerable extent from 1.204 Å (exptl: 1.167 Å – DFT often overestimates bond lengths in open shell systems) to 1.261 Å in the {FeNO}⁸ complex. As a result of the increased trans-effect of NO⁻, the Fe-O_{carboxylate} bond in **19** increases by 0.15 Å. A dramatic change in the Fe-N-O angle was seen from 140.6° (exptl: 148.7°) to 122.4° and, taken with the considerable elongation of the N-O bond by ~0.06 Å, is supportive of more NO-π* occupation in the former SOMO of **18**. Further insight into the nature of the Fe-NO bonding in **19** is gained from a natural population analysis (NPA) on atomic charges in the molecule. Based on NPA, the charge on the Fe center decreased slightly in going from **18** (+1.005) to **19** (+0.882) supporting more electron density about Fe in **19**. A more significant change though is seen in the charge on the NO ligand, which is more negative in **19** (-0.672) versus **18** (-0.230). The NPA results clearly point to an NO-centered reduction in the **18**-to-**19** conversion and are in agreement with the experimental results (ν_{NO} , MB). Taken together, the experimental and DFT results support the LS Fe(II)-NO⁻ ($S = 0$) assignment for complex **19**.

The non-heme {FeNO}⁸ complex **24** offers some insight into the bonding parameters of the Fe-NO unit exhibited in a pseudo-heme coordination sphere.²²³ As usual, DFT analysis (OLYP/STO-TZP) of **24** (singlet is the electronic ground state) starts from the stable {FeNO}⁷ precursor **23**. The Fe-N bond of **23** was calculated to be 1.690 Å (exptl: 1.700) Å, which was shown to shorten slightly upon reduction to 1.681 Å. As expected, the N-O bond increases from 1.183 Å (exptl: 1.171 Å) in **23** to 1.219 Å in {FeNO}⁸ **24**. The near linear Fe-N-O angle observed in **23** (158°) differs more significantly from theory (150°) but this discrepancy has been substantiated due to an effectively barrierless Fe-N-O bending potential. Furthermore, the calculated angle for **24** decreased slightly (142°) after reduction. The transition from **23** to **24** reveals a decrease in the Mulliken charges at the Fe (0.894 to 0.795) and NO (-0.165 to -0.385)

as well as a number of atoms of the LN_4 ligand suggesting the reduction is neither Fe- nor NO-centered. These computed changes upon reduction are similar to those observed in heme $\{\text{FeNO}\}^8$ systems in that the reduction is delocalized over the entire Fe-N-O unit. This behavior is in contrast to what is typically observed in non-heme systems (see **18-to-19** and **20-to-22**)^{220,224} where the reduction occurs primarily on the coordinated nitrosyl lending support to the heme-like character of LN_4 in **24**.²²³ As with heme systems, a limited bonding description can be proposed as intermediate between LS $\text{Fe(II)}\text{-}^1\text{NO}^-$ and LS $\text{Fe(I)}\text{-NO}\cdot$.

The $\{\text{FeNO}\}^8$ moiety has attracted attention as a synthetic target in heme and non-heme model complexes. The direct trapping of HNO has been demonstrated by deoxyMb and highlights one synthetic route to obtain $\{\text{FeHNO}\}^8$ complexes. Alternatively, the chemical and electrochemical reduction of $\{\text{FeNO}\}^7$ is the most common approach. Based on the surprising stability of the MbHNO complex, one can attempt to incorporate design criteria such as secondary-sphere motifs for example H-bonding and aliphatic interactions to stabilize the HNO ligand. For instance Lehnert and coworkers (2013) use the bis-picket fence porphyrin strategy to provide steric protection and possible H-bonding to demonstrate reversible protonation and deprotonation of the NO^- ligand. The reduced species was produced through bulk electrolysis but was not isolable.²³¹ However, the species was described as a LS $\text{Fe(II)}\text{-}^1\text{NO}^-$ complex, consistent with all $\{\text{FeNO}\}^8$ porphyrin model complexes. Recently, Lehnert and coworkers report the first 5C non-heme high-spin (HS) $\{\text{FeNO}\}^7$ ($\text{Fe(III)}\text{-NO}^-$ $S = 3/2$) and $\{\text{FeNO}\}^8$ ($\text{Fe(II)}\text{-NO}^-$ $S = 1$) complexes.²³² These efforts highlight the ability to tune electronics and spin-state of the system in this case through the coordination geometry of a trigonal bipyramidal 5C system. However, the $\{\text{FeNO}\}^8$ complex was not isolable. Nonetheless, understanding what factors lead to the multitude of possible oxidation- and spin-states of the Fe or NO is an

important area of Fe-NO chemistry that is starting to be uncovered. It is anticipated that the reactivity of LS Fe(II)NO⁻ species having a ¹NO⁻ would be very different from that of the HS analogue with ³NO⁻. Thus, establishing criteria that control the oxidation- and spin-state of Fe-NO species in order to access new isolable complexes is a new frontier of Fe-NO chemistry. Accordingly, unraveling the potential reactivity of Fe-NO complexes to deliver HNO or react in a biologically relevant manner may facilitate the design of metal-based HNO donors and other therapeutic compounds.

1.9 Nitrite in Biology

1.9.1 Nitrite Reductase Enzymes

The interconversion of N_yO_x compounds in the nitrogen cycle occurs for two major reasons. First, to produce reduced nitrogen species, namely NH₄⁺, for incorporation into biological molecules such as amino acids and nucleic acids, for the synthesis of proteins and DNA. This process is called assimilation. The second reason is utilization of N_yO_x species as electron donors or acceptors in the respiratory processes of microorganisms, known as dissimilation.⁹ The NO₂⁻ anion is involved in both of these processes and therefore critical to the overall recycling of N-containing species on Earth. With respect to assimilation, the siroheme-containing nitrite reductase enzyme (SCNiR) performs the six-electron reduction of NO₂⁻ to NH₄⁺. The most well-studied form of SCNiR is isolated from the chloroplast of spinach, and contains an active site with one [4Fe-4S] cluster bridged by a cysteinate residue to the siroheme cofactor (Fig. 1.1B). The [4Fe-4S] cluster shuttles electrons between ferredoxin and the siroheme active site.¹¹⁰ Secondary-sphere Arg and Lys residues are conserved and facilitate binding, activation, and reduction of NO₂⁻ through H-bonding and proton delivery.

The mechanism of SCNiR is proposed to be similar to that of the *cc*NiR complex that performs the same net transformation of NO_2^- to NH_4^+ . Importantly, NO_2^- binds to a LS Fe(II) center through its N-atom, assisted by H-bonding through the secondary-sphere residues, a common feature among Fe-containing NiR enzymes (Fig. 1.25). Subsequent protonation and loss of a water molecule affords an Fe(II)- NO^+ or $\{\text{FeNO}\}^6$ complex. This species then undergoes rapid proton and electron transfer to give the Fe(HN(H)OH) species that likely traverses the putative $\{\text{FeHNO}\}^8$ intermediate. Subsequent proton/electron delivery completes the reduction to NH_4^+ .^{111,233-237} As discussed earlier, the mechanism of reduction for *cc*NiR is similar, despite some key differences. One major difference is the electron transfer process. For example, *cc*NiR contains four bis-His-ligated *c* hemes that can store and transfer electrons to the active site.²³⁸ Conversely, the SCNiR enzyme has only one [4Fe-4S] cluster that transfers one electron at a time to the active site. Thus, CSNiR obtains all reducing equivalents through six one-electron donation steps. Another major difference is the active site heme-cofactor. While *cc*NiR contains a *c* heme ligated by a proximal Lys residue, CSNiR has a siroheme ligated by a proximal [4Fe-4S] cluster. It is interesting that both of these distinct enzymes are capable of performing analogous N_2O_x transformations with similar mechanisms, albeit with differing molecular machinery.

A common point between *cc*NiR and SCNiR is that both enzymes maintain bound substrate throughout the proton-coupled electron transfer process. This binding is made possible through the extensive H-bonding network. Moreover, the tuning of local redox potential and release of product are important roles of the secondary-sphere H-bonding network, an important point when considering the release of NO or NH_4^+ .²³⁸ For instance, both the reduction of NO_2^- to NH_4^+ and NO_2^- to NO occur at a heme center. Thus, the release of either NH_4^+ (after six-electron

reduction) or NO (after one-electron reduction) is a critical feature of the H-bonding network in NiR enzymes. This is best illustrated using *cd*₁NiR as an example. Accordingly, *cd*₁NiR reduces NO₂⁻ to NO selectively, but can also perform the four-electron reduction of O₂ to H₂O. Therefore, one might assume that *cd*₁NiR could reduce NO₂⁻ by four-electrons to NH₂OH. However, this reaction does not occur, and is attributed to the H-bond assisted release of NO from the *d*₁ heme.²³⁹

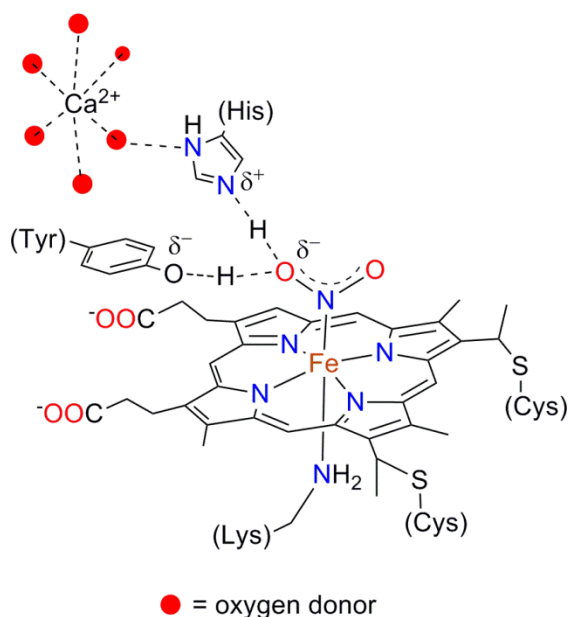


Figure 1.25. Active site for *cc*NiR enzyme illustrating the *c* heme, secondary-sphere H-bonding of the His residue, and calcium binding site.

The dissimilatory pathway for microorganisms contains a multitude of metalloenzymes, yet only three key enzymes reduce NO₂⁻, namely, SCNiR, *cc*NiR and *cd*₁NiR. The latter enzyme does not continue reduction all the way to NH₄⁺, but rather stops at and releases NO. This unique behavior deserves further discussion. The *cd*₁NiR enzyme contains a *c* heme and a *d*₁ heme as an electron relay and active site, respectively. The Fe(III) *d*₁ heme is coordinated to a His residue

and a hydroxide ion on the proximal side that is stabilized by a H-bond from a neighboring Tyr-OH. This state is termed the 6C-closed form of the enzyme. Upon electron transfer from the *c* heme to the *d*₁ heme, a large conformational change in the protein occurs, thus pulling the Tyr-OH away from the now Fe(II)-OH followed by protonation of the hydroxide ion. Consequently, the Fe(II)-H₂O resting state is formed and ready to bind NO₂⁻. Mechanistic proposals suggest that both reduction of the *d*₁ heme and protonation of the secondary sphere His residues must occur for this conformational change to occur. There are two plausible mechanisms for NO₂⁻ reduction at the *d*₁ heme (Fig. 1.26).⁷⁴ One proposed mechanism involves the O-bound nitrito isomer (Fig. 1.26, pathway B). Through this mechanism, a single protonation to the metal bound O of the nitrito ligand facilitates homolytic cleavage of that N-O bond. This immediately releases NO(g) and forms an Fe(III)-OH species, which based on the 6C-closed state of the enzyme (distal Fe(III)-OH) would be a reasonable proposal. However, the only crystallographic data of *cd*₁NiR with NO₂⁻ bound exists in the N-bound nitro form.¹⁹³

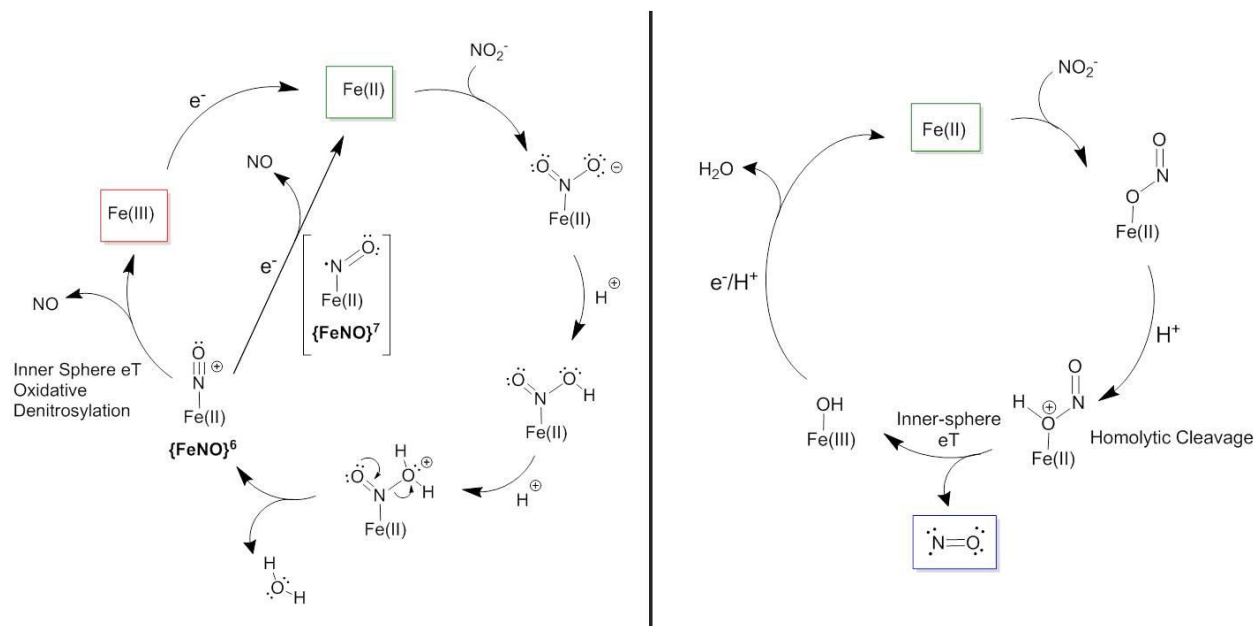


Figure 1.26. Proposed mechanisms for reduction of NO_2^- to NO at $cd_1\text{NiR}$. Left: Pathway A showing the N-bound isomer that can potentially release NO from the $\{\text{FeNO}\}^6$ or $\{\text{FeNO}\}^7$ species after heterolytic cleavage of an N-O bond. Recent evidence supports release from the $\{\text{FeNO}\}^7$ complex. Right: Pathway B showing the single protonation and homolytic N-O bond cleavage mechanism.

The more widely accepted mechanism begins with the coordination of NO_2^- in the nitro form (Fig. 1.26, pathway A). The N-bound isomer is thought to H-bond to the two conserved His-NH residues in the secondary-sphere of the active site and is calculated as the energetically favored isomer.⁷⁴ The His H-bonding and the Fe-to- NO_2^- π -backbonding, assist in elongation and activation of one of the N-O bonds for O-protonation.^{78,240} Subsequent loss of H_2O forms the $\{\text{FeNO}\}^6$ species. At this point though, it is important to consider that a single electron transfer would form an $\{\text{FeNO}\}^7$ complex, and potentially halt catalysis. Although this may be true in most heme proteins, recent evidence suggests that there are several factors supporting that

reduction to the $\{\text{FeNO}\}^7$ species occurs prior to NO dissociation. For instance, the oxidized d_1 heme has two carbonyl groups located on the periphery of the porphyrin structure, as compared to the c heme of $cc\text{NiR}$ (Figs. 1.25 and 1.27). This modulation would have an electronic inductive effect that withdraws electron density from the metal center, thus diminishing the metal-to-ligand π -backbonding and weakening the Fe-NO bond.²⁴¹ The d_1 heme has two anionic pyrrole donors on one side of the porphyrin ring as well as two fully-saturated ring carbons that limit delocalization of the π -system; conversely, the c heme has the anionic pyrroles opposite to one another with a fully-conjugated π -system. These differences in the heme d_1 may also modulate the backbonding and orientation of the NO_2^- or NO species for activation or release, respectively. For instance, the ordering of the d -orbitals in the d_1 heme has been investigated by combined MCD and EPR analysis. It was determined that the Fe(III) d_1 heme has an unusual octahedral d -orbital configuration.²⁴² Typically, Fe(III) hemes maintain the unpaired electron (d^5) in the d_{xz} or d_{yz} orbital, i.e. above the plane of the porphyrin ring. However, the inversion of these t_{2g} orbitals leads to the d_{xy} orbital as the HOMO, thus placing the unpaired electron in the heme plane.²⁴² This localization of the unpaired electron on the heme plane is proposed to limit the π -backbonding ability of the d_1 heme Fe to the NO ligand.

Additional studies that support release of NO from the $\{\text{FeNO}\}^7$ form of $cd_1\text{NiR}$ show that the fully reduced $cd_1\text{NiR}$ has no inhibition of activity when saturated with NO. This result is direct evidence that the Fe(II)-NO interaction is weak.^{241,243,244} Furthermore, it has been shown that NO release is triggered by electron transfer from c heme to the $\{\text{FeNO}\}^6$ d_1 heme.^{244,245} Lastly, if the c heme ligands are mutated from Met/His to His/His, then it is trapped at a redox potential that prevents electron transfer to the d_1 heme. In this case, the $cd_1\text{NiR}$ mutant can reduce NO_2^- but not release NO from the $\{\text{FeNO}\}^6$ state.²⁴⁶ Correspondingly, the $\{\text{FeNO}\}^7$

dissociation rates (k_{off}) for $cd_1\text{NiR}$ were shown to be upwards of 200 s^{-1} , as compared to $\sim 10^{-4}\text{ s}^{-1}$ for other ferrous heme such as Mb, Hb, and sGC, even though the k_{on} is comparable to other heme species ($\sim 10^7\text{-}10^8\text{ M}^{-1}\text{s}^{-1}$).²⁴¹ Thus, NO dissociation occurs at a catalytically relevant rate. Dissociation of NO from the $\{\text{FeNO}\}^7$ unit is facilitated by H-bonding to the nitrosyl, electronics of the d_1 heme, as well as displacement by NO_2^- substrate. Taken together, the electronic state and the secondary-sphere interactions of $cd_1\text{NiR}$ enzyme are finely-tuned to release NO from what would normally be considered a stable Fe-NO species.⁹

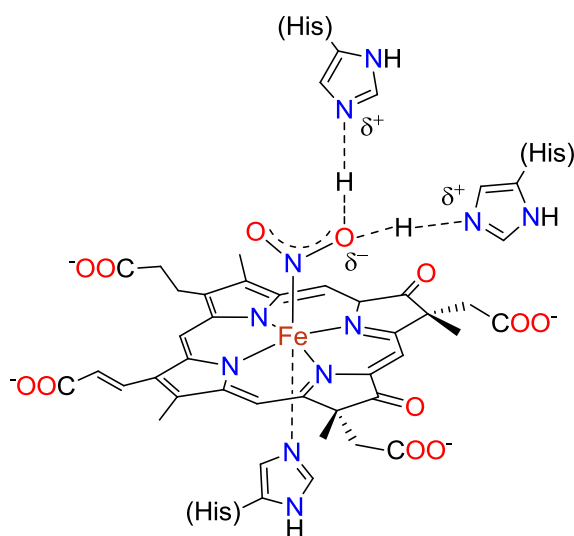


Figure 1.27. Active site for $cd_1\text{NiR}$ enzyme illustrating the d_1 heme and secondary-sphere H-bonding of the His residues.

Collectively, the reduction mechanism of NO_2^- by $cc\text{NiR}$, CSNiR , and $cd_1\text{NiR}$ are nearly analogous up to the point of the $\{\text{FeNO}\}^6$ intermediate, where the former two enzymes reduce the nitrosyl through an $\{\text{FeHNO}\}^8$ intermediate to form NH_4^+ , while the latter enzyme uniquely forms an $\{\text{FeNO}\}^7$ prior to release of NO. The instability of this $\{\text{FeNO}\}^7$ unit is a combination of the electronic structure of the d_1 heme unit as well as a dynamic H-bonding network that can

facilitate substrate binding and then shift to promote product dissociation. The tuned d_1 heme is a substantial cofactor to synthesize.⁹ Therefore, the evolutionary reasoning behind its function must be one of great importance. It is interesting to consider the early evolution of N_yO_x related enzymes and the prevalent architectures in today's higher organisms. In this light, the reduction of NO_2^- to NO at a heme center has traversed through the ages and is prevalent in modern organisms. The function of this transformation stems from energy conversion, but is now understood to be of importance to biological signaling for prokaryotic and eukaryotic life forms. The concept of bacterial signaling, for instance, would suggest that an NiR that produces NO for the purpose of signaling could be considered a bacterial nitric oxide synthase (bNOS). As discussed above, higher organisms do have specific NOSs for the production of NO for signaling in vasculature and neurons; however, discrete genes for the synthesis of NiR enzymes are not found in humans. Current biochemical proposals suggest the NO_2^- conversion to NO is performed by numerous heme-proteins in mammals, as an alternative source of NO to the NOS pathway. Thus, the NO_2^- to NO signaling pathway underscores a fundamental evolutionary requisite involving NO_2^- and heme proteins.

1.9.2 Role of Nitrite in Mammalian Physiology and Interactions with Heme-proteins

The critical roles of NO include: vascular function as a vasodilator and mediator of platelet aggregation; neurological function as a transmitter molecule; immune response function in antimicrobial and antitumor activity; as well as apoptosis and gene expression.^{33,247-252} At the same time, NO becomes a toxic molecule at higher concentration. A typical biological range for NO is 10-100 nM.²⁴⁸ The resulting effects of NO, positive or negative, result from modification of a metal center (heme and [4Fe-4S] clusters) or formation of RSNO. It should be noted that the

formation and reactivity of RSNO is an active area of research. Again, the distinction that RSH and NO do not react spontaneously (as does HNO) holds true due to the fact that $\text{RSH} + \text{NO} \rightarrow \text{RSNO} + \text{H}^+ + \text{e}^-$ and requires a biological oxidant. Thus, a metal center, like Fe(III) cytochrome *c* oxidase (CcO) must mediate this process.²⁵³ Regardless, the synthesis and regulation of NO in biological organisms is one of great importance and requires tight regulation.

Understanding of the NO_2^- pathway to NO has only recently come in to the forefront of biological N_yO_x transformations. An early concept of this transformation was published in 1880 and demonstrated the anaerobic, acid-dependent reduction of NO_2^- to NO and its potential relationship to human physiology.²⁵⁴ It took 73 years for this to be investigated further, in which the study showed relaxation of contracted aortic tissue by addition of NaNO_2 .²⁵⁵ Subsequent studies have detailed the role of the NO_2^- to NO conversion as having cytoprotective behavior during ischemia.^{40,256-260} This supports the role of NO_2^- (0.2 -10 μM physiological levels)¹⁴ as a storage pool for NO that is activated under hypoxic/anoxic conditions (20 and 2 μM O_2 , respectively), conditions that limit the production of NO from the O_2 -dependent NOS enzymes.

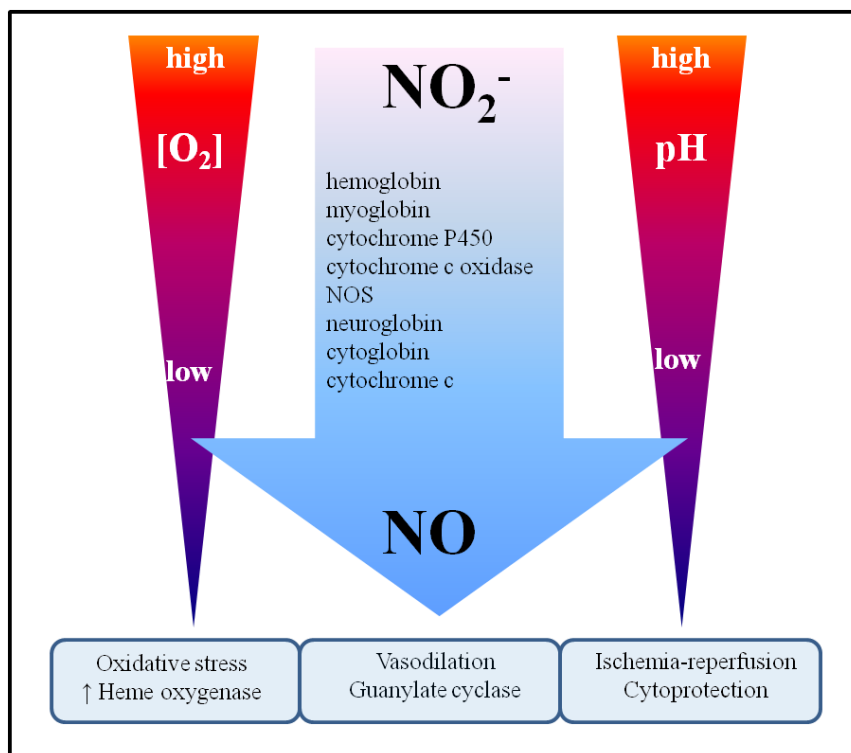


Figure 1.28. Schematic representation of the condition-dependent reduction of NO_2^- to NO proposed to occur through multiple heme-containing proteins and enzymes.

Biological effects of NO_2^- reduction to NO extend further than the common vasodilatory action.^{14,261-263} This conversion is thought to encompass many of the functional roles of NO, under a condition-dependent fashion, i.e. low $[\text{O}_2]$ and increased $[\text{H}^+]$. For instance, angiogenesis and smooth muscle proliferation demonstrate direct cardiovascular effects.^{262,264,265} Moreover, anti-oxidant behavior through gene expression of heme-oxygenase-1 can be considered a NO_2^- dependent signaling pathway to protect against oxidative stress.²⁶⁶ Critically, NO produced through reduction of NO_2^- under hypoxic conditions can regulate mitochondrial respiration, thus the NO-dependent inhibition of the mitochondria can slow O_2 consumption and lessen ROS production.^{259,267-269} In the context of an organ or tissue hypoxia, these combined effects would

increase oxygenated blood flow, regulate O₂ diffusion/consumption, manage ROS, while maintaining an anti-inflammatory environment. Collectively, the condition-dependent (low [O₂], high [H⁺], and reducing), 'emergency' reduction of NO₂⁻ to NO has evolved as a protective mechanism to produce NO in an alternative manner to the O₂-dependent NOS pathway. Provided that there is not yet a known dedicated NiR enzyme in mammals, these important observations proffer the question of how is NO₂⁻ reduced to NO?

Numerous studies have implicated a variety of heme proteins as condition-dependent NO₂⁻ enzymes (Fig. 1.28). For instance, the 5C heme-containing proteins, Hb, Mb, P450,²⁷⁰ CcO,²⁷¹ and NOS²⁷² as well as the 6C neuroglobin (Nb)²⁷³, cytoglobin (Cb),^{274,275} and cytochrome c (Cc),²⁷⁶ have been shown to reduce NO₂⁻ to NO by the general reaction: NO₂⁻ + 2H⁺ + Fe(II)-protein → NO + H₂O + Fe(III)-protein. The majority of reports involving NO₂⁻ reduction by a non-dedicated heme protein involve Hb and Mb. The reaction rates under anaerobic conditions are pH dependent, where Hb reduces NO₂⁻ to NO at $k = 10 \text{ M}^{-1}\text{s}^{-1}$ (pH 6.5) and $\sim 0.1 \text{ M}^{-1}\text{s}^{-1}$ (pH 7.4), while Mb more efficiently performs at pH 7.4 with $k \sim 6\text{-}12 \text{ M}^{-1}\text{s}^{-1}$. Other differences between Hb and Mb are found their P_{50} values of $\sim 3 \text{ }\mu\text{M}$ and $\sim 35 \text{ }\mu\text{M}$ for Mb and Hb, respectively.^{14,125,277-280} These parameters highlight that the Mb protein has a lower affinity for O₂ and exists primarily in its deoxyMb state at low O₂ levels. Moreover, the Mb redox potential (0.046 V vs. NHE) implicates it as a better reducing agent, compared to the Hb T-state (0.17 V vs. NHE).²⁸¹ Both Mb and the R-state of Hb have comparable rates of NO₂⁻ reduction; however, dissociation of NO from the putative {FeNO}⁶ intermediate is approximately an order of magnitude faster from the T-state ($\sim 1 \text{ M}^{-1}\text{s}^{-1}$).²⁸² This highlights a conformational dependence of the Hb protein on its NiR activity. Of course, the Mb monomer

does not have this cooperative factor. Although there are subtle differences in the properties of Hb and Mb, the overall reaction and mechanism of NO release is thought to be similar.

There is clear experimental evidence supporting that isolated Hb and Mb produce NO from NO_2^- under simulated hypoxic conditions.⁹ Experiments involving isolated heart and red blood cells (RBCs) demonstrate response in the presence of NO_2^- indicative of the generation of NO.^{9,14,260,268,278,279,283-290} Furthermore, induced myocardial infarction (heart-attack) in otherwise healthy mice showed that NO_2^- could protect mice against heart-failure. Knockout studies showed that in the absence of Mb, these mice were no longer protected and the overall amount of detectable NO or NO-adducts decreased.^{9,11,279,291,292} However, even with increasing *in vivo* and *in vitro* evidence, the straight forward transformation of $\text{NO}_2^- + 2\text{H}^+ + \text{Fe(II)-protein} \rightarrow \text{NO} + \text{H}_2\text{O} + \text{Fe(III)-protein}$ becomes significantly more complicated in a biological milieu. For instance, the NO formed would be readily trapped by surrounding deoxyMb and deoxyHb that have a k_{on} value of $10^7 \text{ M}^{-1}\text{s}^{-1}$ and a K_d in the low nM range.^{9,278,280,293-299} Moreover, if O_2 is present then it will bind to form Hb(O_2) or Mb(O_2) in which the oxidation of free NO with oxyHb/Mb to NO_3^- occurs at competitive rates up to $k = 10^8 \text{ M}^{-1}\text{s}^{-1}$.^{9,280,294,295,300-303} Due to these kinetic and thermodynamic constraints there have been several proposals that attempt to rationalize the physiological results of apparent NO formation and signaling. The major hurdle is to explain how NO formed inside an RBC can find its way through the membrane and into an endothelial cell or muscle tissue; a point of controversy with respect to Hb due to its primary location in the RBC. With respect to Mb, this is less of an issue of its widespread muscular locale for the Mb monomer.

One proposal suggests the formation of N_2O_3 from reaction of either $[Fe(III)-NO_2^- \leftrightarrow Fe(II)-NO_2\bullet]$ with free $NO\bullet$ or reaction of $[Fe(III)-NO\bullet \leftrightarrow Fe(II)-NO^+]$ with NO_2^- (Fig. 1.29).³⁰⁴⁻
³¹⁰ The formation of N_2O_3 from either pathway would regenerate deoxyHb, and the N_2O_3 formed has little affinity for the Hb and is therefore free to diffuse out of the RBC at which point it can spontaneously hydrolyze to $NO\bullet$ and $NO_2\bullet$. However, this proposal is thermodynamically unfavorable at pH 7 where $\Delta G^{\circ}_{rxn} = 59 \text{ kJ mol}^{-1}$.²⁵³ Accordingly, at a basal NO_2^- concentration of 2.5 μM , this would provide a level of N_2O_3 at $\sim 3 \times 10^{-22} \text{ M}$.²⁵³ Thus, at these extraordinarily low concentrations, hydrolysis reaction of N_2O_3 to give NO may not explain observed physiological responses.

An additional proposal is that the NO formed in the reaction of NO_2^- with deoxyHb occurs in a spatially favorable location, i.e. in a metabolon complex with proteins of the cell membrane, and can diffuse readily outside the RBC. This proposal is reasonable and can be rationalized by the higher affinity of the T-state Hb for the cell membrane, as well as the higher rate of NO release from the T-state. This again implicates a complicated, conformational dependence under allosteric control.^{261,278,292,311,312} Thus, the picture becomes more clear, that under decreasing O_2 levels, the R-state becomes more populated, this being the better NiR-like catalyst. Reaction with NO_2^- and formation of the $\{FeNO\}^6$ intermediate facilitates conformational changes toward the T-state and localization near the cell membrane. Once localized and fully in the T-state, the NO can diffuse through the membrane. One major argument against this proposal is that NO diffusion is controlled by a concentration gradient. Therefore, the NO released at the cell membrane would have a strong affinity for the interior of the RBC and potentially be trapped as the HbFe(II)-NO, however the same argument could be made for outside of the RBC.^{313,314}

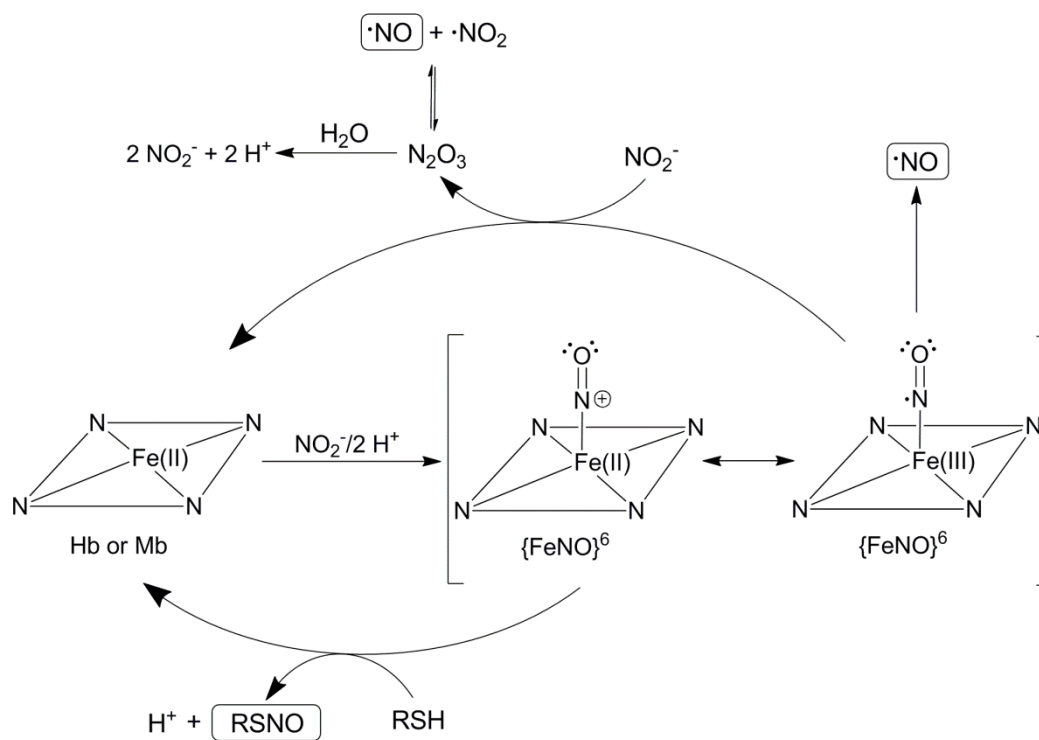
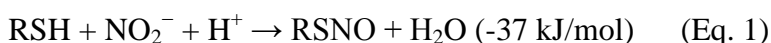
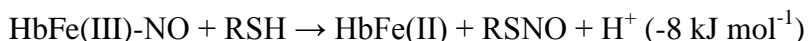


Figure 1.29. Proposed reactive pathways from $\{\text{FeNO}\}^6$ Hb or Mb to produce a vasodilatory response from reduction of NO_2^- . Known vasodilators are shown in boxes.

The last proposal takes into account the formation of the $\{\text{FeNO}\}^6$ species, and possible reaction of RSH to give RSNO, a known vasodilator and storage mechanism for NO (Fig. 1.29).^{253,315} Though tempting, it is not chemically appropriate to consider the reaction of $\text{NO}\cdot$ with $\text{RS}\cdot$ due to the fact that $\text{RS}\cdot + \text{H} \rightleftharpoons \text{R}\cdot + \text{SH}$.^{253,316,317} However, the reaction of $\text{NO}^+ + \text{RSH} \rightarrow \text{RSNO} + \text{H}^+$ is favorable. Likewise, the Hb $\{\text{FeNO}\}^6$ intermediate is formally Fe(III)-NO^+ and the putative reaction of the $\{\text{FeNO}\}^6$ intermediate with a biological thiol becomes very likely. In the presence of H^+ , the net reaction of Hb, NO_2^- , and RSH is favorable (Eq. 1).²⁵³

In this light, both glutathione (GSH) and the β -chain cysteine 93 SH groups may take part in this chemistry.^{318,319} This pathway is reasonable, considering that both GSNO and Hb- β 93Cys-SNO are known compounds and furthermore implicated in cardiovascular signaling related to NO.^{146,320}



The proposed pathways for rationalization of the reduction of NO_2^- and release of NO from the RBC require more experimental work, and would benefit from simpler models of these systems within rigorously controlled systems. With this in mind, the synthesis and characterization of Fe(II)- NO_2 species would allow for the detailed study of Fe(II)- NO_2 with H^+ and RSH to determine if formation of RSNO is viable. Moreover, studies involving the possible generation of N_2O_3 from NO_2^- and NO in the presence of Fe complexes could better support existing proposals. Given the importance of Fe-mediated NO_2^- reduction in the global nitrogen cycle, as well as N_yO_x signaling pathways, the synthesis and characterization of Fe(II)- NO_2 and Fe(III)- NO_2 heme and non-heme complexes have been pursued. Given the context of this dissertation, a review of the heme and non-heme Fe- NO_2 literature is discussed below.

1.10 Heme Fe(NO_2) Model Complexes

Interest in the reactions of heme-enzymes of the nitrogen cycle spawned the early study of the fundamental coordination chemistry of Fe-porphyrin NO_2^- (Fe(por) NO_2) chemistry. Current developments in understanding the NO_2^- signaling pathways and its relationship to Fe

proteins has expanded this area of research. Model compounds of the Fe(II/III)(por) variety have been studied structurally and with an emphasis on the kinetic and thermodynamic properties in their interactions with NO_2^- . Some fundamental studies of their reactivity have been pursued, but primarily with respect to enhanced reductive nitrosylation reactions as well as O-atom transfer (OAT) chemistry. The detailed analysis of Fe(por)NO₂ allows for the determination of specific binding modes and possible reaction mechanisms that may parallel heme-proteins. This insight can help guide researchers toward fundamentally sound and viable hypotheses for how NO_2^- interacts with heme-proteins in biology.

1.10.1 Fe(III)(NO₂)_n Heme Models

Much of the study of [Fe(II/III)(por)(NO₂)_n], where $n = 1$ or 2 , has been spearheaded by the research laboratories of Scheidt and Ford. The early efforts of Scheidt and coworkers (1990's to present) have provided valuable structural insight as well as spin-state and oxidation state analysis. The primary model system used by Scheidt et al. is the picket-fence porphyrin TpivPP (the dianionic $\alpha,\alpha,\alpha,\alpha$ -tetrakis(*o*-pivalamidophenyl)porphinato, Fig. 1.30).³²¹ The use of the picket-fence porphyrin was spurred by a previous study which reported the relative instability of the open-faced porphyrin complexes of Fe(III) with the dianionic TPP, TTP, and OEP species (Figs. 1.20 and 1.30).³²² It should be noted that the isolation of any opened face porphyrin as the [Fe(II/III)(por)(NO₂)_n] species has not been achieved. The synthesis and first structural characterization of an Fe(NO₂)₂ complex, namely [K(18C6)][Fe(NO₂)₂(TpivPP)] (**25**), was achieved by Scheidt and coworkers in 1990.³²¹ Compound **25**, was prepared in chlorobenzene from the [Fe(TpivPP)Tos] (where Tos = tosylate) complex with excess equiv of [K(18C6)][NO₂]. The structural characterization of **25** revealed two NO₂⁻ ligands, coordinated axially through

their respective N-atoms. One NO_2^- ligand is within the protected face of the porphyrin, while the other NO_2^- ligand is exposed. The average Fe- NO_2 distances were reported as 1.970 Å for the NO_2^- inside the picket-fence pocket and 2.001 Å for the NO_2^- on the open-face of the porphyrin (Table 1.6). Notably, there is some asymmetry within the NO_2^- ligands, in that the N-O distances are not the same. This asymmetry may indicate N-O bond activation showing a difference of 0.123 Å in the long N-O bond (1.298 Å) and short N-O bond of (1.175 Å) as compared to the N-O (~1.24 Å) in NaNO_2 . The FTIR spectrum of **25** showed two distinct ν_{NO} bands at 1351 and 1315 cm^{-1} , consistent with an N-bound nitro ligand.⁷⁷ The picket-fence porphyrin increases the overall solution stability and isolable nature of this complex. The greater stability allowed for a determination of binding constants, K_1 and K_2 for the mono- and bis(NO_2) species, reported as 1.49×10^4 and 4.0×10^4 , respectively.³²¹ Moreover, a LS state ($S = 1/2$) was confirmed by EPR spectroscopy, which exhibited a rhombic feature having a relatively narrow g -spread (vide infra). Taken together, the results of this study indicate a high affinity of the Fe(III)(por) system for NO_2^- , and demonstrate a strong preference for Fe(III) to bind two NO_2^- ligands. The LS nature of the Fe in **25**, underscores the strong-field nature of the nitro ligands. Overall, these efforts provide the first structural insight to a Fe(III)(por)(NO_2)₂ complex.³²¹

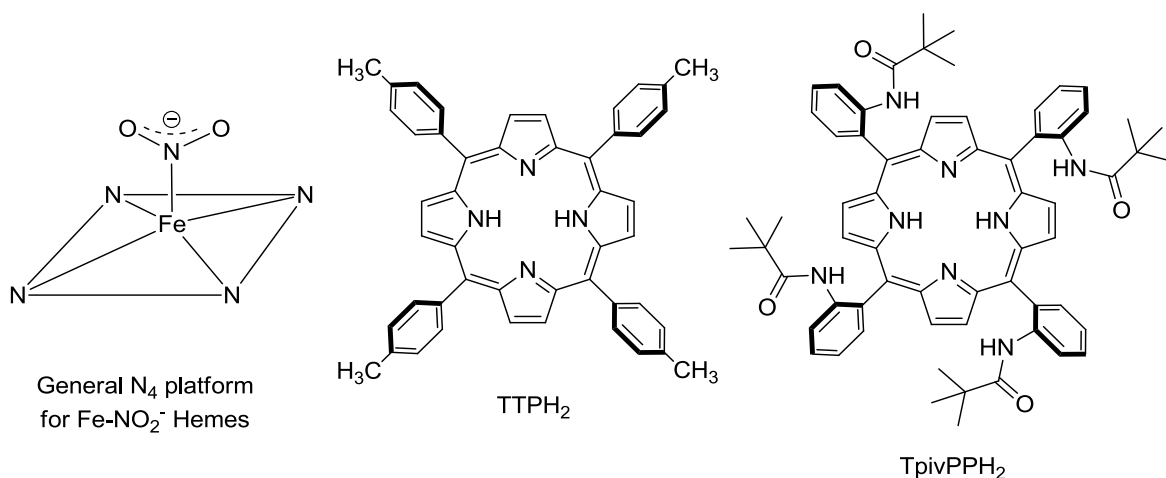


Figure 1.30. The N₄ platform (*left*) represents the general coordination of the FeNO₂ unit in porphyrin-based ligand systems. The porphyrin ligands (*center, right*, H represents dissociable ligand protons) support the Fe(NO₂)_n complexes in [Fe(TTP)(NO₂)], [Fe(TpivPP)(NO₂)₂]⁻ (**25**).

Scheidt and coworkers continued their work with [Fe(NO₂)(L)(TpivPP)], where L = pyridine (Py) (**26**) and imidazole (HIm) (**27**).³²³ The synthesis of these compounds was accomplished by displacement of the exposed NO₂⁻ ligand from **25** with excess Py or HIm in chlorobenzene. These Fe(III) complexes were interrogated similarly to **25** and showed ν_{NO} at 1390/1341 cm⁻¹ for **26**, and 1341/1303 cm⁻¹ for **27**. These values are comparable to **25** and in the appropriate range for an N-bound species.⁷⁷ X-ray crystallographic data confirmed the 6C mononitro complexes with resulting Fe-NO₂ bond lengths that are slightly contracted compared to **25**, with lengths of 1.960 and 1.949 Å for **26** and **27**, respectively. This decrease is due to the weaker π -accepting nature of the neutral N-donors with respect to NO₂⁻, and is further indicated by the longer Fe-N bonds (Fe-Py: 2.093 Å; Fe-HIm: 2.037). The shorter Fe-NO₂ bond lengths exemplify the competition for π -backdonation when two NO₂⁻ ligands compete for the filled metal d π orbital and are thus less effective in π -bonding than in **26** and **27**.³²³

An important bonding feature of the Fe(III)-NO₂⁻ species presents itself when looking at the EPR data obtained for **25**, **26**, and **27** (Table 1.7).^{321,323} The *g*-values for these three species are very similar: *g_z* = 2.67, *g_y* = 2.49, and *g_x* = 1.57; *g_z* = 2.98, *g_y* = 2.37, and *g_x* = 1.35; and *g_z* = 2.87, *g_y* = 2.34, and *g_x* = 1.56 for **25**, **26** and **27**, respectively. The overall spread of these *g*-values indicate a LS *S* = 1/2 system with relatively high-symmetry, i.e. an N₆ octahedral coordination sphere. An important feature is the orbital mixing coefficient, that represents the degree of delocalization of the unpaired electron (*a* = *d_{yz}*, *b* = *d_{yz}*, and *c* = *d_{xy}*). The value of *a*² ranges between 0.90-0.93 for **25-27** indicating that the *d_{yz}* orbital is occupied (> 90%) by the unpaired electron. The high percent localization of the unpaired electron is attributed to the NO₂⁻ ligand. For instance, this value is higher than other LS Fe(III) complexes with two strong-field axial ligands and highlights the significant M→L π-accepting ability of the N-bound NO₂⁻ ligand. Effective π-backdonation requires an occupied *d*-orbital to be perpendicular to the NO₂⁻ plane, furthermore, the known π-donor ability of the HIm and Py ligands of **26** and **27** are maximized if oriented 90° to the NO₂⁻ plane, close to what is observed in the solid-state. These results underscore the effective π-accepting ability of the NO₂⁻ ligand. This interaction orients the *d*-orbitals to optimize the π-overlap between the two axial ligands, one accepting and one donating; importantly, the electronic structure of the Fe-NO₂ unit is dominated by this interaction.

Table 1.6. Electrochemical and Spectroscopic Data of Nitro Heme Systems

Molecule	$E_{1/2}^a$ (V)	$\nu_{\text{NO}_2}^e$ (cm^{-1})	Fe-NO ₂ /Fe-N _{ax} (Å)	N-O _{NO₂} ^h (Å)	Ref
Fe(III)(NO₂)_n					
[Fe(TPivPP)(NO ₂) ₂] ⁻ (25)	-1.20 ^b	1315/1351	2.001 ^f /1.970 ^g	1.298	321,324
[Fe(NO ₂)(Py)(TpivPP)] (26)	-	1341/1390	1.960/2.093	1.233	323
[Fe(NO ₂)(HIm)(TpivPP)] (27)	-	1310/1341	1.949/2.037	1.191	323
[Fe(TpivPP)(SC ₆ HF ₄)(NO ₂)] (28)	-	1352	1.990/2.277	1.228	325
[Fe(TpivPP)(NO)(NO ₂)]	0.30 ^b	-	2.000/1.668	1.226	324,326
[Fe(TTP)(DMS)(NO ₂)] (29)	-	1300/1401 ⁱ	-	-	327
[Fe(TPP)(DMS)(NO ₂)] (30)	-	1302/1399 ⁱ	-	-	327
[Fe(TPP)(NO)(NO ₂)] (31)	-	1464/1303 ^j	-	-	328,329
[Fe(TMPyP)(NO ₂) ₂] ²⁺	-0.29 ^c	-	-	-	330
[Fe(TPP)(NO ₂) ₂]	-0.45 ^d	-	-	-	331
Fe(II)(NO₂)					
[Fe(TpivPP)(NO ₂) ⁻] (32)	-0.92 ^b	-	1.849	1.243	324,332
[Fe(TpivPP)(NO)(NO ₂) ⁻] (33)	0.30 ^b	1305/1346 ^k	2.060/1.840 ^k	1.231 ^k	324,333
[Fe(TpivPP)(CO)(NO ₂) ⁻] (34)	-	1353/1383	2.006/1.782	1.250	334
[Fe(TpivPP)(Py)(NO ₂) ⁻] (35)	-	1289/1354	1.951/2.032	1.257	335
[Fe(TpivPP)(PMS)(NO ₂) ⁻] (36)	-	1295/1349	1.937/2.380	1.242	335

^a $E_{1/2}$ values for the Fe(III)/(II) couple. ^b MeCN vs. SCE. ^c PBS buffered H₂O vs. SCE (pH 7.4). ^d DMF vs. SCE. ^e KBr, RT unless otherwise noted. ^f Nitrite located in picket-fence pocket. ^g Nitrite located on open-face of porphyrin. ^h Average N-O bond. ⁱ Data obtained at 77 K on optically transparent surface of KBr or CaF₂. ^j After irradiation (330 - 500 nm) at 11 K. ^k Two crystalline forms of **33** were obtained, the one in which the NO and NO₂⁻ planes are parallel are shown in table. Values of ν_{NO_2} of 1310 and 1380 cm^{-1} , Fe-NO₂/Fe-N_{ax} = 2.086/1.793 Å, and N-O_{NO₂} = 1.246 Å were obtained for the perpendicular form (see text).

In order to probe the effects of an axial thiolate ligand on **25**, Scheidt and coworkers synthesized $[\text{K}(\text{18C6})(\text{H}_2\text{O})][\text{Fe}(\text{TpivPP})(\text{NO}_2)(\text{SC}_6\text{HF}_4)]$ (**28**) by displacement of the exposed NO_2^- with 2,3,5,6-Tetrafluorothiophenolate (SC_6HF_4).³³⁶ The FTIR data is consistent with an N-bound NO_2^- ligand, with ν_{NO} : 1352 cm^{-1} .⁷⁷ Subsequent EPR studies confirm a LS ($S = 1/2$) rhombic Fe(III) for **28**, consistent with the previously discussed Fe(III) mixed L/ NO_2^- complexes. Structurally, the Fe- NO_2 distance is 1.990 \AA , where the proximal Fe-S thiolate bond length is 2.277 \AA , relatively short as compared to other LS Fe(III)-thiolates having an average Fe-S distance of 2.332 \AA .³³⁶ The ArS^- bond is mutually perpendicular to the NO_2^- plane as is expected for the optimal π -overlap for the donating and accepting ligands, respectively. Interestingly, the orientation of this ArS^- bond is in between two Fe- N_{por} bonds, thus if the N_4 plane is thought of as a square, the ArS^- bond would intersect one face of the square. This is counter to what is normally observed in LS Fe(III)(por)(RS^-) systems, in which the RS^- bond would intersect a corner of the N_4 square plane, i.e. directly beneath an N_{por} (Fig. 1.31).^{337,338} This observation is not a manifestation of sterics, but rather of the relative orientation of the NO_2^- ligand, a phenomenon consistent with compounds **26**, **27**, and **28**.

Compounds **25-28** were also characterized by Mössbauer (MB) spectroscopy (Table 1.7).^{321,323,336} Collectively, the compounds exhibit a narrow range of $\delta = 0.22 - 0.25\text{ mm/s}$ and $\Delta E_{\text{q}} = 2.1 - 2.2\text{ mm/s}$ under zero-field and at 4.2 K . These values correspond to LS Fe(III) for complexes **25-28**. In an applied parallel magnetic field of 8 T , the principal magnetic contribution arises from the LS $[\text{Fe}(\text{III})(\text{TpivPP})(\text{NO}_2)(\text{L})]$ species, with a minor ($\sim 10\%$) contribution from a HS Fe(III) impurity. Using the experimental EPR parameters, an appropriate theoretical fit was determined and confirmed the experimental results. Interestingly, in order to obtain an appropriate fit, the rhombic field axis had to be rotated by 45° about the z-axis, taken as

the porphyrin plane normal. This rotates the $d\pi$ orbitals (d_{yz} and d_{xz}) by $\sim 45^\circ$ such that the plane of these orbitals are now intersecting the face of the N4 square plane, precisely as is seen in the plane of NO_2^- and the axial ligands (Fig. 1.31). Though atypical for porphyrin analysis, all structurally characterized nitro-porphyrins have the NO_2^- plane rotated between $32\text{--}44^\circ$ from the closest M-N_{por} vector.⁶⁴ This phenomenon can be rationalized by the strong π -accepting ability of the NO_2^- ligand that effectively reorients the d_{yz} orbital and dictates the position of the axial ligands for maximal π -donation.³²³

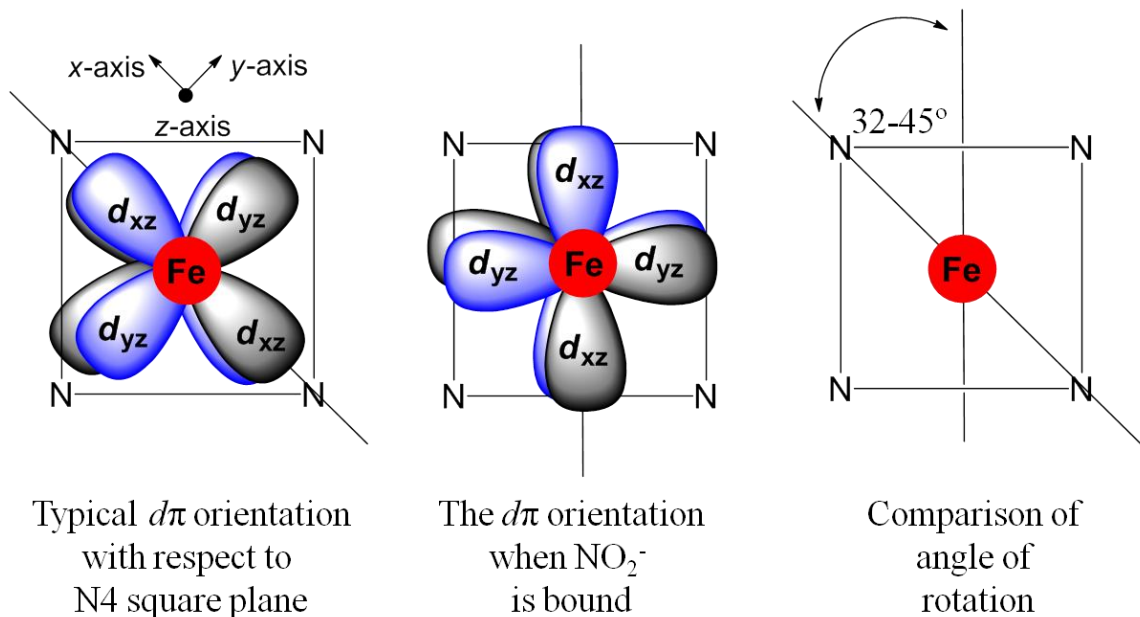


Figure 1.31. Top-down view of an Fe-porphyrin basal plane (looking down the z-axis). The orbital shown represents a $d\pi$ orbital (d_{xz} , d_{yz}) that is above and below the N4 plane. These orbitals are involved in the π -interactions of axial ligands. The typical orientation of these orbitals is shown on the left, however, when NO_2^- is bound, the orbitals rotate $32\text{--}45^\circ$ about the z-axis. This orientation optimizes overlap with the NO_2^- ligand and the other axial ligand for π -interaction.

The binding of NO_2^- through its N atom allows for the most efficient π -overlap, however, the energy difference between the η^1 N-bound and the η^1 O-bound isomer is minimal. In order to experimentally demonstrate this isomerization, Ford and coworkers sought to generate each isomer with $[\text{Fe}(\text{TTP})]$ and $[\text{Fe}(\text{TPP})]$.³²⁷ As previously discussed, isolation of NO_2^- compounds with open-faced Fe-porphyrins is difficult. In order to circumvent this problem, Ford and coworkers sublimed $[\text{Fe}(\text{II})(\text{por})(\text{Py})_2]$ onto a 77 K optically transparent surface of KBr or CaF_2 . This forms a porous porphyrin layer that can then be reacted with gaseous species. In this study, the formation of O-bound $[\text{Fe}(\text{III})(\text{TTP})(\text{ONO})]$ and $[\text{Fe}(\text{III})(\text{TPP})(\text{ONO})]$ species occurs through reaction of the sublimed $[\text{Fe}(\text{II})(\text{por})]$ with NO_2^* to give the nitrito complexes. These 5C species are the starting point for this study and the vibrational analysis clearly shows ν_{NO} of $\sim 1528 \text{ cm}^{-1}$ and $\nu_{\text{NO}} \sim 901 \text{ cm}^{-1}$, with δ_{ONO} of $\sim 750 \text{ cm}^{-1}$, that are typical for an O-bound nitrito species.⁷⁷ Upon gaseous addition of dimethyl sulfide (DMS) or tetrahydrothiophene (THT), a 6C complex is formed. Upon warming to 170 K, a distinct shift occurs in the FTIR to ν_{NO} of $\sim 1403 \text{ cm}^{-1}$ and $\nu_{\text{NO}} \sim 1302 \text{ cm}^{-1}$, with δ_{ONO} of $\sim 809 \text{ cm}^{-1}$. This change in the vibrational spectrum upon addition of DMS and warming corresponds to isomerization from the nitrito complex to the nitro complex, affording $[\text{Fe}(\text{III})(\text{TTP})(\text{NO}_2)(\text{DMS})]$ (**29**) and $[\text{Fe}(\text{III})(\text{TPP})(\text{NO}_2)(\text{DMS})]$ (**30**). Notably, the reaction is completely reversible, where applied vacuum and elevated temperature affords the 5C O-bound isomers.^{328,339-341} Additional studies by the Novozhilova, Coppens, Bagley, and Richter-Addo with the mixed NO_x porphyrin $[\text{Fe}(\text{TPP})(\text{NO})(\text{NO}_2)]$ (**31**) demonstrated the dynamic isomerization of both NO_2^- and NO in this system.³²⁹ The linkage isomers of **31** are promoted by irradiation (330 - 500 nm) at low-T (11 K) in which FTIR analysis indicates nitro-to-nitrito isomerization and may indicate a nitrosyl-to-isonitrosyl, both referring to the N-bound-to-O-bound isomerization of NO and NO_2^- , respectively. With respect

to the nitro-to-nitrito isomers, clear shifts in ν_{NO} 1464, 1303 cm^{-1} , and δ_{ONO} 806 cm^{-1} give way to new bands at 1510 and 935 cm^{-1} consistent with the proposed isomerization that compliment similar experiments by Ford and coworkers.³²⁸ Scheidt and colleagues also investigated the structural parameters of **31** and observed severe disorder in the crystallographic data that obscured definitive analysis.³²⁶ However, the complex $[\text{Fe}(\text{TpivPP})(\text{NO})(\text{NO}_2)]$ was prepared and structurally characterized. This compound showed an axial Fe-NO₂ bond distance of 2.000 Å, and a short Fe-NO distance of 1.668 Å for the $\{\text{FeNO}\}^6$ species (Table 1.6). The LS nature of Fe(III)-NO₂ complexes is again exhibited here in the case of an antiferromagnetically coupled LS $S = 1/2$ Fe(III) center with the $S = 1/2$ NO to give an overall spin of $S = 0$ (Table 1.7). Comparison of the Fe-N distances illustrates that the NO ligand does not impart a strong trans-influence on NO₂⁻, consistent with the dominant bonding of the NO₂⁻ ligand. Moreover, the Fe-NO₂ bond only changes by ~0.06 Å with a variety of different axial ligands (Table 1.6), highlighting little effect of a trans-influence on the NO₂⁻ ligand.

1.10.2 Fe(II)(NO₂) Heme Models

The majority of $[\text{Fe}(\text{por})(\text{NO}_2)_n]$ model complexes are Fe(III), likely due to the inherent reactivity of the Fe(II) counterparts. The first synthesis and structural characterization of a Fe(II)-NO₂ porphyrin complex was accomplished by Scheidt and coworkers. $[[\text{K}(222)]\text{Fe}(\text{TpivPP})(\text{NO}_2)]$ (**32**) was prepared by reduction of $[\text{Fe}(\text{TpivPP})(\text{Tf})]$ with Zn amalgam, followed by addition of ~30 equiv of KNO₂ solubilized by the azacrown ether Kryptofix 222 (4,7,13,16,21,24-Hexaoxa-1,10-diazabicyclo[8.8.8]hexacosane).³³² Despite the excess of KNO₂ added, only the mono-nitro species was isolated. Although no vibrational data was reported, structural characterization shows the 5C complex with NO₂⁻ in the pocket of the

picket fence porphyrin. The short Fe-N_{por} of 1.974 Å and the slight displacement of the Fe from the porphyrin plane of 0.18 Å are indicative of a LS $S = 0$ system. The Fe-NO₂ bond distance is exceptionally short, 1.849 Å, as compared to the Fe(III)-NO₂ porphyrins that range from 1.949 to 2.001 Å (Table 1.6). The NO₂⁻ plane is ~40° rotated toward the face of the N4 square plane, as is observed in Fe(III)-NO₂ complexes. Mössbauer spectroscopy (zero-field, 4.2 K) was utilized in order to obtain a rationale for the unique structural parameters observed. The experimental $\delta = 0.41$ mm/s and $\Delta E_q = 2.28$ mm/s. In an applied field of 8 T, the compound exhibits magnetic splitting typical for an $S = 0$ diamagnetic complex, with a typical δ for LS Fe(II)(por) complexes. However, the large $\Delta E_q = 2.28$ is very unusual for LS Fe(II) hemes, that are normally observed as having $\Delta E_q < 1.5$. For comparison, the 6C [Fe(II)(por)(NO₂)(L)] complexes of Table 1.7 all have ΔE_q close to 1.0, with the exception of **34**. However, complex **32** has ΔE_q more closely resembling that of the 6C [Fe(III)(por)(NO₂)(L)] where ΔE_q ranges from 2.1 - 2.2 mm/s. Such large ΔE_q of the Fe(III) complexes speaks to the relative asymmetry of charge around the Fe nucleus. As observed in the EPR of Fe(III)(por)(NO₂) complexes, there is significant rhombicity in the t_{2g} manifold, namely those capable of $d\pi$ donation (d_{xz} and d_{yz}). Similarly to the Fe(III)(por)NO₂ complexes, the nuclear charge asymmetry also manifests in the Fe(II) complexes, however, in this case it results as a large energy differences in the d_{xz} and d_{yz} . This phenomenon is also observed in [Fe(II)(por)(O₂)] complexes and is thought to arise from asymmetric binding of O₂, which distorts the charge symmetry and imparts significant rhombicity to the nucleus.³⁴² The interesting electronic effects imparted by the NO₂⁻ ligand, may help to explain the lack of structurally characterized Fe(II)(NO₂)₂ species known for porphyrin model complexes, while only 6C Fe(III)(NO₂) have been structurally characterized.

Table 1.7. Spin-state and Spectroscopic Data of Nitro Heme Systems

Molecule	Spin-state	<i>g</i> -values ^a	δ (mm/s)	ΔE_q (mm/s)	Ref
Fe(III)(NO₂)_n					
[Fe(TPivPP)(NO ₂) ₂] ⁻ (25)	LS, <i>S</i> = 1/2	2.67, 2.49, 1.57	0.25 ^b	2.1 ^b	321,323
[Fe(NO ₂)(Py)(TPivPP)] (26)	LS, <i>S</i> = 1/2	2.98, 2.37, 1.35	0.25 ^b	2.1 ^b	323
[Fe(NO ₂)(HIm)(TPivPP)] (27)	LS, <i>S</i> = 1/2	2.87, 2.34, 1.56	-	-	323
[Fe(TpivPP)(SC ₆ H ₄)(NO ₂)] ⁻ (28)	LS, <i>S</i> = 1/2	2.40, 2.30, 1.91	0.22 ^c	2.12 ^c	325
[Fe(TpivPP)(NO)(NO ₂)]	LS, <i>S</i> = 0 ^d	-	0.01 ^c	1.48 ^c	326
[Fe(TPP)(NO)(NO ₂)] (31)	-	-	0.02 ^c	1.37 ^c	326
Fe(II)(NO₂)					
[Fe(TpivPP)(NO ₂)] ⁻ (32)	LS, <i>S</i> = 0	-	0.41 ^b	2.28 ^b	332
[Fe(TpivPP)(NO)(NO ₂)] ⁻ (33)	LS, <i>S</i> = 0	-	0.35 ^{b,e}	1.20 ^{b,e}	333
[Fe(TpivPP)(CO)(NO ₂)] ⁻ (34)	LS, <i>S</i> = 0	-	0.78 ^c	0.32 ^c	334
[Fe(TpivPP)(Py)(NO ₂)] ⁻ (35)	LS, <i>S</i> = 0	-	0.41 ^b	0.93 ^b	335
[Fe(TpivPP)(PMS)(NO ₂)] ⁻ (36)	LS, <i>S</i> = 0	-	0.42 ^b	1.18 ^b	335

^aIn order of *g_z*, *g_y*, and *g_x*, data collected at 5 K. ^bZero-field, 4.2 K, ^cZero-field, 293-295 K

^dSpin-state arises from anti-ferromagnetic coupling of *S* = 1/2 Fe(III) to *S* = 1/2 NO. ^eValues for parallel complex shown in table. Values of 1.78 mm/s and 0.22 mm/s for ΔE_q and δ for the perpendicular compound, respectively, see text.

Scheidt and colleagues followed up their seminal study of **32** by addressing the variability of the π -interaction in 6C coordinate [Fe(II)(TpivPP)(NO₂)(L)]⁻.³³³⁻³³⁵ In this work, the sixth ligand (L) varied from NO (**33**), CO (**34**), Py (**35**), and PMS (**36**), (PMS = pentamethylenesulfide). FTIR data for compounds **33-36** show the ν_{NO} bands are all within the N-bound nitro range of 1383-1280 cm⁻¹ (Table 1.6). The MB parameters of the 6C compounds

34-36 are consistent with LS 6C Fe(II) complexes (Table 1.7). The structural parameters for **34** show an Fe-NO₂ bond length of 2.008 Å. The Fe-NO₂ bond of **34** is elongated by 0.159 Å and the Fe-N_{por} distances expand by ~0.025 Å compared to **32**. These stark changes in ΔE_q and Fe-NO₂ bond length between **32** and **34** demonstrate the variable π -bonding nature of the NO₂⁻ ligand, and infer that NO₂⁻ can modulate the relative strength of its π -bonding profile. This effect in **34-36** is reflected in the Fe-N_{ax} bond distances of 1.785, 2.032, and 2.380 Å, which correlates to the relative strength of the π -acceptors CO >>> Py > PMS, respectively.³³³⁻³³⁵

The mixed axial ligated species [Fe(TpivPP)(NO₂)(NO)]⁻ (**33**) is a case where both ligands can effectively modulate their respective π -bonding profiles. The Fe-N-O angle for the NO ligand can be close to linear, similar to CO, or more bent, similar to a Fe-N-O angle of a bound NO₂⁻ ligand. This angle is largely dependent on oxidation state of the FeNO unit and plays a significant role in the M→L π bonding. Two forms of **33** were obtained through different synthetic routes. One form has the planes of the NO₂⁻ ligand and the NO ligand orthogonal to one another, termed the "perpendicular form". The "parallel form" has these planes in a near parallel orientation. When the axial NO₂⁻ and NO ligands are in the perpendicular form, it allows for maximum sharing of the d_{xz} and d_{yz} orbitals. In this form, the Fe-N-O angle for the nitrosyl ligand is 137.4°. However, in the parallel form, the ligands essentially occupy the same plane, and thus compete directly for the d_{xz} and d_{yz} orbitals. This seemingly minor geometric change has a prominent effect on the MB and FTIR spectroscopy, even though the Fe-N-O angle remains the same. In the perpendicular form the ν_{NO} for the NO₂⁻ is 1380/1310 cm⁻¹ whereas in the parallel form the nitro ligand ν_{NO} is 1346/1305 cm⁻¹. Comparatively, the ν_{NO} for the NO ligand is 1616 and 1668 cm⁻¹ for the perpendicular and parallel forms, respectively. Both the Fe-N-O nitrosyl angle and the stretching frequency range are consistent with the {FeNO}⁷ notation.

The strong trans-influence of NO is imparted to the NO_2^- ligand as is observed in the significant lengthening of the Fe- NO_2 bond by 0.224 Å (average of two forms) from **32** to **33**. The Fe-NO distance of **33** is 1.802, slightly elongated for 6C [Fe(II)(por)(NO)(L)] species that are typically in the 1.73 range.^{54,64} This elongation is due to the NO_2^- ligand, and highlights the strong-field nature of these two NO_x species. The electronic differences in the geometric isomers of **33** show that in perpendicular species $\delta = 0.22$ mm/s and $\Delta E_q = 1.78$ mm/s, as compared to the parallel isomer where $\delta = 0.35$ mm/s and $\Delta E_q = 1.2$ mm/s (zero-field, 4.2 K). As is observed in the [Fe(III)(por)(NO_2)(L)] complexes, similar rhombicity is expected when the ligands occupy perpendicular planes, this maximizes the π -interactions and therefore modulates the $d\pi$ orbitals significantly and imparts the electronic rhombicity. However, when the axial ligands occupy the same plane, the energy separation between the t_{2g} orbitals is lessened, and the overall rhombicity is diminished. Consistent with other Fe(por) NO_2 complexes, the relative plane still intersects the face of the N4 square plane. This suggests that both NO_x axial ligands play a prominent role in defining the orientation of the $d\pi$ -orbitals. This analysis was corroborated by comparing the MB parameters for **33** (parallel) with [Fe(TPP)(NO)] $\delta = 0.35$ mm/s and $\Delta E_q = 1.24$ mm/s (zero-field, 4.2 K). The stark similarity of these MB parameters strongly suggests that NO is dominant in controlling the electronic structure of the [Fe(TpivPP)(NO_2)(NO)]⁻ when the ligands occupy parallel planes.³³³

1.10.3 Theory Fe(II/III)(NO_2) Heme Systems

Computational studies of heme complexes is essential to understanding the electronic structure and relative energies of frontier MOs involved in catalysis. Due to limitations in computational power, these studies must significantly truncate the system at hand. For instance,

to study the mechanism of NO_2^- reduction at a heme site would often require truncating the porphyrin (P) core and axial ligand(s). Moreover, these calculations are often performed in the gas phase. This approach does not take into account the important effects of the surrounding protein such as electrostatic potential, H-bonding, secondary-sphere interactions, or conformational changes. Despite the restrictions, computational modeling can offer the dominant electronic structure of the active site metal-substrate interaction and can contribute to mechanistic understanding.^{78,343,344}

The application of DFT to mono- and bis- NO_2 Fe(II/III)-porphyrin systems has been reported.^{305,345} In these studies, a truncated porphyrin and TpivPP (Fig. 1.30) were used in the presence or absence of an axial N-donor such as Py or His. The initial report by Ghosh and Conradie, using DFT(PW91/TZP), defines the bonding in $[\text{Fe(II/III)(P)(NO}_2)]$ complexes as a σ -donor interaction between the HOMO of NO_2^- and the d_{z^2} orbital of Fe. Additionally, the $[\text{Fe(II/III)(P)(NO}_2)]$ complexes exhibit a π -acceptor interaction into the NO_2^- LUMO from $d\pi$ orbitals of Fe; corresponding to the HOMO and SOMO of Fe(II) and Fe(III) porphyrin species, respectively. The HOMO of $[\text{Fe(II)(P)NO}_2]^-$ has mostly Fe character (77%) with less than 10% of electron density on NO_2^- , and the remaining density distributed on the porphyrin ring. Comparably, the $[\text{Fe(III)(P)NO}_2]$ HOMO is very similar, however, the SOMO show significantly less density on Fe (43%) with 9% on the NO_2^- ligand and an increased contribution from the porphyrin MOs. Structural trends showed a slight lengthening of the Fe- NO_2 bond when going from 5C to 6C complexes containing a *trans* axial ligand. The sixth ligand, pyridine, appears to lengthen the Fe- NO_2 bond by approximately 0.01 Å computationally. The experimental comparison is a lengthening of 0.02 for $[\text{Fe(TpivPP)(NO}_2)]^-$ (**32**) and $[\text{Fe(TpivPP)(Py)(NO}_2)]^-$ (**35**).³³⁵ Additional values from the computational results reveal the Fe- $\text{NO}_2 = 1.885$ Å (expt.

1.849 Å) and N-O = 1.254 Å (expt. 1.243 Å) for **32**; Fe-NO₂ = 2.001 Å (expt. 1.951 Å) and N-O = 1.243 Å (expt. 1.233 Å) for **35**. Overall, the geometry optimized metric parameters agree well with experimental values. However, the calculations showed no preferred orientation of the NO₂⁻ plane with respect to the N₄ square plane of the porphyrin as observed in the solid-state structures of all the porphyrin models. With respect to the electronic structure, all complexes modeled computationally exhibited LS ground-states. The theoretical Fe(III)por complexes displayed very high adiabatic electron affinities of ~2.50 eV for both the 5C and 6C complexes. This value compares to typical values for metalloporphyrins of 1-1.5 eV, and demonstrates the high electron deficiency in these [Fe(III)(por)(NO₂)] complexes. This electronic structure explains the tendency of [Fe(III)(NO₂)] to participate in OAT reactions, (*vide infra*).³⁴⁵

Another DFT study by Ghosh and Conradie aims to rationalize the formation and release of N₂O₃ as the pro-vasodilator in the heme-mediated reduction of NO₂⁻ to NO through an N₂O₃ intermediate species. Computations with the OLYP functional (STO-TZP) reveal high electron affinities of HbFe(III)-NO₂ (2.0 eV) to support its reaction with NO and afford N₂O₃. This was proposed to occur through isomerization to the O-bound nitrito (~7 kcal mol⁻¹ higher energy than the N-bound) and potential non-innocence of this isomer [Fe(III)(ONO)] ↔ [Fe(II)ONO•] as reasoning behind its possible reaction with NO•.³⁰⁵ Experimentally, the O-bound isomer has been observed through X-ray diffraction of Fe(III)Mb and Fe(III)Hb when NO₂⁻ was added to the holo proteins.³⁴⁶ However, crystallographic analysis after addition of a preformed N-bound [Fe(NO₂)(chlorin)] to the apo-Mb protein showed that the N-bound isomer remained (Fig. 1.33).³⁴⁷ These results imply that the secondary-sphere interactions of the Mb His residue can orient the incoming NO₂⁻ ligand to bind through its O-atom. This observation is in good agreement with the relatively low isomerization energy calculated as 5-7 kcal mol⁻¹ between the

O- and N-bound states.^{74,305,348} Additionally, EPR and DFT studies suggest that the two isomers are readily interconvertible in solution.³⁴⁸ These results offer the Mb-ONO complex as a possible intermediate to the formation N_2O_3 from NO_2^- , NO, and Hb, an important reaction that will be discussed in detail below.

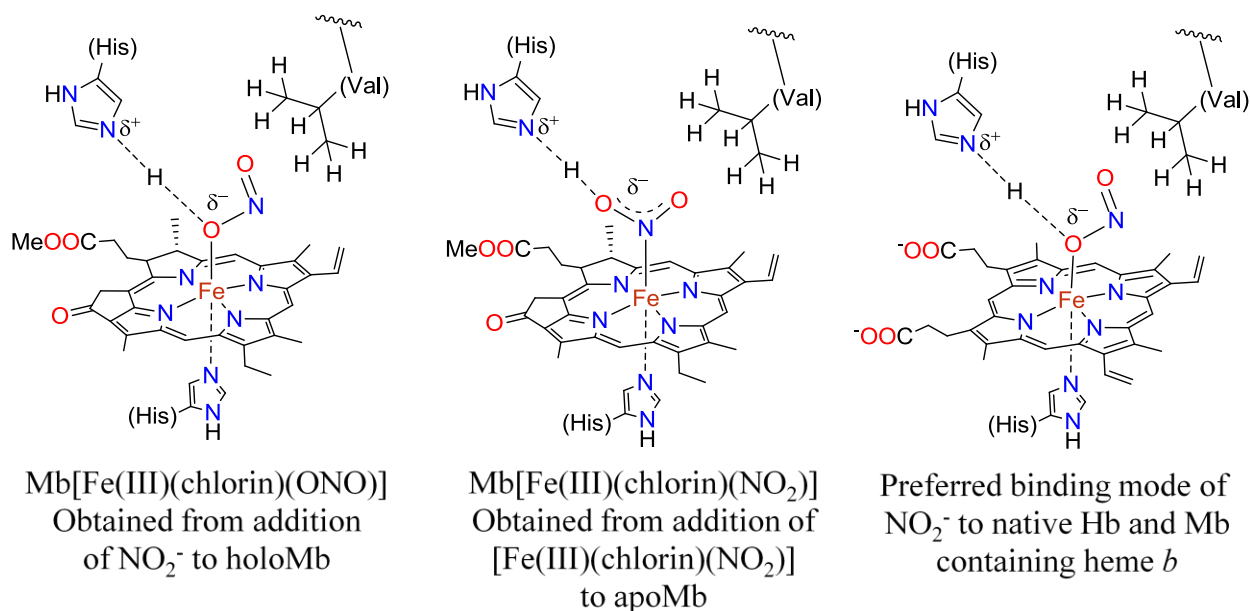


Figure 1.33. Active site representation of the Mb[Fe(III)(chlorin)(ONO)] and Mb[Fe(III)(chlorin)(NO_2)] highlighting the O-bound and N-bound isomers that are dependent on preparation of the protein. The native Hb and Mb prefer to bind NO_2^- in the O-bound form coordinated to the Fe center housed in the heme *b*.

Quantum mechanical/molecular modeling of $cd_1\text{NiR}$ has also been investigated by utilizing crystal structure data from several solved structures of $cd_1\text{NiR}$ in the oxidized state.²⁴⁰ Ranghino and coworkers report the importance of the H-bonding network of the 2 His and 1 Tyr residue as critical for both substrate binding/activation and product dissociation.²⁴⁰ In other computational efforts, Silaghi-Dumitrescu used several theoretical approaches to determine if the

O-bound nitrito isomer is a viable species in the *cd*₁NiR enzyme.⁷⁴ This study used a truncated *d*₁ heme as the porphyrin platform. These results suggest that the N-isomer is again more favorable by 6.0 kcal mol⁻¹ for Fe(II) and 4.5 kcal mol⁻¹ for the Fe(III) complex. Calculated bond lengths for the complex are Fe(II)-NO₂ = 1.96 Å and N-O = 1.25 Å, which agree well with those observed in the enzyme crystal structure of 2.0 and 1.2 Å for the *cd*₁NiR enzyme.¹⁹³ Although this work calculates the Fe(II)-ONO species as a more efficient intermediate than the N-bound isomer, the N-bound isomer is the only one observed in the solid-state of NiR proteins. Moreover, experimental work suggests that *cd*₁NiR forms and releases NO from a metal bound {FeNO}⁷ species, suggestive of the N-bound mechanism (Fig. 1.26). Importantly though, this study may have relevance to the Hb- or Mb-dependent reduction to NO₂⁻.^{76,347,348}

Calculations on the catalytic mechanism of *cc*NiR have been investigated by Einsle and coworkers utilizing the BP86 functional with SV(P) basis set for ligands and the TZV(P) basis set for the Fe center.⁷⁸ In this case, the Fe(por) theoretical model contained a proximal NH₃ to represent the axial Lys residue that coordinates the active site heme.⁷⁸ Based on crystallographic data of proteins and model complexes, the binding of NO₂⁻ was assumed to be N-bound. In the oxidized state, the [Fe(III)(por)(NH₃)(NO₂)] complex is LS *S* = 1/2, and consistent with model complexes.⁶⁴ Additional calculations of the HS *S* = 5/2 state, as well as the O-bound isomer were greater than 10 kcal mol⁻¹ higher in energy. The Fe(III)-NO₂ bond lengths were calculated to be 1.922 Å which is in good agreement with the 1.9 Å Fe(III)-NO₂ length obtained from X-ray data of the oxidized enzyme.⁷⁸ The reduced form of the enzyme could not be crystallized with substrate due to the rapid turnover; however, calculated Fe-NO₂ distances for [Fe(II)(por)(NH₃)(NO₂)]⁻ are 1.932 Å as compared to [Fe(TpivPP)(NO₂)(Py)]⁻ (**35**) with Fe-NO₂

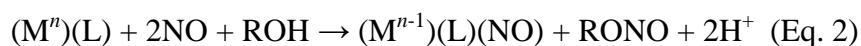
= 1.951 Å.³³⁵ The LS state was also favored by about 8 kcal mol⁻¹ to that of the HS Fe(II) (*S* = 2) state.

Einsle experimentally observed a low affinity of NO₂⁻ for the oxidized form of the enzyme. If considering only an electrostatic interaction, then this observation is counterintuitive. However, the pronounced M→L π-backbonding is enhanced at an electron-rich metal, and may explain the low affinity of NO₂⁻ for Fe(III). Thus, the M→L π-backbonding reveals itself, yet again, as a prominent electronic effect in these systems. Moreover, the reactivity of Fe(II)-NO₂ vs. Fe(III)-NO₂ complexes is highly dependent on the oxidation state of Fe. As is observed in NiR enzymes, the Fe(II)-NO₂ analogue reacts with protons to heterolytically cleave an N-O bond to give H₂O, a formal loss of O²⁻. Conversely, the reactivity of Fe(III)-NO₂ is invariably loss of O-atom. Simply, the two bonding electrons of one N-O bond of NO₂⁻ stay with the electron deficient Fe(III) complex to give a Fe(II)-NO unit or, in the case of the enzyme, leave the Fe(II) complex as H₂O to give an Fe(III)-NO unit. The oxidation state dependent reactivity is of relevance to the biological reduction of NO₂⁻ to NO. Although most commonly thought of as heterolytic N-O bond cleavage and loss of H₂O, model complex studies have indicated that [Fe(III)(por)(NO₂)] species can produce NO and possibly HNO from OAT reactions in aqueous conditions.¹³ Thus, the potential for both reactions to occur under physiological conditions warrants further discussion of the reactive pathways in heme models of Fe(II/III)-NO₂ complexes.

1.11 Reactivity of Fe(II/III)(NO₂) Heme Model Complexes

1.11.1 Reductive Nitrosylation

There is significant interest in the formation of NO from NO₂⁻ in biology; however, due to the great potential for NO to be trapped by Hb and Mb alternative pathways have been proposed to explain how NO could potentially escape these traps and continue towards its signaling role. Porphyrin model complexes have provided detailed reactivity patterns of Fe(por)NO_x that may closely parallel biological systems. One experimental observation is that the presence of NO₂⁻ leads to enhanced rates of reductive nitrosylation (Eq. 2).³⁴⁹



This type of reactivity is common for Fe(por) complexes, in which the complex is reduced by one electron and nitrosylated, with concomitant nitrosation (addition of NO⁺) of ROH (can be H₂O, MeOH, etc.) to give RONO and 2H⁺.³⁵⁰ Such pathways have been observed in the heme proteins Hb and Mb, and are also suggested as a possible nitrosation pathway to afford RSNO (*S*-nitrosothiols) and RNNO (*N*-nitrosoamines).³⁵¹⁻³⁵⁶ For instance, the β-chain-Cys nitrosation of Hb to afford Hb-βCys-SNO has been proposed as the active NO carrier for NO₂⁻ reduction in RBCs.³¹⁹ Thus, the biological importance of the reductive nitrosylation reaction is found in the nucleophilic species that is nitrosated by NO⁺ or Fe-NO⁺. For instance, the following nucleophiles and products could be considered as biologically relevant, H₂O to NO₂⁻, RSH to RSNO, and RNH₂ to RNNO. This divergent reactivity points to the importance of an {FeNO}⁶ species as an electrophile in nitrosation reactions and an intermediate in reductive nitrosylations.

The kinetic study of the reductive nitrosylation of metMb, metHb, and Fe(III)CytC at various pH was conducted by Ford and Hoshini.³⁵⁵ In these studies, the heme-proteins displayed a first-order dependence on [OH⁻], and a complex dependence on [NO]. This observation is

consistent with formation of an electrophilic Fe(II)-NO⁺, an {FeNO}⁶ species, that reacts with [OH⁻] at $k = 1.46 \times 10^3$, 3.2×10^2 , and $3.2 \times 10^3 \text{ M}^{-1}\text{s}^{-1}$ for metMb(NO), metHb(NO), and Fe(III)CytC(NO), respectively. As discussed earlier, the {FeNO}⁶ intermediate is critical in the reduction of NO₂⁻ to NO by FeNiR and other Fe proteins with NiR activity. Similar studies were performed by Ford and coworkers using the [Fe(III)(TPPS)]⁻³ and [Fe(III)(TMPy)]⁺⁵ complexes (Fig. 1.23). It was proposed that NO₂⁻ was formed during the aqueous reaction of Fe(III)(por) with NO. Moreover, it was observed that rate of reductive nitrosylation was enhanced, thus implicating NO₂⁻ is a catalyst for the reaction.³⁵⁷ Mechanistically, this reaction may occur in two ways. One proposal is an outer-sphere mechanism involving the reduction of the {FeNO}⁶ by NO₂⁻ to give the reductive nitrosylation product, {FeNO}⁷, and NO₂•. In the presence of excess NO•, the radical coupling with NO₂• to give N₂O₃ is favored ($\Delta G_{\text{rxn}} = -23 \text{ kJ mol}^{-1}$).^{253,306,307,349} Subsequent hydrolysis of N₂O₃ provides 2 NO₂⁻ and 2 H⁺ thus regenerating the NO₂⁻ catalyst. This proposal is reasonable, although there are some potential drawbacks. One of which is that NO₂⁻ is a poor reducing agent, having a $E^\circ = +1.04 \text{ V vs. NHE}$.⁷¹ Furthermore, Koppenol readily determined that the reaction shown in Eq. 3 of is unfavorable by 88 kJ mol⁻¹.²⁵³ Thus, given the comparable redox potentials of the {FeNO}^{6/7} redox couple for [Fe(III)(TPPS)(NO)]²⁻ (0.591 V vs. NHE) and HbFe(III)NO (~0.5 V vs NHE) an alternative mechanism is more likely.

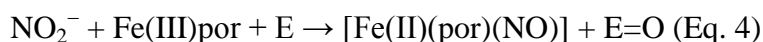


A second mechanistic proposal, in which nucleophilic attack of NO₂⁻ on the {FeNO}⁶ complex leads to the formation of N₂O₃, was made by Ford and coworkers, and further investigated by van Eldik and Jee.³⁰⁹ This mechanistic proposal is supported by the observed dependence of the rate of reductive nitrosylation on the overall charge of the porphyrin. Accordingly, van Eldik compared the observed rate for [Fe(III)por]⁸⁺, [Fe(III)por]⁴⁺,

$[\text{Fe(III)por}]^{4-}$, and $[\text{Fe(III)por}]^{8-}$ of various substituted porphyrins. As expected, the rate of reductive nitrosylation is highest for the most positively charged por species (electron withdrawing) and lowest for the negatively charged species. The electron withdrawing porphyrins increase the electrophilicity of the $\{\text{FeNO}\}^6$ nitrosyl, and undergo nucleophilic attack by NO_2^- more readily. As the outer-sphere electron transfer is thermodynamically unfavorable, this proposal may explain the observed trends. Despite considerable experimental efforts, the exact reasoning behind the enhanced reductive nitrosylation reaction is not fully understood. Similarly, the mechanism of NO_2^- reduction and formation of NO by biological heme proteins is also under debate and remains an important area of research.

1.11.2 Oxygen Atom Transfer from Heme Fe(III)(NO₂)

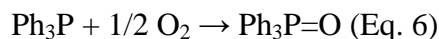
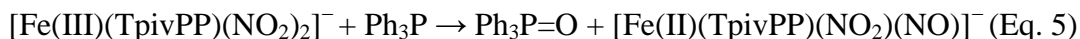
A better understood reaction Fe(III)(por)NO₂ complexes is the OAT reaction. In this reaction the loss of O-atom to a suitable substrate, typically a main group element compound (E), affords oxidized substrate, E=O and the $[\text{Fe(II)(por)(NO)}]$, Eq. 4.



A brief mention of this reactivity was made by Scheidt and coworkers, when they reacted $[\text{Fe(III)(TpivPP)(NO}_2)_2]^-$ (anion of **25**) with 2,3,5,6-tetrafluorothiophenol in chlorobenzene.³³⁶ The result of this reaction was $[\text{Fe(II)(TpivPP)(NO)}]$, however, these authors made no mention of the oxidized S-containing product.³³⁶ Speculation toward formation of sulfenic acid R(S)OH is reasonable, which can react yield RSSR and H₂O.

A complimentary study of OAT from the anion of **25** was performed by Goodwin and coworkers.³²⁴ This report implicates the mixed nitrite/nitrosyl species $[\text{Fe(II)(TpivPP)(NO}_2)(\text{NO})]^-$ (**33**) as an intermediate after OAT. With this intermediate in mind,

the redox chemistry of **33** was studied and from that ΔG values were determined. Based on the known thermodynamics of PPh_3 oxidation, Eq. 6, an overall $\Delta G^\circ_{(E/E=O)}$ can be determined for the OAT to various substrates. This indirect assessment of the driving force of OAT from **25**, allows for an explanation of the OAT activity of **25** with substrates like RSH and Ph_3P , and NO_2^- but not O_2 (Figure 1.32).



From the electrochemical data, the authors report a reversible $E_{1/2}$ for the Fe(III)/(II) couple of **33** at 0.54 V vs. NHE in MeCN. Combined with known values of NO association constants, NO oxidation to NO_2^\bullet , and NO_2^\bullet reduction to NO_2^- , a thermodynamic analysis can be made.³²⁴ Although these results combine gas-phase values and experimental data from various solvents the overall values are expected to be reasonable estimates. From this analysis, the ΔG_{rxn} in Eq. 7 was determined to be $+50 \text{ kJ mol}^{-1}$. However, the $\Delta G^\circ_{(E/E=O)}$ for Eq. 6 is very favorable, at -268 kJ mol^{-1} , thus combining Eq. 6 and 7 affords a net $\Delta G^\circ_{(E/E=O)} = -213 \text{ kJ mol}^{-1}$. Similar analysis can be made for the possible OAT substrates NO_2^- to give NO_3^- and O_2 to give O_3 , which have net $\Delta G^\circ_{(E/E=O)} = -71 \text{ kJ mol}^{-1}$ and $+213 \text{ kJ mol}^{-1}$, respectively.

Scheidt and coworkers report a prolonged stability of $[\text{Fe(TpivPP)(NO}_2)_2]^-$ to O_2 , indicative of the unfavorable $\Delta G^\circ_{(E/E=O)}$.³²¹ Alternatively, the synthesis of $[\text{Fe(TpivPP)(NO}_2)_2]^-$ is performed with excess NO_2^- present, in which the favorable value of -71 kJ mol^{-1} for the OAT to NO_2^- to give NO_3^- (not observed) may indicate a threshold for the predictive nature of this analysis. Counter to this, the open-faced porphyrins like $[\text{Fe(III)(OEP)(Cl)}]^+$ are unstable in the presence of NO_2^- and expected to perform the OAT to give NO_3^- .³²² Taken together, this

thermodynamic analysis is a viable means to determine the potential driving force of OAT from [Fe(III)(por)(NO₂)] complexes and furthermore, highlights the severe difference in reactivity between picket-fence and open-face porphyrins.

One interesting difference in reactivity was demonstrated by Richter-Addo et al., in which they demonstrate the reversible nature of the [Fe(II)(TpivPP)(NO)] to [Fe(III)(TpivPP)(NO₂)] reaction.³⁵⁸ This report was the first to show a reversible nitrosyl-to-nitrite conversion of an {FeNO}⁷ porphyrin. Accordingly, in the presence of O₂ and Py, the nitrosyl species will spontaneously oxidize to the [Fe(III)(TpivPP)(NO₂)] complex. Though, in the presence of an energetically appropriate OAT substrate (Ph₃P) this species can convert back to the [Fe(II)(TpivPP)(NO)]. This reverse reaction does not occur in the OEP system. In fact, the [Fe(OEP)(NO₂)] system has been shown to oxidize O₂ to ozone (O₃), and would convert back to the [Fe(II)(OEP)NO] complex.³⁵⁹ In this context, the [Fe(III)OEP]⁺ system is able to perform OAT to a surprising number of substrates.

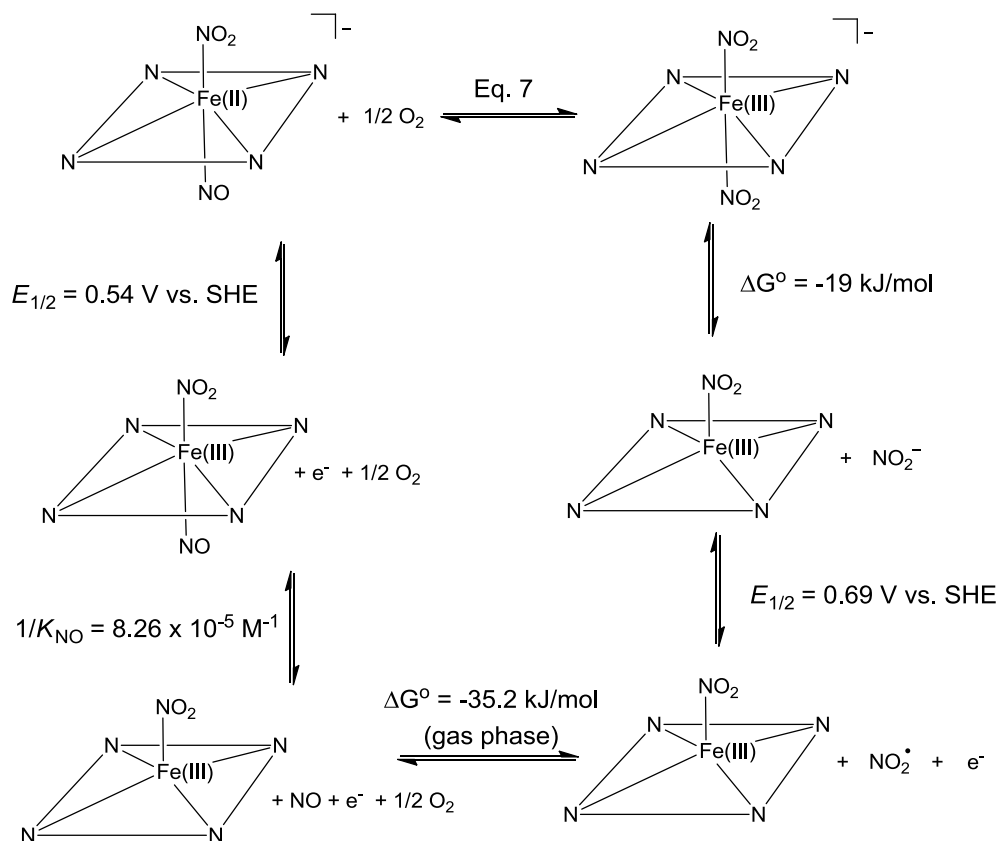
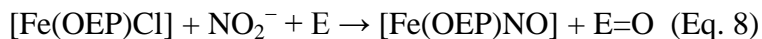


Figure 1.32. Thermodynamic cycle for determination of $\Delta G^\circ_{(E/E=O)}$ for the conversion of $[\text{Fe(II)(TpivPP)(NO)(NO}_2)]^-$ to $[\text{Fe(III)(TpivPP)(NO}_2)_2]^-$.³²⁴

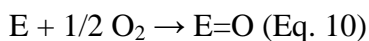
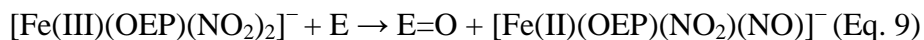
Castro and coworkers have demonstrated that the $[\text{Fe(OEP)Cl}]$ platform has excellent substrate diversity and is high yielding in the OAT reaction.^{359,360} Conditions for the reactions were 4:1 $[\text{Fe(OEP)Cl}]/[\text{K(18C6)}][\text{NO}_2]$ with ~10 equiv of substrate, performed in *N*-methyl-2-pyrrolidone/1% AcOH. The oxidation is proposed to involve an $[\text{Fe(III)(OEP)(NO}_2)]$ species and leads to substrate oxidation with the net reduction of the complex to $[\text{Fe(II)(OEP)(NO)}]$. This report showed OAT to three gaseous substrates, namely NO, CO, and O₂, to afford quantitative transformations to NO₂•, CO₂, and O₃, respectively. The rates of several reactions were determined by spectral monitoring of the conversion of $[\text{Fe(OEP)Cl}]$ to $[\text{Fe(OEP)NO}]$, where the

rate of NO oxidation was highest, and reported as a third order rate, $k = 52,000 \text{ M}^{-2} \text{ s}^{-1}$. This rate is comparable to the readily oxidized Ph_3P where $k = 1300 \text{ M}^{-2} \text{ s}^{-1}$. In addition, the oxidation of aldehydes to carboxylic acids, C-Cl to aldehydes, and C-H to alcohols was reported. The latter two reactions have bond dissociation energies of $\sim 368 \text{ kJ mol}^{-1}$ meaning that a large amount of free energy must be accounted for in the net conversion shown in Eq. 8.



Castro and coworkers do not perform any thermodynamic analysis, but do comment that the high stability of the $[\text{Fe}(\text{OEP})\text{NO}]$ species is likely the driving force of this reaction. Interestingly, the electrochemical characterization by Ryan and coworkers established that $[\text{Fe}(\text{OEP})\text{Cl}]$ can be converted to the bis-nitro complex $[\text{Fe}(\text{OEP})(\text{NO}_2)_2]$ under excess ($\sim 20 \text{ mM}$) NO_2^- .³³¹ Ryan reported a Fe(III)/(II) redox potential of this species at $E_{1/2} = -0.59 \text{ V}$ vs. NHE (DMF). Comparison of this value to the $E_{1/2} = -0.96 \text{ V}$ vs. NHE (MeCN) for Fe(III)/Fe(II) of $[\text{Fe}(\text{TpivPP})(\text{NO}_2)_2]$ shows that the OEP system is more readily reduced by 370 mV and may speak to the greater extent of reactivity observed and the wider range of substrates. The analysis by O'Shea, Wall, and Lin confirm a linear relationship between the redox potential of the $[\text{Fe}(\text{III})/(\text{II})(\text{por})]$ species and the pseudo first-order rate constant.³⁶¹ Accordingly, over the potential range of -0.343 to 0.053 V vs. NHE for Fe(II)/Fe(III) porphyrins, the k_{obs} increased linearly from 2.2×10^{-3} to $13 \times 10^{-3} \text{ M s}^{-1}$ for five different por substrates.³⁶¹

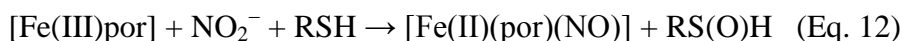
The OAT transfer from $[\text{Fe(III)(OEP)}]^+$ by Castro did not specify as to whether a mono- or bis-nitro species as the active oxidant, however, the tendency for Fe(III) porphyrins to bind NO_2^- is great (K_2 ranges from 60 to 2200 M^{-1} , dependent on solvent/ligand being displaced)³³¹ and cannot be ruled out as the active species. Thus, if the same analysis reported by Goodwin et al. is applied to the OEP system, and the assumption made that an $[\text{Fe(III)(OEP)(NO}_2)_2]^-$ becomes $[\text{Fe(II)(OEP)(NO}_2)(\text{NO})]^-$, then thermodynamic responsibility is no longer on the substrate, but rather the Fe(OEP) system.



For example, the value of $\Delta G^\circ_{(\text{E/E=O})}$ for Eq. 7 (*vide supra*) was determined to be +50 kJ mol^{-1} and therefore the forward progress of the reaction depended on the nature of E in Eq. 10. For Goodwin's work $\text{E} = \text{Ph}_3\text{P}$, having $\Delta G^\circ_{(\text{E/E=O})} = -268 \text{ kJ mol}^{-1}$ and thus an overall favorable reaction. However, if the substrate is toluene, and the reaction is formally C-H activation, then the net free energy difference must come from the more positive reduction potential of $[\text{Fe(III)(OEP)(NO}_2)_2]^-$ and the overall high stability of the $[\text{Fe(OEP)NO}]$. Unfortunately, direct comparison of $[\text{Fe(II)(OEP)(NO}_2)(\text{NO})]^-$ to $[\text{Fe(II)(TpivPP)(NO}_2)(\text{NO})]^-$ is not possible because electrochemical values for the former are not available in the literature. Moreover, the majority of the OAT literature is focused on readily oxidized substrates like Ph_3P , RSR, and RSH. In this context, only $[\text{Fe(OEP)Cl}]$ has been investigated with a wide range of substrates and implicates this NO_2^- -dependent C-H activation as an open area of research for both heme and non-heme complexes.

The reactivity and formation of sulfenic acids (RS(O)H) in biology has emerged as a regulatory mechanism in cellular signaling.³⁶² Oxidation of cysteine residues to Cys-SOH has become a biomarker for oxidant-mediated signaling and disease-related oxidative stress.³⁶² Although, NO_2^- has not been directly linked to OAT of cysteine in biology, the oxidized relative peroxynitrite (ONOO^-), H_2O_2 and ROOH have been implicated.³⁶³ Given the relevance of NO and $\text{O}_2^{\cdot-}$ in the formation of ONOO^- , and the significance of NO_2^- to NO conversion under hypoxic conditions, the biological chemistry of NO_2^- and RS(O)H may have overlapping pathways. Moreover, OAT from a hypothetical Fe(III)- NO_2 heme enzyme to a RSH group could directly give Fe(II)- NO and RS(O)H as a possible mechanism to connect RSH, RS(O)H , NO_2^- and NO . With this concept in mind, Ford and coworkers have pursued the study of OAT from NO_2^- with $[\text{Fe(III)(TPPS)}]^{3-}$ and $[\text{Fe(III)(TMPS)}]^{3-}$ to CysSH and GSH under aqueous conditions (pH ranged from 5.8 - 7.4), where $\text{TMPS} = \text{meso-tetra(sulfonatomesityl)porphyrinato}$.³⁶⁴ A detailed analysis of these reactions confirms that sulfenic acids are formed by Fe(III)-por mediated OAT to thiols, as depicted in Eq. 12. This work was preceded by analogous OAT studies on DMS and a water-soluble derivative of Ph_3P that showed typical OAT reactions to afford DMSO and the phosphine oxide, respectively.³⁶⁵ The RS(O)H species formed were subsequently trapped with dimedone due to the proclivity of the sulfenic acid to form RSSR in the presence of excess RSH (Eq. 13, $\Delta G = -226 \text{ kJ mol}^{-1}$).³⁶⁶ The studies by Ford utilized ~1:50:1,000 equiv of $[\text{Fe(III)(por)}]$, RSH, and NO_2^- , respectively in deoxygenated PBS buffer. Surprisingly, even with 1,000 equiv, the direct binding of NO_2^- was not observed, and the authors attribute this observation to the low affinity of NO_2^- for the $[\text{Fe(III)(TPPS)}]^{3-}$ complex under the exptl. conditions ($K_{\text{NO}_2^-} = 3 \text{ M}^{-1}$).³⁴⁹ Initiation of the reaction by addition of either CysSH or GSH showed clear UV-vis spectral shifts that indicate

formation of [Fe(II)(por)(NO)]. Although the Fe(III)por did not have observable interactions with excess NO₂⁻, titrations of Fe(III)por with RSH did indicate binding of RS⁻ and release of H⁺. Thus, one may propose that the active OAT species may in fact be [Fe(por)(RS)(NO₂)]. However, detailed kinetic analysis confirms that the thiolate-bound species does not contribute to the formation of [Fe(por)NO], but is rather a dead end product. Therefore, the mono-nitro species [Fe(III)(por)(NO₂)] is implicated as the active OAT species and shown to produce CysS(O)H and GS(O)H from NO₂⁻ and the respective thiols.



In a more recent study (2013), Ford and Doctorovich elaborate on the previous OAT studies with water soluble thiols and phosphines.¹³ In this report, the relative instability of the [Fe(II)(por)(NO)] formed after OAT is discussed. It was observed that this species spontaneously regenerated the [Fe(III)(por)] starting complex over ~10 h. This observation highlights, that under the exptl. conditions, the [Fe(II)(por)(NO)] is an active component in a catalytic cycle. The rates of [Fe(III)(por)] regeneration were faster at pH 5.8 than at higher pH, moreover, the gaseous product N₂O was observed. These are intriguing observations and implicate possible formation of an intermediate HNO species. The direct detection of N₂O was made only when the OAT substrate was phosphine, this observation indicates the slower rate of reaction of HNO with excess phosphine than excess thiols. Due to the pH dependence, it was proposed that the [Fe(II)(por)(NO)] complex is protonated to give an [Fe(III)(por)(HNO)] complex, the more labile HNO ligand is lost with subsequent regeneration of the [Fe(III)(por)] starting complex. Trapping experiments proved to be ambiguous in determining HNO formation, however, the use of an HNO-selective electrode allowed for the experimental detection of HNO.³⁶⁷ It should be

noted that the formation of HNO in these studies is catalytic, and about 300 equiv of HNO was formed for every [Fe(III)por].¹³ These exciting studies offer *in vitro* models of the possible chemistry that may occur in the reduction of NO_2^- to NO or possible HNO in a biological setting. Moreover, the possible overlapping biological roles of RS(O)H , NO_2^- , and Fe add yet another degree of complexity to the biological milieu. Clearly, OAT from Fe(III)- NO_2^- is thermodynamically favorable to RSH, but the question remains as to whether or not it is a biological reaction.

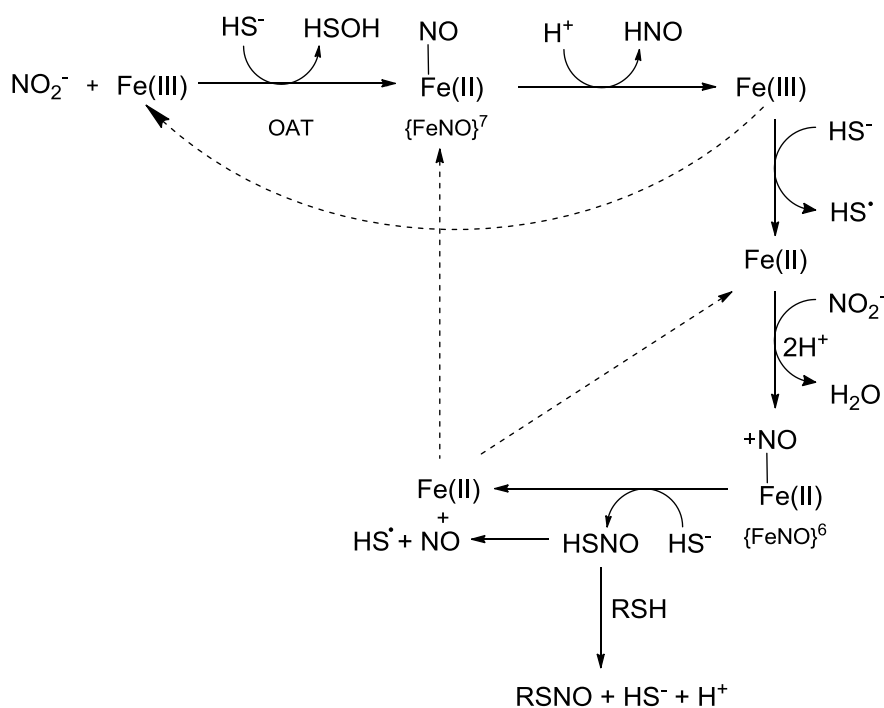


Figure 1.34. Proposed reaction pathways involving NO_2^- , HS^- , and Fe(III)(por) illustrating the possible formation of HNO, HSNO, and NO. If RSH were present, as in $\beta\text{Cys-SH}$ for example, possible S-nitrosylation could occur.

Additional work with a water-soluble Fe(III)por was performed by Ivanović-Burmazović and Filipović.³⁶⁸ This study utilized NO_2^- as an O-atom donor to HS^- to give HSOH and HNO similar to the results by Ford with thiols. However, HSNO can also be formed through the nitrosation of HS^- by the putative $\{\text{FeNO}\}^6$ species formed. Two major pathways are proposed (Fig. 1.34): (i) OAT to HS^- affords the simplest possible sulfenic acid, HSOH^{13} and (ii) HS^- can also serve to reduce the Fe(III)por to Fe(II)por and give HS^\bullet leaving the Fe(II)por to react with NO_2^- affording $\{\text{FeNO}\}^6$ and HSNO after nucleophilic attack by HS^- . Subsequently, HSNO can react with RSH (if present) to give RSNO and regenerate the HS^- , or homolytically cleave to NO^\bullet and HS^\bullet . This chemistry sets the stage for model studies of the possible biological interplay of NO_x and HS-containing species. The potential signaling molecule HSNO is already implicated in the reactions of H_2S with RSNO. For instance, the reaction of an Albumin-SNO with H_2S forms the putative HSNO species which was shown to transfer SNO to the $\beta\text{Cys-SH}$ to give $\beta\text{Cys-SNO}$ of Hb.³⁶⁹ The HSNO molecule can diffuse through membranes and can account for some of the biological signaling and cellular redox regulation associated with $\text{H}_2\text{S}/\text{HS}^-$ and NO .³⁶⁹ The complicated interplay of NO_x and RSH is just beginning to be resolved. Undoubtedly, the use of heme and non-heme models will play an essential role in modeling the physiological interactions of these species with Fe-proteins.

To date, the reactivity of $[\text{Fe}(\text{por})(\text{NO}_2)]$ has almost exclusively involved Fe(III)- NO_2 and OAT reactions to give Fe(II)-NO. This type of reactivity, though possibly relevant to biological transformations of NO_2^- , does not accurately represent the H^+ -dependent reduction of NO_2^- to NO performed by NiR enzymes. It is surprising that the H^+ -dependent reactivity of $[\text{Fe}(\text{II})(\text{por})(\text{NO}_2)]$ has not been more thoroughly investigated; this paucity is due to the proclivity to form stable $\{\text{FeNO}\}^7$ and O-bridged species through a disproportionation process.

Moreover, the cd_1 NiR enzymes that releases NO from an $\{\text{FeNO}\}^7$ complex accomplishes this product release through H-bonding, a feature not always available in porphyrin models. With these facts in mind, non-heme models have gained attention as analogues for NiR-like chemistry.

1.12 Non-heme Fe(NO₂) Model Complexes

1.12.1 Fe(II)(NO₂) Non-heme Models

In comparison to the heme literature, the non-heme Fe-NO₂ literature is sparse. However, the diversity of complexes under this heading is greater due to the variety of ligand frameworks and primary coordination spheres. Similar to heme systems, Fe(III)-NO₂ complexes are more stable, and the N-bound isomers of both Fe(II)- and Fe(III)-NO₂ are typically favored. Non-heme complexes can support all the binding modes of NO₂⁻, a feature not observed in heme complexes. The reactivity of non-heme NO₂⁻ complexes demonstrates both proton-dependent NiR chemistry with Fe(II) and OAT with Fe(III) to generate NO or Fe-NO. In this context, non-heme complexes can serve as modular platforms for the controlled manipulation of electronics, sterics, and secondary-sphere interactions. In many ways, these non-heme species can model the chemistry at Fe(por); however, in some instances unique species that are not possible to obtain with a porphyrin ligand can be characterized and even isolated due to greater flexibility. Although less studied, the non-heme Fe-NO₂ literature illustrates reactivity profiles that are similar to heme models. Due to the diversity of platforms utilized, the reactivity of each complex will be discussed along with its synthesis and characterization.

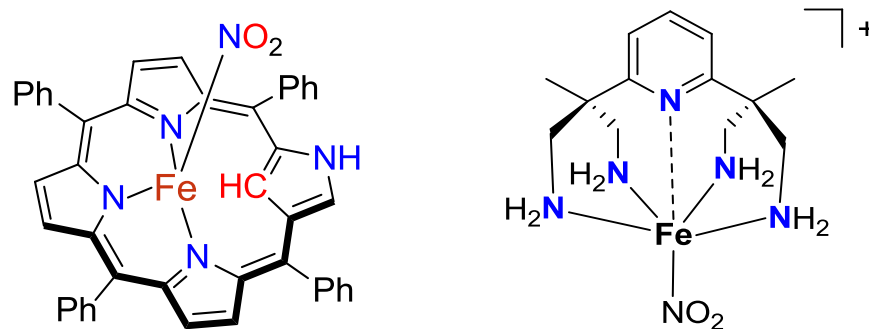


Figure 1.35. The N-confused porphyrin model (*left*) representative of the putative NO_2^- complex of **37**. The PyN4 ligand platform (*right*) and the putative Fe(II)- NO_2^- complex (**38**).

An appropriate transition from heme to non-heme models is the N-confused porphyrin complex $[\text{Fe}(\text{HCTPPH})\text{Br}]$ (**37**).³⁷⁰ This complex is structurally quite similar to the Fe(TPP) system discussed earlier; however, the N-confused system offers a tautomerized pyrrole donor in which the N-H donor is directed to the periphery of the ring, and a C-H group is now directed at the metal (Fig. 1.35). Both functionalities can serve as a source of protons but the latter functional group can become an organometallic donor upon deprotonation, and is thus electronically different from the typical Fe(TPP). The combination of this electronic profile with the internal source of two protons, allowed for the direct reduction of NO_2^- from $[\text{Fe}(\text{HCTPPH})\text{Br}]$ with stoichiometric NO_2^- to give the $\{\text{FeNO}\}^6$ complex $[\text{Fe}(\text{CTPP})\text{NO}]$. The $\{\text{FeNO}\}^6$ complex can be reduced to $\{\text{FeNO}\}^7$ with benzenethiol (PhSH) in CH_2Cl_2 and reversibly oxidized back to $\{\text{FeNO}\}^6$ in the presence of O_2 , and both nitrosyl species were structurally characterized. The N-confused tautomer differs in reactivity of a heme system in several ways, (i) the spontaneous reduction of NO_2^- contrasts the relatively stable coordination

of NO_2^- to $[\text{Fe(II)(TPP)}]$ system (Fig. 1.20), (ii) the reduction of $\{\text{FeNO}\}^6$ by PhSH is very interesting considering the propensity of $\{\text{FeNO}\}^6$ heme complexes to nitrosate RSH and afford RSNO, and (iii) the reaction of the $\{\text{FeNO}\}^7$ complex with O_2 affords $\{\text{FeNO}\}^6$, not Fe(III)-NO_2 , a product observed in the $[\text{Fe(TpivPP)}]$ system.³⁵⁸ Taken together, complex **37** can reduce NO_2^- and stabilize the $\{\text{FeNO}\}^{6/7}$ oxidation states thus making it an NiR functional model complex; however, the instantaneous NO_2^- reactivity precludes any characterization of the putative Fe- NO_2 species. Additionally, the release of NO from Fe was not investigated or suggested, and would be an important feature of this NiR model.

An NiR model produced by Grohmann is the non-heme complex, $[\text{Fe(II/III)PyN4}]$ (where PyN4 = a neutral pentadentate ligand composed of four aliphatic amines appended to a central Py donor (Fig. 1.35)).³⁷¹ The addition of a slight excess of NaNO_2 to a solution of $[\text{Fe(II)(PyN4)Br}]$ afforded the mono-nitro complex $[\text{Fe(II)(PyN4)(NO}_2)]\text{Br}$ (**38**). Complex **38** was well characterized and has ν_{NO} of 1258 and 1219 cm^{-1} that red-shift to 1245 and 1209 cm^{-1} upon ^{15}N -labeling, confirming the species is N-bound. Electrochemical characterization showed a quasi-reversible one-electron wave at -0.07 V vs. Fc^+/Fc (DMSO), and was assigned as the Fe(III/II) redox couple of **38**. Attempts at structural characterization of **38** resulted in the formation of the corresponding $\{\text{FeNO}\}^6$ species. The authors attribute this instability to the presence of adventitious H_2O . Under rigorously dry conditions an unexpected bridging NO_2^- species, $[(\text{Fe(PyN4)})_2(\eta^1\text{-N}:\eta^1\text{-O-NO}_2)]^{3+}$ was observed. This structure is unprecedented, and displays the NO_2^- ligand as bridging between two Fe(II) centers; one Fe N-bound, while the other Fe is coordinated to one O-atom of the NO_2^- ligand. Because this species was crystallized over a period of 7 days, the subsequent reactivity studies are attributed to **38** and not the bridged species. Notably, **38** will spontaneously disproportionate to the $\{\text{FeNO}\}^7$ species over prolonged

time in neutral MeOH solutions. However, reported reactivity through addition of either HBr or HBF₄ in MeOH results in the formation of the {FeNO}⁶ species, consistent with dehydration of the coordinated NO₂⁻. The {FeNO}⁶ complex will slowly convert to {FeNO}⁷ in MeOH, indicative of a disproportionation mechanism. Overall, complex **38** successfully stabilizes NO₂⁻ in the Fe(II) state and controlled reactivity studies demonstrate NiR-like activity; however, NO remains bound to the Fe center. It is possible that NO could be released in the disproportionation reaction, although no mention or characterization of free NO was described.

Another non-heme complex that demonstrates NiR reactivity is the N₄S system, [Fe(S^{Me2}N₄(tren))]⁺, described by the Kovacs group in 2011 (Fig. 1.36).⁷³ This complex, originally designed as a model complex for superoxide reductase (SOR), an enzyme that reduces O₂⁻ to H₂O₂, in a proton-coupled process. Given that both SOR and NiR are proton-dependent reductases, the potential NiR activity of [Fe(S^{Me2}N₄(tren))]⁺ was investigated. Addition of two equiv of NO₂⁻ to an MeCN solution of [Fe(S^{Me2}N₄(tren))]⁺ leads to no observable change in the UV-vis; however, when four equiv of NH₄⁺ was added, a 1:1 mixture of {FeNO}⁷ and [Fe(III)(S^{Me2}N₄(tren)(NO₂))]⁺ (**39**) are formed.⁷³ The general characterization [Fe(II)(S^{Me2}N₄(tren)(NO₂))] was limited, although **39** was well characterized. Complex **39** displays a ν_{NO} of 1478 and 1362 cm⁻¹, consistent with the N-bound isomer. Structural characterization of **39** details the Fe-NO₂ bond = 1.963 Å and an average N-O distance = 1.195 Å. Electrochemical characterization displays a reversible $E_{1/2}$ = -0.480 V vs. SCE (MeCN) for the Fe(III)/Fe(II) couple of the mono-nitro complex. The LS ($S = 1/2$) Fe(III) state was confirmed by solution-state magnetic susceptibility (1.76 BM) and EPR (rhombic feature with $g = 2.18, 2.14, 1.99$). The characterization of **39** is in good agreement with the previously discussed [K(18C6)(H₂O)][Fe(NO₂)(SC₆HF₄)(TpivPP)] (**28**).³³⁶ Despite the stability and isolable

nature of **39**, no reactivity such as OAT was reported. Reaction of the less stable $[\text{Fe(II)}(\text{S}^{\text{Me}_2}\text{N}_4(\text{tren})(\text{NO}_2)]$ was investigated with NH_4^+ and is a disproportionation process leading to $\{\text{FeNO}\}^7$ and Fe(III)-NO_2 ; this pathway is common for proton-dependent reactivity in the absence of a sacrificial electron donor.

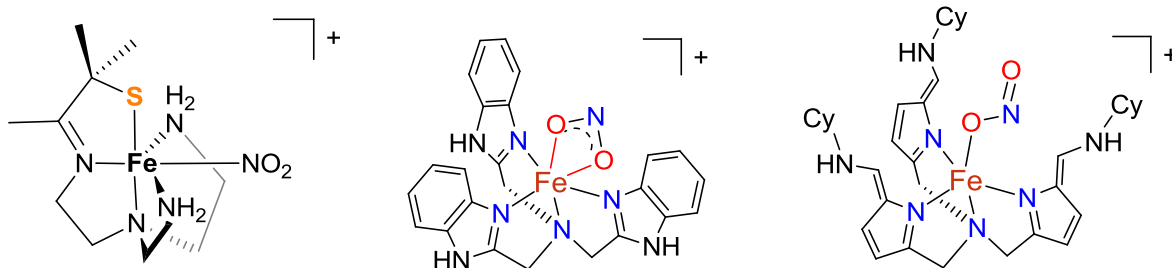


Figure 1.36. Non-heme NiR models $[\text{Fe(III)}(\text{S}^{\text{Me}_2}\text{N}_4(\text{tren})(\text{NO}_2)]^+$ (**39**) (left), $[\text{Fe(II)}(\text{Bim})_3(\eta^2\text{O}_2\text{N})]^+$ (**40**) center, and $[\text{N}(\text{afa}^{\text{Cy}})_3\text{Fe}(\text{ONO})]^+$ (**41**) (right), proposed structure.

Note that all binding modes of NO_2^- are accessible in the non-heme platforms.

Liaw and coworkers synthesized the first example of an O,O-bidentate nitrito coordinated to a non-heme Fe(II) center, namely $[\text{Fe(II)}(\text{Bim})_3(\eta^2\text{O}_2\text{N})]\text{BF}_4$ (**40**), (where Bim = a 4C ligand consisting of three benzimidazole donors branching from a central N, Fig. 1.36).⁷⁵ Though unique to Fe complexes, this binding mode is more relevant to the Cu-NiR enzymes and has never been observed in Fe(por) models or heme proteins. Complex **40** was synthesized in THF with two equiv of NaNO_2 . The crystallographic characterization of **40** displayed the unique binding mode having average Fe-O bonds of 2.221 Å and average N-O bonds of 1.256 Å. The reported ν_{NO} was 1277 cm^{-1} that shifts upon isotopic labeling to 1263 cm^{-1} . These values are very close to the parameters of NaNO_2 and highlight only minor activation of the N-O bonds of **40**. In

the solid-state, the magnetic susceptibility of complex **40** was $\mu_{\text{eff}} = 5.08$ BM (300 K) and 4.2 BM (2 K), consistent with an HS Fe(II) ($S = 2$) complex. This spin-state is unusual for nitrite complexes that are typically LS. These results are indicative of the unique binding mode through the two O-atoms, as σ -donors, and loss of the favorable π -backbonding observed in N-bound isomers. Moreover, the O,O-bidentate nitrito form also appears to affect the reactivity of NO_2^- reduction to NO. Addition of one equiv of AcOH liberates NO, and proposed to occur through protonation of one coordinated O-atom of NO_2^- , followed by isomerization to the Fe- η^1 -OH(N=O) species. Subsequent homolytic cleavage of the O-N=O bond releases NO to afford Fe(III)-OH. The end product of reactivity is the $[[\text{Fe}(\text{Bim})_3]_2(\mu\text{-O})(\mu\text{-CH}_3\text{COO})]^{3+}$ bridged species. This product is a thermodynamic sink, that limits the potential catalytic function of this complex. Importantly, this unusual mechanism may have relevance the reduction of Fe(II)-ONO complex of Hb, Mb, and hemerythrin.

A non-heme complex of similar disposition to **40**, namely $[\text{N}(\text{afa}^{\text{Cy}})_3\text{Fe}(\text{ONO})]^+$ (**41**), was investigated by Fout and colleagues as an NiR model complex (Fig. 1.36).³⁷² This model is supported by a tris(5-cycloiminopyrrol-2-ylmethyl)amine which upon metalation can tautomerize to the aminoazafulvene form (afa).³⁷³ The design of this ligand offers three amines located in the secondary coordination-sphere available for interaction with axial ligands. The reactivity of **41** was investigated by addition of ${}^n\text{Bu}_4\text{NO}_2$ to a THF solution of $[\text{N}(\text{afa}^{\text{Cy}})_3\text{Fe}(\text{OTf})]^+$ (where OTf = trifluoromethanesulfonate). The reaction resulted in the disproportionation of **41** into the $\{\text{FeNO}\}^7$ complex and the oxo species $[\text{N}(\text{afa}^{\text{Cy}})_3\text{Fe}(\text{O})]^+$. Notably, this spontaneous reaction does not require an H^+ source. However, due to the rapid reaction, characterization of the NO_2^- bound species was not possible. In light of this instability, these authors synthesized the Zn(II) analogue of **41** and structurally characterized the O-bound

nitrito complex displaying Zn-O: 2.073 Å and N-O distances: 1.184 and 1.209 Å. Authentic synthesis of the {FeNO}⁷ species confirmed the formation of this product after reaction with NO₂⁻. Although no efforts to prove NO formation were made, this model, similar to **40**, offers a non-heme perspective into the possible routes of NO₂⁻ to NO reduction at Mb and Hb. Compound **41** nicely models the secondary-sphere interactions of the Hb/Mb His residue; moreover, the Fe(III)-O complex is proposed as a possible intermediate in the formation of NO from an O-bound NO₂⁻ complex. Compound **41** and its reactivity with NO₂⁻ contribute to the diversity of non-heme analogues capable of NiR reactivity.

The reported non-heme Fe(II)-NiR models discussed so far utilize H⁺-dependent reactivity for reduction of NO₂⁻ to NO, with the exception of **41**. This approach is consistent with the *cd*₁NiR enzyme and distinguishes Fe(II)-NO₂ complexes from Fe(III)-NO₂; however, complexes **40** and **41** more closely models a possible pathway for NO₂⁻ reduction by Hb and Mb. The non-heme ligands shown in Figures 1.34 and 1.35 have considerable differences. For instance, the primary donor atom is N, but the type of N-donor varies considerably. Moreover, the coordination geometry ranges from square-pyramidal, octahedral, and trigonal bipyramidal. Thus, the diversity of non-heme models allows for all possible isomers of NO₂⁻ coordination, and subsequently the mechanism of H⁺-dependent reduction of NO₂⁻ to NO can also vary. On the other hand, non-heme Fe(III)-NO₂ complexes do not react in an H⁺-dependent manner; instead, the OAT pathway is favored. Accordingly, the synthesis and OAT activity of Fe(III)-NO₂ complexes has been pursued.

1.12.2 Non-heme Fe(III)-NO₂ Models

A non-heme complex having similar structural/electronic disposition to a porphyrin ligand is found in a macrocyclic ligand, L^{Mac} = 6,13-Bis(ethoxycarbonyl)-7,12-dimethylbenzo[*b*]-1,4,8,11-tetrazacyclotetradeca-5,7,12,14-tetraene (Fig. 1.36). This dianionic, diimine N₄ platform, stabilizes the mono(nitro) and bis(nitro) complexes [Fe(III)(L^{Mac})(NO₂)(OH₂)] (**42**) and [Fe(III)(L^{Mac})(NO₂)₂]⁻ (**43**), respectively.³⁷⁴ The bis(nitro) species **43** is purely LS *S* = 1/2; whereas, complex **42** exhibits a spin-crossover phenomenon between the *S* = 1/2 and *S* = 3/2 states. The structural parameters indicate a Fe-NO₂ distance of 1.982 and 2.000 Å for **43**, and 1.963 Å for **42**. Average Fe-N_{eq} distances are about 1.905 Å for both species. Attempts to synthesize the Fe(II)-NO₂ complexes resulted in the formation of the {FeNO}⁷ complex. Interestingly, the {FeNO}⁷ species will react with O₂ in either MeOH or Py to give the Fe(III)-NO₂ complex, as observed in the [Fe(TpivPP)] and other non-heme systems. Further reactivity of complexes **42** and **43** was not suggested, although a better understanding of the potential parallels between heme and non-heme complexes could be gained, given the similar disposition of L^{Mac} to that of a porphyrin.

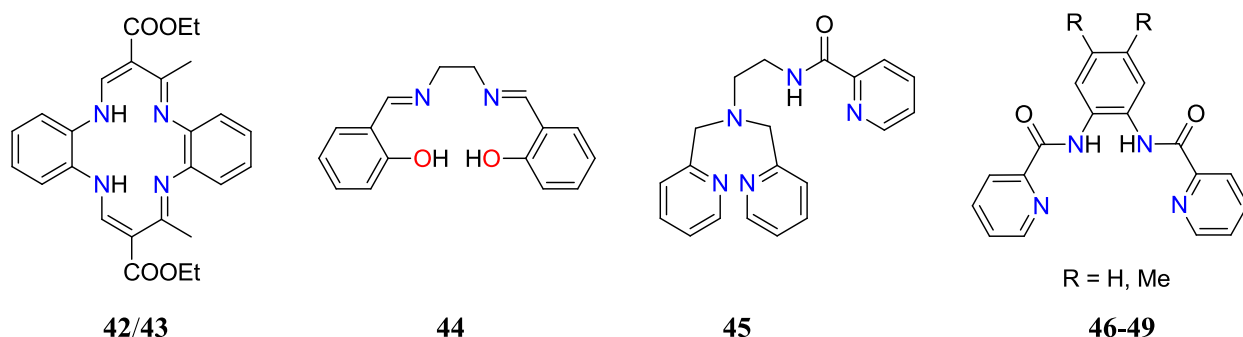


Figure 1.37. Non-heme ligands that support Fe(III)-NO₂ complexes.

The work by Fanning et al. implicated an Fe(III)-NO₂⁻ complex to be involved in Lewis acid catalyzed NO₂⁻ disproportionation with [Fe(salen)(X)], where X = Cl⁻ or NO₃⁻ (Fig. 1.37). The reaction of [Fe(salen)(X)] (**44**), (where salen = dianion of bis(salicylidene)ethylenediamine)) with NO₂⁻ was shown to spontaneously release NO.³⁷⁵ The characterization of the bound NO₂⁻ complexes was not reported, however, release of NO was demonstrated through use of an FTIR gas cell. The net reaction of the complexes was determined to be 2[Fe(III)(salen)] + 3NO₂⁻ → 2NO + [Fe(III)(salen)]₂O + NO₃⁻. Accordingly, the Lewis acid (LA) catalyzed disproportion of 3NO₂⁻ to 2NO, NO₃⁻, and μ-oxo can be accomplished efficiently at ambient temperature without necessitating an OAT substrate like Ph₃P; though NO₂⁻ could act as OAT substrate, similar to what has been reported in porphyrin models.^{322,360} Counter to this, the formation of the [Fe(III)(salen)]₂O species is formally oxy anion (O²⁻) transfer. This type of reactivity is similar to the loss of H₂O, where instead of H⁺, a metal cation supports the O²⁻ transfer to form a μ-oxo species. Observation of NO₃⁻ and μ-oxo support that both O-atom and O²⁻ reaction pathways may occur in this LA catalyzed disproportionation of NO₂⁻. The release of NO in the salen system is noteworthy; however the thermodynamic sink of the [Fe(III)(salen)]₂O species would again, limit catalytic application of this system. Parallels to the reactivity of the mixed heme-Cu model complex of CcO, by Karlin, are evident; in these studies, Cu(II) acts a LA to react with NO₂⁻ to disproportionate to an [por(Fe(III))(μ-O)[Cu(II)]] complex and the {FeNO}⁷ complex [Fe(II)(por)(NO)].³⁷⁶ This end-product is analogous to what is observed for Fe(III)salen system. Although the reactivity discussed differs from NiR activity, it remains an important pathway toward the net reduction of NO₂⁻ to afford NO, and offers mechanistic insight toward NO₂⁻ reduction at CcO.

Mascharak and coworkers have been instrumental in the development of non-heme model complexes capable of stabilizing the Fe(III)-NO₂ unit. One such complex is supported by the PaPy₃ ligand, a 5C species having four neutral N donors and one anionic amide N-donor, where PaPy₃ = *N,N*-bis(2-pyridylmethyl)amine-*N*-ethyl-2-pyridine-2-carboxamide). The ligand wraps around a metal ion such that the amide N is positioned axial to the vacant or solvent coordinated site (Fig. 1.37). Addition of [Fe(DMF)₆](ClO₄)₃ to PaPy₃ in MeCN afforded a dark violet complex that readily reacted with three equiv of NaNO₂ to afford [Fe(PaPy₃)(NO₂)](ClO₄) (**45**).³⁷⁷ The structural characterization details the Fe(III) center in a distorted octahedral geometry, having Fe-NO₂ distance = 2.044 Å, and an axial Fe-N_{amide} = 1.856 Å. The N-O distances are remarkably asymmetric, with one 1.240 Å and the other shorter at 1.182 Å, a difference of 0.058 Å, indicating activation of the N-O bond. The *S* = 1/2 spin-state was confirmed based on the EPR spectrum that displays a rhombic species (*g* = 2.347, 2.212, and 1.902). Moreover, the zero-field MB data collected at 4.2 K display $\Delta E_q = -2.65$ mm/s and $\delta = 0.19$. The large negative values of ΔE_q are indicative of the large valence contribution to the electric field gradient originating from LS *d*⁵ hole in the *t*_{2g} orbitals.³⁷⁸ The OAT reactivity of **45** with Ph₃P was catalytic in the presence of O₂ at 45 - 65 °C in MeCN. The pseudo first-order rate constant and turnover number (TN) was determined to be *k* = 6.72 × 10⁻³ min⁻¹, TN = 37 (45 °C) and *k* = 15.9 × 10⁻³ min⁻¹, TN = 87 (65 °C). These rates are about an order of magnitude slower than those shown for various Fe(III)por species under comparable conditions; however, this system is catalytic unlike the reported Fe(III)por systems that stop at the {FeNO}⁷ species.³⁶¹ In the absence of O₂, the reaction proceeds directly to the [Fe(PaPy₃)(NO)]⁺ {FeNO}⁷ complex with only one equiv of Ph₃P=O produced. The {FeNO}⁷ eventually decomposes to a μ -oxo Fe(III) complex with possible coupling of the NO ligands to N₂O.³⁷⁹ The overall catalytic

behavior is hindered due to the formation of the μ -oxo Fe(III) complex under the reaction conditions. Nonetheless, Mascharak and coworkers demonstrate the first non-heme system capable of catalyzing OAT to Ph₃P. Moreover the reversible conversion from nitrite-to-nitrosyl was a first for non-heme complexes, and indeed parallels the same conversion performed by the [Fe(TpivPP)] system.³⁵⁸

Similar parallels to heme chemistry have been reported by Mascharak with the non-heme system [Fe(Me₂bpb)(NO₂)(X)]ⁿ where Me₂bpb = the dianion of bis(pyridine-2-carboxamido)-4,5-dimethylbenzenediamine (Fig. 1.37).³⁸⁰ For instance, X-ray diffraction analysis displayed both N-bound to O-bound isomers; this observation is indicative of a relatively low isomerization energy, an important phenomenon in observed in heme systems. The bond distances of the isomers are Fe-N_{NO₂} = 2.034 Å and Fe-O_{ONO} = 1.894 Å. Isomerization of coordinated NO₂⁻ from [Fe(Me₂bpb)(NO₂)] was a result of the two methyl substituent groups on the periphery of the ligand. For instance, if the Me group is changed to H then only the N-bound isomer is observed. Moreover, the detailed characterization and reactivity studies were performed on the related [Fe(bpb)(NO₂)(X)]ⁿ, where X = Py (**46**), Cl⁻ (**47**), Br⁻ (**48**), and CN⁻ (**49**); where bpb = the dianion of bis(pyridine-2-carboxamido) benzenediamine (Fig. 1.36).^{380,381} The complexes **47-49** were synthesized from [Fe(bpb)(NO₂)(Py)] (**46**) by ligand exchange with the corresponding Et₄NX salt. The vibrational data for ν_{NO} is only slightly dependent on the axial ligand and is observed at 1384 cm⁻¹ for **46**, **48**, **49**, and 1348 cm⁻¹ for **47**. Compounds **46-49** all exhibit EPR signals at $g = 2.15$, consistent with the LS Fe(III) state ($S = 1/2$). The structural characterization of **46** showed an Fe-NO₂ distance = 1.945 Å and an axial Fe-N_{Py} = 2.032 Å. Additionally a slight elongation is seen between the N-O bonds at 1.211 and 1.245 Å. Complexes **47-49** demonstrate moderate OAT activity with Ph₃P. The catalytic OAT was performed under

pseudo first-order conditions where $k = 1.70 \times 10^{-4}$, 1.50×10^{-4} , and $1.10 \times 10^{-4} \text{ min}^{-1}$ for **47**, **48**, and **49**, respectively. These are about an order of magnitude slower than the PaPy₃ system; accordingly, the decreased rates are attributed to the formation of μ -oxo species and is reflected in the low TNs of ≤ 10 . Interestingly, the rates of OAT are dependent on the σ -donor strength of the axial anion, with the strongest σ -donor having the highest rate of OAT. The reported reactivity of the Fe(bpb) system demonstrates NiR like reactivity of non-heme Fe(III) complexes. Although NO is not released, these platforms are able to perform the nitrosyl-to-nitrite transformation to allow for catalytic OAT.

Taken together, the non-heme NiR models provide a diverse group of Fe-complexes capable of reducing NO_2^- to NO by a variety of mechanisms. This diversity can mimic heme chemistry, but in some instances is divergent from heme-like transformations. Non-heme models allows for investigation and development of new platforms to reduce NO_2^- and the ability to access all coordination isomers of NO_2^- . Moreover, the diverse reactivity pathways proffer alternative approaches to NO_2^- reduction. However, the inability to release NO from these models is a limitation of these systems. Other limitations are disproportionation, and the formation of stable $\{\text{FeNO}\}^{6/7}$, Fe(III)-oxo, and Fe(III)-O-Fe(III) species. Thus, the need to develop non-heme models that avoid stable dead-end species and release NO is an open area of research.

1.13 Research Objective and Purpose

The purpose of this research is to establish the heme-related chemistry of NO_2^- , NO, and HNO on a synthetic non-heme platform. The isolation of Fe-N_yO_x complexes with heme platforms is synthetically challenging due to the inherent instability of these enzymatically

relevant species, which are critical to the global nitrogen cycle and mammalian physiology. Thus, non-heme ligands offer a readily synthesized and systematically tunable platform that can both stabilize N_yO_x species and also transform to model the reaction chemistry of denitrifying metalloenzymes. Moreover, the tunable nature of these systems allows for modulation of sterics, electronics, and both primary/secondary-sphere interactions. Accordingly, detailed insight into the requirements of the stability/reactivity will be addressed. The specific aims of this dissertation are: (i) to synthesize and characterize Fe-NO⁻/HNO complexes and probe their inherent reactivity with biologically relevant molecules such as metalloproteins and thiols. These complexes will offer spectroscopic benchmarks for the M-NO_x community and also be developed as metal-based HNO donors, and (ii) to develop Fe-based complexes for the catalytic reduction of NO₂⁻ to NO for the purpose of developing NO-releasing complexes that can function under physiological conditions.

1.14 References

- (1) Karlin, K. *Science* **1993**, *261*, 701.
- (2) Galloway, J. N. *Bioscience* **2003**, *53*, 341.
- (3) Galloway, J. N. *Biogeochemistry* **2004**, *70*, 153.
- (4) Gruber, N.; Galloway, J. N. *Nature* **2008**, *451*, 293.
- (5) MacLeod, K. C.; Holland, P. L. *Nat. Chem.* **2013**, *5*, 559.
- (6) Peters, J. W.; Stowell, M. H. B.; Soltis, S. M.; Finnegan, M. G.; Johnson, M. K.; Rees, D. C. *Biochemistry* **1997**, *36*, 1181.
- (7) Einsle, O. *J. Biol. Inorg. Chem.* **2014**, *19*, 737.
- (8) *Biological Inorganic Chemistry: Structure and Reactivity*; Bertini, I., Gray, H. B., Stiefel, E. I., Valentine, J. S., Eds.; University Science Books: Sausalito, California, 2007.
- (9) Maia, L. B.; Moura, J. J. G. *Chem. Rev.* **2014**, *114*, 5273.
- (10) Canfield, D. E.; Glazer, A. N.; Falkowski, P. G. *Science* **2010**, *330*, 192.
- (11) Hendgen-Cotta, U. B.; Merx, M. W.; Shiva, S.; Schmitz, J.; Becher, S.; Klare, J. P.; Steinhoff, H. J.; Goedecke, A.; Schrader, J.; Gladwin, M. T.; Kelm, M.; Rassaf, T. *Proc. Natl. Acad. Sci. U.S.A.* **2008**, *105*, 10256.
- (12) Miljkovic, J. L.; Kenkel, I.; Ivanovic-Burmazovic, I.; Filipovic, M. R. *Angew. Chem. Int. Edit.* **2013**, *52*, 12061.
- (13) Heinecke, J. L.; Khin, C.; Pereira, J. C. M.; Suárez, S. A.; Iretskii, A. V.; Doctorovich, F.; Ford, P. C. *J. Am. Chem. Soc.* **2013**, *135*, 4007.
- (14) Cosby, K.; Partovi, K. S.; Crawford, J. H.; Patel, R. P.; Reiter, C. D.; Martyr, S.; Yang, B. K.; Waclawiw, M. A.; Zalos, G.; Xu, X.; Huang, K. T.; Shields, H.; Kim-Shapiro, D. B.; Schechter, A. N.; Cannon, R. O., 3rd; Gladwin, M. T. *Nat. Med.* **2003**, *9*, 1498.
- (15) Butler, A.R.; Megson, I.L. *Chem. Rev.* **2002**, *102*, 1155.
- (16) Zumft, W. G. *Microbiol. Mol. Biol. R.* **1997**, *61*, 533.
- (17) Furchgott, R. F. *Angew. Chem. Int. Ed.* **1999**, *38*, 1870.

- (18) Ignarro, L. J. *Angew. Chem. Int. Ed.* **1999**, 38, 1882.
- (19) Murad, F. *Angew. Chem. Int. Ed.* **1999**, 38, 1856.
- (20) Mulsch, A.; Vanin, A.; Mordvintcev, P.; Hauschildt, S.; Busse, R. *Biochem. J.* **1992**, 288 (Pt 2), 597.
- (21) Clement, B.; Schnorwangen, E.; Kampchen, T.; Mordvintcev, P.; Mulsch, A. *Archiv. der Pharmazie* **1994**, 327, 793.
- (22) Rosen, G. M.; Tsai, P.; Pou, S. *Chem. Rev.* **2002**, 102, 1191.
- (23) van Faassen, E. E.; Bahrami, S.; Feelisch, M.; Hogg, N.; Kelm, M.; Kim-Shapiro, D. B.; Kozlov, A. V.; Li, H.; Lundberg, J. O.; Mason, R.; Nohl, H.; Rassaf, T.; Samouilov, A.; Slama-Schwok, A.; Shiva, S.; Vanin, A. F.; Weitzberg, E.; Zweier, J.; Gladwin, M. T. *Med. Res. Rev.* **2009**, 29, 683.
- (24) Sparacino-Watkins, C. E.; Lai, Y. C.; Gladwin, M. T. *Circulation* **2012**, 125, 2824.
- (25) Kim-Shapiro, D. B.; Gladwin, M. T. *Nitric Oxide-Biol. Ch.* **2014**, 38, 58.
- (26) Miranda, K. M.; Espey, M. G.; Paolocci, N.; Bartberger, M. D.; Colton, C. A.; Wink, D. A. *Free Radical Bio. Med.* **2001**, 31, S72.
- (27) Miranda, K. M.; Nims, R. W.; Thomas, D. D.; Espey, M. G.; Citrin, D.; Bartberger, M. D.; Paolocci, N.; Fukuto, J. M.; Feelisch, M.; Wink, D. A. *J. Inorg. Biochem.* **2003**, 93, 52.
- (28) Miranda, K. M.; Paolocci, N.; Katori, T.; Thomas, D. D.; Wink, D. A. *J. Inorg. Biochem.* **2003**, 96, 49.
- (29) Fukuto, J. M.; Bartberger, M. D.; Dutton, A. S.; Paolocci, N.; Wink, D. A.; Houk, K. N. *Chem. Res. Toxicol.* **2005**, 18, 790.
- (30) Fukuto, J. M.; Dutton, A. S.; Houk, K. N. *Chembiochem* **2005**, 6, 612.
- (31) Fukuto, J. M.; Switzer, C. H.; Miranda, K. M.; Wink, D. A. *Annu. Rev. Pharmacol.* **2005**, 45, 335.
- (32) Miranda, K. M. *Coord. Chem. Rev.* **2005**, 249, 433.
- (33) Irvine, J. C.; Ritchie, R. H.; Favalaro, J. L.; Andrews, K. L.; Widdop, R. E.; Kemp-Harper, B. K. *Trends Pharmacol. Sci.* **2008**, 29, 601.
- (34) Obayashi, E.; Takahashi, S.; Shiro, Y. *J. Am. Chem. Soc.* **1998**, 120, 12964.

- (35) Lehnert, N.; Praneeth, V. K. K.; Paulat, F. *J. Comp. Chem.* **2006**, *27*, 1338.
- (36) McQuarters, A. B.; Wirgau, N. E.; Lehnert, N. *Curr. Opin. Chem. Biol.* **2014**, *19*, 82.
- (37) Irvine, J. C.; Favaloro, J. L.; Kemp-Harper, B. K. *Hypertension* **2003**, *41*, 1301.
- (38) Bartberger, M. D.; Liu, W.; Ford, E.; Miranda, K. M.; Switzer, C.; Fukuto, J. M.; Farmer, P. J.; Wink, D. A.; Houk, K. N. *Proc. Natl. Acad. Sci. U.S.A.* **2002**, *99*, 10958.
- (39) Miller, T. W.; Cherney, M. M.; Lee, A. J.; Francoleon, N. E.; Farmer, P. J.; King, S. B.; Hobbs, A. J.; Miranda, K. M.; Burstyn, J. N.; Fukuto, J. M. *J. Biol. Chem.* **2009**, *284*, 21788.
- (40) Ma, X. L.; Cao, F.; Liu, G. L.; Lopez, B. L.; Christopher, T. A.; Fukuto, J. M.; Wink, D. A.; Feelisch, M. *Proc. Natl. Acad. Sci. U.S.A.* **1999**, *96*, 14617.
- (41) Pagliaro, P.; Mancardi, D.; Rastaldo, R.; Penna, C.; Gattullo, D.; Miranda, K. M.; Feelisch, M.; Wink, D. A.; Kass, D. A.; Paolocci, N. *Free Radical Bio. Med.* **2003**, *34*, 33.
- (42) Nagasawa, H. T.; Fukuto, J. M. *Clin. Pharmacol. Ther.* **1993**, *53*, 158.
- (43) Fukuto, J. M.; Gulati, P.; Nagasawa, H. T. *Biochem. Pharmacol.* **1994**, *47*, 922.
- (44) Nagasawa, H. T.; Kawle, S. P.; Elberling, J. A.; Demaster, E. G.; Fukuto, J. M. *J. Med. Chem.* **1995**, *38*, 1865.
- (45) DeMaster, E. G.; Redfern, B.; Nagasawa, H. T. *Biochem. Pharmacol.* **1998**, *55*, 2007.
- (46) Lopez, B. E.; Rodriguez, C. E.; Pribadi, M.; Cook, N. M.; Shinyashiki, M.; Fukuto, J. M. *Arch. Biochem. Biophys.* **2005**, *442*, 140.
- (47) Smil, V. *Sci. Am.* **1997**, *277*, 76.
- (48) Vitousek, P. M.; Aber, J. D.; Howarth, R. W.; Likens, G. E.; Matson, P. A.; Schindler, D. W.; Schlesinger, W. H.; Tilman, D. G. *Ecol. Appl.* **1997**, *7*, 737.
- (49) Mosier, A.; Kroeze, C.; Nevison, C.; Oenema, O.; Seitzinger, S.; van Cleemput, O. *Nutr. Cycl. Agroecosys.* **1998**, *52*, 225.
- (50) Cameron, K. C.; Di, H. J.; Moir, J. L. *Ann. Appl. Biol.* **2013**, *162*, 145.

- (51) WHO *Background document for development of WHO Guidelines for Drinking-water Quality* **2011**, WHO/SDE/WSH/07.01/16/Rev/1.
- (52) Eisenberg, R.; Meyer, C. D. *Accounts Chem. Res.* **1975**, *8*, 26.
- (53) Richter-Addo, G. B.; Legzdins, P.; Burstyn, J. *Chem. Rev.* **2002**, *102*, 857.
- (54) McCleverty, J. A. *Chem. Rev.* **2004**, *104*, 403.
- (55) Dalby, F. W. *Can. J. Phys.* **1958**, *36*, 1336.
- (56) Farmer, P. J.; Sulc, F. *J. Inorg. Biochem.* **2005**, *99*, 166.
- (57) Bartberger, M. D.; Fukuto, J. M.; Houk, K. N. *Proc. Natl. Acad. Sci. U.S.A.* **2001**, *98*, 2194.
- (58) Donzelli, S.; Espey, M. G.; Thomas, D. D.; Mancardi, D.; Tocchetti, C. G.; Ridnour, L. A.; Paolocci, N.; King, S. B.; Miranda, K. M.; Lazzarino, G.; Fukuto, J. M.; Wink, D. A. *Free Radical Bio. Med.* **2006**, *40*, 1056.
- (59) Shafirovich, V.; Lyman, S. V. *Proc. Natl. Acad. Sci. U.S.A.* **2002**, *99*, 7340.
- (60) Benderskii, V. A.; Krivenko, A. G.; Ponomarev, E. A. *Elektrokhimiya* **1990**, *26*, 318.
- (61) Ghosh, A.; Wondimagegn, T. *J. Am. Chem. Soc.* **2000**, *122*, 8101.
- (62) Wondimagegn, T.; Ghosh, A. *J. Am. Chem. Soc.* **2001**, *123*, 5680.
- (63) Coppens, P.; Novozhilova, I.; Kovalevsky, A. *Chem. Rev.* **2002**, *102*, 861.
- (64) Wyllie, G. R. A.; Scheidt, W. R. *Chem. Rev.* **2002**, *102*, 1067.
- (65) Richter-Addo, G. B.; Legzdins, P. *Metal Nitrosyls*. Oxford University Press, 1992.
- (66) Enemark, J. H.; Feltham, R. D. *Coord. Chem. Rev.* **1974**, *13*, 339.
- (67) Sanders, B.C.; Rhine, M. A.; Harrop, T. C. *Struct. Bonding (Berlin)* **2014**, *160*, 57.
- (68) Truter, M. R. *Nature* **1951**, *168*, 344.
- (69) Truter, M. *Acta Crystallogr.* **1954**, *7*, 73.
- (70) Carpenter, G. B. *Acta Crystallogr.* **1952**, *5*, 132.

- (71) Rosca, V.; Duca, M.; de Groot, M. T.; Koper, M. T. M. *Chem.Rev.* **2009**, *109*, 2209.
- (72) Kato, R.; Rolfe, J. *J. Chem. Phys.* **1967**, *47*, 1901.
- (72) Silaghi-Dumitrescu, R. *Inorg. Chem.* **2004**, *43*, 3715.
- (73) Villar-Acevedo, G.; Nam, E.; Fitch, S.; Benedict, J.; Freudenthal, J.; Kaminsky, W.; Kovacs, J.A. *J. Am. Chem. Soc.* **2011**, *133*, 1419.
- (74) Silaghi-Dumitrescu, R. *Inorg. Chem.* **2004**, *43*, 3715.
- (75) Tsou, C.-C.; Yang, W.-L.; Liaw, W.-F. *J. Am. Chem. Soc.* **2013**, *135*, 18758.
- (76) Xu, N.; Yi, J.; Richter-Addo, G. B. *Inorg. Chem.* **2010**, *49*, 6253.
- (77) Nakamoto, K. *Infrared and Raman spectra of inorganic and coordination compounds.*; John Wiley & Sons, Ltd., 1978.
- (78) Einsle, O.; Messerschmidt, A.; Huber, R.; Kroneck, P. M. H.; Neese, F. *J. Am. Chem. Soc.* **2002**, *124*, 11737.
- (79) Tomita, T.; Haruta, N.; Aki, M.; Kitagawa, T.; Ikeda-Saito, M. *J. Am. Chem. Soc.* **2001**, *123*, 2666.
- (80) Vogel, K. M.; Kozlowski, P. M.; Zgierski, M. Z.; Spiro, T. G. *J. Am. Chem. Soc.* **1999**, *121*, 9915.
- (81) Walker, F. A. *J. Inorg. Biochem.* **2005**, *99*, 216.
- (82) Weichsel, A.; Andersen, J. F.; Champagne, D. E.; Walker, F. A.; Montfort, W. R. *Nat. Struct. Mol. Biol.* **1998**, *5*, 304.
- (83) Harrop, T. C.; Mascharak, P. K. *Acc. Chem. Res.* **2004**, *37*, 253.
- (84) Mascharak, P. K. *Coord. Chem. Rev.* **2002**, *225*, 201.
- (85) Dey, A.; Chow, M.; Taniguchi, K.; Lugo-Mas, P.; Davin, S.; Maeda, M.; Kovacs, J. A.; Odaka, M.; Hodgson, K. O.; Hedman, B.; Solomon, E. I. *J. Am. Chem. Soc.* **2005**, *128*, 533.
- (86) Nagashima, S.; Nakasako, M.; Dohmae, N.; Tsujimura, M.; Takio, K.; Odaka, M.; Yohda, M.; Kamiya, N.; Endo, I. *Nat. Struct. Biol.* **1998**, *5*, 347.
- (87) Bonnet, D.; Artaud, I.; Moali, C.; Pétré, D.; Mansuy, D. *FEBS Lett.* **1997**, *409*, 216.

- (88) Wang, Y.; Averill, B. A. *J. Am. Chem. Soc.* **1996**, *118*, 3972.
- (89) Einsle, O.; Messerschmidt, A.; Stach, P.; Bourenkov, G. P.; Bartunik, H. D.; Huber, R.; Kroneck, P. M. H. *Nature* **1999**, *400*, 476.
- (90) Averill, B. A. *Chem. Rev.* **1996**, *96*, 2951.
- (91) Miller, L. M.; Pedraza, A. J.; Chance, M. R. *Biochemistry* **1997**, *36*, 12199.
- (92) Møller, J. K. S.; Skibsted, L. H. *Chem. Rev.* **2002**, *102*, 1167.
- (93) Linder, D. P.; Rodgers, K. R. *Inorg. Chem.* **2005**, *44*, 1367.
- (94) Benko, B.; Yu, N.-T. *Proc. Natl. Acad. Sci. U.S.A.* **1983**, *80*, 7042.
- (95) Solomon, E. I.; Brunold, T. C.; Davis, M. I.; Kemsley, J. N.; Lee, S.-K.; Lehnert, N.; Neese, F.; Skulan, A. J.; Yang, Y.-S.; Zhou, J. *Chem. Rev.* **1999**, *100*, 235.
- (96) Schenk, G.; Pau, M. Y. M.; Solomon, E. I. *J. Am. Chem. Soc.* **2003**, *126*, 505.
- (97) Brown, C. D.; Neidig, M. L.; Neibergall, M. B.; Lipscomb, J. D.; Solomon, E. I. *J. Am. Chem. Soc.* **2007**, *129*, 7427.
- (98) Diebold, A. R.; Brown-Marshall, C. D.; Neidig, M. L.; Brownlee, J. M.; Moran, G. R.; Solomon, E. I. *J. Am. Chem. Soc.* **2011**, *133*, 18148.
- (99) Orville, A. M.; Chen, V. J.; Kriauciunas, A.; Harpel, M. R.; Fox, B. G.; Munck, E.; Lipscomb, J. D. *Biochemistry* **1992**, *31*, 4602.
- (100) Rodriguez, J. H.; Xia, Y.-M.; Debrunner, P. G. *J. Am. Chem. Soc.* **1999**, *121*, 7846.
- (101) Sheng, Y.; Abreu, I. A.; Cabelli, D. E.; Maroney, M. J.; Miller, A.-F.; Teixeira, M.; Valentine, J. S. *Chem. Rev.* **2014**, *114*, 3854.
- (102) Pierce, B. S.; Gardner, J. D.; Bailey, L. J.; Brunold, T. C.; Fox, B. G. *Biochemistry* **2007**, *46*, 8569.
- (103) Derbyshire, E. R.; Marletta, M. A. *Annu. Rev. Biochem.* **2012**, *81*, 533.
- (104) Russwurm, M.; Koesling, D. *EMBO J.* **2004**, *23*, 4443.
- (105) Winger, J. A.; Marletta, M. A. *Biochemistry* **2005**, *44*, 4083.
- (106) Fernhoff, N. B.; Derbyshire, E. R.; Marletta, M. A. *Proc. Natl. Acad. Sci. U.S.A.* **2009**, *106*, 21602.

- (107) Roy, B.; Garthwaite, J. *Proc. Natl. Acad. Sci. U.S.A.* **2006**, *103*, 12185.
- (108) Fukuto, J. M.; Chiang, K.; Hszieh, R.; Wong, P.; Chaudhuri, G. *J. Pharmacol. Exp. Ther.* **1992**, *263*, 546.
- (109) Hirasawa, M.; Proske, P. A.; Knaff, D. B. *Bba-Bioenergetics* **1994**, *1187*, 80.
- (110) Hirasawa, M.; Tollin, G.; Salamon, Z.; Knaff, D. B. *Bba-Bioenergetics* **1994**, *1185*, 336.
- (111) Setif, P.; Hirasawa, M.; Cassan, N.; Lagoutte, B.; Tripathy, J. N.; Knaff, D. B. *Biochemistry* **2009**, *48*, 2828.
- (112) Shoun, H.; Kim, D. H.; Uchiyama, H.; Sugiyama, J. *FEMS Microbiol. Lett.* **1992**, *94*, 277.
- (113) Saraiva, L. M.; Vicente, J. B.; Teixeira, M. *Adv. Microb. Physiol.* **2004**, *49*, 77.
- (114) Caranto, J. D.; Weitz, A.; Hendrich, M. P.; Kurtz, D. M. *J. Am. Chem. Soc.* **2014**, *136*, 7981.
- (115) Hayashi, T.; Caranto, J. D.; Wampler, D. A.; Kurtz, D. M.; Moenne-Loccoz, P. *Biochemistry* **2010**, *49*, 7040.
- (116) Wasser, I. M.; de Vries, S.; Moenne-Loccoz, P.; Schröder, I.; Karlin, K. D. *Chem. Rev.* **2002**, *102*, 1201.
- (117) Kurtz, J. D. M. *Dalton Trans.* **2007**, 4115.
- (118) Hino, T.; Matsumoto, Y.; Nagano, S.; Sugimoto, H.; Fukumori, Y.; Murata, T.; Iwata, S.; Shiro, Y. *Science* **2010**, *330*, 1666.
- (119) Ye, S. F.; Price, J. C.; Barr, E. W.; Green, M. T.; Bollinger, J. M.; Krebs, C.; Neese, F. *J. Am. Chem. Soc.* **2010**, *132*, 4739.
- (120) Bollinger, J. M.; Price, J. C.; Hoffart, L. M.; Barr, E. W.; Krebs, C. *Eur. J. Inorg. Chem.* **2005**, *2005*, 4245.
- (121) Immoos, C. E.; Sulc, F.; Farmer, P. J.; Czarnecki, K.; Bocian, D. F.; Levina, A.; Aitken, J. B.; Armstrong, R. S.; Lay, P. A. *J. Am. Chem. Soc.* **2005**, *127*, 814.
- (122) Kumar, M. R.; Fukuto, J. M.; Miranda, K. M.; Farmer, P. J. *Inorg. Chem.* **2010**, *49*, 6283.
- (123) Kumar, M. R.; Pervitsky, D.; Chen, L.; Poulos, T.; Kundu, S.; Hargrove, M. S.; Rivera, E. J.; Diaz, A.; Colon, J. L.; Farmer, P. J. *Biochemistry* **2009**, *48*, 5018.

- (124) Lin, R.; Farmer, P. J. *J. Am. Chem. Soc.* **2000**, *122*, 2393.
- (125) Sulc, F.; Immoos, C. E.; Pervitsky, D.; Farmer, P. J. *J. Am. Chem. Soc.* **2004**, *126*, 1096.
- (126) Bayachou, M.; Lin, R.; Cho, W.; Farmer, P. J. *J. Am. Chem. Soc.* **1998**, *120*, 9888.
- (127) Sulc, F.; Fleischer, E.; Farmer, P. J.; Ma, D. J.; La Mar, G. N. *J. Biol. Inorg. Chem.* **2003**, *8*, 348.
- (128) Balasubramanian, S.; Lambright, D. G.; Simmons, J. H.; Gill, S. J.; Boxer, S. G. *Biochemistry* **1994**, *33*, 8355.
- (129) Fukuto, J. M.; Cisneros, C. J.; Kinkade, R. L. *J. Inorg. Biochem.* **2013**, *118*, 201.
- (130) Miranda, K. M.; Ridnour, L.; Esprey, M.; Citrin, D.; Thomas, D.; Mancardi, D.; Donzelli, S.; Wink, D. A.; Katori, T.; Tocchetti, C. G.; Ferlito, M.; Paolocci, N.; Fukuto, J. M. *Prog. Inorg. Chem.* **2005**, *54*, 349.
- (131) Roman, L. J.; Martasek, P.; Masters, B. S. S. *Chem. Rev.* **2002**, *102*, 1179.
- (132) Yoo, J.; Fukuto, J. M. *Biochem. Pharmacol.* **1995**, *50*, 1995.
- (133) Fukuto, J. M.; Wallace, G. C.; Hsieh, R.; Chaudhuri, G. *Biochem. Pharmacol.* **1992**, *43*, 607.
- (134) Fukuto, J. M.; Dutton, A. S.; Houk, K. N. *Chembiochem* **2005**, *6*, 612.
- (135) Rusche, K. M.; Spiering, M. M.; Marletta, M. A. *Biochemistry* **1998**, *37*, 15503.
- (136) Adak, S.; Wang, Q.; Stuehr, D. J. *J. Biol. Chem.* **2000**, *275*, 33554.
- (137) Wei, C. C.; Wang, Z. Q.; Hemann, C.; Hille, R.; Stuehr, D. J. *J. Biol. Chem.* **2003**, *278*, 46668.
- (138) Murphy, M. E.; Sies, H. *Proc. Natl. Acad. Sci. U.S.A.* **1991**, *88*, 10860.
- (139) Alderton, W.; Cooper, C.; Knowles, R. *Biochem. J.* **2001**, *357*, 593.
- (140) Reisz, J. A.; Bechtold, E.; King, S. B. *Dalton Trans.* **2010**, *39*, 5203.
- (141) Donzelli, S.; Espey, M. G.; Flores-Santana, W.; Switzer, C. H.; Yeh, G. C.; Huang, J. M.; Stuehr, D. J.; King, S. B.; Miranda, K. M.; Wink, D. A. *Free Radical Bio. Med.* **2008**, *45*, 578.

- (142) Jackson, M. I.; Fields, H. F.; Lujan, T. S.; Cantrell, M. M.; Lin, J.; Fukuto, J. M. *Arch. Biochem. Biophys.* **2013**, *538*, 120.
- (143) King, S. B. *Curr. Top. Med. Chem.* **2005**, *5*, 665.
- (144) Huang, J.; Sommers, E. M.; Kim-Shapiro, D. B.; King, S. B. *J. Am. Chem. Soc.* **2002**, *124*, 3473.
- (145) Nagasawa, H. T.; DeMaster, E. G.; Redfern, B.; Shirota, F. N.; Goon, J. W. *J. Med. Chem.* **1990**, *33*, 3120.
- (146) Wong, P. S. Y.; Hyun, J.; Fukuto, J. M.; Shirota, F. N.; DeMaster, E. G.; Shoeman, D. W.; Nagasawa, H. T. *Biochemistry* **1998**, *37*, 5362.
- (147) Miranda, K. M.; Nagasawa, H. T.; Toscano, J. P. *Curr. Top. Med. Chem.* **2005**, *5*, 647.
- (148) Shafirovich, V.; Lyman, S. V. *Proc. Natl. Acad. Sci. U.S.A.* **2002**, *99*, 7340.
- (149) Piloty, O. *Ber. Dtsch. Chem. Ges.* **1896**, *29*.
- (150) Angeli, A. *Gazz. Chim. Ital.* **1896**, *26*.
- (151) Miranda, K. M.; Dutton, A. S.; Ridnour, L. A.; Foreman, C. A.; Ford, E.; Paolucci, N.; Katori, T.; Tocchetti, C. G.; Mancardi, D.; Thomas, D. D.; Espey, M. G.; Houk, K. N.; Fukuto, J. M.; Wink, D. A. *J. Am. Chem. Soc.* **2004**, *127*, 722.
- (152) Suárez, S. A.; Martí, M. A.; De Biase, P. M.; Estrin, D. A.; Bari, S. E.; Doctorovich, F. *Polyhedron* **2007**, *26*, 4673.
- (153) Paolucci, N.; Jackson, M. I.; Lopez, B. E.; Miranda, K.; Tocchetti, C. G.; Wink, D. A.; Hobbs, A. J.; Fukuto, J. M. *Pharmacol. Ther.* **2007**, *113*, 442.
- (154) Sha, X.; Isbell, T. S.; Patel, R. P.; Day, C. S.; King, S. B. *J. Am. Chem. Soc.* **2006**, *128*, 9687.
- (155) Cohen, A. D.; Zeng, B.-B.; King, S. B.; Toscano, J. P. *J. Am. Chem. Soc.* **2003**, *125*, 1444.
- (156) Guthrie, D. A.; Kim, N. Y.; Siegler, M. A.; Moore, C. D.; Toscano, J. P. *J. Am. Chem. Soc.* **2012**, *134*, 1962.
- (157) Miranda, K. M.; Katori, T.; Torres de Holding, C. L.; Thomas, L.; Ridnour, L. A.; McLendon, W. J.; Cologna, S. M.; Dutton, A. S.; Champion, H. C.; Mancardi, D.;

- Tocchetti, C. G.; Saavedra, J. E.; Keefer, L. K.; Houk, K. N.; Fukuto, J. M.; Kass, D. A.; Paolocci, N.; Wink, D. A. *J. Med. Chem.* **2005**, *48*, 8220.
- (158) Nelli, S.; Hillen, M.; Buyukafsar, K.; Martin, W. *Brit. J. Pharmacol.* **2000**, *131*, 356.
- (159) Fukuto, J. M.; Switzer, C. H.; Miranda, K. M.; Wink, D. A. *Annu. Rev. Pharmacol. Toxicol.* **2005**, *45*, 335.
- (160) Martí, M. A.; Bari, S. E.; Estrin, D. A.; Doctorovich, F. *J. Am. Chem. Soc.* **2005**, *127*, 4680.
- (161) Shen, B.; English, A. M. *Biochemistry* **2005**, *44*, 14030.
- (162) Paolocci, N.; Saavedra, W. F.; Miranda, K. M.; Martignani, C.; Isoda, T.; Hare, J. M.; Espey, M. G.; Fukuto, J. M.; Feelisch, M.; Wink, D. A.; Kass, D. A. *Proc. Natl. Acad. Sci. U.S.A.* **2001**, *98*, 10463.
- (163) Paolocci, N.; Katori, T.; Champion, H. C.; St John, M. E.; Miranda, K. M.; Fukuto, J. M.; Wink, D. A.; Kass, D. A. *Proc. Natl. Acad. Sci. U.S.A.* **2003**, *100*, 5537.
- (164) Miranda, K. M.; Katori, T.; de Holding, C. L. T.; Thomas, L.; Ridnour, L. A.; MeLendon, W. J.; Cologna, S. M.; Dutton, A. S.; Champion, H. C.; Mancardi, D.; Tocchetti, C. G.; Saavedra, J. E.; Keefer, L. K.; Houk, K. N.; Fukuto, J. M.; Kass, D. A.; Paolocci, N.; Wink, D. A. *J. Med. Chem.* **2005**, *48*, 8220.
- (165) Brain, S. D.; Grant, A. D. *Physiol. Rev.* **2004**, *84*, 903.
- (166) Paolocci, N.; Katori, T.; Belardi, D.; Tocchetti, C. G.; Miranda, K. M.; Wink, D. A.; Kass, D. A. *FASEB J* **2003**, *17*, A1252.
- (167) Tocchetti, C. G.; Wang, W.; Froehlich, J. P.; Huke, S.; Aon, M. A.; Wilson, G. M.; Di Benedetto, G.; O'Rourke, B.; Gao, W. D.; Wink, D. A.; Toscano, J. P.; Zaccolo, M.; Bers, D. M.; Valdivia, H. H.; Cheng, H. P.; Kass, D. A.; Paolocci, N. *Circ. Res.* **2007**, *100*, 96.
- (168) Cheong, E.; Tumbey, V.; Abramson, J.; Salama, G.; Stoyanovsky, D. A. *Cell Calcium* **2005**, *37*, 87.
- (169) Angelo, M.; Hausladen, A.; Singel, D. J.; Stamler, J. S. *Methods Enzymol.* **2008**, *436*, 131.
- (170) Gladwin, M. T.; Grubina, R.; Doyle, M. P. *Acc. Chem. Res.* **2009**, *42*, 157.
- (171) Berto, T. C.; Lehnert, N. *Inorg. Chem.* **2011**, *50*, 7361.

- (172) Hopmann, K. H.; Cardey, B.; Gladwin, M. T.; Kim-Shapiro, D. B.; Ghosh, A. *Chem. Eur. J.* **2011**, *17*, 6348.
- (173) Tolman, W. B. *Activation of Small Molecules: Organometallic and Bioinorganic Perspectives*; Wiley-VCH: Weinheim, 2006.
- (174) Guillard, R.; Kadish, K. M. *Chem. Rev.* **1988**, *88*, 1121.
- (175) Reeder, B. J. *Antioxid. Redox Signaling* **2010**, *13*, 1087.
- (176) Stynes, D. V.; Cleary Stynes, H.; James, B. R.; Ibers, J. A. *J. Am. Chem. Soc.* **1973**, *95*, 4087.
- (177) Wayland, B. B.; Olson, L. W. *J. Am. Chem. Soc.* **1974**, *96*, 6037.
- (178) Scheidt, W. R.; Frisse, M. E. *J. Am. Chem. Soc.* **1975**, *97*, 17.
- (179) Praneeth, V. K. K.; Näther, C.; Peters, G.; Lehnert, N. *Inorg. Chem.* **2006**, *45*, 2795.
- (180) Praneeth, V. K. K.; Neese, F.; Lehnert, N. *Inorg. Chem.* **2005**, *44*, 2570.
- (181) Goodrich, L. E.; Paulat, F.; Praneeth, V. K. K.; Lehnert, N. *Inorg. Chem.* **2010**, *49*, 6293.
- (182) Olson, L. W.; Schaeper, D.; Lançon, D.; Kadish, K. M. *J. Am. Chem. Soc.* **1982**, *104*, 2042.
- (183) Choi, I.-K.; Liu, Y.; Feng, D.; Paeng, K.-J.; Ryan, M. D. *Inorg. Chem.* **1991**, *30*, 1832.
- (184) Fujita, E.; Fajer, J. *J. Am. Chem. Soc.* **1983**, *105*.
- (185) Wei, Z.; Ryan, M. D. *Inorg. Chem.* **2010**, *49*, 6948.
- (186) Liu, Y.; DeSilva, C.; Ryan, M. D. *Inorg. Chim. Acta.* **1997**, *258*, 247.
- (187) Pellegrino, J.; Bari, S. E.; Bikiel, D. E.; Doctorovich, F. *J. Am. Chem. Soc.* **2010**, *132*, 989.
- (188) Barley, M. H.; Takeuchi, K. J.; Meyer, T. J. *J. Am. Chem. Soc.* **1986**, *108*, 5876.
- (189) Barley, M. H.; Rhodes, M. R.; Meyer, T. J. *Inorg. Chem.* **1987**, *26*, 1746.
- (190) Connelly, N. G.; Geiger, W. E. *Chem. Rev.* **1996**, *96*, 877.

- (191) Lançon, D.; Kadish, K. M. *J. Am. Chem. Soc.* **1983**, *105*, 5610.
- (192) Waleh, A.; Ho, N.; Chantranupong, L.; Loew, G. H. *J. Am. Chem. Soc.* **1989**, *111*, 2767.
- (193) Williams, P. A.; Fülöp, V.; Garman, E. F.; Saunders, N. F. W.; Ferguson, S. J.; Hajdu, J. *Nature* **1997**, *389*, 406.
- (194) Silvernail, N. J.; Olmstead, M. M.; Noll, B. C.; Scheidt, W. R. *Inorg. Chem.* **2009**, *48*, 971.
- (195) Wyllie, G. R. A.; Schulz, C. E.; Scheidt, W. R. *Inorg. Chem.* **2003**, *42*, 5722.
- (196) Rich, A. M.; Armstrong, R. S.; Ellis, P. J.; Lay, P. A. *J. Am. Chem. Soc.* **1998**, *120*, 10827.
- (197) Linder, D. P.; Rodgers, K. R. *Inorg. Chem.* **2005**, *44*, 8259.
- (198) Brucker, E. A.; Olson, J. S.; Ikeda-Saito, M.; Phillips, G. N., Jr *Proteins: Struct., Funct., and Genet.* **1998**, *30*, 352.
- (199) Copeland, D. M.; West, A. H.; Richter-Addo, G. B. *Proteins: Struct., Funct., and Genet.* **2003**, *53*, 182.
- (200) Copeland, D. M.; Soares, A. S.; West, A. H.; Richter-Addo, G. B. *J. Inorg. Biochem.* **2006**, *100*.
- (201) Pellegrino, J.; Hübner, R.; Doctorovich, F.; Kaim, W. *Chem. Eur. J.* **2011**, *17*, 7868.
- (202) Grinstaff, M. W.; Hill, M. G.; Birnbaum, E. R.; Schaefer, W. P.; Labinger, J. A.; Gray, H. B. *Inorg. Chem.* **1995**, *34*, 4896.
- (203) Bultitude, J.; Larkworthy, L. F.; Mason, J.; Povey, D. C.; Sandell, B. *Inorg. Chem.* **1984**, *23*, 3629.
- (204) Mason, J.; Larkworthy, L. F.; Moore, E. A. *Chem. Rev.* **2002**, *102*, 913.
- (205) Murphy, W. R., Jr; Takeuchi, K.; Barley, M. H.; Meyer, T. J. *Inorg. Chem.* **1986**, *25*, 1041.
- (206) Murphy, W. R., Jr; Takeuchi, K.; Meyer, T. J. *J. Am. Chem. Soc.* **1982**, *104*, 5817.
- (207) Wilson, R. D.; Ibers, J. A. *Inorg. Chem.* **1979**, *18*, 336.
- (208) Arnold, E. V.; Bohle, D. S. *Methods Enzymol.* **1996**, *269*, 41.

- (209) Bazylinski, D. A.; Goretski, J.; Hollocher, T. C. *J. Am. Chem. Soc.* **1985**, *107*, 7986.
- (210) Bazylinski, D. A.; Hollocher, T. C. *J. Am. Chem. Soc.* **1985**, *107*, 7982.
- (211) Daiber, A.; Nauser, T.; Takaya, N.; Kudo, T.; Weber, P.; Hultschig, C.; Shoun, H.; Ullrich, V. *J. Inorg. Biochem.* **2002**, *88*, 343.
- (212) Sulc, F.; Fleischer, E.; Farmer, P. J.; Ma, D.; La Mar, G. N. *J. Biol. Inorg. Chem.* **2003**, *8*, 348.
- (213) Yu, N.-T.; Kerr, E. A. *In Biological Applications of Raman Spectroscopy*; Wiley: New York, 1988; Vol. 3.
- (214) Scheidt, W. R.; Barabanschikov, A.; Pavlik, J. W.; Silvernail, N. J.; Sage, J. T. *Inorg. Chem.* **2010**, *49*, 6240.
- (215) Di Vaira, M.; Ghilardi, C. A.; Sacconi, L. *Inorg. Chem.* **1976**, *15*, 1555.
- (216) Di Vaira, M.; Tarli, A.; Stoppioni, P.; Sacconi, L. *Cryst. Struct. Comm.* **1975**, *4*, 653.
- (217) Stephens, F. S. *J. Chem. Soc. Dalton Trans.* **1972**, 2257.
- (218) Mašek, J.; Mášlová, E. *Collect. Czech. Chem. Commun.* **1974**, 39.
- (219) González Lebrero, M. C.; Scherlis, D. A.; Estiú, G. L.; Olabe, J. A.; Estrin, D. A. *Inorg. Chem.* **2001**, *40*, 4127.
- (220) Serres, R. G.; Grapperhaus, C. A.; Bothe, E.; Bill, E.; Weyhermüller, T.; Neese, F.; Wieghardt, K. *J. Am. Chem. Soc.* **2004**, *126*, 5138.
- (221) Hauser, C.; Glaser, T.; Bill, E.; Weyhermüller, T.; Wieghardt, K. *J. Am. Chem. Soc.* **2000**, *122*, 4352.
- (222) Schwane, J. D.; Ashby, M. T. *J. Am. Chem. Soc.* **2002**, *124*, 6822.
- (223) Patra, A. K.; Dube, K. S.; Sanders, B. C.; Papaefthymiou, G. C.; Conradie, J.; Ghosh, A.; Harrop, T. C. *Chem. Sci.* **2012**, *3*, 364.
- (224) Montenegro, A. C.; Amorebieta, V. T.; Slep, L. D.; Martín, D. F.; Roncaroli, F.; Murgida, D. H.; Bari, S. E.; Olabe, J. A. *Angew. Chem. Int. Ed.* **2009**, *48*, 4213.
- (225) Conradie, J.; Ghosh, A. *Inorg. Chem.* **2011**, *50*, 4223.

- (226) Turk, J.; Corbett, J. A.; Ramanadham, S.; Bohrer, A.; McDaniel, M. L. *Biochem. Biophys. Res. Commun.* **1993**, *197*, 1458.
- (227) Wong, P. S.-Y.; Hyun, J.; Fukuto, J. M.; Shiota, F. N.; DeMaster, E. G.; Shoeman, D. W.; Nagasawa, H. T. *Biochemistry* **1998**, *37*, 5362.
- (228) Doyle, M. P.; Mahapatro, S. N.; Broene, R. D.; Guy, J. K. *J. Am. Chem. Soc.* **1988**, *110*, 593.
- (229) Boulet, P.; Buchs, M.; Chermette, H.; Daul, C.; Gilardoni, F.; Rogemond, F.; Schläpfer, C. W.; Weber, J. *J. Chem. Phys. A.* **2001**, *105*, 8991.
- (230) Boulet, P.; Buchs, M.; Chermette, H.; Daul, C.; Furet, E.; Gilardoni, F.; Rogemond, F.; Schläpfer, C. W.; Weber, J. *J. Chem. Phys. A.* **2001**, *105*, 8999.
- (231) Goodrich, L. E.; Roy, S.; Alp, E. E.; Zhao, J. Y.; Hu, M. Y.; Lehnert, N. *Inorg. Chem.* **2013**, *52*, 7766.
- (232) Speelman, A. L.; Lehnert, N. *Angew. Chem. Int. Edit.* **2013**, *52*, 12283.
- (233) Hirasawa, M.; Tripathy, J. N.; Sommer, F.; Somasundaram, R.; Chung, J. S.; Nestander, M.; Kruthiventi, M.; Zabet-Moghaddam, M.; Johnson, M. K.; Merchant, S. S.; Allen, J. P.; Knaff, D. B. *Photosynth. Res.* **2010**, *103*, 67.
- (234) Imamura, S.; Terashita, M.; Ohnuma, M.; Maruyama, S.; Minoda, A.; Weber, A. P. M.; Inouye, T.; Sekine, Y.; Fujita, Y.; Omata, T.; Tanaka, K. *Plant Cell Physiol.* **2010**, *51*, 707.
- (235) Nakano, S.; Takahashi, M.; Sakamoto, A.; Morikawa, H.; Katayanagi, K. *Proteins* **2012**, *80*, 2035.
- (236) Kuznetsova, S.; Knaff, D. B.; Hirasawa, M.; Setif, P.; Mattioli, T. A. *Biochemistry* **2004**, *43*, 10765.
- (237) Kuznetsova, S.; Knaff, D. B.; Hirasawa, M.; Lagoutte, B.; Setif, P. *Biochemistry* **2004**, *43*, 510.
- (238) Judd, E. T.; Stein, N.; Pacheco, A. A.; Elliott, S. J. *Biochemistry* **2014**, *53*, 5638.
- (239) Cutruzzolà, F.; Brown, K.; Wilson, E. K.; Bellelli, A.; Arese, M.; Tegoni, M.; Cambillau, C.; Brunori, M. *Proc. Natl. Acad. Sci. U.S.A.* **2001**, *98*, 2232.
- (240) Ranghino, G.; Scorza, E.; Sjögren, T.; Williams, P. A.; Ricci, M.; Hajdu, J. *Biochemistry* **2000**, *39*, 10958.

- (241) Rinaldo, S.; Sam, K. A.; Castiglione, N.; Stelitano, V.; Arcovito, A.; Brunori, M.; Allen, J. W. A.; Ferguson, S. J.; Cutruzzola, F. *Biochem. J.* **2011**, *435*, 217.
- (242) Cheesman, M. R.; Ferguson, S. J.; Moir, J. W. B.; Richardson, D. J.; Zumft, W. G.; Thomson, A. J. *Biochemistry* **1997**, *36*, 16267.
- (243) Rinaldo, S.; Arcovito, A.; Brunori, M.; Cutruzzola, F. *J. Biol. Chem.* **2007**, *282*, 14761.
- (244) Sam, K. A.; Strampraad, M. J. F.; de Vries, S.; Ferguson, S. J. *J. Biol. Chem.* **2008**, *283*, 27403.
- (245) Kobayashi, K.; Koppenhofer, A.; Ferguson, S. J.; Watmough, N. J.; Tagawa, S. *Biochemistry* **2001**, *40*, 8542.
- (246) Zajicek, R. S.; Cartron, M. L.; Ferguson, S. J. *Biochemistry* **2006**, *45*, 11208.
- (247) Fukuto, J. M.; Carrington, S. J.; Tantillo, D. J.; Harrison, J. G.; Ignarro, L. J.; Freeman, B. A.; Chen, A.; Wink, D. A. *Chem. Res. Toxicol.* **2012**, *25*, 769.
- (248) Thomas, D. D.; Ridnour, L. A.; Isenberg, J. S.; Flores-Santana, W.; Switzer, C. H.; Donzelli, S.; Hussain, P.; Vecoli, C.; Paolocci, N.; Ambs, S. *Free Radical Bio. Med.* **2008**, *45*, 18.
- (249) Li, L.; Moore, P. *Biochem. Soc. T.* **2007**, *35*, 1138.
- (250) Moncada, S.; Higgs, E. A. *Br. J. Pharmacol.* **2006**, *147*, S193.
- (251) Wang, P. G.; Xian, M.; Tang, X. P.; Wu, X. J.; Wen, Z.; Cai, T. W.; Janczuk, A. *J. Chem. Rev.* **2002**, *102*, 1091.
- (252) Ignarro, L. J. *Nitric Oxide Biology and Pathobiology*; Academic Press: San Diego, 2000.
- (253) Koppenol, W. H. *Inorg. Chem.* **2012**, *51*, 5637.
- (254) Reichert, E. T. *Am. J. Med. Sci.* **1880**, *80*, 158.
- (255) Furchgott, R. F.; Bhadrakom, S. *J. Pharmacol. Exp. Ther.* **1953**, *108*, 129.
- (256) Thadani, U. *Am. J. Cardiovasc. Drugs* **2014**, *14*, 287.
- (257) Corti, P.; Gladwin, M. T. *Circ. Res.* **2014**, *114*, 1554.
- (258) Shiva, S.; Gladwin, M. T. *Basic Res. Cardiol.* **2009**, *104*, 113.

- (259) Shiva, S.; Sack, M. N.; Greer, J. J.; Duranski, M.; Ringwood, L. A.; Burwell, L.; Wang, X.; MacArthur, P. H.; Shoja, A.; Raghavachari, N.; Calvert, J. W.; Brookes, P. S.; Lefer, D. J.; Gladwin, M. T. *J. Exper. Med.* **2007**, *204*, 2089.
- (260) Duranski, M. R.; Greer, J. J.; Dejam, A.; Jaganmohan, S.; Hogg, N.; Langston, W.; Patel, R. P.; Yet, S. F.; Wang, X.; Kevil, C. G.; Gladwin, M. T.; Lefer, D. J. *J. Clin. Invest.* **2005**, *115*, 1232.
- (261) Crawford, J. H.; Isbell, T. S.; Huang, Z.; Shiva, S.; Chacko, B. K.; Schechter, A. N.; Darley-USmar, V. M.; Kerby, J. D.; Lang, J. D., Jr.; Kraus, D.; Ho, C.; Gladwin, M. T.; Patel, R. P. *Blood* **2006**, *107*, 566.
- (262) Kumar, D.; Branch, B. G.; Pattillo, C. B.; Hood, J.; Thoma, S.; Simpson, S.; Illum, S.; Arora, N.; Chidlow, J. H., Jr.; Langston, W.; Teng, X.; Lefer, D. J.; Patel, R. P.; Kevil, C. G. *Proc. Natl. Acad. Sci. U.S.A.* **2008**, *105*, 7540.
- (263) Cauwels, A.; Buys, E. S.; Thoonen, R.; Geary, L.; Delanghe, J.; Shiva, S.; Brouckaert, P. *J. Exp. Med.* **2009**, *206*, 2915.
- (264) Zuckerbraun, B. S.; George, P.; Gladwin, M. T. *Cardiovasc. Res.* **2011**, *89*, 542.
- (265) Zuckerbraun, B. S.; Shiva, S.; Ifedigbo, E.; Mathier, M. A.; Mollen, K. P.; Rao, J.; Bauer, P. M.; Choi, J. J.; Curtis, E.; Choi, A. M.; Gladwin, M. T. *Circulation* **2010**, *121*, 98.
- (266) Bryan, N. S.; Fernandez, B. O.; Bauer, S. M.; Garcia-Saura, M. F.; Milsom, A. B.; Rassaf, T.; Maloney, R. E.; Bharti, A.; Rodriguez, J.; Feelisch, M. *Nat. Chem. Biol.* **2005**, *1*, 290.
- (267) Cleeter, M. W.; Cooper, J. M.; Darley-USmar, V. M.; Moncada, S.; Schapira, A. H. *FEBS Lett.* **1994**, *345*, 50.
- (268) DeZfulian, C.; Raat, N.; Shiva, S.; Gladwin, M. T. *Cardiovasc. Res.* **2007**, *75*, 327.
- (269) Torres, J.; Darley-USmar, V.; Wilson, M. T. *Biochem. J.* **1995**, *312* (Pt 1), 169.
- (270) Li, H.; Liu, X.; Cui, H.; Chen, Y. R.; Cardounel, A. J.; Zweier, J. L. *J. Biol. Chem.* **2006**, *281*, 12546.
- (271) Castello, P. R.; Woo, D. K.; Ball, K.; Wojcik, J.; Liu, L.; Poyton, R. O. *Proc. Natl. Acad. Sci. U.S.A.* **2008**, *105*, 8203.
- (272) Gautier, C.; van Faassen, E.; Mikula, I.; Martasek, P.; Slama-Schwok, A. *Biochem. Biophys. Res. Commun.* **2006**, *341*, 816.

- (273) Tiso, M.; Tejero, J.; Basu, S.; Azarov, I.; Wang, X.; Simplaceanu, V.; Frizzell, S.; Jayaraman, T.; Geary, L.; Shapiro, C.; Ho, C.; Shiva, S.; Kim-Shapiro, D. B.; Gladwin, M. T. *J. Biol. Chem.* **2011**, *286*, 18277.
- (274) Petersen, M. G.; Dewilde, S.; Fago, A. *J. Inorg. Biochem.* **2008**, *102*, 1777.
- (275) Li, H.; Hemann, C.; Abdelghany, T. M.; El-Mahdy, M. A.; Zweier, J. L. *J. Biol. Chem.* **2012**, *287*, 36623.
- (276) Basu, S.; Azarova, N. A.; Font, M. D.; King, S. B.; Hogg, N.; Gladwin, M. T.; Shiva, S.; Kim-Shapiro, D. B. *J. Biol. Chem.* **2008**, *283*, 32590.
- (277) Gladwin, M. T.; Kim-Shapiro, D. B. *Blood* **2008**, *112*, 2636.
- (278) Huang, Z.; Shiva, S.; Kim-Shapiro, D. B.; Patel, R. P.; Ringwood, L. A.; Irby, C. E.; Huang, K. T.; Ho, C.; Hogg, N.; Schechter, A. N.; Gladwin, M. T. *J Clin. Invest.* **2005**, *115*, 2099.
- (279) Shiva, S.; Huang, Z.; Grubina, R.; Sun, J.; Ringwood, L. A.; MacArthur, P. H.; Xu, X.; Murphy, E.; Darley-Usmar, V. M.; Gladwin, M. T. *Circ. Res.* **2007**, *100*, 654.
- (280) Doyle, M. P.; Pickering, R. A.; DeWeert, T. M.; Hoekstra, J. W.; Pater, D. *J. Biol. Chem.* **1981**, *256*, 12393.
- (281) Ye, J.; Baldwin, R. P. *Anal. Chem.* **1988**, *60*, 2263.
- (282) Gladwin, M. T.; Grubina, R.; Doyle, M. P. *Acc. Chem. Res.* **2009**, *42*, 157.
- (283) Bryan, N. S.; Calvert, J. W.; Elrod, J. W.; Gundewar, S.; Ji, S. Y.; Lefer, D. J. *Proc. Natl. Acad. Sci. U.S.A.* **2007**, *104*, 19144.
- (284) Bryan, N. S.; Calvert, J. W.; Gundewar, S.; Lefer, D. J. *Free Radical Bio. Med.* **2008**, *45*, 468.
- (285) Dejam, A.; Hunter, C. J.; Tremonti, C.; Pluta, R. M.; Hon, Y. Y.; Grimes, G.; Partovi, K.; Pelletier, M. M.; Oldfield, E. H.; Cannon, R. O., 3rd; Schechter, A. N.; Gladwin, M. T. *Circulation* **2007**, *116*, 1821.
- (286) Gladwin, M. T.; Raat, N. J.; Shiva, S.; Dezfulian, C.; Hogg, N.; Kim-Shapiro, D. B.; Patel, R. P. *Am. J. Physiol.-Heart C* **2006**, *291*, H2026.
- (287) Huang, K. T.; Keszler, A.; Patel, N.; Patel, R. P.; Gladwin, M. T.; Kim-Shapiro, D. B.; Hogg, N. *J. Biol. Chem.* **2005**, *280*, 31126.

- (288) Hunter, C. J.; Dejam, A.; Blood, A. B.; Shields, H.; Kim-Shapiro, D. B.; Machado, R. F.; Tarekegn, S.; Mulla, N.; Hopper, A. O.; Schechter, A. N.; Power, G. G.; Gladwin, M. T. *Nat. Med.* **2004**, *10*, 1122.
- (289) Raat, N. J.; Noguchi, A. C.; Liu, V. B.; Raghavachari, N.; Liu, D.; Xu, X.; Shiva, S.; Munson, P. J.; Gladwin, M. T. *Free Radical Bio. Med.* **2009**, *47*, 510.
- (290) Webb, A.; Bond, R.; McLean, P.; Uppal, R.; Benjamin, N.; Ahluwalia, A. *Proc. Natl. Acad. Sci. U.S.A.* **2004**, *101*, 13683.
- (291) Rassaf, T.; Flogel, U.; Drexhage, C.; Hendgen-Cotta, U.; Kelm, M.; Schrader, J. *Circ. Res.* **2007**, *100*, 1749.
- (292) Shiva, S.; Rassaf, T.; Patel, R. P.; Gladwin, M. T. *Cardiovasc. Res.* **2011**, *89*, 566.
- (293) Azizi, F.; Kielbasa, J. E.; Adeyiga, A. M.; Maree, R. D.; Frazier, M.; Yakubu, M.; Shields, H.; King, S. B.; Kim-Shapiro, D. B. *Free Radical Bio. Med.* **2005**, *39*, 145.
- (294) Cassoly, R.; Gibson, Q. *J. Mol. Biol.* **1975**, *91*, 301.
- (295) Eich, R. F.; Li, T.; Lemon, D. D.; Doherty, D. H.; Curry, S. R.; Aitken, J. F.; Mathews, A. J.; Johnson, K. A.; Smith, R. D.; Phillips, G. N., Jr.; Olson, J. S. *Biochemistry* **1996**, *35*, 6976.
- (296) Kharitonov, V. G.; Sharma, V. S.; Magde, D.; Koesling, D. *Biochemistry* **1997**, *36*, 6814.
- (297) Luchsinger, B. P.; Rich, E. N.; Yan, Y.; Williams, E. M.; Stamler, J. S.; Singel, D. *J. J. Inorg. Biochem.* **2005**, *99*, 912.
- (298) Moore, E. G.; Gibson, Q. H. *J. Biol. Chem.* **1976**, *251*, 2788.
- (299) Nienhaus, K.; Palladino, P.; Nienhaus, G. U. *Biochemistry* **2008**, *47*, 935.
- (300) Cooper, C. E. *Biochim. Biophys. Acta* **1999**, *1411*, 290.
- (301) Moncada, S.; Palmer, R. M. J.; Higgs, E. A. *Pharmacol. Rev.* **1991**, *43*, 109.
- (302) Morris, R. J.; Gibson, Q. H. *J. Biol. Chem.* **1980**, *255*, 8050.
- (303) Sharma, V. S.; Traylor, T. G.; Gardiner, R.; Mizukami, H. *Biochemistry* **1987**, *26*, 3837.
- (304) Angelo, M.; Singel, D. J.; Stamler, J. S. *Proc. Natl. Acad. Sci. U.S.A.* **2006**, *103*, 8366.

- (305) Basu, S.; Grubina, R.; Huang, J.; Conradie, J.; Huang, Z.; Jeffers, A.; Jiang, A.; He, X.; Azarov, I.; Seibert, R.; Mehta, A.; Patel, R.; King, S. B.; Hogg, N.; Ghosh, A.; Gladwin, M. T.; Kim-Shapiro, D. B. *Nat. Chem. Biol.* **2007**, *3*, 785.
- (306) Fernandez, B. O.; Ford, P. C. *J. Am. Chem. Soc.* **2003**, *125*, 10510.
- (307) Fernandez, B. O.; Lorkovic, I. M.; Ford, P. C. *Inorg. Chem.* **2003**, *42*, 2.
- (308) Hopmann, K. H.; Cardey, B.; Gladwin, M. T.; Kim-Shapiro, D. B.; Ghosh, A. *Chem. Eur. J.* **2011**, *17*, 6348.
- (309) Jee, J. E.; van Eldik, R. *Inorg. Chem.* **2006**, *45*, 6523.
- (310) Jeffers, A.; Xu, X.; Huang, K. T.; Cho, M.; Hogg, N.; Patel, R. P.; Kim-Shapiro, D. B. *Comp. Biochem. Phys. A.* **2005**, *142*, 130.
- (311) Cantu-Medellin, N.; Vitturi, D. A.; Rodriguez, C.; Murphy, S.; Dorman, S.; Shiva, S.; Zhou, Y.; Jia, Y.; Palmer, A. F.; Patel, R. P. *Nitric Oxide-Biol. Ch.* **2011**, *25*, 59.
- (312) Blood, A. B.; Tiso, M.; Verma, S. T.; Lo, J.; Joshi, M. S.; Azarov, I.; Longo, L. D.; Gladwin, M. T.; Kim-Shapiro, D. B.; Power, G. G. *J. Physiol.-Heart C* **2009**, *296*, H237.
- (313) Lancaster, J. R. *Proc. Natl. Acad. Sci. U.S.A.* **1994**, *91*, 8137.
- (314) Lancaster, J. R., Jr. *Methods Enzymol.* **1996**, *268*, 31.
- (315) Vanin, A. F.; Muller, B.; Alencar, J. L.; Lobysheva, II; Nepveu, F.; Stoclet, J. C. *Nitric Oxide-Biol. Ch.* **2002**, *7*, 194.
- (316) Nauser, T.; Casi, G.; Koppenol, W. H.; Schöneich, C. *J. Phys. Chem. B.* **2008**, *112*, 15034.
- (317) Hofstetter, D.; Nauser, T.; Koppenol, W. H. *Chem. Res. Toxicol.* **2010**, *23*, 1596.
- (318) Gladwin, M. T.; Shelhamer, J. H.; Schechter, A. N.; Pease-Fye, M. E.; Waclawiw, M. A.; Panza, J. A.; Ognibene, F. P.; Cannon, R. O., 3rd *Proc. Natl. Acad. Sci. U.S.A.* **2000**, *97*, 11482.
- (319) Luchsinger, B. P.; Rich, E. N.; Gow, A. J.; Williams, E. M.; Stamler, J. S.; Singel, D. J. *Proc. Natl. Acad. Sci. U.S.A.* **2000**, *97*, 11482. **2003**, *100*, 461.
- (320) Katori, T.; Tocchetti, C. G.; Miranda, K. M.; Mancardi, D.; Toscano, J. P.; Wink, D. A.; Hogg, N.; Paolocci, N. *Circulation* **2004**, *110*, 31.

- (321) Nasri, H.; Goodwin, J. A.; Scheidt, W. R. *Inorg. Chem.* **1990**, *29*, 185.
- (322) Finnegan, M. G.; Lappin, A. G.; Scheidt, W. R. *Inorg. Chem.* **1990**, *29*, 181.
- (323) Nasri, H.; Wang, Y.; Huynh Boi, H.; Walker, F. A.; Scheidt, W. R. *Inorg. Chem.* **1991**, *30*, 1483.
- (324) Frangione, M.; Port, J.; Baldiwala, M.; Judd, A.; Galley, J.; DeVega, M.; Linna, K.; Caron, L.; Anderson, E.; Goodwin, J. A. *Inorg. Chem.* **1997**, *36*, 1904.
- (325) Nasri, H.; Haller, K. J.; Wang, Y.; Huynh Boi, H.; Scheidt, W. R. *Inorg. Chem.* **1992**, *31*, 3459.
- (326) Ellison, M. K.; Schulz, C. E.; Scheidt, W. R. *Inorg. Chem.* **1998**, *38*, 100.
- (327) Kurtikyan, T. S.; Hovhannisyanyan, A. A.; Iretskii, A. V.; Ford, P. C. *Inorg. Chem.* **2009**, *48*, 11236.
- (328) Kurtikyan, T. S.; Hovhannisyanyan, A. A.; Hakobyan, M. E.; Patterson, J. C.; Iretskii, A.; Ford, P. C. *J. Am. Chem. Soc.* **2007**, *129*, 3576.
- (329) Novozhilova, I. V.; Coppens, P.; Lee, J.; Richter-Addo, G. B.; Bagley, K. A. *J. Am. Chem. Soc.* **2006**, *128*, 2093.
- (330) Chi, Y.; Chen, J.; Aoki, K. *Inorg. Chem.* **2004**, *43*, 8437.
- (331) Fernandes, J. B.; Feng, D.; Chang, A.; Keyser, A.; Ryan, M. D. *Inorg. Chem.* **1986**, *25*, 2606.
- (332) Nasri, H.; Wang, Y.; Huynh, B. H.; Scheidt, W. R. *J. Am. Chem. Soc.* **1991**, *113*, 717.
- (333) Nasri, H.; Ellison, M. K.; Chen, S.; Huynh, B. H.; Scheidt, W. R. *J. Am. Chem. Soc.* **1997**, *119*, 6274.
- (334) Nasri, H.; Ellison, M. K.; Shang, M.; Schulz, C. E.; Scheidt, W. R. *Inorg. Chem.* **2004**, *43*, 2932.
- (335) Nasri, H.; Ellison, M. K.; Krebs, C.; Huynh, B. H.; Scheidt, W. R. *J. Am. Chem. Soc.* **2000**, *122*, 10795.
- (336) Nasri, H.; Haller, K. J.; Wang, Y.; Hunyh, B. H.; Scheidt, W. R. *Inorg. Chem.* **1992**, *31*, 3459.
- (337) Schappacher, M.; Ricard, L.; Fischer, J.; Weiss, R.; Bill, E.; Montiel-Montoya, R.; Winkler, H.; Trautwein, A. X. *Eur. J. Biochem.* **1987**, *168*, 419.

- (338) Byrn, M. P.; Strouse, C. E. *J. Am. Chem. Soc.* **1981**, *103*, 2633.
- (339) Kurtikyan, T. S.; Ford, P. C. *Angew. Chem. Int. Ed.* **2006**, *45*, 492.
- (340) Kurtikyan, T. S.; Hovhannisyanyan, A. A.; Gulyan, G. M.; Ford, P. C. *Inorg. Chem.* **2007**, *46*, 7024.
- (341) Paulat, F.; Praneeth, V. K.; Nather, C.; Lehnert, N. *Inorg. Chem.* **2006**, *45*, 2835.
- (342) Boso, B.; Debrunner, P. G.; Wagner, G. C.; Inubushi, T. *Biochim. Biophys. Acta* **1984**, *791*, 244.
- (343) Siegbahn, P. E. M.; Blomberg, M. R. A. *Chem. Rev.* **2000**, *100*, 421.
- (344) Solomon, E. I.; Lowery, M. D. *Science* **1993**, *259*, 1575.
- (345) Conradie, J.; Ghosh, A. *Inorg. Chem.* **2006**, *45*, 4902.
- (346) Yi, J.; Safo, M. K.; Richter-Addo, G. B. *Biochemistry* **2008**, *47*, 8247.
- (347) Yi, J.; Thomas, L. M.; Richter-Addo, G. B. *Angew. Chem. Int. Edit.* **2012**, *51*, 3625.
- (348) Silaghi-Dumitrescu, R.; Svistunenko, D. A.; Cioloboc, D.; Bischin, C.; Scurtu, F.; Cooper, C. E. *Nitric oxide-Biol. Ch.* **2014**, *42*, 32.
- (349) Fernandez, B. O.; Lorkovic, I. M.; Ford, P. C. *Inorg. Chem.* **2004**, *43*, 5393.
- (350) Gwost, D.; Caulton, K. G. *Inorg. Chem.* **1973**, *12*, 2095.
- (351) Chien, J. C. *J. Am. Chem. Soc.* **1969**, *91*, 2166.
- (352) Ford, P. C.; Lorkovic, I. M. *Chem. Rev.* **2002**, *102*, 993.
- (353) Reichenbach, G.; Sabatini, S.; Palombari, R.; Palmerini, C. A. *Nitric Oxide-Biol. Ch.* **2001**, *5*, 395.
- (354) Cabail, M. Z.; Pacheco, A. A. *Inorg. Chem.* **2003**, *42*, 270.
- (355) Hoshino, M.; Maeda, M.; Konishi, R.; Seki, H.; Ford, P. C. *J. Am. Chem. Soc.* **1996**, *118*, 5702.
- (356) Tao, L.; Gao, E.; Bryan, N. S.; Qu, Y.; Liu, H. R.; Hu, A.; Christopher, T. A.; Lopez, B. L.; Yodoi, J.; Koch, W. J.; Feelisch, M.; Ma, X. L. *Proc. Natl. Acad. Sci. U.S.A.* **2004**, *101*, 11471.

- (357) Ford, P. C.; Fernandez, B. O.; Lim, M. D. *Chem. Rev.* **2005**, *105*, 2439.
- (358) Cheng, L.; Powell, D. R.; Khan, M. A.; Richter-Addo, G. B. *Chem. Commun.* **2000**, 2301.
- (359) Castro, C. E. *J. Am. Chem. Soc.* **1996**, *118*, 3984.
- (360) O'Shea, S. K.; Wang, W.; Wade, R. S.; Castro, C. E. *J. Org. Chem.* **1996**, *61*, 6388.
- (361) O'Shea, S.; Wall, T.; Lin, D. *Transition Met. Chem.* **2007**, *32*, 514.
- (362) Gupta, V.; Carroll, K. S. *Biochim. Biophys. Acta* **2014**, *1840*, 847.
- (363) Poole, L. B.; Karplus, P. A.; Claiborne, A. *Annu Rev Pharmacol* **2004**, *44*, 325.
- (364) Heinecke, J.; Ford, P. C. *J. Am. Chem. Soc.* **2010**, *132*, 9240.
- (365) Khin, C.; Heinecke, J.; Ford, P. C. *J. Am. Chem. Soc.* **2008**, *130*, 13830.
- (366) Holm, R. H. *Chem. Rev.* **1987**, *87*, 1401.
- (367) Suárez, S. n. A.; Fonticelli, M. H.; Rubert, A. A.; de la Llave, E.; Scherlis, D. n.; Salvarezza, R. C.; Martí, M. A.; Doctorovich, F. *Inorg. Chem.* **2010**, *49*, 6955.
- (368) Miljkovic, J.; Kenkel, I.; Ivanovic-Burmazovic, I.; Filipovic, M. R. *Angew. Chem. Int. Ed.* **2013**, *52*, 12061.
- (369) Filipovic, M. R.; Miljkovic, J. L.; Nauser, T.; Royzen, M.; Klos, K.; Shubina, T.; Koppenol, W. H.; Lippard, S. J.; Ivanović-Burmazović, I. *J. Am. Chem. Soc.* **2012**, *134*, 12016.
- (370) Ching, W.-M.; Chuang, C.-H.; Wu, C.-W.; Peng, C.-H.; Hung, C.-H. *J. Am. Chem. Soc.* **2009**, *131*, 7952.
- (371) López, J. P.; Heinemann, F. W.; Prakash, R.; Hess, B. A.; Horner, O.; Jeandey, C.; Oddou, J.-L.; Latour, J.-M.; Grohmann, A. *Chem. Eur. J.* **2002**, *8*, 5709.
- (372) Matson, E. M.; Park, Y. J.; Fout, A. R. *J. Am. Chem. Soc.* **2014**, *136*, 17398.
- (373) Matson, E. M.; Bertke, J. A.; Fout, A. R. *Inorg. Chem.* **2014**, *53*, 4450.
- (374) Weber, B.; Kapplinger, I.; Gorls, H.; Jager, E. G. *Eur. J. Inorg. Chem.* **2005**, 2794.
- (375) Ankers, D. L.; Fanning, J. C. *Polyhedron* **2001**, *20*, 623.

- (376) Hematian, S.; Siegler, M. A.; Karlin, K. D. *J Biol. Inorg. Chem.* **2014**, *19*, 515.
- (377) Patra, A. K.; Afshar, R. K.; Rowland, J. M.; Olmstead, M. M.; Mascharak, P. K. *Angew. Chem. Int. Ed.* **2003**, *42*, 4517.
- (378) Patra, A. K.; Rowland, J. M.; Marlin, D. S.; Bill, E.; Olmstead, M. M.; Mascharak, P. K. *Inorg. Chem.* **2003**, *42*, 6812.
- (379) Feig, A. L.; Bautista, M. T.; Lippard, S. J. *Inorg. Chem.* **1996**, *35*, 6892.
- (380) Rose, M. J.; Patra, A. K.; Olmstead, M. M.; Mascharak, P. K. *Inorg. Chim. Acta* **2010**, *363*, 2715.
- (381) Afshar, R. K.; Eroy-Reveles, A. A.; Olmstead, M. M.; Mascharak, P. K. *Inorg. Chem.* **2006**, *45*, 10347.

CHAPTER 2

SYNTHESIS, PROPERTIES, AND REACTIVITY OF A SERIES OF NON-HEME {FeNO}^{7/8} COMPLEXES: IMPLICATIONS FOR Fe-NITROXYL COORDINATION¹

¹ B. C. Sanders, A. K. Patra, and T. C. Harrop *J. Inorg. Biochem.*, **2013**, *118*, 115-127.
Reprinted here with permission of Elsevier Publishing

2.1 Abstract

The biochemical properties of nitroxyl (HNO/NO⁻) are distinct from nitric oxide (NO). Metal centers, particularly Fe, appear as suitable sites of HNO activity, both for generation and targeting. Furthermore, reduced Fe-NO⁻/Fe-HNO or {FeNO}⁸ (Enemark-Feltham notation) species offer unique bonding profiles that are of fundamental importance. Given the unique chemical properties of {FeNO}⁸ systems, we describe herein the synthesis and properties of {FeNO}⁷ and {FeNO}⁸ non-heme complexes containing pyrrole donors that display heme-like properties, namely [Fe(LN₄^R)(NO)] (R = C₆H₄ or Ph for **3**; and R = 4,5-Cl₂C₆H₂ or PhCl for **4**) and K[Fe(LN₄^R)(NO)] (R = Ph for **5**; R = PhCl for **6**). X-ray crystallography establishes that the Fe-N-O angle is ~ 155° for **3**, which is atypical for low-spin square-pyramidal {FeNO}⁷ species. Both **3** and **4** display ν_{NO} at ~ 1700 cm⁻¹ in the IR and reversible diffusion-controlled cyclic voltammograms (CVs) (E_{1/2} = ~ -1.20 V vs. Fc/Fc⁺ in MeCN) suggesting that the {FeNO}⁸ compounds **5** and **6** are stable on the CV timescale. Reduction of **3** and **4** with stoichiometric KC₈ provided the {FeNO}⁸ compounds **5** and **6** in near quantitative yield, which were characterized by the shift in ν_{NO} to 1667 and ~ 1580 cm⁻¹, respectively. While ν_{NO} for **6** is consistent with FeNO reduction, ν_{NO} for **5** appears more indicative of ligand-based reduction. Complexes **5** and **6** are compared to the previously reported {FeNO}⁸ complex, [Fe(LN₄)(NO)]⁻ (**7**). Reactivity studies of **5** and **6** demonstrate HNO-like chemistry in their reactions with ferric porphyrins [Fe^{III}(TPP)X] (X = Cl⁻, OTf⁻) to form [Fe(TPP)(NO)] in stoichiometric yield via a transnitrosylation pathway. Moreover, the reactivity of {FeNO}^{7/8} compounds with stoichiometric *p*-chlorobenzenethiol results in the formation of dinitrosyl iron complexes (DNICs) in an oxidation-state dependent manner.

2.2 Introduction

The one-electron reduced analogue of nitric oxide (NO•), termed a nitroxyl or nitrosyl hydride (HNO or NO⁻ depending on the pH; pK_a = 11.6),^{1,2} has received special attention of late including a recent thematic issue of the *Journal of Inorganic Biochemistry* (2013). Most research on this enigmatic inorganic small molecule stems from its potential as a therapeutic.³ For example, HNO has been shown to increase myocardial contractility, i.e., the strength of heart muscle tissue, and thus represents a promising drug for heart failure.⁴⁻⁶ In fact, HNO is already clinically approved for other disease treatments. This includes the HNO-donor molecule cyanamide (*N*-hydroxycyanamide is the actual HNO-donor), which has shown to be an effective anti-alcoholism drug by disturbing alcohol metabolism through inhibiting the enzyme aldehyde dehydrogenase.^{7,8} The mechanism of action of HNO appears to be through its interactions with thiol-containing biomolecules,⁹⁻¹¹ and ferric heme proteins.^{1,12-16} While the endogenous production of HNO has not been clearly established, there is evidence of its formation from nitric oxide synthase (NOS) in the absence of its biopterin cofactor.¹⁷ Additionally, iron-coordinated HNO/NO⁻ are proposed intermediates of the enzymes involved in denitrification, namely nitrite reductase (NiR) and nitric oxide reductase (NOR).^{12,18-21} However, the basic chemistry and biology of this small molecule is challenging to study. The short half-life of HNO, due to the self-condensation reaction to form nitrous oxide (N₂O) and water, necessitates the use of reliable HNO-donor molecules to understand its fundamental biochemical reactions.^{1,3,14,17,22,23} The most commonly employed HNO-donors are Angeli's salt (Na₂N₂O₃),^{24,25} derivatives of Piloty's acid (sulfohydroxamic acids),^{3,26} and others^{27,28} making this quite an active area of research in the HNO field. As such, there still remains much to be answered in terms of the chemistry and biology of HNO.

Table 2.1. Electrochemical and Spectroscopic Data of {FeNO}⁸ Systems.

Complex	$E_{1/2}$ (V) ^a	ν_{NO} (cm ⁻¹)	$\Delta\nu_{\text{NO}}$ (cm ⁻¹) ^b	Ref
[Fe(LN ₄ ^{Ph})(NO)] ⁻ (5)	-0.83 ^c	1667 ^d	-43	this work
[Fe(LN ₄ ^{PhCl})(NO)] ⁻ (6)	-0.76 ^c	~1580 ^d	-140	this work
[Fe(LN ₄ ^{Pr})(NO)] ⁻ (7)	-0.98 ^c	1604 ^d	-100	43
[Fe(TPP)(NO)] ⁻	-0.93 ^e	1496 ^f	-185	31,33
[Fe(OEP)(NO)] ⁻	-1.08 ^g	1441 ^f	-229	59
[Fe(TFPPBr ₈)(NO)] ⁻	-0.19 ^e	~1550 ^d	-176	34
<i>trans</i> -[Fe(NO)(cyclam-ac)]	-0.99 ^c	1271 ^c	-336	42
[Fe(CN) ₅ (HNO)] ³⁻	-1.00 ^h	1380, 1304 ^h	-268	41

^aData represents the $E_{1/2}$ value for the {FeNO}^{7/8} redox couple employing the isolated {FeNO}⁷ complexes and normalized to the saturated calomel reference electrode (SCE) based on information found in Geiger.²⁹ ^bDenotes the change in N-O stretching frequency upon reduction from {FeNO}⁷-to-{FeNO}⁸. ^cMeCN. ^dKBr. ^eCH₂Cl₂. ^fTHF-d₈. ^gTHF. ^hH₂O.

First-row transition metals, especially iron, appear to be among the most likely sites for the potential endogenous generation and targets of HNO.^{1,3,12,15,17,18,30} Metal-NO complexes are typically defined by the notation of Enemark and Feltham (E-F notation) that describes the total number of electrons in this delocalized bond as a post-superscript, designated as {MNO}ⁿ.³¹ Iron nitroxy complexes proposed to form in denitrifying enzymes are thus classified as {FeNO}⁸ or {FeHNO}⁸ depending on the pH. Despite their importance in defining the fundamental coordination chemistry of HNO with Fe in biology, there remains a paucity of information on this class of iron-nitrosyls.

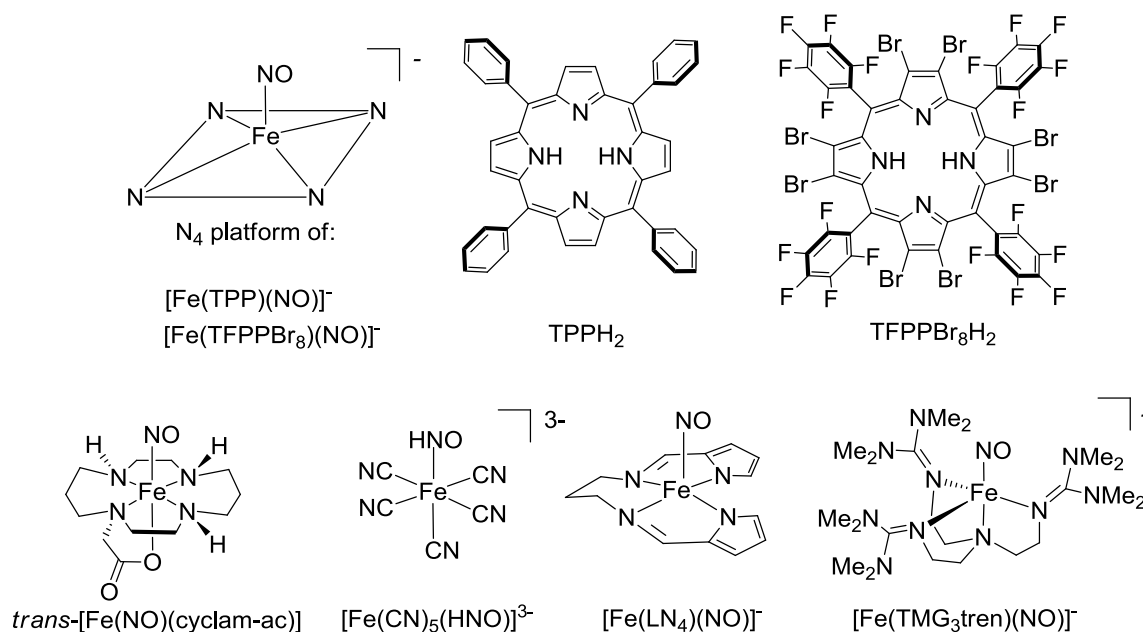


Figure 2.1 Representative structures of reported low molecular weight $\{Fe(H)NO\}^8$ coordination complexes.

The pioneering work by Kadish and Ryan on the $\{FeNO\}^8$ complexes of tetraphenylporphyrin (TPP) and octaethylporphyrin (OEP) represent the first foray into this unique E-F notation (Fig. 2.1, Table 1).³²⁻³⁴ Both $[Fe(TPP)(NO)]^-$ and $[Fe(OEP)(NO)]^-$ were studied *in situ* by spectroelectrochemistry where they displayed reversible $\{FeNO\}^7/\{FeNO\}^8$ redox couples at relatively low potentials (~ -1 V vs. SCE) in a variety of solvents (Table 1).³²⁻³⁴ While these derivatives were never isolated as discrete solids (even after exhaustive electrolysis), vibrational data (Table 1) was obtained on these systems, which exhibited NO stretching frequencies (ν_{NO}) at ~ 1500 cm^{-1} .³² The first and only isolated heme $\{FeNO\}^8$ analogue, $[Co(Cp)_2][Fe(TFPPBr_8)(NO)]$ (Fig. 2.1), was reported in 2010 by Doctorovich and coworkers.^{35,36} Extensive halogenation of the TPP framework resulted in a significant stabilization of this $\{FeNO\}^8$ derivative and is represented by the cathodic shift in $E_{1/2}$ to -0.20 V (vs. SCE in CH_2Cl_2) and corresponding blue-shift in ν_{NO} to ~ 1550 cm^{-1} from the TPP derivative.³⁵ Additional theoretical work by Lehnert and Rodgers have also helped establish the

structural and spectroscopic features of heme $\{\text{Fe}(\text{H})\text{NO}\}^8$ complexes although no small molecule has been characterized by any structural methods.^{37,38} Farmer's group, however, was successful in obtaining structural information on the $\{\text{FeHNO}\}^8$ complex with myoglobin, which is apparently very stable.³⁹⁻⁴¹ The X-ray absorption experiments revealed Fe-N and N-O lengths of 1.82 and 1.24 Å, respectively, with a severely bent Fe-N-O angle of 131°. ³⁹ These values were largely in agreement with theoretical calculations for small molecules with diamagnetic ground states. Non-heme examples of $\{\text{FeNO}\}^8$ are even rarer with a total of four such reported complexes,^{42,43} to date (2015) and only one being isolable.⁴⁴ The extensive spectroscopic studies by Wieghardt on $[\text{Fe}(\text{cyclam-ac})(\text{NO})]$ represent the first reported non-heme derivative.⁴³ While these studies were performed on *in situ* generated material at low temperature, they were the first to include Mössbauer studies on an $\{\text{FeNO}\}^8$ complex (δ : 0.41 mm/s, ΔE_Q : 1.69 mm/s) and report the lowest ν_{NO} (1271 cm^{-1}) of all $\{\text{FeNO}\}^8$ complexes.⁴³ These values were consistent with a low-spin (LS) Fe(II) ($S = 0$) coordinated to singlet $^1\text{NO}^-$ ($S = 0$). The IR value is in-line with another non-heme $\{\text{FeHNO}\}^8$ complex, $[\text{Fe}(\text{CN})_5(\text{HNO})]^{3-}$ (Fig. 2.1), which displays a ν_{NO} of 1380 cm^{-1} .⁴² The only non-heme protein $\{\text{FeNO}\}^8$ example has been produced by cryoreduction of the $\{\text{FeNO}\}^7$ adduct of the taurine/ α -ketoglutarate dioxygenase (TauD) enzyme.⁴⁵ This study was the first and is still the only to report a paramagnetic $\{\text{FeNO}\}^8$ species from an extensive theoretical calibration of valid bonding models with experimental Mössbauer parameters (δ : 1.07 mm/s, ΔE_Q : 2.39 mm/s). These results contrast those obtained for $[\text{Fe}(\text{cyclam-ac})(\text{NO})]$ due to the triplet ground state of TauD- $\{\text{FeNO}\}^8$ that has been assigned as a high-spin (HS) Fe(II) ($S = 2$) antiferromagnetically coupled to triplet $^3\text{NO}^-$ ($S = 1$). Moreover, the first $S = 1$ $\{\text{FeNO}\}^8$ complex was reported by Lehnert, namely $[\text{Fe}(\text{TMG}_3\text{tren})(\text{NO})](\text{OTf})$ (Fig. 2.1). Similar to TauD, it was characterized as HS Fe ($S = 2$) antiferromagnetically-coupled

to an $S = 1$ NO^- ligand.⁴⁶ This small collection of reported $\{\text{Fe}(\text{H})\text{NO}\}^8$ complexes has led to some general properties of $\{\text{FeNO}\}^8$: (i) the preference of $S = 0$ (diamagnetic) ground states (TauD and $[\text{Fe}(\text{TMG3tren})(\text{NO})](\text{OTf})$ being the only outliers) suggestive of a coordinated singlet nitroxyl or nitroxyl anion (^1HNO or $^1\text{NO}^-$); (ii) ν_{NO} values $\sim 1500\text{ cm}^{-1}$ for heme; $\sim 1300\text{ cm}^{-1}$ for non-heme with the exception of MbHNO (ν_{NO} : 1385 cm^{-1})^{39,47}; and (iii) low $E_{1/2}$ values for the $\{\text{FeNO}\}^7/\{\text{FeNO}\}^8$ redox couple $\sim -1\text{ V}$ (vs. SCE) with one noted exception in $[\text{Fe}(\text{TPFFBr}_8)(\text{NO})]$. Although several theoretical and spectroscopic examinations have shed some insight on the elusive $\{\text{FeNO}\}^8$ species, the reactivity of these systems has not been thoroughly explored.

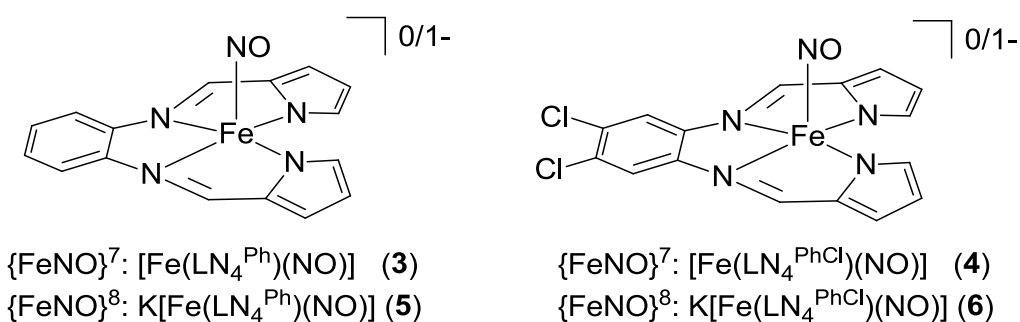


Figure 2.2 Iron nitrosyl complexes reported in this work.

As part of our continuing efforts to establish the defining features of this unique class of iron-nitrosyls and a means of understanding biological Fe-nitroxyl interactions, we describe herein the synthesis and properties of several iron coordination complexes utilizing a heme-like diimine/dipyrroloide N_4 supporting ligand, namely $(\text{Et}_4\text{N})[\text{Fe}(\text{LN}_4^{\text{Ph}})\text{Cl}]$ (1), $(\text{Et}_4\text{N})[\text{Fe}(\text{LN}_4^{\text{PhCl}})\text{Cl}]$ (2), $[\text{Fe}(\text{LN}_4^{\text{Ph}})(\text{NO})]$ (3), $[\text{Fe}(\text{LN}_4^{\text{PhCl}})(\text{NO})]$ (4), $\text{K}[\text{Fe}(\text{LN}_4^{\text{Ph}})(\text{NO})]$ (5), and $\text{K}[\text{Fe}(\text{LN}_4^{\text{PhCl}})(\text{NO})]$ (6) (Figure 2.2). We previously published a detailed account of the

synthesis and properties of the first isolable non-heme $\{\text{FeNO}\}^8$ complex, $[\text{Co}(\text{Cp}^*)_2][\text{Fe}(\text{LN}_4^{\text{Pr}})(\text{NO})]$ (**7**), where we established its nitroxyl-like reactivity with met-myoglobin under pseudo-physiological conditions.⁴⁴ Seeking to add to the list of isolable $\{\text{FeNO}\}^8$ complexes, we describe in this work new $\{\text{FeNO}\}^8$ complexes based on similar ligand backbones with subtle electronic/structural differences as a logical extension of our previous study. The objective of the present contribution was to define new synthetic strategies to access Fe-nitroxyls and to understand the fundamental spectroscopic, structural, and reaction chemistry of isolable $\{\text{FeNO}\}^8$ systems. The long-term goal is to utilize this knowledge in (i) establishing spectroscopic benchmarks for Fe-(H)NO intermediates traversed in biological denitrification and (ii) the development of metal-based HNO donors with therapeutic applications.

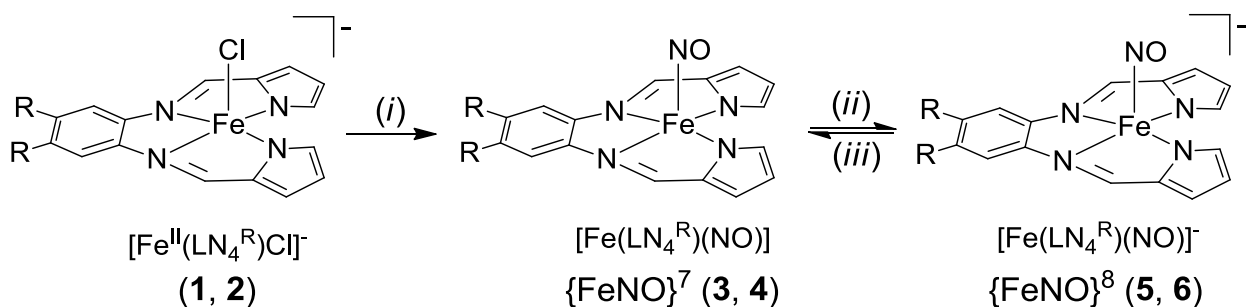
2.3 Results and Discussion

2.3.1 Synthesis of $\{\text{FeNO}\}^7$ complexes

Coordination of HNO or its anion to Fe has been proposed in several heme and non-heme systems as described previously.^{32,33,35,36,42-45,48} Although the list is sparse, the collective use of porphyrin and cyclam N-ligands has been a popular choice in the construction of $\{\text{FeNO}\}^8$ complexes. In this regard, we chose to utilize non-macrocyclic but pseudo-planar N_4 -ligand platforms with electronically variable peripheral atoms, denoted as $\text{LN}_4^{\text{R}}\text{H}_2$ (H represents dissociable pyrrole protons; R is defined above), for the synthesis of FeNO complexes in this work. The presence of the pyrrolide N-donors in these ligand frames replicate the electronic properties provided by porphyrins/hemes, but in a non-macrocyclic, i.e., non-heme environment. These ligands thus represent hybrid heme/non-heme constructs that would allow one to achieve $\{\text{FeNO}\}^8$ with the relatively weak π -basic pyrrolide-N, but with the coordination flexibility of a

non-heme system. Indeed, such ligands have been used in the construction of high-valent iron-oxos^{49,50} and vanadium-N₂O⁵¹ coordination complexes. Collectively, our strategy was to synthesize {FeNO}⁷ complexes by introduction of NO(g) to Fe(II) precursor complexes, namely (Et₄N)[Fe(LN₄^R)Cl] (**1** and **2**), and then reduce the {FeNO}⁷ species (**3** and **4**) chemically or electrochemically to obtain the {FeNO}⁸ complexes (**5** and **6**, Scheme 2.1).

Scheme 2.1. Synthetic Routes for {FeNO}^{7/8} Complexes.^a



^a (i) NO(g), MeCN, RT; (ii) KC₈, acetone, RT or [Co(Cp*)₂], toluene, RT; (iii) FcPF₆, MeCN, RT. R groups defined in Figure 2.2.

The $\{\text{FeNO}\}^7$ complexes were synthesized by direct $\text{NO}(\text{g})$ purge into MeCN solutions of the precursor molecules, $(\text{Et}_4\text{N})[\text{Fe}(\text{LN}_4^{\text{Ph}})\text{Cl}]$ (**1**) and $(\text{Et}_4\text{N})[\text{Fe}(\text{LN}_4^{\text{PhCl}})\text{Cl}]$ (**2**), to afford $[\text{Fe}(\text{LN}_4^{\text{Ph}})(\text{NO})]$ (**3**) and $[\text{Fe}(\text{LN}_4^{\text{PhCl}})(\text{NO})]$ (**4**), respectively, as red-brown solids in ~80% yield at RT (Scheme 2.1). Complexes **3** and **4** readily precipitated from MeCN upon formation, which allowed for straightforward isolation and purification of the $\{\text{FeNO}\}^7$ product. Particularly, **3** precipitated as a fine microcrystalline solid due to its partial solubility in MeCN, whereas **4** came out of solution as an amorphous powder with limited MeCN solubility. Complexes **3** and **4** appear to be relatively stable with respect to air or excess $\text{NO}(\text{g})$ purge and thus can be handled safely under ambient conditions.

2.3.2 X-ray crystal structure of $[\text{Fe}(\text{LN}_4^{\text{Ph}})(\text{NO})]$ (**3**)

Single crystals of $\{\text{FeNO}\}^7$ complex **3** were grown from slow diffusion of pentane into a toluene solution of **3** at $-20\text{ }^\circ\text{C}$ over the course of three days. There are two unique molecules in the asymmetric unit of **3** which are nearly isostructural (Fig. 2.1 and S1) and their metric parameters are reported below (Table 2.2) and the supporting information (Table S2). No significant close contacts are observed between the molecules; however, there appears to be a weak interaction between the nitrosyl N (N5) of one molecule and the phenyl carbon (C23) of another (N5-C23: 3.125 \AA ; sum of the van der Waals radii for N and C: 3.25 \AA ;⁵² Fig. S2) suggestive of $\text{N}_\pi\text{-C}_\pi$ overlap. The Fe center in **3** is coordinated in a square-pyramidal (Sq-Py) geometry from the planar $[\text{LN}_4^{\text{Ph}}]^{2-}$ ligand comprising the basal plane and N-coordinated NO in the axial position (Fig. 2.3). This polyhedral assignment is demonstrated by a τ value of nearly 0 (τ_{avg} [average of two independent molecules] = 0.025 for **3**), where τ is the trigonal distortion parameter as defined by Addison and Reedijk.⁵³ The metric parameters (Table 2.2) of the complex are

consistent with a LS Fe center, especially the Fe-L distances that are all less than 2 Å. The Fe-N_{imine} bonds (avg: 1.926 Å) are slightly shorter than the corresponding Fe-N_{pyrrole} bonds (avg: 1.966 Å). These distances appear to be a bit contracted, but mostly consistent with other five-coordinate (5C) Sq-Py {FeNO}⁷ complexes such as [Fe(TPP)(NO)] and [Fe(OEP)(NO)], which display average Fe-N_{pyrrole} distances of ~2.00-2.01 Å.^{30,54} Although the N_{pyrrole} is generally considered as a stronger-field ligand than N_{imine}, the resulting distances in the structure of **3** presumably arise from the significantly acute bite angle of the phenylenediimine portion of LN₄ (avg. N_{imine}-Fe-N_{imine}: 81.89°) versus the more open angle of the N_{pyrrole}-Fe-N_{pyrrole} (avg: 104.22°). In contrast, the similarly disposed {FeNO}⁷ complex [Fe(LN₄^{Pr})(NO)] (**7**), containing a propyl linker between the diimine donors, displays shorter Fe-N_{pyrrole} (avg: 1.945 Å) versus Fe-N_{imine} (avg: 1.984 Å) bonds.⁴⁴ It is possible that the greater flexibility in the ligand frame of **7** allows for electronic influences of the N-donor to be more representative in the bond length due to the relaxed and non-conjugated coordination i.e. the N_{imine}-Fe-N_{imine} (avg: 90.10°) and N_{pyrrole}-Fe-N_{pyrrole} (avg: 95.39°) angles are more ideal. The Fe center in **3** is situated slightly above the plane defined by the four N-ligands of LN₄ by 0.41 Å and is reflected in the bond angles of *trans* N-donors (in the basal plane) e.g. N2-Fe1-N4: 152.05°, which are significantly less than the 180° expected for a perfect square-pyramid.

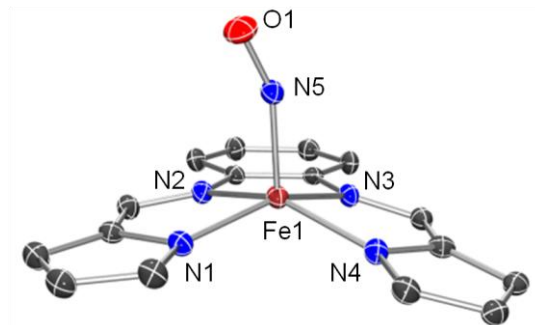


Figure 2.3 ORTEP diagram of $[\text{Fe}(\text{LN}_4^{\text{Ph}})(\text{NO})]$ (**3**) (one unique molecule) at 50% thermal probability ellipsoids for all non-hydrogen atoms with the atom labeling scheme. Selected bond distances and angles are given in Table 2.2.

Table 2.2 Selected bond distances (\AA) and bond angles (deg) for one of the two unique molecules of $[\text{Fe}(\text{LN}_4^{\text{Ph}})(\text{NO})]$ (**3**) as depicted in Fig. 2.3. See Table S2 and Fig. S1 for metric parameters of the other unique molecule.

$[\text{Fe}(\text{LN}_4^{\text{Ph}})(\text{NO})]$ (3)	
Fe1-N1	1.960(3)
Fe1-N2	1.918(3)
Fe1-N3	1.928(3)
Fe1-N4	1.986(3)
Fe1-N5	1.694(3)
N5-O1	1.150(4)
O1-N5-Fe1	155.6(3)
N1-Fe1-N2	81.97(12)
N1-Fe1-N3	153.72(12)
N1-Fe1-N4	104.40(12)
N1-Fe1-N5	95.90(13)
N2-Fe1-N3	81.84(12)
N2-Fe1-N4	152.05(12)
N2-Fe1-N5	101.41(13)
N3-Fe1-N4	81.36(12)
N3-Fe1-N5	107.51(13)
N4-Fe1-N5	104.87(13)

The metric parameters associated with the Fe-N-O unit are often indicative of the nature of the Fe and NO in this highly delocalized bond. Complex **3** displays features that are mostly characteristic of other 5C Sq-Py {FeNO}⁷ complexes (*vide supra*); however, some differences are noted. Analogous to other {FeNO}⁷ complexes,^{30,54-56} the Fe-N (avg: 1.696 Å) and N-O (avg: 1.150 Å) distances are short and generally consistent with a LS-Fe(II)-NO• assignment for this complex (*vide infra*). The Fe-N-O angle (avg: 154.4°) is bent from linearity, which is somewhat representative for this class of nitrosyls and reflective of a radical localized on the nitrogen atom of NO and verified by the N-hyperfine coupling to g_z in the EPR spectrum (*vide infra*). However, the average Fe-N-O angles in similar LS 5C {FeNO}⁷ complexes are more bent (Fe-N-O ~140°),^{30,55} ~ 15° less than the angle found in complex **3**. Thus, complex **3** is certainly an outlier with respect to the Fe-N-O angle. This deviation should be reflected in the ν_{NO} stretching frequency in the IR; however, the IR spectra of **3** and **4** are quite in-line with other {FeNO}⁷ complexes (*vide infra*). Indeed, computations by Ghosh⁵⁷ and Lehnert³⁷ for a variety of LS ($S = 1/2$) heme and non-heme 5C systems suggest that this linearity is due to significant d_z - p_z mixing which alleviates repulsion between the σ lone pair on NO and the Fe d_z^2 -based HOMO. The DFT results by Ghosh revealed a positive correlation between the Fe-N-O angle and the percentage of Fe p_z in the HOMO and a negative correlation with the Fe-N distance in several theoretical 5C Sq-Py LS {FeNO}⁷ derivatives. That is, the larger Fe-N-O angle leads to greater % p , less electron repulsion, and greater Fe-N(O) overlap (or contracted Fe-N bond). In using these theoretical results with those experimentally obtained for complex **3** i.e. its Fe-N-O angle of ~ 155°, one would estimate 8-9% Fe p_z character in its HOMO and an Fe-N distance of ~1.68-1.69. The Fe-N distance obtained from the theoretical correlation line fits well with the experimental value. Thus, the independently reported theoretical results have been somewhat validated by our

experiments. Accordingly, the more bent angle typically observed in 5C {FeNO}⁷ hemes (avg: 144°) correlate with ~ 3-4% Fe *p_z*-character in the HOMO and an Fe-N distance of ~ 1.73 Å (compare with avg: 1.73 Å from experiment).^{30,54-56,58} Taken together, our experiments, in combination with theoretical results by others,^{37,57} suggest that 5C {FeNO}⁷ complexes are better described as LS-Fe(I)-NO⁺, likely in resonance with LS-Fe(II)-NO• owing to the highly delocalized nature of this bond.

2.4 Spectroscopic and Electrochemical Properties of {FeNO}⁷ Complexes

2.4.1 {FeNO}⁷ Spectroscopic Properties.

In addition to the structural characterization of **3**, various spectroscopic measurements on {FeNO}⁷ complexes **3** and **4** were performed. Generally, FTIR spectroscopy is employed to gauge the strength of the N-O and M-N(O) bonding in metal-nitrosyls. In particular, the intense N-O stretching frequency (ν_{NO}) can be particularly informative in MNO systems, but should be interpreted with caution.³⁰ For example, the solid-state ν_{NO} values for **3** and **4** are observed at 1698 and 1720 cm⁻¹ (KBr), respectively (Fig. 2.4 for **4**). These values do not appear to shift significantly in the solution-state in a variety of weak-/non-coordinating solvents (~ 1720 cm⁻¹), but red-shift for **4** ~15 cm⁻¹ (1705 cm⁻¹) in donor solvents such as MeCN and DMSO, indicative of potential solvent coordination in these solutions. Predictably, the ν_{NO} of **4** is blue-shifted from **3** due to the electron withdrawing nature of the peripheral Cl groups on the ligand resulting in decreased Fe π -back-donation into the NO π^* MO.^{30,37,59}

The average ν_{NO} values for 5C Sq-Py complexes also appear in this range (1630-1690 cm^{-1}).^{30,55} When $^{15}\text{NO}(\text{g})$ is used in the preparation of **3** and **4**, the ν_{NO} values shift in agreement with the classic harmonic oscillator model, ν_{NO} : 1667 cm^{-1} (KBr, $\Delta\nu_{\text{NO}}$: 31 cm^{-1}) for **3** and ν_{NO} : 1686 cm^{-1} (KBr, $\Delta\nu_{\text{NO}}$: 34 cm^{-1}) for **4** (Fig. 2.4 for **4**- ^{15}NO).

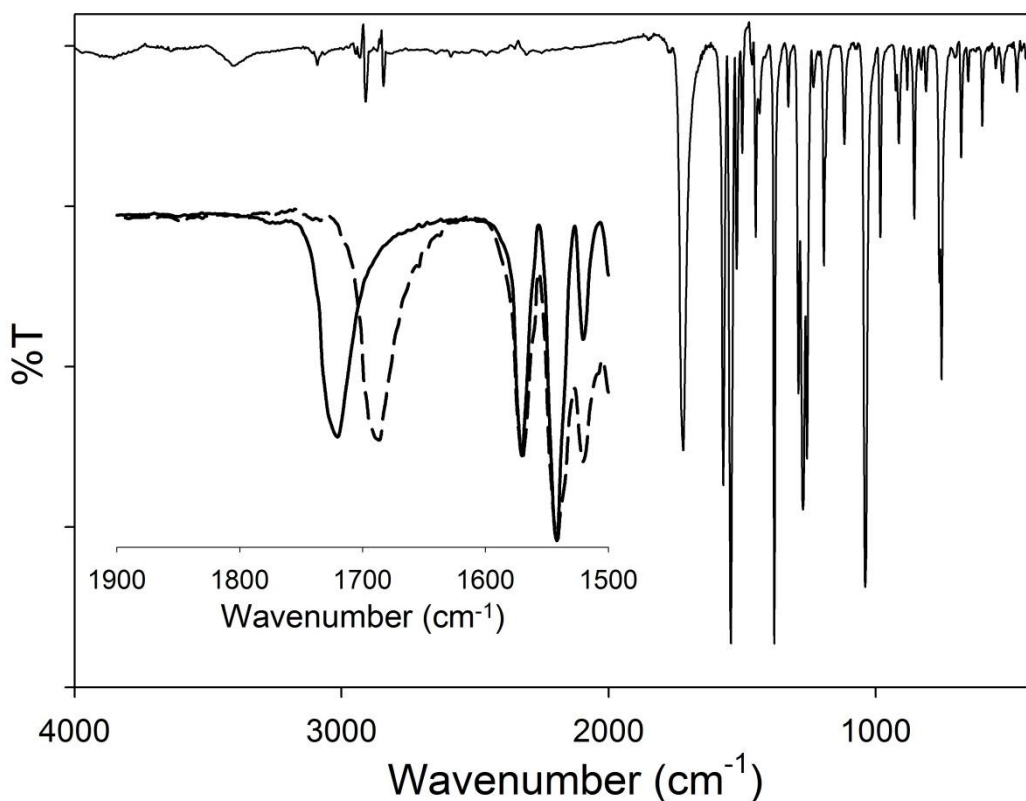


Figure 2.4 FTIR spectra of $[\text{Fe}(\text{LN}_4^{\text{PhCl}})(\text{NO})]$ (**4**) (solid line) and $[\text{Fe}(\text{LN}_4^{\text{PhCl}})(^{15}\text{NO})]$ (**4**- ^{15}NO) (dashed line; inset) in a KBr matrix.

The 5C $\{\text{FeNO}\}^7$ complexes **3** and **4** are paramagnetic and display magnetic properties that are consistent with a doublet electronic ground state ($S = 1/2$), which is typical for this class of iron-nitrosyls.^{30,54} This assignment has been confirmed by magnetic moment measurements (see Experimental) and X-band EPR spectroscopy. For example, EPR measurements (10 K, 3:1 toluene/MeCN) on **3** and **4** reveal an axial feature at $g \sim 2.07$ - 2.01 consistent with the high

symmetry of these Fe-N₄-NO complexes (see Supporting Information, Fig. S3 for complex **4**). Additionally, hyperfine coupling to the $I = 1$ nucleus of the NO nitrogen with $A \sim 16$ G is observed in the g_z component. DFT calculations^{37,44} have shown that this hyperfine coupling is actually representative of minority spin-density localized on N with the majority spin localized on Fe and consistent with an LS-Fe(I)-NO⁺ description (*vide supra*). Complexes **3** and **4** are red-brown in color in organic solvents such as DMF and THF displaying similar UV-vis spectral features with an intense $\lambda_{\text{max}} \sim 350$ nm and a visible shoulder at ~ 470 nm. The electronic transitions at 350 and 470 nm have been tentatively assigned as π - π^* from the ligand frame and MLCT, respectively. There appears to be little difference in the UV-vis spectrum when the solvent dielectric is changed to DMF indicating that the electronic structure is similar in coordinating and weak-/non-coordinating solvent at 298 K.

2.4.2 Electrochemical Properties.

The electrochemical properties of MNO systems are of principal importance since the general goal of our research is to utilize the changes in the MNO redox levels to access underexplored E-F notations in metal-nitrosyls and, more specifically, the {FeNO}⁸ state in this contribution. It is therefore a general requirement to construct molecules that display reversible/diffusion-controlled MNO redox couples in order to synthesize an {FeNO}⁸ complex from an {FeNO}⁷ precursor. Indeed, the cyclic voltammograms (CVs) of **3** and **4** revealed this property. For example, the CV of **3** and **4** in MeCN/RT displayed a reversible $E_{1/2}$ at -1.23 V (ΔE_p : 0.110 V) and -1.16 V (ΔE_p : 0.078 V) (both vs. Fc⁺/Fc; or -0.83 and -0.76 V, respectively vs. SCE²⁹), respectively (Fig. 2.5). Differential pulse voltammetry (DPV) further confirmed the CV results (Fig. 2.5). As expected, the $E_{1/2}$ for **3** is 70 mV more negative and thus more difficult

to reduce than **4** due to the electron-withdrawing nature of the Cl substituents on the ligand. These values compare favorably with the $\{\text{FeNO}\}^7/\{\text{FeNO}\}^8$ redox couples for $[\text{Fe}(\text{TPP})(\text{NO})]$ (-0.93 V vs. SCE in CH_2Cl_2) and $[\text{Fe}(\text{OEP})(\text{NO})]$ (-1.08 V vs. SCE in THF, Table 2.1), but are significantly and expectedly more negative than the halogenated FeNO complex $[\text{Fe}(\text{TFPPBr}_8)(\text{NO})]$ (-0.19 V vs. SCE in CH_2Cl_2) (Table 1). The electrochemical results thus confirm that the $\{\text{FeNO}\}^8$ oxidation state is accessible with minimal structural rearrangement within these ligand architectures.

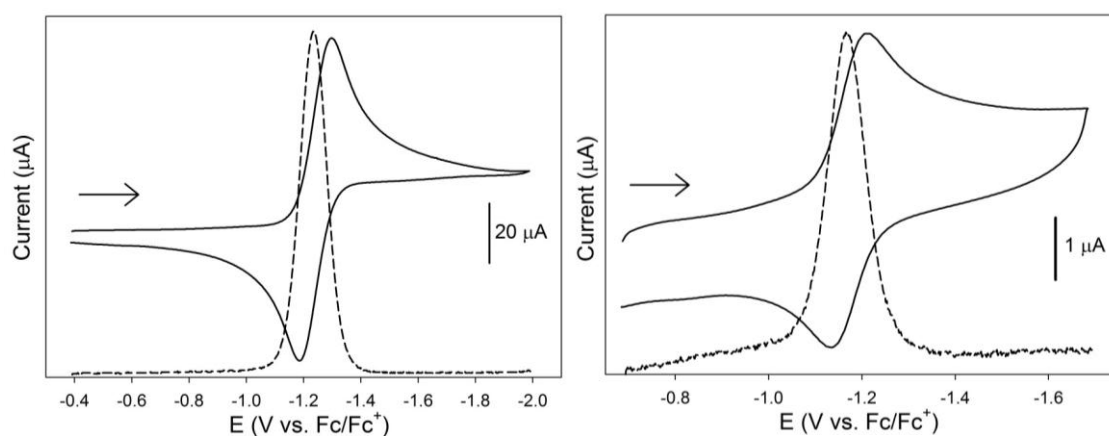


Figure 2.5 *Left*: Cyclic voltammogram (solid line) and differential pulse voltammogram (dashed line) of a 10 mM MeCN solution of $[\text{Fe}(\text{LN}_4^{\text{Ph}})(\text{NO})]$ (**3**) *Right*: Cyclic voltammogram (solid line) and differential pulse voltammogram (dashed line) of a 1 mM MeCN solution of $[\text{Fe}(\text{LN}_4^{\text{PhCl}})(\text{NO})]$ (**4**). Conditions: 0.1 M $n\text{Bu}_4\text{NPF}_6$ supporting electrolyte, glassy carbon working electrode, Pt-wire counter electrode, 100 mV/s scan speed, RT). Arrow displays direction of scan.

2.5 Synthesis and Spectroscopic Properties of {FeNO}⁸ Complexes

2.5.1 Synthesis of {FeNO}⁸ complexes

The {FeNO}⁸ complexes were synthesized via chemical reduction of the {FeNO}⁷ complexes **3** and **4** to generate [Fe(LN₄^{Ph})(NO)]⁻ (anion of **5**) and [Fe(LN₄^{PhCl})(NO)]⁻ (anion of **6**), respectively, where the cation depends on the reductant used in the synthesis (Scheme 2.1). In previous accounts by our lab⁴⁴ and others,³⁵ this reduction has been accomplished using cobaltocene [Co(Cp)₂] or decamethylcobaltocene [Co(Cp*)₂] as reducing agents with the selection being dependent on the potential of the {FeNO}⁷/_{{FeNO}⁸ redox couple. These metallocene reductants work reasonably well, but the necessity to often purify [Co(Cp*)₂] and the insolubility of the resulting {FeNO}⁸ as the [Co(Cp*)₂]⁺ salt complicated the synthesis. For example, Geiger and Connelly recommend that [Co(Cp)₂] be sublimed before use, stored in the dark at -10 °C, and used within 10 days.²⁹ Regardless, reaction of complexes **3** or **4** with [Co(Cp*)₂] in toluene at RT resulted in respectable yields of the {FeNO}⁸ complexes, [Co(Cp*)₂][Fe(LN₄^{Ph})(NO)] (^{Cp*}**5**) and [Co(Cp*)₂][Fe(LN₄^{PhCl})(NO)] (^{Cp*}**6**), which precipitated from the reaction medium. The non-methylated [Co(Cp)₂] would presumably afford a more polar aprotic-soluble cobaltocenium salt, but could not be used since it is not strong enough of a reducing agent. Although this synthesis was successful in our hands, the need for constant purification of the metallocene led us to select other chemical reductants. Thus, inspired by classic reagents used in organometallic reactions, we employed potassium graphite (KC₈) as the reducing agent. Similarly, the {FeNO}⁸ complexes K[Fe(LN₄^{Ph})(NO)] (**5**) and K[Fe(LN₄^{PhCl})(NO)] (**6**) were obtained by reaction of stoichiometric KC₈ with acetone solutions of **3** and **4**, respectively. It is important to point out that *stoichiometric* KC₈ should be employed in the synthesis as excess leads to disparate reactivity and multiple reduced species probably}

associated with the imine functionality, which is well documented for this reductant.^{60,61} The yields are nearly quantitative and the resulting {FeNO}⁸ complexes display reasonable solubility in most organic solvents such as MeCN. Additional benefits of this synthetic route include the relative insolubility of the graphite by-product, which is easily separated from the FeNO complex by simple filtration. However, unlike **3** and **4**, compounds **5** and **6** are air-sensitive materials that require anaerobic conditions for workup, storage, and characterization.

2.5.2. {FeNO}⁸ Spectroscopic Properties

As described above, vibrational spectroscopy is one of the principal methods of MNO complex characterization, and vibrational measurements on {FeNO}⁸ complexes are rare (Table 2.1). Additionally, one would expect significant changes in ν_{NO} among {MNO}ⁿ redox isomers depending on the extent of NO-based redox. Indeed, complexes **5** and **6** display shifted ν_{NO} bands from their parent oxidized complexes **3** and **4**, albeit to a different extent. For example, the solid-state IR spectrum of **5** displayed ν_{NO} at 1667 cm⁻¹ (identified by ¹⁵N isotopic labeling), which is only 43 cm⁻¹ away from the parent {FeNO}⁷ complex **3**. This value appears to be more consistent with a ligand-based reduction instead of {FeNO} unit reduction although this result may be more indicative of a thermally accessible triplet excited state (*vide infra*). A ligand based reduction would not be too surprising given the highly delocalized nature of the LN₄ scaffold, which is evidenced by the disparate C-C bond distances in the X-ray structure especially in the pyrrolide ring. The ν_{NO} band of **6**; however, shifted significantly from parent **4** (1720 cm⁻¹) to ~ 1580 cm⁻¹ (approximate due to overlap with LN₄ $\nu_{\text{C=N}}$ bands, Fig. 2.6). Both **5** and **6** also display ν_{CO} values at 1705 cm⁻¹ that are similar to metal-coordinated acetone complexes (ν_{CO} : 1660-1700 cm⁻¹).⁶² The presence of acetone was also confirmed by elemental analysis (see

Experimental) and mass spectrometry measurements (*vide infra*). Analogous to other $\{\text{FeNO}\}^8$ complexes,³⁵ the ν_{NO} is obstructed from ligand vibrational bands. The ν_{NO} value for **6** thus supports reduction in the FeNO unit due to increased occupancy of π^* orbitals on NO from its $\{\text{FeNO}\}^7$ precursor **4**. These values are also consistent with other heme $\{\text{FeNO}\}^8$ complexes that have been synthesized or studied by high-level DFT calculations (Table 2.1). They are, however, quite higher than the corresponding values for non-heme $\{\text{FeNO}\}^8$ systems (avg: 1300 cm^{-1}) suggesting that the electronic nature of the LN_4 frame in **6** is more heme-like.

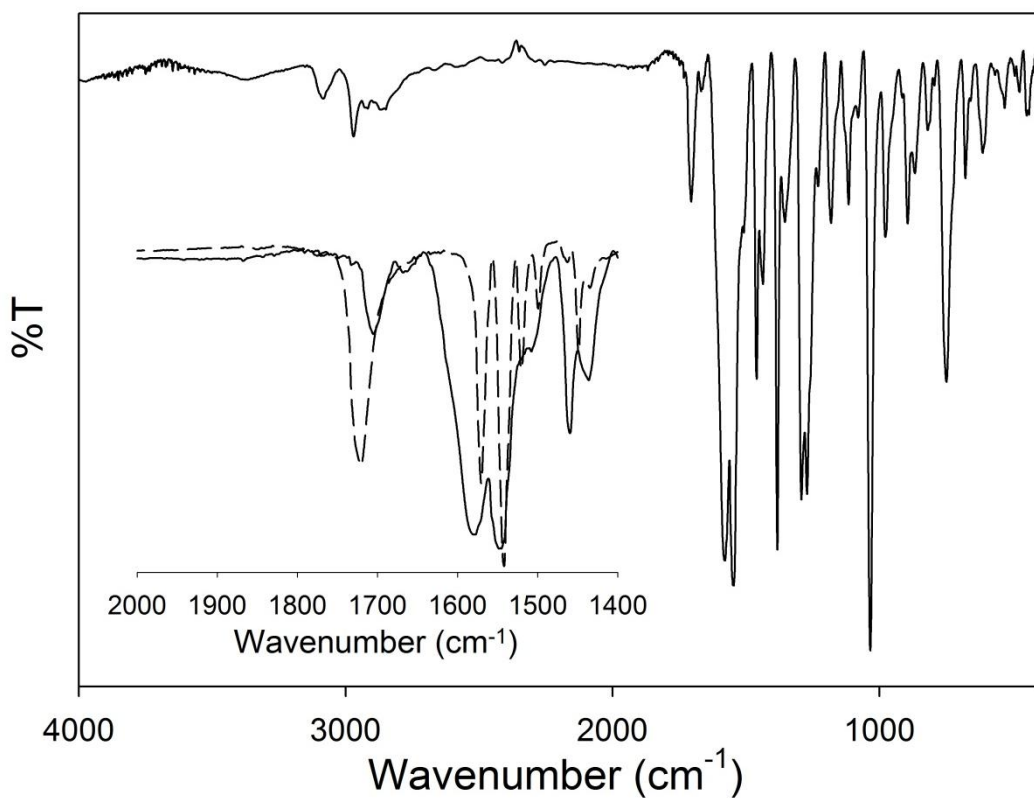


Figure 2.6 FTIR spectra of $\text{K}[\text{Fe}(\text{LN}_4^{\text{PhCl}})(\text{NO})]$ (solid line) (**6**) and $[\text{Fe}(\text{LN}_4^{\text{PhCl}})(\text{NO})]$ (dashed line; inset) (**4**) in a KBr matrix. Peak at 1705 cm^{-1} in **6** represents coordinated acetone ν_{CO} .

High-resolution FTMS (HRMS) studies were also performed to confirm the identity of the $\{\text{FeNO}\}^8$ complexes. Single crystals of such systems have been difficult to grow due to the reactive nature of these complexes (*vide infra*). Thus, HRMS would provide further confirmation of these elusive metal nitrosyls. The HRMS (negative ion mode) experiments do provide such evidence, as the molecular ion peak $[\text{M}]^-$ for **5** (m/z : 346.0385; calcd: 346.0386) does appear with the appropriate isotope pattern (Supporting Information Section). Complex **6**, on the other hand, only displayed peaks consistent with $[\text{M} + \text{acetone}]^-$ (m/z : 472.0000; calcd: 472.0026) and $[\text{M} + \text{acetone} - \text{H}]^-$ (m/z : 470.9967; calcd: 470.9947) with the latter being the predominant species. The ^{15}N isotopomers were also examined and support the formulation predicted. To the best of our knowledge, the MS studies on the $\text{Fe-LN}_4^{\text{R}}\text{-NO}$ systems⁴⁴ represent the only MS measurements performed on such FeNO complexes.

Other spectroscopic methods were employed to characterize complexes **5** and **6**. Both **5** and **6** demonstrate excellent solubility in a variety of organic solvents such as acetone, MeCN, and DMF affording red-brown colored solutions; moderate solubility is observed in non-polar solvents such as THF. The UV-vis spectrum of the $\{\text{FeNO}\}^8$ complex **6** is similar in shape to $\{\text{FeNO}\}^7$ complex **4** with some minor changes (Fig. 2.7). To date (2015), all reported non-heme $\{\text{FeNO}\}^8$ complexes have been reported as diamagnetic with the exception of one compound;⁴⁶ however, this description represents a small sample size ($N = 4$) as the majority of these systems have only been characterized *in situ*. This property suggests that, if we assign the coordinated NO as a nitroxyl anion, the $\text{LS-Fe(II)-}^1\text{NO}^-$ would be the favorable assignment for $\{\text{FeNO}\}^8$. Complex **6** displays a complex ^1H NMR spectrum that is consistent with a diamagnetic system (see Supporting Information). The complexity presumably arises from ligation/deligation of solvent (*vide infra*) or structural rearrangement of the LN_4 ligand around the Fe center. In

contrast, the ^1H NMR of **5** is observable, but appears broad in nature and consistent with a paramagnetic material. The NMR broadness is attributed to formation of an unknown species upon complex dissolution and/or a thermally accessible higher spin-state (i.e. $^3\text{NO}^-$ versus $^1\text{NO}^-$ or ligand reduction). We favor this description since ν_{NO} of **5** matches quite well with calculated ν_{NO} values for 6C $\{\text{FeNO}\}^8$ complexes, which range from 1612-1777 cm^{-1} for $[\text{Fe}(\text{P})(\text{Im})(\text{NO})]^-$ complexes in the $S = 1$ state.^{37,38} Additionally, a paramagnetic triplet ground state has been assigned to the $\{\text{FeNO}\}^8$ adduct of the non-heme TauD system suggesting that higher spin manifolds may be accessible for **5**.⁴⁵ Although the extra stability of the $\{\text{FeNO}\}^8$ in **6** is not quite significant from an electrochemical vantage point (~ 100 mV), perhaps the presence of the Cl substituents lower the energy of the ligand π -orbitals just enough to prevent parallel spin occupation and/or ligand reduction. Collectively, it appears that heme-based $\{\text{FeNO}\}^8$ complexes and **6** display ν_{NO} : 1500-1600 cm^{-1} and generally prefer to be ground state singlets. However, non-heme $\{\text{FeNO}\}^8$ systems (excluding the examples reported here and elsewhere⁴⁴) display $\nu_{\text{NO}} \sim 1300$ cm^{-1} . This data suggests an oxidation state assignment of LS-Fe(II)- $^1\text{NO}^-$ for non-heme $\{\text{FeNO}\}^8$ and more of a resonance LS-Fe(II)- $^1\text{NO}^- \leftrightarrow$ LS-Fe(I)-NO \bullet description for heme $\{\text{FeNO}\}^8$.

2.6 Reactivity of $\{\text{FeNO}\}^7$ and $\{\text{FeNO}\}^8$ Complexes

The reactivity of $\{\text{FeNO}\}^8$ complexes have received little attention with the exception of the protonation studies by Doctorovich on $[\text{Fe}(\text{TFPPBr}_8)(\text{NO})]^-$,³⁵ which was shown to liberate $\text{H}_2(\text{g})$ and reform the $\{\text{FeNO}\}^7$ complex via a transient $\{\text{FeHNO}\}^8$ complex. As the reactivity of $\{\text{FeNO}\}^8$ systems is underexplored and of fundamental importance with respect to the biological fate of HNO/ NO^- , we have initiated such reactivity studies in the present contribution. Due to

principal reduction of the {FeNO} unit in **6**, the majority of our reactivity discussion is focused on this system; however, reactions with **5** (a complex more consistent with ligand-based reduction or paramagnetic spin-state) were also performed and resulted in nearly parallel outcomes.

In the absence of structural characterization of **5** or **6** and to support the electrochemical results, the conversion of the {FeNO}⁸ complexes back to their oxidized {FeNO}⁷ counterparts was performed. For instance, treatment of an MeCN solution of the {FeNO}⁸ complexes **5** or **6** with a stoichiometric amount of ferrocenium hexafluorophosphate resulted in quantitative formation of the corresponding {FeNO}⁷ complexes **3** and **4** as monitored by FTIR spectroscopy. The reversibility of the FeNO redox states is depicted in Scheme 2.1. Thus, the {FeNO}^{7/8} complexes (**3/5** or **4/6**) are chemically and electrochemically interconvertible.

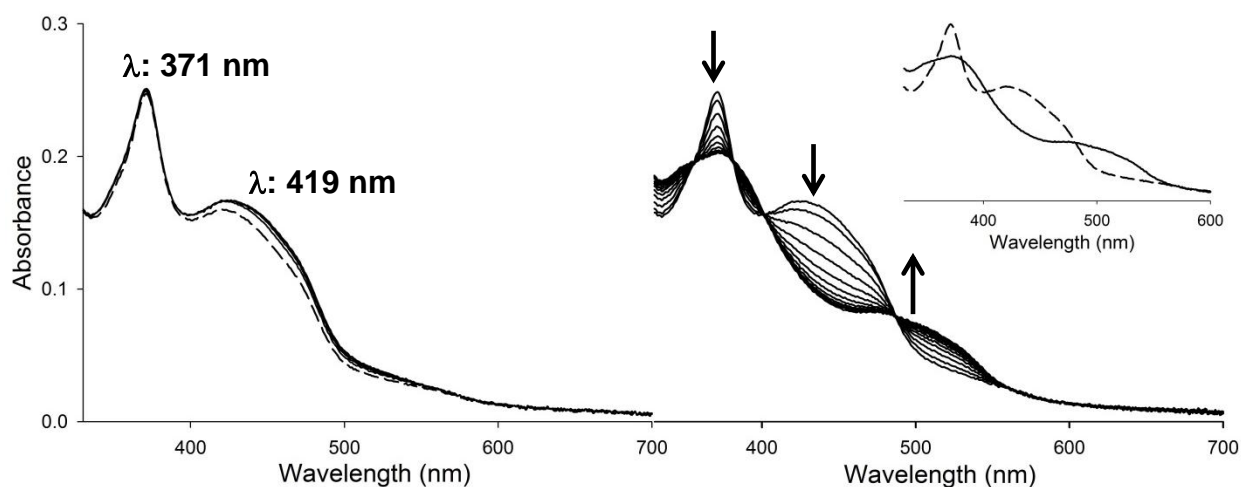


Figure 2.7 UV-vis spectral monitor of an 8.33 μM THF solution of $\text{K}[\text{Fe}(\text{LN}_4^{\text{PhCl}})(\text{NO})]$ (**6**) at 298 K. *Left*: UV-vis monitor of **6** upon initial dissolution (dashed line) and subsequent traces (solid lines) for 15, 30, 45, and 60 min thereafter. *Right*: continuation of spectral monitor on the left only at 1 h intervals (total time = 12 h); inset depicts first (dashed line) and last (solid line) scan. Arrows illustrate the direction of change.

The difficulty in the isolation of single crystals of $\{\text{FeNO}\}^8$ derivatives likely derives from the inherent reactivity of these systems. For example, Kadish and Olson reported that exhaustive electrolysis of the $\{\text{FeNO}\}^8$ complex of TPP simply resulted in isolation of the starting $\{\text{FeNO}\}^7$ species.³⁴ This outcome is likely due to the presence of some protic material in the non-polar CH_2Cl_2 solvent that resulted in the reaction of H^+ with the formed $\{\text{FeNO}\}^8$ complex in an analogous fashion to what is observed by Doctorovich.³⁵ The inherent reactivity of this class of iron-nitrosyls at least provides some explanation for the lack of isolable $\{\text{FeNO}\}^8$ complexes in the literature. Previously, our group reported that the structurally similar $\{\text{FeNO}\}^8$ complex **7** undergoes disproportionation reactions in MeCN or THF to yield the $\{\text{FeNO}\}^7$ complex and an Fe(I)- N_2 species. This reaction takes nearly 13 h to go to completion.⁴⁴ Thus, complex **7** could still be used as a potential nitroxyl donor providing that release of nitroxyl is faster than disproportionation. We hypothesized that this reaction may be a common feature for $\{\text{FeNO}\}^8$ species at least with the LN_4 type of ligand platform. As expected, when a THF solution of **6** was monitored by UV-vis spectroscopy (298 K), distinct changes in the visible region were observed with a decrease in the λ_{max} at 371 and 419 nm and new bands appearing at λ_{max} of 361 and 481 nm over the course of 9 h (Fig. 2.7). Complex **6** is thus more reactive than **7**. There appears to be little change in the UV-vis over the course of ~ 2 h indicating modest solution stability of the $\{\text{FeNO}\}^8$ complex (Fig. 2.7). Additionally, several isosbestic points are present in the spectrum during this process at 359, 384, 403 and 490 nm supporting a clean transformation with the final trace displaying bands at 361 and 481 nm, which appear to be indicative of the $\{\text{FeNO}\}^7$ complex **4**. FTIR analysis of this reaction also revealed the ν_{NO} bands of **4**, which further confirmed formation of the $\{\text{FeNO}\}^7$ complex. Further examination of the UV-vis experiments indicate that $\{\text{FeNO}\}^7$ **4** is obtained in quantitative yield, which eliminates a

disproportionation reaction. This result suggests that a simple oxidation is taking place over prolonged storage of **6** in solution to result in **4** and reduction of the solvent. Another path to obtain $\{\text{FeNO}\}^7$ from $\{\text{FeNO}\}^8$ would be via protonation as demonstrated by Doctorovich³⁵ as described above; however, this reaction seems unlikely under the anhydrous/anaerobic conditions employed. Complex **5** also undergoes a similar reactivity profile in THF but appears to form the $\{\text{FeNO}\}^7$ species more rapidly (6 h).

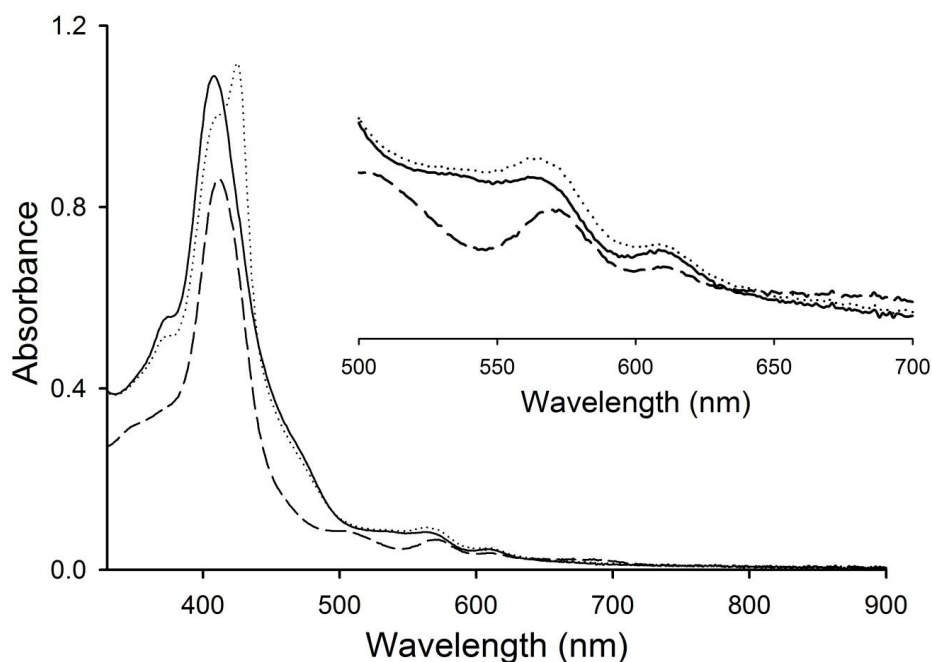


Figure 2.8 UV-vis spectrum of an 8.33 μM THF solution of $[\text{Fe}(\text{TPP})\text{Cl}]$ (dashed line), 1 min after (dotted line), and 1 h after (solid line) the addition of 1 mol-equiv of $\text{K}[\text{Fe}(\text{LN}_4^{\text{PhCl}})(\text{NO})]$ (**6**) at 298 K. *Inset*: expansion of the Q-band region of the spectrum.

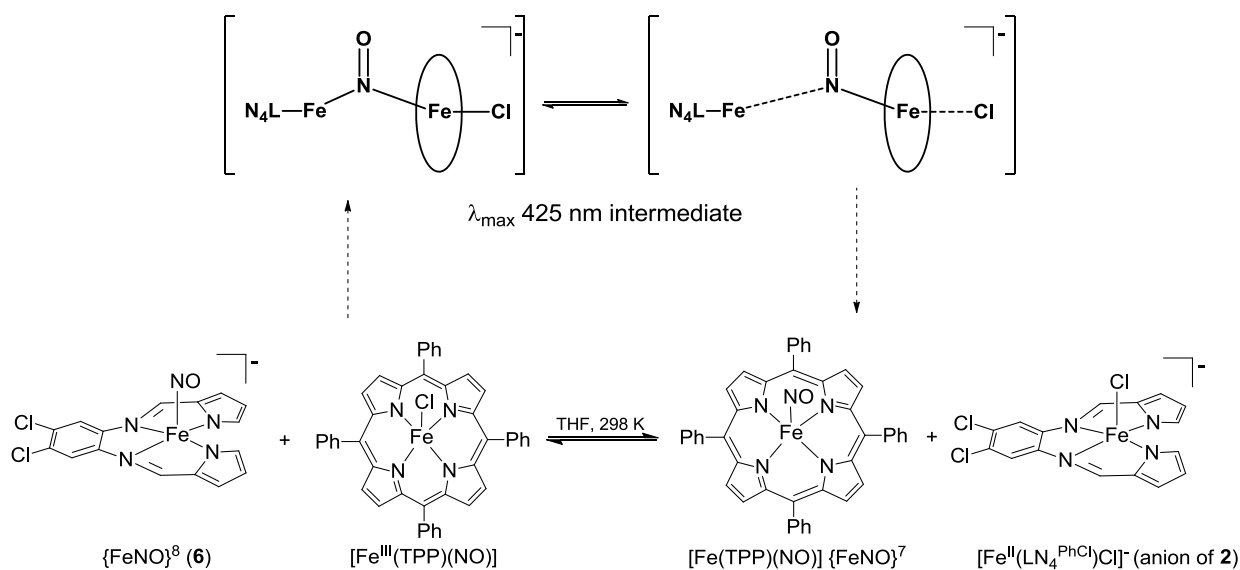
The established reductive nitrosylation⁶³ reaction of HNO with ferric hemes is among the most sensitive chemical tests for HNO-releasing molecules where HNO provides both the electron and NO to form an $\{\text{FeNO}\}^7$ ferrous-NO heme.^{40,64,65} Additionally, M(III)-porphyrin complexes have been demonstrated as efficient traps for HNO.^{64,66,67} To test whether complexes

such as **6** could react in a similar manner, we explored the interaction of these $\{\text{FeNO}\}^8$ complexes with the ferric heme analogue $[\text{Fe}(\text{TPP})\text{Cl}]$ under dark conditions to prevent any ill-defined photochemistry. The reaction of a THF solution of $[\text{Fe}(\text{TPP})\text{Cl}]$ at 298 K with stoichiometric amounts of the $\{\text{FeNO}\}^8$ complexes was monitored by UV-vis and IR spectroscopies. Addition of the $\{\text{FeNO}\}^8$ complex **6** to $[\text{Fe}(\text{TPP})\text{Cl}]$ (1:1 ratio) resulted in several changes in the UV-vis spectrum, which are ultimately consistent with formation of the $\{\text{FeNO}\}^7$ porphyrin complex, $[\text{Fe}(\text{TPP})(\text{NO})]$, after ~ 1 h (Fig. 2.8). The trace after 1 min addition of **6** displayed a red-shift in the Soret band of $[\text{Fe}(\text{TPP})\text{Cl}]$ from 412 nm to 425 nm with a significant increase in absorbance. Spectral changes such as this have been attributed to several transformations of $[\text{Fe}(\text{TPP})\text{Cl}]$. For example, a similar shift has been observed in the photo-reduction of $[\text{Fe}(\text{TPP})\text{Cl}]$ in MeOH to form what is assigned as the 6C bis-solvato complex, $[\text{Fe}(\text{TPP})(\text{MeOH})_2]$.^{68,69} While a reduced solvato species is possible in the reported reaction, we must note that the 6C complex described above was formed in MeOH and is only stable on the millisecond timescale. In contrast, these reactions were performed in weakly coordinating THF and the λ_{max} : 425 nm species is observed on the minute timescale. Additionally, authentic $[\text{Fe}^{\text{II}}(\text{TPP})]$ has been prepared in THF by Darensbourg and coworkers where they report a Soret λ_{max} of 412 nm,⁷⁰ which eliminates this species. This spectral change may, however, suggest the formation of a transient 6C $\{\text{FeNO}\}^7$ -porphyrin complex. In fact, the 6C complex, $[\text{Fe}(\text{TPP})(\text{NO})(\text{MI})]$, prepared by Lehnert's group⁵⁸ has a Soret absorption band at 425 nm and Q-bands at 538 and 600 nm in CH_2Cl_2 . The intermediate we form displayed λ_{max} at 425, 537, and 606 nm, which is slightly red-shifted and more intense from the final trace with λ_{max} at 407, 540, 609 nm and in-line with authentic $[\text{Fe}(\text{TPP})(\text{NO})]$ (λ_{max} : 405, 543, 614 nm in CH_2Cl_2 [68]). The slight shifts in UV-vis values are due to the different solvent (THF in this account) as well as

influences of the $[\text{Fe}(\text{LN}_4^{\text{PhCl}})\text{Cl}]^-$ chromophore byproduct. When $[\text{Fe}(\text{TPP})\text{OTf}]$ was prepared⁷¹ and subjected to the same conditions used for $[\text{Fe}(\text{TPP})\text{Cl}] + \mathbf{6}$, a similar 425 nm band is observed in the first spectral trace. Though the OTf^- anion is considered to be a weaker field ligand than Cl^- , previous reports describe $[\text{Fe}(\text{TPP})\text{OTf}]$ as a 5C species instead of an ion pair.^{71,72} Since the resulting UV-vis spectral changes were nearly identical to that of compound $\mathbf{6}$ with $[\text{Fe}(\text{TPP})\text{Cl}]$, we propose that the net NO^- transfer is occurring through a similar mechanism with both 5C ferric porphyrins. Moreover, an identical intermediate was observed in the reaction of $\mathbf{7}$ with $[\text{Fe}(\text{TPP})\text{Cl}]$, (Fig. S18). As previously reported, complex $\mathbf{7}$ has been used to transfer NO^-/HNO to metMb, resulting in a reductive nitrosylation.⁴⁴ The $[\text{Fe}(\text{TPP})\text{Cl}]$ is a free Fe-porphyrin and therefore available for possible bridging interactions, whereas the heme of metMb is buried in a protein matrix. Thus, a potential mechanism could involve formation of a binary complex where the NO ligand of $\mathbf{6}$ bridges the two reactants to form a $[\text{P-Fe}(\mu\text{NO})\text{Fe-L}]^-$ intermediate (Scheme 2.2). This species is comparable to the intermediate observed in the transnitrosation of thiolates with nitrosothiols (RSNO) where attack of the nucleophilic thiolate anion on the electrophilic RSNO produces the anionic $\text{RSN}(\text{O})\text{SR}^-$ intermediate.^{73,74} This type of NO-transfer has been postulated to be involved in safe NO-trafficking, which never involves the release of free NO. By analogy, the process described here would be defined as a “transnitroxylation” where the coordinated NO^- is transferred from one molecule to another without involving free NO^- . Electron transfer and nitrosylation take place through the bridge i.e. an inner-sphere mechanism and the 6C intermediate decays to yield the more stable 5C $[\text{Fe}(\text{TPP})(\text{NO})]$ complex and $\mathbf{2}$ perhaps via a monomeric $[\text{Fe}^{\text{II}}(\text{TPP})(\text{NO})\text{Cl}]$ complex after splitting the bridge (Scheme 2.2). The identity of the 425 nm intermediate could be any of these 6C FeNO complexes. Therefore, the net reaction would be: $[\text{Fe}(\text{LN}_4^{\text{R}})(\text{NO})]^-$ (anion of $\mathbf{6}$) +

$[\text{Fe}(\text{TPP})\text{Cl}] \rightarrow [\text{Fe}(\text{TPP})(\text{NO})] + [\text{Fe}(\text{LN}_4^{\text{R}})\text{Cl}]^-$ (anion of **2**). Further support for this chemistry comes from IR analysis. The FTIR spectrum of the bulk reaction mixture of $[\text{Fe}(\text{TPP})\text{Cl}]/\text{complex } \mathbf{6}$ (1:1) confirmed this postulate and the only ν_{NO} bands observed are from $[\text{Fe}(\text{TPP})(\text{NO})]$ (ν_{NO} : 1701 cm^{-1} in KBr), which shifted when **6- ^{15}N O** was used (ν_{NO} : 1669 cm^{-1} in KBr) (see the Supporting Information). Furthermore, the UV-vis spectrum of independently-prepared complex **2** and $[\text{Fe}(\text{TPP})(\text{NO})]$ (mixed in a 1:1 ratio) in THF at 298 K nearly resembles the final spectrum of the reaction described above (see Supporting Information). The control reaction of $[\text{Fe}(\text{TPP})\text{Cl}]$ with the $\{\text{FeNO}\}^7$ complexes **3** and **4** also appear to generate $[\text{Fe}(\text{TPP})(\text{NO})]$; however, the reaction time is long (> 12 h) and incomplete according to IR and UV-vis spectroscopies. Additionally, Darensbourg observes a similar reaction of $[\text{Fe}(\text{TPP})\text{Cl}]$ or $[\text{Fe}(\text{OEP})\text{Cl}]$ with a 5C $\{\text{FeNO}\}^7$ - N_2S_2 complex that also takes place over a similar (24-72 h) timescale.⁷⁰ Thus, while $\{\text{FeNO}\}^7$ can ultimately result in the same product as with $\{\text{FeNO}\}^8$ (**5** and **6**) and dinitrosyl iron complexes (DNICs, the reactions studied by Darensbourg), the reaction path appears very different.

Scheme 2.2. Proposed reaction path and transnitrosylation intermediates (bracketed) in the reaction of $\{\text{FeNO}\}^8$ complex with $[\text{Fe}^{\text{III}}(\text{TPP})\text{Cl}]$. Oval represents porphyrin in intermediate complex. A similar reaction path is proposed with $[\text{Fe}^{\text{III}}(\text{TPP})\text{OTf}]$ (Fig. S17).



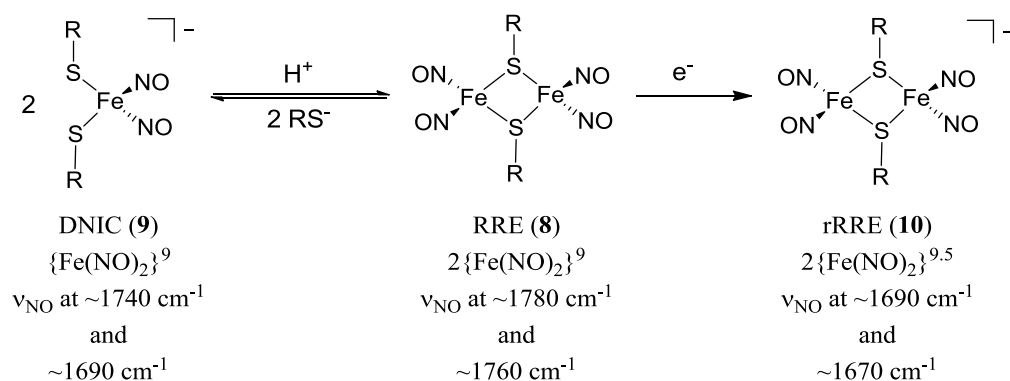
Reactivity of $\{\text{FeNO}\}^7$ with *p*-chlorobenzenethiol²

The proposed targets for HNO in biology are Fe(III)-hemes and thiols. Because of this, we sought to also investigate the reactivity of thiols with $\{\text{FeNO}\}^{7/8}$ complexes. The results of these studies demonstrate that $\{\text{FeNO}\}^7$ complexes (**3** and **4**) and $\{\text{FeNO}\}^8$ complexes (**5** and **6**) rearrange to bi- and mononuclear dinitrosyl iron complexes (DNICs), respectively, when reacted with an aromatic thiol such as *p*-chlorobenzenethiol ($p\text{-ClArSH} = \text{RSH}$). Our observations suggest that the $\{\text{FeNO}\}^7$ species react with *p*-ClArSH in THF to give Roussin's Red Esters, namely $[\text{Fe}_2(\mu\text{-RS})_2(\text{NO})_4]$, whereas the $\{\text{FeNO}\}^8$ species afford the DNIC $[\text{Fe}(p\text{-ClArSH})_2(\text{NO})_2]^-$. It is known that in solution the DNIC and RRE species are in an equilibrium

² Unpublished results and discussion related to the research found in the citation of footnote 1.

with each other that is dependent on pH and $[RS^-]$ (Scheme 2.3).^{75,76} However, the divergence between DNIC and RRE end-products in this study appears to be dependent on the oxidation state of the FeNO unit. These results underscore the reduced nature of the $\{FeNO\}^8$ complexes **5** and **6**.

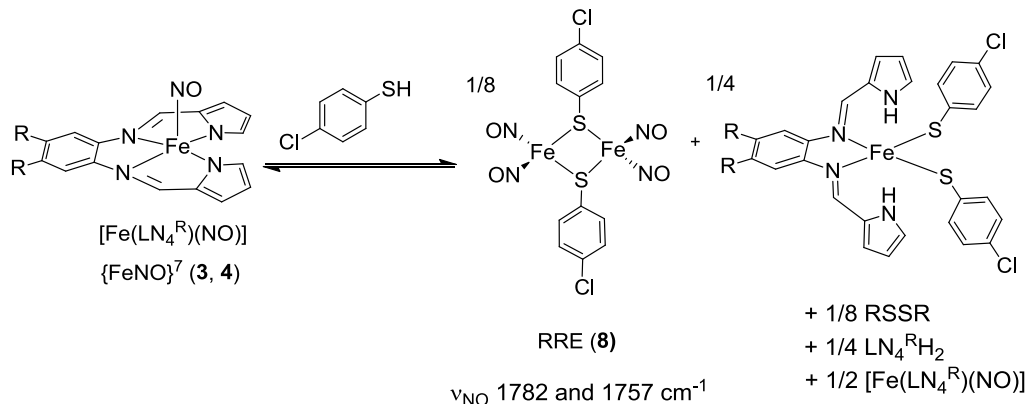
Scheme 2.3. Equilibrium between Dinitrosyl Iron Complex (DNIC) and Roussin's Red Ester (RRE) and reduction of RRE to the reduced RRE (rRRE). RS = anion of *p*-ClArSH.



The $\{FeNO\}^7$ complexes **3** and **4** were reacted with one-equivalent of *p*-ClArSH in THF under anaerobic conditions. The results point to the partial formation of $[Fe_2(\mu-RS)_2(NO)_4]$ (**8**) based on the appearance of ν_{NO} at 1782 and 1757 cm^{-1} , consistent with the previously reported neutral RRE supported by aromatic thiolates (Fig. S23).⁷⁶ Moreover, analogous studies performed with the $\{FeNO\}^7$ complex of $[Fe(LN_4^{Pf})NO]$ also resulted in formation of this RRE.⁷⁷ Although the $\{FeNO\}^7$ species do react with *p*-ClArSH, the process appears to be incomplete over 1 h, which is indicated by the strong ν_{NO} at 1699 and 1721 cm^{-1} , corresponding to the $\{FeNO\}^7$ starting materials of **3** and **4**, respectively. Importantly, the 1H NMR (C_6D_6) of the Et_2O soluble material from the reaction workup exhibited the presence of two aromatic

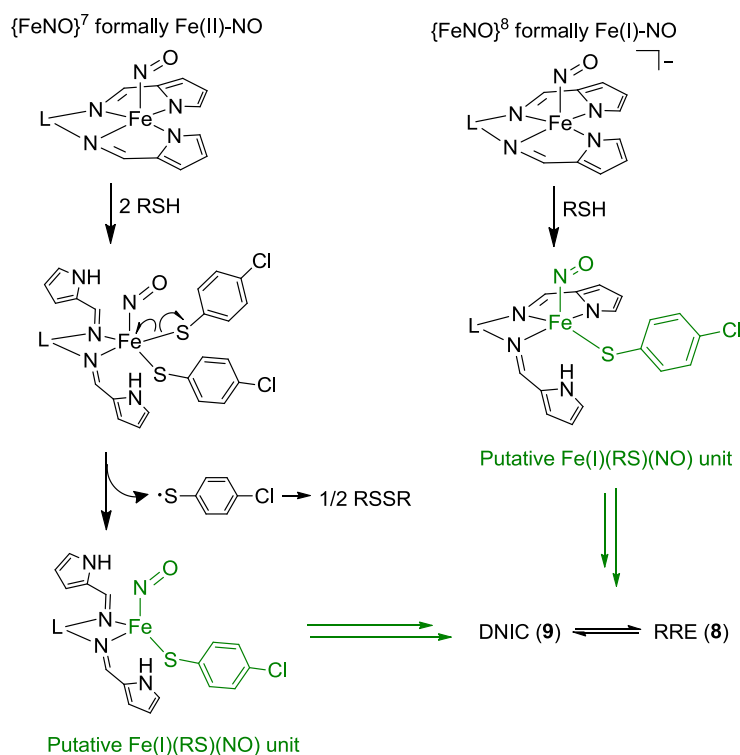
doublets. These signals were confirmed to be the disulfide of *p*-ClArSH (RSSR) by authentic synthesis (Fig. S19). Separation and isolation of all products was problematic due to the similar solubility properties of the neutral {FeNO}⁷ and RRE products. However, based on the speciation, it appears that only ~0.5 equiv of {FeNO}⁷ react with one equiv of *p*-ClArSH. A proposed balanced reaction is shown in Scheme 2.4. The scheme shows that the Fe center can be removed from the LN₄²⁻ platform. The mechanism of this process is not currently known; however, recent work involving Co derivatives of the same ligands reporting the H⁺-dependent reactivity of {CoNO}⁸ complexes, may involve protonation at the Co(III)-NO⁻ nitrosyl and the pyrrole LN₄²⁻ ligand.⁷⁸ The {CoNO}⁸ series are accurately described as Co(III)-NO⁻, but the nitrosyl of the {FeNO}⁷ complexes are considerably less basic and more accurately described as Fe(II)-NO• ↔ Fe(I)-NO⁺. One mechanistic proposal may involve the concomitant deprotonation and coordination of two *p*-ClArSH with subsequent protonation and dissociation of the pyrrolide ligands. This reaction would result in the 5C complex, [Fe(II)(LN₄H₂)(NO)(RS)₂]. Recent studies on DNIC formation suggest that the common intermediate in formation of RRE or DNIC from Cys, FeSO₄ and NO is [Fe(II)(NO)(RS)₂] an {FeNO}⁷ species.⁷⁵ This complex is then thought to lose RS• to form RSSR and the [Fe(I)(NO)(RS)]⁻, an {FeNO}⁸ complex and precursor to DNIC. By analogy, the [Fe(II)(LN₄H₂)(NO)(RS)₂] may lose RS• to provide the reduced [Fe(I)(LN₄H₂)(NO)(RS)], which can then lead to formation of RRE (**8**) or DNIC (**9**).

Scheme 2.4 Equilibrium between $\{\text{FeNO}\}^7$ and $p\text{-ClArSH}$.



Alternatively, the intermediate complex, $[\text{Fe}(\text{II})(\text{LN}_4\text{H}_2)(\text{NO})(\text{RS})_2]$, could disproportionate to give 0.5 equiv $[\text{Fe}(\text{II})(\text{LN}_4\text{H}_2)(\text{RS})_2]$ and the 0.5 equiv $[\text{Fe}(\text{II})(\text{LN}_4\text{H}_2)(\text{NO})_2(\text{RS})_2]$, a 6C DNIC. Analogously, the complex $[\text{Fe}(\text{II})(\text{LN}_4\text{H}_2)(\text{NO})_2(\text{RS})_2]$ could undergo internal electron transfer from one of the bound thiolates to give $[\text{Fe}(\text{I})(\text{LN}_4\text{H}_2)(\text{NO})_2(\text{RS})]$ and RSSR (Scheme 2.5). At this point, the Fe(I) DNIC, $[\text{Fe}(\text{I})(\text{LN}_4\text{H}_2)(\text{NO})_2(\text{RS})]$, could combine to form the RRE product. Either mechanism would imply that the electron equivalents required to convert $\{\text{FeNO}\}^7$ (formally Fe(II)) to $\{\text{Fe}(\text{NO})_2\}^9$ (formally Fe(I)) must come from the thiol and its ultimate formation of disulfide. As a result of RSSR formation, the total amount of thiol in the system is diminished and therefore the known equilibrium shown in Scheme 2.3 favors the RRE product.^{75,76,79}

Scheme 2.5 Illustrating possible mechanism for DNIC and RRE formation from $\{\text{FeNO}\}^{7/8}$ complexes. Where L = Ph, PhCl, and propyl groups of complexes **3/5**, **4/6**, and **7**, respectively. RSH = *p*-ClArSH; RS = *p*-ClArS⁻; RSSR = disulfide of *p*-ClArSH.



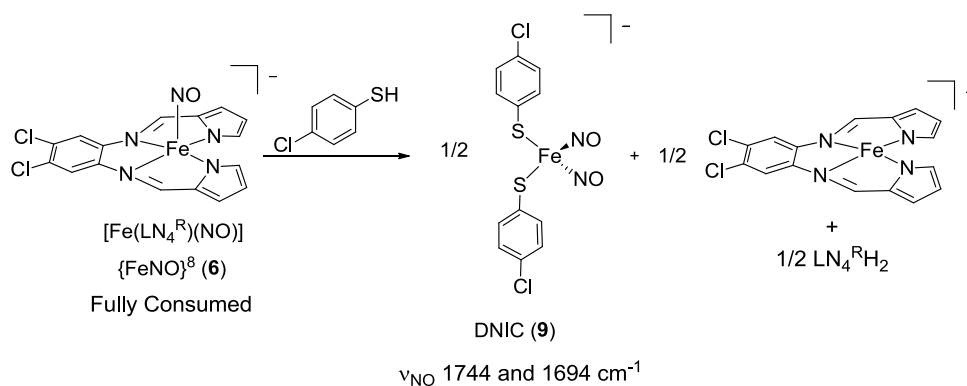
Reactivity of $\{\text{FeNO}\}^8$ with *p*-chlorobenzenethiol³

The reaction of the $\{\text{FeNO}\}^8$ complex **6** with *p*-ClArSH in MeCN led to the formation of DNIC, namely $\text{Co}(\text{Cp}^*)_2[\text{Fe}(\text{RS})_2(\text{NO})_2]$ (**9**). Similar reactivity was performed in THF with analogous results. The FTIR spectrum of **9** revealed two strong $\nu_{\text{NO}} = 1744$ and 1694 cm^{-1} (Fig. 2.10). These values are consistent with previously reported anionic DNIC complexes with aromatic thiolates, and an authentic synthesis of $\text{Et}_4\text{N}[\text{Fe}(\text{NO})_2(\text{ClArS})_2]$.^{76,79,80} Compound **9** was readily separable from the reaction mixture due to its sparing solubility in THF, and was isolated

³ Unpublished results and discussion related to the research found in the citation of footnote 1.

in 85% yield. Additional characterization of **9** by ESI-MS(-) displayed peaks with $m/z = 371.8$ and 401.8, consistent with the ions of $[\text{Fe}(\text{RS})_2(\text{NO})]^-$ and $[\text{Fe}(\text{RS})_2(\text{NO})_2]^-$ (**9**), respectively.⁸⁰ The UV-vis absorption of **9** showed a characteristic broad absorbance bands at 475 and 799 nm that are in-line DNIC complex, (Fig. 2.9).

Scheme 2.6 Proposed product formation from reaction of **6** with RSH.



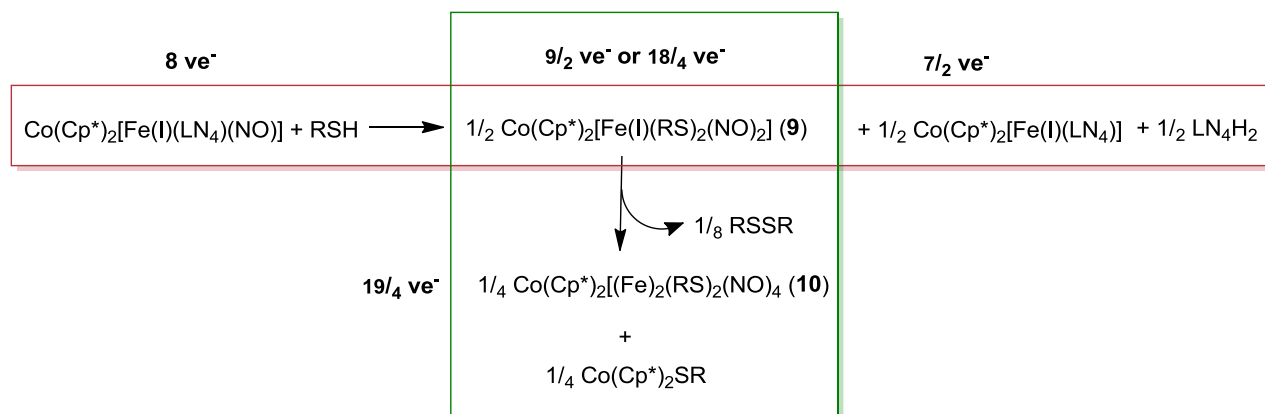
Analysis of the Et₂O-soluble material after workup provided evidence for free LN₄^{PhCl} based on ¹H NMR and FTIR (Fig. S20). Identification of these products is consistent with protonation and dissociation of the LN₄^{PhCl} ligand. However, there is no indication of RSSR formation in the ¹H NMR. This observation may point to a difference in the reactivity between the {FeNO}⁷ and {FeNO}⁸ complexes, implicating disulfide formation as a requisite to form the Fe(I) DNIC. In the case of {FeNO}⁷, this may occur within the putative 5C complex $[\text{Fe}(\text{II})(\text{LN}_4\text{H}_2)(\text{NO})(\text{RS})_2]$ to ultimately give $[\text{Fe}(\text{I})(\text{LN}_4\text{H}_2)(\text{NO})(\text{RS})]$ and RS• prior to formation of RRE (**8**). Differing from this, the {FeNO}⁸ unit is formally between Fe(II)-NO⁻ ↔ Fe(I)-NO•, thus only one equiv of RSH must bind to the metal center to afford the 5C $[\text{Fe}(\text{I})(\text{LN}_4\text{H})(\text{NO})(\text{RS})]^-$. Subsequent combination of the LN₄-stabilized $[\text{Fe}(\text{I})(\text{NO})(\text{RS})]$ unit would lead to formation of DNIC without the formation of RSSR.

The difference in reactivity between $\{\text{FeNO}\}^7$ and $\{\text{FeNO}\}^8$ with RSH stems from the reduced nature of the $\{\text{FeNO}\}^8$ complex. It is clear that a thermodynamic minimum for the $[\text{Fe}(\text{LN}_4^{\text{R}})(\text{NO})]^{0/-}$ complexes with RSH is some version of a DNIC or RRE complex. This type of reactivity of a 5C non-heme $\{\text{FeNO}\}^8$ complex has not been observed. Importantly, biological DNICs have been observed *in vivo*, yet the formation of these compounds is not fully understood. As discussed above, a current theory evokes formation of $[\text{Fe}(\text{II})(\text{NO})(\text{RS})_2]$ and loss of $\text{RS}\cdot$ to afford the reduced $[\text{Fe}(\text{I})(\text{NO})(\text{RS})]$ unit as the common precursor to DNIC or RRE.⁷⁵ Provided that the $\{\text{FeNO}\}^7$ species require formation of RSSR can explain the preference towards the RRE product due to the lack of available RS^- . Similarly, the lack of RSSR in the $\{\text{FeNO}\}^8$ reactions indicates that the electron equivalents are present, speaking to the reduced nature of the Fe-NO unit. Taken together, these results highlight that: (i) $\{\text{FeNO}\}^7$ complexes are more stable to RSH reactivity due to the observation of unreacted starting material, where as >85% of the NO containing material was consumed from the $\{\text{FeNO}\}^8$ reactions; (ii) the observation that $\{\text{FeNO}\}^7$ complexes favor RRE (**8**) formation, whereas $\{\text{FeNO}\}^8$ species favor DNIC (**9**) formation, which result from the one-electron reduced nature of the starting $\{\text{FeNO}\}^8$ complex; and (iii) both the $\{\text{FeNO}\}^7$ and $\{\text{FeNO}\}^8$ reaction pathways may have a common intermediate, namely the putative LN_4H_n -stabilized $[\text{Fe}(\text{I})(\text{NO})(\text{RS})]$ complex.

Reactivity of $[\text{Co}(\text{Cp}^*)_2][\text{Fe}(\text{LN}_4^{\text{Pr}})(\text{NO})]$ (**7**) $\{\text{FeNO}\}^8$ with *p*-chlorobenzenethiol and glutathione⁴

We continue our investigations into the reactivity of non-heme $\{\text{FeNO}\}^8$ complexes by studying the reaction of $[\text{Co}(\text{Cp}^*)_2][\text{Fe}(\text{LN}_4^{\text{Pr}})(\text{NO})]$ (**7**) with the *p*-ClArSH and glutathione (GSH). Complex **7** was shown to transfer HNO to metMb under buffered aqueous conditions.⁴⁴ However, in the presence of GSH, the HNO transfer was inhibited. This inhibition is due to either trapping of HNO by GSH to form sulfinamide, $\text{GS}(\text{O})\text{NH}_2$, or by formation of a thiolate bound Fe complex, e.g., a DNIC. Therefore, to better understand the fate of **7** in the presence of thiols, stoichiometric reactions with RSH and GSH were pursued.

Scheme 2.7 Analysis of products formed in reaction of **7** with RSH = *p*-ClArSH; $\text{Co}(\text{Cp}^*)_2 =$ decamethylcobaltacenium cation; $\text{ve}^- =$ valence electrons. The red box indicates one forward reaction to give the DNIC **9**, and the green box indicates another forward reaction of **9** going to rRRE **10**.



⁴ Unpublished results and discussion related to the research found in the citation of footnote 1.

Complex **7** reacted with RSH in MeCN to afford a mixture of DNIC species. A systematic workup through a series of different polarity solvents allowed for quantification and identification of nearly all species present. From this, the major NO-containing products are identified as the anionic DNIC (**9**) and the reduced Roussin's red ester (rRRE), **10** (Scheme 2.7). Compound **9** was identified by FTIR (1744 and 1694 cm^{-1} , Fig. 2.10), ESI-MS ($m/z = 402.0$), and UV-vis (383, 475, and 799 nm, Fig. 2.9) and isolated in 28% yield. These results are congruous with an authentic synthesis of $\text{Et}_4\text{N}[\text{Fe}(p\text{-ClArS})_2(\text{NO})_2]$ and are analogous to the product obtained from reactions of **5** and **6** with RSH. One noted difference is that the reaction of RSH with **7** also afforded rRRE **10**, 98% yield. Compound **10** was characterized by FTIR ($\nu_{\text{NO}} = 1683$ and 1667 cm^{-1}) and are clearly distinguishable from the ν_{NO} of **9** (Fig. 2.10). These ν_{NO} values red-shift from those seen in RRE **8**, which is in-line with the more reduced nature of **10**, and agrees well with other rRRE complexes.⁸¹ The UV-vis profile for **10** has characteristic absorbance bands at 652 and 971 nm that are comparable to peptide-bound rRRE complexes (Fig. 2.9).⁸² The rRRE complex **10** is expected to be paramagnetic. Accordingly, the EPR spectrum showed an axial feature centered at $g = 2.03$, with no observable hyperfine coupling under the experimental parameters used (Fig. S24). These results are indicative of an $S = 1/2$ rRRE complex in which the unpaired electron is predominantly delocalized over the 2Fe-2S system. Moreover, the EPR signal differs from that observed for the $S = 1/2$ $\{\text{FeNO}\}^7$ species **4**. Characterization of other products include the initial MeCN precipitate, which is currently assigned as $[\text{Co}(\text{Cp}^*)_2][\text{SR}]$ salt based on FTIR, and is present in 98% yield using the stoichiometry of Scheme 2.7. Moreover, ^1H NMR of the Et_2O -soluble material confirmed the presence of LN_4H_2 isolated in 95% yield (Fig. S21).

One major Fe-containing product, $[\text{Co}(\text{Cp}^*)_2][\text{Fe}(\text{I})(\text{LN}_4^{\text{Pr}})]$, is tentatively assigned but is supported by the previously reported complex, namely $[\text{Co}(\text{Cp}^*)_2][\text{Fe}(\text{I})(\text{LN}_4^{\text{Pr}})(\text{N}_2)]$, that was observed in the disproportionation studies of **7**.⁴⁴

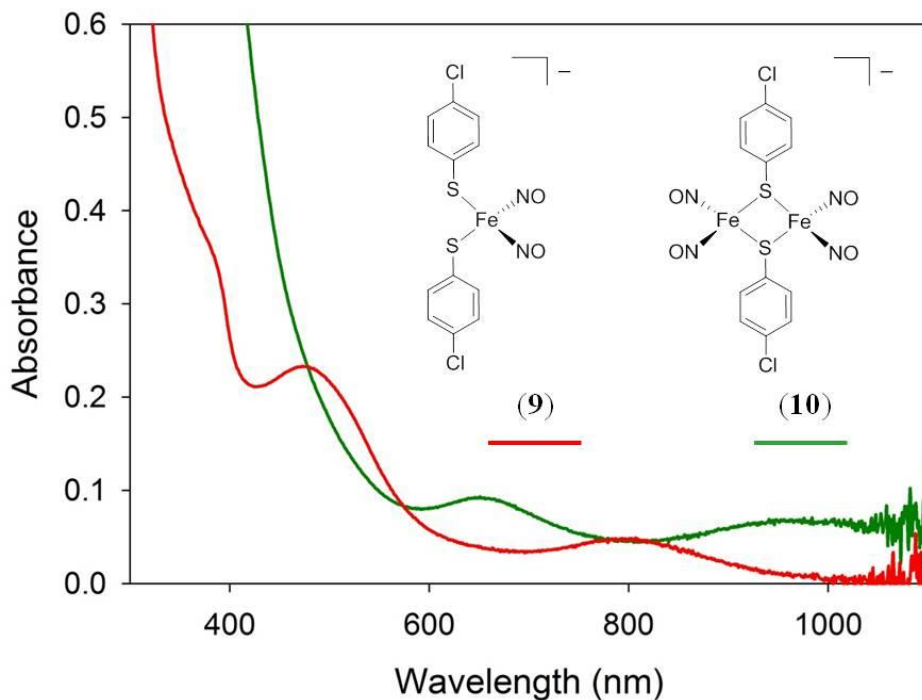


Figure 2.9. UV-vis (qualitative, MeCN, RT) comparison of DNIC (**9**, red trace) and rRRE (**10**, green trace)

The analysis shown in Scheme 2.7 is balanced; however, there are additional pathways that may interconnect various species and affect the overall equation. For instance, the transformation shown in the green box (Scheme 2.7) requires electron transfer. Importantly, this is not the straightforward equilibrium that is observed between DNIC (**9**) and RRE (**8**), but rather a forward progressing reaction, likely driven by the insolubility of the $[\text{Co}(\text{Cp}^*)_2][\text{SR}]$. As shown in Scheme 2.7, the valence electron count requires $1/4$ of an electron to balance the equation, accordingly this may come from dissociation of $1/4 \text{ RS}\cdot$ from **9** to give $1/8 \text{ RSSR} + 1/4$

e^- . This occurs, presumably, through an inner-sphere mechanism, similarly to what is proposed with $\{\text{FeNO}\}^7$ reactivity discussed above. This type of reductive elimination has been proposed for the formation of DNIC and RRE, and may apply here to the formation of rRRE.⁷⁵ However, the reduced complex, $[\text{Co}(\text{Cp}^*)_2][\text{Fe}(\text{I})(\text{LN}_4)]$, could also serve as a reducing agent.

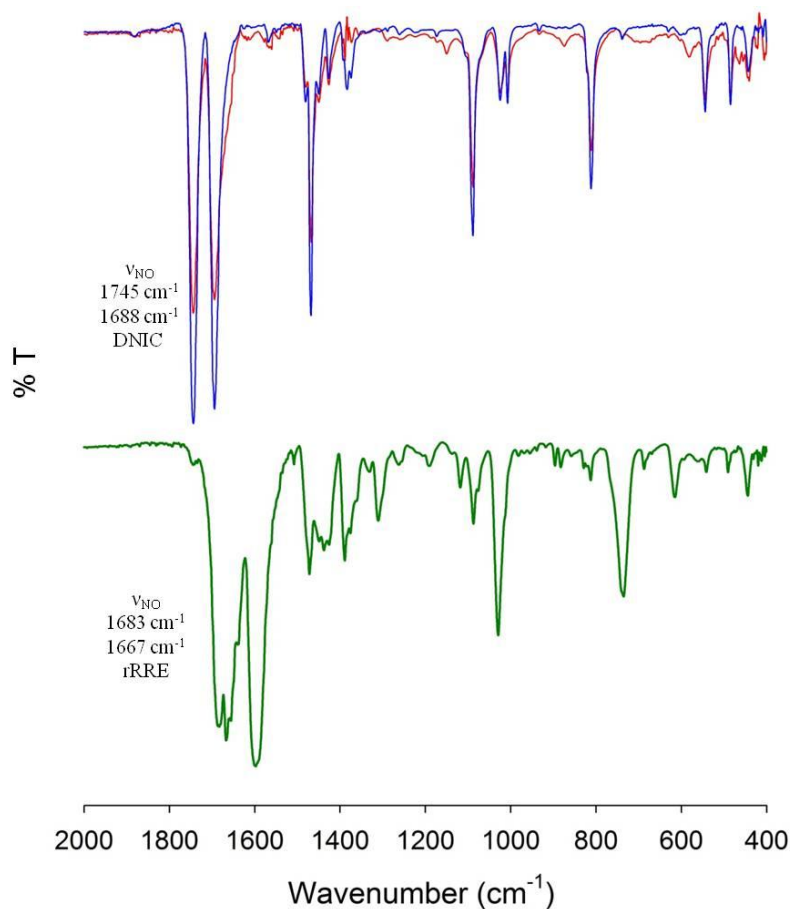


Figure 2.10 FTIR (KBr, RT) of the DNIC (**9**) from reaction of **6** (red trace) and **7** (blue trace) with *p*-ClArSH; and FTIR of rRRE (**10**) from reaction of **7** (green trace) with *p*-ClArSH.

Mechanistically, the analysis discussed above for the $\{\text{FeNO}\}^8$ complexes **5** and **6** is applicable here, inferring the formation of the putative $[\text{Fe}(\text{RS})(\text{NO})]$ unit that eventually leads to formation of DNIC (Scheme 2.5). However, it is unclear exactly why the formation of rRRE (**10**) is favored for **7**, but not observed in the reactions of **5** or **6**. One rationale is that complex **7** has the most negative redox potential (Table 1) and may facilitate formation of the highly reduced complex **10**. However, it is unclear as to which species, **9** or **10**, is formed first.

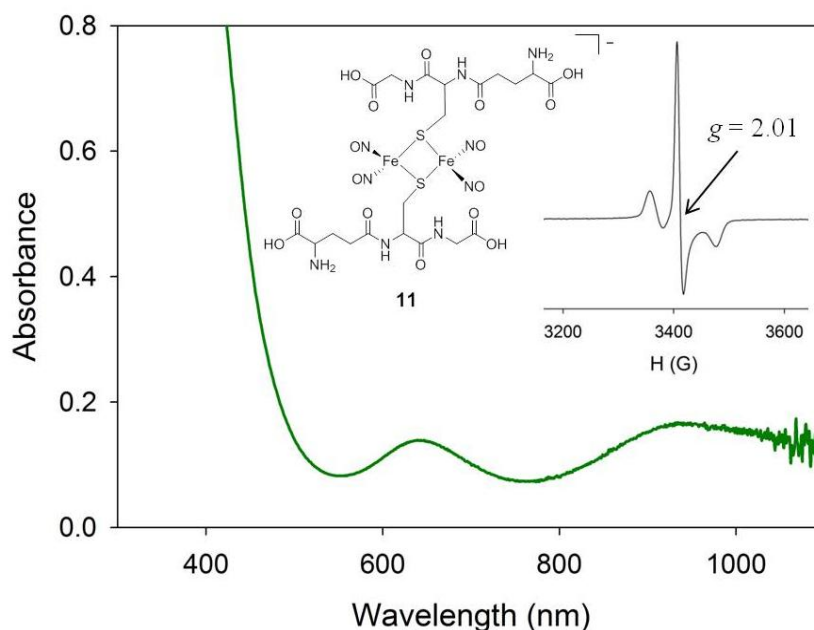


Figure 2.11 UV-vis (qualitative, milli-Q H_2O) of rRRE complex **11** (green trace) formed from reaction of **7** with GSH. *Inset:* EPR spectrum of **11**. Data collected on a 5 mM 10:1 (milli-Q H_2O :MeCN) solution of **11**. Experimental parameters: $T = 20$ K, Microwave Power = 1.00×10^{-2} mW, Frequency = 9.582 GHz. Mod. Amp.: 6.48 G.

The reaction of **7** with RSH in organic solvents primarily leads to formation of **10**. Therefore, we aimed to investigate the reactivity of **7** with a biologically relevant thiol, namely GSH, in aqueous conditions. The reaction was performed by adding an MeCN aliquot of **7** to an aqueous solution of GSH in 1:1 stoichiometry. This resulted in the immediate formation of a green colored solution. UV-vis analysis showed $\lambda_{\text{max}} = 643$ and 952 nm (Fig. 2.11), characteristic of a rRRE species, assigned as $[\text{Co}(\text{Cp}^*)_2][(\text{Fe})_2(\text{GS})_2(\text{NO})_4]$ (**11**). Moreover, EPR analysis of the green solution confirmed the paramagnetic $S = 1/2$ species with $g = 2.01$ (Fig. 2.11). The EPR spectra of **10** and **11** are very similar and confirms the formation of rRRE from **7** in both organic and aqueous conditions.

Taken together, the reaction of **7** with RSH and GSH favors the formation of rRRE (**10**), thus distinguishing **7** from **5** and **6**, that only produce **9**. This type of reactivity may support the formation of DNIC species (e.g. **8**, **9**, and **10**) from reduced Fe-NO complexes in biology. For instance, paramagnetic DNICs like **9** have been observed in biological samples and are thought to safely transport and deliver NO.⁸³ These species arise from chelatable Fe, NO, and biological thiols. However, the standard interpretation of DNIC formation comes from Fe(II), NO, and thiols, which must inevitably be reduced (through disulfide formation) to afford the known Fe(I) DNIC. Thus, an alternative route involving the reaction of thiols with a preformed Fe(I)-NO species, $\{\text{FeNO}\}^8$, could circumvent disulfide formation. Thus, it is possible that free HNO could be trapped at a protein-bound Fe(II) center, to afford an $\{\text{Fe}(\text{H})\text{NO}\}^8$ complex, which in the presence of GSH, for example, may lead to formation of DNIC. This suggests that DNICs may arise from HNO, and explain the overlapping biological responses of HNO and NO, such as vasodilation.

2.7. Conclusions

The following are the summary of the main findings of this work:

- (i) We have described the synthesis and characterization of several non-heme FeNO complexes supported by the planar LN₄ diimine-dypyrrolide ligand framework, which represent new examples of the {FeNO}⁷ (**3** and **4**) and {FeNO}⁸ (**5** and **6**) class of metal nitrosyls in hybrid heme architectures. The synthesis of the rare {FeNO}⁸-type complexes **5** and **6** could be achieved by stoichiometric chemical reduction with [Co(Cp*)₂] or KC₈. These {FeNO}⁸ species add to the small list of this type of FeNO complex that can be isolated under standard lab conditions.
- (ii) The {FeNO}⁷ complexes display spectroscopic and structural properties that are mostly consistent with other 5C FeNO species in this class. One particular outlying feature was demonstrated in the X-ray crystal structure of **3**, which afforded an atypical Fe-N-O angle of ~ 155° for this E-F notation. This unusual metric parameter has been explained with respect to the relative amount of Fe *p_z* character in the largely *d_z²*-based HOMO of this and similarly disposed 5C {FeNO}⁷ complexes. Independent calculations by another group have assigned the oxidation states in such systems as LS-Fe(I)-NO⁺ (*S* = 1/2) with majority spin-density on Fe.
- (iii) The electrochemical properties of {FeNO}⁷ complexes **3** and **4** are fairly similar exhibiting reversible and diffusion-controlled redox potentials for the {FeNO}^{7/8} couple at -1.23 and -1.16 V (vs. Fc/Fc⁺ in MeCN), respectively. The electrochemical data highlight the accessibility and stability of {FeNO}⁸ from suitable {FeNO}⁷ precursor molecules.

- (iv) Consistent with the electrochemical picture obtained, chemical reduction to obtain $\{\text{FeNO}\}^8$ complexes **5** and **6** was relatively straightforward if some precaution is followed. This reduction is also reversible and the corresponding $\{\text{FeNO}\}^7$ complexes **3** and **4** could be re-obtained with ferrocenium oxidants. Complex **5** afforded a ν_{NO} value $\sim 50 \text{ cm}^{-1}$ less than the parent $\{\text{FeNO}\}^7$ complex **3**, which is suggestive of a ligand-based reduction/higher spin-state derivative. Other measurements (NMR) are consistent with this assessment. Complex **6**, on the other hand, afforded a ν_{NO} red-shift of $\sim 140 \text{ cm}^{-1}$ to 1580 cm^{-1} from **4** that was more consistent with $\{\text{FeNO}\}$ unit reduction.
- (v) These air-sensitive $\{\text{FeNO}\}^8$ materials appear to be indefinitely stable in the solid-state when stored under anaerobic/anhydrous conditions in the dark. Their solution-state solubility is different resulting in slow re-oxidation to the $\{\text{FeNO}\}^7$ derivatives **3** and **4** over the course of 6-9 h in both polar and apolar organic solvents. The ultimate explanation behind this reactivity is unknown at present, but it is consistent with the label for this class of FeNO systems as “elusive”. However, it is important to point out that these are slow processes with respect to the potential for such molecules to serve as HNO sources.
- (vi) Complexes **5**, **6**, and **7** exhibit nitroxyl-like reactivity with the ferric porphyrin complex, $[\text{Fe}(\text{TPP})\text{Cl}]$, to afford $[\text{Fe}(\text{TPP})(\text{NO})]$ in stoichiometric yield. UV-vis monitoring of this reaction suggests that a potential 6C $\{\text{FeNO}\}^7$ is an intermediate traversed in the reaction path via a “transnitroxylation” process.
- (vii) Complexes **5**, **6**, and **7** react differently from their $\{\text{FeNO}\}^7$ counterparts in the presence of thiols. Though all the complexes discussed form DNICs, the reaction

pathway appears to be dependent on the oxidation state (reduced nature) of the Fe-NO unit.

In sum, unraveling the chemistry of iron-nitroxyl/{FeNO}⁸ derivatives is challenging as they represent synthetic targets that are difficult to achieve and maintain. Once stabilized, at least to some extent, they offer new avenues of MNO reactivity that have never been explored. To the best of our knowledge a “transnitroxylation” process has not been proposed before (in stark contrast to transnitrosation), presumably due to a lack of reasonably well-characterized and stable Fe-nitroxyl systems. We expect systems like these and others will ultimately be used as synthetic analogues of biological Fe-nitroxyls and HNO-donors with therapeutic application.

2.8 Materials and methods

2.8.1 General Information

All reagents were procured from commercial suppliers and used as received unless otherwise noted. Research grade nitric oxide gas, (NO(g), UHP, 99.5%) was obtained from Matheson Tri-Gas. The NO(g) was purified by passage through an Ascarite II[®] column (sodium hydroxide-coated silica, purchased from Aldrich) and handled under anaerobic conditions. ¹⁵NO(g) (¹⁵N, ≥ 98%) was purchased from Cambridge Isotope Laboratories and used without further purification. Acetonitrile (MeCN), methylene chloride (CH₂Cl₂), tetrahydrofuran (THF), diethyl ether (Et₂O) and pentane were purified by passage through activated alumina columns using an MBraun MB-SPS solvent purification system and stored over 3 Å molecular sieves under a nitrogen (N₂) atmosphere before use. *N,N*-dimethylformamide (DMF) was purified with a VAC solvent purifier containing 4 Å molecular sieves and was stored under similar conditions.

Anhydrous MeOH and EtOH was obtained by distilling the alcohol from $\text{Mg}(\text{OR})_2$ ($\text{R} = \text{Me}$ for MeOH, Et for EtOH) and stored under N_2 . Toluene was purified by stirring overnight with 3 Å molecular sieves, then distilling from CaH_2 , which was finally stored over 3 Å molecular sieves. Acetone was dried by stirring over 3 Å molecular sieves for 24 h, which was decanted and stored under N_2 . All solvents were filtered to remove sieve particulate with a 0.45 μm nylon filter immediately before use. The Fe(II) salt, $(\text{Et}_4\text{N})_2[\text{FeCl}_4]$,⁸⁴ and $\{\text{FeNO}\}^7$ complex $[\text{Fe}(\text{TPP})(\text{NO})]$,⁸⁵ were prepared according to the published procedures. All reactions were performed under an inert atmosphere of N_2 using standard Schlenk-line techniques or in an MBraun Labmaster glovebox under an atmosphere of purified N_2 . All reactions and measurements involving $\text{NO}(\text{g})$ and the FeNO complexes were performed in the dark with minimal light exposure by wrapping the reaction flasks/vials with aluminum foil to avoid any photochemical reactions.

2.8.2 Physical Methods

FTIR spectra were collected with a ThermoNicolet 6700 spectrophotometer running the OMNIC software. Samples were run as solids as KBr pellets in a stream of dry N_2 . Solution FTIR spectra were obtained using a demountable airtight liquid IR cell from Graseby-Specac with CaF_2 windows and 0.1 Teflon mm spacers. All FTIR samples were prepared inside a glovebox. The closed liquid cell was taken out of the box and spectra were acquired immediately. Room temperature (RT) solid-state magnetic susceptibility measurements were performed with a Johnson Matthey magnetic susceptibility balance. Solution-state susceptibility measurements were performed at 298 K using the Evans method on a Varian Unity Inova 500 MHz NMR spectrometer.⁸⁶ X-band (9.60 GHz) EPR spectra were obtained on a Bruker ESP

300E EPR spectrometer controlled with a Bruker microwave bridge at 10 K. The EPR was equipped with a continuous-flow liquid He cryostat and a temperature controller (ESR 9) made by Oxford Instruments, Inc. Electronic absorption spectra were run at 298 K using a Cary-50 UV-vis spectrophotometer containing a Quantum Northwest TC 125 temperature control unit. The UV-vis samples were prepared anaerobically in gas-tight Teflon-lined screw cap quartz cells with an optical pathlength of 1 cm. Electrochemistry measurements were performed with a PAR Model 273A potentiostat using a Ag/Ag⁺ (0.01 M AgNO₃/0.1 M ⁿBu₄NPF₆ in CH₃CN) reference electrode, Pt-wire counter electrode, and a Glassy Carbon working milli-electrode (diameter = 2 mm) under an Ar atmosphere. Measurements were performed at ambient temperature using 1.0-10.0 mM analyte in various solvents containing 0.1 M ⁿBu₄NPF₆ as the supporting electrolyte. Ferrocene (Fc) was used as an internal standard and all potentials are reported relative to the Fc⁺/Fc couple. ¹H and ¹³C NMR spectra were recorded in the listed deuterated solvent on a 400 MHz Bruker BZH 400/52 NMR spectrometer or a Varian Unity Inova 500 MHz NMR at 298 K with chemical shifts referenced to TMS or residual protio signal of the deuterated solvent as previously reported.⁸⁷ Low resolution ESI-MS data were collected on a Perkin Elmer Sciex API I Plus quadrupole mass spectrometer, whereas high resolution ESI-MS data were collected using a Bruker Daltonics 9.4 T APEXQh FT-ICRM. Elemental microanalysis for C, H, and N were performed by QTI-Intertek (Whitehouse, NJ) or Columbia Analytical Services (Tucson, AZ). For some complexes, notably **5-6**, residual solvent is present in the microanalysis and is consistent with what is observed for these compounds in their solid-state IR spectra.

2.8.3 Synthesis of Compounds

(N¹E,N²E)-N¹,N²-bis((1H-pyrrol-2-yl)methylene)-benzene-1,2-diamine (LN₄H₂^{Ph})

To an anaerobic solution of 1,2-phenylenediamine (2.161 g, 19.98 mmol) in 25 mL of MeCN was added a 25 mL MeCN solution containing 3.801 g (39.97 mmol) of pyrrole-2-carboxaldehyde followed by addition of activated 3 Å molecular sieves (15% w/v). The brown solution mixture was refluxed for 24 h and allowed to cool to RT before workup. Once cooled the red mixture was filtered (sieves and insoluble yellow product) and the insolubles were washed with CHCl₃. The red filtrate was concentrated under vacuum to afford a red amorphous paste that was dried for several hours under reduced pressure prior to trituration with ~30 mL of Et₂O. The insoluble yellow material was filtered, washed with cold Et₂O, and dried under vacuum to afford 3.255 g (12.36 mmol, 62%) of product. mp: 197-199 °C. ¹H NMR (400 MHz, CDCl₃, δ from TMS): 12.34 (br, 1H, NH), 7.68 (s, 1H, CH=N), 7.25 (t, 1H, Ar-H), 7.07 (dd, 1H, Ar-H), 6.40 (d, 1H, Ar-H Pyrrole), 6.23 (s, 1H, Ar-H Pyrrole), 6.01 (t, 1H, Ar-H Pyrrole). ¹³C NMR (100.6 MHz, CDCl₃): 150.7 (CH=N), 145.9 (Ar-C), 131.0 (Ar-C), 126.8 (Ar-C), 123.9 (Ar-C), 119.1 (Ar-C), 117.3 (Ar-C), 109.7 (Ar-C). FTIR (KBr matrix), ν_{max} (cm⁻¹): 3445 (w), 3141 (m), 3085 (w), 2970 (w), 2855 (w), 2746 (w), 1617 (vs), 1574 (s), 1549 (m), 1485 (w), 1442 (m), 1412 (s), 1336 (m), 1310 (m), 1275 (w), 1247 (w), 1211 (m), 1189 (w), 1160 (w), 1138 (m), 1094 (s), 1036 (s), 1026 (s), 971 (w), 966 (w), 884 (m), 877 (m), 846 (m), 801 (w), 783 (w), 742 (s), 659 (w), 608 (m), 579 (w), 551 (m). LRMS-ESI (*m/z*): [M + H]⁺ calcd for C₁₆H₁₅N₄, 263.1; found, 263.2.

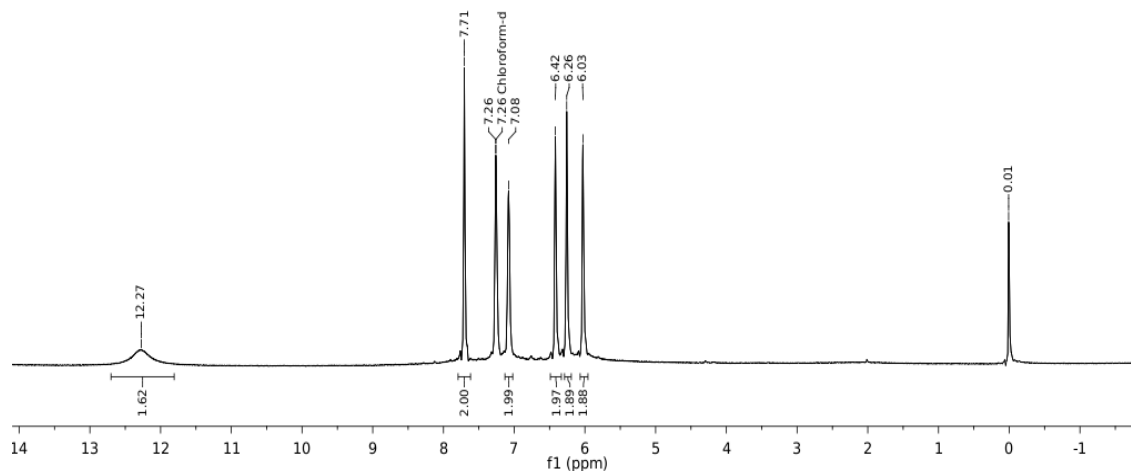


Figure 2.12. ^1H NMR of $\text{LN}_4\text{H}_2^{\text{Ph}}$, CDCl_3 , TMS, RT.

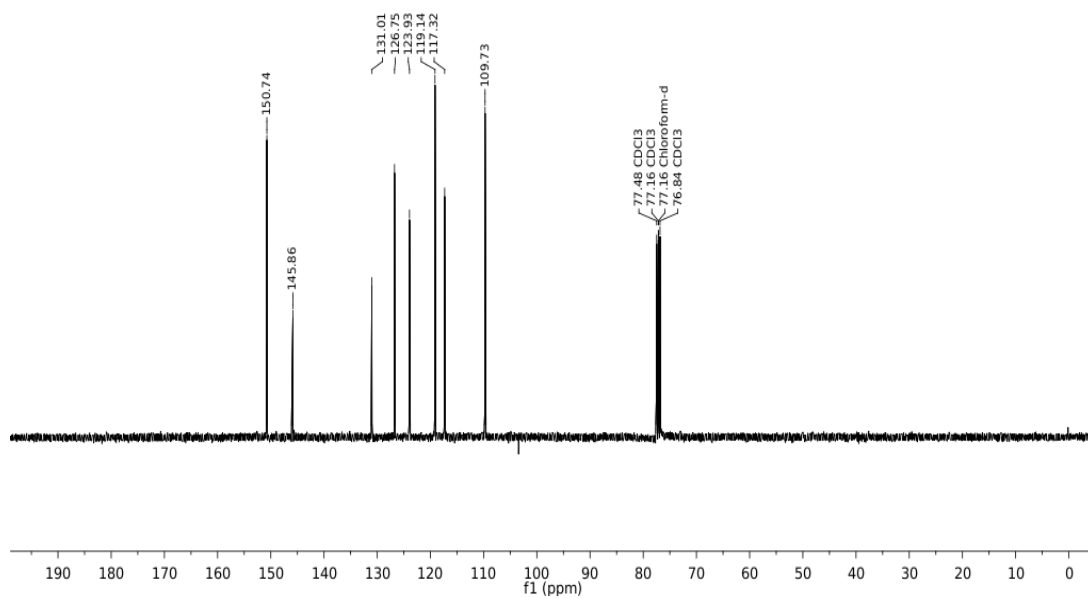


Figure 2.13. ^{13}C NMR of $\text{LN}_4\text{H}_2^{\text{Ph}}$, CDCl_3 , TMS, RT.

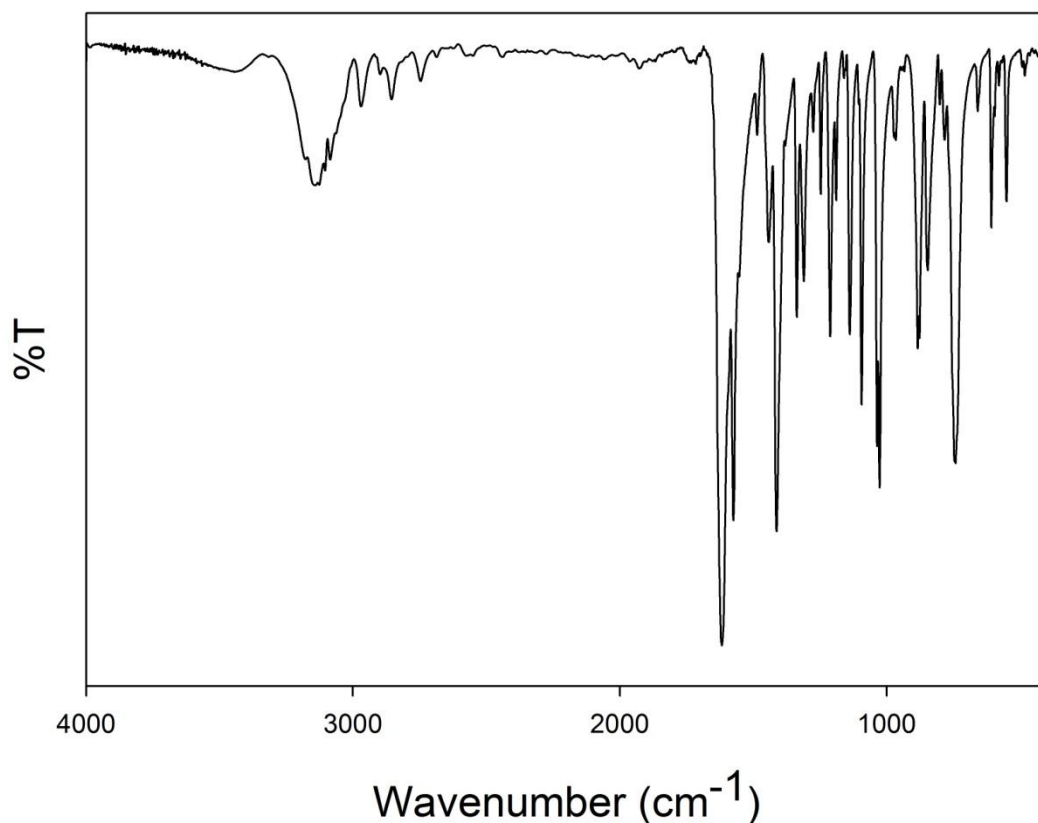


Figure 2.14. FTIR (KBr) of $\text{LN}_4\text{H}_2^{\text{Ph}}$.

(N¹E,N²E)-N¹,N²-bis((1H-pyrrol-2-yl)methylene)-4,5-dichlorobenzene-1,2-diamine (LN₄H₂^{PhCl})

Under anaerobic conditions, a 5 mL MeCN solution of 1.004 g (5.671 mmol) of 4,5-dichlorobenzene-1,2-diamine was added to a 5 mL MeCN solution containing 1.074 g (11.29 mmol) of pyrrole-2-carboxaldehyde in the presence of 3 Å molecular sieves (15% w/v). This solution was then refluxed overnight at 70 °C for 20 h resulting in a black-to-deep-red color change over the reflux period. Cooling the resulting mixture to RT resulted in the precipitation of a dark insoluble material. The insolubles (product and sieves) were filtered through a glass frit, thoroughly washed with CHCl_3 , and the filtrate was concentrated and dried in vacuo to a dark

red paste. The material was then redissolved in minimal MeCN (~10 mL) and kept at -5 °C to induce precipitation of the desired product. The procedure of concentration, dissolution in minimal MeCN, and precipitation was repeated three times to afford the dark red-brown solid product (1.110 g, 3.341 mmol, 59%). mp: 191-194 °C. ¹H NMR (400 MHz, CDCl₃, δ from residual protio solvent): 11.87 (br, 0.7H, NH, integrates slightly low due to the exchangeable nature of the pyrrole proton), 7.64 (s, 1H, CH=N), 7.16 (s, 1H, Ar-H), 6.48 (d, 1H, Ar-H Pyrrole), 6.38 (d, 1H, Ar-H Pyrrole), 6.10 (t, 2H, Ar-H Pyrrole). ¹³C NMR (100.6 MHz, CDCl₃): 151.5 (CH=N), 145.3 (Ar-C), 130.6 (Ar-C), 129.6 (Ar-C), 124.5 (Ar-C), 120.7 (Ar-C), 118.8 (Ar-C) 110.6 (Ar-C). FTIR (KBr matrix), ν_{max} (cm⁻¹): 3446 (w), 3140 (w), 2967 (w), 2890 (w), 2847 (w), 2745 (w), 1611 (vs), 1567 (m), 1484 (w), 1471 (w), 1435 (w), 1413 (s), 1374 (w), 1355 (m), 1331 (m), 1312 (m), 1263 (w), 1245 (w), 1223 (w), 1163 (m), 1126 (s), 1092 (m), 1032 (s), 961 (w), 887 (m), 856 (w), 831 (w), 808 (w), 741 (m), 678 (w), 652 (w), 605 (m), 594 (m), 505 (w), 497 (w), 440 (w), 429 (w). LRMS-ESI (m/z): [M + H]⁺ calcd for C₁₆H₁₃Cl₂N₄, 331.1; found, 331.2.

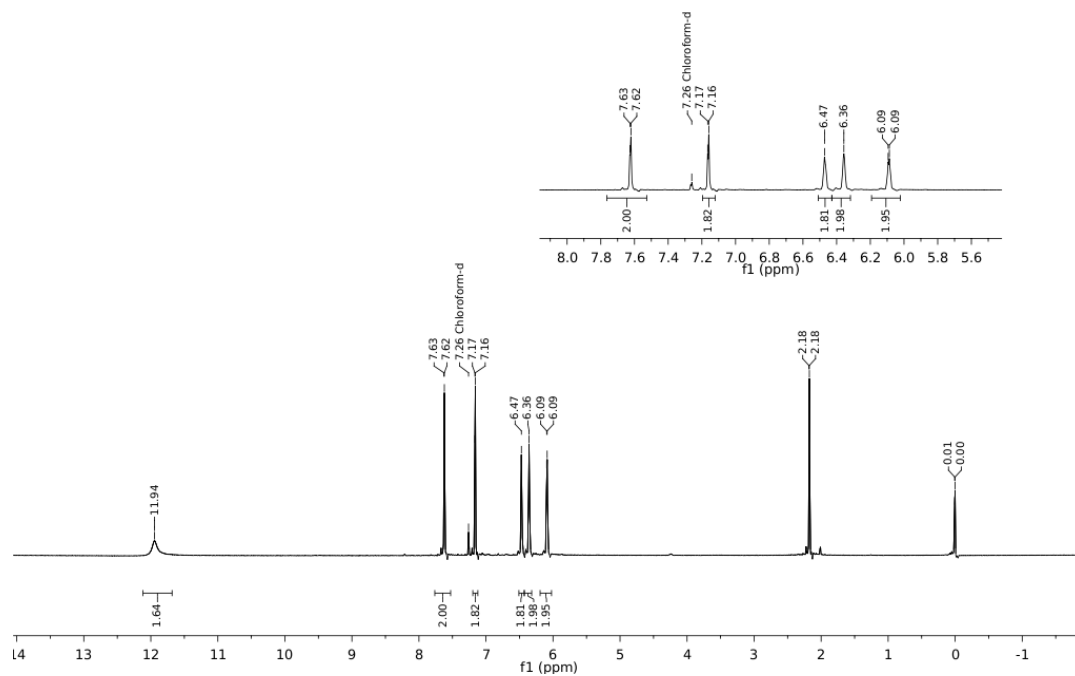


Figure 2.15. ^1H NMR of $\text{LN}_4\text{H}_2^{\text{PhCl}}$, CDCl_3 , TMS, RT.

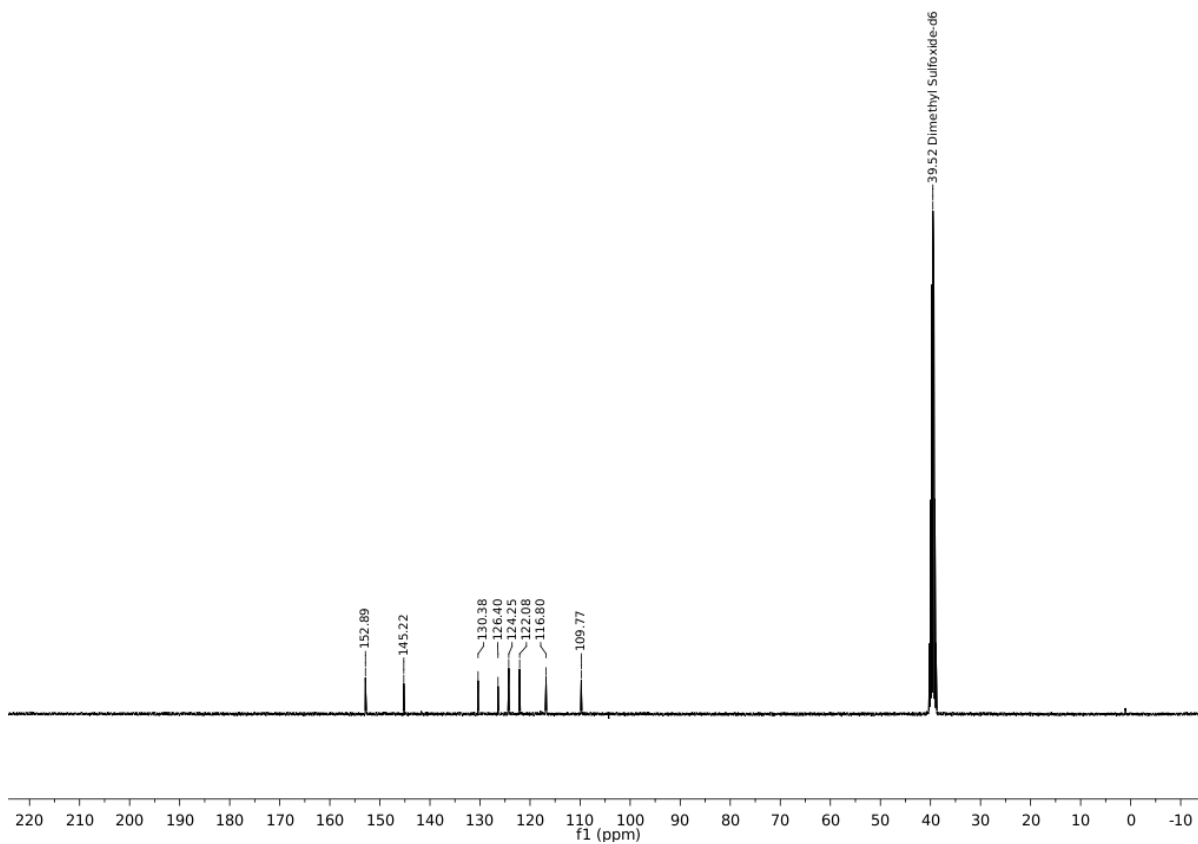


Figure 2.16. ^{13}C NMR of $\text{LN}_4\text{H}_2^{\text{PhCl}}$, DMSO-d_6 , TMS, RT.

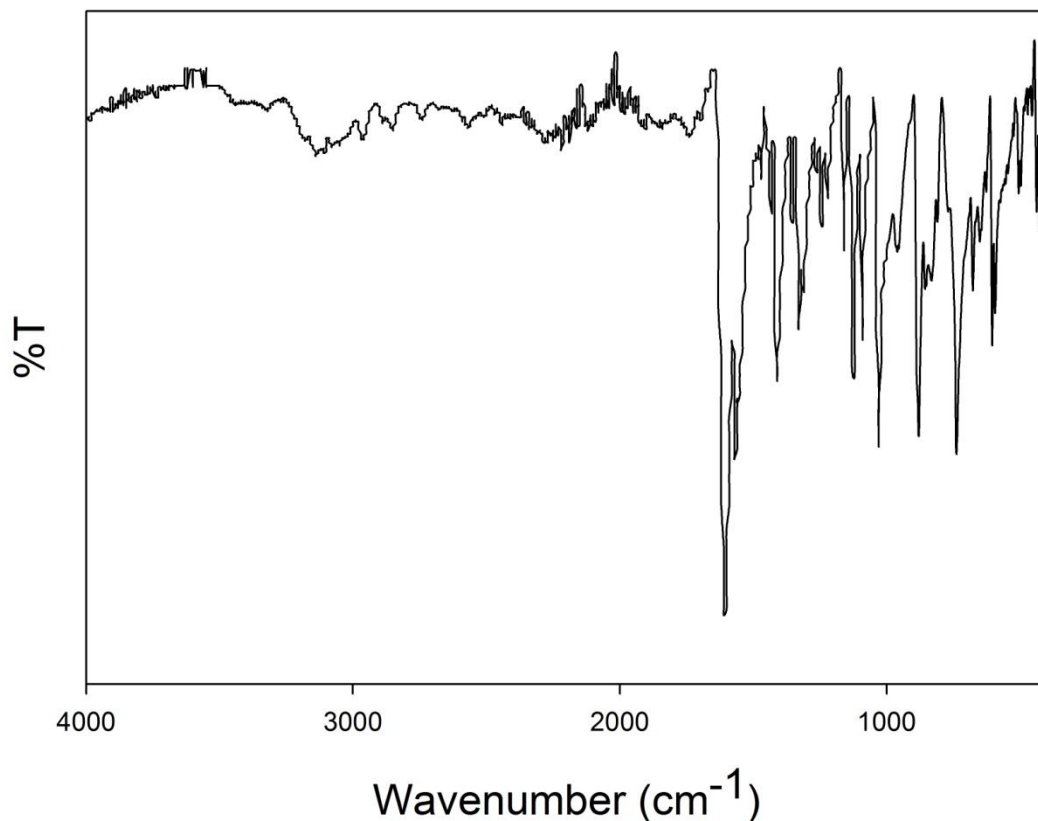
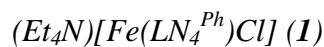


Figure 2.17. FTIR (ATR) of $\text{LN}_4\text{H}_2^{\text{PhCl}}$.



To a batch of $\text{LN}_4\text{H}_2^{\text{Ph}}$ (0.2500 g, 0.9531 mmol) dispersed in 5 mL of dry MeCN was added a 3 mL MeCN slurry of NaH (0.0457 g, 1.904 mmol), resulting in $\text{H}_2(\text{g})$ evolution and a color change from orange-yellow to bright yellow indicative of ligand deprotonation. To ensure complete deprotonation, an occasional vacuum was applied while stirring for ~ 15 min. To this reaction mixture was then added a 10 mL MeCN solution of $(\text{Et}_4\text{N})_2[\text{FeCl}_4]$ (0.4366 g, 0.9529 mmol) resulting in formation of a pale gray-white precipitate (NaCl) and a solution color change to dark brown-yellow. The reaction mixture was stirred for another 2 h at RT, which resulted in no further change. The solution was filtered of insolubles and the homogeneous dark filtrate was

stripped of MeCN and treated with ~ 20 mL of THF to precipitate any excess Et₄NCl. The THF insolubles were filtered, washed with THF, and the dark filtrate was concentrated and dried under vacuum resulting in **1** as a shiny dark solid (0.3582 g, 0.7434 mmol, 78%). FTIR (KBr matrix), ν_{\max} (cm⁻¹): 3062 (w), 2975 (w), 2945 (w), 1589 (vs), 1557 (vs), 1481 (w), 1462 (m), 1437 (m), 1383 (s), 1288 (s), 1219 (m), 1183 (m), 1169 (m), 1100 (w), 1077 (w), 1027 (vs), 969 (m), 891 (m), 870 (m), 787 (m), 743 (s), 684 (w), 608 (m), 591 (m), 578 (m), 551 (w), 531 (w), 480 (w). UV-vis (THF, 298 K), λ_{\max} , nm (ϵ , M⁻¹ cm⁻¹): 313 (12,900), 364 (27,000), 414 (16,200). Anal. Calcd for C₂₄H₃₂N₅ClFe•0.5 H₂O: C, 58.73; H, 6.78; N, 14.27. Found: C, 58.76; H, 6.44; N, 13.92.

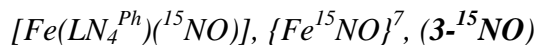
(Et₄N)[Fe(LN₄^{PhCl})Cl] (2)

To a batch of LN₄H₂^{PhCl} (0.3001 g, 0.9061 mmol) dispersed in 8 mL of MeCN was added a 3 mL MeCN slurry of NaH (0.0435 g, 1.813 mmol), which resulted in H₂(g) evolution and a dark brown-green solution indicative of ligand deprotonation. To ensure complete deprotonation, an occasional vacuum was applied while stirring the solution for ~15 min. To this solution was then added a 5 mL MeCN slurry of (Et₄N)₂[FeCl₄] (0.4151 g, 0.9060 mmol) resulting in formation of a pale gray-white precipitate (NaCl) and a solution color change to dark brown-yellow. The reaction mixture was stirred for another 2 h at RT, which resulted in no further change. The solution was then filtered to obtain a homogeneous dark filtrate. The filtrate was stripped to dryness, and treated with 20 mL of THF to precipitate any free Et₄NCl. The THF insolubles were filtered, washed with THF, and the dark filtrate was concentrated and dried under vacuum resulting in a shiny dark black solid (0.4500 g 0.8171 mmol, 90%). FTIR (KBr matrix), ν_{\max} (cm⁻¹): 3080 (w), 2975 (w), 2945 (w), 1578 (vs), 1541 (vs), 1481 (w), 1457 (m),

1444 (m), 1434 (m), 1383 (s), 1292 (s), 1280 (s), 1254 (s), 1184 (m), 1170 (m), 1119 (m), 1076 (w), 1029 (s), 998 (m), 970 (m), 891 (m), 867 (m), 809 (w), 784 (w), 758 (m), 745 (s), 683 (w), 672 (w), 609 (m), 538 (w), 493 (w), 447 (m). UV-vis (THF, 298 K), λ_{max} , nm (ϵ , $\text{M}^{-1} \text{cm}^{-1}$): 324 sh (14,000), 370 (33,000), 430 (23,000). Anal. Calcd. for $\text{C}_{24}\text{H}_{30}\text{Cl}_3\text{FeN}_5 \cdot 0.75 \text{H}_2\text{O}$: C, 51.09; H, 5.63; N, 12.41. Found: C, 51.19; H, 5.72; N, 12.10.

$[\text{Fe}(\text{LN}_4^{\text{Ph}})(\text{NO})], \{\text{FeNO}\}^7$ (**3**)

To an 8 mL MeCN solution of **1** (0.5951 g, 1.235 mmol) was purged NO(g) for 2 min at RT. The resulting solution changed immediately from brown-yellow to red-brown with concomitant precipitation of a dark microcrystalline solid. The reaction mixture was then stirred for 30 min at RT under an atmosphere of NO. After this time, excess NO(g) was removed in vacuo and replaced with N_2 and this solution was then placed in a -20°C refrigerator for 1 h to precipitate more material. The microcrystalline product was filtered, washed with 6 mL of cold MeCN, and dried under vacuum to yield 0.351 g (1.01 mmol, 82%) of product. X-ray quality red crystals were grown by slow diffusion of pentane into a toluene solution of the complex at -20°C . FTIR (KBr matrix), ν_{max} (cm^{-1}): 3088 (w), 3059 (w), 2999 (w), 1698 (vs, ν_{NO}), 1583 (m), 1549 (s), 1506 (m), 1460 (w), 1443 (w), 1379 (s), 1323 (m), 1290 (s), 1256 (m), 1193 (m), 1170 (w), 1153 (w), 1077 (w), 1034 (s), 984 (m), 929 (m), 893 (m), 847 (w), 819 (w), 780 (m), 743 (s), 678 (m), 636 (w), 623 (m), 602 (m), 548 (w), 477 (w), 434 (w), 419 (w). FTIR (solution); ν_{NO} (cm^{-1}): 1705 (MeCN); 1716 (2-MeTHF); 1716 (toluene); 1716 (CH_2Cl_2); μ_{eff} (solution, 298 K): 2.4 BM in $\text{DMSO}-d_6$. UV-vis (THF, 298 K), λ_{max} , nm (ϵ , $\text{M}^{-1} \text{cm}^{-1}$): 309 sh (16,000), 359 (24,000), 469 (10,000). Anal. Calcd for $\text{C}_{16}\text{H}_{12}\text{FeN}_5\text{O}$: C, 55.52; H, 3.49; N, 20.23. Found: C, 55.27; H, 3.08; N, 20.24.

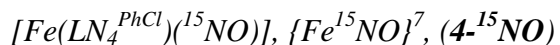


The isotopically-labeled complex was prepared in a similar procedure as **3** except for using $^{15}NO(g)$ and 0.561 g (1.164 mmol) of **1**. Yield: 0.3550 g (1.025 mmol, 88%). FTIR, ν_{NO} (cm^{-1}): 1667 (KBr matrix, $\Delta\nu_{NO}$ from natural abundant isotope in **3**: 31 cm^{-1}); 1680 (MeCN, $\Delta\nu_{NO}$: 25 cm^{-1}); 1681 (2-MeTHF, $\Delta\nu_{NO}$: 35 cm^{-1}); 1684 (toluene, $\Delta\nu_{NO}$: 32 cm^{-1}); 1685 (CH_2Cl_2 , $\Delta\nu_{NO}$: 31 cm^{-1}).

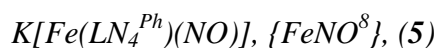


To a 10 mL MeCN solution containing 0.1401 g (0.2544 mmol) of **2** was purged a stream of purified $NO(g)$ for 2 min at RT under dark conditions. Immediately upon introduction of $NO(g)$, a dark burgundy powdered solid appeared and the solution became red-burgundy in color. The reaction mixture was then stirred for 30 min at RT under an atmosphere of NO in the headspace of the flask. After this time, excess $NO(g)$ was removed in vacuo and replaced with N_2 . This solution was then placed in a -20 °C refrigerator for 1 h to precipitate more material. Finally, the powdered solid was filtered, washed with 3 mL of cold MeCN, and dried under vacuum to afford 0.0852 g (0.2048 mmol, 81%) of product. FTIR (KBr matrix), ν_{max} (cm^{-1}): 2922 (w), 1772 (w), 1720 (s, ν_{NO}), 1570 (s), 1542 (s), 1520 (s), 1500 (m), 1462 (w), 1449 (m), 1379 (s), 1327 (w), 1289 (m), 1272 (s), 1258 (m), 1193 (w), 1116 (w), 1039 (s), 982 (w), 924 (w), 912 (w), 881 (w), 854 (w), 810 (w), 752 (m), 679 (w), 653 (w), 600 (w), 549 (w), 522 (w), 470 (w), 424 (w). FTIR (solution); ν_{NO} (cm^{-1}): 1722 (CH_2Cl_2); 1716 (THF); 1702 (DMSO). μ_{eff} (solution-state, 298 K): 2.1 BM in $DMSO-d_6$. UV-vis (DMF, 298 K), λ_{max} , nm (ϵ , $M^{-1} cm^{-1}$): 317 sh (22,000), 361 (31,000), 478 sh (12,000); (THF, 298 K), λ_{max} , nm (ϵ , $M^{-1} cm^{-1}$): 319 sh

(14,000), 361 (21,000), 480 (8600). Anal. Calcd for C₁₆H₁₀Cl₂FeN₅O: C, 46.30; H, 2.43; N, 16.87. Found: C, 46.43; H, 2.57; N, 16.53.

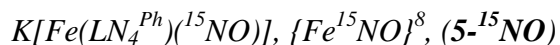


The isotopically-labeled complex **4-¹⁵NO** was prepared analogously to **4** except for using 0.1660 g (0.3014 mmol) of **4** dissolved in 5 mL of MeCN and ¹⁵NO(g). Yield: 0.0951 g (0.2291 mmol, 76%). FTIR, ν_{NO} (cm⁻¹): 1686 (KBr matrix, $\Delta\nu_{NO}$: 34 cm⁻¹); 1684 (THF, $\Delta\nu_{NO}$: 32 cm⁻¹); 1663 (DMSO, $\Delta\nu_{NO}$: 39 cm⁻¹).



To a dark mixture of compound **3** (0.2000 g, 0.5778 mmol) in 5 mL of acetone was added K₂C₈ (0.0850 g, 0.6288 mmol), which immediately formed a dark-red homogeneous solution (apart from the insoluble graphite). This mixture was allowed to stir for an additional 5 min prior to removal of the graphite by filtration. The filtrate was concentrated and treated with 2 × 5 mL of Et₂O, which was decanted from the solid. The material was collected and dried to afford 0.2001 g (0.5194 mmol, 90%) of a dark-red solid product. FTIR (KBr matrix), ν_{max} (cm⁻¹): 3435 (w), 3069 (w), 2958 (w), 2917 (m), 2849 (m), 1705 (m, ν_{CO}), 1667 (m, ν_{NO}), 1589 (s), 1553 (s), 1463 (m), 1442 (w), 1382 (s), 1355 (m), 1285 (s), 1256 (m), 1223 (w), 1175 (w), 1092 (w), 1032 (s), 972 (w), 892 (w), 872 (w), 801 (w), 743 (s), 679 (w), 603 (w), 579 (w), 532 (w), 481 (w). UV-vis (THF, 298 K), λ_{max} , nm (ϵ , M⁻¹ cm⁻¹): 364 (21,300), 409 (12,700), 455 sh (8000). Anal. Calcd for C₁₆H₁₂FeKN₅O•acetone: C, 51.48; H, 4.09; N, 15.80. Found: C, 52.54; H, 3.75; N, 15.41. Compound may contain trace graphite (C₈) from workup resulting in the higher than

expected percent C. Complex **5** was also prepared as the $[\text{Co}(\text{Cp}^*)_2]^+$ salt by reduction with $\text{Co}(\text{Cp}^*)_2$ according to previously published work.⁴⁴



The isotopically-labeled complex **5-¹⁵NO** was prepared analogously to **5** except for using 0.0901 g (0.2603 mmol) of **3-¹⁵NO** dissolved in 3 mL of acetone and 0.0385 g (0.2848 mmol) of KC_8 . Yield: 0.0871 g (0.2261 mmol, 87%). FTIR, ν_{NO} (cm^{-1}): 1629 (KBr matrix, $\Delta\nu_{\text{NO}}$: 38 cm^{-1}).



To a dark red heterogeneous mixture of **4** (0.1200) g, 0.2891 mmol) in 3 mL of acetone was added KC_8 (0.0430 g, 0.3180 mmol), which immediately formed a homogeneous (apart from C_8) darkened solution. This mixture was stirred for an additional 5 min at which point the insoluble C_8 was removed by vacuum filtration and the acetone soluble filtrate was concentrated to dryness. The dark residue was charged with 3 mL of Et_2O and stirred for 5 min followed by decantation. This procedure was repeated three times at which point the material was dried under vacuum to afford 0.1150 g (0.2631 mmol, 91%) of dark solid product. FTIR (KBr matrix), ν_{max} (cm^{-1}): 3084 (w), 2971 (w) 2923 (w), 2853 (w), 1705 (m, ν_{CO}), 1579 (s, ν_{NO} , $\nu_{\text{C=N}}$), 1545 (s), 1460 (m), 1436 (m), 1382 (s), 1354 (m), 1292 (s), 1271 (s), 1228 (w), 1181 (m), 1115 (m), 1080 (w), 1034 (s), 978 (m), 913 (w), 894 (m), 864 (w), 819 (w), 794 (w), 749 (s), 678 (m), 657 (w), 613 (m), 531 (w), 492 (w), 475 (w), 448 (w). UV-vis (THF, 298 K), λ_{max} , nm (ϵ , $\text{M}^{-1} \text{cm}^{-1}$): 371 (24,000), 419 (16,300), 471 sh (10,300). Anal. Calcd for $\text{C}_{16}\text{H}_{10}\text{Cl}_2\text{FeKN}_5\text{O}\cdot 1.25 \text{ acetone}\cdot 0.5 \text{ H}_2\text{O}$: C, 44.28; H, 3.48; N, 13.07. Found: C, 44.05; H, 3.25; N, 12.83.

$K[Fe(LN_4^{PhCl})(NO)]$ (**6-¹⁵NO**)

The isotopically-labeled complex **6-¹⁵NO** was prepared analogously to **6** except for using 0.0982 g (0.2366 mmol) of **4-¹⁵NO** dissolved in 3 mL of acetone and 0.0351 g (0.2597 mmol) of KC_8 . Yield: 0.0951 g (0.2094 mmol, 89%). FTIR, ν_{NO} (cm^{-1}): Obscured due to overlap with $\nu_{C=N}$. Complex **6** was also prepared as the $[Co(Cp^*)_2]^+$ salt by reduction with $Co(Cp^*)_2$ according to previously published work.⁴⁴

2.8.4 Reactivity Studies

*Chemical Oxidation of $K[Fe(LN_4^{Ph})(NO)]$ (**5**)*

To a 1 mL MeCN solution of complex **5** (0.0225 g, 0.0584 mmol) was added a 1 mL MeCN solution containing 0.0192 g (0.0580 mmol) of ferrocenium hexafluorophosphate ($FcPF_6$). Addition of the oxidant resulted in immediate precipitation of a dark material and the solution color became more pale. This heterogeneous solution was stirred for 30 min at RT, which resulted in no further change. The solution was concentrated to dryness and treated with 2 mL of MeOH to separate and yield 0.0178 g (0.0514 mmol, 89%) of the $\{FeNO\}^7$ complex **3**. The FTIR spectrum (KBr) of this solid is consistent with authentic **3** (ν_{NO} : 1698 cm^{-1}).

*Chemical Oxidation of $K[Fe(LN_4^{PhCl})(NO)]$ (**6**)*

This reaction and workup was performed analogously to the oxidation of **5** except for using 0.0409 g (0.0901 mmol) of **6** and 0.0298 g (0.0900 mmol) of $FcPF_6$. The addition of $FcPF_6$ resulted in a burgundy-red insoluble material, which after workup yielded 0.0322 g (0.0776 mmol, 86%) of $\{FeNO\}^7$ complex **4**. The FTIR spectrum (KBr) of this solid is consistent with authentic **4** (ν_{NO} : 1720 cm^{-1}).

UV-vis Monitoring of the Reaction of {FeNO}⁷ and {FeNO}⁸ Compounds with [Fe(TPP)Cl]⁵

A 1 mM stock solution of [Fe(TPP)Cl] in THF was prepared anaerobically and in the dark. Addition of a 0.025 mL aliquot of the [Fe(TPP)Cl] stock to 2.975 mL of THF resulted in an 8.33 μM working solution of [Fe(TPP)Cl]. After a THF blank was recorded at 298 K, the spectrum of the working solution was recorded. The UV-vis spectrum thus obtained was consistent with literature⁸⁸ and was monitored over 15 min resulting in no observable change. To this cuvette was then added a 0.025 mL aliquot of a 1 mM stock of the {FeNO}⁷ (**3** or **4** in THF) or {FeNO}⁸ (**5** or **6** in acetone, **7** in MeCN) compounds (1:1 ratio of [Fe(TPP)Cl]/{FeNO}^{7/8}) to initiate the reaction. The reaction mixture was allowed to equilibrate at 298 K for 1 min and the spectrum was recorded. Subsequent UV-vis spectra were recorded at 298 K until no further change was observed.

*UV-vis Monitoring of the Reaction of K[Fe(LN₄^{PhCl})NO] (**6**) with [Fe(TPP)OTf].*

The UV-Vis reactions of **6** with [Fe(TPP)OTf] were performed analogously to those with [Fe(TPP)Cl] from section 2.4.3. The [Fe(TPP)OTf] was obtained by literature methods,⁷¹ and compared well to known spectroscopic data including UV-vis (Fig. S16) and FTIR.^{71,72}

Reaction of {FeNO}⁷ and {FeNO}⁸ Compounds with [Fe(TPP)Cl]

The bulk reactivity studies were performed using 0.0200 g of [Fe(TPP)Cl] (0.0284 mmol) and a stoichiometric equiv of the respective {FeNO}⁷ (**3/3-¹⁵NO** or **4/4-¹⁵NO**) and {FeNO}⁸ (**5/5-¹⁵NO** or **6/6-¹⁵NO**) species. A solution of [Fe(TPP)Cl] was prepared either in 2 mL of THF (for {FeNO}⁷ complexes **3** or **4**) or 2 mL of THF/acetone (1%) (for {FeNO}⁸ **5** or **6**) to mimic the UV-vis conditions. To these [Fe(TPP)Cl] solutions were added a 1 mL THF (**3** or **4**) or

⁵ Unpublished experimental section with respect to complex **7**, and related to the research found in reference 43.

THF/acetone (1%) (**5** or **6**) solution containing the $\{\text{FeNO}\}^7$ or $\{\text{FeNO}\}^8$ species, respectively. The reaction was stirred at RT and in the dark for 2 h at which point the solvent was removed in vacuo to afford a dark brown-purple residue, which was characterized by FTIR. Pure $[\text{Fe}(\text{TPP})(\text{NO})]$ was isolated by treating the brown-purple mixture with ~2 mL of MeOH, which resulted in isolable product. Example yields: 0.0171 g (0.0243 mmol, 86%) and 0.0186 g (0.0264 mmol, 93%) of purple solid corresponding to $[\text{Fe}(\text{TPP})(\text{NO})]$ and $[\text{Fe}(\text{TPP})(^{15}\text{NO})]$ from the reaction of $[\text{Fe}(\text{TPP})\text{Cl}]$ with **6** and **6-¹⁵NO**, respectively.

*Reaction of $\{\text{FeNO}\}^7$ and $\{\text{FeNO}\}^8$ Compounds with *p*-ClArSH⁶*

The bulk reactions of *p*-ClArSH with $\{\text{FeNO}\}^7$ complexes **3**, **4**, and **7**, were performed at ~10 mM concentrations of $\{\text{FeNO}\}^7$ with stoichiometric *p*-ClArSH in 4.8 mL solution of THF. A typical procedure used 20 mg (0.0482 mmol) of **4** dissolved in 4.82 mL of THF. To this was added a 1 mL THF solution containing 7 mg (0.0484 mmol) of *p*-ClArSH. The reaction was stirred at RT under N₂ for 1 h with little observable change. The solution was concentrated and treated with Et₂O to afford a pale red-brown colored Et₂O solution and a similarly colored Et₂O insoluble portion that were nearly identical to one another by FTIR. The ν_{NO} data obtained from these reactions compared well to known spectroscopic data for RRE.⁷⁶

The bulk reaction of **6** with *p*-ClArSH was performed by adding 2.1 mg (0.0145 mmol) of *p*-ClArSH dissolved in 200 μL of THF to complex **6** (10.8 mg, 0.0145 mmol) dissolved in 1 mL of THF. The resulting solution was stirred for 45 min at RT, then placed in a -25 °C freezer to facilitate precipitation. The solution was filtered to give 4.1 mg (0.0059 mmol, 81%) of $[\text{Co}(\text{Cp}^*)_2][\text{Fe}(\text{RS})_2(\text{NO})_2]$. The THF filtrate was concentrated under vacuum and subjected to an Et₂O extraction 5 \times 3 mL. Characterization of the Et₂O-insoluble material showed a mixture of

⁶ Unpublished experimental section related to the research found in citation of footnote 1.

products (FTIR) including DNIC (**9**). The Et₂O-soluble portion was concentrated to give 2.1 mg of a pale-yellow paste. The ¹H NMR spectrum of this material indicated the presence of free LN₄^{PhCl}H₂.

Reaction of [Co(Cp)₂][Fe(LN₄)(NO)] (**7**) {FeNO}⁸ Compounds with *p*-ClArSH⁷*

A 1 mL MeCN solution of *p*-ClArSH (23.9 mg, 0.1652 mmol) was prepared and set aside. Complex **7** (100 mg, 0.1652 mmol) was dissolved in 3 mL of MeCN with immediate stirring to give a dark purple colored solution. The *p*-ClArSH solution was added rapidly within 30 s from dissolution of the {FeNO}⁸ complex. Upon addition of *p*-ClArSH, an instantaneous color change from dark purple to a dark green was observed. The reaction mixture was stirred for an additional 1 hour at RT. Precipitation occurred over the course of the hour and this material was filtered to give a light-brown solid (20 mg, 0.0423 mmol of Co(Cp*)₂SR, 98%) and a green homogeneous filtrate. The green filtrate was placed into a -25 °C freezer overnight, affording a red-purple solid identified as [Co(Cp*)₂][Fe(*p*-ClArS)₂(NO)₂] (17 mg, 0.0232 mmol, 28%). The MeCN was removed from the green filtrate by vacuum and the residue was taken up in 10 mL of THF to afford a green solution and a red-orange precipitate. This was again filtered to separate the insoluble material, which was washed with 3 × 3 mL of THF to afford an orange solid, of [Co(Cp*)₂][Fe(LN₄)] after drying under vacuum (35 mg, 0.0572 mmol, 69%). The green THF filtrate was then concentrated under vacuum and subjected to an Et₂O extraction (5 × 3 mL) that was stirred vigorously each time, followed by carefully decanting the yellow solution from the gummy green material. The Et₂O-soluble portion was concentrated under vacuum to afford 18 mg of LN₄H₂ (0.0788 mmol, 95%). The green material eventually solidified to a green powder identified to be [Co(Cp*)₂][Fe₂(μ-*p*-ClArS)₂(NO)₄] (34 mg, 0.0401 mmol, 97%).

⁷ Unpublished experimental section with respect to complex **7**, and related to the research found in reference 43.

Reaction of Co(Cp)₂[Fe(LN₄)(NO)] (7) {FeNO}⁸ Compounds with GSH⁸*

To 900 μL solution of GSH (1.6 mg, 0.0051 mmol) in milli-Q H₂O was added a 100 μL MeCN aliquot of **7** (3.2 mg, 0.0051 mmol). The solution instantly turned to a green color. UV-vis and EPR analysis was performed and indicate formation of [Co(Cp*)₂][Fe₂(μ -GS)₂(NO)₄]

2.9 Supporting Information

X-ray Crystallographic Data Collection and Structure Solution and Refinement

Dark-red crystals of [Fe(LN₄^{Ph})(NO)] (**3**) were grown under anaerobic conditions by slow diffusion of pentane into a toluene solution of **3** at -20 °C. Suitable crystals were mounted on a glass fiber. All geometric and intensity data were measured at 100 K on a Bruker SMART APEX II CCD X-ray diffractometer system equipped with graphite-monochromatic Mo K α radiation (λ = 0.71073 Å) with increasing ω (width 0.5° per frame) at a scan speed of 10 s/frame controlled by the SMART software package.⁸⁹ The intensity data were corrected for Lorentz-polarization effects and for absorption⁹⁰ and integrated with the SAINT software. Empirical absorption corrections were applied to structures using the SADABS program.⁹¹ The structures were solved by direct methods with refinement by full-matrix least-squares based on F² using the SHELXTL-97 software⁹² incorporated in the SHELXTL 6.1 software package.⁹³ The atom of O(2) bonded to N(10) on the terminal NO group was found disordered in two sets labeled as O(2) (one set) and O(2') (another set), respectively (Fig. S1). Each of these two sets is divided using the PART commands and proper restraints. The set of O(2) has 60% occupancy while the other O(2') has 40% occupancy. The hydrogen atoms were fixed in their calculated positions and refined using a riding model. All non-hydrogen atoms were refined anisotropically. Selected crystal data and

⁸ Unpublished discussion with respect to complex **7**, and related to the research found in reference 43.

metric parameters for complex **3** are summarized in Tables S1 and S2. Selected bond distances and angles for one unique molecule of complex **3** are given in Table 2.1. Perspective views of the complexes were obtained using ORTEP.⁹⁴ An ORTEP view of complex **3** showing the disordered O atom is illustrated in Fig. S1.

Table S1. Summary of crystal data and intensity collection and structure refinement parameters for [Fe(LN₄^{Ph})(NO)] (**3**).

Parameters	3
Formula	C ₁₆ H ₁₂ FeN ₅ O
Formula weight	346.14
Crystal system	Triclinic
Space group	<i>P</i> -1
Crystal color, habit	Red rectangle
<i>a</i> , Å	8.8924(7)
<i>b</i> , Å	9.4766(7)
<i>c</i> , Å	17.5997(13)
α , deg	95.7930(10)
β , deg	95.3610(10)
γ , deg	102.0640(10)
<i>V</i> , Å ³	1432.93(19)
<i>Z</i>	4
ρ_{calcd} , g/cm ⁻³	1.605
<i>T</i> , K	100(1)
abs coeff, μ , mm ⁻¹	1.064
θ limits, deg	2.34-26.00
total no. of data	16729
no. of unique data	5627
no. of parameters	425
GOF on F ²	1.087
<i>R</i> ₁ , ^[a] %	4.63
<i>wR</i> ₂ , ^[b] %	5.67
max, min peaks, e/Å ³	1.588, -0.799

$${}^a R_1 = \frac{\sum ||F_o| - |F_c||}{\sum |F_o|}; {}^b wR_2 = \left\{ \frac{\sum [w(F_o^2 - F_c^2)^2]}{\sum [w(F_o^2)^2]} \right\}^{1/2}.$$

Table S2. Selected bond distances (Å) and bond angles (deg) for both unique molecules in the asymmetric unit of [Fe(LN₄^{Ph})(NO)] (**3**). Molecule 1 is depicted in Fig. 2.3 of the main text.

[Fe(LN ₄ ^{Ph})(NO)] (3)			
Molecule 1		Molecule 2	
Fe1-N1	1.960(3)	Fe2-N6	1.964(3)
Fe1-N2	1.918(3)	Fe2-N7	1.935(3)
Fe1-N3	1.928(3)	Fe2-N8	1.922(3)
Fe1-N4	1.986(3)	Fe2-N9	1.954(3)
Fe1-N5	1.694(3)	Fe2-N10	1.695(3)
N5-O1	1.150(4)	N10-O2	1.161(8)
O1-N5-Fe1	155.6(3)	N10-O2'	1.146(11)
N1-Fe1-N2	81.97(12)	O2-N10-Fe2	157.0(6)
N1-Fe1-N3	153.72(12)	O2'-N10-Fe2	153.5(16)
N1-Fe1-N4	104.40(12)	N6-Fe2-N7	81.54(11)
N1-Fe1-N5	95.90(13)	N6-Fe2-N8	151.62(11)
N2-Fe1-N3	81.84(12)	N6-Fe2-N9	104.03(12)
N2-Fe1-N4	152.05(12)	N6-Fe2-N10	105.10(12)
N2-Fe1-N5	101.41(13)	N7-Fe2-N8	81.49(11)
N3-Fe1-N4	81.36(12)	N7-Fe2-N9	152.90(11)
N3-Fe1-N5	107.51(13)	N7-Fe2-N10	104.94(12)
N4-Fe1-N5	104.87(13)	N8-Fe2-N9	81.94(11)
		N8-Fe2-N10	101.15(12)
		N9-Fe2-N10	99.21(12)

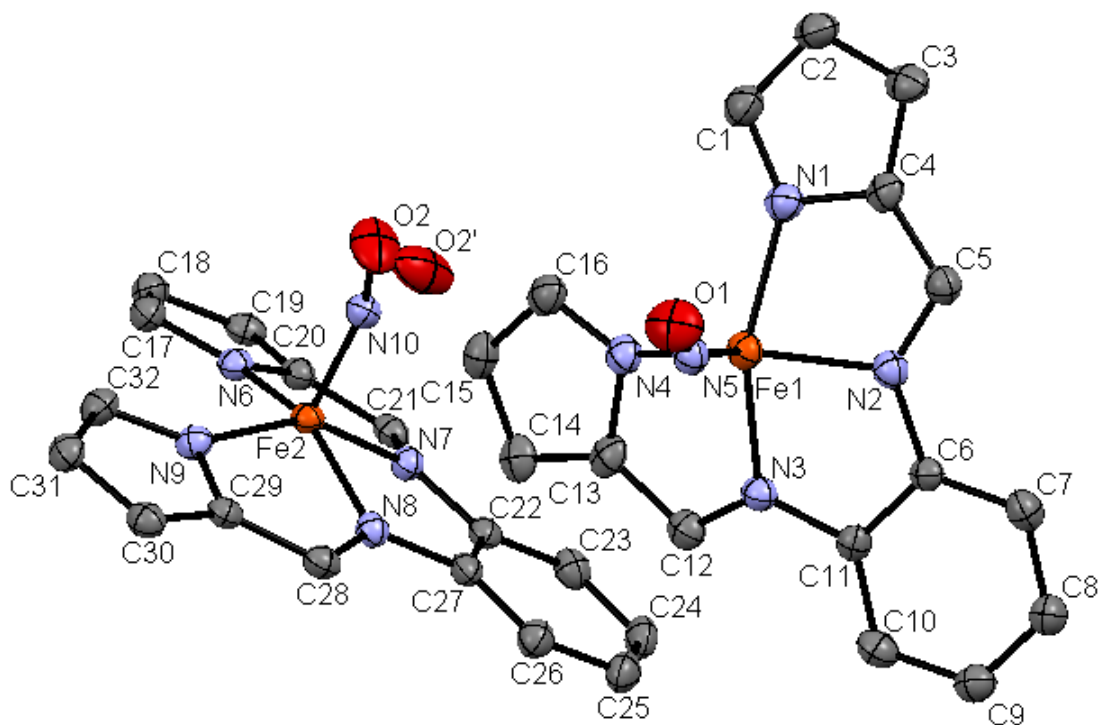


Fig. S1. Unit cell of **3** at 50% thermal probability ellipsoids for all non-hydrogen atoms showing the two unique molecules in the asymmetric unit. Disordered oxygen atom in one unique molecule is depicted and labeled as O2 and O2' with 60 and 40% occupancy, respectively. Atom labeling: C (grey), N (blue), O (red), Fe (orange).

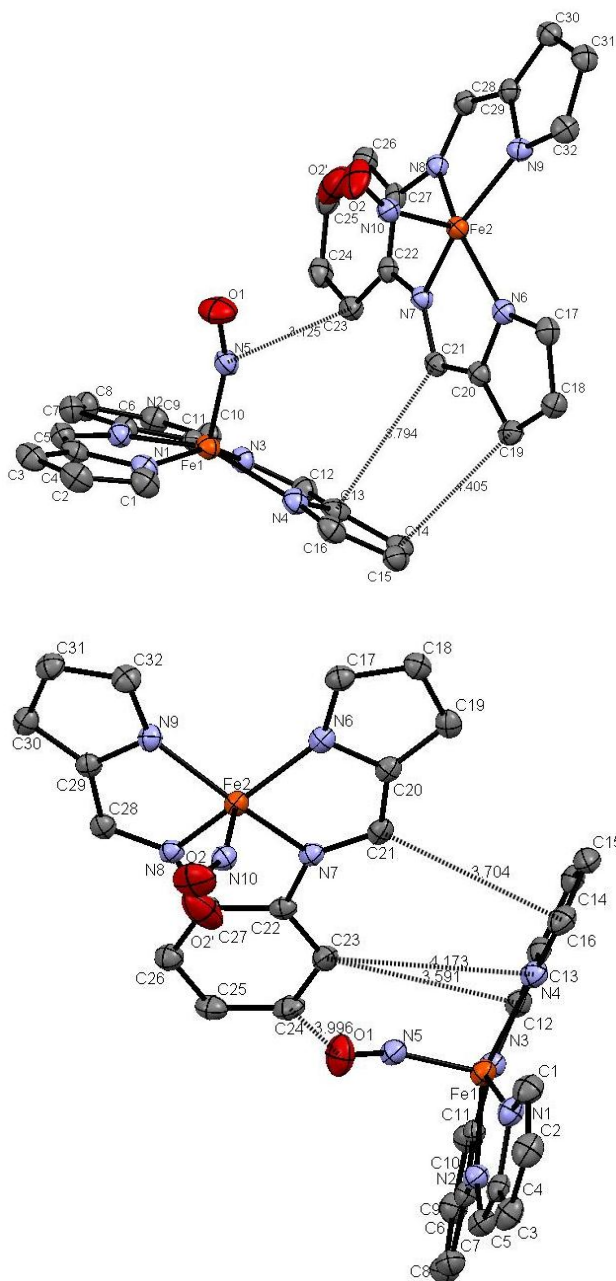


Fig. S2. Different orientations of the unit cell of **3** as in Fig. S1. Selected interatomic distances are given for atoms that appear to be in close contact. A careful analysis of the structure reveals that only one particular bond distance is less than the sum of the van der Waals radii of the selected atoms, C23-N5 (top): 3.125 Å (van der Waals sum: 3.25 Å).

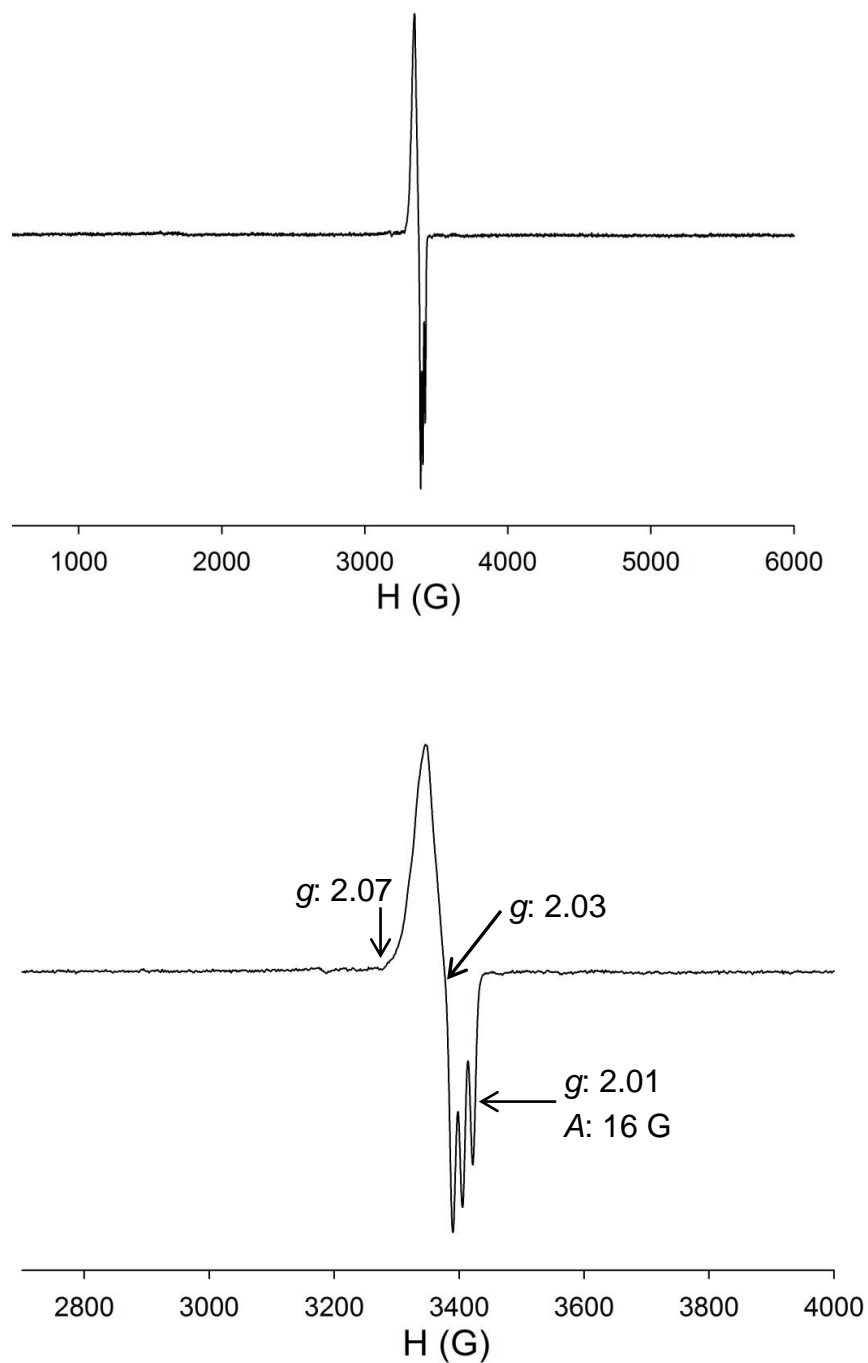


Fig. S3. EPR spectrum of $[\text{Fe}(\text{LN}_4^{\text{PhCl}})(\text{NO})]$ (**4**) in a 1:3 MeCN/toluene glass at 10 K. Top: full trace. Bottom: expansion. Selected g -values and ^{14}N hyperfine coupling constants are indicated. Spectrometer settings: microwave frequency, 9.58 GHz; microwave power, 1.0 mW; modulation frequency, 100 kHz; modulation amplitude, 6.31 G.

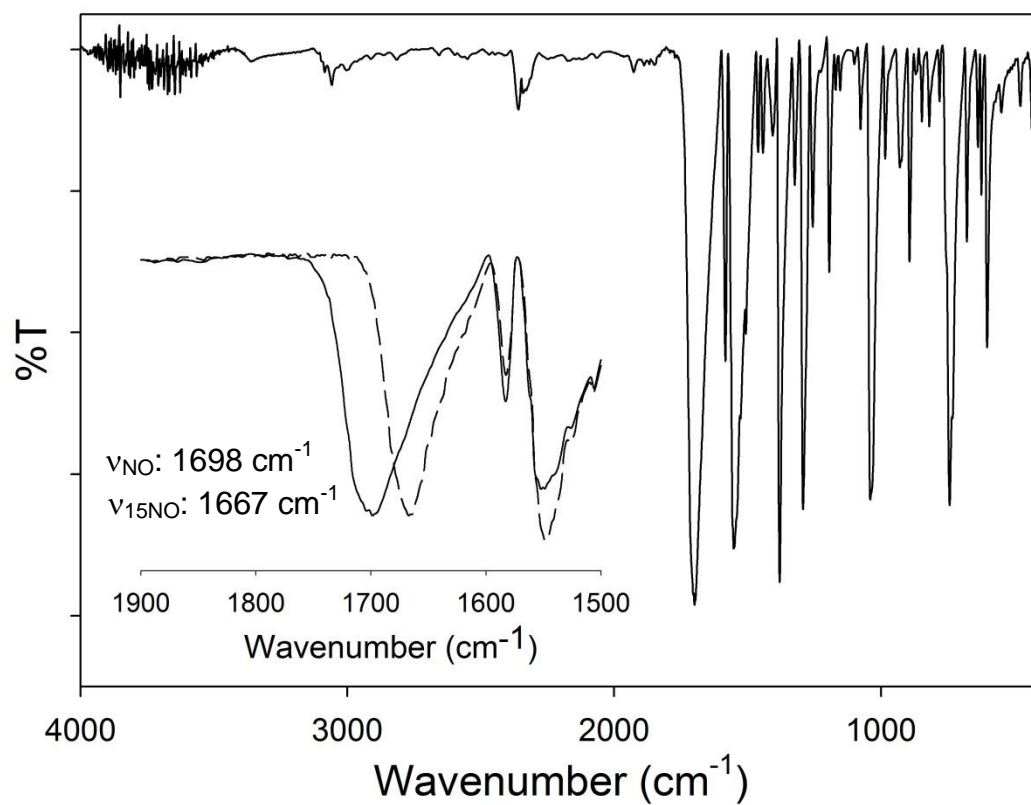


Fig. S4. FTIR spectra of [Fe(LN₄^{Ph})(NO)] (solid line) (**3**) and [Fe(LN₄^{Ph})(¹⁵NO)] (dashed line; inset) (**3**-¹⁵NO) in a KBr matrix.

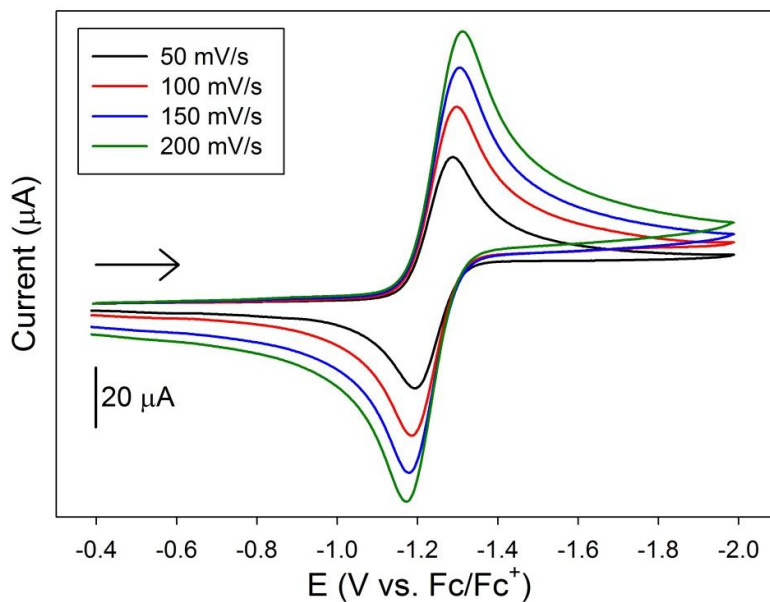


Fig. S5. Cyclic voltammograms of a 10 mM MeCN solution of $[\text{Fe}(\text{LN}_4^{\text{Ph}})(\text{NO})]$ (**3**) at different scan rates as indicated in the inset (0.1 M $n\text{Bu}_4\text{NPF}_6$ supporting electrolyte, glassy carbon working electrode, Pt-wire counter electrode, RT). Arrow displays direction of scan.

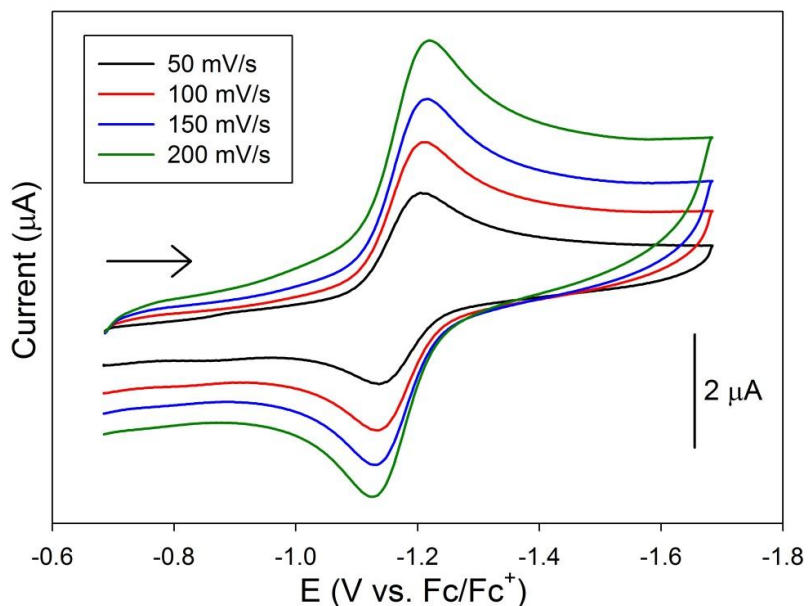


Fig. S6. Cyclic voltammograms of a 1 mM MeCN solution of $[\text{Fe}(\text{LN}_4^{\text{PhCl}})(\text{NO})]$ (**4**) at different scan rates as indicated in the inset (0.1 M $n\text{Bu}_4\text{NPF}_6$ supporting electrolyte, glassy carbon working electrode, Pt-wire counter electrode, RT). Arrow displays direction of scan.

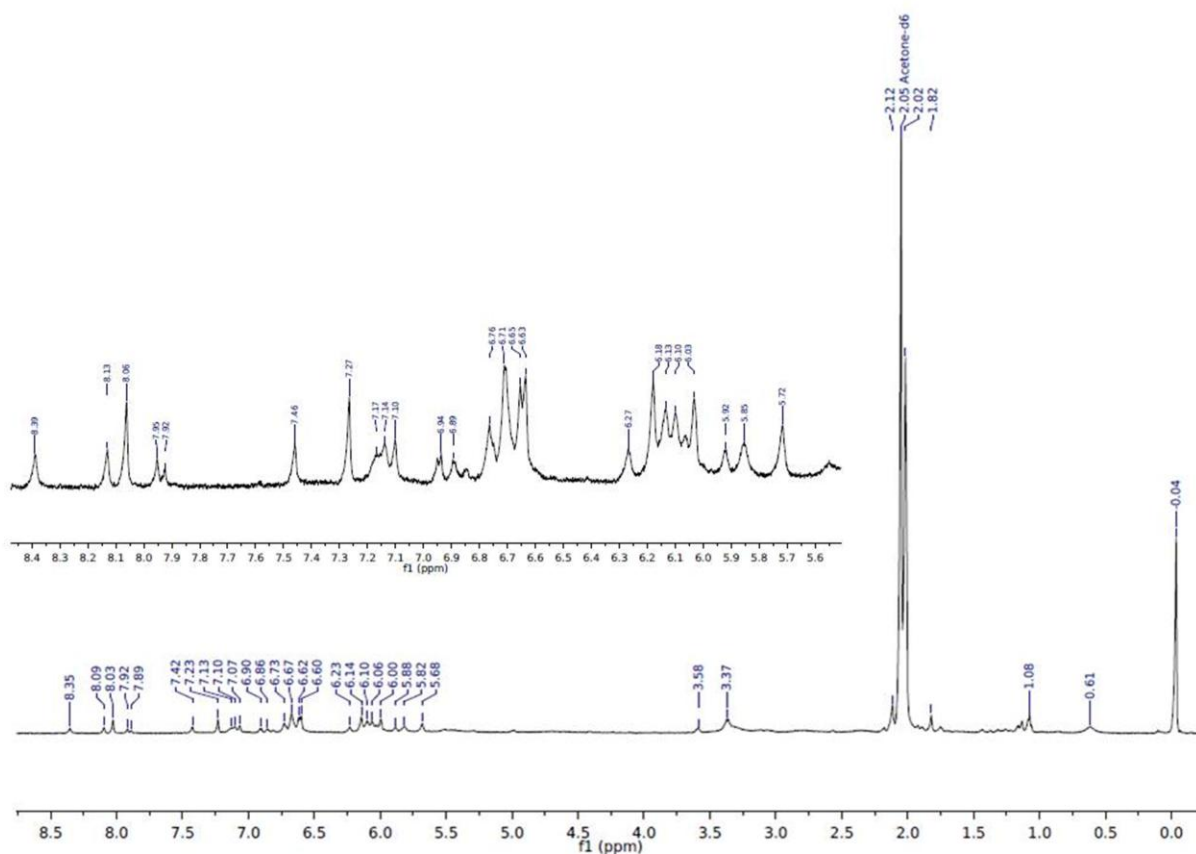


Fig. S7. Full spectrum and aromatic region (inset) of the ¹H-NMR spectrum obtained from K[Fe(LN₄^{PhCl})(NO)] (**6**) in acetone-*d*₆ at 298 K. Peaks at 2.02 and 2.05 ppm are from coordinated and residual acetone. The overall complexity of this spectrum highlights the dynamic nature of {FeNO}⁸ species such as **6** in solution.

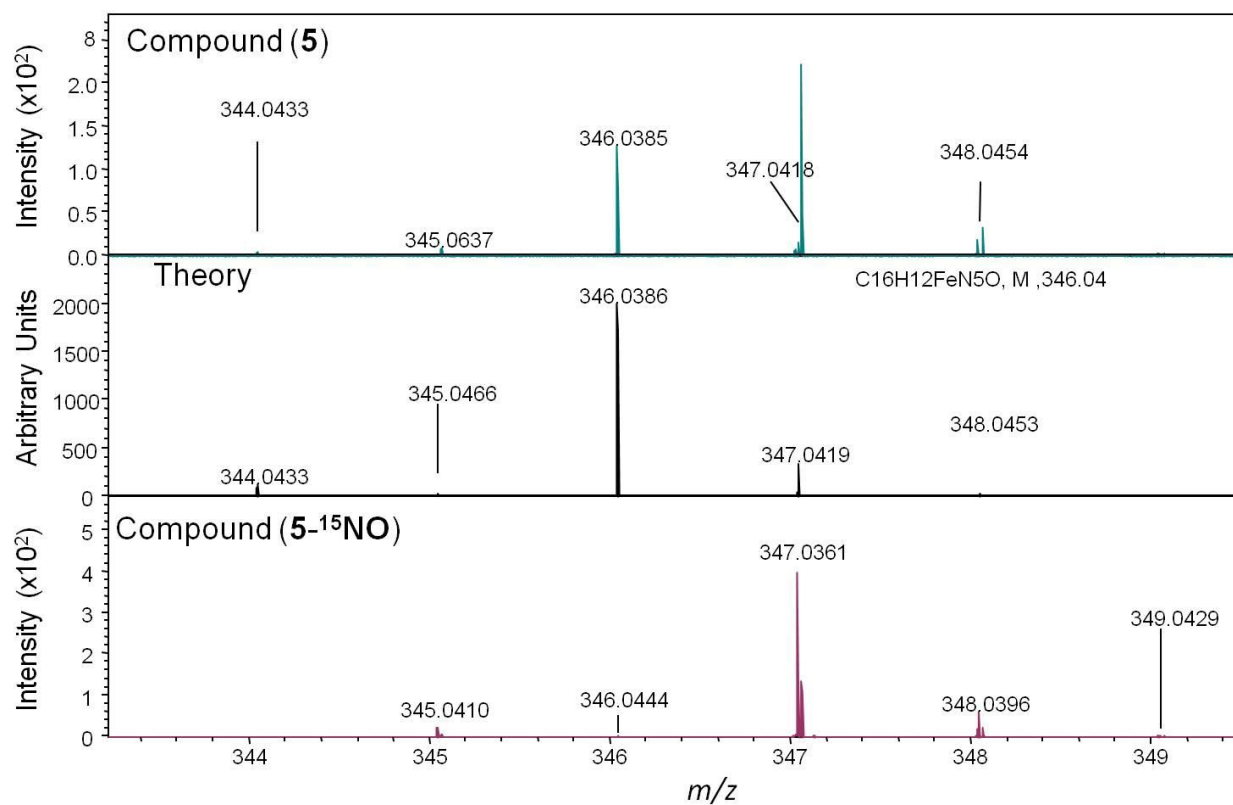


Fig. S8. FT-ICR-MS of an acetone solution of $\text{K}[\text{Fe}(\text{LN}_4^{\text{Ph}})(\text{NO})]$ (**5**) (*top*) and (**5-¹⁵N**) (*bottom*) in negative-ion mode with theoretical MS for natural abundant isotope (*middle*).

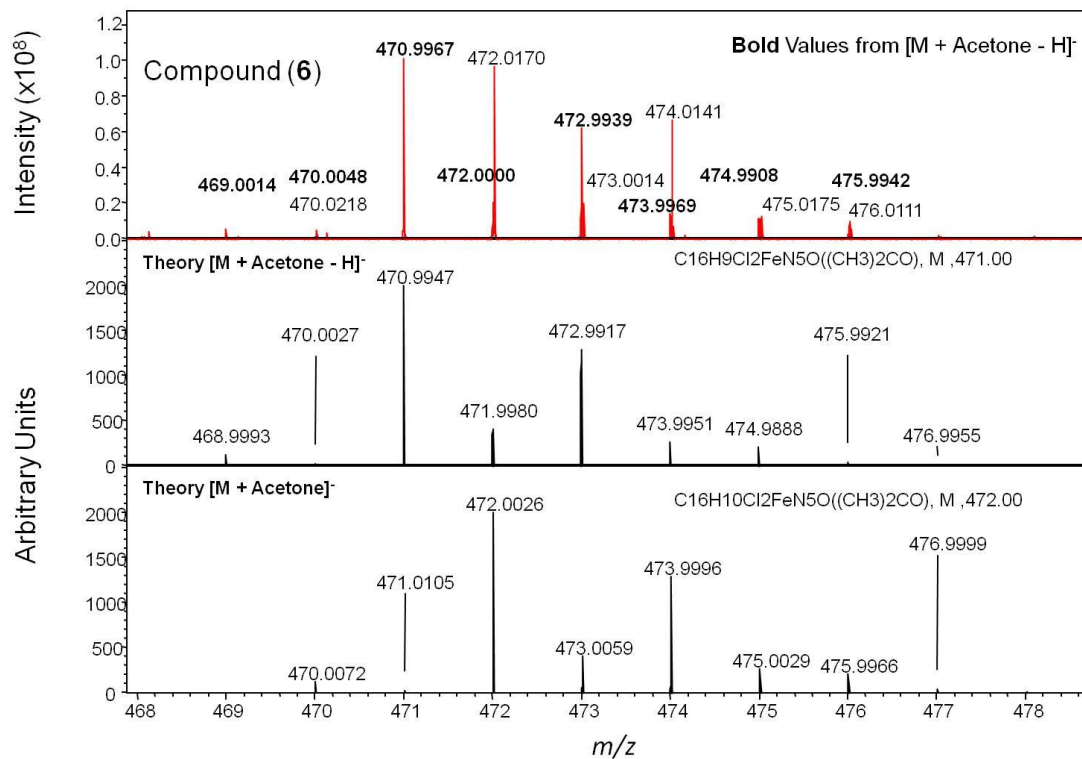


Fig. S9. FT-ICR-MS of an acetone solution of $\text{K}[\text{Fe}(\text{LN}_4^{\text{PhCl}})(\text{NO})]$ (**6**) (*top*) in negative-ion mode alongside the theoretical MS (*middle* and *bottom*) of the two major species observed. The experimental MS shows an overlapping mass series for what has been assigned as $[\text{M} + \text{acetone} - \text{H}]^-$ and $[\text{M} + \text{acetone}]^-$.

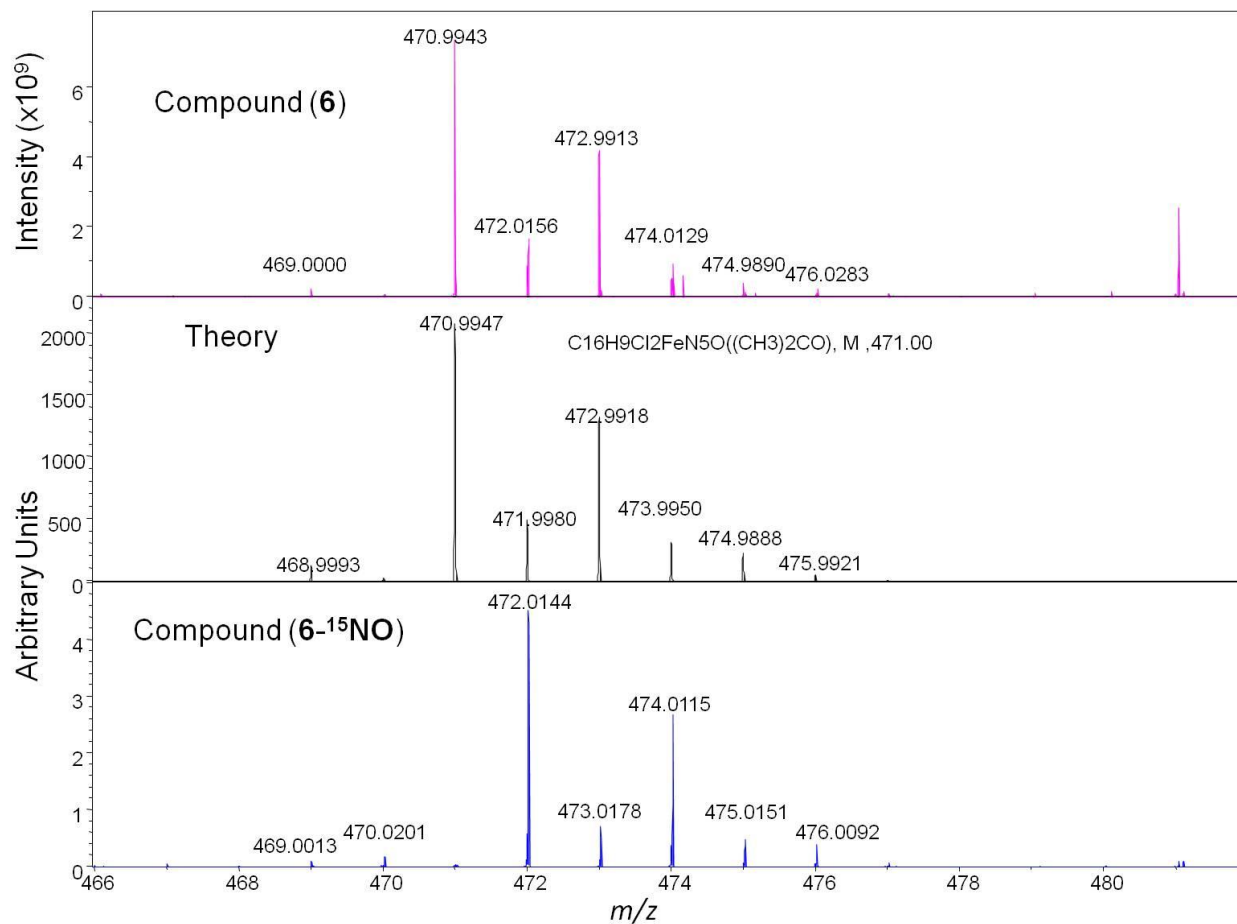


Fig. S10. FT-ICR-MS of an acetone solution of $\text{K}[\text{Fe}(\text{LN}_4^{\text{PhCl}})(\text{NO})]$ (**6**) (*top*) and (**6- ^{15}N O**) (*bottom*) in negative-ion mode with theoretical MS for natural abundant isotope (*middle*). The experimental MS shows an overlapping mass series for what has been assigned as $[\text{M} + \text{acetone} - \text{H}]^-$.

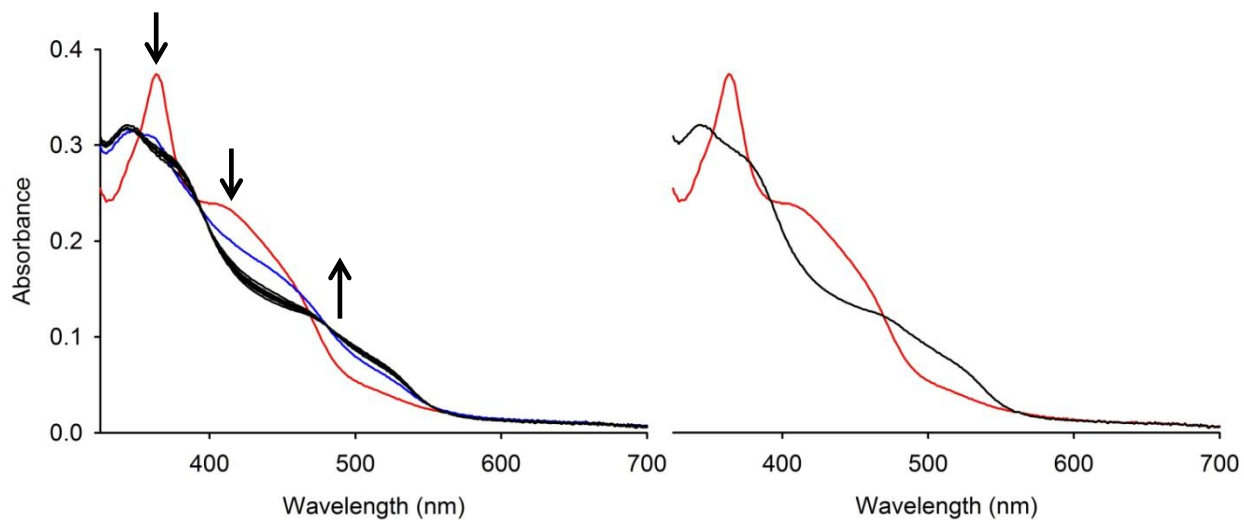


Fig. S11. UV-vis spectral monitoring of an 8.33 μM THF solution of $\text{K}[\text{Fe}(\text{LN}_4^{\text{Ph}})(\text{NO})]$ (**5**) at 298 K for 12 h. *Left:* UV-vis of **5** upon initial dissolution (red) and subsequent traces (blue line: 1 h; black lines: every 1 h for 6 h – no change after this point). *Right:* Depicts the first (red) and 12 h trace (black). Arrows illustrate direction of change.

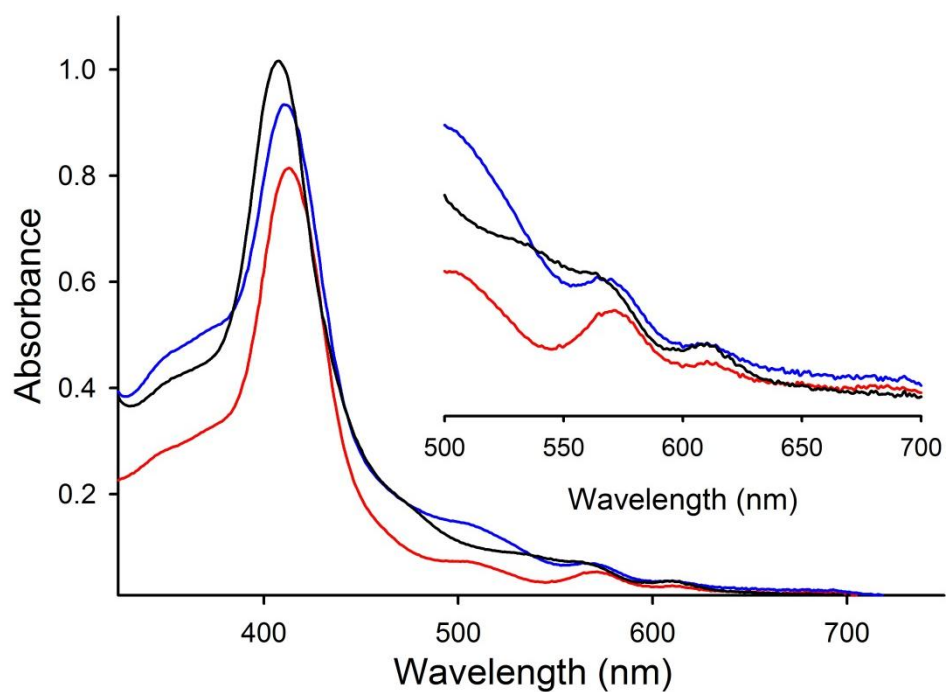


Fig. S12. UV-vis spectral monitoring of an 8.33 μM THF solution of $[\text{Fe}(\text{TPP})\text{Cl}]$ with 1 mol-equiv of $[\text{Fe}(\text{LN}_4^{\text{PhCl}})(\text{NO})]$ (**4**; $\{\text{FeNO}\}^7$ complex) at 298 K. $[\text{Fe}(\text{TPP})\text{Cl}]$ before (red trace) and after addition of **4** (1 min: blue trace; 12 h: black trace). *Inset*: expansion of the Q-band region of the spectrum.

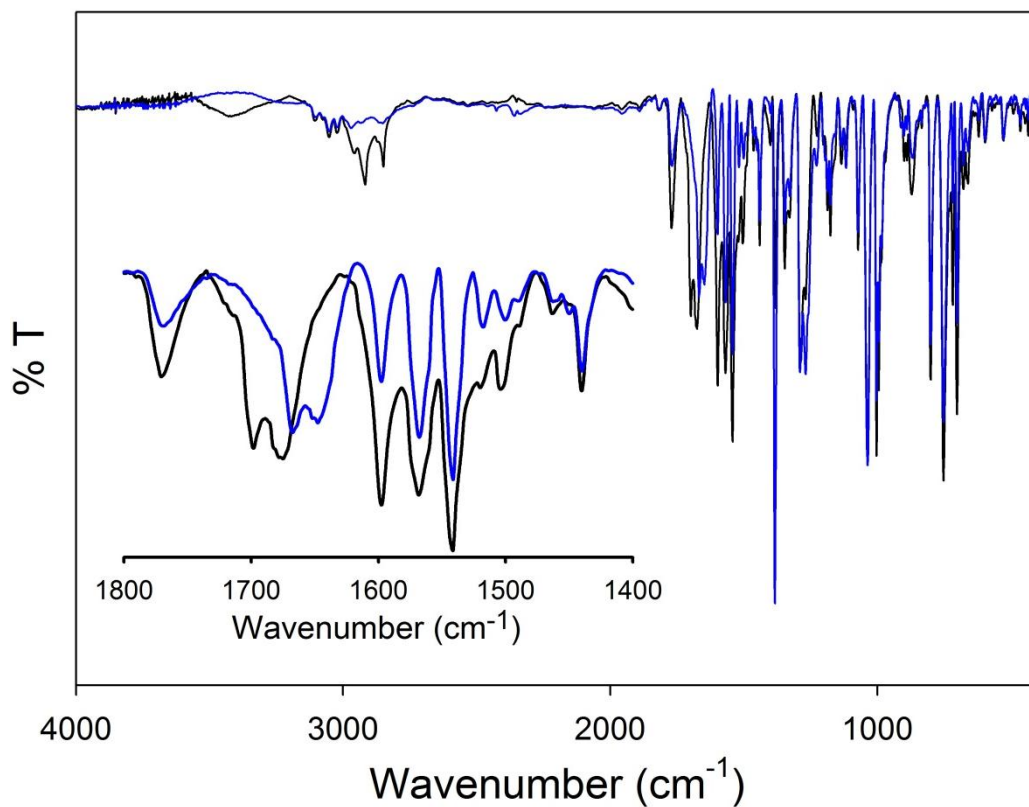


Fig. S13. FTIR analysis of the bulk reactivity products obtained from the reaction of a 1:1 THF solution of [Fe(TPP)Cl] with [Fe(LN₄^{PhCl})(NO)] (**4**) (black) and [Fe(LN₄^{PhCl})(¹⁵NO)] (**4-¹⁵NO**) (blue). *Inset:* expanded region from 1800 to 1400 cm⁻¹ where two isotope-sensitive bands are observed at 1698/1675 cm⁻¹ (¹⁴N-black) and 1666/1648 cm⁻¹ (¹⁵N-blue) that are consistent with [Fe(TPP)(NO)]; see Scheidt and coworkers *Inorg. Chem.* **2009**, *48*, 971 and Fig. S14 for explanation of the two ν_{NO} bands.

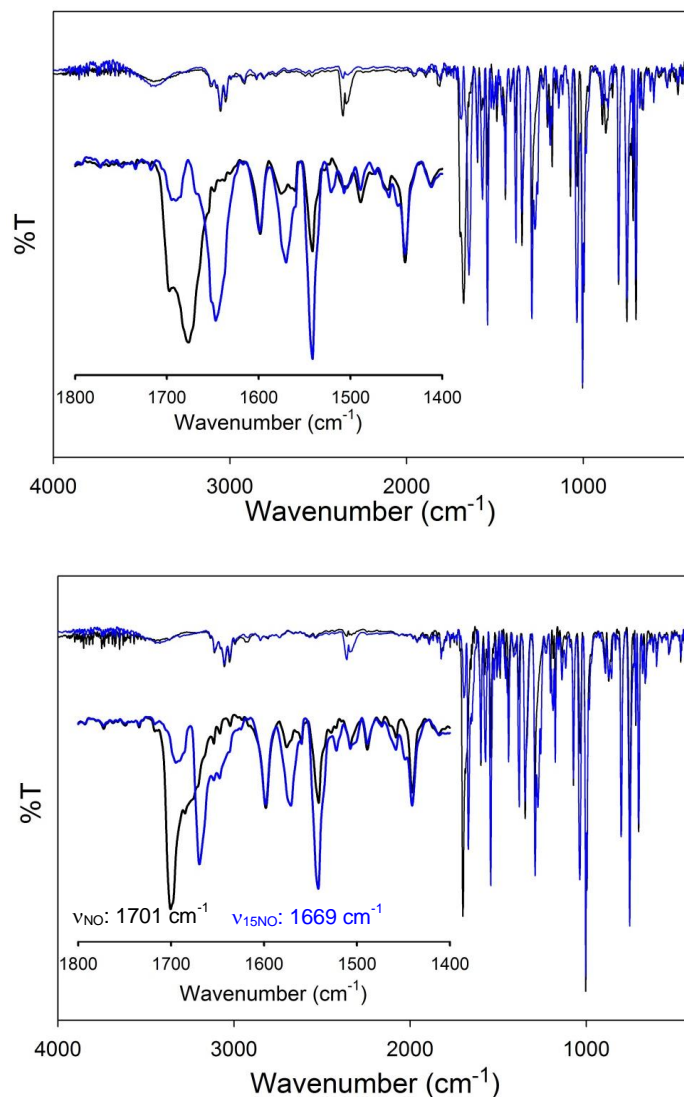


Fig. S14. FTIR analysis of the bulk reactivity products obtained from the reaction of a 1:1 THF solution of $[\text{Fe}(\text{TPP})\text{Cl}]$ with $\text{K}[\text{Fe}(\text{LN}_4^{\text{PhCl}})(\text{NO})]$ (**6**) (black) and $\text{K}[\text{Fe}(\text{LN}_4^{\text{PhCl}})(^{15}\text{NO})]$ (**6- ^{15}NO**) (blue). *Insets:* expanded region from 1800 to 1400 cm^{-1} . *Top:* two ν_{NO} bands featured at 1697/1675 cm^{-1} (^{14}N -black) and 1666/1647 cm^{-1} (^{15}N -blue). *Bottom:* after heating the KBr pellet in a 150 °C oven for 1 h, one major band consistent with $[\text{Fe}(\text{TPP})(\text{NO})]$ resulted; see Scheidt and coworkers *Inorg. Chem.* **2009**, *48*, 971 where they note, that if KBr is not thoroughly dry, an additional ν_{NO} appears at 1677 cm^{-1} . As performed here, this band is irreversibly converted on heating of the KBr pellet to the $\sim 1700 \text{ cm}^{-1}$ band typically associated with this complex.

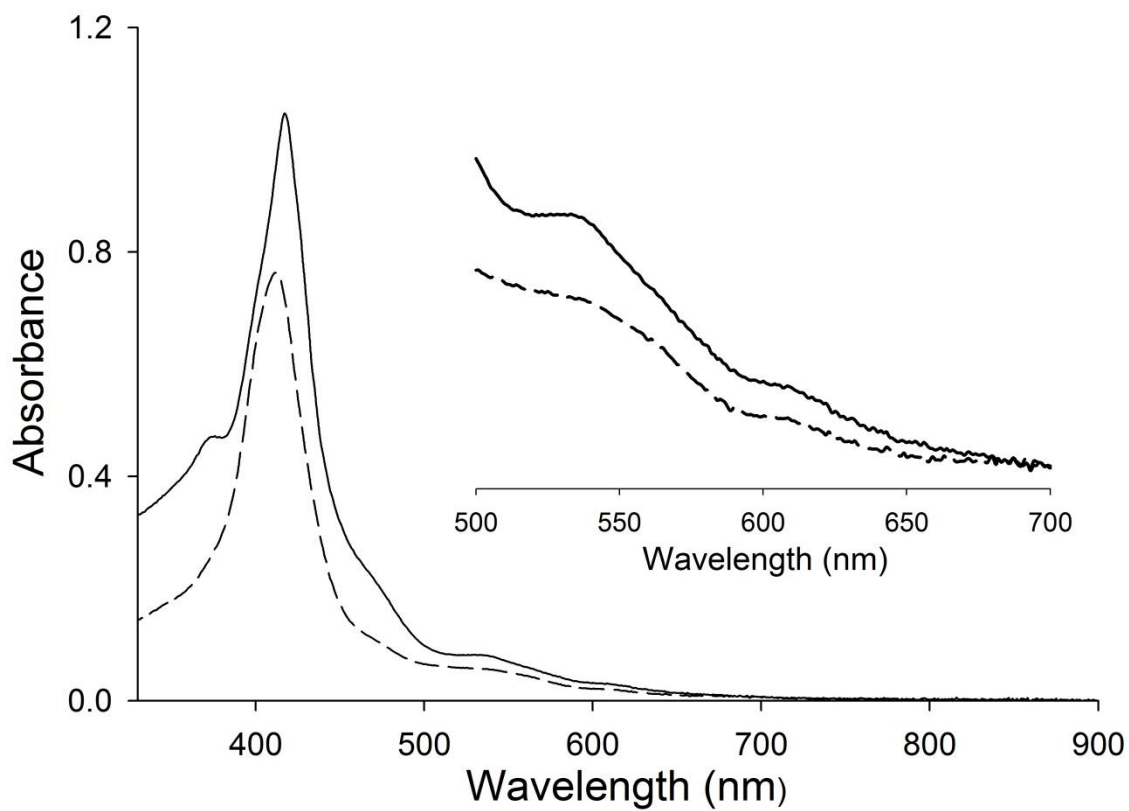


Fig. S15. UV-Vis spectra of an 8.33 μM THF solution of [Fe(TPP)(NO)] (dashed line) and upon addition of 1 mol-equiv of (Et₄N)[Fe(LN₄^{Ph})Cl] (**2**) at 298 K (solid line, 1 min mixing).

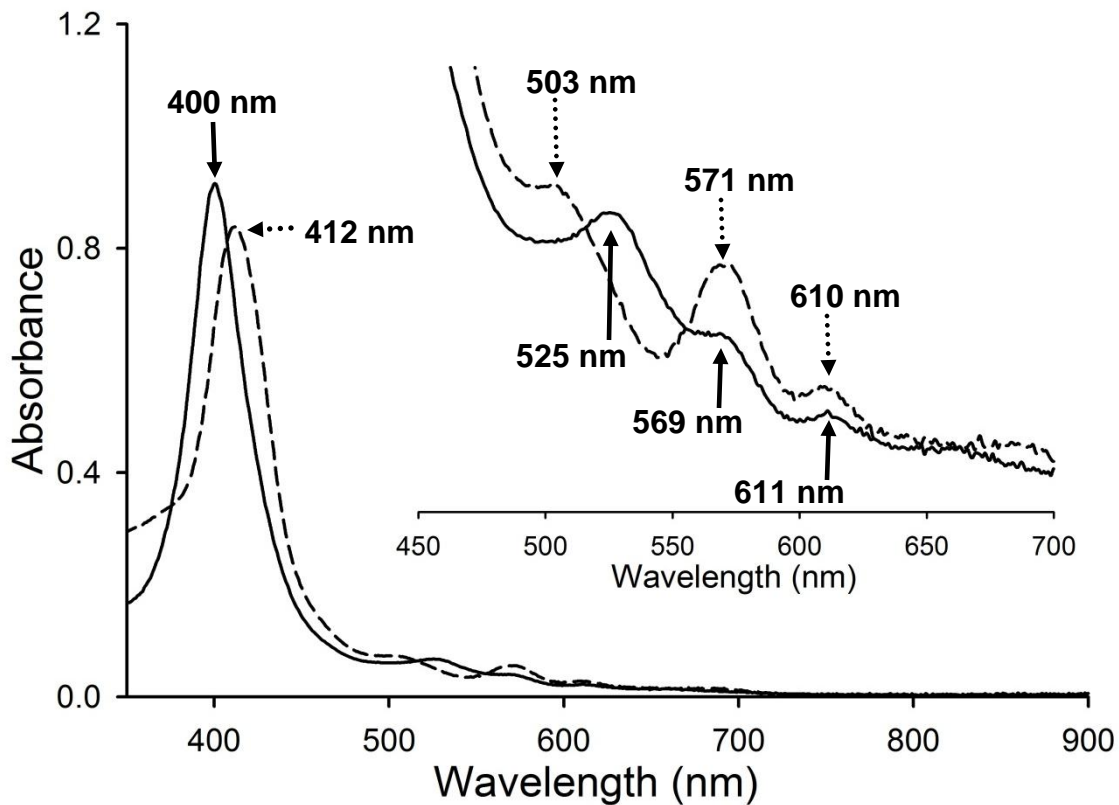


Fig. S16. UV-vis spectra of 8.33 μM THF solutions of $[\text{Fe}(\text{TPP})\text{Cl}]$ (dashed line) and $[\text{Fe}(\text{TPP})\text{OTf}]$ (solid line) at 298 K. *Inset:* expansion of the Q-band region of the spectrum. Arrows are coded according to the spectrum they represent.

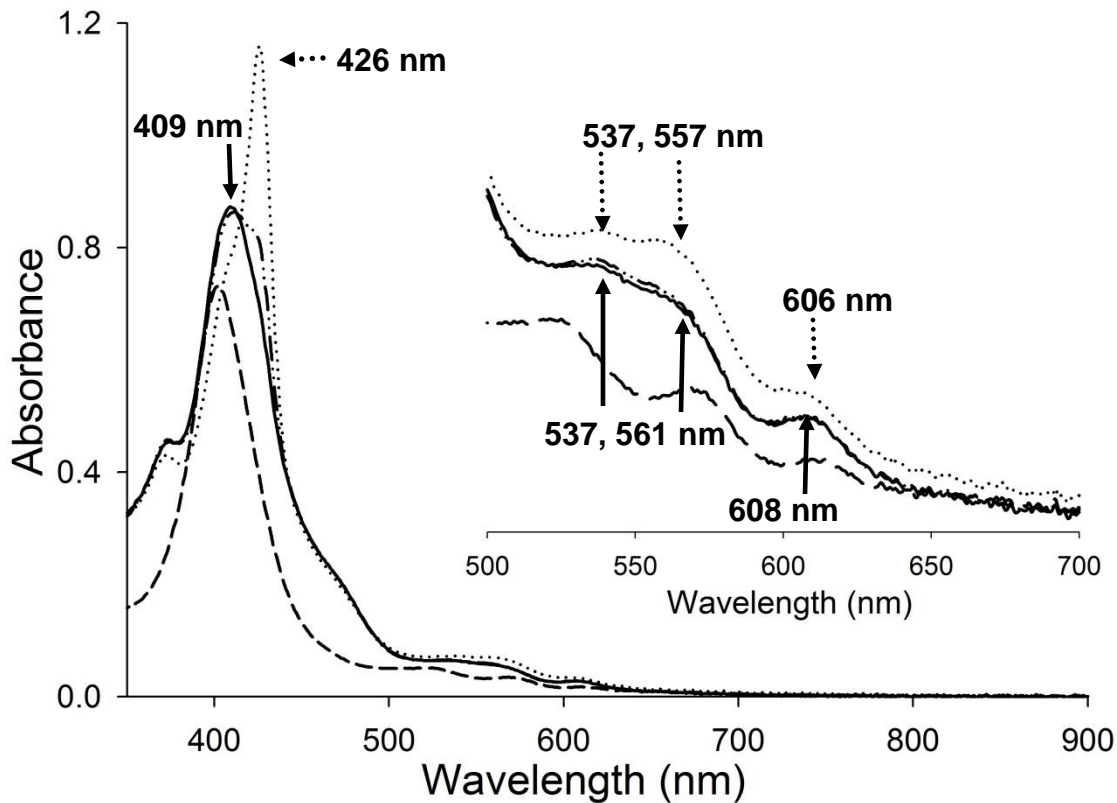


Fig. S17. UV-vis spectra of an 8.33 μM THF solution of [Fe(TPP)OTf] (dashed line), 1 min. after (dotted line), 1 h after (dash-dot-dot line), and 2 h after (solid line) the addition of 1 mol-equiv of K[Fe(LN₄^{PhCl})(NO)] (6) at 298 K. Note that the 1 h and 2 h traces are nearly superimposable. *Inset:* expansion of the Q-band region of the spectrum. Arrows for the 1 min and 2 h traces are provided and coded according to the spectrum they represent.

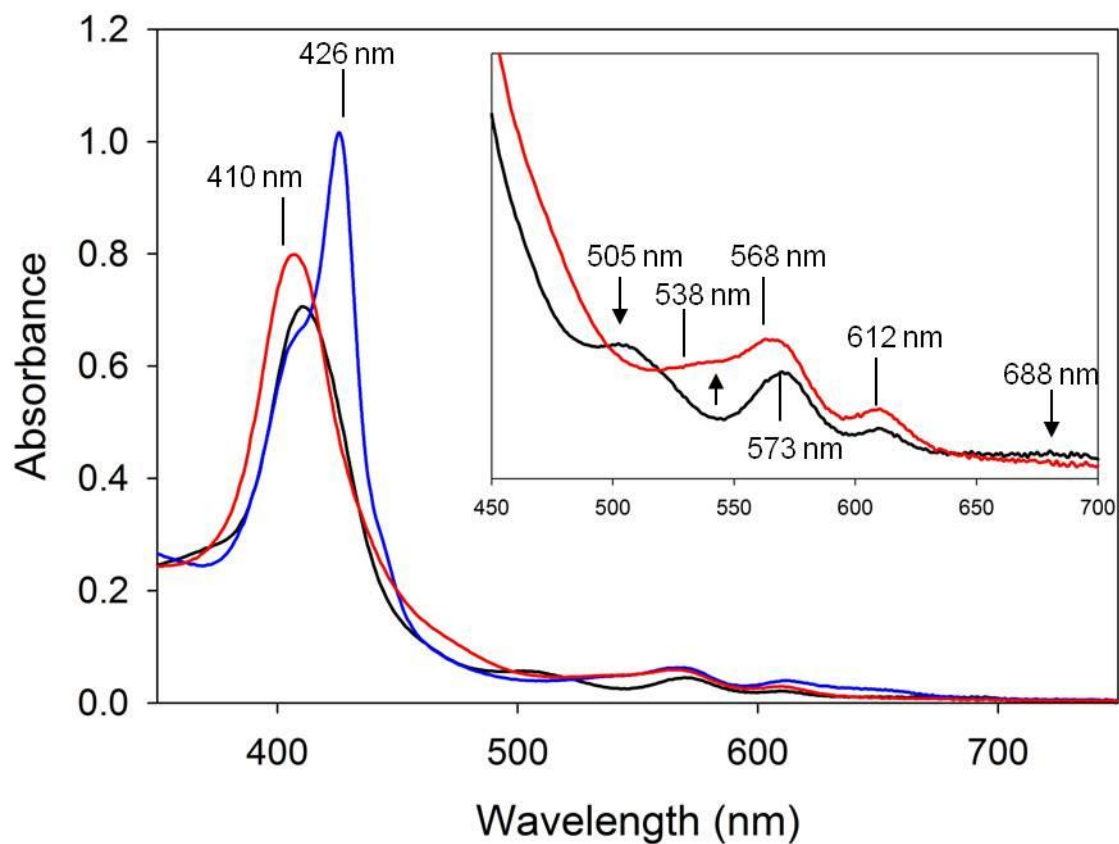


Figure S18. UV-vis spectra of an 8.33 μM THF solution of [Fe(TPP)Cl] (black line), 1 min. after (blue line), and 2 h after (red line) the addition of 1 mol-equiv of [Co(Cp*)₂][Fe(LN₄)(NO)] (**7**) at 298 K. *Inset:* expansion of the Q-band region of the spectrum.

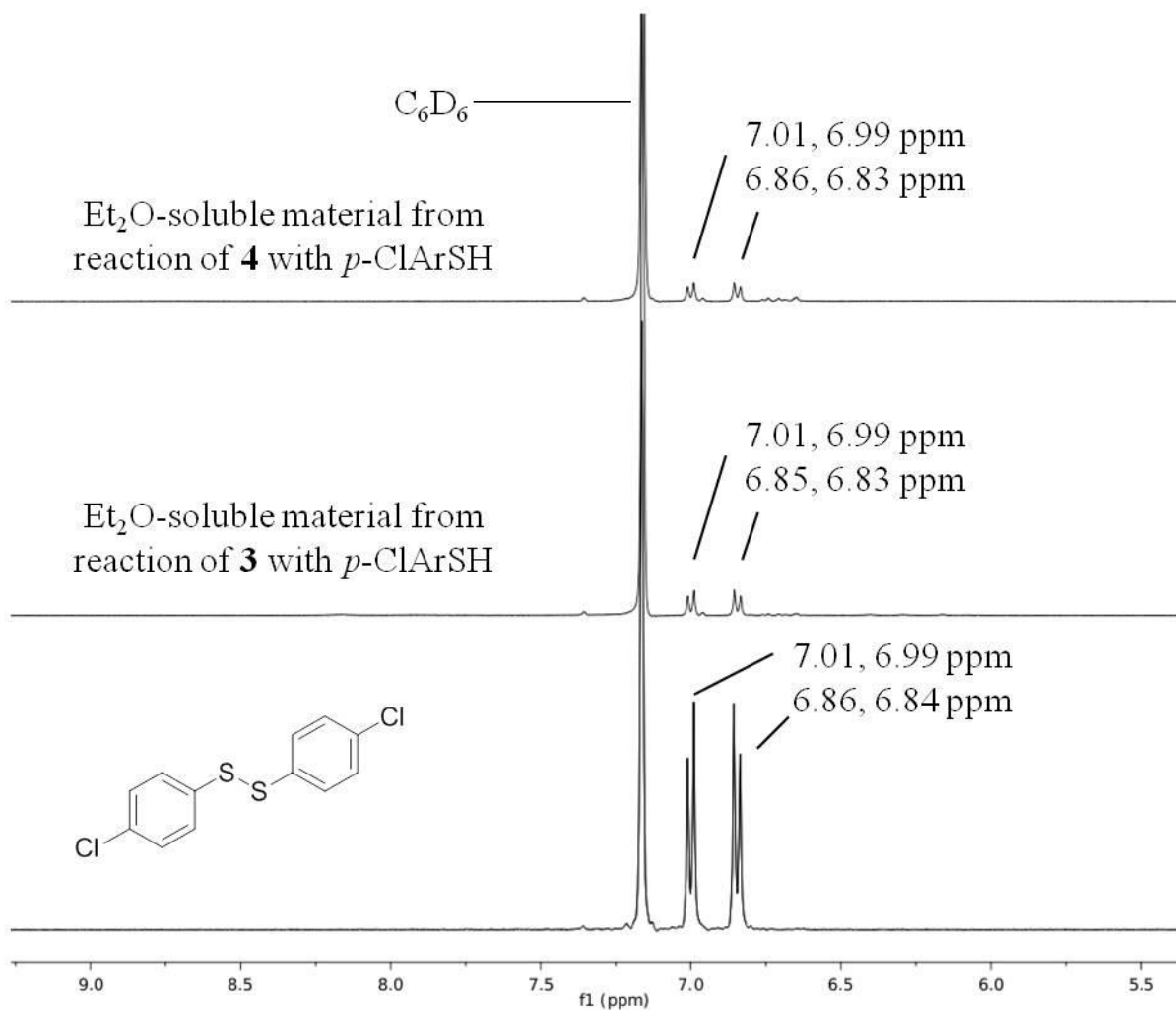


Figure S19. Aromatic region of the ¹H NMR (C₆D₆, RT) of the Et₂O-soluble material from the reactions of **3** and **4** with *p*-ClArSH as compared to an authentic sample of disulfide.

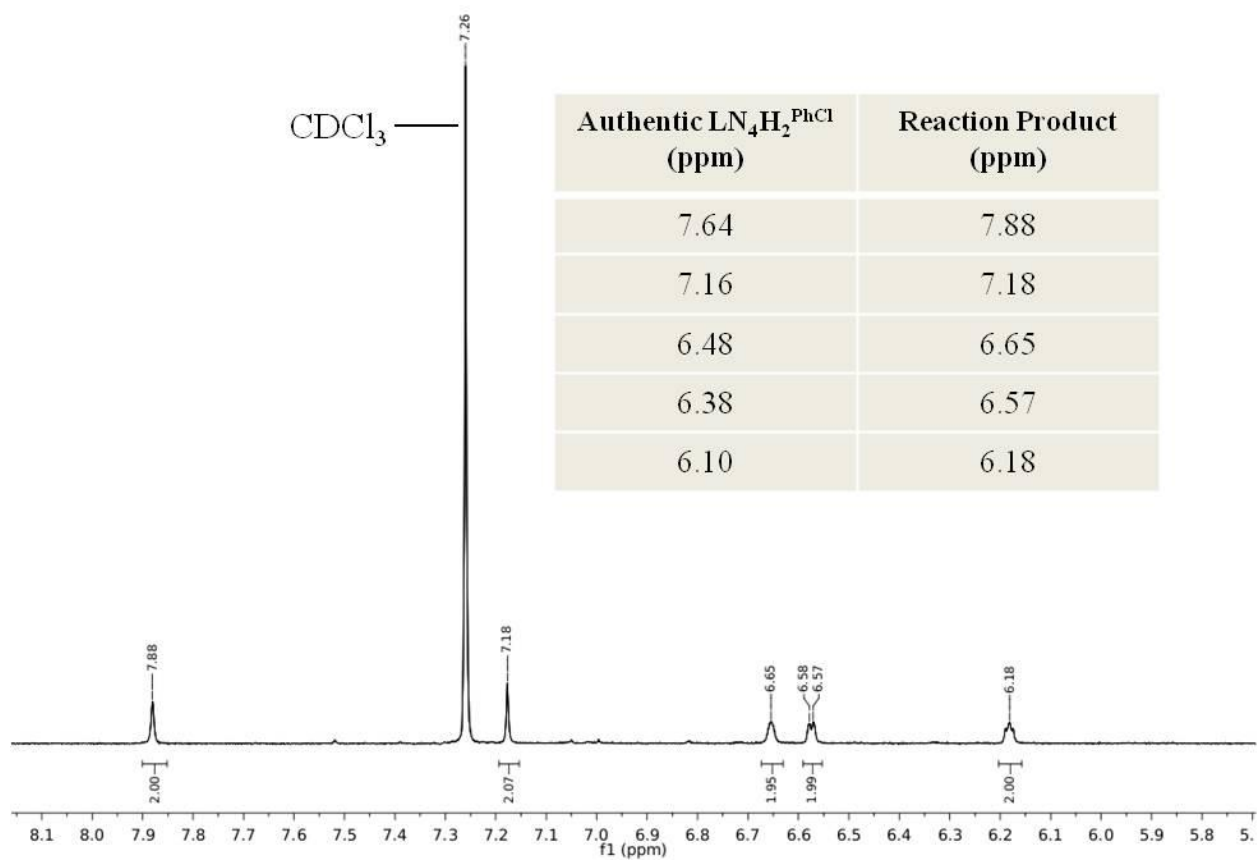


Figure S20. ¹H NMR (CDCl₃, RT) of the Et₂O-soluble material from the reactions of **6** with *p*-ClArSH as compared to authentic LN₄H₂^{PhCl}.

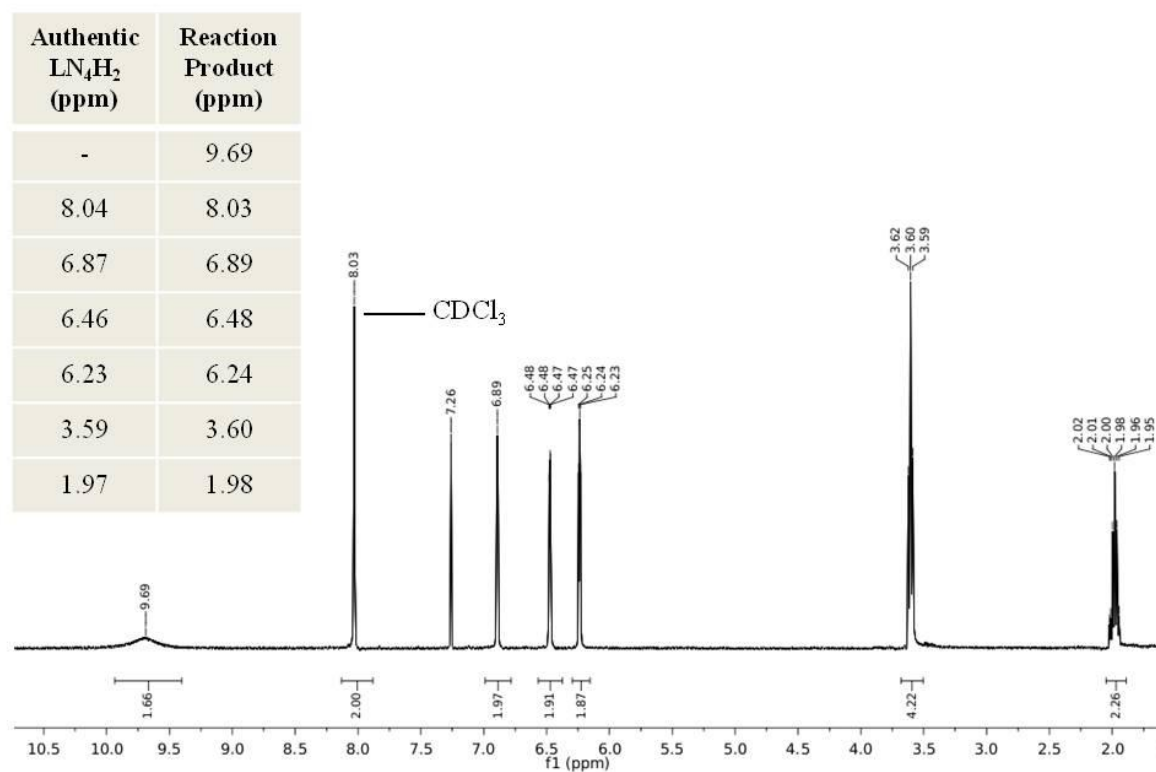


Figure S21. ¹H NMR (CDCl₃, RT) of the Et₂O-soluble material from the reactions of **7** with *p*-ClArSH as compared to authentic LN₄H₂.

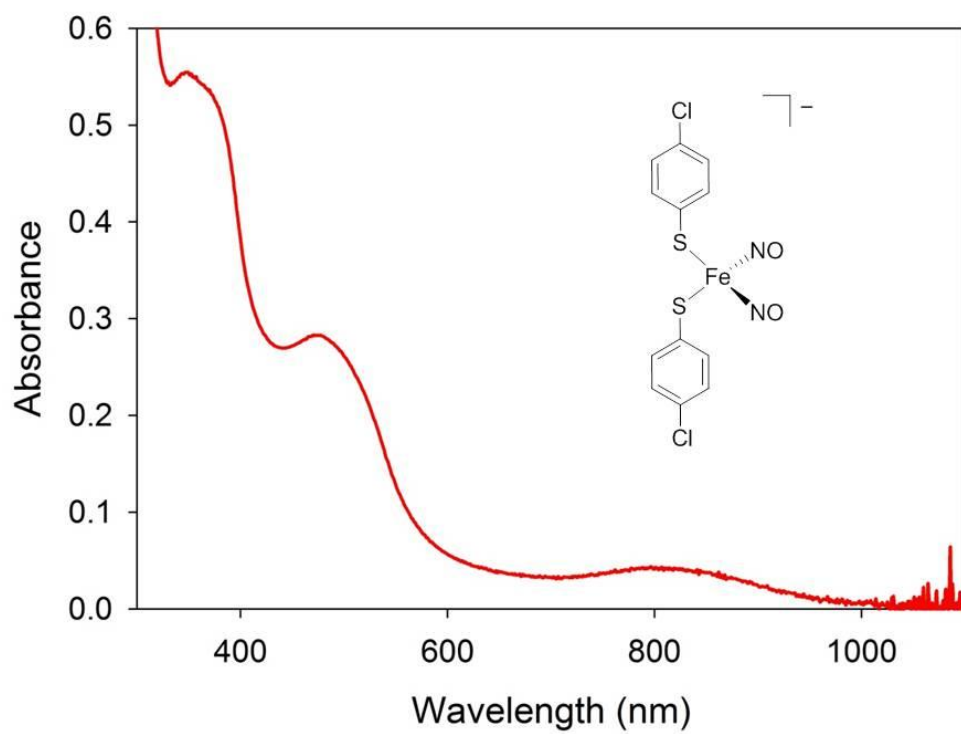


Figure S22. UV-vis (qualitative, MeCN, RT) of the Co(Cp*)₂ salt of DNIC (**9**) obtained from the reaction of **6** with *p*-ClArSH.

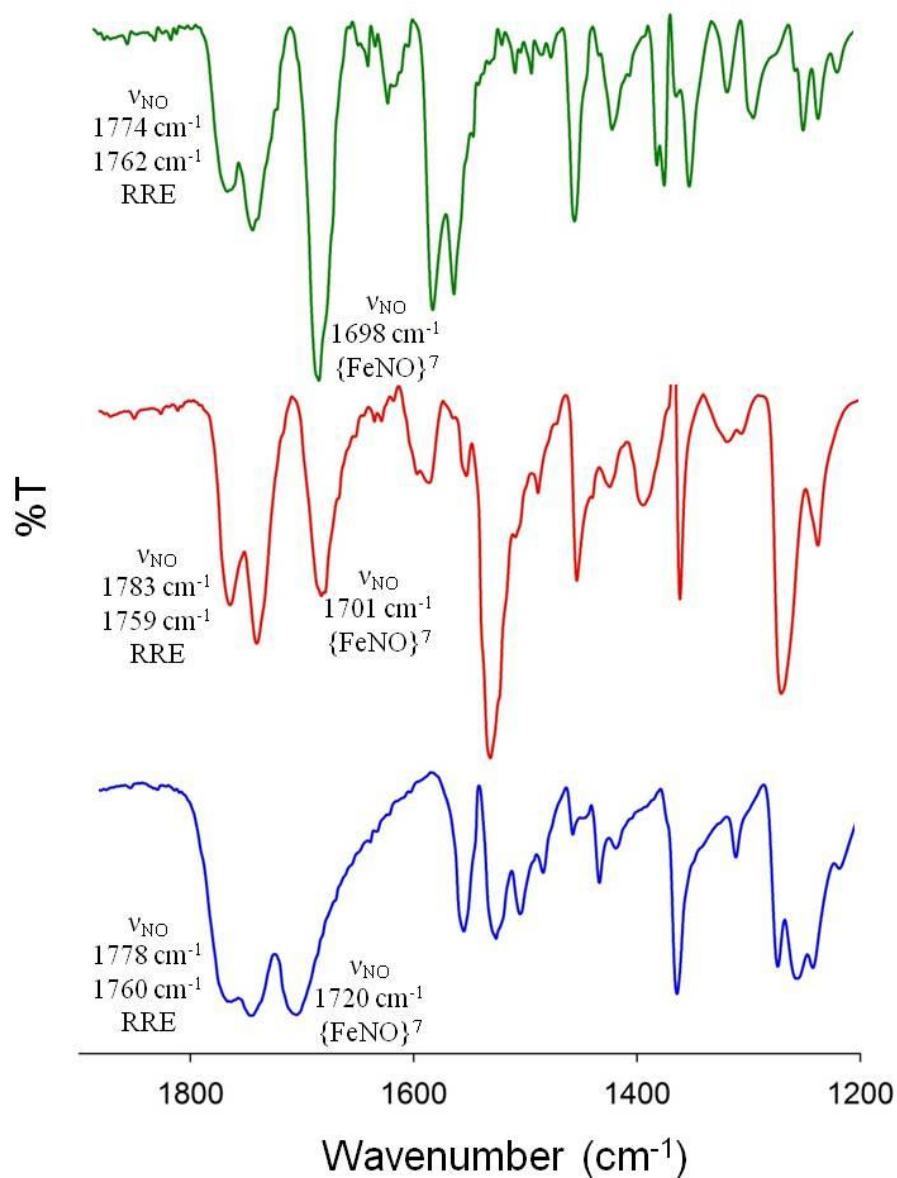


Figure S23. FTIR (KBr, RT) of the Et₂O-insoluble material from the reaction of the {FeNO}⁷ complexes: [Fe(LN₄^{pr})NO] (green trace), **3** (red trace), and **4** (blue trace). The ν_{NO} values are indicative of RRE (**8**) formation and unreacted {FeNO}⁷ starting material.

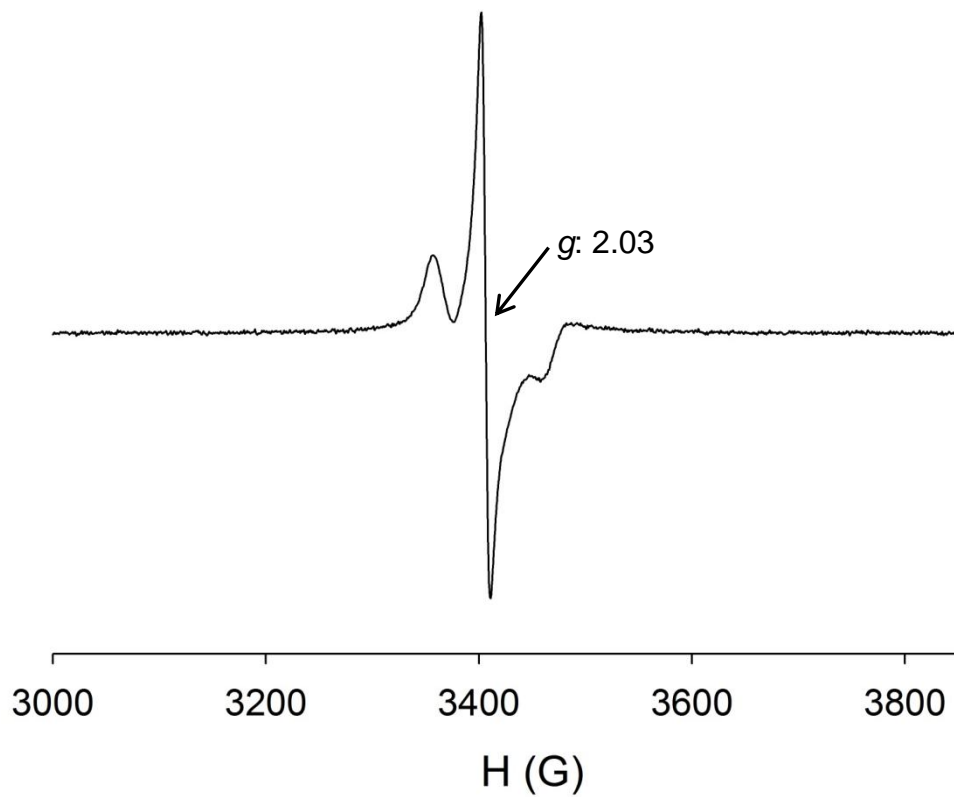


Figure S24. EPR spectrum of **10**. Data collected on a 5 mM 3:1 (MeCN:toluene) solution of **10**. Experimental parameters: $T = 20$ K, microwave power = 2.02×10^{-4} mW, frequency = 9.6 GHz, modulation amplitude = 6.48 G.

2.10 References

- (1) Miranda, K. M. *Coord. Chem. Rev.* **2005**, *249*, 433.
- (2) Bartberger, M. D.; Liu, W.; Ford, E.; Miranda, K. M.; Switzer, C.; Fukuto, J. M.; Farmer, P. J.; Wink, D. A.; Houk, K. N. *Proc. Natl. Acad. Sci. USA* **2002**, *99*, 10958.
- (3) Irvine, J. C.; Ritchie, R. H.; Favaloro, J. L.; Andrews, K. L.; Widdop, R. E.; Kemp-Harper, B. K. *Trends Pharmacol. Sci.* **2008**, *29*, 601.
- (4) Miranda, K. M.; Paolocci, N.; Katori, T.; Thomas, D. D.; Ford, E.; Bartberger, M. D.; Espey, M. G.; Kass, D. A.; Feelisch, M.; Fukuto, J. M.; Wink, D. A. *Proc. Natl. Acad. Sci. USA* **2003**, *100*, 9196.
- (5) Paolocci, N.; Katori, T.; Champion, H. C.; St. John, M. E.; Miranda, K. M.; Fukuto, J. M.; Wink, D. A.; Kass, D. A. *Proc. Natl. Acad. Sci. USA* **2003**, *100*, 5537.
- (6) Wink, D. A.; Miranda, K. M.; Katori, T.; Mancardi, D.; Thomas, D. D.; Ridnour, L.; Espey, M. G.; Feelisch, M.; Colton, C. A.; Fukuto, J. M.; Pagliaro, P.; Kass, D. A.; Paolocci, N. *Am. J. Physiol.; Heart Circ. Physiol.* **2003**, *285*, H2264.
- (7) Nagasawa, H. T.; DeMaster, E. G.; Redfern, B.; Shirota, F. N.; Goon, D. J. W. *J. Med. Chem.* **1990**, *33*, 3120.
- (8) Nagasawa, H. T.; Kawle, S. P.; Elberling, J. A.; DeMaster, E. G.; Fukuto, J. M. *J. Med. Chem.* **1995**, *38*, 1865.
- (9) Doyle, M. P.; Mahapatro, S. N.; Broene, R. D.; Guy, J. K. *J. Am. Chem. Soc.* **1988**, *110*, 593.
- (10) Turk, J.; Corbett, J. A.; Ramanadham, S.; Bohrer, A.; McDaniel, M. L. *Biochem. Biophys. Res. Commun.* **1993**, *197*, 1458.
- (11) Wong, P. S.-Y.; Hyun, J.; Fukuto, J. M.; Shirota, F. N.; DeMaster, E. G.; Shoeman, D. W.; Nagasawa, H. T. *Biochemistry* **1998**, *37*, 5362.
- (12) Farmer, P. J.; Sulc, F. *J. Inorg. Biochem.* **2005**, *99*, 166.
- (13) Kumar, M. R.; Fukuto, J. M.; Miranda, K. M.; Farmer, P. J. *Inorg Chem* **2010**, *49*, 6283.
- (14) Miranda, K. M.; Katori, T.; Torres de Holding, C. L.; Thomas, L.; Ridnour, L. A.; McLendon, W. J.; Cologna, S. M.; Dutton, A. S.; Champion, H. C.; Mancardi, D.;

- Tocchetti, C. G.; Saavedra, J. E.; Keefer, L. K.; Houk, K. N.; Fukuto, J. M.; Kass, D. A.; Paolocci, N.; Wink, D. A. *J. Med. Chem.* **2005**, *48*, 8220.
- (15) Miranda, K. M.; Nims, R. W.; Thomas, D. D.; Espey, M. G.; Citrin, D.; Barberger, M. D.; Paolocci, N.; Fukuto, J. M.; Feelisch, M.; Wink, D. A. *J. Inorg. Biochem.* **2003**, *93*, 52.
- (16) Doctorovich, F.; Bikiel, D.; Pellegrino, J.; Suárez, S. A.; Larsen, A.; Martí, M. A. *Coord. Chem. Rev.* **2011**, *255*, 2764.
- (17) Fukuto, J. M.; Dutton, A. S.; Houk, K. N. *ChemBioChem* **2005**, *6*, 612.
- (18) Averill, B. A. *Chem. Rev.* **1996**, *96*, 2951.
- (19) Daiber, A.; Nauser, T.; Takaya, N.; Kudo, T.; Weber, P.; Hultschig, C.; Shoun, H.; Ullrich, V. *J. Inorg. Biochem.* **2002**, *88*, 343.
- (20) Zumft, W. G. *J. Inorg. Biochem.* **2005**, *99*, 194.
- (21) Schopfer, M. P.; Wang, J.; Karlin, K. D. *Inorg. Chem.* **2010**, *49*, 6267.
- (22) Shafirovich, V.; Lyman, S. V. *Proc. Natl. Acad. Sci. USA* **2002**, *99*, 7340.
- (23) Miranda, K. M.; Nagasawa, H. T.; Toscano, J. P. *Curr. Top. Med. Chem.* **2005**, *5*, 649.
- (24) Angeli, A.; Angelico, A.; Scurti, F. *Chem. Zentralbl.* **1902**, *73*, 691.
- (25) Angeli, A. *Gazz. Chim. Ital.* **1903**, *33*, 245.
- (26) Paolocci, N.; Jackson, M. I.; Lopez, B. E.; Miranda, K.; Tocchetti, C. G.; Wink, D. A.; Hobbs, A. J.; Fukuto, J. M. *Pharmacol. Ther.* **2007**, *113*, 442.
- (27) Andrei, D.; Salmon, D. J.; Donzelli, S.; Wahab, A.; Klose, J. R.; Citro, M. L.; Saavedra, J. E.; Wink, D. A.; Miranda, K. M.; Keefer, L. K. *J. Am. Chem. Soc.* **2010**, *132*, 16526.
- (28) Guthrie, D. A.; Kim, N. Y.; Siegler, M. A.; Moore, C. D.; Toscano, J. P. *J. Am. Chem. Soc.* **2012**, *134*, 1962.
- (29) Connelly, N. G.; Geiger, W. E. *Chem. Rev.* **1996**, *96*, 877.
- (30) McCleverty, J. A. *Chem. Rev.* **2004**, *104*, 403.
- (31) Enemark, J. H.; Feltham, R. D. *Coord. Chem. Rev.* **1974**, *13*, 339.

- (32) Choi, I.-K.; Liu, Y.; Feng, D.; Paeng, K.-J.; Ryan, M. D. *Inorg. Chem.* **1991**, *30*, 1832.
- (33) Lançon, D.; Kadish, K. M. *J. Am. Chem. Soc.* **1983**, *105*, 5610.
- (34) Olson, L. W.; Schaeper, D.; Lançon, D.; Kadish, K. M. *J. Am. Chem. Soc.* **1982**, *104*, 2042.
- (35) Pellegrino, J.; Bari, S. E.; Bikiel, D. E.; Doctorovich, F. *J. Am. Chem. Soc.* **2010**, *132*, 989.
- (36) Pellegrino, J.; Hübner, R.; Doctorovich, F.; Kaim, W. *Chem. Eur. J.* **2011**, *17*, 7868.
- (37) Lehnert, N.; Praneeth, V. K. K.; Paulat, F. *J. Comput. Chem.* **2006**, *27*, 1338.
- (38) Linder, D. P.; Rodgers, K. R. *Inorg. Chem.* **2005**, *44*, 8259.
- (39) Immoos, C. E.; Sulc, F.; Farmer, P. J.; Czarnecki, K.; Bocian, D. F.; Levina, A.; Aitken, J. B.; Armstrong, R. S.; Lay, P. A. *J. Am. Chem. Soc.* **2005**, *127*, 814.
- (40) Sulc, F.; Immoos, C. E.; Pervitsky, D.; Farmer, P. J. *J. Am. Chem. Soc.* **2004**, *126*, 1096.
- (41) Lin, R.; Farmer, P. J. *J. Am. Chem. Soc.* **2000**, *122*, 2393.
- (42) Montenegro, A. C.; Amorebieta, V. T.; Slep, L. D.; Martín, D. F.; Roncaroli, F.; Murgida, D. H.; Bari, S. E.; Olabe, J. A. *Angew. Chem. Int. Ed.* **2009**, *48*, 4213.
- (43) Serres, R. G.; Grapperhaus, C. A.; Bothe, E.; Bill, E.; Weyhermüller, T.; Neese, F.; Wieghardt, K. *J. Am. Chem. Soc.* **2004**, *126*, 5138.
- (44) Patra, A. K.; Dube, K. S.; Sanders, B. C.; Papaefthymiou, G. C.; Conradie, J.; Ghosh, A.; Harrop, T. C. *Chem. Sci.* **2012**, *3*, 364.
- (45) Ye, S.; Price, J. C.; Barr, E. W.; Green, M. T.; Bollinger, J. M., Jr.; Krebs, C.; Neese, F. *J. Am. Chem. Soc.* **2010**, *132*, 4739.
- (46) Speelman, A. L.; Lehnert, N. *Angew. Chem. Int. Edit.* **2013**, *52*, 12283.
- (47) Bayachou, M.; Lin, R.; Cho, W.; Farmer, P. J. *J. Am. Chem. Soc.* **1998**, *120*, 9888.
- (48) Wei, Z.; Ryan, M. D. *Inorg. Chem.* **2010**, *49*, 6948.
- (49) Harman, W. H.; Chang, C. J. *J. Am. Chem. Soc.* **2007**, *129*, 15128.

- (50) Bigi, J. P.; Harman, W. H.; Lassalle-Kaiser, B.; Robles, D. M.; Stich, T. A.; Yano, J.; Britt, R. D.; Chang, C. J. *J. Am. Chem. Soc.* **2012**, *134*, 1536.
- (51) Piro, N. A.; Lichterman, M. F.; Harman, W. H.; Chang, C. J. *J. Am. Chem. Soc.* **2011**, *133*, 2108.
- (52) Bondi, A. *J. Phys. Chem.* **1964**, *68*, 441.
- (53) Addison, A. W.; Rao, T. N.; Reedijk, J.; van Rijn, J.; Verschoor, G. C. *J. Chem. Soc., Dalton Trans.* **1984**, 1349.
- (54) Goodrich, L. E.; Paulat, F.; Praneeth, V. K. K.; Lehnert, N. *Inorg. Chem.* **2010**, *49*, 6293.
- (55) Wyllie, G. R. A.; Scheidt, W. R. *Chem. Rev.* **2002**, *102*, 1067.
- (56) Wyllie, G. R. A.; Schulz, C. E.; Scheidt, W. R. *Inorg. Chem.* **2003**, *42*, 5722.
- (57) Conradie, J.; Ghosh, A. *Inorg. Chem.* **2011**, *50*, 4223.
- (58) Praneeth, V. K. K.; Näther, C.; Peters, G.; Lehnert, N. *Inorg. Chem.* **2006**, *45*, 2795.
- (59) Vogel, K. M.; Kozlowski, P. M.; Zgierski, M. Z.; Spiro, T. G. *J. Am. Chem. Soc.* **1999**, *121*, 9915.
- (60) Bergbreiter, D. E.; Killough, J. M. *J. Am. Chem. Soc.* **1978**, *100*, 2126.
- (61) Savoia, D.; Trombini, C.; Umani-Ronchi, A. *Pure Appl. Chem.* **1985**, *57*, 1887.
- (62) Kilner, C. A.; Halcrow, M. A. *Acta. Crystallogr.* **2006**, *C62*, m437.
- (63) Gwost, D.; Caulton, K. G. *Inorg. Chem.* **1973**, *12*, 2095.
- (64) Bari, S. E.; Martí, M. A.; Amorebieta, V. T.; Estrin, D. A.; Doctorovich, F. *J. Am. Chem. Soc.* **2003**, *125*, 15272.
- (65) Bazyliniski, D. A.; Hollocher, T. C. *J. Am. Chem. Soc.* **1985**, *107*, 7982.
- (66) Martí, M. A.; Bari, S. E.; Estrin, D. A.; Doctorovich, F. *J. Am. Chem. Soc.* **2005**, *127*, 4680.
- (67) Suárez, S. A.; Martí, M. A.; De Biase, P. M.; Estrin, D. A.; Bari, S. E.; Doctorovich, F. *Polyhedron* **2007**, *26*, 4673.
- (68) Hoshino, M.; Baba, T. *J. Am. Chem. Soc.* **1998**, *120*, 6820.

- (69) Zhu, X.-Q.; Zhang, J.-Y.; Mei, L.-R.; Cheng, J.-P. *Org. Lett.* **2006**, *8*, 3065.
- (70) Chiang, C.-Y.; Darensbourg, M. Y. *J. Biol. Inorg. Chem.* **2006**, *11*, 359.
- (71) Reed, C. A.; Mashiko, T.; Bentley, S. P.; Kastner, M. E.; Scheidt, W. R.; Spartalian, K.; Lang, G. *J. Am. Chem. Soc.* **1979**, *101*, 2948.
- (72) Boersma, A. D.; Goff, H. M. *Inorg. Chem.* **1982**, *21*, 581.
- (73) Houk, K. N.; Hietbrink, B. N.; Bartberger, M. D.; McCarren, P. R.; Choi, B. Y.; Voyksner, R. D.; Stamler, J. S.; Toone, E. J. *J. Am. Chem. Soc.* **2003**, *125*, 6972.
- (74) Perissinotti, L. L.; Turjanski, A. G.; Estrin, D. A.; Doctorovich, F. *J. Am. Chem. Soc.* **2005**, *127*, 486.
- (75) Pereira, J. C.; Iretskii, A. V.; Han, R. M.; Ford, P. C. *J. Am. Chem. Soc.* **2015**, *137*, 328.
- (76) Hung, M. C.; Tsai, M. C.; Lee, G. H.; Liaw, W. F. *Inorg. Chem.* **2006**, *45*, 6041.
- (77) Patra, A. K.; Harrop, T. C. *Unpublished Results*.
- (78) Rhine, M. A.; Rodrigues, A. V.; Urbauer, R. J. B.; Urbauer, J. L.; Stemmler, T. L.; Harrop, T. C. *J. Am. Chem. Soc.* **2014**, *136*, 12560.
- (79) Tsai, M. L.; Liaw, W. F. *Inorg. Chem.* **2006**, *45*, 6583.
- (80) Sanders, B. C.; Hassan, S. M.; Harrop, T. C. *J. Am. Chem. Soc.* **2014**, *136*, 10230.
- (81) Wang, R.; Camacho-Fernandez, M. A.; Xu, W.; Zhang, J.; Li, L. *Dalton Trans.* **2009**, 777.
- (82) Lin, Z.-S.; Lo, F.-C.; Li, C.-H.; Chen, C.-H.; Huang, W.-N.; Hsu, I. J.; Lee, J.-F.; Horng, J.-C.; Liaw, W.-F. *Inorg. Chem.* **2011**, *50*, 10417.
- (83) Butler, A. R.; Megson, I. L. *Chem. Rev.* **2002**, *102*, 1155.
- (84) Gill, N. S.; Taylor, F. B. *Inorg. Synth.* **1967**, *9*, 136.
- (85) Scheidt, W. R.; Frisse, M. E. *J. Am. Chem. Soc.* **1975**, *97*, 17.
- (86) Sur, S. K. *J. Magn. Reson.* **1989**, *82*, 169.
- (87) Fulmer, G. R.; Miller, A. J. M.; Sherden, N. H.; Gottlieb, H. E.; Nudelman, A.; Stoltz, B. M.; Bercaw, J. E.; Goldberg, K. I. *Organometallics* **2010**, *29*, 2176.

- (88) Walker, F. A.; Lo, M.-W.; Ree, M. T. *J. Am. Chem. Soc.* **1976**, 98, 5552.
- (89) SMART v5.626: Software for the CCD Detector System; Bruker AXS: Madison WI **2000**.
- (90) Walker, N.; Stuart, D. *Acta. Crystallogr.* **1983**, A39, 158.
- (91) Sheldrick, G. M. *SADABS, Area Detector Absorption Correction, University of Göttingen, Göttingen, Germany, 2001*.
- (92) Sheldrick, G. M. *SHELX-97, Program for Refinement of Crystal Structures, University of Göttingen, Göttingen, Germany, 1997*.
- (93) Sheldrick, G. M. *SHELXTL 6.1, Crystallographic Computing System, Siemens Analytical X-Ray Instruments, Madison, WI, 2000*.
- (94) Burnett, M. N.; Johnson, C. K. *ORTEP-III, Report ORNL - 6895; Oak Ridge National Laboratory: Oak Ridge, TN, 1996*.

CHAPTER 3

NO₂⁻ ACTIVATION AND REDUCTION TO NO BY A NON-HEME Fe-(NO₂)₂ COMPLEX¹

¹ B. C. Sanders, S. M. Hassan, and T. C. Harrop, *J. Am. Chem. Soc.*, **2014**, *136*, 10230-10233.
Reprinted here with permission of the American Chemical Society.

3.1 Abstract

The selective reduction of nitrite (NO_2^-) to nitric oxide (NO) is a fundamentally important chemical transformation related to environmental remediation of NO_x and mammalian blood flow. We report the synthesis and characterization of two non-heme Fe complexes, $[\text{Fe}(\text{LN}_4^{\text{Im}})(\text{MeCN})_2](\text{BF}_4)_2$ (**1**^{MeCN}) and $[\text{Fe}(\text{LN}_4^{\text{Im}})(\text{NO}_2)_2]$ (**2**), geared towards understanding the NO_2^- to NO conversion. Complex **2** represents the first structurally characterized Fe(II) complex with two axial NO_2^- ligands that functions as a nitrite reduction catalyst.

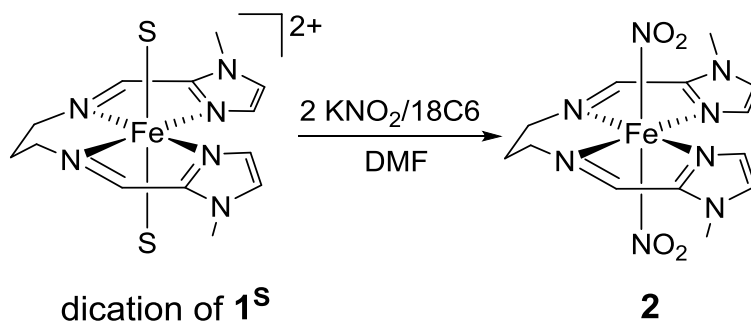
3.2 Introduction

While the physiological properties of nitric oxide (NO) have been established over the past four decades,¹⁻³ several other small inorganic molecules have emerged that exhibit important biological activities. This list includes reactive nitrogen species (RNS) such as nitrite (NO_2^-)⁴⁻⁸ and nitroxyl (HNO)^{9,10} and S-containing molecules such as hydrogen sulfide (H_2S).^{11,12} In particular, the biochemical properties of NO_2^- have been the focus of recent research efforts, which stems from its role in the global nitrogen cycle and its potential therapeutic use in diseases related to blood flow.⁴⁻⁸ For example, the overuse of nitrogen-rich fertilizers has led to an increase in nitrate (NO_3^-) and NO_2^- concentrations to toxic levels in water runoff.¹³ Thus, removal of these nitrogen oxides by denitrifying bacteria or synthetic catalysts is a key process in municipal water treatment.¹⁴ Additionally, in vivo vascular levels of NO_2^- approach high μM where it serves as an emergency storage pool of NO.¹⁵⁻¹⁷ The two proton, one electron reduction of NO_2^- to NO is effectively carried out in microbes by nitrite reductase enzymes (NiR: $\text{NO}_2^- + 2\text{H}^+ + \text{e}^- \rightarrow \text{NO} + \text{H}_2\text{O}$) utilizing type 2 Cu or heme-Fe (*cd*₁) cofactors.⁶ Although no such human NiR exists, several heme proteins have demonstrated NiR activity under hypoxic conditions.² These studies emphasize nitrite's role as an alternative (nitric oxide synthase (NOS) independent) reservoir of NO during times of stress. Indeed, this activity has been observed in several mammalian proteins including deoxyhemoglobin, endothelial NOS, and cytochrome *c* oxidase.⁴ This property emphasizes the significant role Fe-containing proteins play in the physiological equilibrium between NO_2^- and NO.

Due to the environmental and physiological importance of the NO_2^- -to-NO conversion, several groups have pursued synthetic analogues of NiRs.⁹⁻¹⁰ Examples of functional Cu-NiR^{18-20,21-27} analogues are greater than their Fe counterparts.²⁸⁻³² This absence is because of the

tendency to form Fe reaction by-products that halt the catalytic cycle including oxo-bridged Fe(III)-O-Fe(III) and ‘inert’ {FeNO}⁷ derivatives.²⁸⁻³² Encouraged by our findings in non-heme-mediated reduction of NO with pyrrole ligands, we transitioned to the design of NO₂⁻ reduction catalysts.^{33,34} We thus synthesized a planar, neutral, imine/imidazole, N₄-ligand (LN₄^{Im}) to permit the binding of NO₂⁻ ligands in vacant or solvent-bound axial positions (Scheme 3.1). We hypothesized that the decreased basicity of LN₄^{Im} would circumvent the formation of stable {FeNO}⁷ products and facilitate catalytic reduction of NO₂⁻. Herein, we report the synthesis, structure and properties of [Fe(LN₄^{Im})(MeCN)₂](BF₄)₂ (**1**^{MeCN}) and [Fe(LN₄^{Im})(NO₂)₂] (**2**) (Scheme 3.1). To our knowledge, **2** is the first example of a non-heme Fe(II)-(NO₂)₂ complex that exhibits catalytic NiR activity.

Scheme 3.1. Synthesis of **2** (S = solvent ligands)



3.3 Spectroscopic and Reactive Studies of Complex **1**^{MeCN} and **2**

Complex **1**^{MeCN} was synthesized by treating an MeCN solution of LN₄^{Im} with [Fe(H₂O)₆](BF₄)₂ (1:1) affording the red Fe(II) complex (λ_{max} : 478 nm in MeCN, Fig. S4 in the Supporting Information = SI) in 92% yield. Complex **1**^{MeCN} has been characterized by various spectroscopies and X-ray diffraction (Fig. 3.1) to support its formulation (see the SI). Complex **1**

reacted readily with KNO_2 (1:2, solubilized with 18-crown-6 ether = 18C6) in DMF to result in precipitation of the violet N-bound (nitro) species **2** in 85% yield (Scheme 3.1). Spectroscopic features in the UV-vis (λ_{max} : 574 nm in MeCN, Fig. S4) and FTIR (^{15}N -sensitive peaks at 1327, 1281, and 813 cm^{-1} , KBr, Fig. S3)³⁵ are consistent with its formation. The isolation of **2** from stoichiometric addition of NO_2^- is noteworthy as reacting an Fe(II)-P (where P = porphyrin) complex with excess NO_2^- only results in the mono-nitro derivative.³⁶ This observation has been attributed to the strong π -accepting ability of NO_2^- and is exemplified by the low-spin (LS) nature of Fe in the Fe-P- NO_2 complex. Complex **2** is no exception to the LS trend; however, the binding of the second axial NO_2^- group is a first in Fe(II) heme and non-heme systems. The π -acidity of NO_2^- in **2** is likely buffered by the neutral, less basic LN_4^{Im} . In contrast, Fe-P complexes with other anionic axial ligands are typically high-spin.¹³

3.3.1 X-Ray Crystal Structures of **1** and **2**

X-ray crystallographic analysis revealed distorted octahedral Fe(II) centers from the four basal plane N-donors of LN_4^{Im} and two MeCN or NO_2^- axial ligands for **1**^{MeCN} and **2**, respectively (Fig. 3.1). The bond distances for **1**^{MeCN} and **2** are similar with Fe- N_{imine} (avg: 1.962 Å for **1**; 1.940 Å for **2**) and Fe- $\text{N}_{\text{imidazole}}$ (avg: 1.992 Å for **1**; 1.996 Å for **2**) lengths supportive of the LS nature of Fe(II). The axial Fe-NCMe distance (avg: 1.935 Å) in **1**^{MeCN} is shorter than the Fe- NO_2 distance (avg: 1.964 Å) in **2** reflective of the better π -accepting ability of nitrile versus nitrite. Comparison of the Fe- NO_2 distance in **2** with Fe(II)-P- NO_2 complexes emphasizes the highly variable nature of the π -bonding in the NO_2^- ligand. For example, the Fe- NO_2 distance of **2** is longer than the Fe- NO_2 distance in the five-coordinate Fe(II)-P- NO_2 complex (1.849 Å)³⁶ and ccNiR (1.9 Å, Fe(III) form),³⁷ but is similar to that found in six-coordinate Fe(II)-P- NO_2

complexes (avg: 1.988 Å).³⁸ This structural discrepancy in five- versus six-coordinate Fe-NO₂ complexes has been attributed to the trans influence i.e. competition for the *dπ* orbitals of Fe.³⁹ For comparison, the only Fe-axial-dinitro complex that has been characterized by X-ray diffraction is an Fe(III)-P species with Fe-NO₂(avg): 1.985 Å.⁴⁰ Complex **2** is thus the first structurally characterized Fe(II)-axial-dinitro complex and shares metric similarities to six-coordinate mono-nitro Fe(II)-P-NO₂ complexes. The unique N-O distances in **2** (one long: 1.285 Å; one short: 1.222 Å) are symptomatic of the diminished π -delocalization in the O-N-O molecule and underscores the potential lability of these bonds (vide infra).

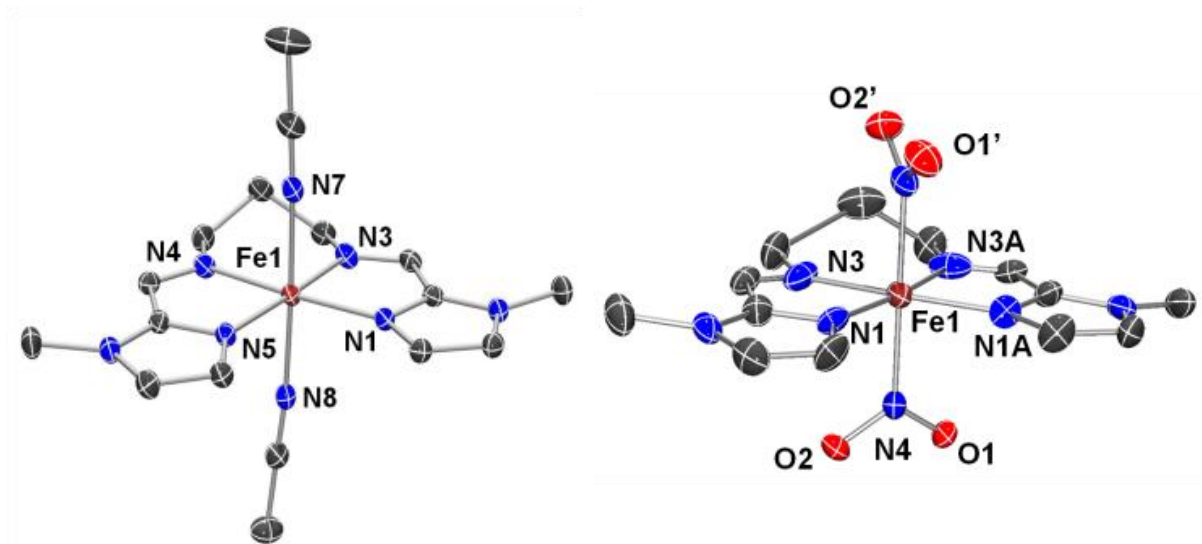
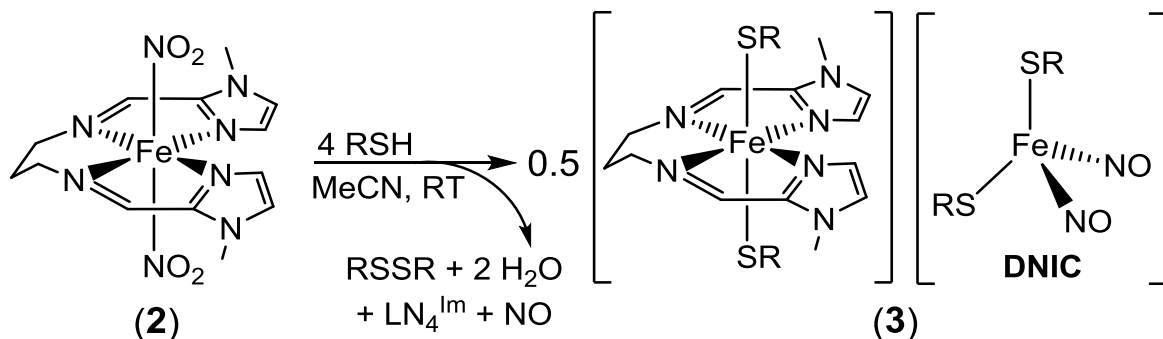


Figure 3.1. ORTEP of **1**^{MeCN} (left) and **2** (right) with 50% thermal probability for all non-hydrogen atoms. MeCN and PhCN solvent of crystallization for **1**^{MeCN} and **2**, respectively, have been omitted for clarity.

3.4 Reactivity Studies of **2**

The unprecedented Fe(NO₂)₂ axial ligation in **2** prompted us to explore its reaction chemistry with thiols since they could function as H⁺ and e⁻ sources for reduction of coordinated NO₂⁻. Reaction of **2** with *p*-chlorobenzenethiol (1:4; *p*-ClArSH = RSH, pK_a: 9-10 in DMSO⁴¹) resulted in the tetrahedral dinitrosyl iron complex (DNIC), [Fe(SAr-*p*-Cl)₂(NO)₂]⁻ (anion of **3**, MeCN, room temperature = RT, see Scheme 3.2). Fractional precipitation of the reaction mixture allowed us to characterize the products formed. After reacting **2** with RSH (1:4) for 24 h, the solvent was removed and the dark residue was treated with Et₂O to afford an insoluble dark-red solid. Spectroscopic analysis of this solid by FTIR (ν_{NO}: 1743, 1692 cm⁻¹, KBr), UV-vis (λ_{max}: 487, 790 nm, MeCN), and ESI-MS(-) is consistent with DNIC.⁴²⁻⁴⁴ This assignment was further verified by comparing these parameters to that of independently prepared **3** (Et₄N⁺ salt, Figs. S5-S7). ESI-MS(+) of this solid confirmed that the cation of **3** is the Fe(III) complex [Fe(LN₄^{lm})(SR)₂]⁺ (Fig. S8-S9). The organic soluble materials comprised of the disulfide of *p*-Cl-ArSH (*p*-Cl-ArSSAr-*p*-Cl or RSSR) and free LN₄^{lm} based on ¹H NMR comparison to authentic samples. From this evidence, one mechanistic proposal involves the stepwise heterolytic cleavage of the N-O bonds in **2** and formation of a transient mononitrosyl {FeNO}⁷ iron complex (MNIC). All RSH equivalents serve as H⁺ sources; half reduces the {FeNO} unit (generating RSSR) and the other half becomes ligand. Recent work from Kim demonstrated that Fe-thiolate MNICs disproportionate into DNIC and 2Fe-2S clusters in the presence of excess thiol.⁴⁵ A similar fate in the present reaction thus appears reasonable. Moreover, thiol (not thiolate) is necessary for the observed conversion as addition of (Et₄N)(SAr-*p*-Cl) to an MeCN solution of **2** does not yield DNIC. Thus, a proton-coupled redox event accounts for the chemistry in Scheme 3.2.

Scheme 3.2. Reaction of **2** with RSH (R: *p*-ClArSH)



The **2** and RSH reaction represents a new path to NO formation and interception via the DNIC. Indeed, studies in the early 1980s revealed the *in vivo* formation of protein-bound DNICs when rats were fed diets high in nitrite salts.^{46,47} DNIC formation is in contrast to the reaction of Fe(III)-P-NO₂ complexes with thiols, which yield the corresponding {FeNO}⁷ and sulfenic acid (RS=OH) through an O-atom transfer (OAT) mechanism.⁴⁸⁻⁵⁰ No evidence for S-oxygenates was observed in the **2** and RSH reaction demonstrating the difference in chemistry between Fe(III)- and Fe(II)-NO₂ complexes. Moreover, addition of 25 mol-equiv of the classic O-atom acceptor PPh₃^{49,51} resulted in no reaction with **2** under identical conditions (Fig. S10). Although thiol-induced rearrangement of the coordination sphere of **2** to yield **3** halts catalytic NO₂⁻ reduction, the chemistry is indicative of the NiR activity of **2** in the presence of a weak acid, a previously uninvestigated H⁺/e⁻ source for reduction of Fe(II)-NO₂ complexes.

To circumvent DNIC formation, we tested the NiR activity of **2** using an acid with a non-coordinating conjugate base in combination with *p*-ClArSH as the sacrificial reductant. Reaction of **2** with a 1:1 mixture of tosic acid hydrate (TsOH•H₂O; *p*K_a: 8.6, MeCN⁵²)/*p*-ClArSH (1:2:2, net: 2H⁺, 1 e⁻ per bound NO₂⁻) resulted in immediate color change of the MeCN solution from

violet to red. The first indication that this pathway was different from the thiol-only reaction was from fractional precipitation of the reaction mixture. For example, removal of the MeCN solvent followed by treatment of the dark residue with Et₂O, afforded the red insoluble Fe-containing product, [Fe(II)(LN₄^{Im})(MeCN)₂](OTs)₂ (tosylate salt of **1**^{MeCN}) in 73% yield (UV-vis, FTIR, and ESI-MS(+)). The FTIR of the Et₂O-insoluble compound displayed no ν_{NO} peaks attributed to DNIC.⁵³ Furthermore, ¹H NMR analysis of the Et₂O-soluble portion indicated only RSSR (85%). Further insight regarding the fate of the NO₂⁻ ligands of **2** was obtained through GC-MS analysis of the reaction headspace. Sampling the headspace after mixing **2** with RSH/TsOH (1:2:2) under identical conditions revealed the presence of a peak in the GC ($t_r = 1.79$ min) whose corresponding MS (m/z : 29.9) was consistent with NO (Fig. S11). There was no evidence for other nitrogen oxide compounds (i.e. N₂O, NO₂). Control experiments with NO₂⁻ resulted in ~10% of the NO observed in the **2**-promoted reduction highlighting its requirement in the NO₂⁻-to-NO conversion. An identical GC-MS experiment with ¹⁵N-labeled **2**^{15N} exhibited m/z : 30.9 (¹⁵NO) to further corroborate NO formation from **2** (Fig. S12). To quantify released NO(g), vial-to-vial NO-trapping reactions were performed with the Co^{II}-P complex [Co(T(-OMe)PP)] (where T(-OMe)PP = 5,10,15,20,-tetrakis(4-methoxyphenyl)-21*H*,23*H*-porphine) to generate the corresponding {CoNO}⁸ complex [Co(T(-OMe)PP)(NO)].²⁴ Performing this experiment with **2** and RSH/TsOH (1:2:2) resulted in stoichiometric conversion of [Co(T(-OMe)PP)] to the {CoNO}⁸ complex as monitored by UV-vis (λ_{max} : 418, 540 nm, CH₂Cl₂) and FTIR (ν_{NO} : 1697 cm⁻¹; $\nu_{15\text{NO}}$: 1667 cm⁻¹ using **2**^{15N}, KBr, Fig. S13-14).

The release of NO from the reaction of **2** and RSH/TsOH, coupled with the isolation of **1**^{MeCN}, suggested we could reform **2** by addition of NO₂⁻ to the reaction mixture and demonstrate turnover. Thus, formation of NO was monitored by GC-MS under identical conditions (vide

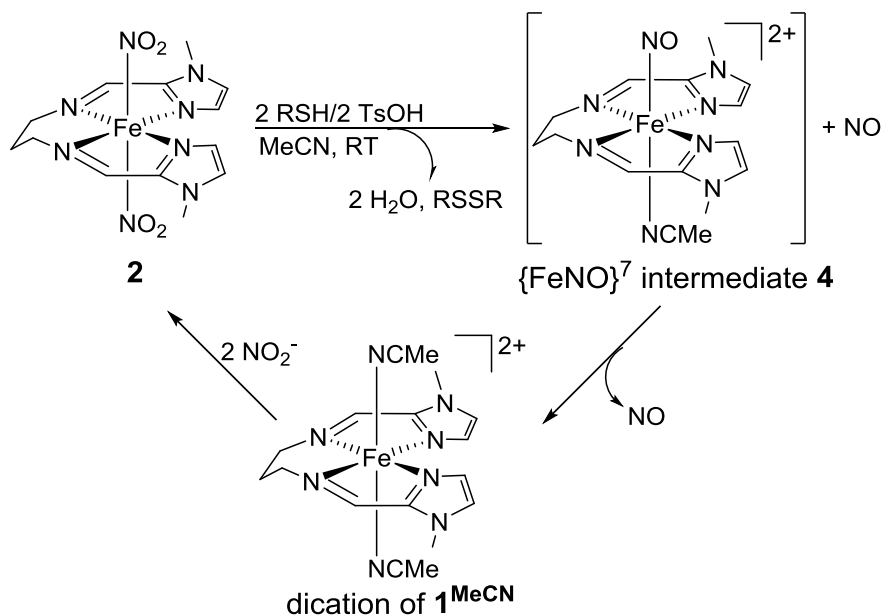
supra). After 15 min, 2 mol-equiv of NO_2^- were added to the mixture to displace any coordinated NO and regenerate **2**. GC-MS analysis of the reaction headspace at this point verified the presence of NO (Fig. S15). After this measurement, the headspace was removed under vacuum and refilled with N_2 to provide an NO-free baseline in the GC. Subsequent iterations of this cycle (three total) demonstrated turnover of NO_2^- to NO via **2** and RSH/ H^+ , generation of **1**^{MeCN}, and lastly reformation of **2** with added NO_2^- . Notably, the Fe-catalyst **2** is recoverable after three cycles in 80% yield.²⁶ Overall, these results provide strong support that **2** is a functional NiR model.

NO formation from Fe- NO_2 complexes occurs through three mechanisms: (i) OAT to an acceptor molecule (E) to produce the $\{\text{FeNO}\}^7$ product and $\text{E}=\text{O}$;^{48,49,51} (ii) H^+ -assisted reduction and heterolysis of the N-O bond through loss of O^{2-} (as H_2O ; μ -oxo bridge when Lewis acid (Cu^{I}) used in place of H^+) and formation of an $\{\text{FeNO}\}^7$ complex (via transient $\{\text{FeNO}\}^6$);²⁸⁻³¹ and (iii) H^+ -assisted reduction and homolysis of the N-O bond to afford Fe(III)-OH and NO.³² Not surprisingly, we can rule out (i), as excess PPh_3 does not react with **2** (vide supra). Pathway (iii) can also be eliminated since this route generally requires an *O*-bound (nitrito) NO_2^- ligand. X-ray crystallographic analysis of **2** under several different growth conditions always resulted in N-bound nitrite ligands. The IR spectrum of **2** is also suggestive of nitro coordination.³⁵ Taken together, (ii) is the most reasonable path.

A probable mechanism emerges and is supported by several lines of evidence (Scheme 3.3). Bulk workup and analysis of the reaction of **2** and RSH/TsOH reveals formation of **1**^{MeCN} (Et_2O -insoluble) and RSSR (Et_2O -soluble) in ~80% yield. Furthermore, trapping of NO from this reaction with Co^{II} -P establishes the stoichiometric release of NO. In the absence of an NO acceptor, mechanism (ii) would suggest an $\{\text{FeNO}\}^7$ (**4** in Scheme 3.3) or $\{\text{Fe}(\text{NO})_2\}^8$

intermediate is likely traversed. Our results support the former. First, the $\{\text{Fe}(\text{NO})_2\}^8$ formulation has only been proposed as a *transient* (low temperature) intermediate in three instances.⁵⁴⁻⁵⁶ Second, attempts at synthesizing this FeNO species by reacting NO with **1** only result in a product with one strong ν_{NO} stretch in the IR ($\sim 1700\text{ cm}^{-1}$),⁵⁷ which is consistent with $\{\text{FeNO}\}^7$ complexes in similar coordination environments.^{58,59} Finally, in situ monitoring of the **2** and RSH/TsOH reaction revealed IR and UV-vis features that resemble independently prepared **4** (Fig. S16). We hypothesized that the Fe-NO bond in **4** would be particularly labile. This logic stems from the decreased basicity of LN_4^{Im} (compared to a previously reported $\{\text{FeNO}\}^7$ complex with pyrrole ligands)^{33,34} making the Fe center less of a π -donor. Also, LN_4^{Im} bears some resemblance, in an electronic sense, to the neutral N4Py ligand (N4Py = *N,N*-bis(2-pyridylmethyl)-(N-(bis-2-pyridylmethyl)amine)) whose corresponding $\{\text{FeNO}\}^7$ complex exhibits a *labile* Fe-NO bond.⁶⁰ The Fe-NO bond lability in **4** is further confirmed in its synthesis as application of vacuum or simple dissolution in donor solvents ultimately yields **1**^S making isolation of analytically pure **4** difficult.

Scheme 3.3. Reaction Path of **2** with RSH/TsOH



3.5 Conclusions

In summary, we report the synthesis and properties of two non-heme Fe(II) complexes with special emphasis on the dinitro complex **2**, which displays stoichiometric and catalytic NiR activity. To our knowledge, **2** represents the first non-heme complex that demonstrates selective turnover of NO_2^- into NO. Additionally, **2** is the first structurally characterized example of a non-heme complex with *trans* coordinated nitro ligands.

3.6 Materials and Methods

3.6.1 General Information

Only information that differs from Chapter 2 General Information section has been included. Potassium nitrite (KNO_2) was procured from Aldrich and dried at 323 K under vacuum for 4 h before use. ^{15}N labeled sodium nitrite ($\text{Na}^{15}\text{NO}_2$) was purchased from Cambridge Isotope Labs and used without further purification. Methanol (MeOH) was dried over 3 Å molecular sieves and degassed by three freeze-pump-thaw cycles. The Et_4N^+ salt of *para*-

chlorobenzenethiol (Et₄NSAr-*p*-Cl) and its corresponding disulfide (*p*-Cl-ArSSAr-*p*-Cl or RSSR) were prepared and checked according to the literature procedure.⁶¹⁻⁶³

3.6.2 Physical Methods

Only information that differs from Chapter 2 Physical Methods section has been included. GC-MS experiments were performed on a Varian 4000 GC/MS/MS. The GC was equipped with a Varian VF-5 capillary column and a TCD detector. Samples were injected as 100 μ L aliquots in splitless mode using a Hamilton gas-tight syringe. The following oven temperature profile was used with He carrier gas: T was raised from 50 to 155 °C at a rate of 10 °C/min followed by a ramp to 260 °C at a rate of 30 °C/min. Elemental microanalyses for C, H, and N were performed by QTI-Intertek (Whitehouse, NJ).

3.6.3 Synthesis of Compounds

(1E,1'E)-N,N'-(propane-1,3-diyl)bis(1-(1-methyl-1H-imidazol-2-yl)methanimine) (LN₄^{Im})

To a 6 mL MeCN solution containing 1-methyl-2-imidazole carboxaldehyde (1.000 g, 9.082 mmol) was added a colorless 5 mL MeCN solution of 1,3-diaminopropane (0.3365 g, 4.540 mmol) affording a pale yellow solution. This mixture was sealed with a septum and stirred at 50 °C for 8 h resulting in no further change. This solution was then diluted with 20 mL of MeCN, dried with anhydrous MgSO₄, filtered, and the filtrate was concentrated under reduced pressure at 70 °C for 4 h. This workup afforded the product as a light-brown oil (1.102 g, 4.266 mmol, 94%). ¹H NMR (400 MHz, CDCl₃, δ from TMS): 8.35 (s, 2H, CH=N), 7.11 (s, 2H, ImH), 6.93 (s, 2H, ImH), 4.00 (s, 6H, N-CH₃), 3.70 (t, 4H, NCH₂CH₂CH₂N), 2.04 (p, 2H, NCH₂CH₂CH₂N). ¹³C NMR (100.6 MHz, CDCl₃, δ from solvent): 153.43 (CH=N), 143.23 (ImC), 129.14 (ImC), 124.75 (ImC), 59.46 (NCH₂CH₂CH₂N), 35.35 (NCH₃), 32.38

(NCH₂CH₂CH₂N). A peak at 38 ppm that we have not identified consistently appears in the ¹³C NMR of all preparations of this ligand. This minor impurity has not affected the synthesis of the corresponding Fe(II) complexes (vide infra). FTIR (ATR), ν_{max} (cm⁻¹): 3102 (w), 2941 (m), 2864 (m), 2838 (m), 1680 (m), 1647 (vs, $\nu_{\text{C=N}}$), 1518 (w), 1475 (s), 1435 (s), 1413 (m), 1367 (m), 1318 (w), 1286 (m), 1228 (w), 1206 (w), 1148 (m), 1110 (w), 1082 (m), 1056 (m), 1021 (w), 965 (w), 920 (m), 755 (s), 732 (m), 707 (m), 689 (m), 663 (w), 628 (w), 616 (w), 567 (w), 522 (w), 511 (w), 452 (w). LRMS-ESI (m/z): [M + H]⁺ calcd for C₁₃H₁₉N₆ (relative abundance), 259.2 (100), 260.2 (16.5), 261.2 (1.3); found, 259.2 (100), 260.2 (16.7), 261.2 (1.4).

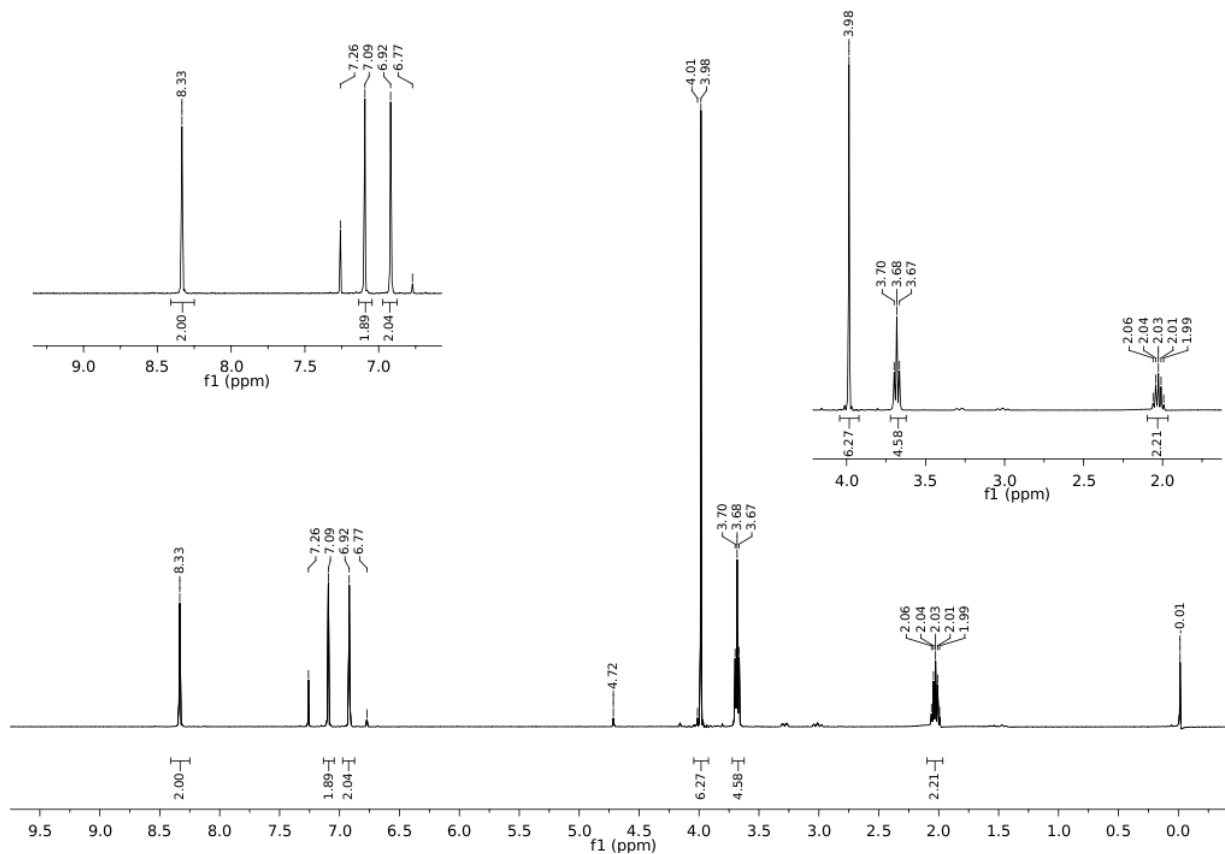


Figure 3.2. ¹H NMR of LN₄^{Im}, CDCl₃, TMS, RT.

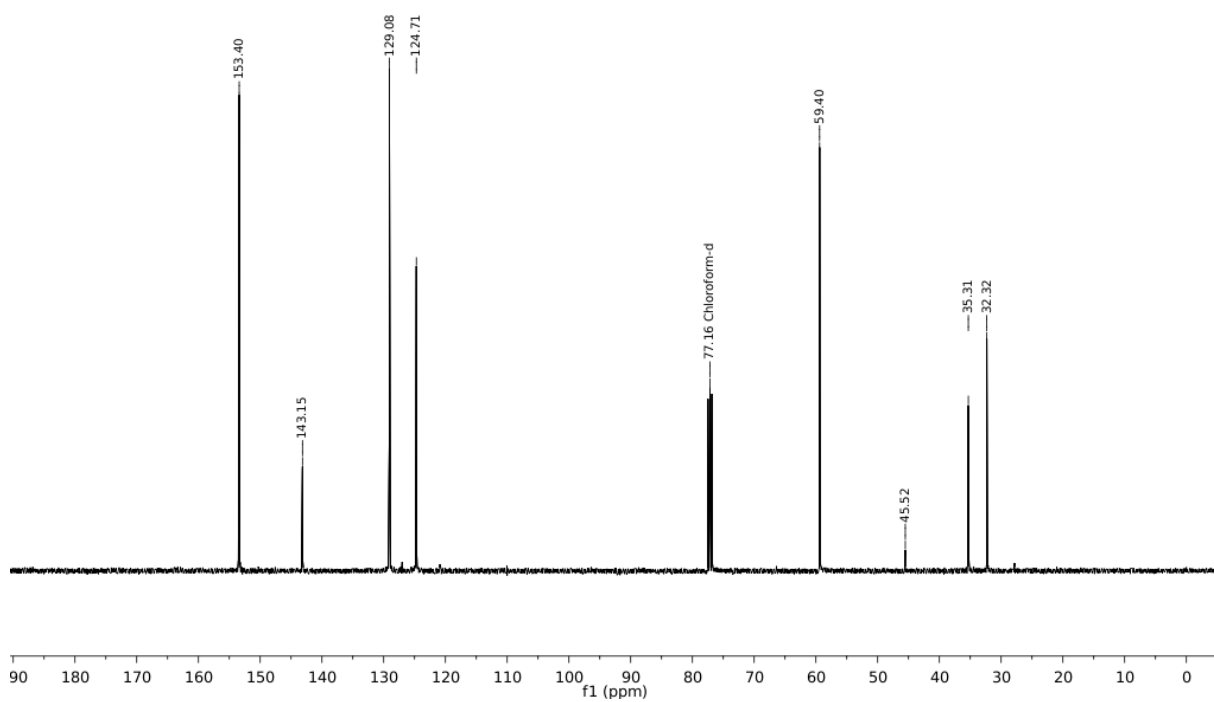


Figure 3.3. ^{13}C NMR of LN_4^{Im} , CDCl_3 , RT.

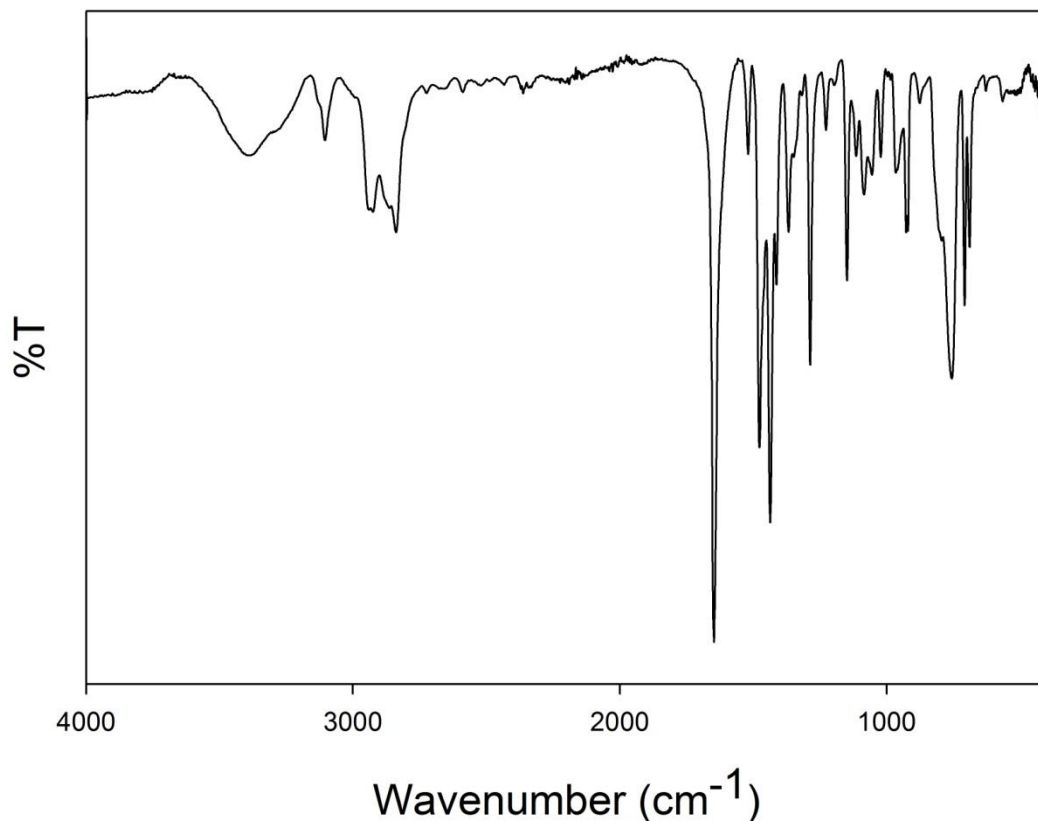
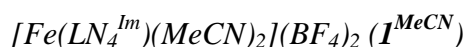


Figure 3.4. FTIR (KBr) of LN_4^{Im} .



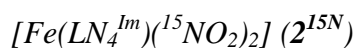
To a 4 mL MeCN solution containing 0.2500 g (0.9678 mmol) of LN_4^{Im} was added a 2 mL MeCN solution containing 0.3267 g (0.9679 mmol) of $[\text{Fe}(\text{H}_2\text{O})_6](\text{BF}_4)_2$. Upon mixing, the color instantly changed from pale-yellow to dark-red indicative of complex formation. The homogeneous solution was stirred an additional 1 h at RT with no further changes. The solvent was then removed from the flask under reduced pressure to afford the dark-red solid product (0.5051 g, 0.8863 mmol, 92%). Diffraction quality crystals were grown from diffusion of Et_2O into an MeCN solution of $\mathbf{1}^{\text{MeCN}}$ at $-25\text{ }^\circ\text{C}$. FTIR (KBr pellet), ν_{max} (cm^{-1}): 3470 (m), 3269 (w), 3208 (w), 3155 (w), 3012 (w), 2947 (w), 2876 (w), 2313 (m, $\nu_{\text{C}\equiv\text{N}}$), 2284 (m, $\nu_{\text{C}\equiv\text{N}}$), 1660 (m),

1628 (m), 1542 (w), 1496 (s), 1455 (s), 1427 (s), 1374 (m), 1346 (w), 1292 (m), 1065 (vs, ν_{BF}), 878 (w), 843 (w), 780 (m), 765 (m), 711 (w), 666 (w), 625 (w), 579 (w), 521 (m). UV-vis (MeCN, 298 K), λ_{max} , nm (ϵ , $\text{M}^{-1} \text{cm}^{-1}$): 478 (3,300); 456 (2,700). LRMS-ESI (m/z): $[\text{M} - 2 \text{MeCN} - 2 \text{BF}_4]^{2+}$ calcd for $\text{C}_{13}\text{H}_{18}\text{FeN}_6$ (relative abundance), 157.1 (100), 157.6 (18.8), 156.1 (6.4); found, 157.0 (100), 157.5 (15.7), 156.0 (6.5). μ_{eff} (solid-state, 298 K) 0 BM (negative R reading). μ_{eff} (solution, 298 K): 2.60 BM in CD_3CN . Non-zero μ_{eff} values have been observed with other low-spin Fe(II) complexes, which have been attributed to trace Fe impurities and/or a thermally-accessible singlet-to-triplet transition.⁶⁴⁻⁶⁶ Anal. Calcd for $\text{C}_{17}\text{H}_{24}\text{B}_2\text{F}_8\text{FeN}_8$: C, 35.83; H, 4.25; N, 19.66. Found: C, 35.71; H, 4.18; N, 19.73.

[Fe(LN₄^{Im})(NO₂)₂] (2)

To a deep-red DMF solution (5 mL) containing 0.3000 g (0.5264 mmol) of **1**^{MeCN} was added a homogeneous DMF solution (1 mL) containing 0.0986 g (1.16 mmol) of KNO_2 and 0.3200 g (1.211 mmol) of 18-Crown-6 (18C6). Immediately upon addition of the KNO_2 /18C6 solution, the deep-red color instantly turned dark-purple with the concomitant precipitation of a similar colored solid. This mixture was stirred for an additional 2 h at RT with no further changes. At this point the mixture was placed in a $-25\text{ }^\circ\text{C}$ freezer to facilitate precipitation. After 2 h at $-25\text{ }^\circ\text{C}$, the solution was filtered and washed with 3×5 mL of Et_2O to yield the dark-purple solid product (0.1818 g, 0.4476 mmol, 85%). FTIR (KBr pellet), ν_{max} (cm^{-1}): 3435 (w), 3133 (w), 3115 (w), 2993 (w), 2929 (w), 2848 (w), 1666 (vs, ν_{CO} DMF), 1582 (s), 1536 (w), 1489 (w), 1459 (m), 1424 (w), 1389 (w), 1379 (w), 1327 (vs, ν_{NO_2}), 1312 (vs, sh), 1281 (vs, ν_{NO_2}), 1205 (w), 1184 (m), 1113 (w), 1097 (w), 1081 (w), 977 (w), 932 (w), 888 (w), 863 (w), 813 (m, δ_{NO_2}), 759 (w), 713 (w), 665 (m), 622 (w), 599 (w), 506 (w), 464 (w). UV-vis (1 mM KNO_2 /18C6, MeCN, 298 K) λ_{max} , nm (ϵ , $\text{M}^{-1} \text{cm}^{-1}$): 410 (1,200), 540 (4,800), 574 (6,600).

LRMS-ESI (m/z): $[M - \text{NO}_2]^+$ calcd. for $\text{C}_{13}\text{H}_{18}\text{FeN}_7\text{O}_2$ (relative abundance), 360.1 (100.0), 361.1 (19.2), 358.1 (6.4), 362.1 (2.5); found, 360.0 (100.0), 361.0 (19.1), 358.1 (6.8), 362.0 (2.8). LR-MALDI-TOF (m/z): found, 360.3 (100.0), 361.3 (19.5), 358.3 (5.2). μ_{eff} (solid-state, 298 K) 0 BM (negative R reading). μ_{eff} (solution, 298 K): 0.82 BM in $\text{DMSO-}d_6$ with 1 mM $\text{KNO}_2/18\text{C}6$. See above.⁶⁴⁻⁶⁶ Anal. Calcd for $\text{C}_{13}\text{H}_{18}\text{FeN}_8\text{O}_4$: C, 38.44; H, 4.47; N, 27.59. Found: C, 38.83; H, 4.68; N, 26.17. As seen in the IR, this compound contains residual DMF and H_2O even after vacuum drying, which results in the lower than expected percent N.



The isotopically-labeled complex $[\text{Fe}(\text{LN}_4^{\text{Im}})(^{15}\text{NO}_2)_2] (\mathbf{2}^{15\text{N}})$ was prepared analogously to **2** except for using 0.0875 g (0.1535 mmol) of **1**, 0.0226 g (0.3229 mmol) of $\text{Na}^{15}\text{NO}_2$, and 0.0893 g (0.3378 mmol) of 18C6. Yield: 0.0520 g (0.1274 mmol, 83%). FTIR (KBr pellet), ν_{max} of isotope-sensitive peaks (cm^{-1}): 1291 (vs, $\Delta\nu_{\text{NO}_2} = 36 \text{ cm}^{-1}$), 1257 (vs, $\Delta\nu_{\text{NO}_2} = 24 \text{ cm}^{-1}$), 807 (s, $\Delta\delta_{\text{NO}_2} = 6 \text{ cm}^{-1}$).

Attempted Synthesis of $[\text{Fe}(\text{LN}_4^{\text{Im}})(\text{NO})](\text{BF}_4)_2 (\mathbf{4})$

Method A: To a red MeOH solution (5 mL) of **1** (100.0 mg, 0.1755 mmol) was purged $\text{NO}(\text{g})$ (90 s) under anaerobic conditions. This reaction was allowed to stir under NO headspace for 2 h during which time a green colored solution formed. After 2 h, a gas-tight syringe was used to remove a solution aliquot for analysis by solution-phase FTIR. To the bulk solution was added 4 mL of Et_2O by syringe and a green solid was filtered through an air-free frit, washed with Et_2O and flushed with N_2 to dry the solid and avoid loss of coordinated NO to yield 0.173 g of green solid. Percent yield was not calculated since the nature of the green species as being $\{\text{FeNO}\}^7$ is speculative due to the lability of the Fe-NO bond. The isolated green solid slowly

returned to a red color overnight, even under dry, anaerobic conditions. FTIR (MeOH), ν_{NO} (cm^{-1}): 1797 (w), 1704 (vs). FTIR (KBr), ν_{NO} (cm^{-1}): 1840 (w), 1764 (vs). UV-vis (MeOH, 298 K), λ_{max} , nm : 504, 597.

Method B: To a red MeCN solution (6 mL) of **1** (130.0 mg, 0.2281 mmol) was purged NO(g) (90 s) under anaerobic conditions. In situ characterization gave similar results, but clearly a mixture of **1**^{MeCN} and **4** according to UV-vis and IR. FTIR (MeCN), ν_{NO} (cm^{-1}): 1807 (w), 1699 (vs). A total of 0.1010 g (0.1772 mmol, 78% recovery) of **1**^{MeCN} recovered after in situ characterization followed by concentration under vacuum.

*Et₄N[Fe(SAr-*p*-Cl)₂(NO)₂]*

To a 5 mL MeCN solution of (Et₄N)₂[Fe(SAr-*p*-Cl)₄], synthesized according to a literature procedure⁴³ (0.185 g, 0.208 mmol) was purged NO(g) for 90 s. Addition of NO(g) resulted in a distinct darkening of the green heterogeneous solution to a red-purple homogenous solution. The flask was removed of all volatiles and the dark residue was washed with Et₂O to afford 0.0692 g of dark solid (0.130 mmol, 63%). FTIR (KBr pellet), ν_{NO} (cm^{-1}): 1753 (vs), 1702 (vs). UV-vis (MeCN, 298 K) λ_{max} , nm: 378, 471, 798. LRMS-ESI (m/z): [M]⁻ calcd. for C₁₂H₈Cl₂FeN₂O₂S₂ (relative abundance), 401.9 (100.0), 403.9 (72.8), 402.9 (17.7), 405.9 (17.1), 404.9 (12.7); found, 401.8 (100.0), 403.8 (74.1), 402.9 (17.5), 405.8 (16.5), 404.8 (12.3).

3.6.4 Reactivity Studies

*Reaction of 2 with para-chlorobenzenethiol (HSAr-*p*-Cl)*

To a 10 mL anaerobic MeCN solution of **2** (40.0 mg, 0.0985 mmol) was added a 1.0 mL MeCN solution of HSAr-*p*-Cl (57.0 mg, 0.394 mmol). The resulting solution showed no

immediate change. The reaction mixture stirred at RT for 24 h. After 24 h, the red-purple colored solution was concentrated under vacuum and stirred with 10 mL of Et₂O to afford an Et₂O-insoluble dark-red compound (28.0 mg). The Et₂O-soluble material was light-red in color and was taken to dryness and then treated with 10 mL of pentane. A pentane-insoluble dark red material formed that was again treated with Et₂O (5 mL) to afford a red solid (8 mg, compound 3; total of 36.0 mg, 0.0360 mmol, 37%). The pentane-soluble was also taken to dryness resulting in a white solid, which revealed a mixture of the disulfide of HSAr-*p*-Cl and free LN₄^{Im} (49 mg). The products from this reaction were characterized by FTIR, UV-vis, ¹H NMR and ESI-MS.

*Reaction of 2 with TsOH•H₂O/HSAr-*p*-Cl*

To a 15 mL anaerobic MeCN solution of **2** (30.0 mg, 0.0739 mmol) was added an 0.800 mL MeCN solution containing 28.1 mg (0.148 mmol) of TosOH•H₂O and 21.4 mg (0.148 mmol) HSAr-*p*-Cl that were mixed 30 s prior to addition. Immediately upon addition, the reaction turned from dark-purple to a pale-red color. This reaction was stirred for 15 min at RT while the red color became darker. After this time, the volatiles were removed under vacuum to afford a red solid. Subsequent addition of 5 mL of Et₂O and stirring afforded a red solid that was identified to be [Fe(LN₄^{Im})(MeCN)₂](OTs)₂ (tosylate salt of **1**^{MeCN}, 40.0 mg, 0.0542 mmol, 73%). The Et₂O-soluble portion contained the disulfide of HSAr-*p*-Cl (18.0 mg, 0.0627 mmol, 85%). The products from this reaction were characterized by FTIR, UV-vis, ¹H NMR, and ESI-MS.

*In situ formation of [Fe(LN₄^{Im})(NO)](OTs)₂ from **2***

To a purple MeCN solution (7 mL) of **2** (15.0 mg, 0.0369 mmol) was added a 400 μ L MeCN solution containing 14.1 mg (0.074 mmol) of TosOH•H₂O and 10.7 mg (0.0740 mmol) HSAr-*p*-Cl (mixed 30 s prior to addition). This reaction was stirred for 2 h prior to analysis. LRMS-ESI (*m/z*): [{M + H + H₂O + OTs} - 2 X]⁺ calcd. for C₂₀H₂₈FeN₈O₆S (relative abundance), 564.1 (100.0), 565.1 (28.2), 566.1 (9.9); found, 564.1 (100.0), 565.2 (31.4), 566.1 (14.6). FTIR (MeCN), ν_{NO} (cm⁻¹): 1787 (w), 1685 (vs).

*Detection of NO assay with [Co(T(-OMe)PP)] and **2***

A 10 mL, 1 mM stock solution of [Co(T(-OMe)PP)] was prepared in CH₂Cl₂ and placed into a large vial (see Fig. S13). In a smaller vial was prepared a 5 mL MeCN solution of **2** (1.0 mM). The smaller vial was gently placed into the larger vial containing [Co(T(-OMe)PP)], keeping the two solutions separate (see Fig. S13). The entire reaction vessel was sealed with a septum. To the inner vial containing **2** was added a 0.800 mL MeCN solution containing two mol-equivs each of HSAr-*p*-Cl and TosOH•H₂O through the septum. The inner vial was allowed to react for 15 min prior to the addition of two mol-equivs of KNO₂/18C6. The reaction was monitored by UV-vis by removing 0.100 mL aliquots of the [Co(T(-OMe)PP)] outer vial solution and adding 10 μ L to a cuvette containing 3 mL of CH₂Cl₂. The reaction was kept sealed for 24 h prior to workup and analysis by FTIR.

*Assay with [Co(T(-OMe)PP)] and **2**^{15N}*

This reaction was performed under similar as with **2** with the exception of using 5 mL of a 1 mM stock solution of **2**^{15N}.

GC-MS

This reaction was performed in a 10 mL Schlenk flask. To a 10 mL MeCN solution of **2** (20.0 mg, 0.0492 mmol) was added an 0.800 mL aliquot of an MeCN solution containing 18.7 mg (0.0983 mmol) of TosOH•H₂O and 14.2 mg (0.0982 mmol) of HSAr-*p*-Cl that were mixed 30 s prior to addition. The solution was stirred for 5 min before addition of 0.400 mL of a DMF solution containing KNO₂ (8.4 mg, 0.099 mmol) and 18C6 (26.0 mg, 0.0984 mmol). The solution rapidly returned back to its original purple color. At t = 30 min after initiation of the reaction, 100 μL of headspace gas was removed and injected into the GC-MS for analysis. After confirmation of NO in the headspace, the flask was subjected to intermittent vacuum and refilling with N₂. After removal of NO from a previous cycle, GC-MS of the headspace was performed in order to provide a baseline level of an NO free headspace over the reaction mixture. This process was repeated three times over the course of 3 h (Fig. S15). After completion of the three cycles, four equiv of KNO₂ (16.8 mg, 0.198 mmol) and 18C6 (52.0 mg, 0.197 mmol) in 3 mL of DMF were added to the reaction mixture. MeCN was removed to leave DMF and the solution was cooled overnight (-25 °C), filtered and the resulting violet-colored solid was washed with Et₂O and dried to give 16.0 mg of **2** (0.0394 mmol, 80%).

UV-vis Studies

*Reaction of 2 with TsOH•H₂O/HSAr-*p*-Cl (1:1:1)*

A 1 mM stock solution of **2** was prepared by dissolving 4.062 mg (0.01000 mmol) of **2** into 10 mL of MeCN. To a UV-vis cuvette containing 3.00 mL of MeCN was added 0.750 mL of stock **2**; cuvette concentration = 0.200 mM. To the cuvette was then added 0.075 mL of a 9-10 mM stock of both TosOH•H₂O (8.50 mg (0.0447 mmol) in 5 mL of MeCN) and HSAr-*p*-Cl

(7.20 mg (0.0498 mmol) in 5 mL of MeCN). Overall: ~one mol-equiv each with respect to **2**. Reagents were mixed under anaerobic conditions and then monitored by UV-vis at 298 K within 60 s of addition.

Reaction of 2 with TsOH•H₂O/HSAr-p-Cl (1:2:2)

Analogous conditions used in the 1:1:1 study except 0.150 mL each of the TosOH•H₂O and HSAr-p-Cl stock solutions were used. Overall: ~two mol-equivalents each with respect to **2**.

Reaction of 2 with HSAr-p-Cl

Analogous conditions used in the 1:1:1 study except only 0.300 mL of the thiol stock solution was used. Overall: four mol-equivalents with respect to **2**.

Reaction of 2 with PPh₃

A 0.250 mL aliquot from a 1 mM stock solution of **2** was added to a UV-vis cuvette containing 3.00 mL of MeCN; cuvette concentration = 0.077 mM. To this solution was added a 0.250 mL aliquot of a 25 mM stock of PPh₃ in MeCN (32.79 mg (0.1250 mmol) in 5 mL MeCN). Overall: 25 mol-equivalents with respect to **2**. The reaction was monitored for 24 h at 298 K.

Reaction of 2 with Et₄NSAr-p-Cl

A 0.750 mL aliquot from a 1 mM stock solution of **2** was added to a cuvette containing 3.00 mL of MeCN cuvette concentration = 0.200 mM. To this solution was added a 0.075 mL MeCN aliquot (one mol-equiv) of a 10 mM stock of Et₄NSAr-p-Cl (13.7 mg (0.0500 mmol) in 5

mL MeCN). Subsequent additions of 0.075 mL (two total mol-equiv) and 0.600 mL (10 total mol-equiv) were monitored at 298 K.

3.7 Supporting Information

X-ray Crystallographic Data Collection and Structure Solution and Refinement.

Red crystals of $[\text{Fe}(\text{LN}_4^{\text{Im}})(\text{MeCN})_2]\cdot\text{MeCN}$ ($\mathbf{1}^{\text{MeCN}}\cdot\text{MeCN}$) were grown under anaerobic conditions by slow diffusion of Et_2O into an MeCN solution of $\mathbf{1}^{\text{MeCN}}$ at $-25\text{ }^\circ\text{C}$. Purple crystals of $[\text{Fe}(\text{LN}_4^{\text{Im}})(\text{NO}_2)_2]\cdot 0.5\text{PhCN}$ ($\mathbf{2}\cdot 0.5\text{PhCN}$) were grown under anaerobic conditions by slow diffusion of Et_2O into a PhCN solution of $\mathbf{2}$ at $-25\text{ }^\circ\text{C}$. Suitable crystals were mounted on a glass fiber. The X-ray intensity data were measured at 100 K on a Bruker SMART APEX II X-ray diffractometer system with graphite-monochromated Mo $\text{K}\alpha$ radiation ($\lambda = 0.71073\text{ \AA}$) using ω -scan technique controlled by the SMART software package.⁶⁷ The data were collected in 1464 frames with 10 s exposure times. The data were corrected for Lorentz and polarization effects⁶⁸ and integrated with the manufacturer's SAINT software. Absorption corrections were applied with the program SADABS.⁶⁹ Subsequent solution and refinement was performed using the SHELXTL 6.1 solution package operating on a Pentium computer.^{70,71} The structure was solved by direct methods using the SHELXTL 6.1 software package.^{70,71} Non-hydrogen atomic scattering factors were taken from the literature tabulations.⁷² Selected data and refinement parameters for $\mathbf{1}^{\text{MeCN}}$ and $\mathbf{2}$ are summarized in Table S1. Selected bond distances and angles for $\mathbf{1}^{\text{MeCN}}$ and $\mathbf{2}$ are given in Table S2. Perspective views of the complexes were obtained using ORTEP.⁷³ For the cation of $\mathbf{1}^{\text{MeCN}}$, three carbon atoms (C6, C7, C8) were found disordered in two sets. Each of these sets was divided using the PART commands with proper restraints and refined occupancies. The set C6, C7, C8 has 47.82% occupancy, while the set C6', C7', C8' has

52.18% occupancy. In **2**, the atoms from several fragments in the molecule were found disordered in the adjacent positions in two sets of each. Each of these sets was divided using the PART commands with proper restraints and refined occupancies. The disordered atoms are labeled as follows with refined occupancies for each set. For fragment 1: N1, C1, C2, N2, C3, C4, C5 (55.34% occupancy) and N1', C1', C2', N2', C3', C4', C5' (44.66% occupancy). For fragment 2: C6 (50% occupancy) and C6' (50% occupancy). For fragment 3: O1, O2 (50% occupancy) and O1', O2' (50% occupancies).

Table S1. Summary of crystal data and intensity collection and structure refinement parameters for [Fe(LN₄^{Im})(MeCN)₂](BF₄)₂•MeCN (**1**^{MeCN}•MeCN) and [Fe(LN₄^{Im})(NO₂)₂]•PhCN (**2**•PhCN).

Parameters	1 ^{MeCN} •MeCN	2 •PhCN
Formula	C ₁₉ H ₂₇ N ₉ B ₂ F ₈ Fe	C ₂₀ H ₂₃ N ₉ O ₄ Fe
Formula weight	610.97	509.32
Crystal system	Monoclinic	Trigonal
Space group	<i>P2₁/n</i>	<i>P3₂21</i>
Crystal color, habit	Red	Purple
<i>a</i> , Å	10.9135(6)	14.1554(14)
<i>b</i> , Å	21.3956(12)	14.1554(14)
<i>c</i> , Å	11.3491(7)	9.8070(10)
<i>α</i> , deg	90	90
<i>β</i> , deg	98.6690(10)	90
<i>γ</i> , deg	90	120
<i>V</i> , Å ³	2619.7(3)	1701.8(4)
<i>Z</i>	4	3
ρ_{calcd} , g/cm ³	1.549	1.491
<i>T</i> , K	100	100
abs coeff, μ (Mo K α), mm ⁻¹	0.661	0.712
θ limits, deg	2.05 to 30.00	2.660 to 27.472
total no. of data	39771	22766
no. of unique data	7629	2622
no. of parameters	383	234
GOF of F ²	1.034	1.056
<i>R</i> ₁ , ^[a] %	3.31	4.28
<i>wR</i> ₂ , ^[b] %	9.00	10.79
max, min peaks, e/Å ³	0.605, -0.570	0.462, -0.378

$$^a R_1 = \sum |F_o| - |F_c| / \sum |F_o| ; ^b wR_2 = \{\sum [w(F_o^2 - F_c^2)] / \sum [w(F_o^2)]\}^{1/2}$$

Table S2. Selected bond distances (Å) and bond angles (deg) for [Fe(LN₄^{Im})(MeCN)₂](BF₄)₂•MeCN (1^{MeCN}•MeCN) and [Fe(LN₄^{Im})(NO₂)₂]•PhCN (2•PhCN).

1 ^{MeCN} •MeCN		2•PhCN	
Fe1-N7	1.9313(11)	Fe1-N3	1.940(4)
Fe1-N8	1.9390(11)	Fe1-N1	1.931(15)
Fe1-N3	1.9615(11)	Fe1-N1'	2.061(16)
Fe1-N4	1.9619(10)	Fe1-N4	1.964(3)
Fe1-N1	1.9893(10)		
Fe1-N5	1.9943(10)	N4-O1	1.212(6)
		N4-O1'	1.232(7)
N7-Fe1-N8	177.83(4)	N4-O2	1.284(6)
N7-Fe1-N3	89.53(5)	N4-O2'	1.286(7)
N8-Fe1-N3	92.04(5)		
N7-Fe1-N4	88.28(5)	N3-Fe1-N3A	95.8(3)
N8-Fe1-N4	90.08(5)	N3-Fe1-N1	77.5(5)
N3-Fe1-N4	95.19(5)	N3-Fe1-N1A	173.2(5)
N7-Fe1-N1	90.17(4)	N1-Fe1-N1A	109.3(10)
N8-Fe1-N1	91.54(4)	N3-Fe1-N4A	89.98(15)
N3-Fe1-N1	81.72(4)	N1-Fe1-N4A	90.9(11)
N4-Fe1-N1	176.55(4)	N3-Fe1-N4	90.24(15)
N7-Fe1-N5	90.39(4)	N1-Fe1-N4	88.9(11)
N8-Fe1-N5	87.97(4)	N4A-Fe1-N4	179.7(2)
N3-Fe1-N5	177.10(4)	N3A-Fe1-N1'	177.9(5)
N4-Fe1-N5	81.91(4)	N3-Fe1-N1'	86.3(5)
N1-Fe1-N5	101.18(4)	N4-Fe1-N1'	90.0(12)
		N4A-Fe1-N1'	89.7(11)
		N1'A-Fe1-N1'	91.6(10)
		O1-N4-O2	117.7(4)
		O1'-N4-O2'	117.1(5)
		O1-N4-Fe1	122.5(3)
		O1'-N4-Fe1	122.7(4)
		O2-N4-Fe1	119.8(3)
		O2'-N4-Fe1	120.0(4)

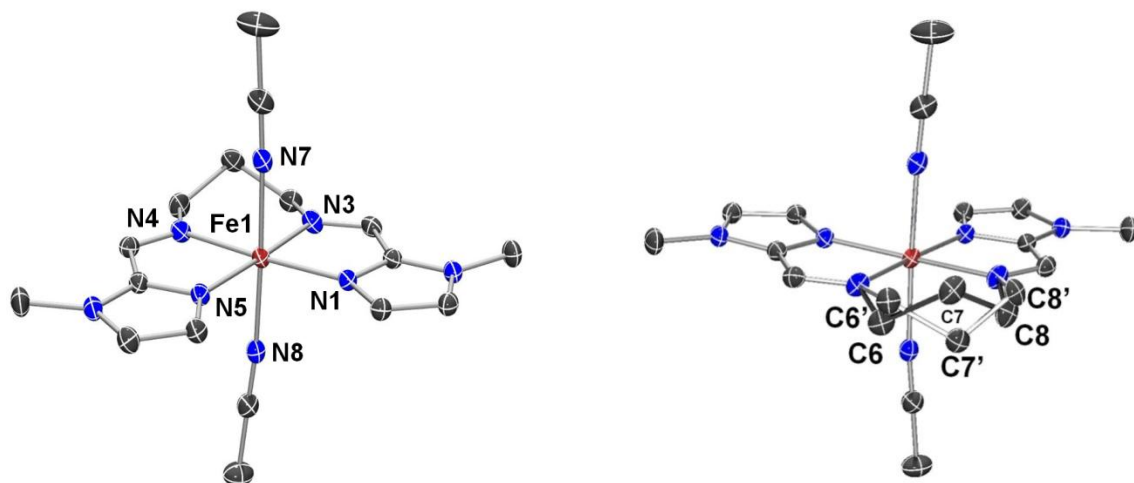


Figure S1. ORTEP of the dication of $[\text{Fe}(\text{LN}_4^{\text{Im}})(\text{MeCN})_2](\text{BF}_4)_2$ (1^{MeCN}) (left) (50% thermal probability for all non-hydrogen atoms). Alternative view showing disorder in the C atoms of the propyl linker (C6, C7, C8) (right). MeCN solvent of crystallization has been omitted for clarity.

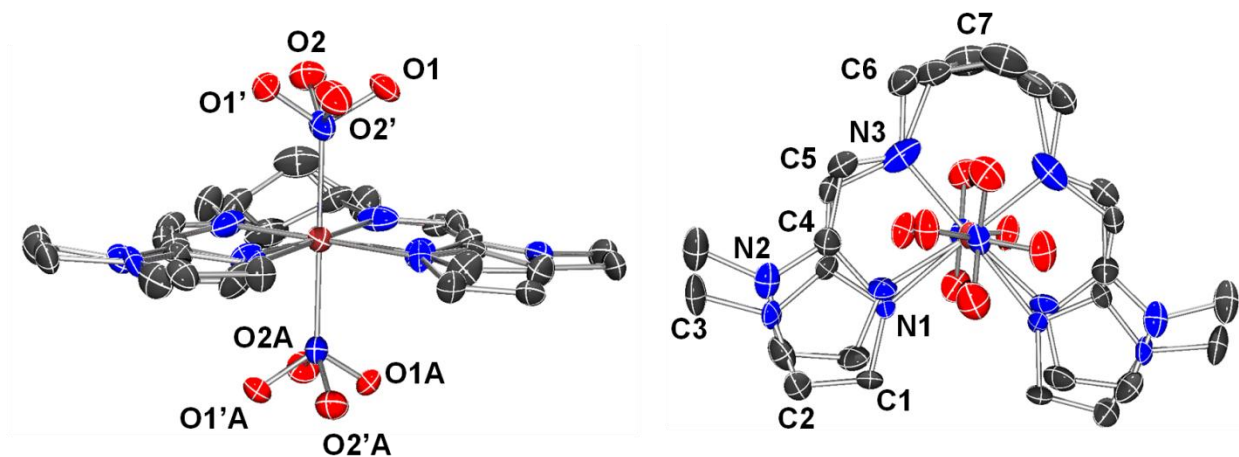


Figure S2. Alternative views of the ORTEP of $[\text{Fe}(\text{LN}_4^{\text{Im}})(\text{NO}_2)_2]$ (2) (50% thermal probability for all non-hydrogen atoms) showing rotational disorder in the N-O bonds of coordinated nitrite (left) and disorder in the imidazole (N1, N2, C1, C2, C3, C4, C5) and propyl chain (C6, C7) (right). PhCN solvent of crystallization has been omitted for clarity.

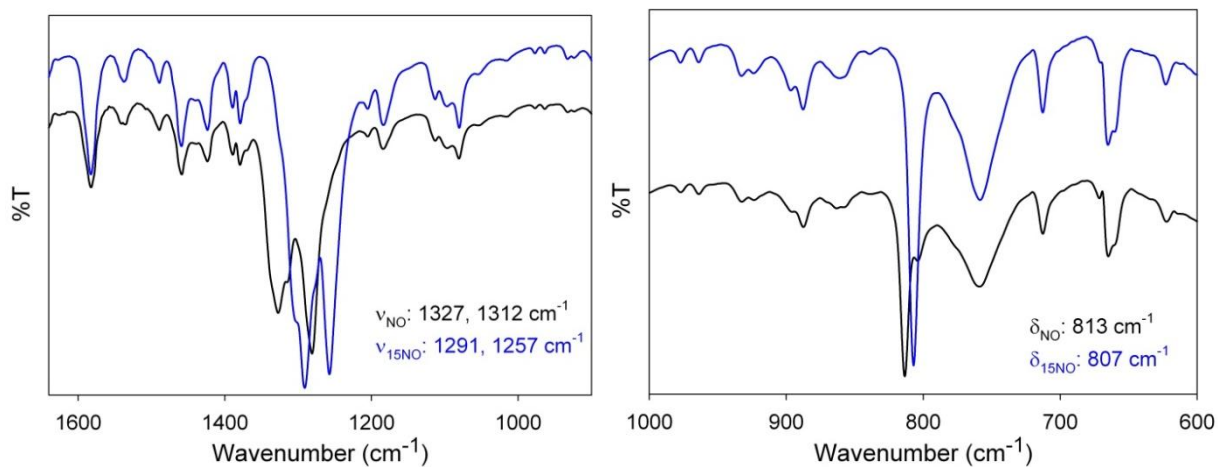


Figure S3. Solid-state FTIR spectra of **2** (black trace) and **2**^{15N} (blue trace) showing isotope-sensitive ν_{NO} (left) and δ_{ONO} (right) peaks (KBr matrix).

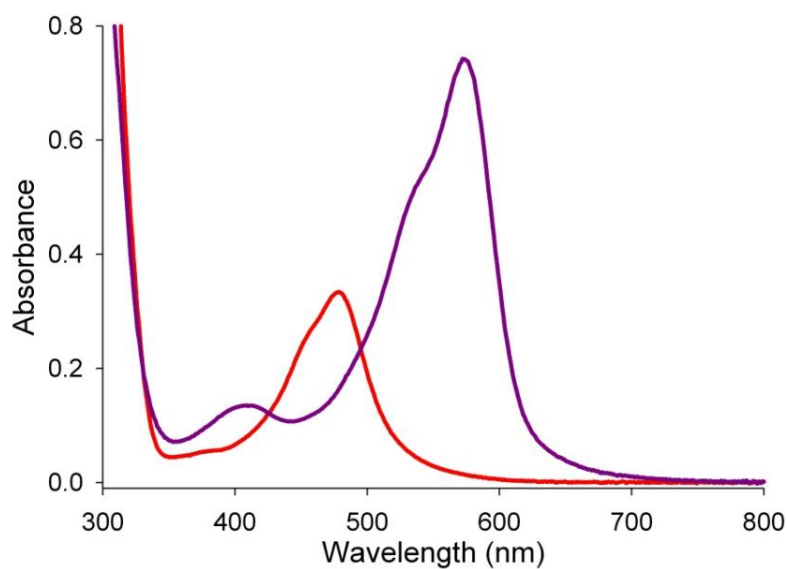


Figure S4. UV-vis spectra of **1**^{MeCN} (red) and **2** (purple) in MeCN at 298 K.

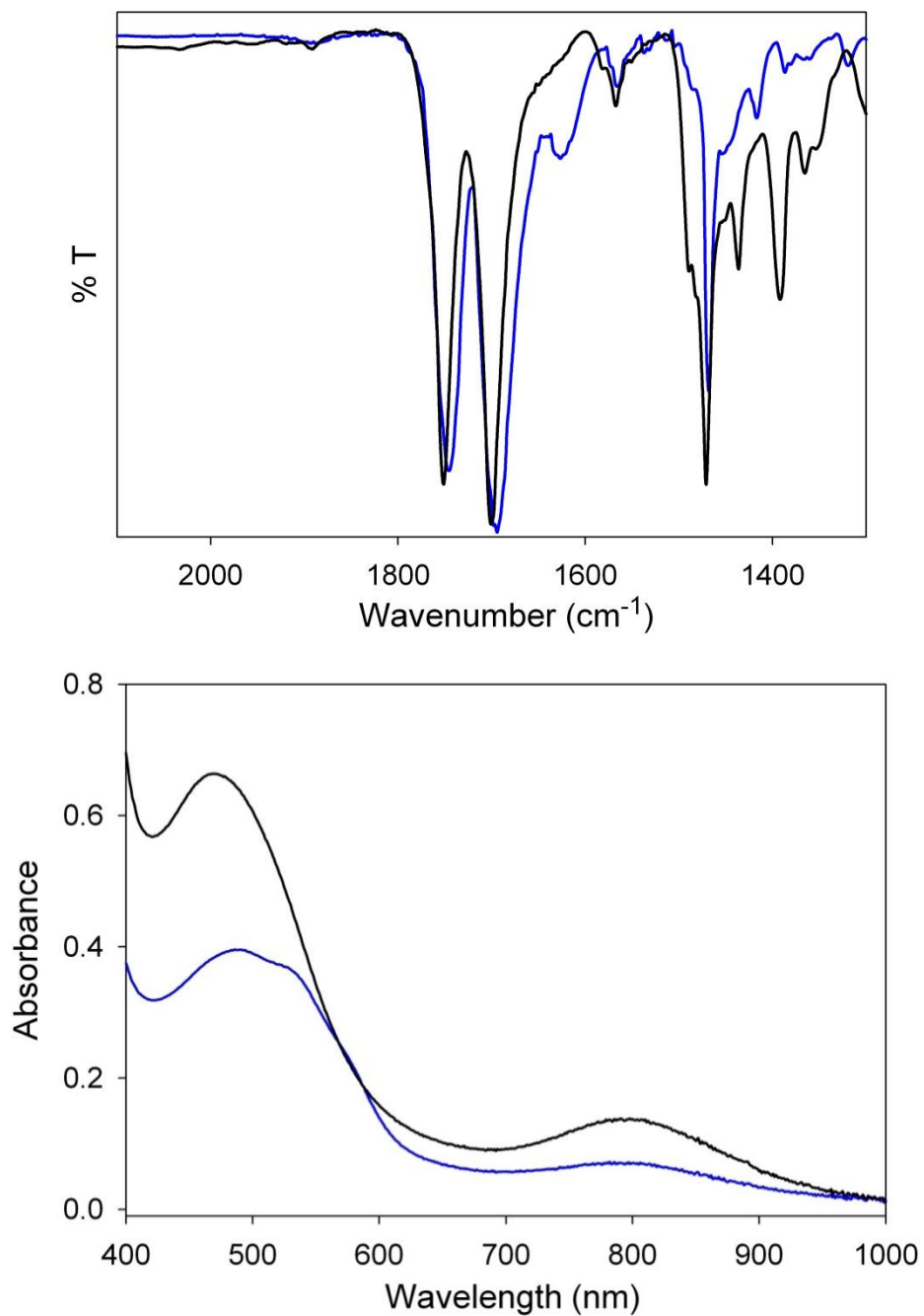


Figure S5. Comparison of DNIC (anion of **3**) formed from bulk reactivity of **2** with *p*-Cl-ArSH (1:4, blue trace) with independently synthesized DNIC (Et₄N)[Fe(SAr-*p*-Cl)₂(NO)₂] (black trace). *Top*: Solid-state FTIR (KBr matrix). *Bottom*: UV-vis in MeCN, 298 K. Shoulder at 530 nm is attributed to the cation of **3**, [Fe(LN₄^{Im})(SR)₂]⁺.

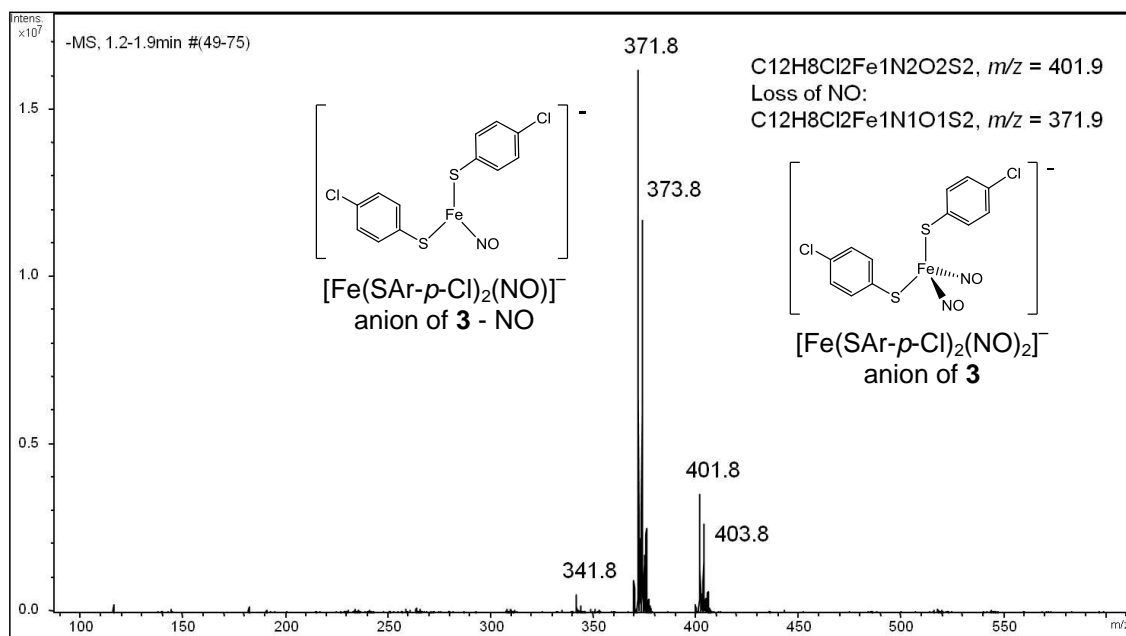


Figure S6. Low-resolution ESI-MS (negative mode) of DNIC from the reaction of p -Cl-ArSH and **2** (4:1; MeCN). Peak at m/z : 401.8 corresponds to anion of **3** $[\text{Fe}(\text{SAr-}p\text{-Cl})_2(\text{NO})_2]^-$. Peak at m/z : 371.8 corresponds to anion of **3-NO** ($[\text{Fe}(\text{SAr-}p\text{-Cl})_2(\text{NO})]^-$).

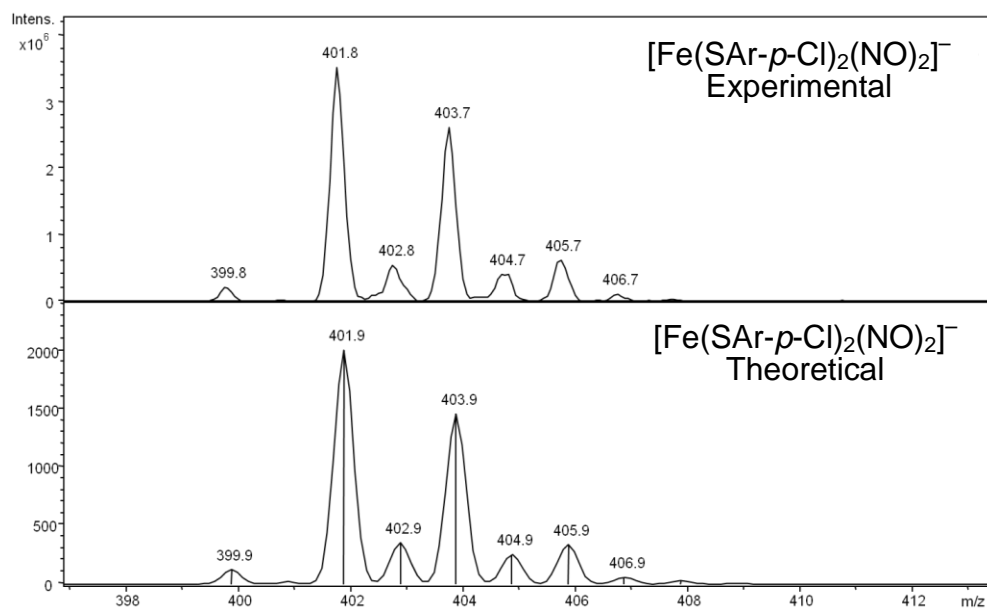


Figure S7. *Top*: Zoom-in of low-resolution ESI-MS (negative mode) peak at m/z : 401.8 from Figure S6. *Bottom*: Theoretical MS for anion of **3**.

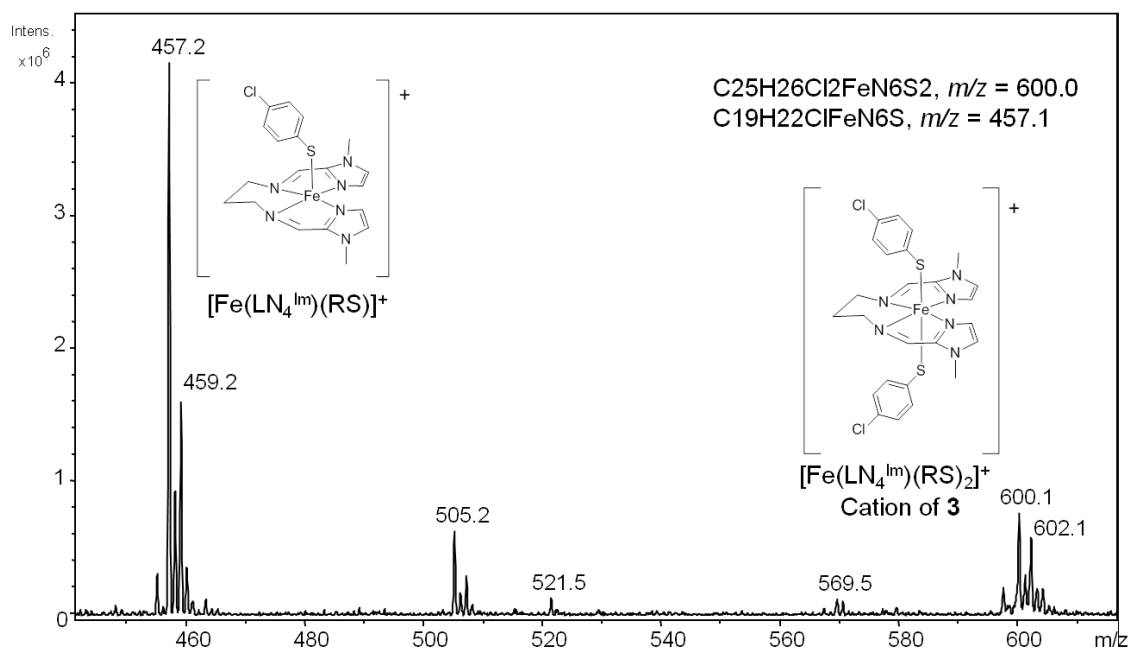


Figure S8. Low-resolution ESI-MS (positive mode) from the reaction of *p*-Cl-ArSH and **2** (4:1; MeCN). Peak at *m/z*: 600.1 corresponds to cation of **3** $[\text{Fe}(\text{LN}_4^{\text{Im}})(\text{SAr-}p\text{-Cl})_2]^+$. Peak at *m/z*: 457.2 corresponds to cation of **3** - SR ($[\text{Fe}(\text{LN}_4^{\text{Im}})(\text{SAr-}p\text{-Cl})]^+$).

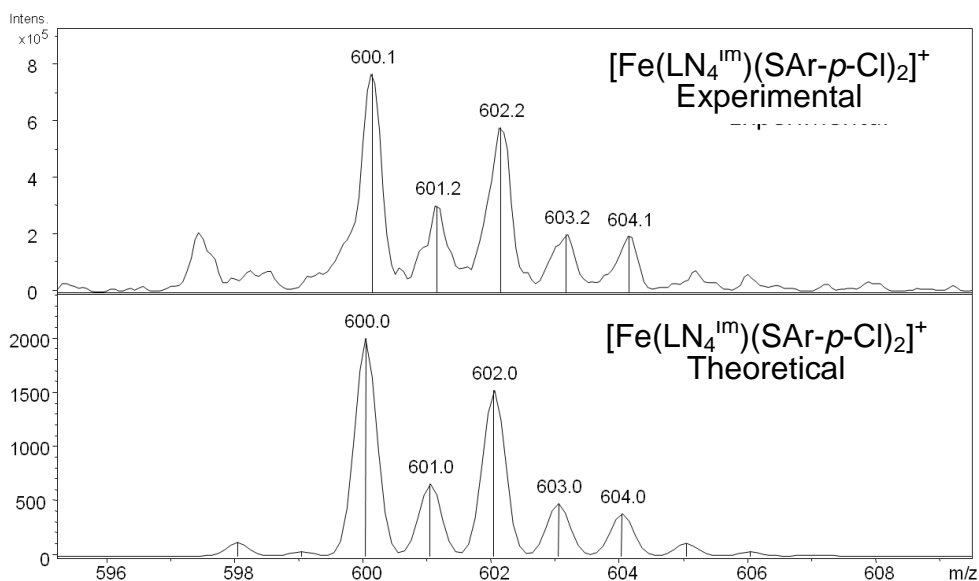


Figure S9. *Top*: Zoom-in of low-resolution ESI-MS (positive mode) peak at *m/z*: 600.1 from Figure S8. *Bottom*: Theoretical MS for cation of **3**.

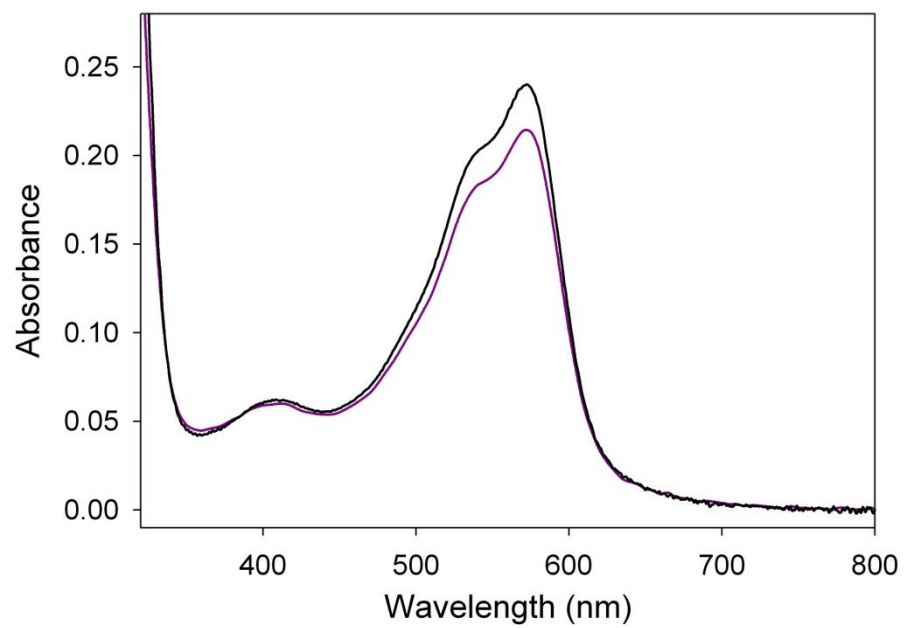


Figure S10. UV-vis spectrum of a 0.031 mM MeCN solution of **2** (black trace) and after 24 h reaction with 25 mol-equiv of PPh₃ (purple trace) at 298 K.

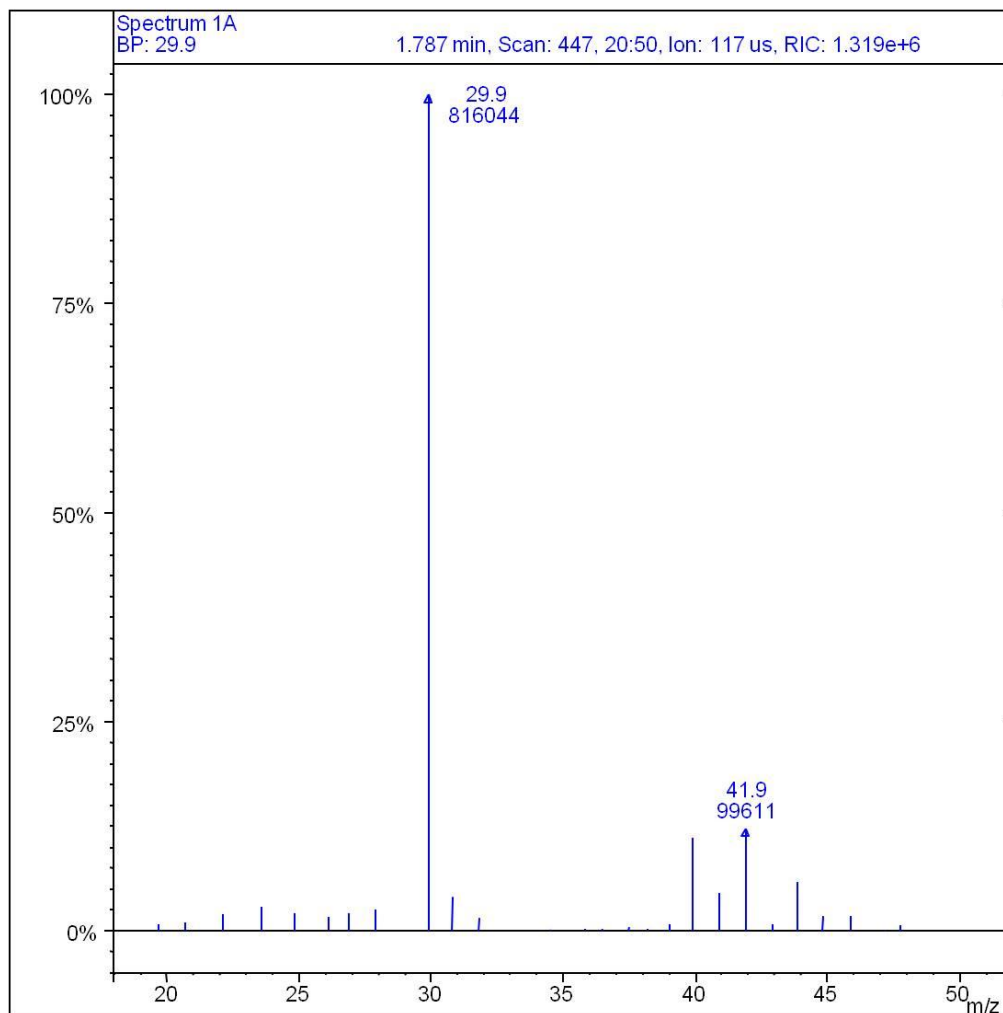
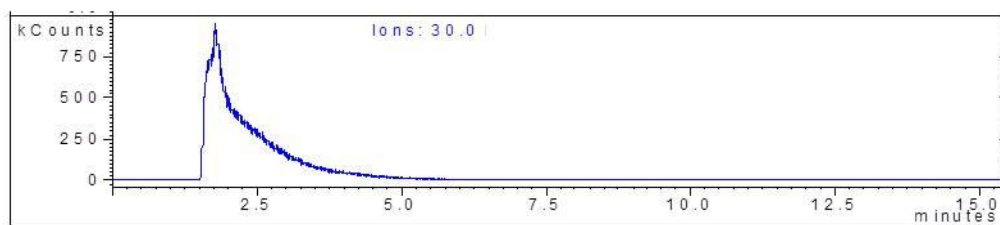


Figure S11. *Top:* GC of the reaction of **2** and *p*-Cl-ArSH/TosOH•H₂O (1:2:2) in MeCN at RT. *Bottom:* EI-MS of *t* = 1.79 min peak for *m/z*: 29.9 corresponding to NO. Peaks clustered at *m/z*: 40 corresponds to MeCN as is observed in blank solvent headspace.

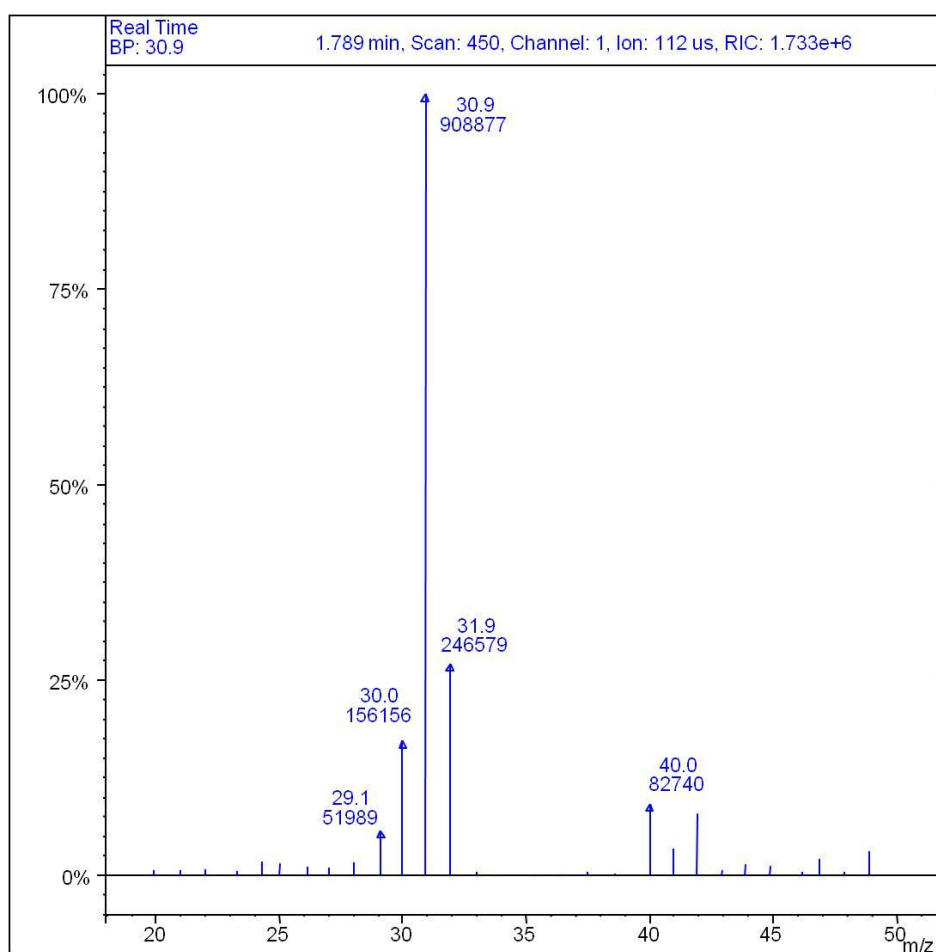
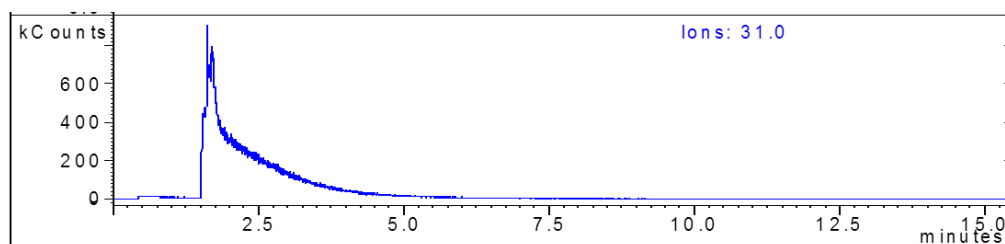


Figure S12. *Top:* GC of the reaction of 2^{15}N and $p\text{-Cl-ArSH/TosOH}\cdot\text{H}_2\text{O}$ (1:2:2) in MeCN at RT. *Bottom:* EI-MS of $t = 1.79$ min peak for m/z : 30.9 corresponding to ^{15}NO . Peaks clustered at m/z : 40 corresponds to MeCN as is observed in blank solvent headspace.

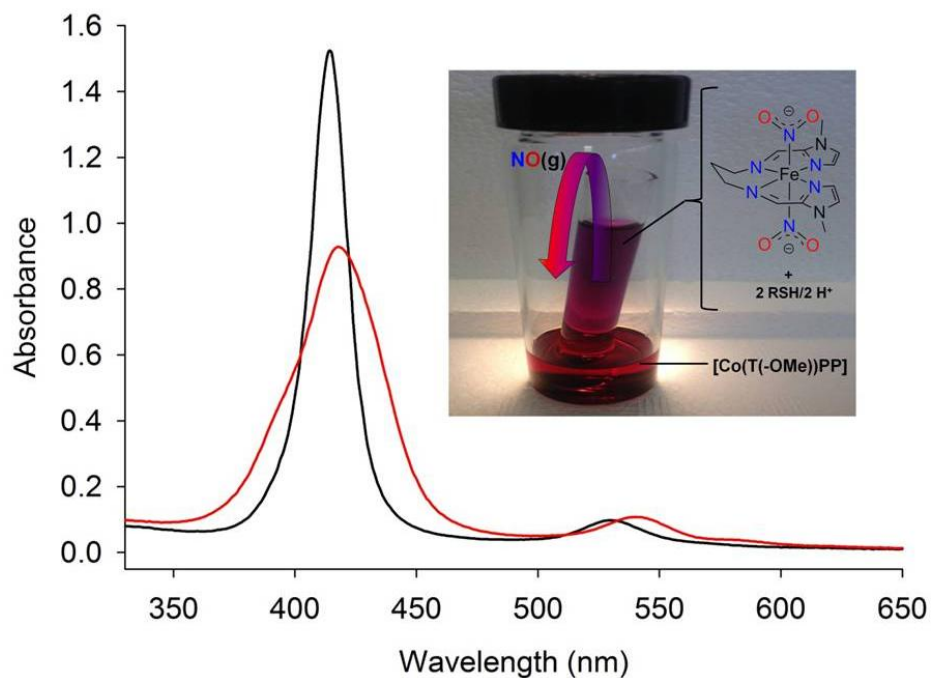


Figure S13. UV-vis of [Co(T(-OMe)PP)] (13 μ M in CH₂Cl₂, 298 K, black trace) and after reacting with NO produced from mixing **2** and *p*-Cl-ArSH/TosOH•H₂O (1:2:2, MeCN, 18 h, inner vial - see inset) to form the {CoNO}⁸ complex [Co(T(-OMe)PP)(NO)] (red trace). *Inset:* Setup of NO trapping experiment.

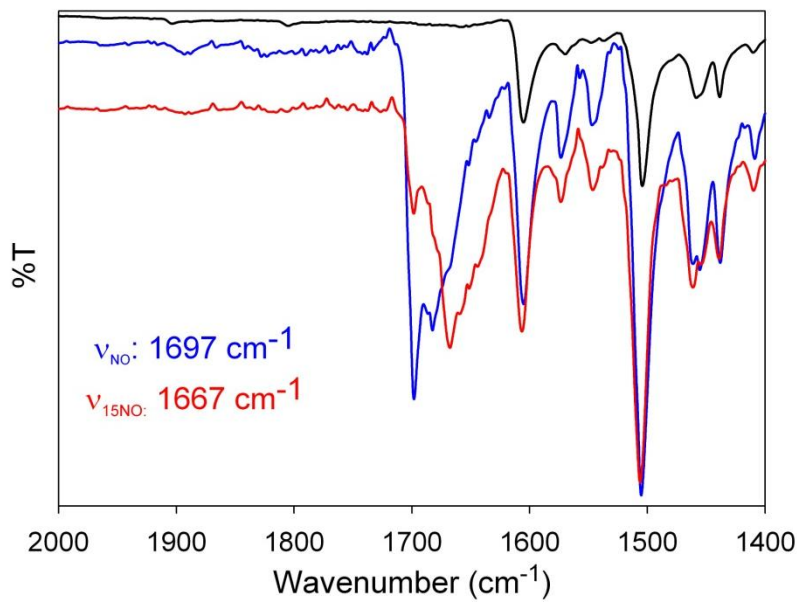


Figure S14. FTIR (KBr matrix) of the reaction from Fig. S13 demonstrating formation of [Co(T(-OMe)PP)(NO)] from reaction of [Co(T(-OMe)PP)] with NO produced from **2** and *p*-Cl-ArSH/TosOH•H₂O (1:2:2). IR of [Co(T(-OMe)PP)] (black trace) and {CoNO}⁸ from using **2** (blue trace) or **2**^{15N} (red trace).

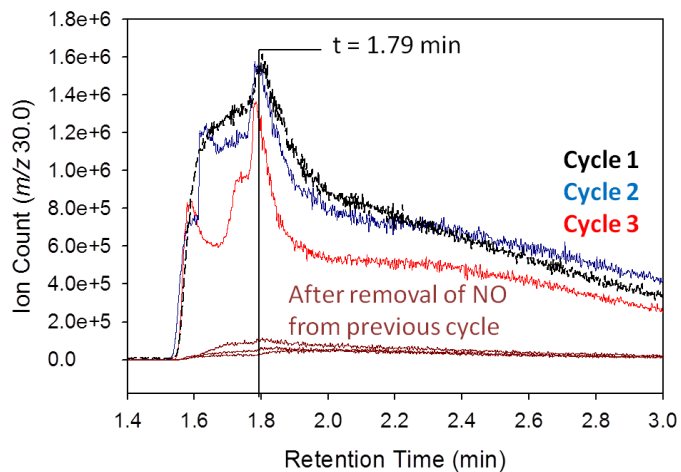


Figure S15. GC headspace analysis of the reaction of **2** and *p*-Cl-ArSH/TosOH•H₂O (1:2:2) in MeCN at RT demonstrating the iterative cycles of NO formation. Dark-red traces indicate NO-free environment after application of vacuum and N₂ purge. First addition (black trace), second addition (blue trace), and third addition (red trace) of *p*-Cl-ArSH/TosOH•H₂O to **2**.

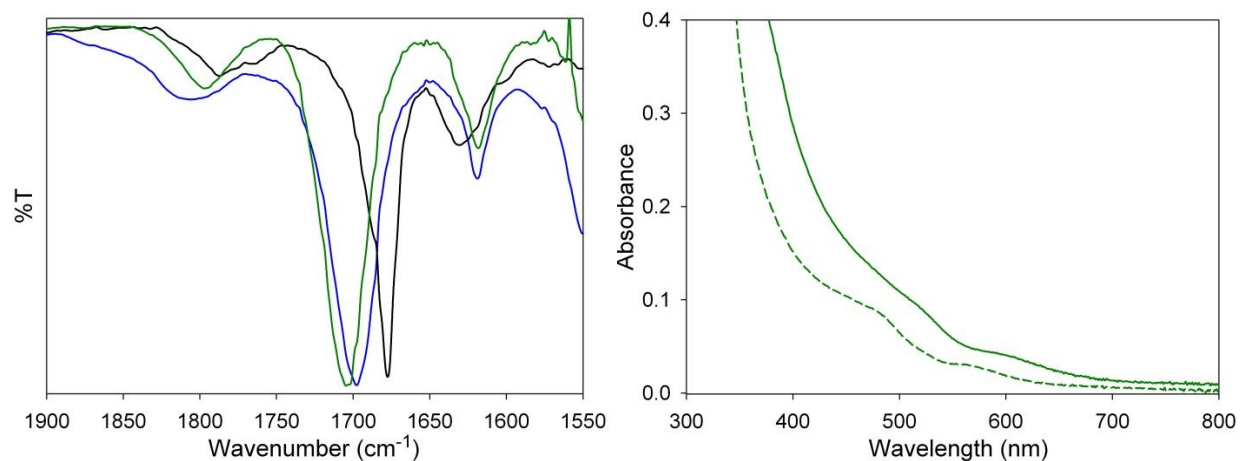


Figure S16. *Left:* FTIR of **4** from purge of NO into MeCN (blue trace) or MeOH (green trace) solutions of **1**. *In situ* FTIR of the MeCN solution of **2** and TsOH•H₂O/HSAr-*p*-Cl (1:2:2) (black trace) after 2 h mixing. *Right:* Qualitative UV-vis of **4** from purge of NO into MeOH solution of **1** (solid trace) and the MeCN solution of **2** and TsOH•H₂O/HSAr-*p*-Cl (1:2:2) after 2 h mixing (dashed trace).

3.8 References

- (1) Ignarro, L. J. *Nitric Oxide Biology and Pathobiology*; Academic Press: San Diego, 2000.
- (2) Moncada, S.; Higgs, E. A. *Br. J. Pharm.* **2006**, *147*, S193.
- (3) Hill, B. G.; Dranka, B. P.; Bailey, S. M.; Lancaster, J. R., Jr.; Darley-Usmar, V. M. *J. Biol. Chem.* **2010**, *285*, 19699.
- (4) van Faassen, E. E.; Bahrami, S.; Feelisch, M.; Hogg, N.; Kelm, M.; Kim-Shapiro, D. B.; Kozlov, A. V.; Li, H.; Lundberg, J. O.; Mason, R.; Nohl, H.; Rassaf, T.; Samouilov, A.; Slama-Schwok, A.; Shiva, S.; Vanin, A. F.; Weitzberg, E.; Zweier, J.; Gladwin, M. T. *Med. Res. Rev.* **2009**, *29*, 683.
- (5) Lundberg, J. O.; Weitzberg, E.; Gladwin, M. T. *Nat. Rev. Drug. Discov.* **2008**, *7*, 156.
- (6) Maia, L. B.; Moura, J. J. G. *Chem. Rev.* **2014**, *114*, 5273..
- (7) Gladwin, M. T.; Grubina, R.; Doyle, M. P. *Acc. Chem. Res.* **2009**, *42*, 157.
- (8) Ormerod, J. O. M.; Ashrafian, H.; Maher, A. R.; Arif, S.; Steeples, V.; Born, G. V. R.; Egginton, S.; Feelisch, M.; Watkins, H.; Frenneaux, M. P. *Cardiovasc. Res.* **2011**, *89*, 560.
- (9) Fukuto, J. M.; Cisneros, C. J.; Kinkade, R. L. *J. Inorg. Biochem.* **2013**, *118*, 201.
- (10) Sanders, B.C.; Rhine, M. A.; Harrop, T. C. *Struct. Bonding (Berlin)* **2014**, *160*, 57.
- (11) Wang, R. *Physiol. Rev.* **2012**, *92*, 791.
- (12) Kabil, O.; Banerjee, R. *J. Biol. Chem.* **2010**, *285*, 21903.
- (13) WHO Background document for development of WHO Guidelines for Drinking-water Quality **2011**, WHO/SDE/WSH/07.01/16/Rev/1.
- (14) Grant, S. B.; Saphores, J.-D.; Feldman, D. L.; Hamilton, A. J.; Fletcher, T. D.; Cook, P. L. M.; Stewardson, M.; Sanders, B. F.; Levin, L. A.; Ambrose, R. F.; Deletic, A.; Brown, R.; Jiang, S. C.; Rosso, D.; Cooper, W. J.; Marusic, I. *Science* **2012**, *337*, 681.
- (15) Dezfulian, C.; Raat, N.; Shiva, S.; Gladwin, M. T. *Cardiovasc. Res.* **2007**, *75*, 327.

- (16) Pattillo, C. B.; Bir, S.; Rajaram, V.; Kevil, C. G. *Cardiovasc. Res.* **2011**, *89*, 533.
- (17) Duranski, M. R.; Greer, J. J. M.; Dejam, A.; Jaganmohan, S.; Hogg, N.; Langston, W.; Patel, R. P.; Yet, S.-F.; Wang, X.; Kevil, C. G.; Gladwin, M. T.; Lefer, D. J. *J. Clin. Invest.* **2005**, *115*, 1232.
- (18) Tolman, W. B. *J. Biol. Inorg. Chem.* **2006**, *11*, 261.
- (19) Wasser, I. M.; de Vries, S.; Moënné-Loccoz, P.; Schröder, I.; Karlin, K. D. *Chem. Rev.* **2002**, *102*, 1201.
- (20) Woollard-Shore, J. G.; Holland, J. P.; Jones, M. W.; Dilworth, J. R. *Dalton Trans.* **2010**, *39*, 1576.
- (21) Chen, C. S.; Yeh, W. Y. *Chem. Commun.* **2010**, *46*, 3098.
- (22) Chuang, W.-J.; Lin, I.-J.; Chen, H.-Y.; Chang, Y.-L.; Hsu, S. C. N. *Inorg. Chem.* **2010**, *49*, 5377.
- (23) Kujime, M.; Izumi, C.; Tomura, M.; Hada, M.; Fujii, H. *J. Am. Chem. Soc.* **2008**, *130*, 6088.
- (24) Kumar, M.; Dixon, N. A.; Merkle, A. C.; Zeller, M.; Lehnert, N.; Papish, E. T. *Inorg. Chem.* **2012**, *51*, 7004.
- (25) Maji, R. C.; Barman, S. K.; Roy, S.; Chatterjee, S. K.; Bowles, F. L.; Olmstead, M. M.; Patra, A. K. *Inorg. Chem.* **2013**, *52*, 11084.
- (26) Halfen, J. A.; Tolman, W. B. *J. Am. Chem. Soc.* **1994**, *116*, 5475.
- (27) Halfen, J. A.; Mahapatra, S.; Wilkinson, E. C.; Gengenbach, A. J.; Young, V. G. J.; Que, L. J.; Tolman, W. B. *J. Am. Chem. Soc.* **1996**, *118*, 763.
- (28) Ching, W.-M.; Chuang, C.-H.; Wu, C.-W.; Peng, C.-H.; Hung, C.-H. *J. Am. Chem. Soc.* **2009**, *131*, 7952.
- (29) Harris, T. D.; Betley, T. A. *J. Am. Chem. Soc.* **2011**, *133*, 13852.
- (30) López, J. P.; Heinemann, F. W.; Prakash, R.; Hess, B. A.; Horner, O.; Jeandey, C.; Oddou, J.-L.; Latour, J.-M.; Grohmann, A. *Chem-Eur J* **2002**, *8*, 5709.
- (31) Villar-Acevedo, G.; Nam, E.; Fitch, S.; Benedict, J.; Freudenthal, J.; Kaminsky, W.; Kovacs, J. A. *J. Am. Chem. Soc.* **2011**, *133*, 1419.
- (32) Tsou, C.-C.; Yang, W.-L.; Liaw, W.-F. *J. Am. Chem. Soc.* **2013**, *135*, 18758.

- (33) Patra, A. K.; Dube, K. S.; Sanders, B. C.; Papaefthymiou, G. C.; Conradie, J.; Ghosh, A.; Harrop, T. C. *Chem. Sci.* **2012**, *3*, 364.
- (34) Sanders, B. C.; Patra, A. K.; Harrop, T. C. *J. Inorg. Biochem.* **2013**, *118*, 115.
- (35) Nakamoto, K. *Infrared and Raman Spectra of Inorganic and Coordination Compounds.*; John Wiley & Sons, Ltd., 1978.
- (36) Nasri, H.; Wang, Y.; Huynh, B. H.; Scheidt, W. R. *J. Am. Chem. Soc.* **1991**, *113*, 717.
- (37) Einsle, O.; Messerschmidt, A.; Huber, R.; Kroneck, P. M. H.; Neese, F. *J. Am. Chem. Soc.* **2002**, *124*, 11737.
- (38) Nasri, H.; Ellison, M. K.; Krebs, C.; Huynh, B. H.; Scheidt, W. R. *J. Am. Chem. Soc.* **2000**, *122*, 10795.
- (39) Optimal π -overlap between Fe and NO_2^- results when the two O-N-O planes are orthogonal to each other to interact separately with the d_{xz} and d_{yz} orbitals. The rotational disorder of the NO_2^- ligands in **2** makes it impossible to comment on such an orientation.
- (40) Nasri, H.; Goodwin, J. A.; Scheidt, W. R. *Inorg. Chem.* **1990**, *29*, 185.
- (41) Bordwell, F. G.; Hughes, D. L. *J. Org. Chem.* **1982**, *47*, 3224.
- (42) Hung, M.-C.; Tsai, M.-C.; Lee, G.-H.; Liaw, W.-F. *Inorg. Chem.* **2006**, *45*, 6041.
- (43) Harrop, T. C.; Tonzetich, Z. J.; Reisner, E.; Lippard, S. J. *J. Am. Chem. Soc.* **2008**, *130*, 15602.
- (44) Tsai, F.-T.; Kuo, T.-S.; Liaw, W.-F. *J. Am. Chem. Soc.* **2009**, *131*, 3426.
- (45) Fitzpatrick, J.; Kalyvas, H.; Filipovic, M. R.; Ivanović-Burmazović, I.; MacDonald, J. C.; Shearer, J.; Kim, E. *J. Am. Chem. Soc.* **2014**, *136*, 7229.
- (46) Woolum, J. C.; Commoner, B. *Biochim. Biophys. Acta* **1970**, *201*, 131.
- (47) The H^+ -assisted reaction of free NO_2^- with RSH yields the corresponding S-nitrosothiol (RSNO, see Koppenol, W. H. *Inorg. Chem.* **2011**, *51*, 5637), which is a potential source of NO. Mixing **2** with Ph_3CSNO (1:2) in MeCN for 18 h resulted in no DNIC.
- (48) Heinecke, J.; Ford, P. C. *J. Am. Chem. Soc.* **2010**, *132*, 9240.

- (49) Heinecke, J. L.; Khin, C.; Pereira, J. C. M.; Suárez, S. A.; Iretskii, A. V.; Doctorovich, F.; Ford, P. C. *J. Am. Chem. Soc.* **2013**, *135*, 4007.
- (50) Nasri, H.; Haller, K. J.; Wang, Y.; Huynh, B. H.; Scheidt, W. R. *Inorg. Chem.* **1992**, *31*, 3459.
- (51) Patra, A. K.; Afshar, R. K.; Rowland, J. M.; Olmstead, M. M.; Mascharak, P. K. *Angew. Chem. Int. Ed.* **2003**, *42*, 4517.
- (52) Kütt, A.; Leito, I.; Kaljurand, I.; Sooväli, L.; Vlasov, V. M.; Yagupolskii, L. M.; Koppel, I. A. *J. Org. Chem.* **2006**, *71*, 2829.
- (53) Trace amounts of the dinuclear species, $[\text{Fe}_2(\mu\text{-SR})_2(\text{NO})_4]$ = Roussin's red ester, are observed in the IR and likely accounts for the less than stoichiometric recovery of **2**.
- (54) Patterson, J. C.; Lorković, I. M.; Ford, P. C. *Inorg. Chem.* **2003**, *42*, 4902.
- (55) Wang, J.; Schopfer, M. P.; Sarjeant, A. A. N.; Karlin, K. D. *J. Am. Chem. Soc.* **2009**, *131*, 450.
- (56) Lorković, I.; Ford, P. C. *J. Am. Chem. Soc.* **2000**, *122*, 6516.
- (57) Weak ν_{NO} signals at $\sim 1800\text{ cm}^{-1}$ are observed in attempted preparations of **4**. While this may be assigned to an $\{\text{Fe}(\text{NO})_2\}^8$ complex, its low intensity with respect to the strong peak at $\sim 1700\text{ cm}^{-1}$ leads us to think otherwise. It is possible that a mixture of five- and six-coordinate $\{\text{FeNO}\}^7$ is present, which have very different ν_{NO} values (see Lehnert or ref 59).
- (58) McCleverty, J. A. *Chem. Rev.* **2004**, *104*, 403.
- (59) Goodrich, L. E.; Paulat, F.; Praneeth, V. K. K.; Lehnert, N. *Inorg. Chem.* **2010**, *49*, 6293.
- (60) McQuilken, A. C.; Ha, Y.; Sutherlin, K. D.; Siegler, M. A.; Hodgson, K. O.; Hedman, B.; Solomon, E. I.; Jameson, G. N. L.; Goldberg, D. P. *J. Am. Chem. Soc.* **2013**, *135*, 14024.
- (61) Palermo, R. E.; Power, P. P.; Holm, R. H. *Inorg. Chem.* **1982**, *21*, 173.
- (62) Rosenfield, S. G.; Armstrong, W. H.; Mascharak, P. K. *Inorg. Chem.* **1986**, *25*, 3014.
- (63) Harrop, T. C.; Olmstead, M. M.; Mascharak, P. K. *Inorg. Chim. Acta.* **2002**, *338*, 189.

- (64) Holm, R. H.; Pinolet, L. H.; Lewis, R. A. *J. Am. Chem. Soc.* **1971**, *93*, 360.
- (65) Wieghardt, K.; Kueppers, H. J.; Weiss, J. *Inorg. Chem.* **1985**, *24*, 3067.
- (66) Widger, L. R.; Davies, C. G.; Yang, T.; Siegler, M. A.; Troeppner, O.; Jameson, G. N. L.; Ivanović-Burmazović, I.; Goldberg, D. P. *J. Am. Chem. Soc.* **2014**, *136*, 2699.
- (67) SMART v5.626: Software for the CCD Detector System; Bruker AXS: Madison WI, **2000**.
- (68) Walker, N.; Stuart, D. *Acta Crystallogr. A.* **1983**, *39*, 158.
- (69) Sheldrick, G. M. *SADABS, Area Detector Absorption Correction, University of Göttingen, Göttingen, Germany*, **2001**.
- (70) Sheldrick, G. M. *SHELX-97, Program for Refinement of Crystal Structures, University of Göttingen, Göttingen, Germany*, **1997**.
- (71) Sheldrick, G. M. *SHELXTL 6.1, Crystallographic Computing System, Siemens Analytical X-Ray Instruments, Madison, WI*, **2000**.
- (72) Cromer, D. T.; Waber, J. T. *International Tables for X-ray Crystallography*; The Kynoch Press: Birmingham, England, 1974; Vol. IV, Table 2.2B.
- (73) Burnett, M. N.; Johnson, C. K. *ORTEP-III, Report ORNL - 6895; Oak Ridge National Laboratory: Oak Ridge, TN*, **1996**.

CHAPTER 4

PROGRESS TOWARDS CONTROLLING SECONDARY-SPHERE INTERACTIONS IN A Fe-(NO₂)₂ COMPLEX

4.1 Abstract

The influence of secondary-sphere interactions in metalloenzymes is of critical importance to the reactivity and selectivity of enzymatic chemical transformations. This holds true for heme-dependent nitrite reductase (NiR) enzymes that can either reduce nitrite (NO₂⁻) to nitric oxide (NO) or much further to ammonium (NH₄⁺). In these enzymes, secondary-sphere residues serve to orient substrate, provide proton equivalents, and dictate the path towards NO or NH₄⁺. Given the importance of the NO₂⁻ to NO transformation within mammalian physiology, we have advanced our previous efforts in the non-heme NiR model complexes to include secondary-sphere modulation. Herein, we report our efforts in designing NiR model complexes [Fe(LN₄^{Im})(MeCN)₂]²⁺ (**1**); [Fe(LN₄^{Im})(NO₂)₂] (**2**); [Fe(LN₄^{Morph})]²⁺ (**3**); [Fe(LN₄^{Morph})(NO₂)₂] (**4**); and [Fe(LN₄)(NO₂)]⁻ (**5**) and discuss the implications of installed secondary-sphere moieties.

4.2 Introduction

The interaction of NO_2^- with Fe is an important feature of the heme-dependent reduction of NO_2^- , a critical reaction with relevance to the global nitrogen cycle, environmental remediation, and cardiovascular maintenance. However, other important interactions that promote catalysis, namely H-bonding and proton delivery, are based in the secondary-coordination sphere of nitrite reductase (NiR) enzymes. The H-bonding network in the NiRs is made up of His, Arg, and Tyr residues, that dictate the course of NO_2^- reduction to either NO, in the case of cytochrome *cd*₁ NiR (*cd*₁NiR), or NH_4^+ with respect to both siroheme-containing NiR (SCNiR) and cytochrome c NiR (*cc*NiR). Non-polar contacts also play relevant roles in the orientation of axial heme ligands. For example, distal Val residues in myoglobin (Mb) direct O_2 , HNO, and NO_2^- when bound to Fe.¹⁻³ Accordingly, the secondary-sphere amino acids in heme-proteins affect the overall charge, sterics, pH, substrate specificity, and substrate binding/activation. For instance, non-dedicated proteins that exhibit NiR activity such as hemoglobin (Hb) and Mb have been shown to bind NO_2^- and produce NO under hypoxic conditions a proposed emergency source of NO.⁴⁻⁷ Current mechanistic proposals suggest that the secondary-sphere network in Hb/Mb favors the η^1 -O-bound (nitrito) isomer through a combined H-bond (His) and non-polar (Val) interaction.^{3,8-10} Presumably, this pathway can avoid stable FeNO adducts of Hb and Mb, but is in contrast to the commonly accepted N-bound (nitro) isomer observed in dedicated NiR enzymes.¹¹

The NO-producing *cd*₁NiR has been shown to traverse an $\{\text{FeNO}\}^7$ state prior to product formation. The release of NO from what is typically a stable Fe-NO adduct is facilitated by H-bonding.¹² Alternatively, differing secondary-sphere networks found in SCNiR and *cc*NiR maintain the NO_x bound to Fe throughout a series of reduction and protonation events to

ultimately produce NH_4^+ .^{13,14} Electrostatic repulsion of NH_4^+ and the positively charged residues in the heme-pocket push the product out of the active site. Secondary-sphere networks are also important to substrate specificity and activity. For example, *cd₁NiR* can reduce both NO_2^- and O_2 . Upon mutation of secondary-sphere His residues to Ala, the K_m for NO_2^- became indeterminable, and the rate of NO production decreased by two orders of magnitude, whereas O_2 affinity increased.¹² Similarly, site-directed mutation of distal residues in Mb can direct reactivity from O_2 binding (globin) to O_2 activation (peroxidase) indicating that the reactivity profile of a protein can be altered by changes in the secondary-sphere.¹⁵ These examples highlight several major points: (i) substrate orientation can be directed through secondary-sphere H-bonding; (ii) charge of the active site is dictated by secondary-sphere residues and can facilitate activation of the enzyme, substrate binding, and product release; and (iii) non-covalent contacts in the secondary-coordination sphere, such as H-bonding and hydrophobic interactions, are key to enzymatic chemical transformations. Modulation of these features can enhance or alter reactivity.

Another important feature of the secondary-sphere matrix is steric protection. This was realized by Collman and coworkers in their utilization of "picket-fence" porphyrins in the study of O_2 adducts of heme model complexes.¹⁶⁻¹⁸ Since then, appending secondary-sphere steric protection has been utilized in countless metalloporphyrins¹⁹⁻²² and other small molecule complexes.^{23,24} Moreover, the ability to add H-bond donors,²⁵⁻³⁰ proton relays,^{31,32} and Lewis acid moieties^{33,34} has led to various activities for non-porphyrin complexes with respect to NO_2^- reduction, CO_2 reduction, O_2 activation, C-C bond formation, and H_2 reduction/oxidation. With respect to NO_2^- activation, the heterobimetallic complex, $[\mu(\text{NO}_2)\text{Co}(\text{doen})\text{Mg}(\text{Me}_3\text{TACN})]$ supports NO_2^- N-bound to Co(I) and O-bound to the secondary-sphere Mg^{2+} (where *doen* =

dioxime/diimine and Me₃TACN = *N,N,N'*-trimethyl-1,4,7-triazacyclononane). The use of this scaffold allowed for isolation of a Co(I)-NO₂ complex, a previously uncharacterized adduct; additionally, this complex was capable of the electrocatalytic conversion of NO₂⁻ to N₂O. The accessibility of challenging species such as Co(I)-NO₂ and {CoNO}⁹ traversed along the catalytic cycle was attributed to the secondary-sphere Lewis acid functionality of this complex.³³ Thus, the synthetic incorporation of such functionality can drastically change the reactivity profile and efficiency of small molecule catalysts. Combined, these efforts described above aim to utilize secondary-sphere design concepts perceived in natural metalloenzymes.

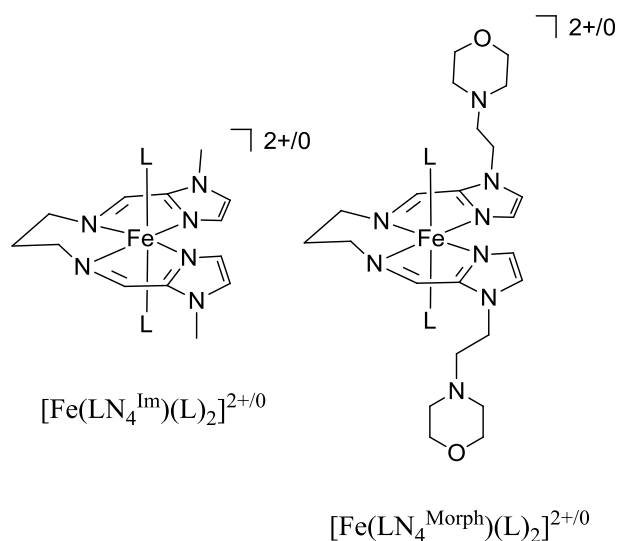


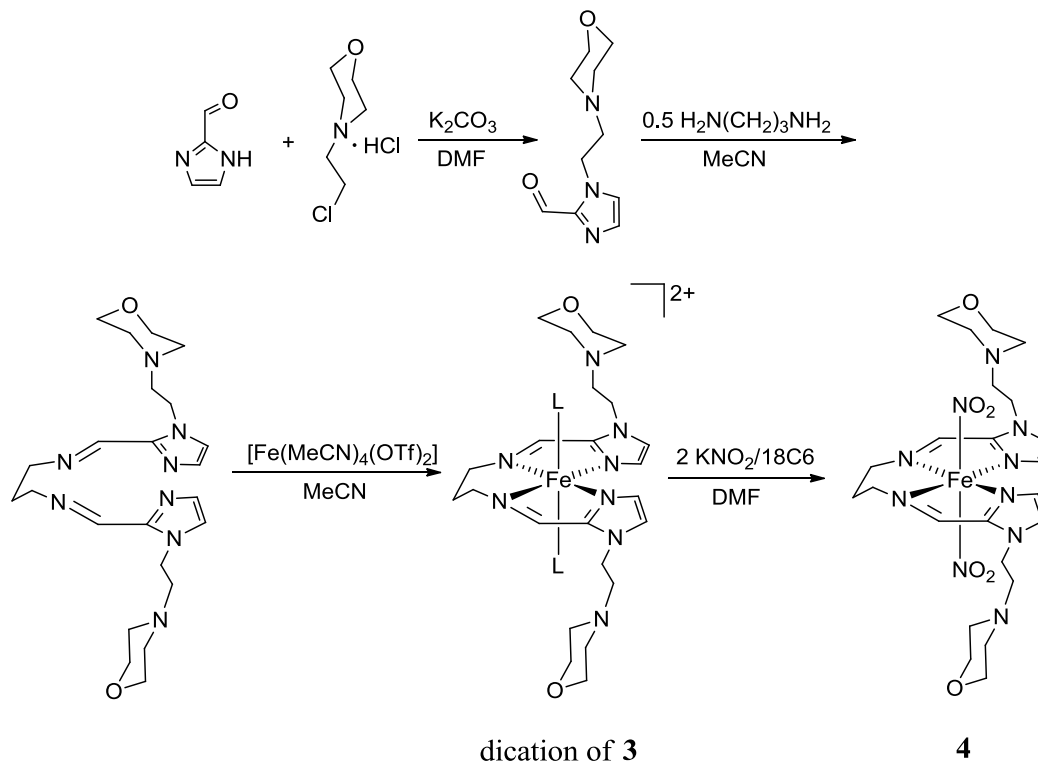
Figure 4.1. Fe complexes of LN₄^{Im} and LN₄^{Morph} ligands present in this work, L = MeCN, OTf⁻ or NO₂⁻.

In our continuing work to develop non-heme NiR catalysts, we have embarked on modulating the secondary-sphere interactions of our previously reported complexes, [Fe(LN₄^{Im})(MeCN)₂](BF₄)₂ (**1**) and [Fe(LN₄^{Im})(NO₂)₂] (**2**).³⁵ The objective of this work is to increase the catalytic competence of systems **1** and **2** by providing proton relays, steric protection

and the potential for stabilization of reactive intermediates, through the controlled manipulation of the secondary-sphere. In this current work, we installed two morpholine appendages on the periphery of the ligand backbone of LN_4^{Im} . It is our hypothesis that these moieties will be capable of H-bonding/proton donation and non-covalent interaction with axial ligands such as NO_2^- . Once coordinated, the neutral and planar ligand ($\text{LN}_4^{\text{Morph}}$) allows for two open coordination sites in the axial positions. The use of an imidazole donor provides a straightforward point to install secondary-sphere moieties (Scheme 1).

Our previous studies involving non-heme $\{\text{FeNO}\}^{7/8}$ complexes of a pyrrole-based ligand (LN_4H_2 , also used in complex **5**) support very stable $\{\text{FeNO}\}^7$ species and isolable $\{\text{FeNO}\}^8$ complexes.³⁶ We attribute this stability, in part, to the strength of the bis-pyrrolide donors that increase the π -basicity of the metal and encourage π -backbonding interactions between the Fe-NO unit. Counter to this, the use of neutral imidazole ligands (LN_4^{Im}) weakens the metal-to-ligand (M \rightarrow L) backbonding effect. Thus, we anticipate weaker Fe-NO interactions, a necessity for release of NO post-nitrite reduction. Herein we present our results toward the design and implementation of controlled secondary-sphere interactions in the pursuit of non-heme NiR model complexes capable of releasing NO.

Scheme 4.1. Synthesis of **3** and **4** (L = MeCN or OTf)



4.3 Synthesis, Spectroscopic, and Reactive Studies of Complexes 3 and 4

Encouraged by previous results, we sought to modify the secondary-coordination sphere of **1** and **2** by incorporating two appended morpholine groups on the ligand periphery. We accomplished this by covalent modification of the 3-position of imidazole 2-carboxaldehyde with 4-(2-chloroethyl)morpholine in DMF (Scheme 4.1). Combination of the functionalized aldehyde and 1,3-diaminopropane in MeCN affords 1-(2-morpholinoethyl)-1*H*-imidazole-2-carbaldehyde (LN_4^{Morph} , 66%, 2 steps). Complex 3^{OTf} was prepared by addition of an MeCN solution of LN_4^{Morph} to a solution of $[Fe(MeCN)_4(OTf)_2]$ (1:1, OTf = trifluoromethylsulfonate).³⁷ Coordination of Fe(II) is apparent due to the dark-red color change that occurred instantaneously.

The λ_{max} : 476 nm was the first spectroscopic feature suggesting that the Fe(II) center of **3** occupies a similar primary-coordination environment to that of **1** (Figure 4.2).³⁵ ESI-MS(+) analysis confirms the presence of the molecular ion $[\text{Fe}(\text{LN}_4^{\text{Morph}})(\text{OTf})]^+$ (Figure S1). Analysis of **3**^{OTf} by FTIR (KBr) suggested a possible mixture of OTf⁻ and MeCN bound complexes due to the very weak intensity of (ν_{CN} : 2280 and 2247 cm^{-1}) as compared to the similarly prepared $[\text{Fe}(\text{LN}_4^{\text{Morph}})(\text{MeCN})_2](\text{BF}_4)_2$ (**3**^{BF4}) (ν_{CN} : 2282 and 2252 cm^{-1} , Figure S2). It appears that in the bulk solid-state that two OTf⁻ are bound to Fe. By comparison, the ν_{CN} of **1**^{OTf} are identical in energy and intensity to **1**^{BF4} supporting that MeCN is coordinated in both complexes (Figure S3). This observation supports favorable secondary-sphere interactions between the morpholine appendages of **3** and OTf⁻, which we anticipate will be similar to NO₂⁻. Accordingly, the stabilizing interaction is strong enough to favor a weaker ligand (OTf⁻) over MeCN, at least in the solid state. In solution however, the estimated ϵ values for **1**^{OTf} and **3**^{OTf} (Figure 4.2) are nearly identical, supporting two axial MeCN ligands as observed in **1**^{BF4} and **3**^{BF4}.

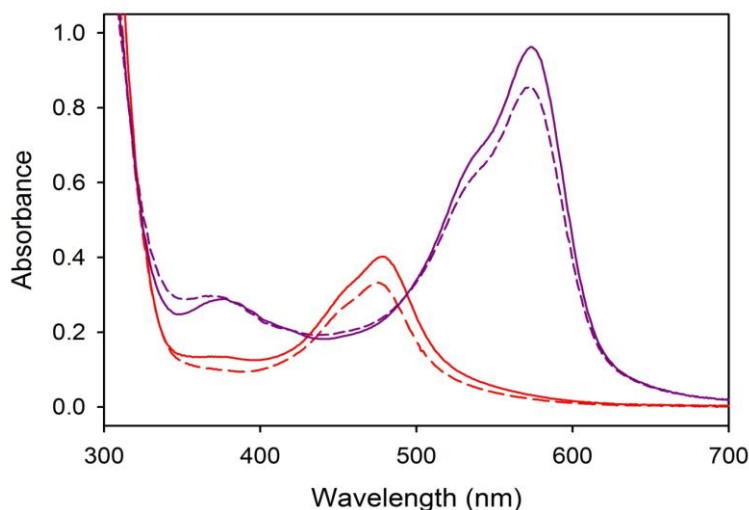


Figure 4.2. UV-vis spectra of 100 μM MeCN solution of **1**^{OTf} (red solid line), **2** (purple solid line), **3**^{OTf} (red dashed line), and **4** (purple dashed line) in MeCN at 298 K. Compounds **2** and **4** contain 10 mM ⁿBu₄NNO₂.

Magnetic measurements (solution-state, CD₃CN, 20 °C) indicate that **1**^{BF₄} and **10**^{Tf} are of intermediate spin (IS) state, $S = 1$, with μ_{eff} value of 2.60 and 2.59 BM, respectively. Complex **3**^{OTf} also appears to be IS, although the μ_{eff} value of 3.28 BM suggest a possible equilibrium between MeCN and OTf⁻. For example, other non-heme ferrous complexes with bound OTf⁻ such as [Fe(TPA)(OTf)₂], [Fe(*iso*-bpmen)(OTf)₂], and [Fe(Me₆-tren)OTf]OTf have solution-state μ_{eff} values of 5.35 BM (CDCl₃), 5.32 BM (CD₂Cl₂), and 4.92 BM (CD₂Cl₂), respectively (where TPA = tris(2-pyridylmethyl)amine; *iso*-bpmen = *iso*-bispyridylmethyl)ethylenediamine; and Me₆-tren = tris(2-dimethylaminoethyl)amine)) indicative of HS Fe(III) centers.^{38,39} Thus, a significantly higher μ_{eff} would be anticipated for an OTf⁻ bound species, which suggests that the MeCN-bound complex predominates in solution. However, OTf⁻ binds more favorably to **3**^{OTf}

over $\mathbf{1}^{\text{OTf}}$. Notably, the ^1H NMR spectra of $\mathbf{1}^{\text{OTf}}$ and $\mathbf{3}^{\text{OTf}}$ are representative of paramagnetically-shifted and broadened absorbances between $\sim 50 - 15$ ppm for both $\mathbf{1}^{\text{OTf}}$ and $\mathbf{3}^{\text{OTf}}$ (Figure S4), in agreement with the μ_{eff} measurements.

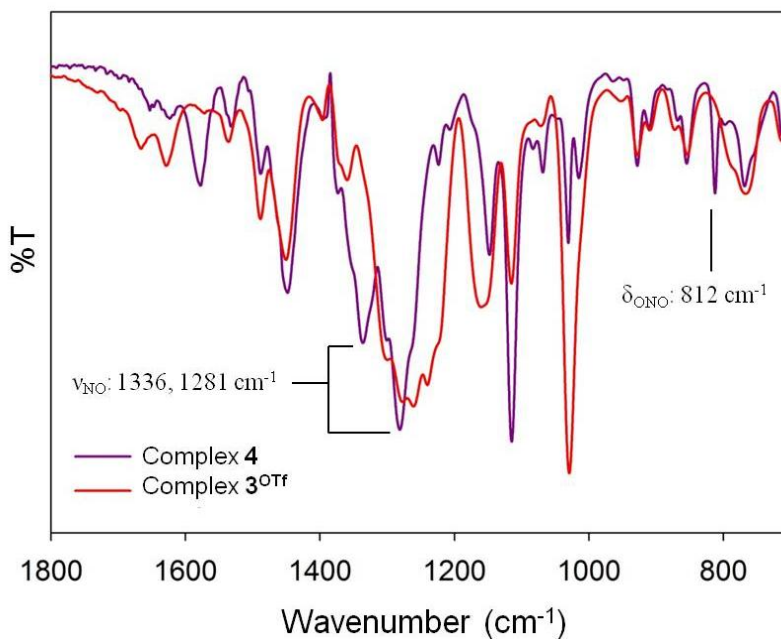


Figure 4.3. FTIR (KBr) comparison of $\mathbf{3}^{\text{OTf}}$ and $\mathbf{4}$.

Upon addition of $[\text{K}(\text{18C6})]\text{NO}_2$ to an MeCN solution of $\mathbf{3}^{\text{OTf}}$ or $\mathbf{3}^{\text{BF}_4}$, the deep-red color rapidly became violet, indicative of NO_2^- coordination, where 18C6 = 1,4,7,10,13,16-hexaoxacyclooctadecane. Overnight diffusion of Et_2O affords $[\text{Fe}(\text{LN}_4^{\text{Morph}})(\text{NO}_2)_2]$ ($\mathbf{4}$) as a dark-violet solid with a λ_{max} of 571 nm and a 540 nm shoulder (Figure 4.2). The observed absorbance UV-vis spectrum is analogous to $\mathbf{2}$ and compares well to those observed for 6C $[\text{Fe}(\text{por})(\text{NO}_2)(\text{L})]$ complexes, in which the λ_{max} ranges from 533-580 nm (ϵ : 4500-16000 $\text{M}^{-1} \text{cm}^{-1}$) in chlorobenzene.⁴⁰ The visible absorbance of $\mathbf{4}$ is in-line with a charge-transfer band and assigned as M→L CT consistent with the π -accepting ability of the NO_2^- ligand.¹³ Distinct absorbance in the IR for $\mathbf{4}$ indicate bound NO_2^- with ν_{NO} : 1336 and 1281 cm^{-1} and δ_{ONO} : 812 cm^{-1}

¹. Consistent with **2**, complex **4** appears to bind two NO₂⁻ as N-bound nitro ligands. Additional characterization by ESI-MS(+) indicated the presence of [Fe(LN₄^{Morph})(NO₂)⁺ (*m/z* 558.4, Figure S6), characteristic of the loss of one NO₂⁻ under ionization conditions. Solution-state magnetic measurements (5:1 ⁿBu₄NNO₂:**3**^{OTf}) show a significant change in μ_{eff} from 3.28 BM of **3**^{OTf} to 0.51 BM, suggestive of a low-spin (LS) Fe(II) center in **4**. Comparatively, complex **2** exhibits a μ_{eff} of 0.82 BM (DMSO-*d*₆, 298 K) but is (*S* = 0) in the solid-state based on X-ray diffraction results and a solid-state μ_{eff} measurements. The ¹H NMR of **3**^{OTf} also changes drastically upon addition of ⁿBu₄NNO₂, with complete disappearance of the downfield resonances and appearance of new peaks in the diamagnetic region (~13 - 0 ppm, Figure S7). The resonances corresponding to the imine (*HC=N*) and aromatic (*Im-H*) are still broadened in comparison to the many methylene groups of **4**, and may represent a slight local paramagnetism in the conjugated network.

4.3.1 X-Ray Crystal Structures of **3**^{BF₄} and **3**^{OTf}

A complimentary synthesis of **3**^{BF₄} can be accomplished by using [Fe(H₂O)₆](BF₄)₂ to afford [Fe(LN₄^{Morph})(MeCN)₂](BF₄)₂ (**3**^{BF₄}). X-ray crystallographic analysis of **3**^{BF₄} shows the Fe(II) center housed in a distorted octahedral geometry comprised of the four basal plane N-donors from LN₄^{Morph} and two axial MeCN ligands. The bond distances for **1**^{BF₄} and **3**^{BF₄} are similar with Fe-N_{imine} (avg: 1.962 Å for **1**^{BF₄}; 1.944 Å for **3**^{BF₄}) and Fe-N_{imidazole} (avg: 1.992 Å for **1**; 1.985 Å for **3**^{BF₄}), supportive of LS Fe(II) in both complexes (Table S2). The N7 and N8 nitrogens of morpholine are protonated in **3**^{BF₄}, which may occur during crystallization due to the excess H₂O associated with [Fe(H₂O)₆](BF₄)₂ (Figure 4.4). We anticipate the pK_a of the internal

morpholinium acid to be similar to N-methylmorpholine and triethylamine with pK_a values of 7.4 and 10.7 in H_2O , respectively.⁴¹ The morpholine appendage extends away from the metal center and axial MeCN ligands. Presumably due to electrostatic repulsion between the Fe(II) center and the two morpholinium arms. The protonated state of the ligand offers an important glimpse into the potential proton donor functionality of the LN_4^{Morph} system (Figure 4.4).

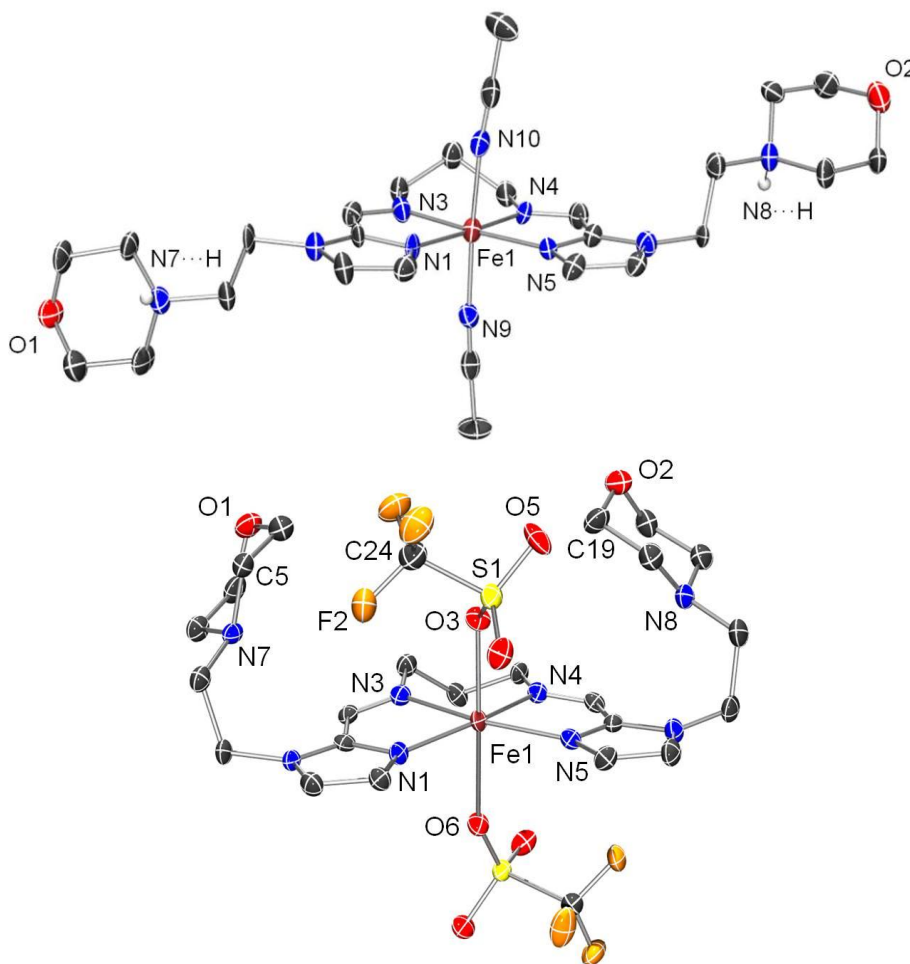


Figure 4.4. ORTEP of 3^{BF_4} (top) and 3^{OTf} (bottom) with 50% thermal probability for all non-hydrogen atoms. Protons have been modeled in their ideal positions for N7 and N8 of 3^{BF_4} . The MeCN solvent of crystallization and BF_4^- counter anions have been omitted in 3^{BF_4} for clarity; hydrogen atoms have been omitted for clarity.

In an attempt to avoid protonation of the morpholine adducts, the anhydrous $[\text{Fe}(\text{MeCN})_4(\text{OTf})_2]$ salt was used for metalation to produce $[\text{Fe}(\text{LN}_4^{\text{Morph}})(\text{OTf})_2]$ ($\mathbf{3}^{\text{OTf}}$).³⁷ Under analogous crystallization conditions to $\mathbf{3}^{\text{BF}_4}$, complex $\mathbf{3}^{\text{OTf}}$ formed pale-red colored crystals suitable for X-ray diffraction. The bond distances for $\mathbf{3}^{\text{BF}_4}$ and $\mathbf{3}^{\text{OTf}}$ are quite different (Table S2), and reflective of the μ_{eff} values obtained (vide supra). For instance, the Fe-N_{imine} (avg: 2.178 Å for $\mathbf{3}^{\text{OTf}}$) is considerably elongated from $\mathbf{3}^{\text{BF}_4}$, with $\Delta\text{Fe-N}_{\text{imine}}$: 0.234 Å. Similarly, the Fe-N_{imidazole} (avg: 2.124 Å for $\mathbf{3}^{\text{OTf}}$) also increases ($\Delta\text{Fe-N}_{\text{imine}}$: 0.132 Å). The axial Fe-O_{OTf} bonds are also lengthened (avg: 2.218 Å for $\mathbf{3}^{\text{OTf}}$) from axial MeCN ligands of $\mathbf{3}^{\text{BF}_4}$ (avg: 1.927 Å). Taken together, the structural parameters for $\mathbf{3}^{\text{OTf}}$ suggest a HS Fe(II) center, whereas $\mathbf{3}^{\text{BF}_4}$ is LS Fe(II). Therefore, the spin-state of $\mathbf{3}$ is dependent on the *trans*-axial ligands. A comparable system having *cis* MeCN ligands, $[\text{Fe}(\text{TPA})(\text{MeCN})_2]$ (Fe-N avg: 1.956 Å) is LS, whereas the analogue $[\text{Fe}(\text{TPA})(\text{OTf})_2]$ (Fe-N avg: 2.178 Å; Fe-O_{OTf} avg: 2.102 Å) is HS (TPA = tris(2-pyridylmethyl)amine). Moreover, the Fe-O_{OTf} lengths of $\mathbf{3}^{\text{OTf}}$ are consistent with those of $[\text{Fe}(\text{TPA})(\text{OTf})_2]$ (avg: 2.102 Å), $[\text{Fe}(\text{iso-bpmen})(\text{OTf})_2]$ (avg: 2.164 Å), and $[\text{Fe}(\text{Me}_6\text{-tren})(\text{OTf})]\text{OTf}$ (2.043 Å), which are all HS species.^{38,39}

The axial sites in $\mathbf{3}^{\text{OTf}}$ differ due to the influence of the morpholine arms, in which both occupy the secondary-sphere of one face (proximal) of the FeN₄ plane (Figure 4.4). The effect is apparent in the Fe-O_{OTf} bond distance of 2.187 Å for Fe-O₃ (proximal) and 2.248 for Fe-O₆ (distal). The notable $\Delta\text{Fe-O}_{\text{OTf}}$ of 0.061 Å in $\mathbf{3}^{\text{OTf}}$ compares to complexes $\mathbf{1}^{\text{BF}_4}$, $\mathbf{3}^{\text{BF}_4}$, and $\mathbf{2}$ having $\Delta\text{Fe-N}_{\text{MeCN}}$: 0.008 Å, $\Delta\text{Fe-N}_{\text{MeCN}}$: 0.018 Å, and $\Delta\text{Fe-N}_{\text{NO}_2}$: 0.001 Å for the bis(MeCN) and bis(NO₂) axial ligands, respectively. A similar contraction of the proximal ligand has also been observed in the $[\text{K}(\text{18C6})][\text{Fe}(\text{TpivPP})(\text{NO}_2)_2]$ complex which supports two axial NO₂⁻ ligands having Fe-N_{NO₂}: 1.970 Å (proximal) and 2.001 Å (distal); with $\Delta\text{Fe-N}_{\text{NO}_2}$: 0.031 Å

(where TpivPP = *meso*-tetra($\alpha,\alpha,\alpha,\alpha$ -*o*-pivaloylamidophenyl)porphyrin). However, there is no contact of NO_2^- with the picket-fence periphery consistent with the observation that TpivPP does not interact with bound small molecules like NO_2^- or O_2 .^{17,20} Counter to this observation, the proximal OTf of $\mathbf{3}^{\text{OTf}}$ has several close contacts to the morpholine ring. These contacts appear to be both hydrophobic and weakly polar interactions. For instance, the closest interaction is between O5 of OTf proximal and H-C19 of the morpholine ring, having an O---H distance of 2.494 Å and C---O distance of 3.103 Å, both within the sum of their van der Waals radii of 2.72 and 3.22 Å, respectively (Figure 4.4). In addition, the H-C5 of the adjacent morpholine is in close contact to F-C24 from the CF_3 moiety. This H---F contact is 2.515 Å (van der Waals radii: 2.67 Å) and indicative of a non-polar interaction. Distances between the N_{morph} and Fe-bound O3 atom are 5.210 Å and 4.717 Å. The large difference between these two occurs due to the much bulkier CF_3 group occupying one side of the secondary-sphere space. The average Fe- N_{morph} distance is 5.296 Å, a value much longer than that observed in the well studied H_2 evolving catalyst, $[\text{Ni}(\text{P}^{\text{Cy}}_2\text{N}^{\text{Bz}}_2)_2](\text{BF}_4)_2$ (where $\text{P}^{\text{Cy}}_2\text{N}^{\text{Bz}}_2 = 1,5\text{-dibenzyl-}3,7\text{-dicyclohexyl-}1,5,3,7\text{-diazadiphosphocyclooctane}$), in which the pendant amine is 3.3-3.4 Å away from Ni;³² however, the Ni-H---H-N interaction requires much closer proximity between pendant amine and the metal center. In $\mathbf{3}^{\text{OTf}}$, the morpholine rings are directed toward the propyl-linker of $\text{LN}_4^{\text{Morph}}$; this orientation seems to avoid electronic repulsion between the aromatic imidazole ring and the lone-pair of N_{morph} . Taken together, the structure of $\mathbf{3}^{\text{OTf}}$ provides a first look at the secondary-sphere impact of the appended morpholine moieties.

The metric parameters obtained from the two crystal structures, $\mathbf{3}^{\text{BF}_4}$ and $\mathbf{3}^{\text{OTf}}$, clearly indicate a dynamic range of motion for the morpholine appendages. Moreover, $\mathbf{3}^{\text{BF}_4}$ demonstrates that protonation of N_{morph} is possible and may suggest proton donor ability not

available in **1** and **2**. Protonation of N_{morph} causes electrostatic repulsion of the morpholine rings, observed in **3**^{BF₄} and offers an upper limit on the distance from axial ligand to morpholine. Alternatively, **3**^{OTf} presents much closer interactions between axially-coordinated OTf⁻ and morpholine. There is clear steric repulsion between OTf and morpholine; therefore, the nature of secondary-sphere influence for smaller ligands such as NO and NO₂⁻ remains unknown and are currently under investigation.

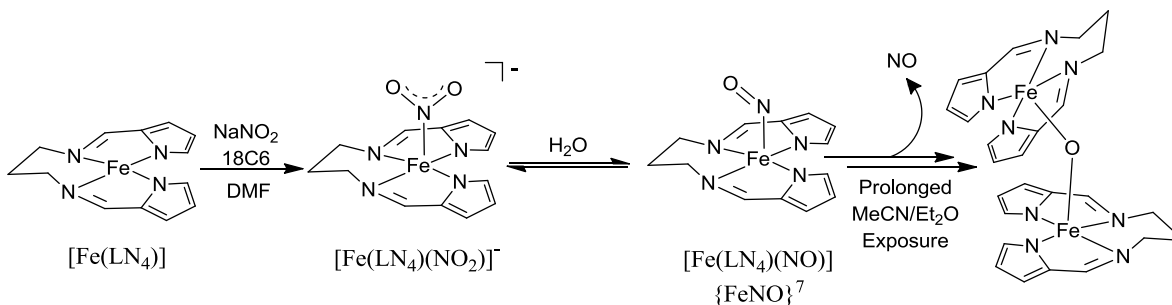
4.4 Reactivity Studies of **2**, **4**, and **5**

*Reactivity of **5***

Our initial endeavors into the reaction of NO₂⁻ with a non-heme Fe(II) pyrrolide complex began with the synthesis of [Na(18C6)][Fe(LN₄)(NO₂)] (**5**). Addition of [Na(18C6)]NO₂ to a DMF solution of [Fe(LN₄)] affords a dark-brown solid after workup. Characterization of **5** includes ESI-MS(-) which shows [Fe(LN₄)(NO₂)]⁻ (m/z 328.0) as the base peak, and a strong intensity peak appears in the FTIR (ν_{NO} : ~1253 cm⁻¹). This value for ν_{NO} is suggestive of an N-bound NO₂⁻ ligand participating in strong M→L π -backbonding; as compared to the ν_{NO} for **2** and **4** (~1330 and 1280 cm⁻¹). It is important to note that the appearance of ν_{NO} from the {FeNO}⁷ complex of this ligand at 1698 cm⁻¹ is also present in our preparations of **5**. This observation supports the spontaneous reduction of NO₂⁻ to NO presumably due to the presence of adventitious H₂O. An analogous synthesis with Na¹⁵NO₂ showed formation of a new shoulder ($\nu_{15\text{NO}}$: 1208 cm⁻¹) as well as the red-shifted {FeNO}⁷ ($\nu_{15\text{NO}}$: 1664 cm⁻¹) confirming that NO is formed from added NO₂⁻ (Figure S8). Electrochemical analysis (CV) of **5** a reversible wave with $E_{1/2}$ value of -1.18 V vs. Fc⁺/Fc, that is currently assigned as the Fe(III/II) couple for **5** (Figure S9). Also present in this CV is a reversible $E_{1/2}$ of -1.41 vs. Fc⁺/Fc that corresponds to the

$\{\text{FeNO}\}^{7/8}$ couple of $[\text{Fe}(\text{LN}_4)(\text{NO})]$.³⁶ Attempts to crystallize **5** (MeCN/Et₂O, -25 °C) resulted in formation of $[(\text{Fe}(\text{LN}_4))_2\mu\text{-O}]$ (Figure S10). FTIR of the crystalline material indicated loss of absorbance in the ν_{NO} region for both Fe(II)-NO and Fe(II)-NO₂⁻ and appearance of new peaks corresponding to ν_{FeO} at 857 and 871 cm⁻¹ (Figure S8) Therefore, it appears that **5** spontaneously reduces NO₂⁻. The ultimate fate of the reaction is μ -oxo, and without added electrons, the remaining products are likely NO and H₂O (Scheme 4.2). Thus, the mechanism of reduction would formally occur as loss of oxy anion (O²⁻) as water or as μ -oxo. Similar reduction of NO₂⁻ has been observed elsewhere, however, the O-bound isomer is implicated in this type of reactivity.^{29,42} The spontaneous reaction of **5** with NO₂⁻ to give $\{\text{FeNO}\}^7$ and/or μ -oxo has been observed in small molecule iron complexes in the literature.⁴³⁻⁴⁶ This pathway is driven by the inherent stability of $\{\text{FeNO}\}^7$ and Fe(III)-O-Fe(III) complexes. Therefore, to release NO from a stable Fe complex, one must destabilize the Fe-NO bond through modulation of π -backbonding and/or secondary-sphere interactions; the same features in the porphyrin ligand of *cd*₁NiR that releases NO from an $\{\text{FeNO}\}^7$ state.¹² Given our interest in designing NiR model complexes, we first investigated the reactivity of **1**^{BF₄} and **3**^{BF₄} with NO(g).

Scheme 4.2. Proposed scheme for the reduction of NO₂⁻ by **5**.



Reactivity of **1** and **3** with NO(g)

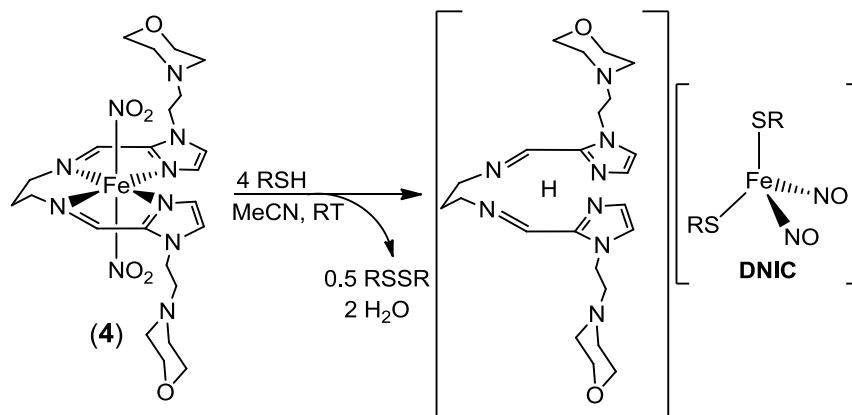
Introduction of excess NO(g) to complex **1**^{BF₄} affords a red to brown-green color change, indicative of NO coordination. The stability of these complexes is very low, however, and application of vacuum returns the solution to its red color in solvents such as MeCN. In more weakly coordinating alcohol solvents, the {FeNO}⁷ complex is more stable. After applied vacuum, the red complex showed a ν_{NO} at 1767 cm⁻¹ (KBr), and is tentatively assigned as [Fe(LN₄^{Im})(NO)](BF₄)₂. This compares with the solution-state FTIR values of ~1700 cm⁻¹ collected in situ characterization of the reaction of **1** with NO(g) in MeCN or MeOH. In the solid-state, ν_{NO} is considerably higher in energy than the corresponding pyrrole analog, [Fe(LN₄)(NO)] (ν_{NO} : 1698 cm⁻¹, KBr), demonstrating π -basicity of the Fe. Analysis of [Fe(LN₄^{Im})(NO)](BF₄)₂ by EPR (EtOH, 10 K) did indicate the presence of a paramagnetic species, consistent with an {FeNO}⁷ complex ($g = 2.04$, Figure S11).

Similarly, synthesis of the NO-adduct of **3**^{BF₄} was also attempted in MeOH. This resulted in parallel observations to that of **1**, although, attempts to isolate the {FeNO}⁷ complex only gave back **3**^{BF₄} in MeOH. It appears that the morpholine appendages do not stabilize the NO ligand. In fact, it appears that the NO complex is less stable, an ideal feature for catalytic NO release. A very weak ν_{NO} is observed at 1791 cm⁻¹ and supports the weak interaction between **3**^{BF₄} and NO. The instability of complexes **1** and **3** with NO is an important feature of these complexes that has been implemented through use of imidazole donors in place of pyrrole. Moreover, we anticipate that this weakly bound NO can be readily displaced by NO₂⁻ or MeCN under our NO₂⁻-to-NO reduction conditions (vide infra). This feature allows for avoidance of stable Fe-NO adducts that can halt additional turnover of NO₂⁻ reduction.

Reactivity of **4** with thiols

Complex **4** reacts with *p*-chlorobenzenethiol in MeCN (1:4; *p*-ClArSH = RSH, pK_a : 9-10 in DMSO⁴⁹) to afford the familiar tetrahedral dinitrosyl iron complex (DNIC), $[\text{Fe}(\textit{p}\text{-ClArSH})_2(\text{NO})_2]^-$ in 81% yield. DNIC formation was confirmed by FTIR (ν_{NO} : 1745 and 1698 cm^{-1}), UV-vis (λ_{max} : 377, 488, and 798 nm), and ESI-MS(-) (m/z 371.8), corresponding to $[\text{Fe}(\textit{p}\text{-ClArSH})\text{NO}]^-$. After workup, the Et₂O-soluble material was characterized by FTIR and ¹H NMR and supports formation of the disulfide of *p*-ClArSH (~50% yield). However, there was only ~1% of free LN₄^{Morph} present based on ¹H NMR integration. This result differs from the reactivity of **2** in which both DNIC and free ligand were isolated in ~50% yield. This observation corroborates that protonated LN₄^{Morph} is the counter-cation of DNIC as ESI-MS(+) revealed $[\text{LN}_4^{\text{Morph}}\text{H}]^+$ (m/z 457.3). Therefore, the major product of **4** with RSH is $(\text{LN}_4^{\text{Morph}}\text{H})[\text{Fe}(\textit{p}\text{-ClArSH})_2(\text{NO})_2]$. It is difficult to imagine that $[\text{LN}_4^{\text{Morph}}\text{H}]^+$ to be a non-coordinating counter-cation, and perhaps in solution the Fe center is in equilibrium between DNIC and LN₄^{Morph} with formation of RS⁻/RSH. These results suggest a different reaction pathway from that of **2**, and may implicate the morpholine appendages as reason for this new reactivity. Further investigation of the potential interactions of $(\text{LN}_4^{\text{Morph}}\text{H})[\text{Fe}(\textit{p}\text{-ClArSH})_2(\text{NO})_2]$ and the reason for its formation are currently under way. Additionally, future work regarding the electrochemical reactivity of **2** and **4** is also underway.

Scheme 4.3. Reaction of **4** with RSH (R: *p*-ClArSH)



OAT reactions of electrochemically-generated Fe(III) complex

Compound **1**^{BF₄} exhibits an oxidation event (E_{ox} : 0.58 V vs. Fc/Fc⁺) corresponding to the irreversible Fe(III)/Fe(II) couple. Upon addition of NO₂⁻, these events become considerably more negative by ~630 mV indicative of anion coordination. Moreover, the reversibility of this couple increases with added NO₂⁻. The reversible redox event for **2** is shown in Figure S12. Notably, the $E_{1/2}$ of **2** is -0.087 V vs. Fc/Fc⁺ (0.32 V vs. SCE; $\Delta E_p = 0.094$ V; $R^2 = 0.995$ for i^p vs. $v^{1/2}$).⁴⁷ This $E_{1/2}$ value is much more positive when compared to [Fe(TPP)(NO₂)₂]⁻ (-0.45 V vs. SCE) and [Fe(OEP)(NO₂)₂]⁻ (-0.83 V vs. SCE). We attribute this positive shift in $E_{1/2}$ value to the relative charge of the neutral LN₄ platforms, compared to the dianionic porphyrins. The Fe(III)/Fe(II) couple of complex **5**, the pyrrolidine-based complex, is in better agreement with the porphyrin complexes, and is observed at -0.78 V vs. SCE.

The use of spectroelectrochemistry provides insight into the relative stability of the putative [Fe(LN₄^{Im})(NO₂)₂]⁺. Upon holding the cell potential at 0.5 V vs. Ag/AgNO₃ in MeCN, the characteristic absorbance of **2** rapidly decreases with isosbestic behavior over ~90 s and appears with similar intensity at 389 nm (Figure 4.5). If the potential is held for longer than 90 s,

a new absorbance at 389 nm begins to decrease with concomitant appearance of a peak at 477 nm, consistent with formation of **1** (Figure S12). Once back at open circuit potential, the absorbance of **2** returns, through an intermediate species (λ_{max} : 493 and 533 nm), however only to about half its original intensity, implying that a portion of NO_2^- has been consumed.

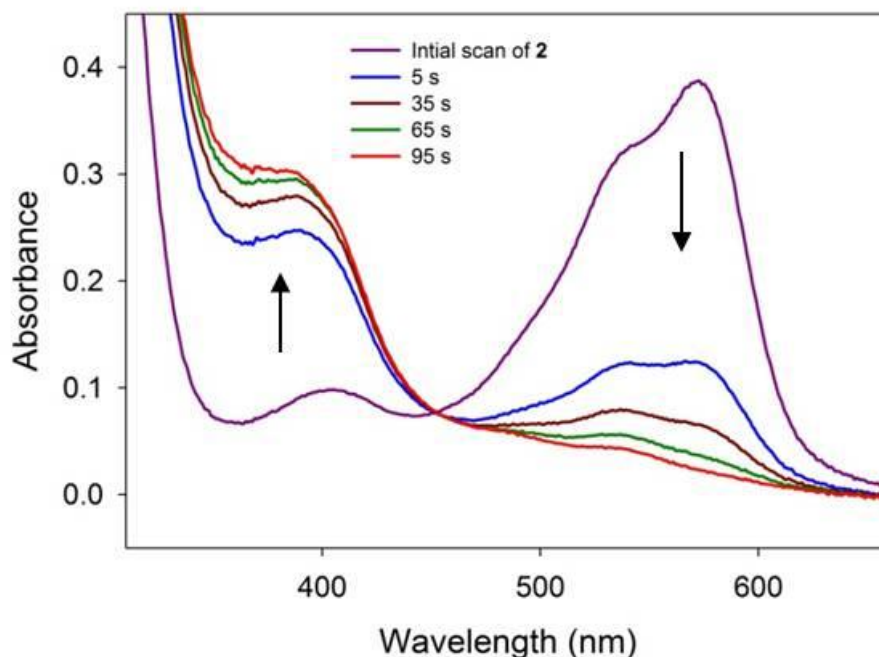
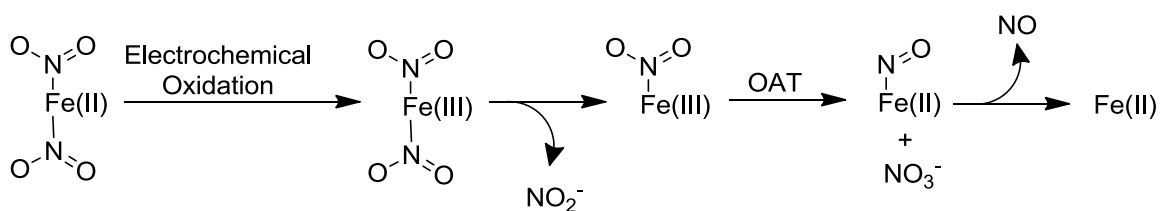


Figure 4.5. UV-vis spectroelectrochemical analysis of **2** in MeCN (0.1 M Et_4NPF_6 supporting electrolyte, Pt-mesh working electrode, Pt-wire counter electrode, RT). UV-vis spectrum shows the initial scan of **2** before and after applied potential of 0.5 V vs. Ag/AgNO_3 .

One possible explanation for these observations is that bulk oxidation forms the $[\text{Fe}(\text{III})(\text{LN}_4^{\text{Im}})(\text{NO}_2)_2]^+$ complex (λ_{max} : 389 nm) followed by an O-atom transfer (OAT) to NO_2^- to give NO_3^- and NO. This explanation may account for the difficulty in isolating of $[\text{Fe}(\text{III})(\text{LN}_4^{\text{Im}})(\text{NO}_2)_2]^+$ through bulk chemical oxidation of **2**. In addition, the OAT to NO_2^- has been reported in $\text{Fe}(\text{III})(\text{por})\text{NO}_2$ complexes.⁴⁸ Accordingly, if OAT is occurring then one would

expect formation of $[\text{Fe}(\text{LN}_4^{\text{Im}})(\text{NO})]^{2+}$, which will release NO to give **1** (λ_{max} : 477 nm, $E_{1/2}$: 0.58 V vs. Fc/Fc⁺). As shown in Scheme 4.3, NO_2^- may come off of the $\text{Fe}(\text{III})(\text{NO}_2)_2$ complex, thus providing OAT substrate. However, it appears that under the conditions used that not all the NO_2^- was consumed, and upon return to open circuit potential, NO_2^- binds back to the $\text{Fe}(\text{II})\text{LN}_4$ species through the mono(NO_2) intermediate (λ_{max} : 493 and 533 nm) en route to partial reformation of **2**. These initial electrochemical reactivity studies provide a possible route to NO_2^- reduction through an OAT mechanism. Importantly, complex **2** demonstrates the ability to reduce NO_2^- by two distinct pathways; (i) OAT and (ii) loss of oxy-anion as H_2O , for $\text{Fe}(\text{III})\text{-NO}_2$ and $\text{Fe}(\text{II})\text{-NO}_2$, respectively. Future studies in the presence of a suitable OAT acceptor substrates such as Ph_3P may provide a means for electrocatalytic reduction of NO_2^- to NO at low over-potential. Moreover, complex **2** is stable at negative potentials, ranging from -0.1 to -0.5 V vs. AgNO_3/Ag . Therefore, the ability to add a proton source without the need for sacrificial electron donors may be possible. If so, complexes **2** and **4** could perform NO_2^- reduction through both OAT and H^+ -dependent reaction pathways.

Scheme 4.3. Possible electrochemical reduction of NO_2^- through OAT with **2**.



4.5 Conclusions and Future Outlook

The installation of secondary-sphere modulators in **3** and **4** clearly affects the chemical properties of these complexes when compared to **1** and **2**. The major implications of this

modification are seen in the protonated $\mathbf{3}^{\text{BF}_4}$ and the OTf-bound $\mathbf{3}^{\text{OTf}}$, in which the potential for proton relays and non-covalent secondary-sphere interactions are displayed, respectively. Moreover, binding of OTf⁻ over an MeCN ligand is not observed in **1** and is an observation that can only be attributed to added stability of the morpholine/OTf interactions, thus offering the first direct indication for secondary-sphere effects. Complex **4** is spectroscopically similar to **2**, suggestive of no immediate effects on NO₂⁻ coordination or binding mode. However, we anticipate that differences in the reactivity of **2** and **4**, will become apparent as this work continues to move forward.

Importantly, complex **3** provides the initial platform for the future design of related ligands. As has been demonstrated, the imidazole donors provide both appropriate donor strength for NO release, as well as a synthetic handle for installation of secondary-sphere moieties. Thus, one can envision a series of ligands in which the secondary-sphere can be modulated to incorporate in various proton donors, Lewis acids, and/or steric protection. Moreover, incorporation of additional metal-binding sites in the secondary-sphere of Fe could lead to multimetallic catalysts. With this in mind, the rational design of these ligands may dictate the corresponding chemistry that occurs at the metal center, without changing the primary-coordination sphere. This type of reactivity control is seen in natural heme-proteins and remains an important area of development in synthetic model complexes.

4.6 Materials and Methods

4.6.1 General Information

See General Information section for Chapter 3 Part A.

4.6.2 Physical Methods

See Physical Methods section for Chapter 3 Part A. The electrochemical cell/cuvette, Pt-mesh electrode, and Pt reference electrode were purchased through ALS Co., Ltd, and connected to a μ Autolab Type III potentiostat/galvonostat. Electrochemical parameters were controlled through Autolab GPES software. UV-vis spectra were collected with the UV-vis and software listed in Chapter 3 Part A.

4.6.3 Synthesis of Compounds

(1-(2-morpholinoethyl)-1H-imidazole-2-carbaldehyde)

To a 20 mL DMF solution was added 4-(2-chloroethyl)morpholine (1.000 g, 0.0054 mmol), 1H-imidazole-2-carbaldehyde (0.6223 g, 0.0065 mmol), NaI (0.8900 g, 0.0059 mmol), and K_2CO_3 (1.642 g, 0.0119 mmol). The reaction vessel was fit with a reflux condenser and the light-brown colored solution and insoluble K_2CO_3 were stirred and heated to 110 °C for 8 h. After this time, the solution became dark-brown color with some white insoluble material. The solution was filtered and concentrated by short-path distillation to give a dark-brown oil. The oil was dissolved in EtOAc (60 mL) and washed with saturated $NaHCO_3$ (3×100 mL), deionized H_2O (3×100 mL), and brine (3×100 mL). The layer was dried with anhydrous $MgSO_4$ and concentrated to a dark-brown oil. (0.7908 g, 0.0038 mmol, 70%). 1H NMR (400 MHz, $CDCl_3$, δ from solvent): 9.80 (s, 1H, *HCO*), 7.27 (s, 1H, *ImH*), 7.23 (s, 1H, *ImH*), 4.50 (t, 2H, $J = 8$ Hz, *CH*₂), 3.65 (t, 2H, $J = 6$ Hz, *CH*₂), 2.68 (t, 2H, $J = 8$ Hz, *CH*₂), 2.47 (t, 2H, $J = 8$ Hz, *CH*₂). ^{13}C NMR (100.6 MHz, $CDCl_3$, δ from solvent): 182.11 (*HCO*), 143.26 (*C1*, *Im*), 131.52 (*ImC*), 126.81 (*ImC*), 66.90 (*CH*₂), 58.74 (*CH*₂), 53.65 (*CH*₂), 44.68 (*CH*₂). FTIR (ATR), ν_{max} (cm^{-1}): 3107 (w), 2958 (m), 2850 (m), 2810 (m), 1674 (s), 1506 (w), 1474 (m), 1453 (m), 1407 (s), 1358

(w), 1334 (m), 1299 (m), 1274 (m), 1262 (m), 1208 (w), 1148 (m), 1113 (s), 1069 (m), 1035 (m), 1009 (m), 930 (m), 915 (m), 868 (m), 855 (m), 760 (s), 690 (m), 675 (w), 622 (w), 609 (m).
 LRMS-ESI (m/z): $[M + H]^+$ calcd for $C_{10}H_{16}N_3O_2$ (% relative abundance), 210.1 (100), 211.1 (12.2), 212.1 (1.1); found, 210.2 (100), 211.2 (12.3), 212.2 (1.4).

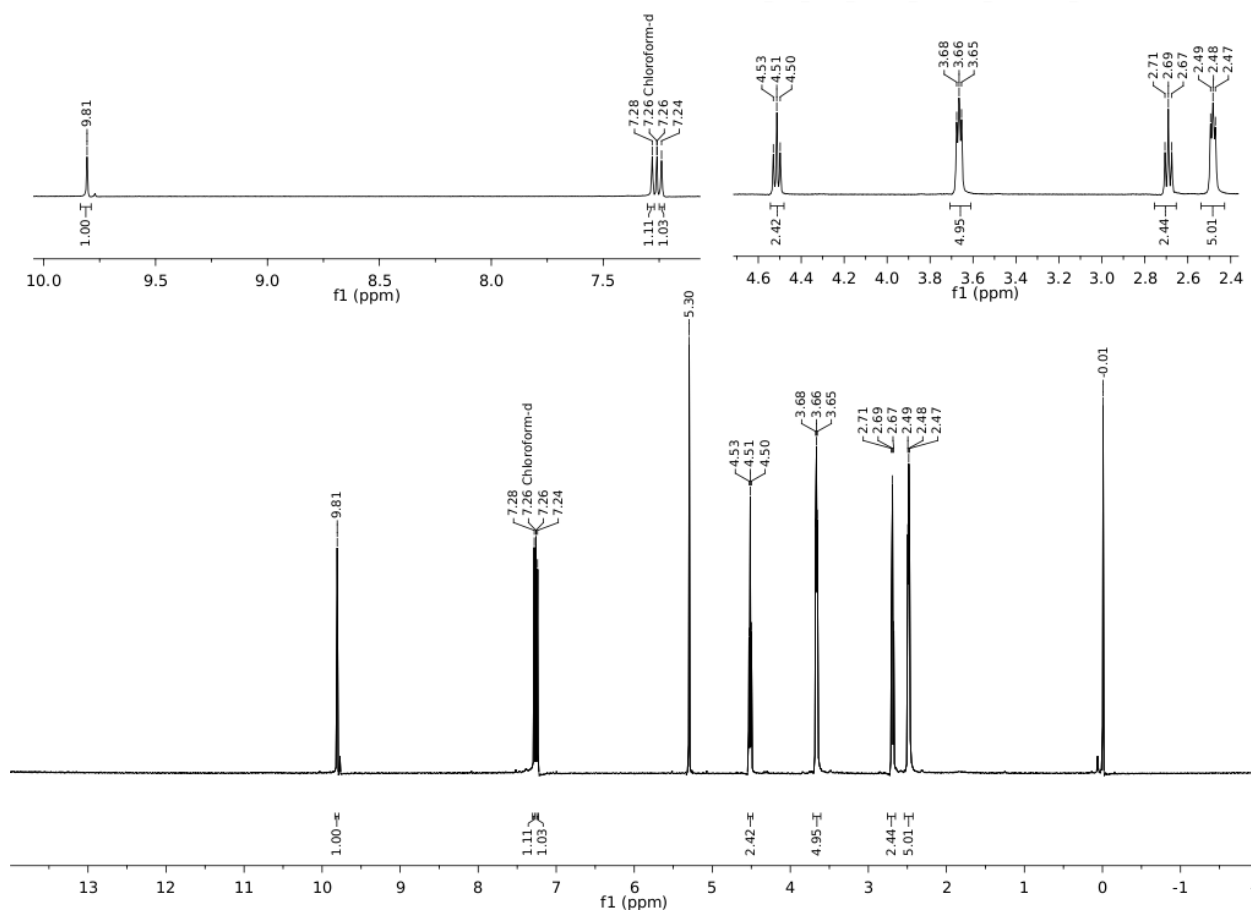


Figure 4.6. 1H NMR of (1-(2-morpholinoethyl)-1H-imidazole-2-carbaldehyde), $CDCl_3$, TMS, RT

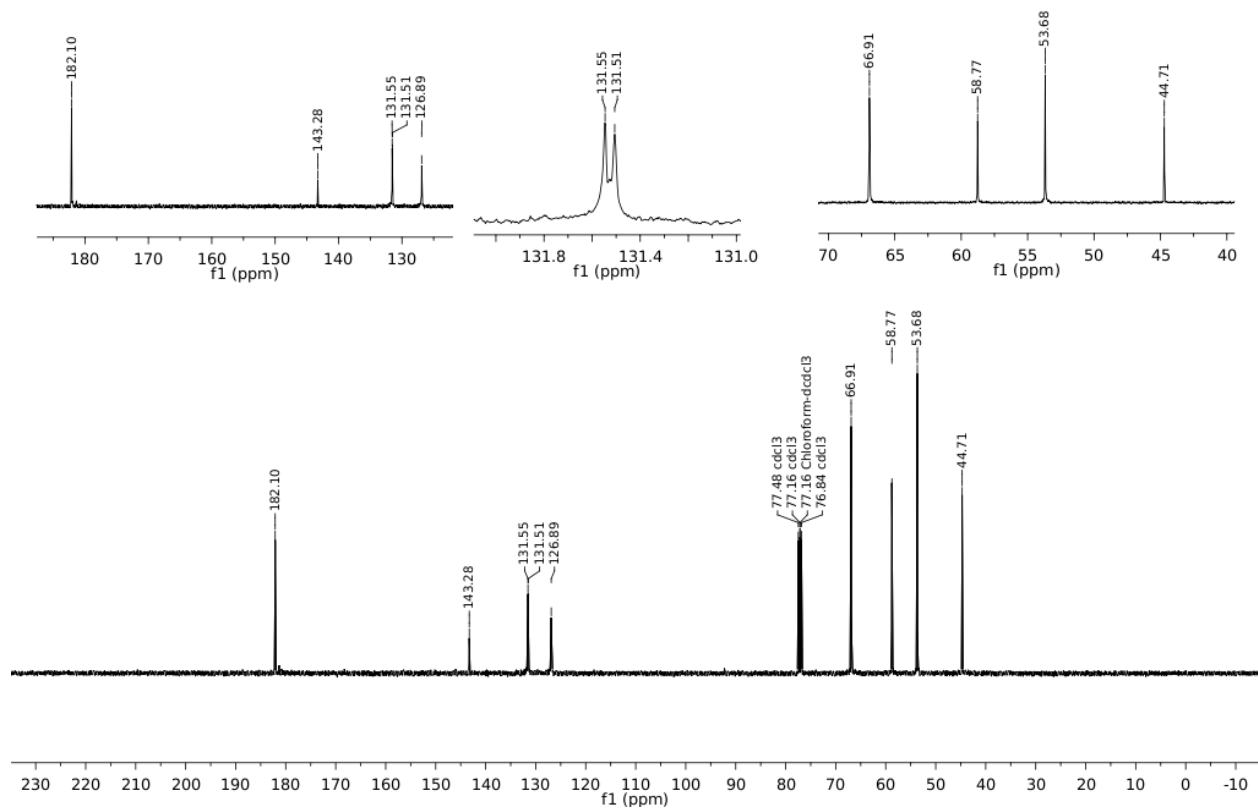


Figure 4.7. ^{13}C NMR of (1-(2-morpholinoethyl)-1H-imidazole-2-carbaldehyde), CDCl_3 , TMS, RT.

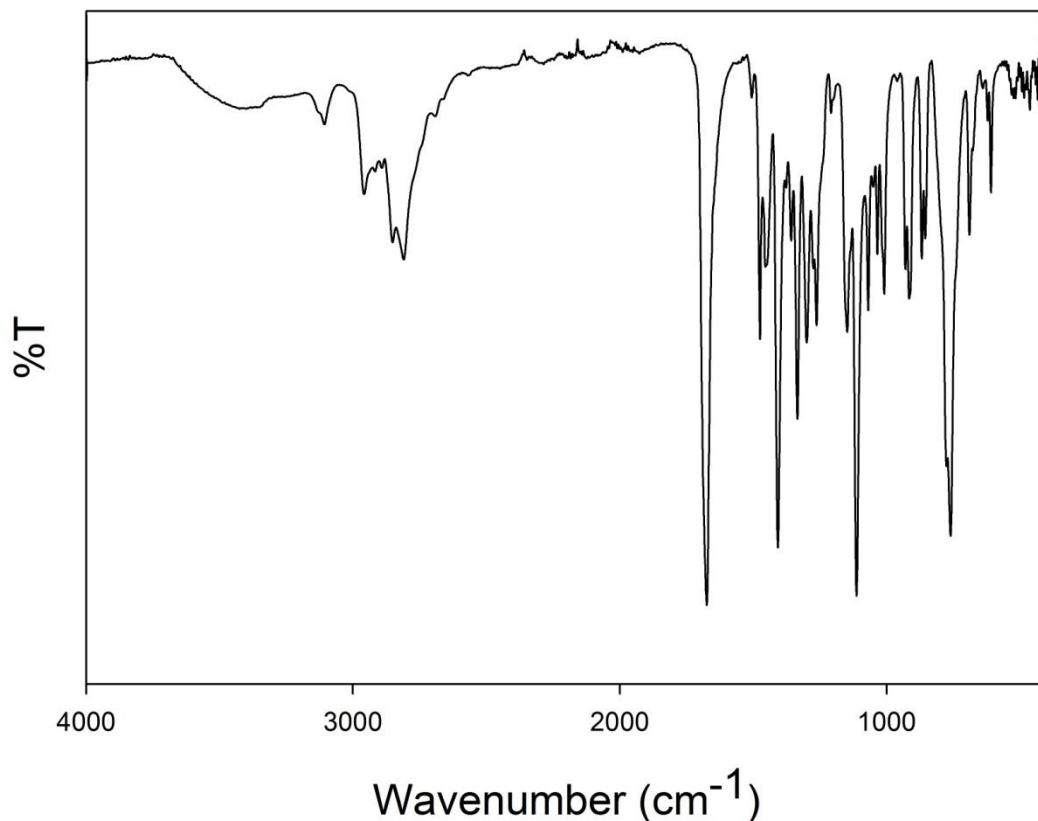


Figure 4.8. FTIR (ATR) of 1-(2-morpholinoethyl)-1H-imidazole-2-carbaldehyde).

*((N¹Z,N³E)-N¹,N³-bis((1-(2-morpholinoethyl)-1H-imidazol-2-yl)methylene)propane-1,3-diamine)
(LN₄^{Morph})*

To a 5 mL MeCN solution of 1-(2-morpholinoethyl)-1H-imidazole-2-carbaldehyde (0.2928 g, 0.0014 mmol) was added 1,3-diaminopropane (0.0519 g, 0.0584 mL, 0.0007 mmol). The flask was fit with a condenser and the temperature was brought to 60° C for 18 h. After this time, the solvent was removed by rotary evaporation to leave a yellow-brown oil. The oil was dissolved in 40 mL of EtOAc and washed with neutral deionized water to remove any unreacted material. The EtOAc soluble portion was dried with anhydrous MgSO₄, filtered, and concentrated to an amber oil (0.651 mmol, 0.297 g, 93%). ¹H NMR (400 MHz, CDCl₃, δ from

solvent): 8.31 (s, 1H, HC=N), 7.10 (s, 1H, ImH), 7.03 (s, 1H, ImH), 4.57 (t, 4H, ImNCH₂CH₂NMorpholine), $J = 8$ Hz, 2CH₂), 3.66 (m, 12H:8H from morpholine CH₂ and 4H from backbone, NCH₂), 2.67 (4.57 (t, 4H, ImNCH₂CH₂ Nmorpholine), 2.47 (t, 8H, CH₂ from morpholine), 2.02 (t, 2H, CH₂ backbone NCH₂CH₂CH₂N). ¹³C NMR (100.6 MHz, CDCl₃, δ from solvent): 153.62 (HC=N), 142.65 (C1, Im), 129.37 (ImC), 124.28 (ImC), 67.02 (CH₂), 59.53 (CH₂), 58.88 (CH₂), 53.87 (CH₂), 44.68 (CH₂), 32.42 (CH₂). FTIR (ATR), ν_{\max} (cm⁻¹): 3103 (w), 2937 (m), 2887 (m), 2850 (m), 2808 (m), 1646 (s), 1512 (w), 1471 (s), 1434 (s), 1357 (m), 1323 (w), 1334 (m), 1294 (s), 1274 (m), 1263 (m), 1206 (w), 1146 (m), 1113 (s), 1069 (m), 1034 (m), 1008 (m), 929 (m), 913 (m), 868 (s), 856 (m), 800 (m), 762 (s), 708 (s), 674 (w), 636 (w), 621 (w), 609 (m), 571 (w), 521 (w), 491 (w), 471 (w). LRMS-ESI (m/z): [M + H]⁺ calcd for C₂₃H₃₆N₈O₂ (% relative abundance), 457.3 (100), 458.3 (28.3), 459.3 (4.3); found, 457.3 (100), 458.3 (30.4), 459.3 (3.3).

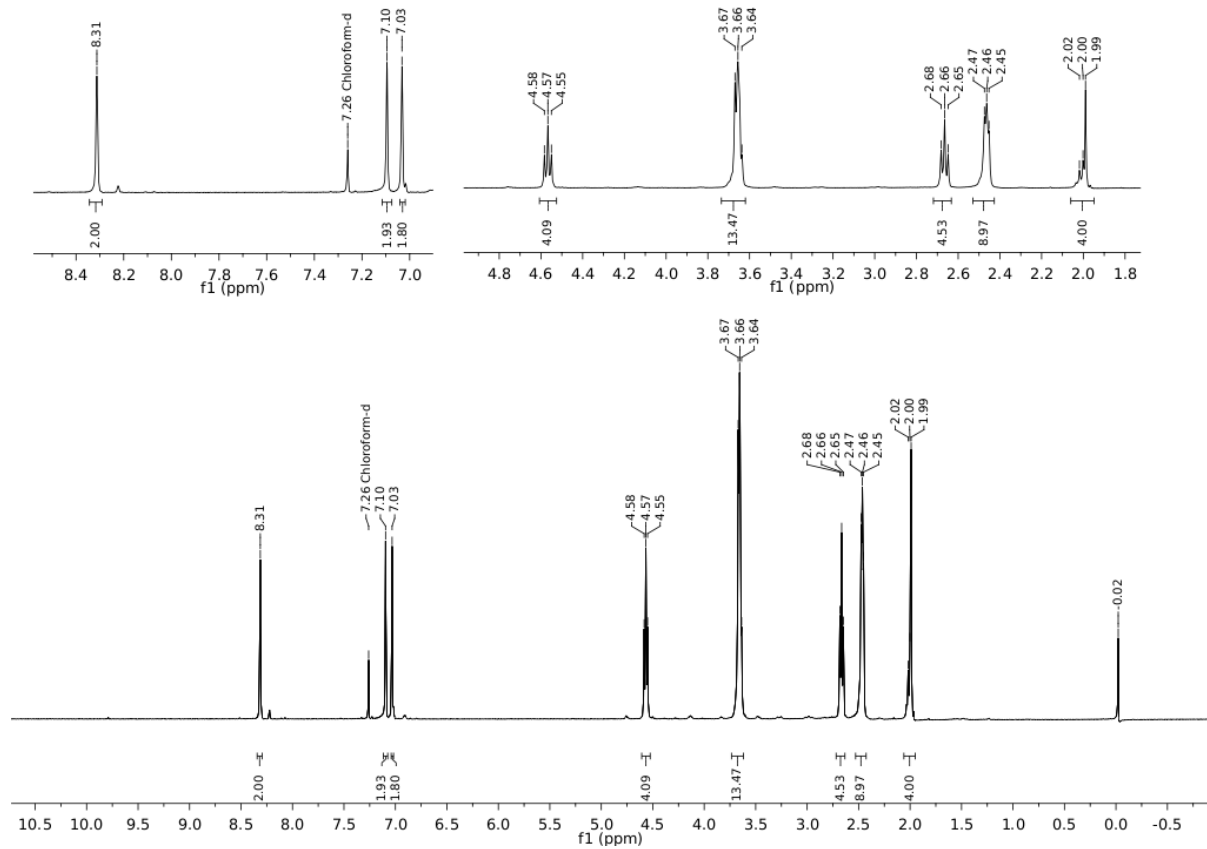


Figure 4.9. ¹H NMR ¹³C NMR of LN₄^{Morph}, CDCl₃, RT.

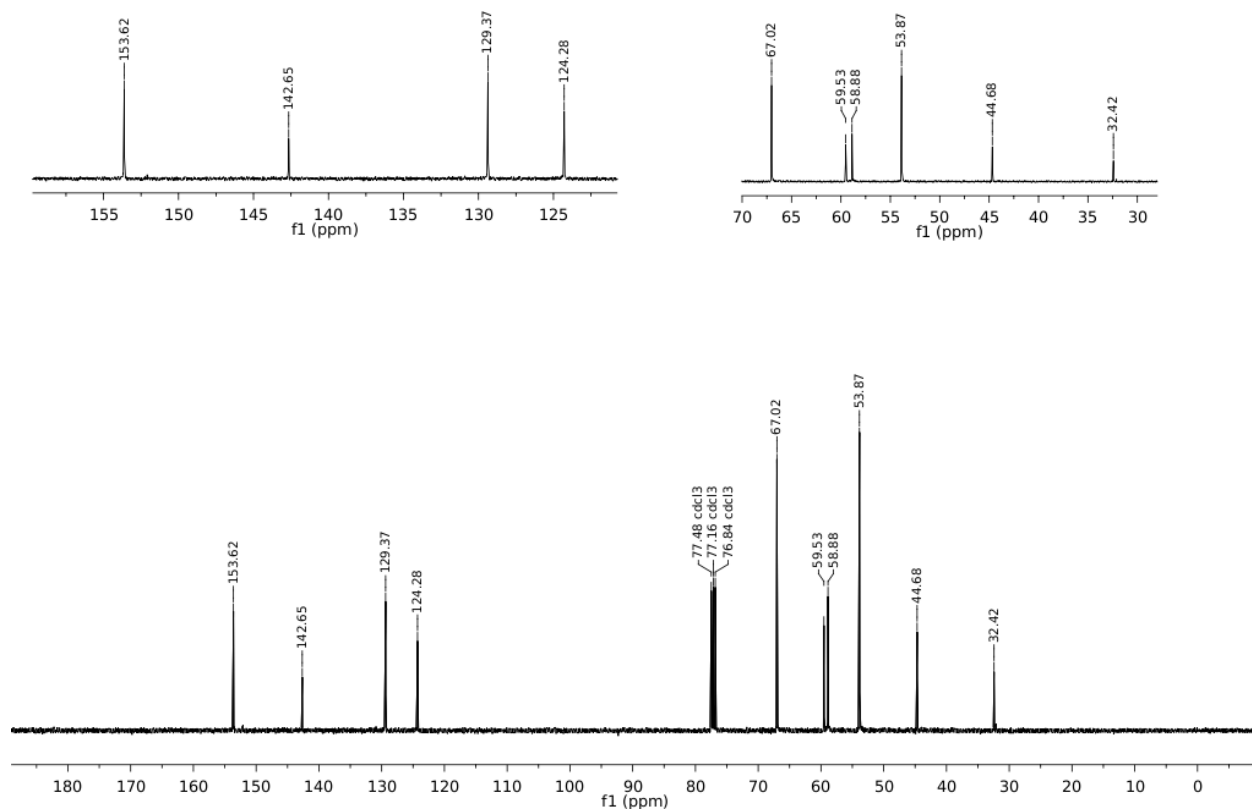


Figure 4.10. ^{13}C NMR of $\text{LN}_4^{\text{Morph}}$, CDCl_3 , RT.

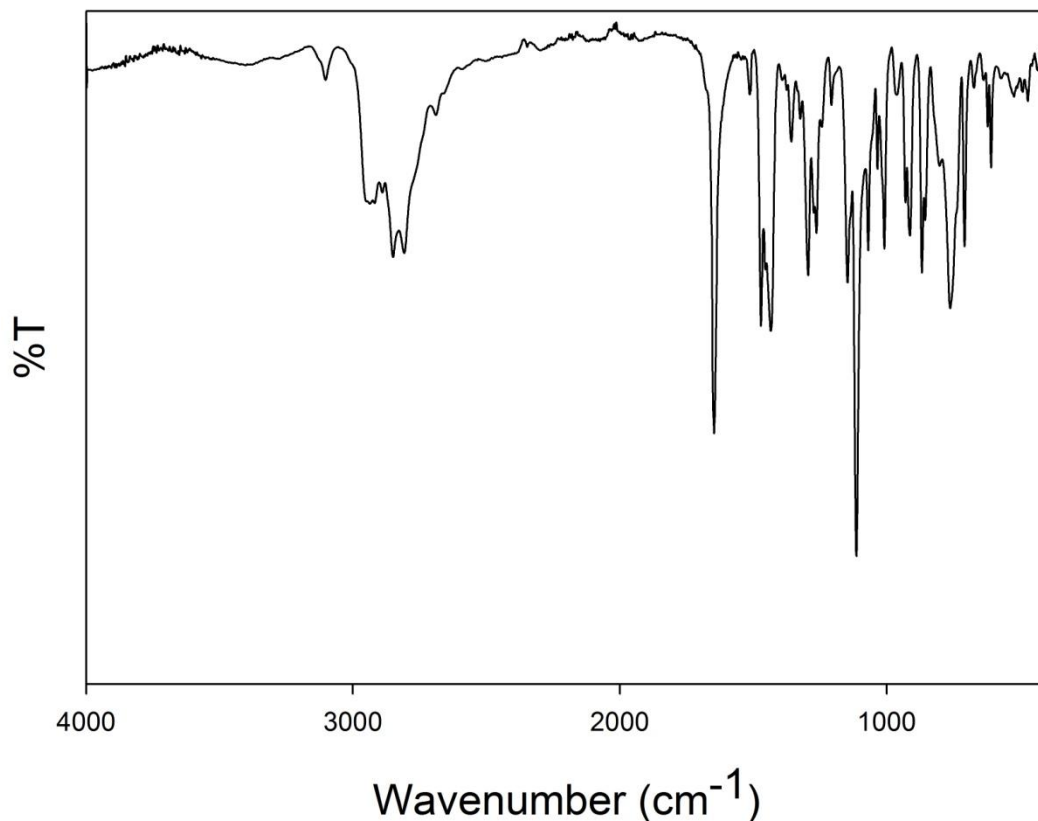
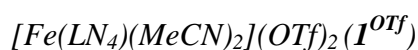


Figure 4.11. FTIR (ATR) of $\text{LN}_4^{\text{Morph}}$.

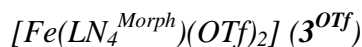


The synthesis of $\mathbf{1}^{\text{BF}_4}$ and $\mathbf{2}$ have been reported in previous work.³⁵ An analogous synthetic procedure from $\mathbf{1}^{\text{BF}_4}$ is used for $\mathbf{1}^{\text{OTf}}$ though $[\text{Fe}(\text{MeCN})_2(\text{OTf})_2]$ is used in place of $[\text{Fe}(\text{H}_2\text{O})_6](\text{BF}_4)_2$ to afford $[\text{Fe}(\text{LN}_4^{\text{Im}})(\text{MeCN})_2](\text{OTf})_2$ in 82% yield.³⁷ FTIR (KBr pellet), ν_{max} (cm^{-1}): 3411 (w), 3130 (m), 2944 (m), 2874 (w), 2310 (w), 2281 (m, $\nu_{\text{C}\equiv\text{N}}$), 2253 (m, $\nu_{\text{C}\equiv\text{N}}$), 1667 (m), 1629 (m), 1582 (w), 1542 (m), 1494 (s), 1455 (s), 1426 (s), 1391 (m), 1289 (vs), 1277 (vs), 1260 (vs), 1238 (vs), 1224 (vs), 1162 (vs), 1088 (w), 1030 (vs), 962 (m), 876 (m), 846 (m), 760 (s), 710 (m), 666 (m), 638 (vs), 573 (m), 517 (s). UV-vis (MeCN, 298 K), λ_{max} , nm: 476 and 455

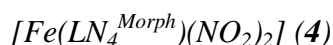
sh. LRMS-ESI (m/z): [$\{M - 2 \text{ MeCN} - 1 \text{ OTf}\}^{1+}$ calcd for $\text{C}_{14}\text{H}_{18}\text{F}_3\text{FeN}_6\text{O}_3\text{S}$ (relative abundance), 463.0 (100), 464.0 (20.4), 461.1 (6.4), 465.0 (5.4); found, 463.0 (100), 464.0 (17.0), 461.0 (5.9), 465.0 (6.1). μ_{eff} (solution, 293 K): 2.59 BM in CD_3CN . Non-zero μ_{eff} values have been observed with other low-spin Fe(II) complexes, which have been attributed to trace Fe impurities and/or a thermally-accessible singlet-to-triplet transition.⁵⁰⁻⁵²



To a 4 mL MeCN solution containing 0.1000 g (0.2190 mmol) of $\text{LN}_4^{\text{Morph}}$ was added a 2 mL MeCN solution containing 0.0813 g (0.2409 mmol) of $[\text{Fe}(\text{H}_2\text{O})_6](\text{BF}_4)_2$. Upon mixing, the color instantly changed from pale-yellow to dark-red indicative of complex formation. The homogeneous solution was stirred an additional 1 h at RT with no further changes. The solvent was then removed from the flask under reduced pressure to afford the dark-red solid product (0.1564 g, 0.2037 mmol, 93%). Diffraction quality crystals were grown from diffusion of Et_2O into an MeCN solution of $\mathbf{3}^{\text{MeCN}}$ at $-25\text{ }^\circ\text{C}$ that afforded the protonated morpholine product, $[\text{Fe}(\text{LN}_4^{\text{MorphH}_2})(\text{MeCN})_2](\text{BF}_4)_4$. FTIR (KBr pellet), ν_{max} (cm^{-1}): 3443 (m), 3150 (m), 2925 (m), 2854 (w), 2282 (m, $\nu_{\text{C}\equiv\text{N}}$), 2252 (m, $\nu_{\text{C}\equiv\text{N}}$), 1746 (w), 1660 (m), 1627 (m), 1537 (w), 1488 (m), 1450 (s), 1327 (w), 1304 (m), 1285 (m), 1263 (w), 1061 (vs, ν_{BF}), 929 (w), 907 (w), 874 (w), 854 (w), 765 (m), 714 (w), 521 (m). UV-vis (MeCN, 298 K), λ_{max} , nm: 477 and 455 sh. LRMS-ESI (m/z): [$\{M - 2 \text{ MeCN} - 2 \text{ BF}_4 + \text{H}_3\text{O}\}^{1+}$ calcd for $\text{C}_{23}\text{H}_{39}\text{FeN}_8\text{O}_3$ (relative abundance), 531.2 (100), 532.3 (25.5), 529.3 (6.4); found, 531.3 (100.0), 532.3 (31.2), 533.3 (4.8).



To a 4 mL MeCN solution containing 0.3000 g (0.6570 mmol) of LN_4^{Morph} was added a 3 mL MeCN solution containing 0.3008 g (0.6899 mmol) of $[Fe(MeCN)_4(OTf)_2]$.³⁷ Upon mixing, the color instantly changed from pale-yellow to dark-red indicative of complex formation. The homogeneous solution was stirred an additional 1 h at RT with no further changes. The solvent was then removed from the flask under reduced pressure to afford the dark-red solid product (0.4490 g, 0.5345 mmol, 84%). Diffraction quality crystals were grown from diffusion of Et_2O into an MeCN solution of **3** at -25 °C afforded the complex $[Fe(LN_4^{Morph})(OTf)_2]$. FTIR (KBr pellet), ν_{max} (cm^{-1}): 3125 (m), 2961 (m), 2854 (m), 2817 (w), 2279 (vw, $\nu_{C\equiv N}$), 2249 (vw, $\nu_{C\equiv N}$), 1666 (m), 1629 (m), 1536 (w), 1488 (s), 1450 (s), 1396 (w), 1359 (m), 1300 (vs, $\nu_{S=O}$), 1276 (vs, $\nu_{S=O}$), 1260 (vs, $\nu_{S=O}$), 1240 (vs, $\nu_{S=O}$), 1221 (vs, $\nu_{S=O}$), 1161 (s), 1115 (s), 1029 (vs), 928 (m), 910 (w), 872 (w), 854 (m), 767 (m), 713 (m), 637 (vs), 574 (m), 517 (m), 425 (s). UV-vis (MeCN, 298 K), λ_{max} , nm: 476 and 454 sh. LRMS-ESI (m/z): [$\{M - 2 MeCN - OTf\}^{1+}$ calcd for $C_{24}H_{36}F_3FeN_8O_5S$ (relative abundance), 661.2 (100), 662.2 (32.6), 663.2 (11.0); found, 661.1 (100), 662.1 (30.4), 663.1 (9.6). μ_{eff} (solution, 293 K): 3.28 BM in CD_3CN .



To a deep-red DMF solution (1 mL) containing 0.1000 g (0.1234 mmol) of $\mathbf{3}^{OTf}$ was added a homogeneous DMF solution (1 mL) containing 0.0210 g (0.2470 mmol) of KNO_2 and 0.0661 g (0.2500 mmol) of 18C6. Immediately upon addition of the $[K(18C6)]NO_2$ solution, the deep-red color instantly turned dark-purple. The solution was stirred for an additional 2 h at RT with no further changes. After this time, the solution was placed in a five dram vial and Et_2O was diffused overnight to give 0.0460 g (0.0761 mmol, 62%) of **4** after filtering and drying the dark-

violet solid. FTIR (KBr pellet), ν_{\max} (cm^{-1}): 3446 (w), 3116 (w), 2954 (m), 2916 (m), 2849 (m), 2811 (m), 1623 (w), 1578 (m), 1532 (w), 1488 (m), 1448 (s), 1394 (w), 1373 (w), 1336 (vs, ν_{NO_2}), 1299 (vs, ν_{NO_2}), 1281 (vs, ν_{NO_2}), 1223 (w), 1148 (s), 1115 (vs), 1083 (w), 1068 (m), 1031 (m), 1015 (w), 928 (m), 867 (w), 855 (w), 812 (m, δ_{NO_2}), 768 (m), 712 (w), 637 (s), 609 (w), 572 (w), 517 (w). UV-vis (1 mM ${}^n\text{Bu}_4\text{NNO}_2$, MeCN, 298 K) λ_{\max} , nm 410, 540, 574. LRMS-ESI (m/z): $[\text{M} - \text{NO}_2]^+$ calcd. for $\text{C}_{23}\text{H}_{36}\text{FeN}_9\text{O}_4$ (relative abundance), 558.2 (100.0), 559.2 (31.0), 556.2 (6.4), 560.2 (5.8); found, 558.4 (100.0), 559.4 (33.8), 556.4 (6.1), 560.3 (7.1). μ_{eff} (solution, 293 K): 0.51 BM in CD_3CN with five equiv of ${}^n\text{Bu}_4\text{NNO}_2$. Non-zero μ_{eff} values have been observed with other low-spin Fe(II) complexes, which have been attributed to trace Fe impurities and/or a thermally-accessible singlet-to-triplet transition.⁵⁰⁻⁵²

[Fe(LN₄)]

The synthesis and characterization of (N^1E, N^3E)- N^1, N^3 -bis((1H-pyrrol-2-yl)methylene)propane-1,3-diamine (LN_4H_2) have been reported in previous work.³⁶ To a heterogeneous solution of LN_4H_2 (0.3000 g, 1.314 mmol) prepared in 9 mL of MeCN was added two equivs. of an NaH slurry (0.0631 g, 2.628 mmol) in 2 mL MeCN while stirring. During a period of 20 min, intermittent vacuum was applied to remove $\text{H}_2(\text{g})$, which afforded a pink wine-colored homogeneous solution. At this point, the $[\text{Na}_2\text{LN}_4]$ solution was treated with one equiv of $[\text{Fe}(\text{H}_2\text{O})_6](\text{BF}_4)_2$ (0.4435 g, 1.314 mmol) as a homogeneous solution in 3 mL of MeCN while stirring vigorously. Immediately upon mixing a brown-colored solution appeared with concomitant precipitation of a light-colored amorphous material. This mixture was stirred for an additional 2 h with no further change. The MeCN was evaporated under reduced pressure to afford a dark solid material. The residue was treated with 3×5 mL of CH_2Cl_2 to precipitate

NaBF₄. The CH₂Cl₂ insoluble, white solid material was filtered and dried to afford 0.2790 g (2.537 mmol, 97%) of NaBF₄ (0.2890 g expected for 2.628 mmol NaBF₄). The CH₂Cl₂ filtrate was then concentrated and treated with 5 mL of Et₂O to afford 0.2891 g (1.025 mmol, 78%) of a brown solid after filtration. FTIR (KBr matrix), ν_{\max} (cm⁻¹): 3246 (w), 3084 (w), 2916 (w), 2848 (w), 1599 (vs), 1508 (w), 1435 (m), 1392 (m), 1361 (m), 1332 (w), 1310 (m), 1263 (w), 1191 (w), 1116 (w), 1073 (w), 1031 (s), 895 (w), 882 (w), 739 (s), 612 (w).

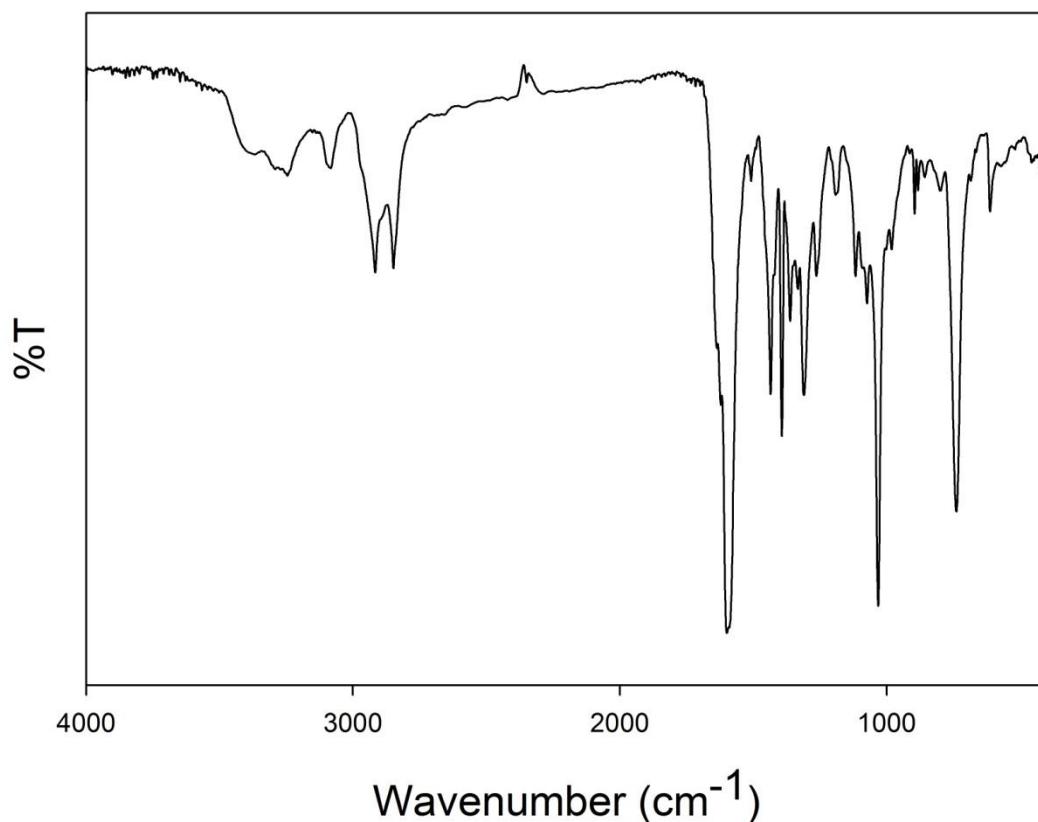
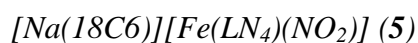


Figure 4.12. FTIR (KBr) of [Fe(LN₄)].



To a 3 mL DMF solution of [Fe(LN₄)] (0.1000 g, 0.3545 mmol) was added a 1 mL DMF solution of KNO₂ (0.0269 g, 0.3899 mmol) and 18C6 (0.1124 g, 0.4254 mmol). Upon addition, a

slight color change from brown to red-brown occurred with no observed precipitation. This solution was stirred for an additional 1 h before removing DMF by short-path distillation. The residue was washed with 3×10 mL of Et₂O to afford a brown solid (0.1767 g of a mixture of **5** and {FeNO}⁷). FTIR (KBr matrix), ν_{\max} (cm⁻¹): 3445 (m), 3089 (w), 2908 (m), 2870 (s), 1699 (m, ν_{NO} , {FeNO}⁷), 1657 (w), 1605 (vs), 1586 (vs), 1470 (m), 1453 (m), 1435 (m), 1391 (m), 1364 (m), 1353 (m), 1252 (s, ν_{NO}), 1108 (vs), 1031 (s), 951 (m), 896 (w), 835 (w), 828 (w, δ_{NO_2}), 798 (w), 734 (s), 681 (w), 610 (w). UV-vis (MeCN, 298 K), λ_{\max} , nm: 293, 513, 708. LRMS-ESI (m/z): [M – Na(18C6)]⁻ calcd. for C₁₃H₁₄FeN₅O₂ (relative abundance), 328.0 (100.0), 329.1 (16.6); found, 328.0 (100.0), 329.0 (22.6).

[Na(18C6)][Fe(LN₄)(¹⁵NO₂)]

The isotopically-labeled complex [Na(18C6)][Fe(LN₄)(¹⁵NO₂)] was prepared analogously to **5** except for using 0.1000 g (0.3545 mmol) of [Fe(LN₄)], 0.0248 g (0.3545 mmol) of Na¹⁵NO₂, and 0.1031 g (0.3899 mmol) of 18C6. Yield: 0.0520 g (0.2907 mmol, 82%). FTIR (KBr pellet), ν_{\max} of isotope-sensitive peaks (cm⁻¹): 1208 (s, sh, $\Delta\nu_{\text{NO}_2} = \sim 42$ cm⁻¹), 821 (w, $\Delta\delta_{\text{NO}_2} = 7$ cm⁻¹).

4.6.4 Reactivity Studies

NO Reactivity

The reactivity of **1**^{BF₄} is reported in Chapter 3 Part A. For **3**^{BF₄}, 0.0500 g (0.0651 mmol) was dissolved in 3 mL of MeOH and NO(g) was purged directly into the solution for 90 s. This resulted in a rapid color change from red to brown-green. After applying vacuum, the color went

back to the starting red instantly. The solution was concentrated and characterized by FTIR and indicated reformation of $\mathbf{3}^{\text{BF}_4}$.

Spectroelectrochemistry

A 3 mL, 10 mM MeCN (0.1 M Bu₄NPF₆) solution was prepared anaerobically and added to the cuvette with a syringe fixed with a 0.45 μm filter. The cuvette was kept under positive N₂ pressure through a direct gas purge in to the cuvette headspace. The potential was held at +0.5 V vs. AgNO₃/Ag for ~90 s while scans were recorded every 30 s for 5 min total. Observations are described in the text.

Reactivity of 4 with para-chlorobenzenethiol (HSAr-p-Cl).

To a 2 mL anaerobic MeCN solution of **4** (20.0 mg, 0.0331 mmol) was added a 1.0 mL MeCN solution of HSAr-*p*-Cl (19.1 mg, 0.1324 mmol). The resulting solution showed no immediate change. The reaction mixture stirred at RT for 24 h. After 24 h, the red-purple colored solution was concentrated under vacuum and stirred with 10 mL of Et₂O to afford an Et₂O-insoluble dark-red compound (23.0 mg, 0.0267 mmol, 81%) currently assigned as (LN₄^{MorphH})[Fe(*p*-ClArS)₂(NO)₂]. The Et₂O-soluble material was concentrated to a pale solid (10.0 mg, 0.0348 mmol, 53% based on RSH equivs.) and characterized by ¹H NMR, which revealed a mixture of the disulfide of HSAr-*p*-Cl and ~1% of free LN₄^{Morph} based on integration. The products from this reaction were characterized by FTIR, UV-vis, ¹H NMR and ESI-MS.

4.7 Supporting Information

X-ray Crystallographic Data Collection and Structure Solution and Refinement.

Red crystals of $[\text{Fe}(\text{LN}_4^{\text{MorphH2}})(\text{MeCN})_2](\text{BF}_4)_4 \cdot 4\text{MeCN}$ ($\mathbf{3}^{\text{BF}_4} \cdot 4\text{MeCN}$) were grown under anaerobic conditions by slow diffusion of Et_2O into an MeCN solution of $\mathbf{3}^{\text{BF}_4}$ at $-25\text{ }^\circ\text{C}$. Pale-red crystals of $[\text{Fe}(\text{LN}_4^{\text{Morph}})(\text{OTf})_2]$ ($\mathbf{3}^{\text{OTf}}$) were grown under anaerobic conditions by slow diffusion of Et_2O into a MeCN solution of $\mathbf{3}^{\text{OTf}}$ at $-25\text{ }^\circ\text{C}$. Suitable crystals were mounted on a glass fiber. The X-ray intensity data were measured at 100 K on a Bruker SMART APEX II X-ray diffractometer system with graphite-monochromated Mo $K\alpha$ radiation ($\lambda = 0.71073\text{ \AA}$) using ω -scan technique controlled by the SMART software package.⁵³ The data were collected in 1464 frames with 10 s exposure times. The data were corrected for Lorentz and polarization effects⁵⁴ and integrated with the manufacturer's SAINT software. Absorption corrections were applied with the program SADABS.⁵⁵ Subsequent solution and refinement was performed using the SHELXTL 6.1 solution package operating on a Pentium computer.^{56,57} The structure was solved by direct methods using the SHELXTL 6.1 software package.^{56,57} Non-hydrogen atomic scattering factors were taken from the literature tabulations.⁵⁸ Except for two hydrogen atoms H(7) and H(8) bonded with the atoms N(7) and N(8) that were located from difference Fourier map and refined with proper restraints, the rest of the hydrogen atom positions were calculated and allowed to ride on the carbon to which they are bonded assuming a C–H bond length of $m\text{ \AA}$ ($m = 0.95$ for CH groups, $m = 0.99$ for CH_2 groups, $m = 0.98$ for CH_3 groups). Hydrogen atom temperature factors were fixed at n ($n = 1.2$ for CH and CH_2 groups, $n = 1.5$ for CH_3 groups) times the isotropic temperature factor of the C-atom to which they are bonded. Selected data and refinement parameters for $\mathbf{3}^{\text{BF}_4}$ and $\mathbf{3}^{\text{OTf}}$ are summarized in Table S1. Selected bond distances and angles for $\mathbf{3}^{\text{BF}_4}$ and $\mathbf{3}^{\text{OTf}}$ are given in Table S2. Perspective views of the complexes were obtained using ORTEP.⁵⁹

Table S1. Summary of crystal data and intensity collection and structure refinement parameters for $[\text{Fe}(\text{LN}_4^{\text{Morph}})(\text{MeCN})_2](\text{BF}_4)_2 \cdot \text{MeCN}$ (**3^{BF4}**•4MeCN) and $[\text{Fe}(\text{LN}_4^{\text{Morph}})(\text{OTf})_2]$.

Parameters	3^{BF4} •4MeCN	3^{OTf}
Formula	C ₃₅ H ₅₆ B ₄ F ₁₆ Fe N ₁₄ O ₂	C ₂₅ H ₃₆ F ₆ FeN ₈ O ₈ S ₂
Formula weight	1108.0	810.6
Crystal system	Triclinic	Triclinic
Space group	<i>P</i> -1	<i>P</i> -1
Crystal color, habit	Red	Pale-red
<i>a</i> , Å	11.132(2)	9.976(3)
<i>b</i> , Å	15.575(3)	12.342(4)
<i>c</i> , Å	16.803(3)	15.142(5)
α , deg	103.997(4)	66.846(5)
β , deg	104.405(4)	88.148(5)
γ , deg	108.096(3)	72.580(5)
<i>V</i> , Å ³	2515.7(9)	1627.8(9)
<i>Z</i>	2	2
ρ_{calcd} , g/cm ³	1.463	1.654
<i>T</i> , K	100	100
abs coeff, μ (Mo K α), mm ⁻¹	0.407	0.687
θ limits, deg	1.999 to 25.500	2.378 to 26.022
total no. of data	21607	19375
no. of unique data	9390	6405
no. of parameters	664	234
GOF of F ²	1.000	0.998
R_1 , ^[a] %	8.28	6.85
wR_2 , ^[b] %	13.18	15.12
max, min peaks, e/Å ³	0.7456, 0.6233	0.7454, 0.5895

$$^a R_1 = \sum |F_o| - |F_c| / \sum |F_o| ; ^b wR_2 = \{\sum [w(F_o^2 - F_c^2)^2] / \sum [w(F_o^2)^2]\}^{1/2}$$

Table S2. Selected bond distances (Å) and bond angles (deg) for [Fe(LN₄^{MorphH2})(MeCN)₂](BF₄)₄•4MeCN (**3^{BF4}**•4MeCN) and [Fe(LN₄^{Morph})(OTf)₂] (**3^{OTf}**).

3^{BF4} •4MeCN		3^{OTf}	
Fe1-N9	1.917(6)	Fe1-O3	2.187(4)
Fe-N10	1.936(6)	Fe-O6	2.249(4)
Fe1-N4	1.936(6)	Fe1-N4	2.188(4)
Fe1-N3	1.952(6)	Fe1-N3	2.168(4)
Fe1-N5	1.977(6)	Fe1-N5	2.110(4)
Fe-N1	1.993(6)	Fe-N1	2.138(4)
N1-Fe1-N10	90.4	N1-Fe1-O3	92.02
N3-Fe1-N10	91.0	N3-Fe1-O3	90.70
N4-Fe1-N10	89.0	N4-Fe1- O3	94.55
N5-Fe1-N10	87.3	N5-Fe1- O3	90.49
N1-Fe1-N9	92.0	N1-Fe1-O6	85.32
N3-Fe1-N9	91.7	N3-Fe1-O6	90.79
N4-Fe1-N9	88.7	N4-Fe1-O6	88.56
N5-Fe1-N9	89.9	N5-Fe1-O6	88.79
N10-Fe1-N9	176.6	O3-Fe1-O6	176.6
N1-Fe1-N3	81.8	N1-Fe1-N3	77.83
N3-Fe1-N4	95.0	N3-Fe1-N4	87.57
N4-Fe1-N5	81.7	N4-Fe1-N5	78.59
N5-Fe1-N1	101.5	N5-Fe1-N1	115.91

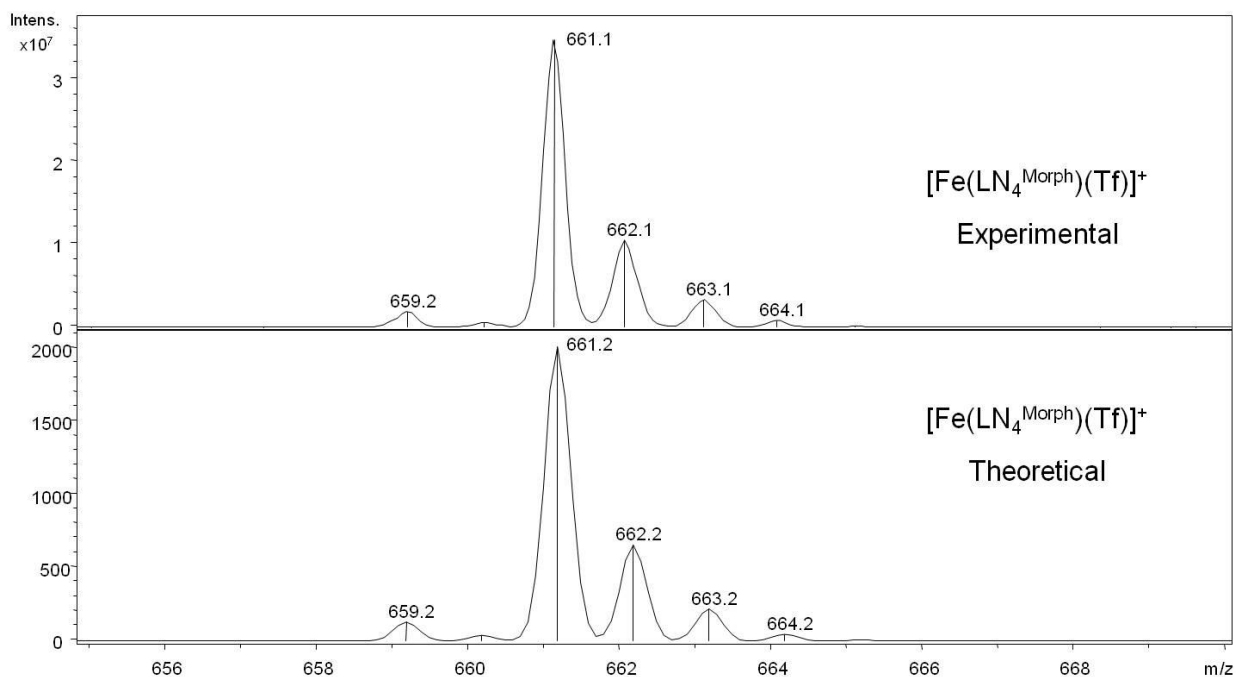
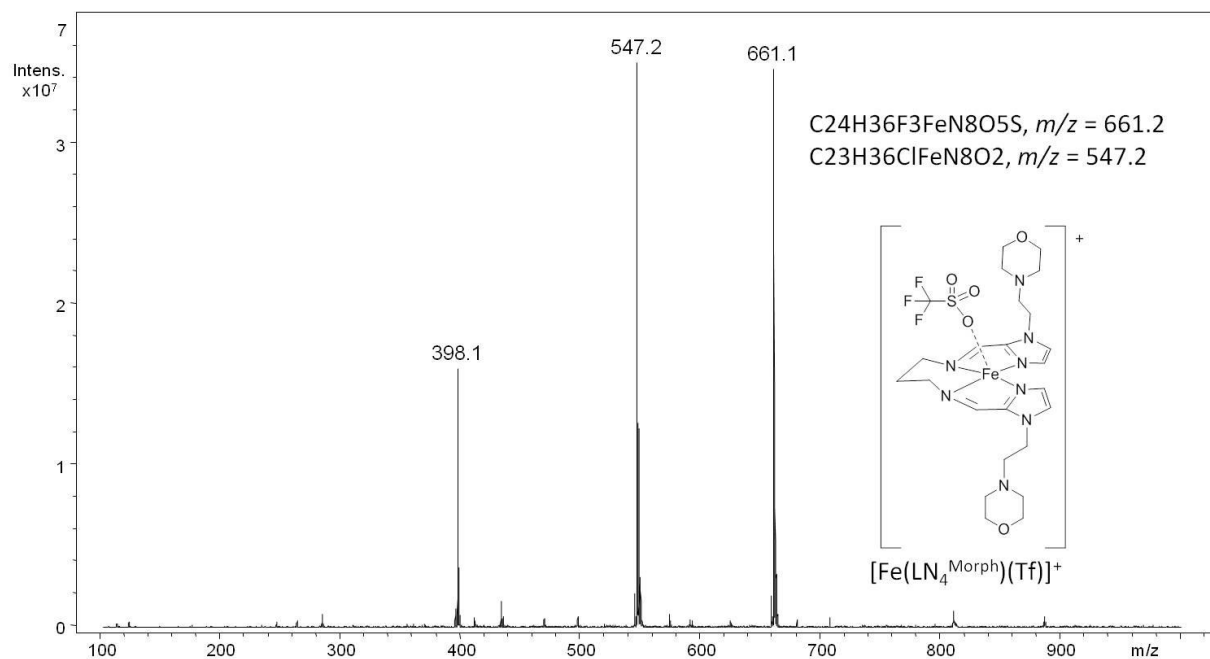


Figure S1. Low-resolution ESI-MS (positive mode) from the reaction of **3** (MeCN). Peak at m/z : 661.1 corresponds to the cation of **3** $[Fe(LN_4^{Morph})(OTf)]^+$. Peak at m/z : 547.2 corresponds to the cation $[Fe(LN_4^{Morph})(Cl)]^+$ presumably from contamination of Cl^- in ESI-MS experiment. *Bottom:* Theoretical MS for cation of **3**, $[Fe(LN_4^{Morph})(OTf)]^+$.

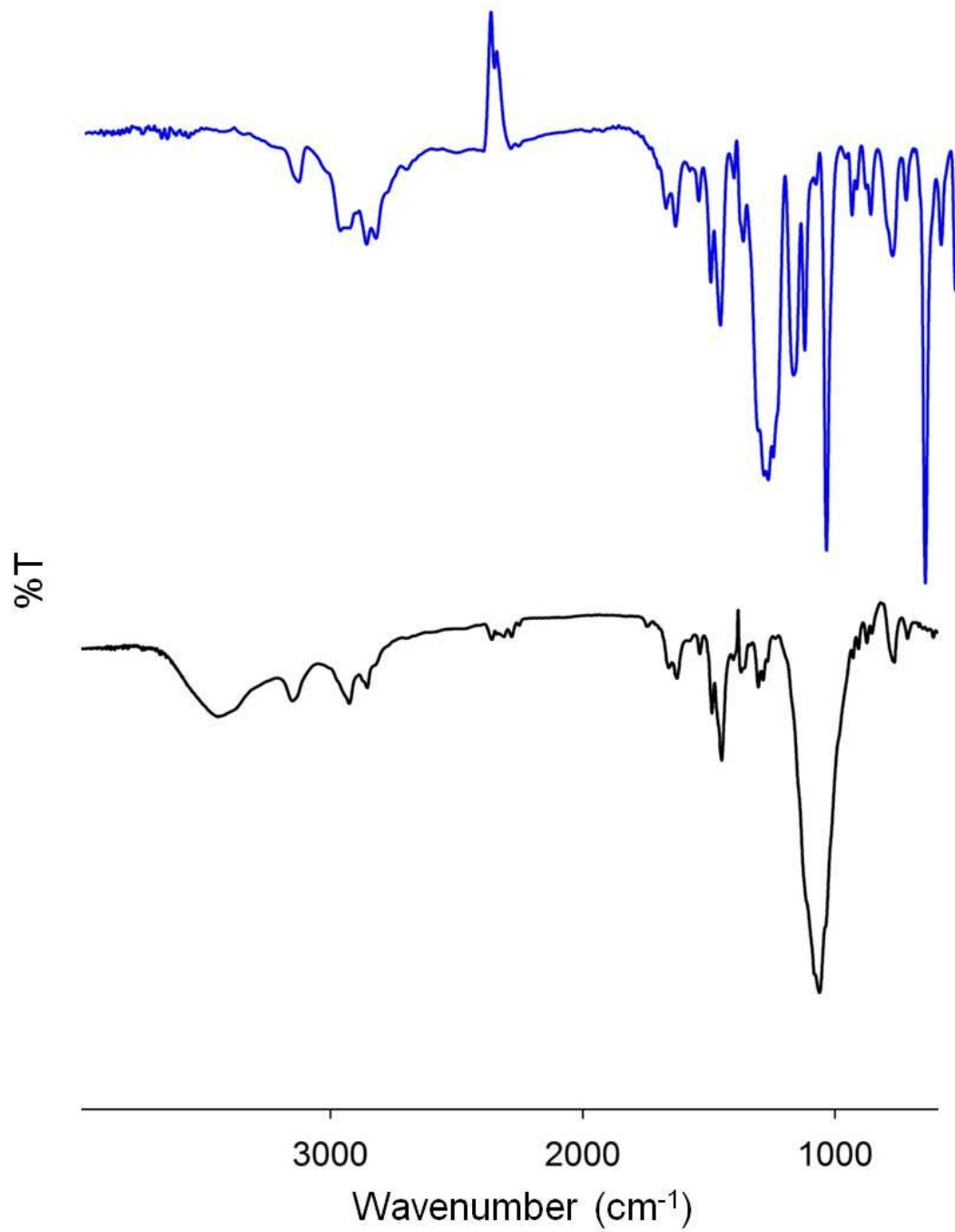


Figure S2. FTIR (KBr, RT) of **3^{OTf}** (blue trace) and **3^{BF4}** (black trace).

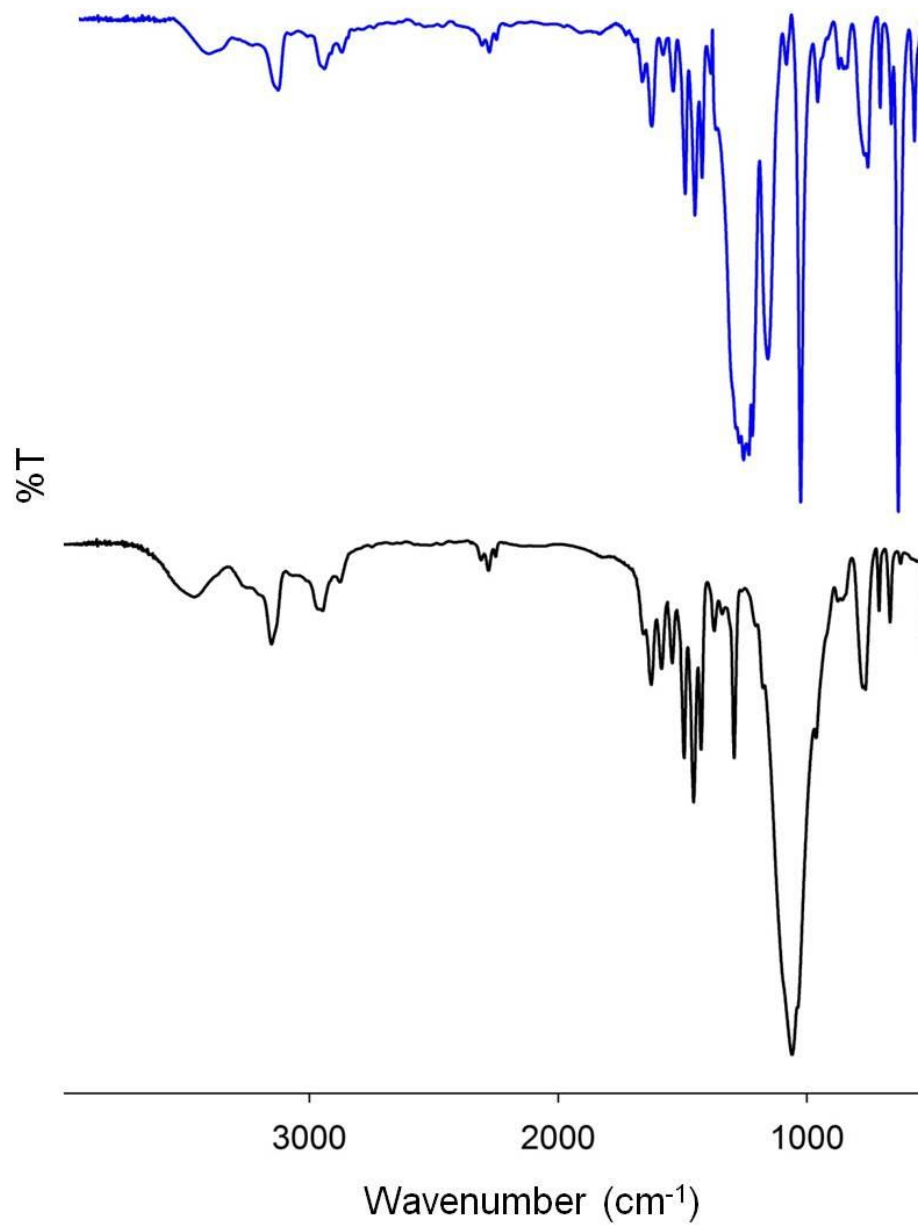


Figure S3. FTIR (KBr, RT) of **1**^{OTf} (blue trace) and **1**^{BF4} (black trace).

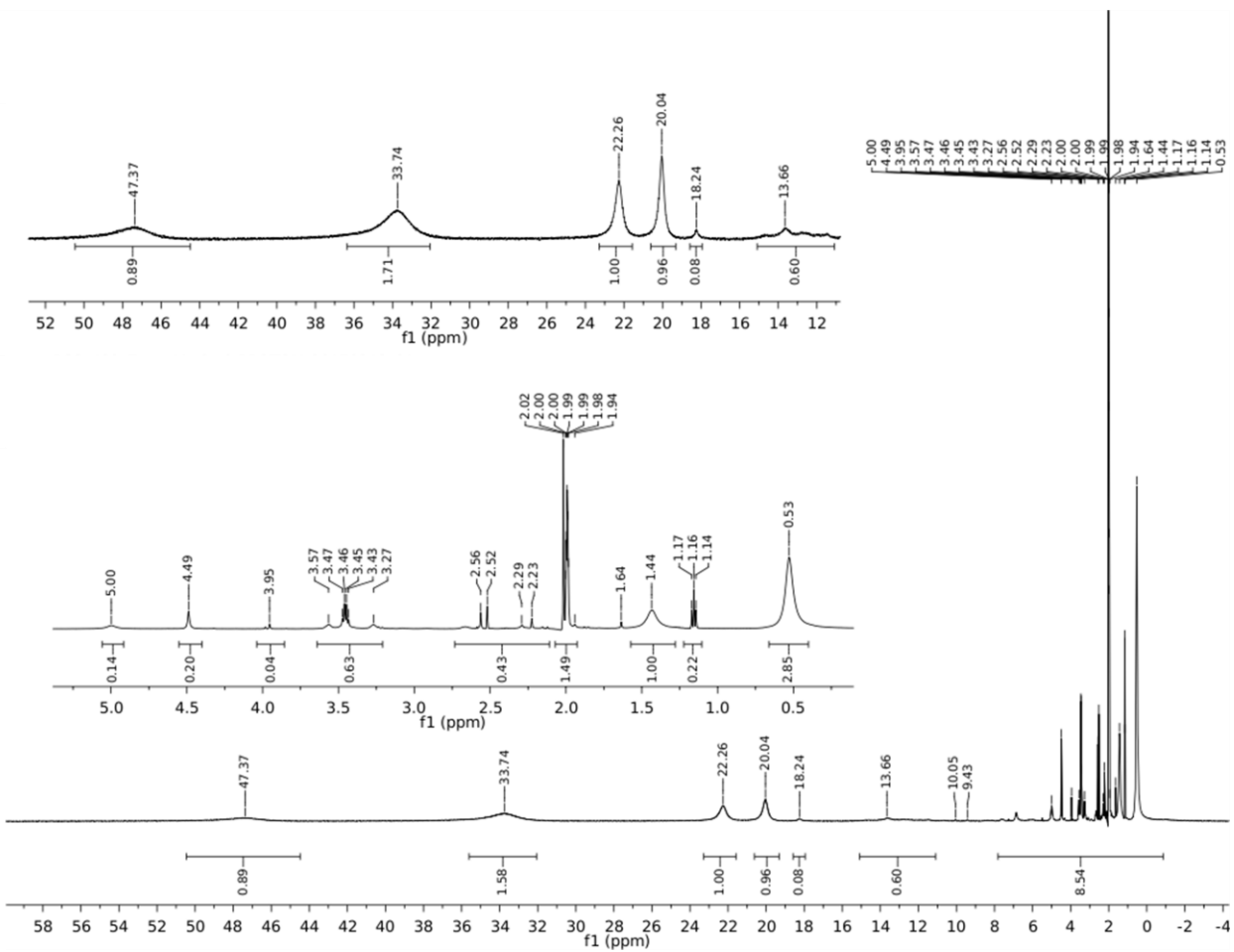


Figure S4. ^1H NMR of 1^{OTf} indicating downfield resonances due to paramagnetism.

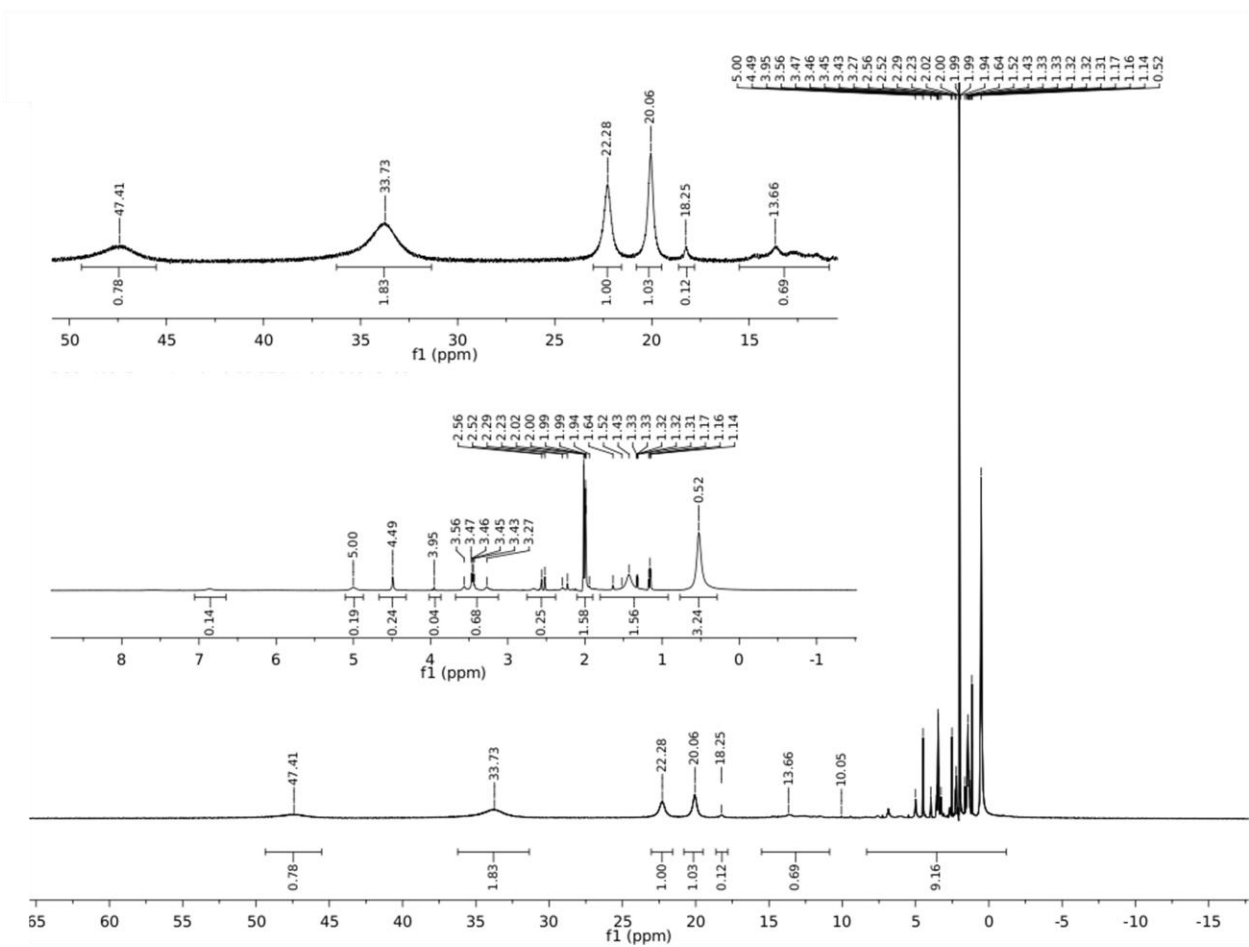


Figure S5. ^1H NMR of 3^{OTf} indicating downfield resonances due to paramagnetism.

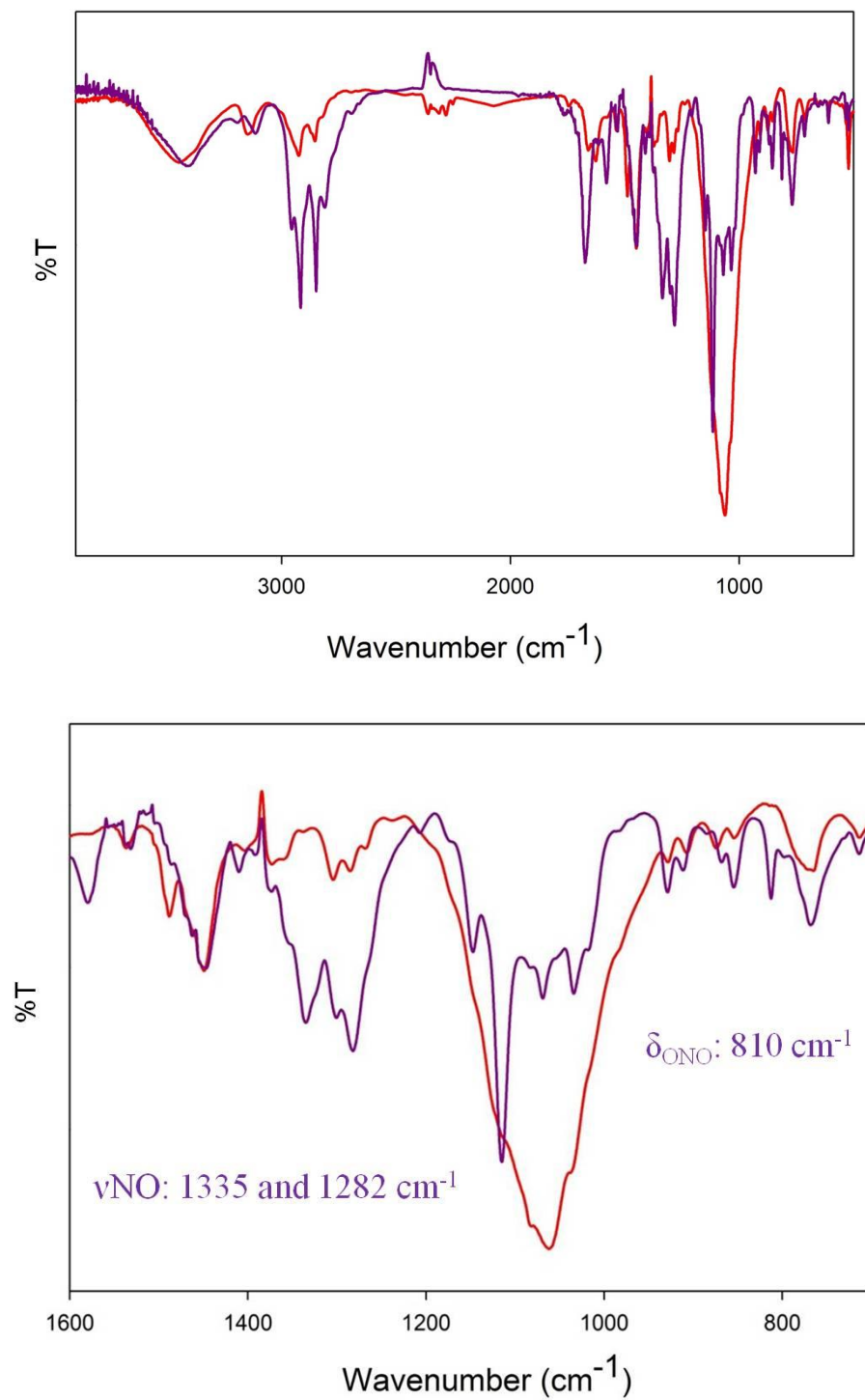


Figure S6. Top: Solid-state FTIR spectra of 3^{BF_4} (red trace) and **4** (purple trace). Bottom: Zoom-in (1600-700 cm⁻¹) showing ν_{NO} region and δ_{ONO} region (KBr matrix).

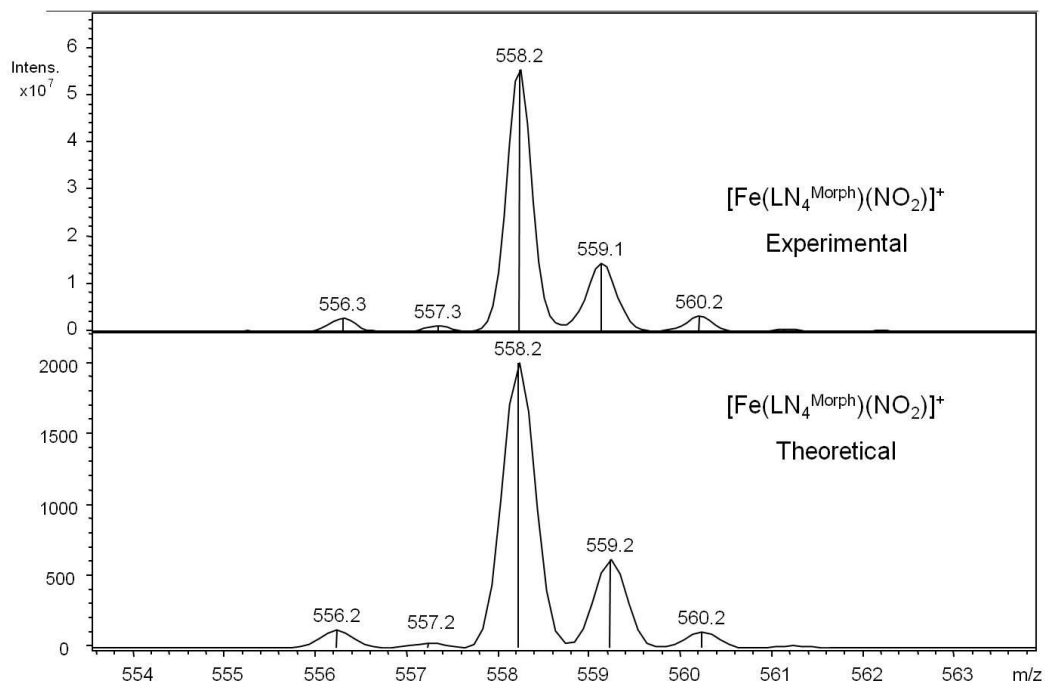
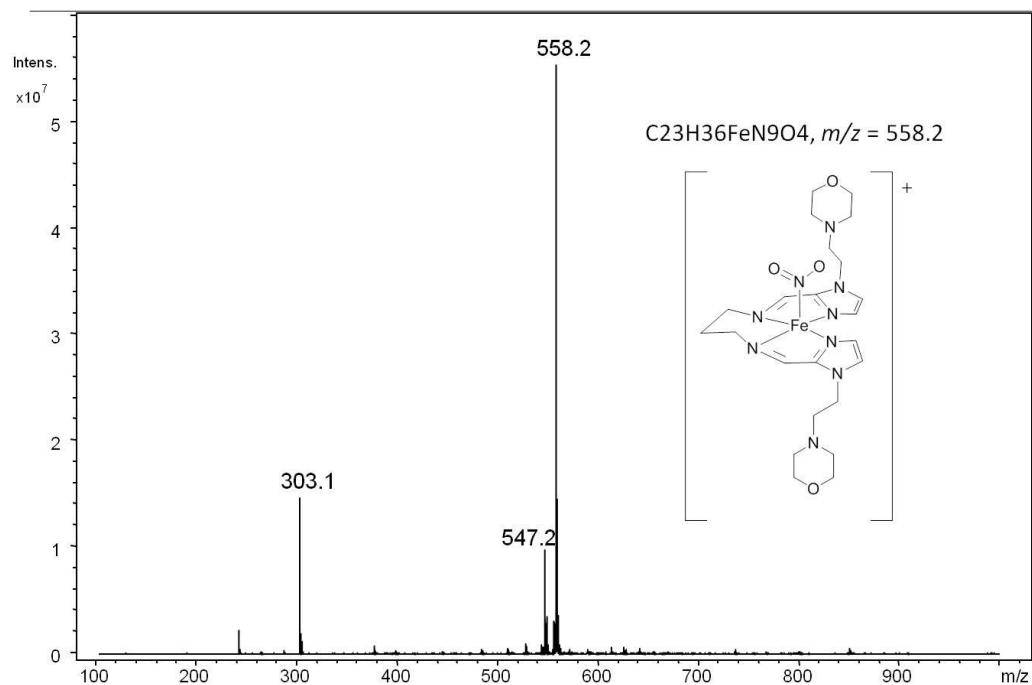


Figure S7. Top: LRESI-MS of **4**. Bottom: Experimental and theoretical fit for $[Fe(LN_4^{Morph})(NO_2)]^+$.

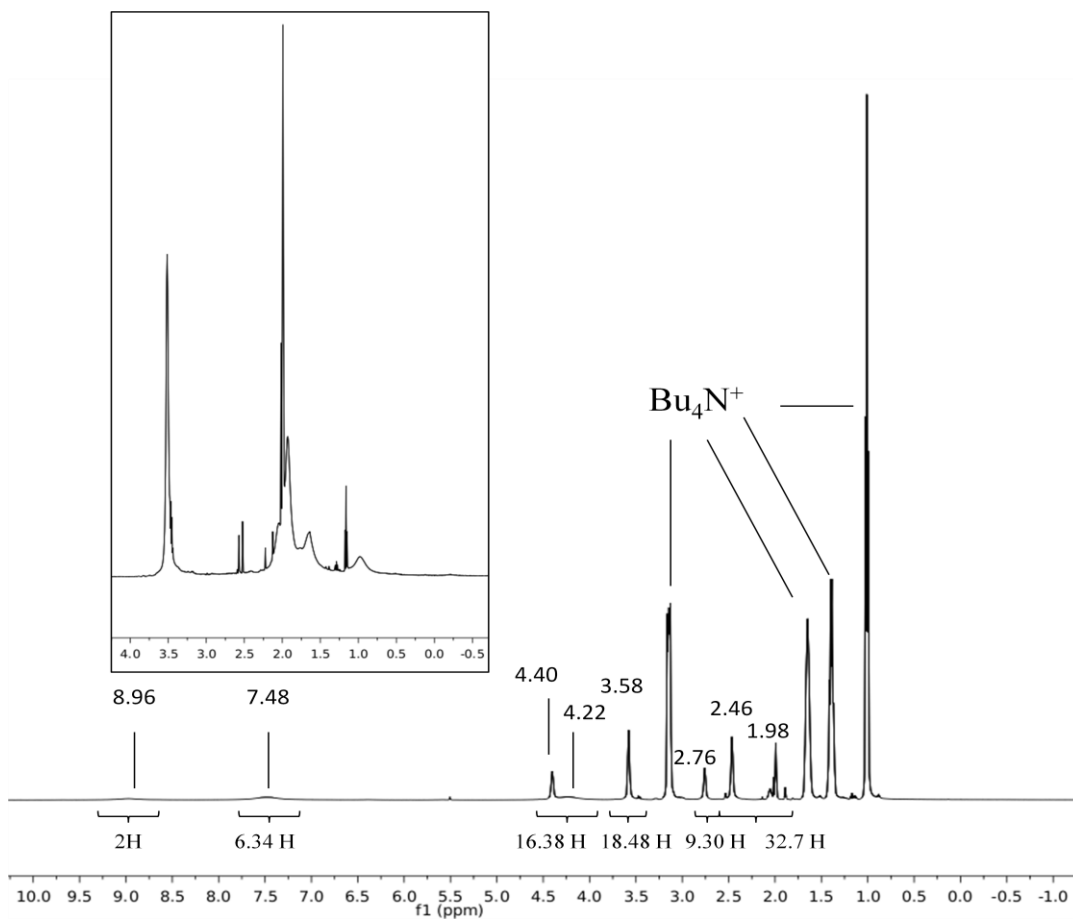


Figure S8. ^1H NMR of $\mathbf{3}^{\text{OTf}}$ and ${}^n\text{Bu}_4\text{NNO}_2$. Inset: diamagnetic region of $\mathbf{3}^{\text{OTf}}$ before ${}^n\text{Bu}_4\text{NNO}_2$.

CD_3CN , 20 $^\circ\text{C}$.

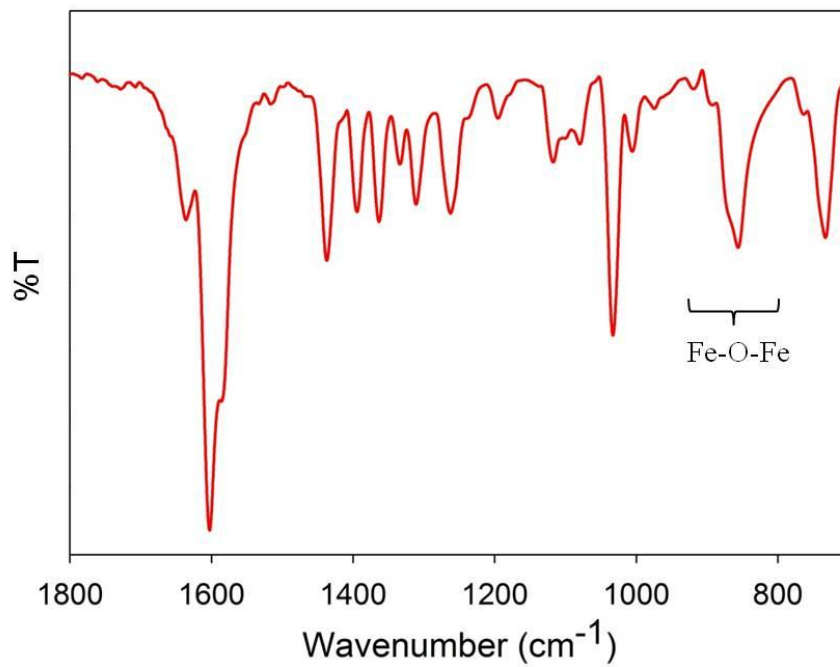
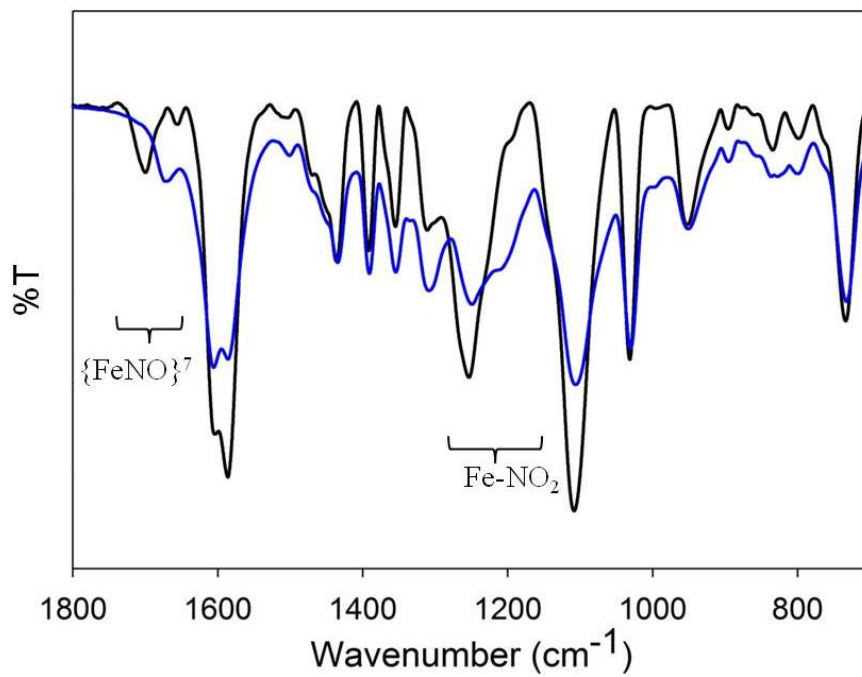


Figure S9. Top: FTIR (KBr, RT) of **5** (black trace) and **5**^{15NO₂} (blue trace) indicating the isotope sensitive bands of {FeNO}⁷ Fe-NO₂. Bottom: FTIR of crystals grown from **5**, indicating the ν_{FeO} region.

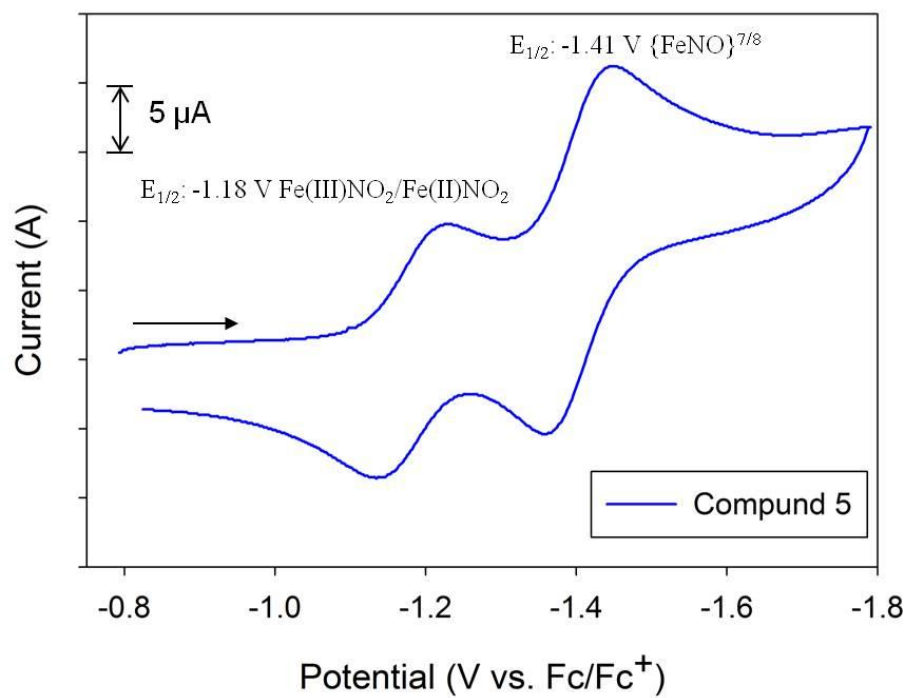


Figure S10. CV of compound **5** (0.1 M $n\text{-Bu}_4\text{NPF}_6$ supporting electrolyte, glassy carbon working electrode, Pt-wire counter electrode, RT). Arrow displays direction of scan.

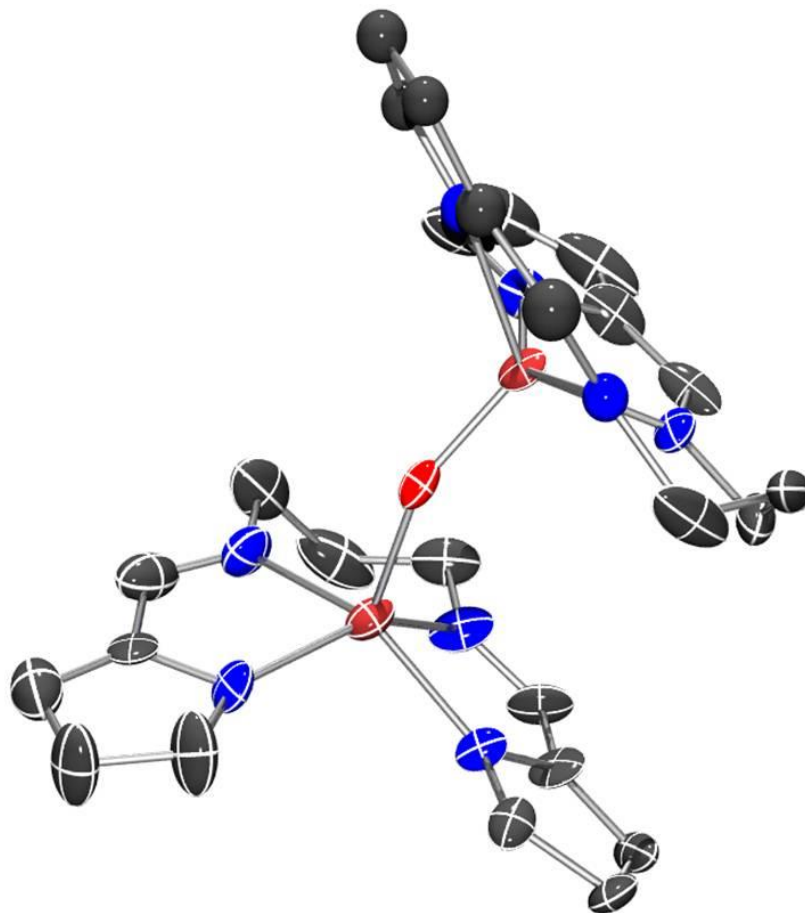


Figure S11. ORTEP representation of the material formed upon crystallization attempts of **5**. The collected diffraction data for this complex is of low-quality and not all atoms could be anisotropically refined ($R_{int} = 0.252$).

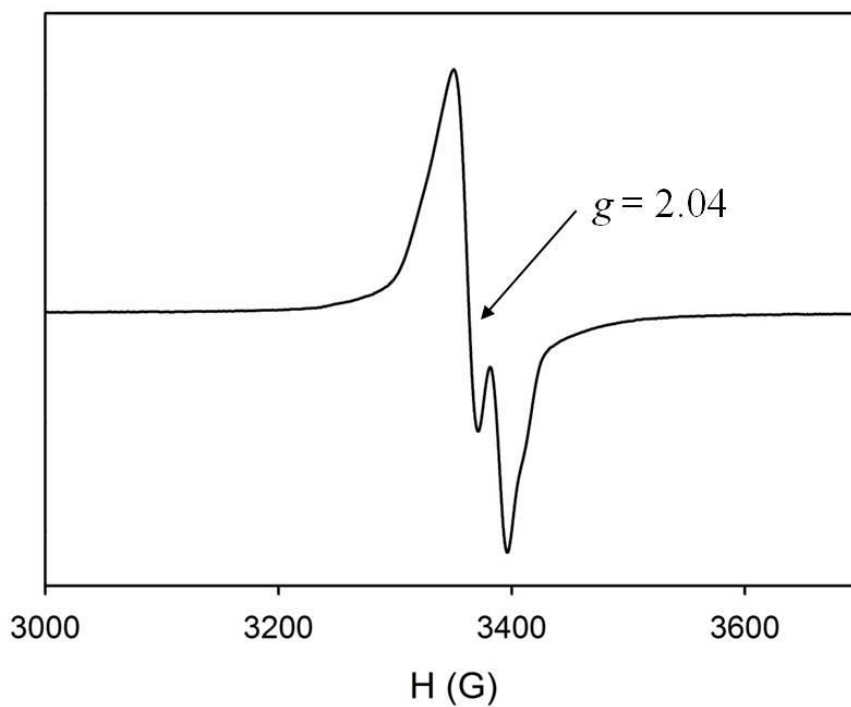


Figure S12. EPR spectrum of $[\text{Fe}(\text{LN}_4^{\text{Im}})(\text{NO})](\text{BF}_4)_2$ in an EtOH glass at 10 K. Selected g -values and ^{14}N hyperfine coupling constants are indicated. Spectrometer settings: microwave frequency, 9.58 GHz; microwave power, 1.0 mW; modulation frequency, 100 kHz; modulation amplitude, 6.31 G.

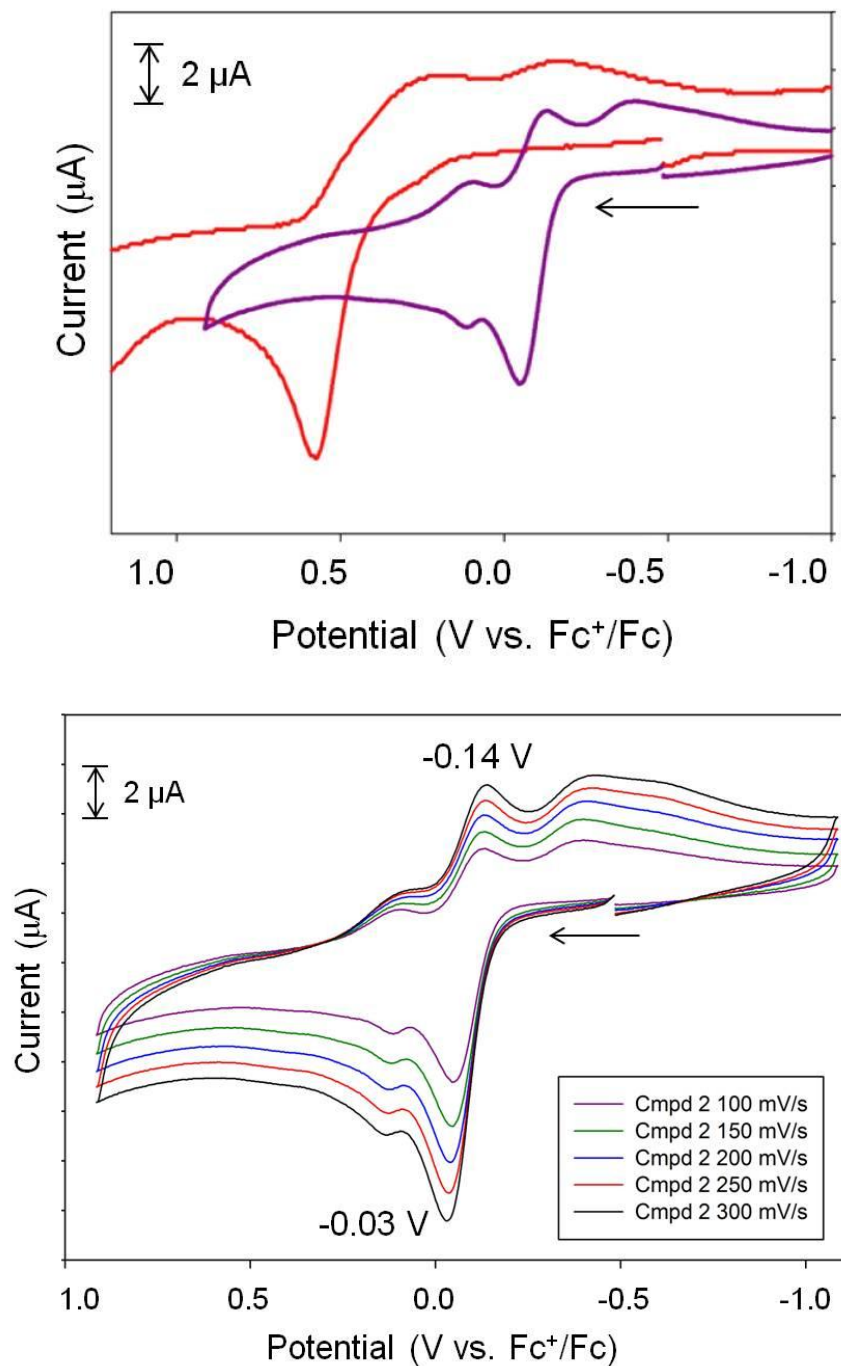


Figure S13. Top: Cyclic voltammograms (CVs) of **1** (red) and **2** (purple). Bottom: CVs of a 1 mM MeCN solution of **2** at different scan rates as indicated in the inset (0.1 M ⁿBu₄NPF₆ supporting electrolyte, glassy carbon working electrode, Pt-wire counter electrode, RT). Arrow displays direction of scan.

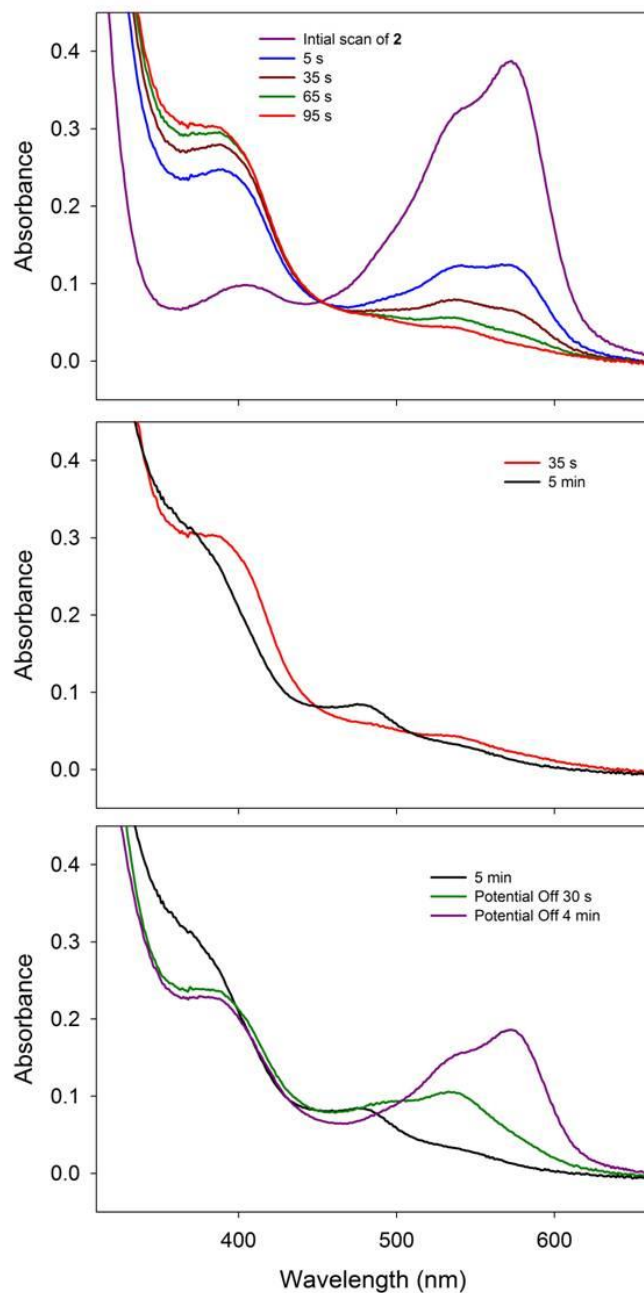


Figure S14. UV-vis spectroelectrochemical analysis of **2** in MeCN (0.1 M Et₄NPF₆), RT. Top: initial scan of **2** before (purple) applied potential and after being held at a potential of 0.5 V vs. Ag⁺/Ag. Center: conversion of 386 nm peak (red trace) into **1** (477 nm, black trace). Bottom: final scan at 0.5 V vs. Ag⁺/Ag (black trace), then 30 s after (green trace) and 4 min after potential is turned off (purple trace).

4.8 References

- (1) Farmer, P. J.; Sulc, F. *Free Radical Bio. Med.* **2002**, *33*, S375.
- (2) Immoos, C. E.; Sulc, F.; Farmer, P. J.; Czarnecki, K.; Bocian, D. F.; Levina, A.; Aitken, J. B.; Armstrong, R. S.; Lay, P. A. *J. Am. Chem. Soc.* **2005**, *127*, 814.
- (3) Yi, J.; Safo, M. K.; Richter-Addo, G. B. *Biochemistry* **2008**, *47*, 8247.
- (4) Cosby, K.; Partovi, K. S.; Crawford, J. H.; Patel, R. P.; Reiter, C. D.; Martyr, S.; Yang, B. K.; Waclawiw, M. A.; Zalos, G.; Xu, X.; Huang, K. T.; Shields, H.; Kim-Shapiro, D. B.; Schechter, A. N.; Cannon, R. O., III; Gladwin, M. T. *Nat. Med.* **2003**, *9*, 1498.
- (5) Shiva, S.; Huang, Z.; Grubina, R.; Sun, J.; Ringwood, L. A.; MacArthur, P. H.; Xu, X.; Murphy, E.; Darley-Usmar, V. M.; Gladwin, M. T. *Circ. Res.* **2007**, *100*, 654.
- (6) Sinha, S. S.; Shiva, S.; Gladwin, M. T. *Trends Cardiovas. Med.* **2008**, *18*, 163.
- (7) Sparacino-Watkins, C. E.; Lai, Y. C.; Gladwin, M. T. *Circulation* **2012**, *125*, 2824.
- (8) Xu, N.; Yi, J.; Richter-Addo, G. B. *Inorg. Chem.* **2010**, *49*, 6253.
- (9) Yi, J.; Orville, A. M.; Skinner, J. M.; Skinner, M. J.; Richter-Addo, G. B. *Biochemistry* **2010**, *49*, 5969.
- (10) Yi, J.; Thomas, L. M.; Richter-Addo, G. B. *Angew. Chem. Int. Ed.* **2012**, *51*, 3625.
- (11) Silaghi-Dumitrescu, R. *Inorg. Chem.* **2004**, *43*, 3715.
- (12) Cutruzzola, F.; Brown, K.; Wilson, E. K.; Bellelli, A.; Arese, M.; Tegoni, M.; Cambillau, C.; Brunori, M. *Proc. Natl. Acad. Sci. U.S.A.* **2001**, *98*, 2232.
- (13) Einsle, O.; Messerschmidt, A.; Huber, R.; Kroneck, P. M. H.; Neese, F. *J. Am. Chem. Soc.* **2002**, *124*, 11737.
- (14) Einsle, O.; Messerschmidt, A.; Stach, P.; Bourenkov, G. P.; Bartunik, H. D.; Huber, R.; Kroneck, P. M. *Nature* **1999**, *400*, 476.
- (15) Ozaki, S.-i.; Roach, M. P.; Matsui, T.; Watanabe, Y. *Acc. Chem. Res.* **2001**, *34*, 818.

- (16) Collman, J. P.; Gagne, R. R.; Reed, C. A.; Robinson, W. T.; Rodley, G. A. *Proc. Natl. Acad. Sci. U.S.A.* **1974**, *71*, 1326.
- (17) Collman, J. P.; Gagne, R. R.; Reed, C.; Halbert, T. R.; Lang, G.; Robinson, W. T. *J. Am. Chem. Soc.* **1975**, *97*, 1427.
- (18) Collman, J. P.; Fu, L. *Acc. Chem. Res.* **1999**, *32*, 455.
- (19) *Biological Inorganic Chemistry: Structure and Reactivity*; Bertini, I., Gray, H. B., Stiefel, E. I., Valentine, J. S., Eds.; University Science Books: Sausalito, California, 2007.
- (20) Nasri, H.; Goodwin, J. A.; Scheidt, W. R. *Inorg. Chem.* **1990**, *29*, 185.
- (21) Nasri, H.; Wang, Y.; Huynh B. H.; Walker, F. A.; Scheidt, W. R. *Inorg. Chem.* **1991**, *30*, 1483.
- (22) Wyllie, G. R. A.; Scheidt, W. R. *Chem. Rev.* **2002**, *102*, 1067.
- (23) Speelman, A. L.; Lehnert, N. *Angew. Chem. Int. Edit.* **2013**, *52*, 12283.
- (24) Crabtree, R. H. *New. J. Chem.* **2011**, *35*, 18.
- (25) Kumar, M.; Dixon, N. A.; Merkle, A. C.; Zeller, M.; Lehnert, N.; Papish, E. T. *Inorg. Chem.* **2012**, *51*, 7004.
- (26) Sahu, S.; Widger, L. R.; Quesne, M. G.; de Visser, S. P.; Matsumura, H.; Moënné-Loccoz, P.; Siegler, M. A.; Goldberg, D. P. *J. Am. Chem. Soc.* **2013**, *135*, 10590.
- (27) Schmeier, T. J.; Dobereiner, G. E.; Crabtree, R. H.; Hazari, N. *J. Am. Chem. Soc.* **2011**, *133*, 9274.
- (28) Matson, E. M.; Bertke, J. A.; Fout, A. R. *Inorg. Chem.* **2014**, *53*, 4450.
- (29) Matson, E. M.; Park, Y. J.; Fout, A. R. *J. Am. Chem. Soc.* **2014**, *136*, 17398.
- (30) Shook, R. L.; Borovik, A. S. *Inorg. Chem.* **2010**, *49*, 3646.
- (31) DuBois, R. M.; DuBois, D. L. *Chem. Soc. Rev.* **2009**, *38*, 62.
- (32) Wilson, A. D.; Newell, R. H.; McNevin, M. J.; Muckerman, J. T.; DuBois, R. M.; DuBois, D. L. *J. Am. Chem. Soc.* **2005**, *128*, 358.
- (33) Uyeda, C.; Peters, J. C. *J. Am. Chem. Soc.* **2013**, *135*, 12023.

- (34) Miller, A. J. M.; Labinger, J. A.; Bercaw, J. E. *J. Am. Chem. Soc.* **2008**, *130*, 11874.
- (35) Sanders, B. C.; Hassan, S. M.; Harrop, T. C. *J. Am. Chem. Soc.* **2014**, *136*, 10230.
- (36) Patra, A. K.; Dube, K. S.; Sanders, B. C.; Papaefthymiou, G. C.; Conradie, J.; Ghosh, A.; Harrop, T. C. *Chem. Sci.* **2012**, *3*, 364.
- (37) Hagen, K. S. *Inorg. Chem.* **2000**, *39*, 5867.
- (38) Diebold, A.; Hagen, K. S. *Inorg. Chem.* **1998**, *37*, 215.
- (39) Britovsek, G. J.; England, J.; White, A. J. *Inorg. Chem.* **2005**, *44*, 8125.
- (40) Nasri, H.; Ellison, M. K.; Chen, S.; Huynh, B. H.; Scheidt, W. R. *J. Am. Chem. Soc.* **1997**, *119*, 6274.
- (41) Hall, H. K. *J. Am. Chem. Soc.* **1957**, *79*, 5441.
- (42) Hematian, S.; Siegler, M. A.; Karlin, K. D. *J. Biol. Inorg. Chem.* **2014**, *19*, 515.
- (43) Ching, W.-M.; Chuang, C.-H.; Wu, C.-W.; Peng, C.-H.; Hung, C.-H. *J. Am. Chem. Soc.* **2009**, *131*, 7952.
- (44) Harris, T. D.; Betley, T. A. *J. Am. Chem. Soc.* **2011**, *133*, 13852.
- (45) López, J. P.; Heinemann, F. W.; Prakash, R.; Hess, B. A.; Horner, O.; Jeandey, C.; Oddou, J.-L.; Latour, J.-M.; Grohmann, A. *Chem. Eur. J.* **2002**, *8*, 5709.
- (46) Villar-Acevedo, G.; Nam, E.; Fitch, S.; Benedict, J.; Freudenthal, J.; Kaminsky, W.; Kovacs, J. A. *J. Am. Chem. Soc.* **2011**, *133*, 1419.
- (47) Connelly, N. G.; Geiger, W. E. *Chem. Rev.* **1996**, *96*, 877.
- (48) Finnegan, M. G.; Lappin, A. G.; Scheidt, W. R. *Inorg. Chem.* **1990**, *29*, 181.
- (49) Bordwell, F. G.; Hughes, D. L. *J. Org. Chem.* **1982**, *47*, 3224.
- (50) Holm, R. H.; Pinolet, L. H.; Lewis, R. A. *J. Am. Chem. Soc.* **1971**, *93*, 360.
- (51) Wieghardt, K.; Kueppers, H. J.; Weiss, J. *Inorg. Chem.* **1985**, *24*, 3067.
- (52) Widger, L. R.; Davies, C. G.; Yang, T.; Siegler, M. A.; Troepfner, O.; Jameson, G. N. L.; Ivanović-Burmazović, I.; Goldberg, D. P. *J. Am. Chem. Soc.* **2014**, *136*, 2699.

- (53) SMART v5.626: Software for the CCD Detector System; Bruker AXS: Madison WI **2000**.
- (54) Walker, N.; Stuart, D. *Acta Crystallogr. A*. **1983**, 39, 158.
- (55) Sheldrick, G. M. *SADABS, Area Detector Absorption Correction, University of Göttingen, Göttingen, Germany*, **2001**.
- (56) Sheldrick, G. M. *SHELX-97, Program for Refinement of Crystal Structures, University of Göttingen, Göttingen, Germany*, **1997**.
- (57) Sheldrick, G. M. *SHELXTL 6.1, Crystallographic Computing System, Siemens Analytical X-Ray Instruments, Madison, WI*, **2000**.
- (58) Cromer, D. T.; Waber, J. T. *International Tables for X-ray Crystallography*; The Kynoch Press: Birmingham, England, 1974; Vol. IV, Table 2.2B.
- (59) Burnett, M. N.; Johnson, C. K. *ORTEP-III, Report ORNL - 6895; Oak Ridge National Laboratory: Oak Ridge, TN*, **1996**.

CHAPTER 5

CONCLUSIONS

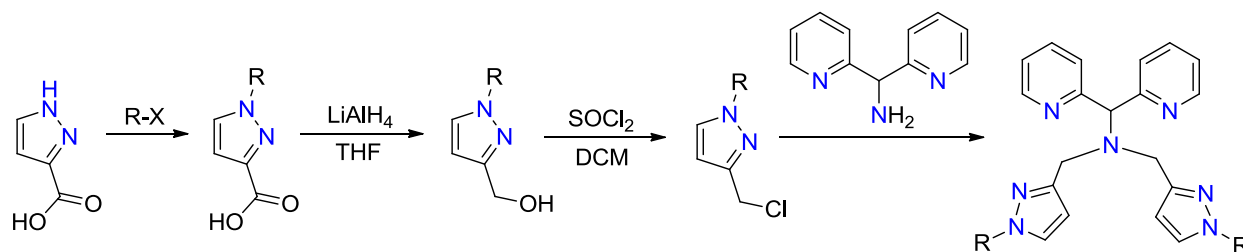
We have successfully designed, developed, and implemented non-heme complexes as NO_2^- reduction catalysts and NO^-/HNO donors. In addition, we have developed the groundwork for future generations of non-heme Fe- NO_2 and Fe-NO complexes with respect to 5-coordinate ligands (5C) and secondary-sphere interactions. In this work, the ligands are non-heme; however, much of the enzymatic chemistry our systems aim to model is in fact, heme-dependent. Even more so, the LN_4 and LN_5 platforms utilized in this work could more accurately be described as psuedo-heme given the coordination geometry and donor disposition (i.e. neutral N, imidazole, and anionic pyrrole). Although similar to heme systems, these non-heme systems allow for the stabilization/isolation of complexes such as $\text{Fe(II)(NO}_2)_2$ and Fe(II)-NO^- , that are fleeting in heme models. Moreover, the ability to isolate such complexes allows for the detailed characterization and controlled reactivity studies. With this in mind, we have synthesized and isolated a series of $\{\text{FeNO}\}^8$ complexes, a rare oxidation-state for Fe-nitrosyls, and demonstrated the first metal-based NO^-/HNO donor to Fe-porphyrins (por) and metmyoglobin (metMb). Furthermore, the reactivity of $\{\text{FeNO}\}^{7/8}$ complexes with thiols like *p*-chlorobenzenethiol (*p*-ClArSH) and glutathione (GSH) have detailed the potential for reduced non-heme Fe-NO species to transform into dinitrosyl iron complexes (DNICs); the latter species being known for storage and transport of NO in biology.

With respect to NO_2^- reduction, we have synthesized and structurally characterized the first $\text{Fe(II)(NO}_2)_2$ complex in which the NO_2^- ligands are bound *trans* to each other. In addition, the controlled reactivity studies with *p*-ClArSH allowed for the impressive transformation from an $\text{Fe(II)(NO}_2)_2$ to an Fe(I)(NO)_2 DNIC. Importantly, this transformation formally requires four H^+ and three e^- , and is the first of its kind to implicate Fe-NO_2^- as a source of physiological DNIC. Moreover, the first demonstration of catalytic reduction of NO_2^- to NO on a non-heme platform was demonstrated in this work. This catalytic reactivity is a step forward in the ability to reduce NO_2^- under mild conditions; moreover, this work demonstrates how the rational design of a ligand can avoid catalytically doomed species such as stable $\{\text{FeNO}\}^7$ and Fe(III)-O-Fe(III) .

Inspired by metalloenzymes, the latter portion of this dissertation focused on the development of new ligands that are 5C or have secondary-sphere modulators. With respect to the latter, we have shown a proof-of-principle that installation of morpholine appendages to the periphery of an LN_4 platform can indeed modulate the secondary-sphere, and in turn, affect the chemical properties of the complex. Though the implications of this new system have not yet been fully realized, it is our hypothesis that modulating the secondary-sphere will increase the catalytic competence of our systems with respect to NO_2^- reduction catalysts, as well as stabilize Fe-NO^- complexes for future HNO donor scaffolds. Similar to this, the implementation of 5C ligands is expected to afford more control over the Fe-NO_x chemistry of these non-heme complexes. Given the modular design of these systems, the ability to conceptualize and develop new complexes is nearly unlimited. With this in mind, the future of this project is to rationally design new ligands with the intent to install secondary-sphere modulators. This can be accomplished from the $[\text{Fe}(\text{LN}_4^{\text{Morph}})(\text{L})_2]^{n+}$ system; however the N of morpholine is disposed to be relatively far away from the secondary-sphere of the axial site. Provided with the ease at

which the imidazole-NH can be modified, any number of secondary-sphere modulators can be envisioned. Additionally, the development of new 5C ligands can also be realized, for instance preliminary reactions suggest that N2Py2Im is synthetically achievable. In this light, the development of 5C ligands and their Fe-NO_x complexes remains an important, yet under investigated area of research. Moreover, the design and implementation of secondary-sphere modulation in the 5C systems is also possible. Though hypothetical, this may be achieved through the synthetic incorporation of pyrazole donors (Scheme 5.1). In conclusion, we have provided the basis for development of a toolbox of readily synthesized Fe-NO_x complexes. Utilizing such systems will inevitably facilitate the understanding and development of new technologies surrounding the chemistry of Fe and NO_x.

Scheme 5.1. Proposed synthetic route from a commercially available pyrazole acid to a 5C ligand having secondary-sphere modulators (R).



APPENDIX A

NON-HEME NO_x COMPLEXES WITH FIVE-COORDINATE N-LIGANDS

A.1. Introduction

The pursuit of enzymatic model complexes utilizing non-heme ligand scaffolds has allowed for an in-depth spectroscopic and mechanistic insight into the activation of small molecules. Of particular interest is O₂ activation and hydrocarbon oxidation chemistry.¹⁻⁷ A popular five-coordinate (5C) non-heme ligand is N4Py (**1**) (where N4Py = *N,N*-bis(2-pyridylmethyl)-*N*-(bis-2-pyridylmethyl)amine, Scheme A.1, see section A.5.).¹ The Fe complexes of **1** can stabilize an Fe(IV)=O capable of C-H activation through H-atom abstraction and O-atom transfer (OAT) to form alcohols, carbonyl groups, and epoxides on a variety of substrate molecules.⁷ This chemistry has been well-studied due to the parallels to oxygenase enzymes like cytochrome P450 and TauD (where TauD = taurine/ α -ketoglutarate dioxygenase), and furthermore, as a model for the Fe-bleomycin complex, a naturally occurring oxidation catalyst capable of selective DNA cleavage.^{2,7,8} The synthesis and study of these biomimetic non-heme complexes and their O₂ reactivity has broadened the understanding of oxygenase enzymes. Apart from oxygenase chemistry, however, the Fe-N4Py platform has not been studied with respect to activation of other small molecules such as NO_x. As of 2015 only one study involving an Fe-N4Py complex, namely [Fe(N4Py)(MeCN)](BF₄)₂ (**2**^{BF₄}) and its reaction with NO to give [Fe(N4Py)(NO)](BF₄)₂ (**3**) has been reported by Goldberg and coworkers.⁹ In their

efforts to model cysteine dioxygenase, the substitution of a Py from **1** for a thiolate donor affords the N3PyS⁻ system. Comparison of the {FeNO}⁷ derivatives of the [Fe(N4Py)]²⁺ and [Fe(N3PyS)]⁺ detailed photorelease of NO(g) from the thiolate bound complex, but not from complex **3**.⁹ In addition, both [Fe(N3PyS)(NO)]⁺ and [Fe(N4Py)(NO)]²⁺ complexes exhibit reversible {FeNO}^{6/7} and {FeNO}^{7/8} redox couples. Apart from these studies, the investigation of **2** and its reactivity toward NO_x complexes is underrepresented in the literature; moreover, the potential of **2** as a NO₂⁻ reduction catalyst or as an {FeNO}⁸ based HNO donor has not been pursued. In this work we continue our efforts in controlling the reactivity of non-heme Fe-NO₂ species and aim to expand our work to 5C ligands that afford 6C [Fe(N4Py)NO₂]ⁿ⁺ complexes. This modification will limit the coordination chemistry of NO₂⁻ to one open axial site, thus offering more control over the reactivity. This appendix describes our initial work towards developing new NO₂⁻ reduction catalysts through the synthesis of **1** and its corresponding Fe complexes **2**, **3**, and [Fe(N4Py)(NO₂)](BPh₄) (**4**) (Fig. A.1). In addition, progress towards the synthesis of a novel 5C ligand, namely N2Py2Im (**5**, Scheme A.1) is discussed in the experimental section (A.6.).

A.2. Synthesis and Characterization

The synthesis and characterization of compounds **1**, **2**, and **3** have been reported previously.^{1,9,10} In our studies we opted to obtain **1** from di(pyridin-2-yl)methanamine and picolyl chloride hydrochloride in DMF with K₂CO₃/KI in 77% yield (Scheme A.1).¹ Complexes **2** and **3** were prepared from published procedures and compare well to the reported characterization.⁹ The synthesis and characterization of these molecules is reported in section A.6.

The reaction of **1** with $[\text{Fe}(\text{H}_2\text{O})_6](\text{BF}_4)_2$ in MeCN affords a red-colored solution of $\mathbf{2}^{\text{BF}_4}$ (λ_{max} : 375 and 454 nm, Fig. A.2). The BF_4^- anion can be readily exchanged in the reaction with NaBPh_4 in 3:2 MeOH:MeCN precipitates $\mathbf{2}^{\text{BPh}_4}$ in 87% yield. Comparison of the FTIR spectra indicate the loss of BF_4^- (ν_{BF} 1058 cm^{-1}) and appearance of new bands associated with BPh_4^- (765, 737, 704 cm^{-1}). The UV-vis of $\mathbf{2}^{\text{BF}_4}$ and $\mathbf{2}^{\text{BPh}_4}$ in MeCN (λ_{max} : 377 and 455 nm) are nearly identical and characteristic of the metal-to-ligand charge-transfer bands (MLCT) as assigned in previous reports.¹¹ ESI-MS(+) of $\mathbf{2}^{\text{BF}_4}$ revealed the molecular ion (m/z 442.1) that corresponds to a reduced complex $\{[\text{Fe}(\text{N4Py})(\text{H}_2\text{O})] + \text{H}\}^+$ and indicates reduction of the complex under ionization conditions. An analogous phenomenon is observed for other neutral LN_4 platforms discussed in Chapters 3 and 4 of this dissertation. In negative-ion mode, however, the ESI-MS of $\mathbf{2}^{\text{BF}_4}$ displays $[[\text{Fe}(\text{N4Py})](\text{BF}_4)_3]^-$ (m/z 684.0), indicating the appropriate oxidation state of Fe(II). The ^1H NMR spectra of $\mathbf{2}^{\text{BF}_4}$ and $\mathbf{2}^{\text{BPh}_4}$ in CD_3CN exhibit sharp resonances, indicative of a low-spin (LS), $S = 0$ state (Figs. A23 and A25). Notably, the two H atoms of the methylene groups in **2** become non-equivalent (4.39 and 4.29 ppm) and undergo geminal splitting with a large coupling constant ($J = 15$ Hz); comparable to what has been reported previously for **1**, where $J = 18$ Hz.¹ This offers a direct indication for metal coordination. Complex **2** remains diamagnetic in 1:1 ($\text{CD}_3\text{CN}:\text{CD}_3\text{OD}$). However, when the analogous ^1H NMR experiment is performed in DMSO-d_6 , the complex becomes paramagnetic, as apparent from the dramatically shifted ^1H -resonances (100 to -10 ppm, Fig. A.3). This demonstrates that in weaker donor solvents, $[\text{Fe}(\text{N4Py})(\text{Sol})]^{2+}$ becomes high-spin (HS).¹¹ Corresponding solution-state magnetic susceptibility measurements of $\mathbf{2}^{\text{BPh}_4}$ indicate a $\mu_{\text{eff}} = 4.98$ BM, consistent with an $S = 2$ Fe(II) center. The quintet manifold for $[\text{Fe}(\text{N4Py})(\text{Sol})]^{2+}$ is consistent with those previously reported

in aqueous conditions in which a spin-state equilibrium between the singlet and quintet state was proposed.¹¹

The addition of [K(18C6)]NO₂ to a 1:1 MeCN:MeOH solution of **2**^{BF₄} afforded the NO₂⁻ complex **4** 86% yield after anion exchange with NaBPh₄ and precipitation from MeOH. Complex **4** can also be obtained from **2**^{BPh₄}. The UV-vis spectrum of **4** displays a similar morphology to that of **2**, but the MLCT bands are shifted to lower-energy (λ_{max} : 390 and 474 nm), thus indicating coordination of NO₂⁻ (Fig. A.2). Analysis of **4** by FTIR supports NO₂⁻ coordination in the N-bound nitro form, with ν_{NO} : 1320 and 1284 cm⁻¹ (**4**^{15NO₂} shows $\nu_{15\text{NO}}$: 1302 and 1261 cm⁻¹; $\Delta\nu_{\text{NO}}$: 18 and 23 cm⁻¹, respectively, Fig. A.4). Additional support for the formation of **4** is found in the ESI-MS(+) in which the molecular ion [Fe(N4Py)(NO₂)⁺ is seen at m/z 469.1 (**4**^{15NO₂} shows m/z 470.2). Complex **4** exhibits a broadened and shifted ¹H NMR spectrum different from **2** in CD₃CN. Addition of 10 equiv of NaNO₂ to **2**^{BPh₄} in DMSO-d₆ resulted in the loss of downfield resonances between 100 and -10 ppm to give resonances within 10-0 ppm (Fig. A.3). The strong-field nature of the N-bound NO₂⁻ ligand should favor a LS Fe(II) center and explains the shift in the observed resonances. Though one may anticipate the return of a purely diamagnetic complex, slight paramagnetism in the solution-state has been observed in other non-heme nitro complexes that are otherwise determined to be LS.¹² Because the observed paramagnetism is dependent on the presence of NO₂⁻, several possibilities may explain the apparent paramagnetism of **4**. First, NO₂⁻ may spontaneously reacts with **2** to give a paramagnetic species such as, [Fe(III)(N4Py)] and/or an {FeNO}⁷ complex, that could form through a disproportionation mechanism. However, the stability of **4** appears to dispel this possibility. Secondly, the NO₂⁻ ligand could isomerize between the N-bound and O-bound states, in which the O-bound isomer may promote a HS complex due to the weaker ligand field.

Therefore, the spin-state equilibrium may depend on the binding-mode of the NO_2^- ligand. Lastly, the NO_2^- may remain N-bound, in which case, a thermally-accessible singlet-to-triplet transition may explain the slight paramagnetism of **4** in solution.¹³⁻¹⁵

A.3. Reactivity Studies

To test its capacity as an NiR functional model, the addition of two equiv of tosic acid (TsOH) to **4** in MeCN was performed. Accordingly, a slight color change from red to red-orange occurred, consistent with loss of NO_2^- and coordination of MeCN. Analysis of the bulk material by FTIR (KBr) supports the consumption of NO_2^- through absence of the ν_{NO} : 1320 and 1283 cm^{-1} . Importantly, a new peak appears at 1660 cm^{-1} appears and is suggestive of ν_{NO} from the $\{\text{FeNO}\}^7$ complex **3**. Authentic synthesis of **3** indicates ν_{NO} : 1678 cm^{-1} (KBr). The discrepancy between these two values is not understood, however, an analogous study using **4**^{15NO2} indicates a red-shift from 1663 to 1624 cm^{-1} ($\Delta\nu_{\text{NO}}$: 39 cm^{-1} , Fig. A.5). ESI-MS(+) displayed m/z . 594.2 which corresponds to the molecular ion $[\text{Fe}(\text{N4Py})(\text{OTs})]^+$ indicative of an Fe(II) complex, but no signal from an Fe-NO complex was observed. This is similar to the ESI-MS(+) of **3** that also does not indicate an Fe-NO species, and attests to the lability of the NO molecule in **3** under ionization conditions.⁹

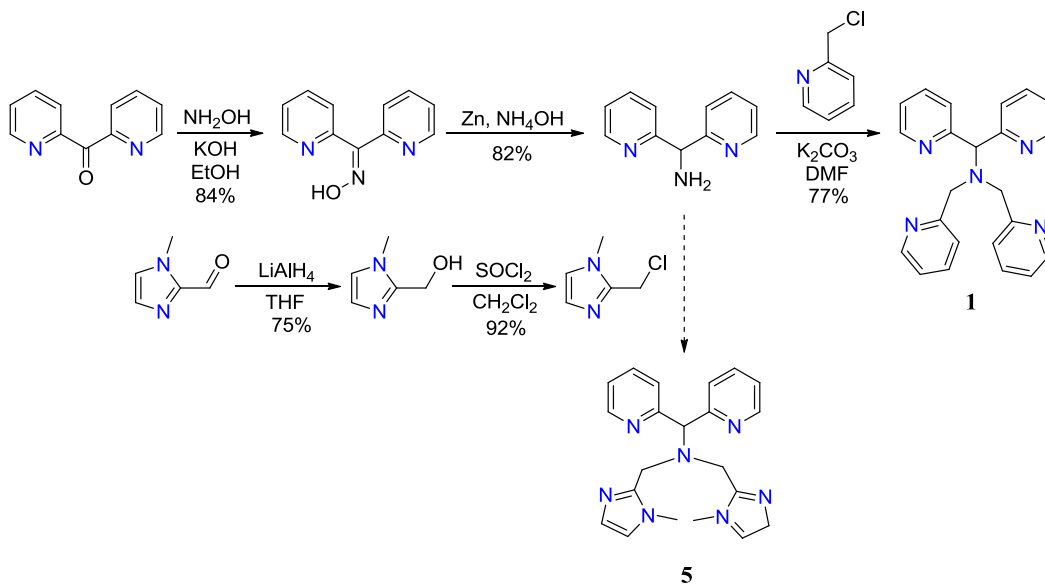
The consumption of NO_2^- is apparent from FTIR and ESI-MS, thus a likely explanation for the observed reactivity of **4** is an H^+ -dependent reduction of NO_2^- to NO. This may occur through formation of an $\{\text{FeNO}\}^6$ species, followed by electron transfer to give the observed $\{\text{FeNO}\}^7$ complex. Under these conditions, a disproportionation is the likely pathway, and occurs due to the requisite bimolecular interaction for electron transfer to occur, thus giving a mixture of 0.5 $[\text{Fe(III)(N4Py)(MeCN)}]^{3+}$ and 0.5 $[\text{Fe(II)(N4Py)(NO)}]^{2+}$ (Scheme A.2) Taken together, these preliminary results offer the first insight into the Fe(II)N4Py system as a potential candidate for the reduction of NO_2^- to NO.

A.4. Conclusions and Future Directions

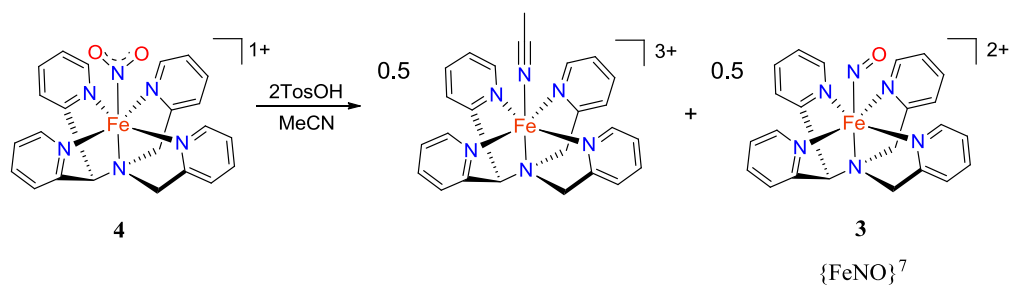
These initial studies into the reactive nature of Fe(N4Py) with NO_2^- begin our exploration into the controlled reduction of NO_2^- to NO with 5C non-heme ligands, thus building on our previous effort with 4C ligands. Future work on these systems would require a more detailed look into the reaction of **4** with various proton and electron donors. Moreover, the spin-state equilibrium of **4** in solution may be better understood through a temperature dependent study of the NO_2^- isomerization. The ability of the Fe(N4Py) system to stabilize high oxidation state species suggests that the Fe(III)- NO_2 complexes may be readily attainable. Thus, divergent reactivity of Fe(II)- NO_2 vs. Fe(III)- NO_2 may be realized on such a platform.

A.5. Schemes and Figures

Scheme A.1. Synthetic routes to **1** and **5**. Dashed arrow indicates an attempted reaction in which the product has not been isolated and fully characterized.



Scheme A.2. Proposed H^+ -dependent disproportionation of **4** to $[Fe(III)(N4Py)(MeCN)]^{3+}$ and **3**.



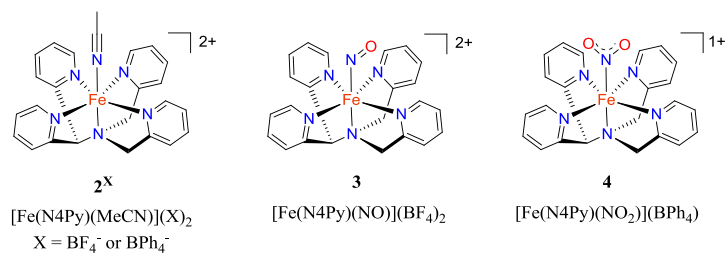


Figure A.1. $[\text{Fe}(\text{N4Py})(\text{L})]^{n+}$ complexes discussed in Appendix 1.

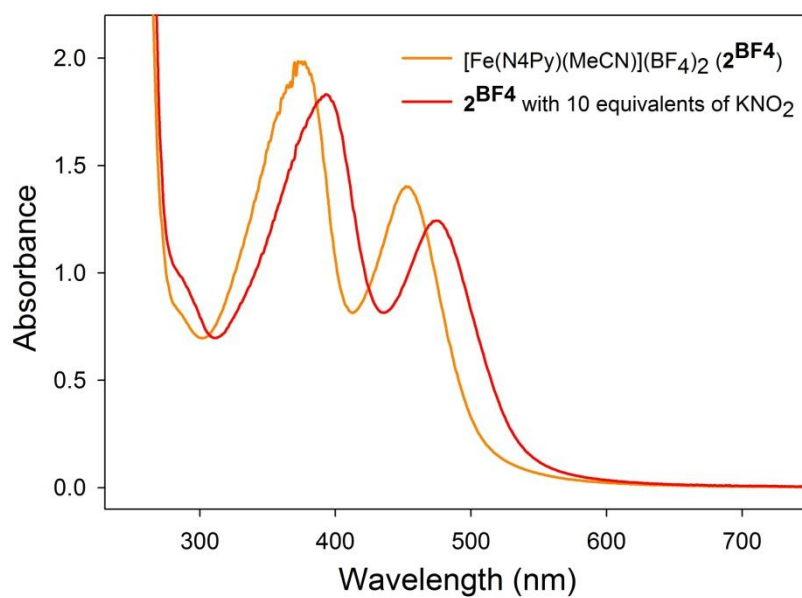


Figure A.2. UV-vis of 2^{BF_4} (orange trace) and 2^{BF_4} with 10 equiv of NaNO_2 , MeCN, 25 °C.

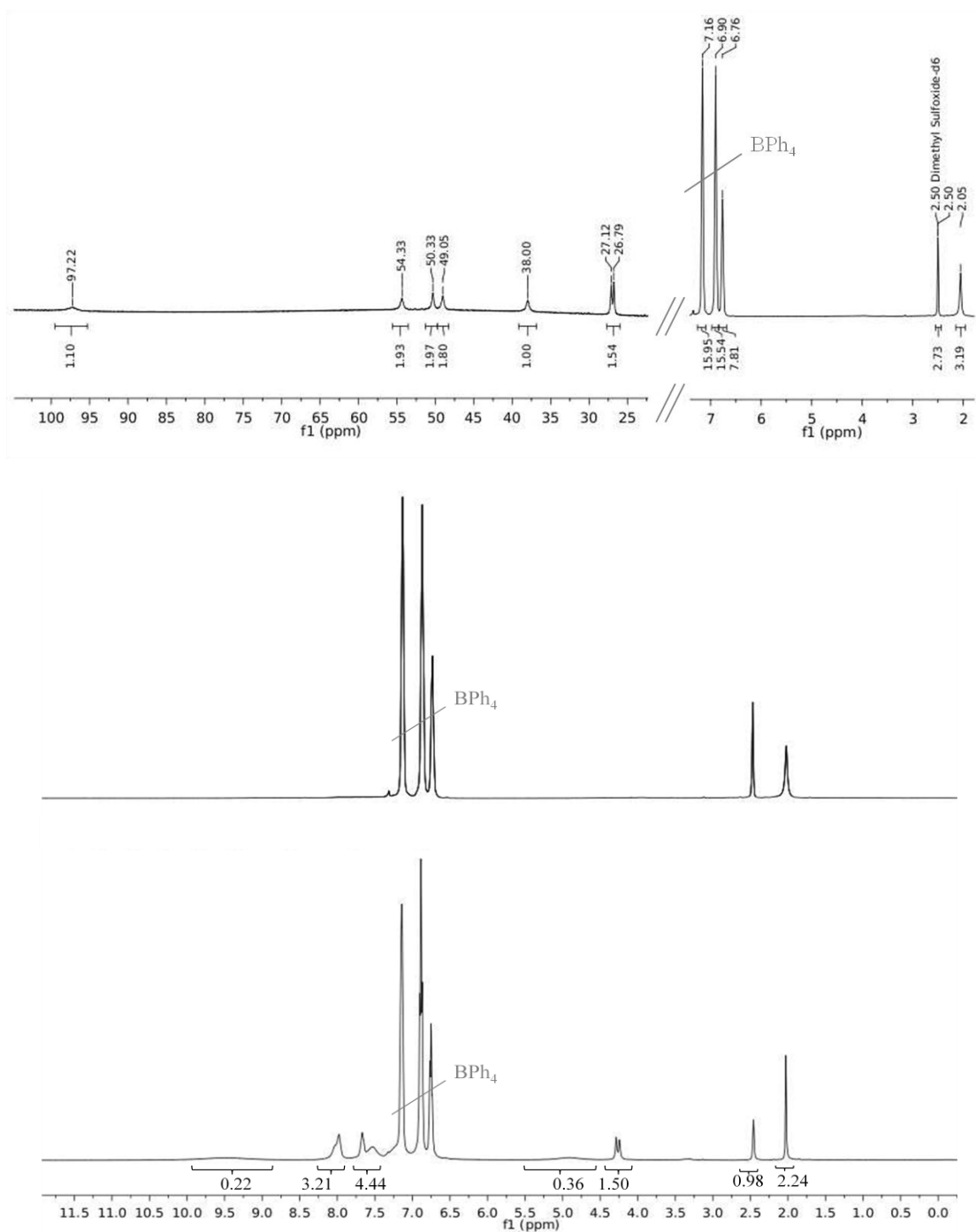


Figure A.3. Top: ^1H NMR of 2^{BPh_4} in DMSO-d_6 ; center: zoom-in of the region between 12 and 0 ppm of 2^{BPh_4} before addition of 10 equiv NaNO_2 ; bottom: 2^{BPh_4} after addition of 10 equiv NaNO_2 . The integration for BPh_4 was held constant in both experiments.

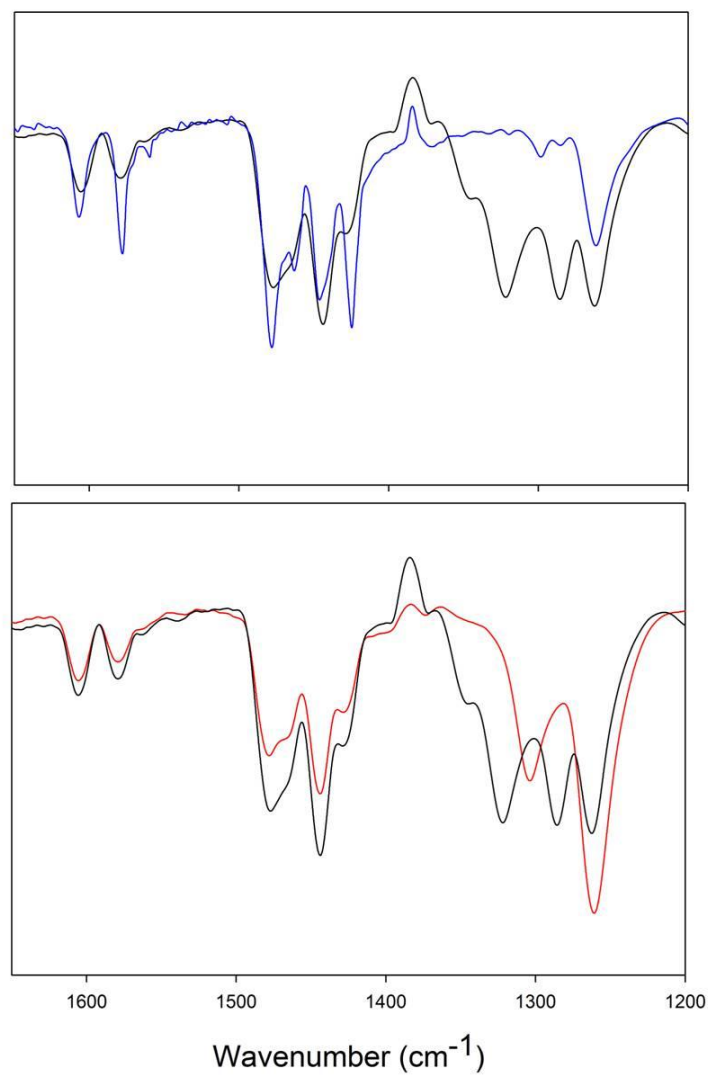


Figure A.4. FTIR of **4** (black trace) and **4**^{15NO₂} (red trace) indicating the isotopically sensitive bands in the ν_{NO} region.

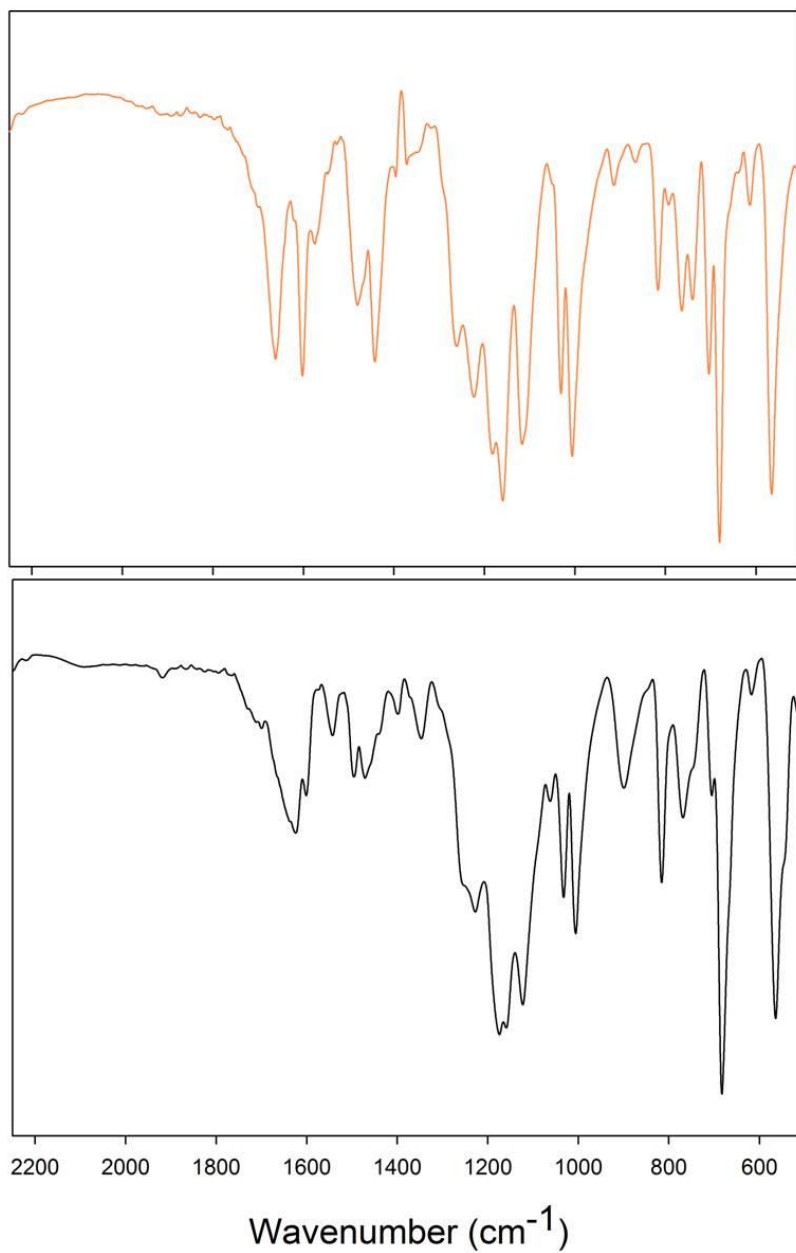


Figure A.5. FTIR of the reaction products from **4** (orange trace) and **4**^{15NO₂} (black trace) with TsOH, MeCN, RT.

A.6. Experimental Section

General Information.

See Chapter 2, Section 2.8.

Physical Methods.

See Chapter 2, Section 2.8.

Synthesis of Compounds

Di(pyridin-2-yl)methanone oxime hydrate

The synthesis of this compound has been reported previously.¹⁰ This procedure was used with the following reagent amounts: di(pyridin-2-yl)methanone (2.000 g, 10.86 mmol), hydroxylamine hydrochloride (1.132 g, 16.29 mmol), KOH (3.046 g, 54.3 mmol), EtOH (5 mL). Prior to the workup, place the solution into a 500 mL beaker due to the tendency of CO₂ evolution and product precipitation to foam out of a smaller vessel. Once the compound has precipitated, the addition of more H₂O can help to stir and wash the material prior to filtering. After workup, the solution was filtered and the solid was collected, dried under reduced pressure, and placed in a dessicator overnight to afford a pale-pink powder (1.977 g, 9.102 mmol, 84%). ¹H NMR (400 MHz, CDCl₃, δ from solvent): 16.2 (s, 1H, *HON*), 8.63 (t, 2H, *J* = 6 Hz, *PyH*), 7.87 (t, 1H, *J* = 8 Hz, *PyH*), 7.82 (m, 2H, *PyH*), 7.65 (t, 1H, *J* = 8 Hz, *PyH*), 7.45 (t, 1H, *J* = 6 Hz, *PyH*), 7.35 (t, 1H, *PyH*), 1.74 (s, *H*₂O hydrate). ¹³C NMR (100.6 MHz, CDCl₃, δ from solvent): 154.64 (q, *C=N*_{oxime}), 151.41 (q, *CN*, *Py*), 150.65 (q, *CN*, *Py*), 148.73 (t, *HCN*, *Py*), 146.12 (t, *HCN*, *Py*), 137.91 (t, *HC*, *Py*), 137.30 (t, *HC*, *Py*), 125.23 (t, *HC*, *Py*), 124.99 (t, *HC*, *Py*), 124.43 (t, *HC*, *Py*), 123.47 (t, *HC*, *Py*). FTIR (ATR), ν_{\max} (cm⁻¹): 3346 (s), 2989 (m), 2762 (m), 1665 (w), 1620 (w), 1592 (s), 1566 (m), 1475 (s), 1432 (s), 1337 (m), 1283 (m), 1238 (w),

1200 (w), 1153 (m), 1096 (m), 1050 (m), 1017 (s), 999 (vs), 970 (m), 994 (vs), 903 (m), 790 (vs), 759 (m), 749 (m), 690 (m), 658 (m), 622 (m), 579 (w), 494 (w), 458 (w), 415 (m). LRMS-ESI (m/z): $[M - H_2O + H]^+$ calcd for $C_{11}H_{10}N_3O$ (% relative abundance), 200.1 (100), 201.1 (13.2); found, 200.2 (100), 201.2 (12.1).

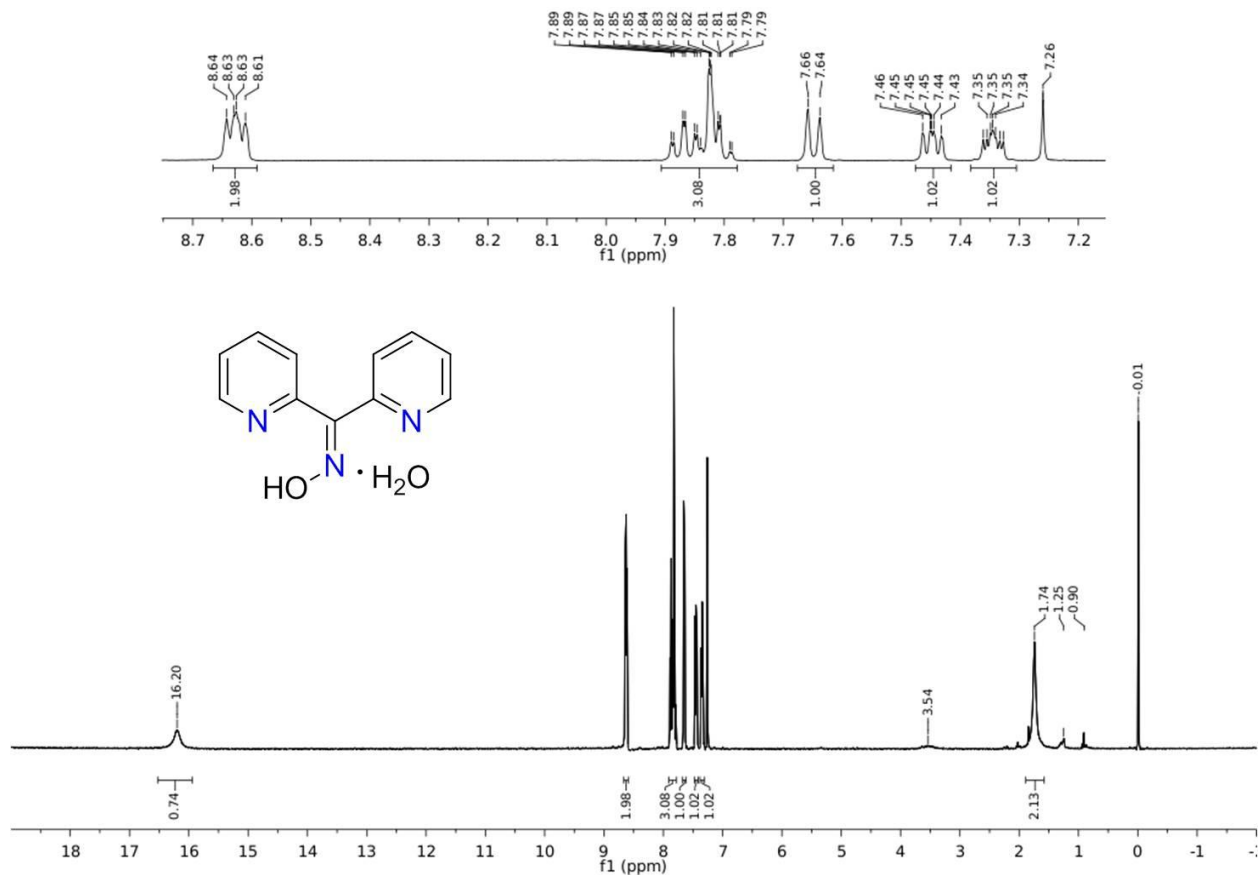


Figure A.6. 1H NMR of di(pyridin-2-yl)methanone oxime hydrate, $CDCl_3$, TMS, RT. Due to the hydrogen bonding of the H_2O hydrate, the symmetry of this molecule is lost and therefore each proton is unique.

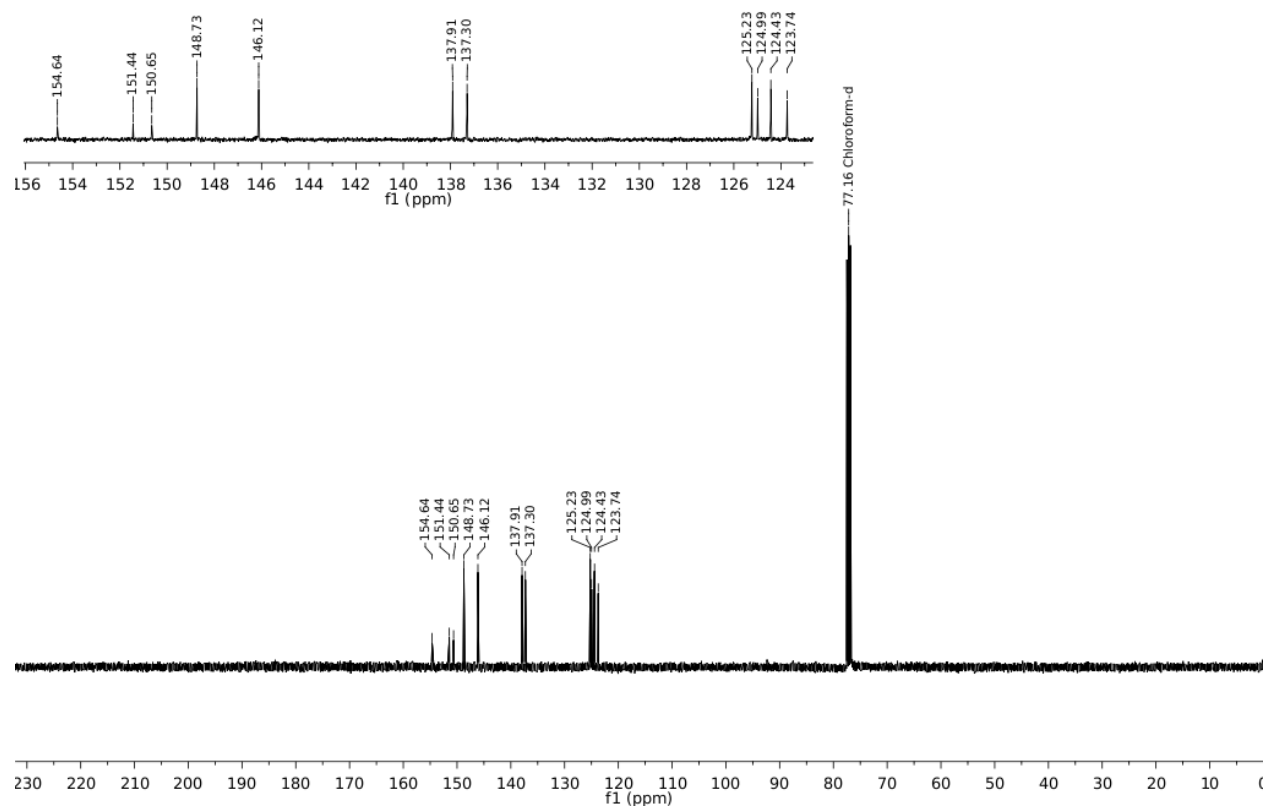


Figure A.7. ^{13}C NMR of di(pyridin-2-yl)methanone oxime hydrate, CDCl_3 , TMS, RT. Due to the hydrogen bonding of the H_2O hydrate, the symmetry of this molecule is lost and therefore each carbon is unique.

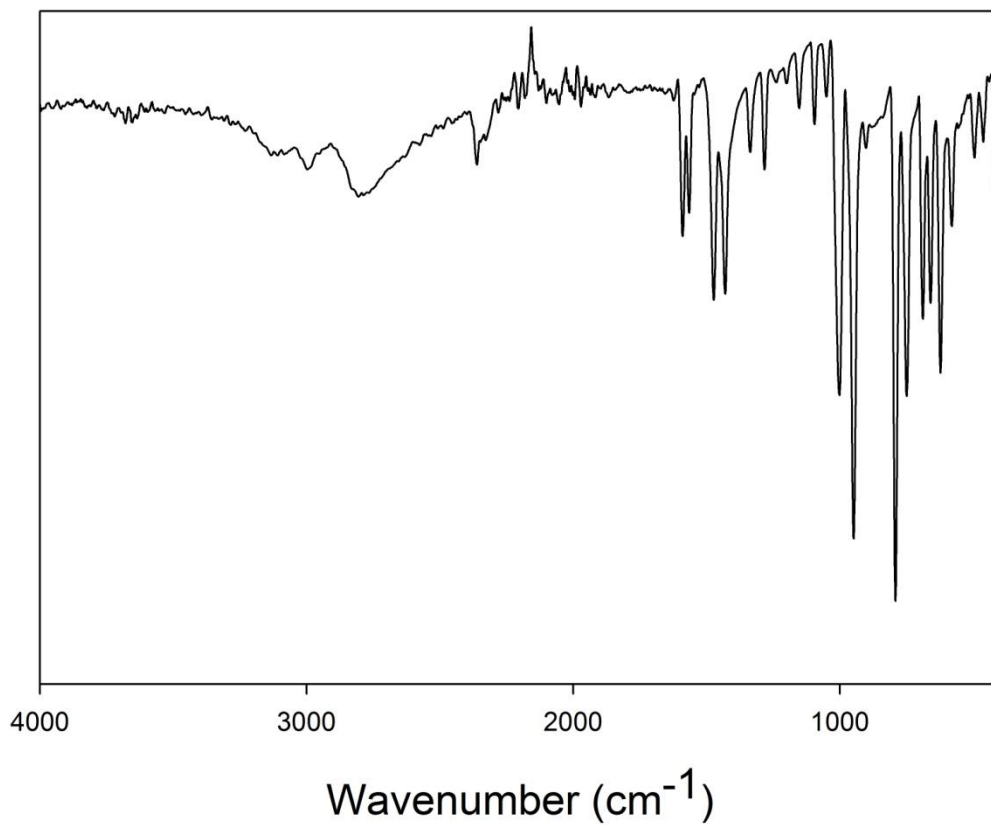


Figure A.8. FTIR (ATR) of di(pyridin-2-yl)methanone oxime hydrate, RT.

Di(pyridin-2-yl)methanamine

The synthesis of this compound has been reported previously.¹⁰ This procedure was used with the following reagent amounts: di(pyridin-2-yl)methanone oxime hydrate (1.802 g, 8.665 mmol), 30% aqueous ammonia (12.5 mL), Zn powder (2.055 g, 37.20 mmol), NH₄OAc (0.9453 g, 17.30 mmol), EtOH:H₂O (30 mL, 1:1 v/v). A short-path distillation unit was used for purification of the final product (see Fig. A.9 below). The distillate was collected to give a slightly-yellow transparent syrup (1.311 g, 7.079 mmol, 82%) ¹H NMR (400 MHz, CDCl₃, δ from solvent): 8.50 (d, 2H, *J* = 4 Hz, HCN, Py), 7.56 (td, 2H, *J* = 8 Hz, CH, Py), 7.34 (d, 2H, *J* = 4 Hz, CH, Py), 7.08 (t, 2H, *J* = 4 Hz, CH, Py), 5.27 (s, 1H H₂N-CH), 2.40 (s, 2H, H₂N-CH). ¹³C NMR (100.6 MHz, CDCl₃, δ from solvent): 162.82 (q, CN, Py), 149.19 (t, HCN, Py), 136.63 (t, HCN, Py), 122.08 (t, HCN, Py), 121.77 (t, HCN, Py), 62.39 (t, HC-NH₂, Py). FTIR (ATR), ν_{\max} (cm⁻¹): 3362 (w), 3279 (w), 3049 (m), 3005 (w), 1585 (s), 1567 (s), 1468 (m), 1431 (s), 1373 (w), 1318 (w), 1299 (w), 1269 (w), 1214 (w), 1198 (w), 1147 (m), 1092 (w), 1074 (w), 1046 (m), 993 (m), 917 (m), 888 (m), 819 (m), 747 (vs), 659 (m), 634 (m), 604 (s), 556 (m), 469 (w). LRMS-ESI (*m/z*): [M + H]⁺ calcd for C₁₁H₁₂N₃ (% relative abundance), 186.1 (100), 187.1 (13.1); found, 186.2 (100), 187.3 (11.0).

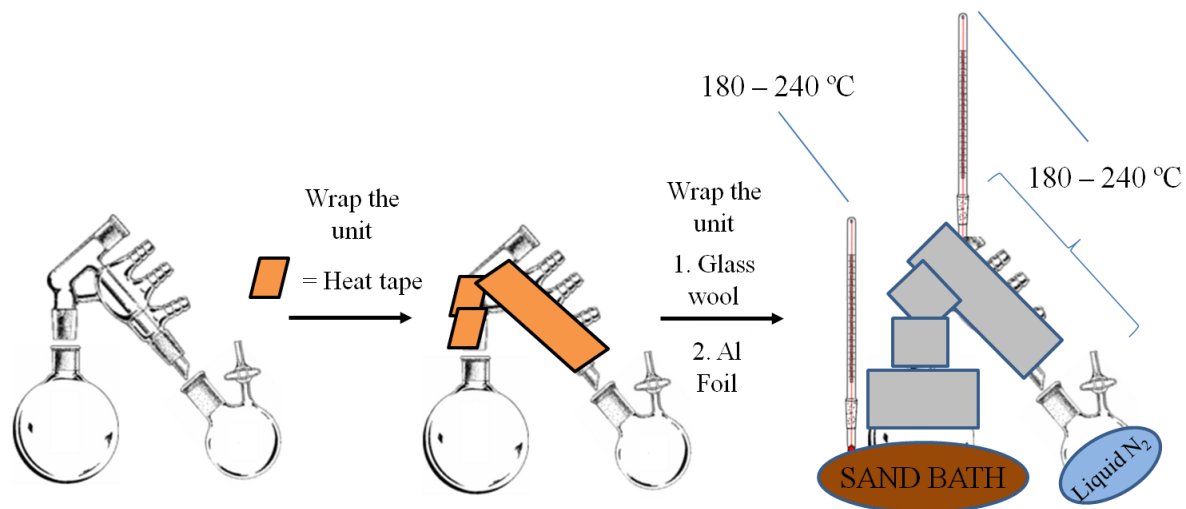


Figure A.9. Schematic depiction of the distillation unit used in the purification of di(pyridin-2-yl)methanamine. A thermometer is placed in the sand bath and next to the wrapped heat tape in order to monitor temperature.

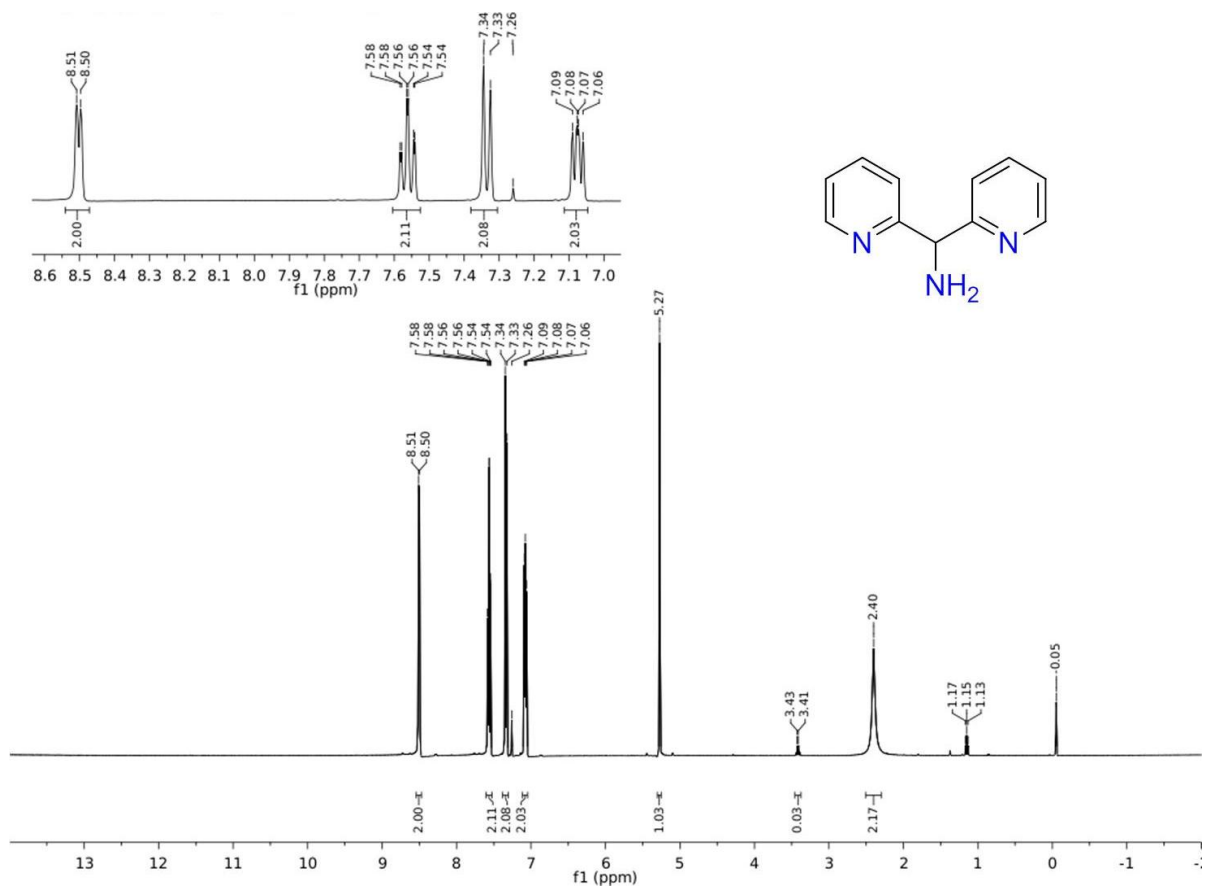


Figure A.10. ¹H NMR of di(pyridin-2-yl)methanamine, CDCl₃, TMS, RT.

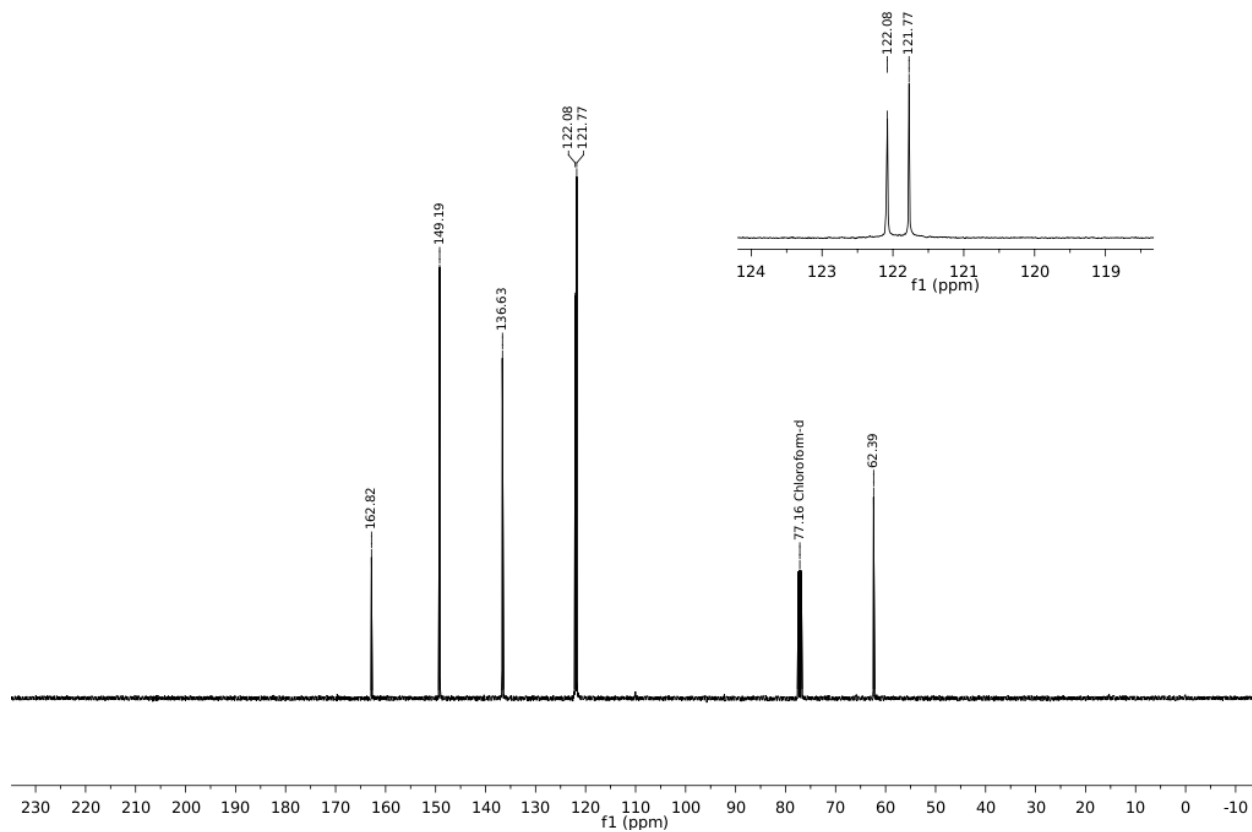


Figure A.11. ^{13}C NMR of di(pyridin-2-yl)methanamine, CDCl_3 , TMS, RT.

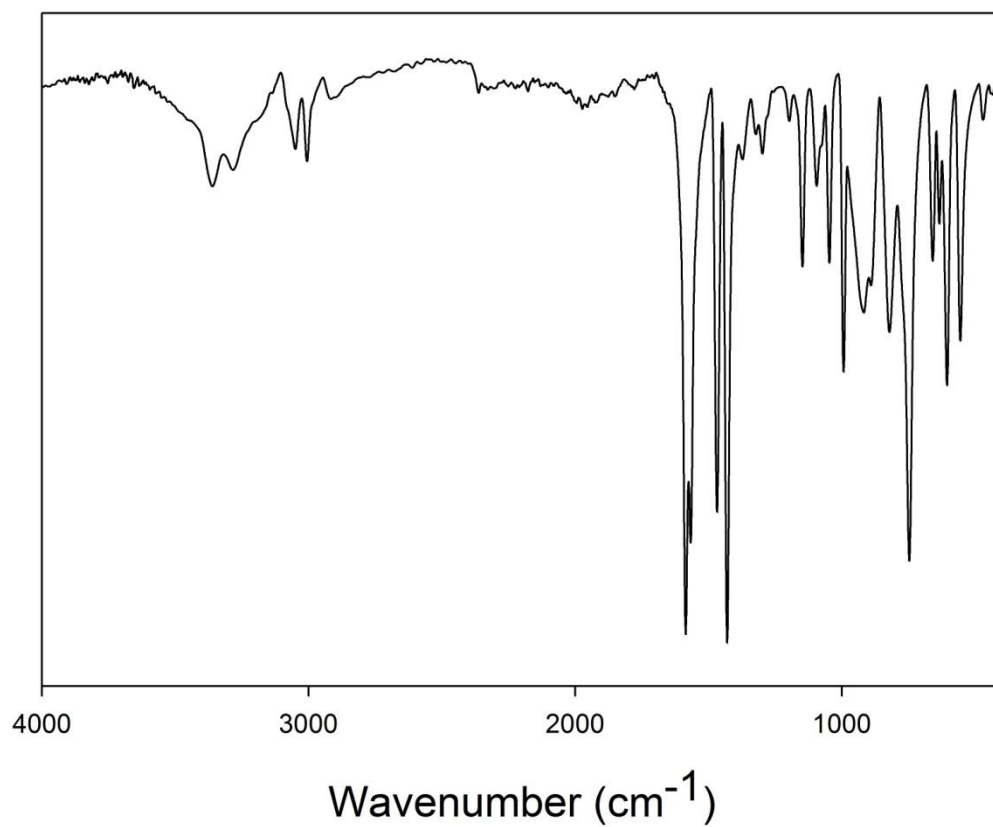


Figure A.12. FTIR (ATR) of di(pyridin-2-yl)methanamine, RT.

(1-methyl-1H-imidazol-2-yl)methanol

The synthesis of this compound has been reported previously.¹⁶ This procedure was used with the following reagent amounts: 1-methyl-1H-imidazole-2-carbaldehyde (2.000 g, 18.16 mmol), LiAlH₄ (0.7600 g, 20.00 mmol). After workup, the material was crystallized from EtOAc and hexanes to give a white solid (1.531 g, 13.54 mmol, 75%). ¹H NMR (400 MHz, CDCl₃, δ from solvent): 6.86 (s, 1H, *H*Im), 6.81 (s, 1H, *H*Im), 5.80 (s, br, 1H, CH₂OH), 4.63 (s, 2H, CH₂OH), 3.72 (s, 3H, N-CH₃). ¹³C NMR (100.6 MHz, CDCl₃, δ from solvent): 148.20 (q, CCH₂OH, Im), 126.51 (t, HC, Im), 121.47 (t, HC, Im), 55.48 (s, CH₂COH), 32.88 (p, N-CH₃). FTIR (ATR), ν_{max} (cm⁻¹): 3134 (m), 3113 (m), 2936 (m), 2813 (m), 1597 (w), 1497 (s), 1492 (s), 1438 (m), 1421 (m), 1360 (m), 1282 (m), 1246 (s), 1192 (m), 1145 (s), 1018 (vs), 962 (s), 931 (m), 848 (m), 793 (m), 784 (s), 752 (s), 744 (vs), 700 (s), 651 (s), 627 (m), 431 (s). LRMS-ESI (*m/z*): [M + H]⁺ calcd for C₅H₉N₂O (% relative abundance), 113.1 (100), 114.1 (6.3); found, 113.2 (100), 114.3 (6.5).

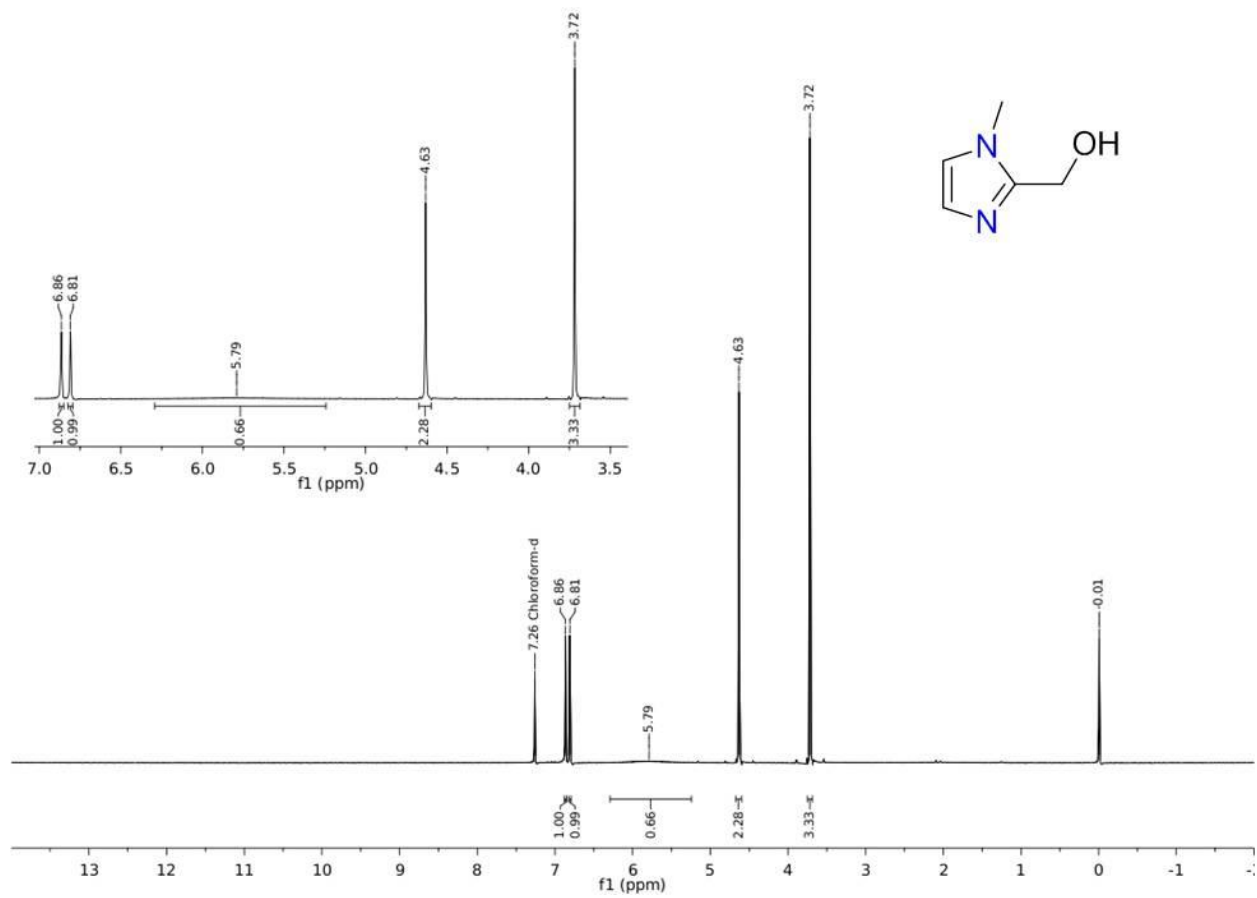


Figure A.13. ¹H NMR of (1-methyl-1H-imidazol-2-yl)methanol, CDCl₃, TMS, RT.

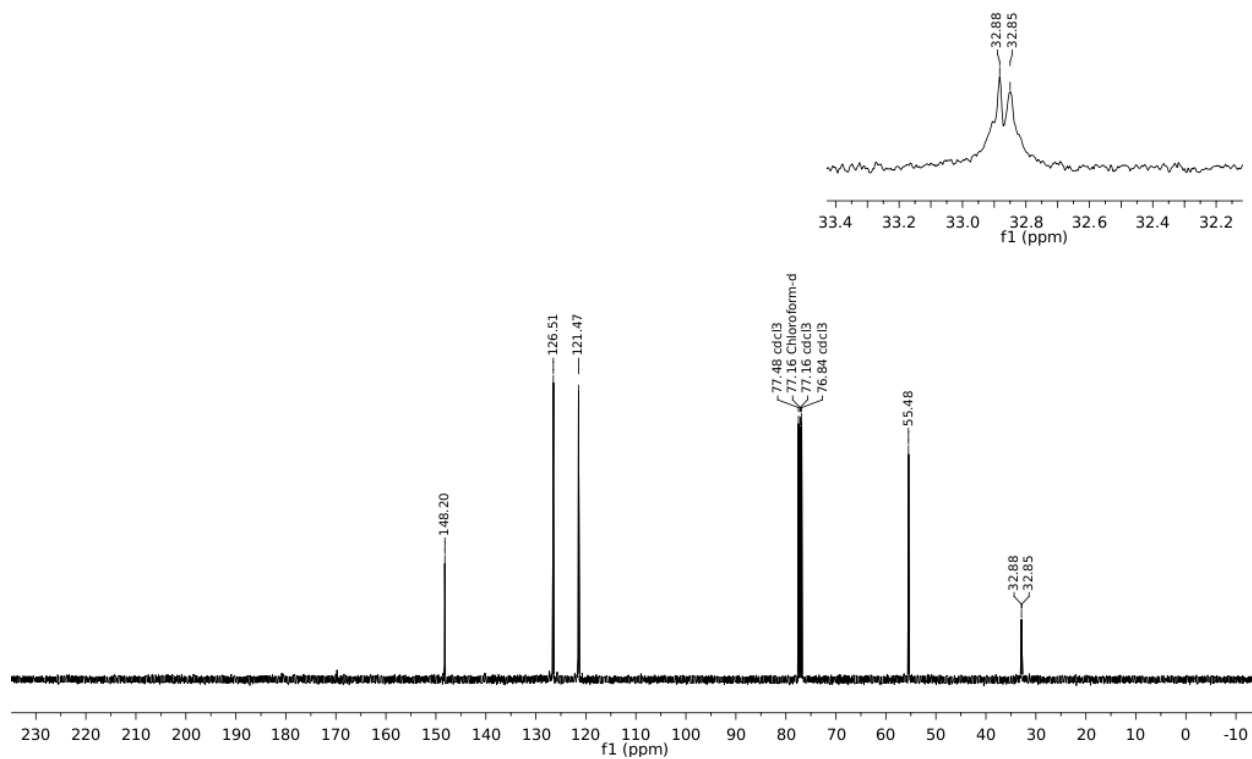


Figure A.14. ^{13}C NMR of (1-methyl-1H-imidazol-2-yl)methanol, CDCl_3 , TMS, RT. Two peaks are observed for the methylene carbon at 32.88 and 32.85 ppm and are possibly due to stable rotomers on the NMR time-scale.

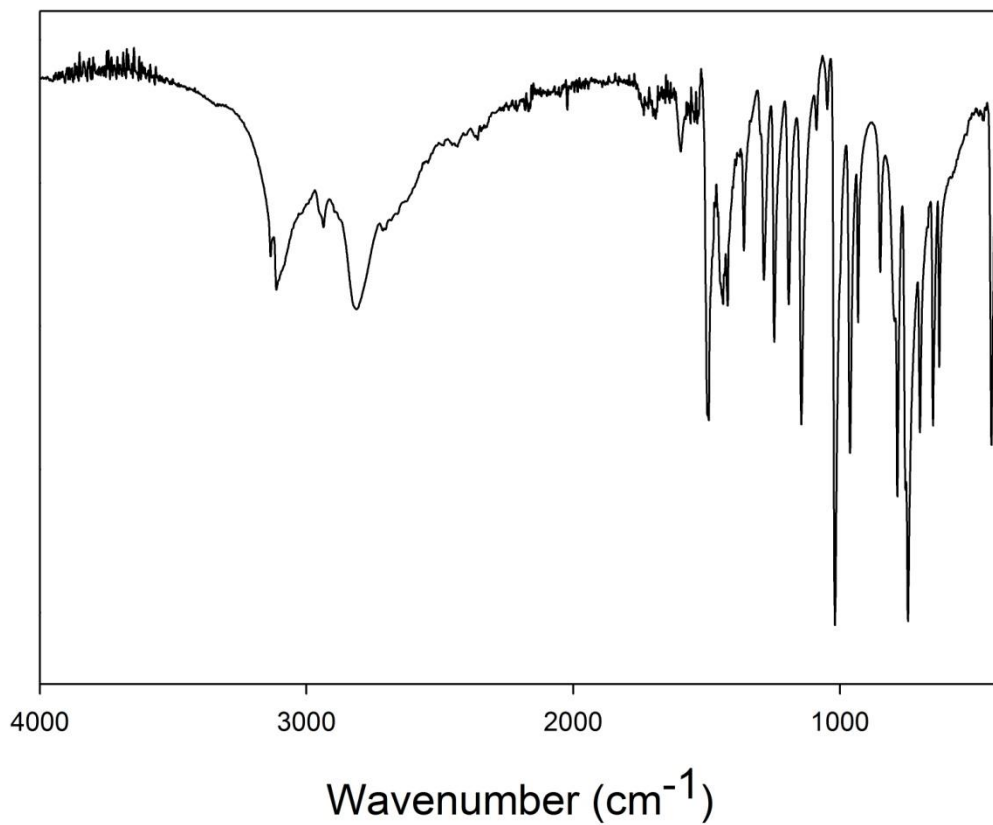


Figure A.15. FTIR (ATR) of (1-methyl-1H-imidazol-2-yl)methanol, RT.

2-(chloromethyl)-1-methyl-1H-imidazole hydrochloride

To a 10 mL solution of neat SOCl_2 at 0 °C was added a 5 mL solution of (1-methyl-1H-imidazol-2-yl)methanol (1.330 g, 11.86 mmol) in CH_2Cl_2 . This was stirred at RT for 1 h while direct N_2 purge removed any volatiles. Once concentrated to SOCl_2 volume, a short-path distillation unit was used to remove excess SOCl_2 . Once dry, 5 mL of CH_2Cl_2 was added to co-evaporate remaining SOCl_2 . This was repeated three times. The resulting powder was stirred in 20 mL of Et_2O before filtering and drying under vacuum to afford a pale tan solid (1.820 g, 10.90 mmol, 92%). ^1H NMR (400 MHz, $(\text{CD}_3)_2\text{SO}$, δ from solvent): 7.82 (d, 1H, $J = 4$ Hz, *H*Im), 7.72 (d, 1H, $J = 4$ Hz, *H*Im), 5.23 (s, br, 2H, CH_2Cl), 3.89 (s, 3H, N- CH_3). ^{13}C NMR (100.6 MHz, $(\text{CD}_3)_2\text{SO}$, δ from solvent): 141.39 (q, CCH_2Cl , Im), 124.70 (t, HC, Im), 119.11 (t, HC, Im), 34.24 (s, CH_2CCl), 31.58 (p, N- CH_3). FTIR (ATR), ν_{max} (cm^{-1}): 3403 (w), 3146 (m), 3107 (m), 2996 (m), 2945 (m), 2531 (w), 2466 (w), 2420 (m), 1859 (s), 1812 (m), 1757 (w), 1660 (w), 1593 (s), 1529 (s), 1479 (m), 1452 (w), 1432 (w), 1422 (w), 1394 (s), 1342 (w), 1301 (m), 1267 (s), 1216 (vs), 1176 (m), 1107 (w), 1079 (s), 1045 (m), 940 (s), 926 (s), 902 (m), 879 (s), 776 (vs), 756 (s), 745 (vs), 658 (s), 624 (vs), 581 (m). LRMS-ESI (m/z): $[\text{M} + \text{H}]^+$ calcd for $\text{C}_5\text{H}_8\text{N}_2\text{Cl}$ (% relative abundance), 131.0. (100), 133.0 (32.1), 132.0 (6.2), found, 131.2 (100), 133.2 (31.0), 131.2 (6.3).

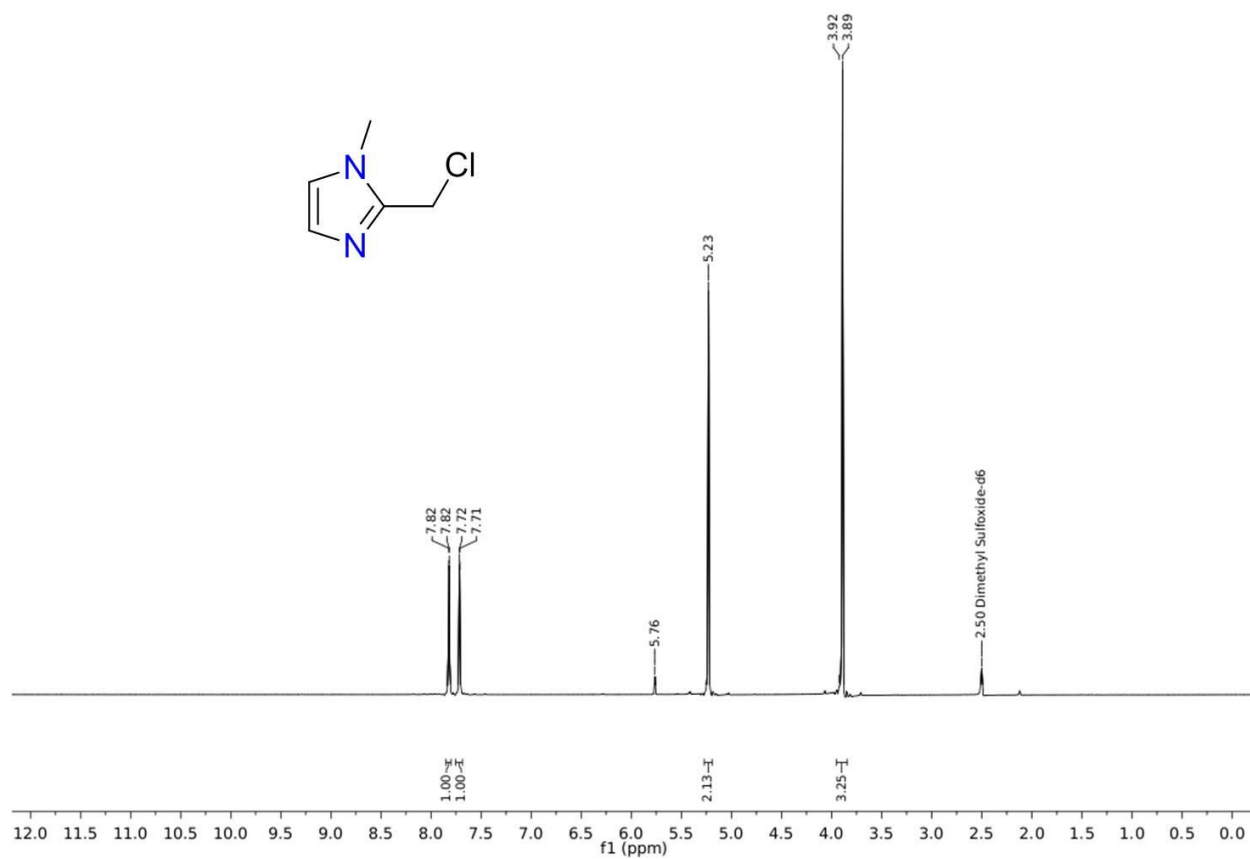


Figure A.16. ¹H NMR of 2-(chloromethyl)-1-methyl-1H-imidazole hydrochloride, DMSO-d₆, TMS, RT.

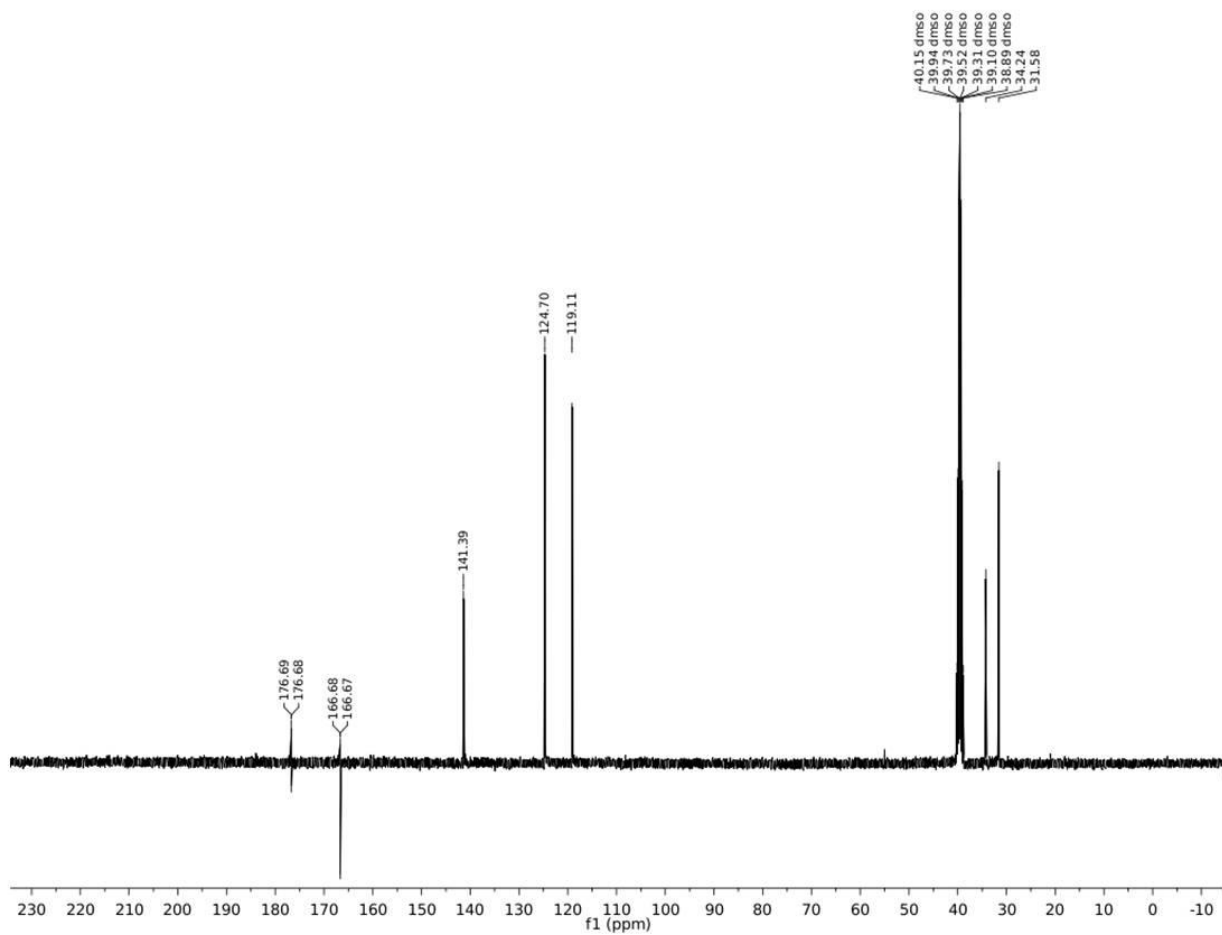


Figure A.17. ^{13}C NMR of 2-(chloromethyl)-1-methyl-1H-imidazole hydrochloride, DMSO- d_6 , TMS, RT. Peaks seen at 176.69 and 166.69 are artifacts of the experiment.

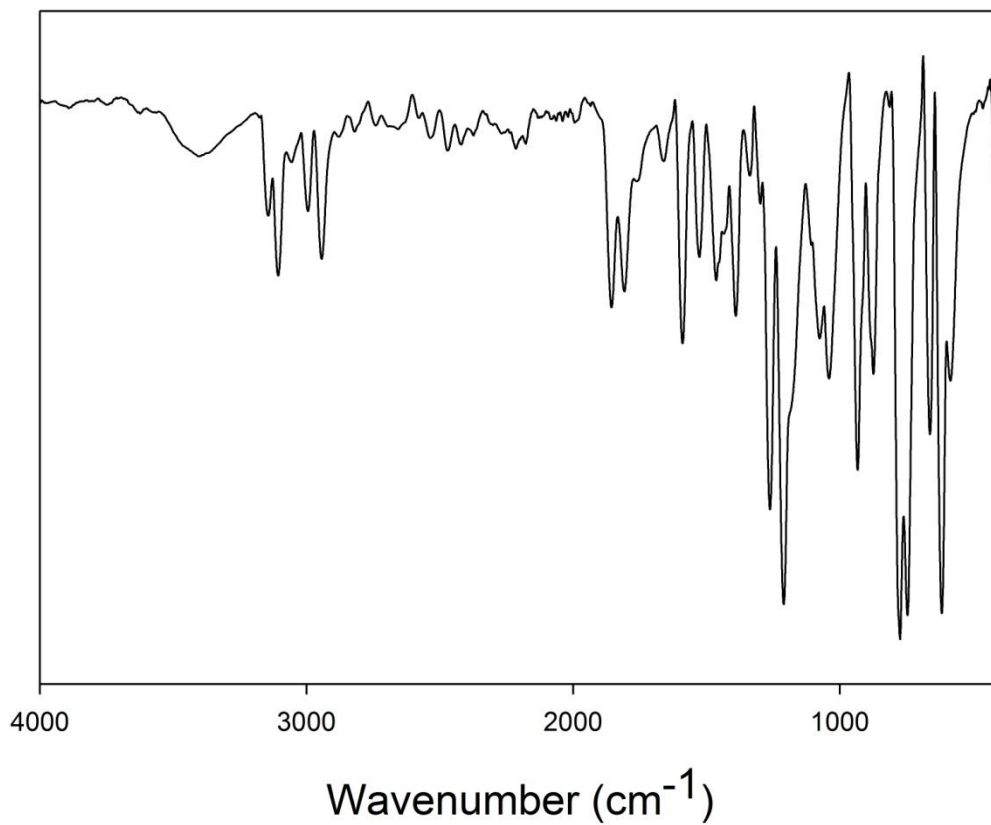


Figure A.18. FTIR (ATR) of 2-(chloromethyl)-1-methyl-1H-imidazole hydrochloride, CDCl₃, TMS, RT.

N4Py (I).

To a 30 mL DMF solution of picolyl chloride hydrochloride (0.7438 g, 4.536 mmol) was added solid K_2CO_3 (2.388 g, 17.28 mmol), a 2 mL DMF aliquot of di(pyridin-2-yl)methanamine (0.4000 g, 2.160 mmol), followed by KI (0.8300 g, 5.000 mmol). The mixture was heated under reflux for 8 h during which a the initial yellow solution became dark red. The solution was brought to ambient temperature and the DMF was removed by short-path distillation. The residue was extracted with 5×20 mL of EtOAc. The EtOAc-soluble portion was then washed with DI water, saturated $NaHCO_3$, and brine. The EtOAc was concentrated under reduced pressure to give a dark red syrup. The crude material was purified by column chromatography (silica, 0-5% MeOH in CH_2Cl_2) to afford a dark red syrup (0.6080 g, 1.655 mmol, 77%). 1H NMR (400 MHz, $CDCl_3$, δ from solvent): 8.57 (d, 2H, $J = 5$ Hz, *HPy*), 8.49 (d, 2H, $J = 5$ Hz, *HPy*), 7.65 (m, 8H, *HPy*), 7.14 (t, 2H, $J = 8$ Hz *HPy*), 7.09 (t, 2H, $J = 5$ Hz *HPy*), 5.34 (s, 1H, *HCN*), 3.97 (s, 4H, $2CH_2$). ^{13}C NMR (100.6 MHz, $CDCl_3$, δ from solvent): 160.1 (q, *CN*, *Py*), 160.0 (q, *CN*, *Py*), 149.4 (t, *HC*, *Py*), 149.4 (t, *HC*, *Py*), 136.4 (t, *HC*, *Py*), 136.4 (t, *HC*, *Py*) 124.0 (t, *HC*, *Py*), 123.0 (t, *HC*, *Py*), 122.2 (t, *HC*, *Py*), 121.9 (t, *HC*, *Py*), 72.1 (t, *HCN*), 57.4 (s, CH_2). FTIR (ATR), ν_{max} (cm^{-1}): 3371 (w), 3048 (w), 3005 (w), 2927 (w), 2838 (4), 1676 (w), 1585 (s), 1568 (s), 1506 (w), 1469 (s), 1430 (s), 1362 (m), 1312 (w), 1247 (w), 1147 (m), 1121 (m), 1089 (m), 1048 (m), 994 (m), 954 (m), 880 (w), 784 (m), 748 (s), 694 (m), 650 (w), 631 (m), 556 (m). 511 (w). LRMS-ESI (m/z): $[M + H]^+$ calcd for $C_{23}H_{22}N_5$ (% relative abundance), 368.2 (100), 369.2 (27.0), 370.2 (3.5), found, 368.4 (100), 369.4 (25.2), 370.4 (3.4); $[M + Na]^+$ calcd for $C_{23}H_{21}N_5Na$ (% relative abundance), 390.2 (100), 391.2 (27.0), 392.2 (3.5), found, 390.4 (100), 391.4 (24.7), 392.4 (4.0).

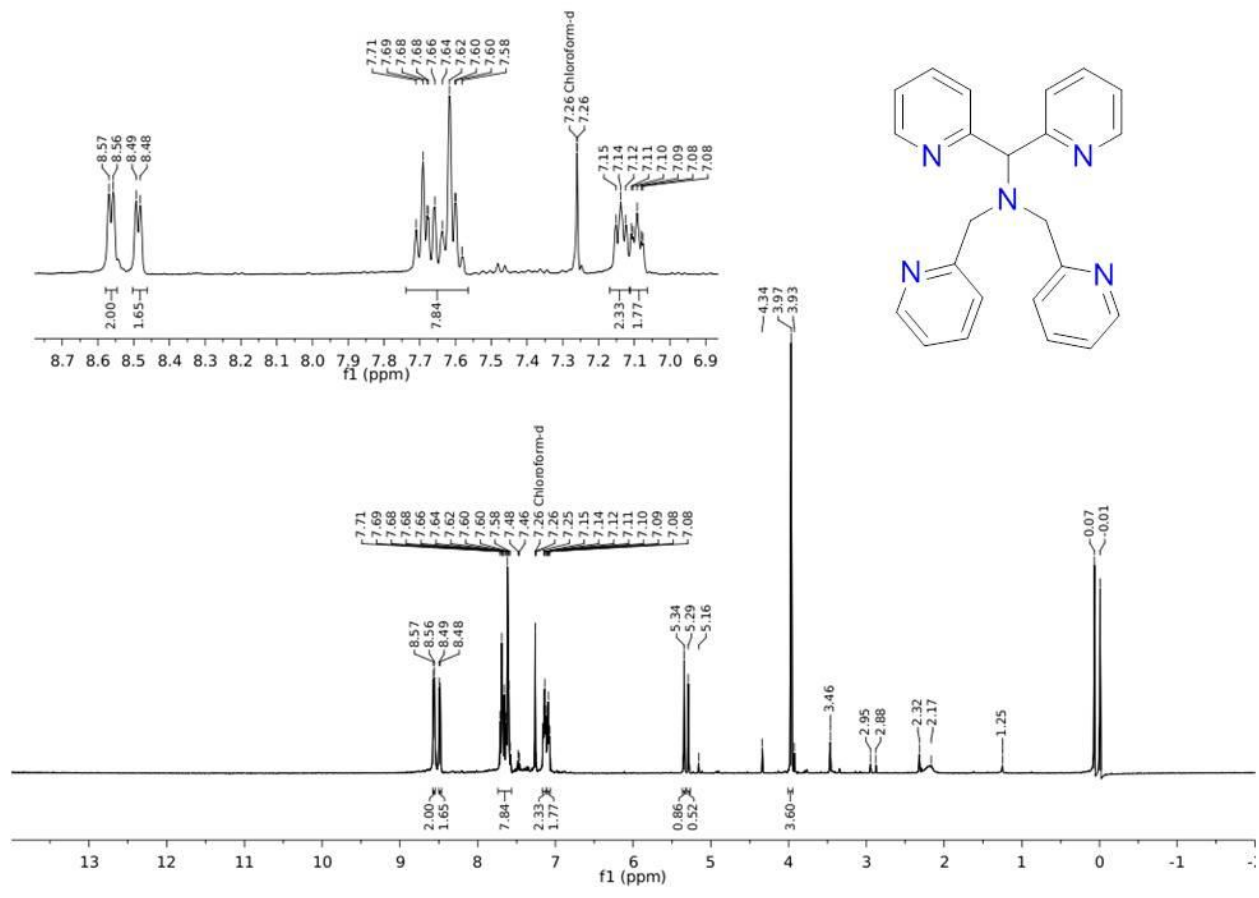


Figure A.19. ^1H NMR of **1** in CDCl_3 , TMS, RT.

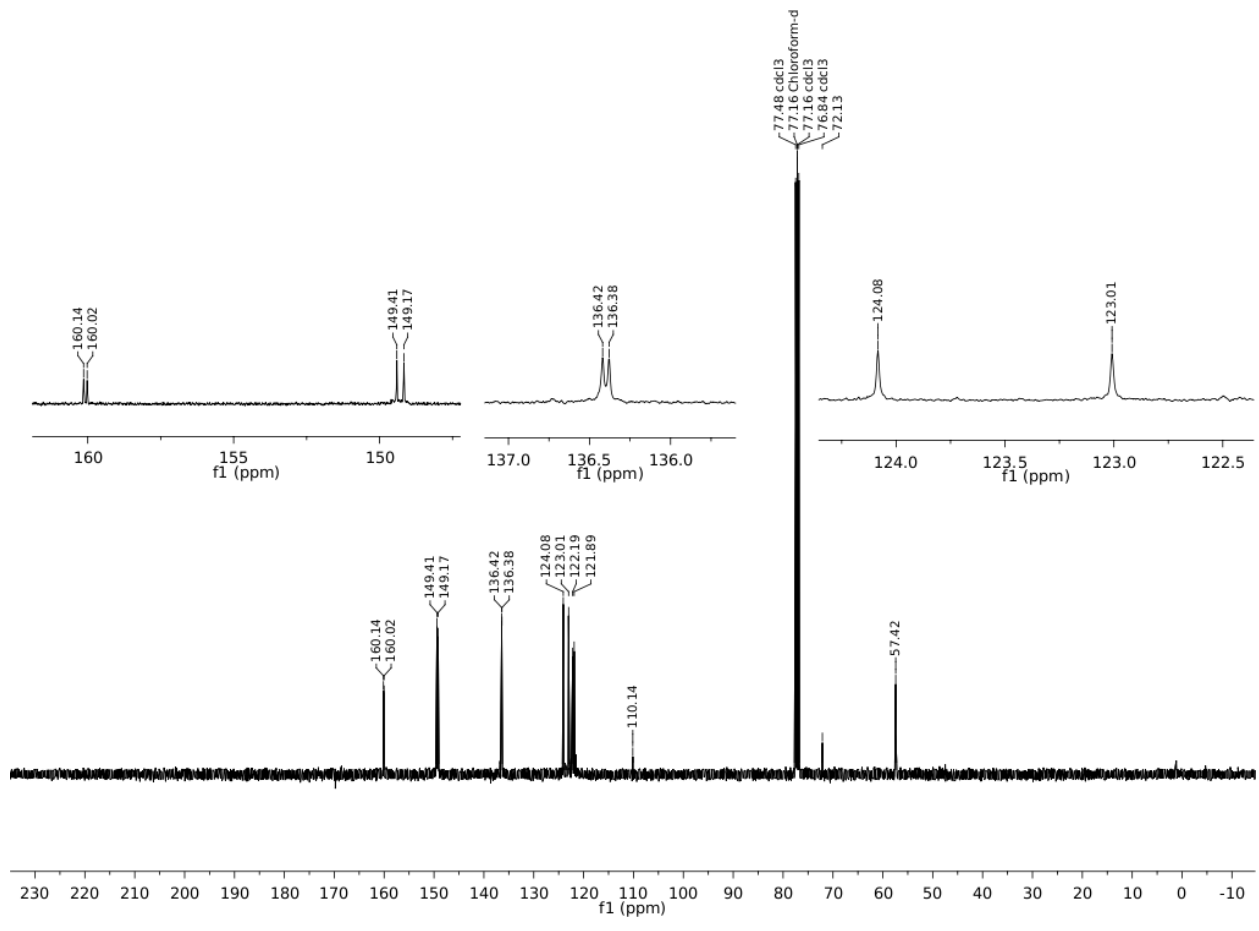


Figure A.20. ^{13}C NMR of 1.

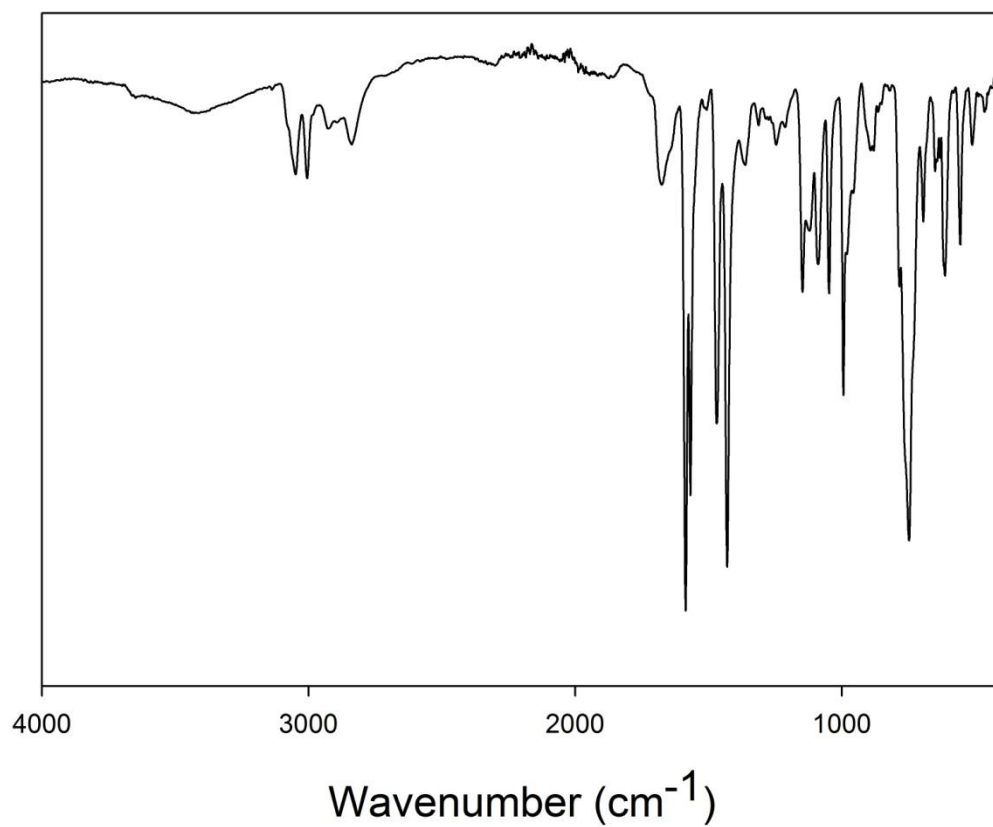


Figure A.21. FTIR (ATR) of 1.

N2Py2Im (5)

The N2Py2Im ligand can be prepared from the reaction of 2-(chloromethyl)-1-methyl-1H-imidazole hydrochloride with di(pyridin-2-yl)methanamine in a similar fashion to **1** except without reflux, under refluxing conditions more side-products are formed. To a 3 mL DMF solution of di(pyridin-2-yl)methanamine (0.4280 g, 2.311 mmol) was added 2-(chloromethyl)-1-methyl-1H-imidazole hydrochloride (0.7719 g, 4.622 mmol) and K₂CO₃ (1.916 g, 13.87 mmol), then KI (0.9591 g, 5.778 mmol) was added. The solution was stirred for 72 h to give a dark red-brown solution with light insolubles (presumably K₂CO₃). After 72 h, the DMF was removed by short-path distillation, followed by extraction with 5 × 30 mL CH₂Cl₂. The dark red solution was concentrated and purified by column chromatography (silica, 0-5% MeOH in CH₂Cl₂) to afford a dark red syrup. The material is not completely free of impurities and requires further purification. However, ¹H NMR and ESI-MS indicate the presence of the desired compound.

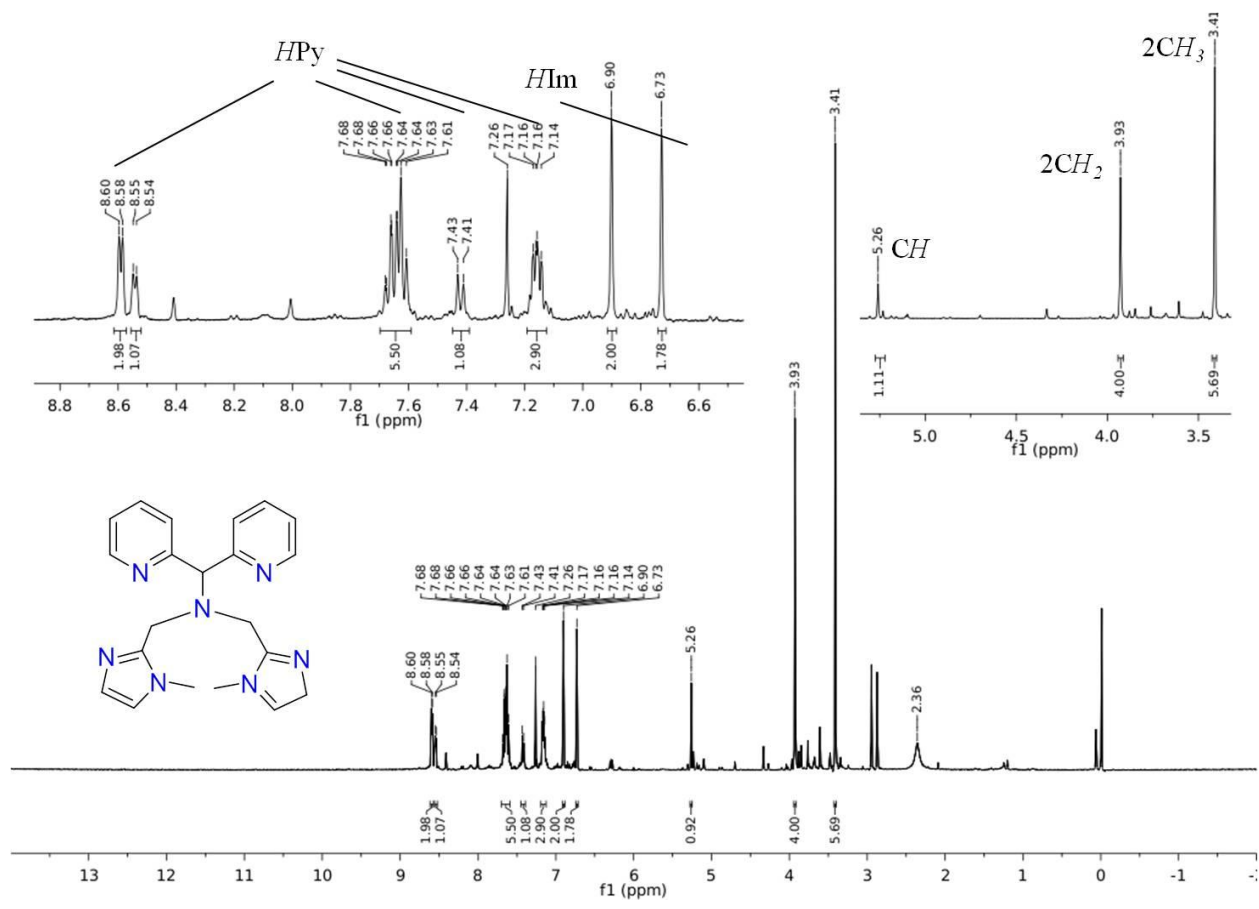


Figure A.22. ¹H NMR of 5 after column.



Compound 2^{BF_4} has been synthesized in previous reports.⁹ To a 4 mL MeCN solution containing 0.1000 g (0.2722 mmol) of **1** was added a 1 mL MeCN solution containing 0.0919 g (0.2722 mmol) of $[Fe(H_2O)_6](BF_4)_2$. Upon mixing, the color instantly became a more intense red color. The homogeneous solution was stirred an additional 1 h at RT with no further changes. The solvent was then removed from the flask under reduced pressure, washed with 3×5 mL of Et_2O , and dried to afford an orange-red solid product (0.1546 g, 0.2423 mmol, 89%). 1H NMR (400 MHz, CD_3CN , δ from solvent): 9.04 (d, 2H, $J = 5$ Hz, *HPy*), 8.90 (d, 2H, $J = 5$ Hz, *HPy*), 7.94 (t, 2H, $J = 8$ Hz, *HPy*), 7.88 (d, 2H, $J = 10$ Hz, *HPy*), 7.68 (t, 2H, $J = 8$ Hz *HPy*), 7.35 (dd, 4H, $J = 5$ Hz, *HPy*), 7.07 (d, 2H, $J = 5$ Hz), 6.33 (s, 1H, *H*CN), 4.39 (d, 2H, $J = 15$ Hz, *CH*₂), 4.29 (d, 2H, $J = 15$ Hz, *CH*₂), 1.96 (s, 3H, coordinated MeCN). FTIR (KBr pellet), ν_{max} (cm^{-1}): 3440 (m), 3109 (w), 3073 (w), 2246 (w, $\nu_{C\equiv N}$), 1629 (m), 1605 (m), 1478 (m), 1463 (m), 1446 (m), 1288 (w), 1058 (vs, ν_{BF}), 918 (w), 776 (s), 725 (w), 655 (w), 581 (w), 521 (w). UV-vis (MeCN, 298 K), λ_{max} , nm: 375 and 454. LRMS-ESI (m/z): [$\{M - MeCN - 2 BF_4 + H_3O\}^+$] calcd for $C_{23}H_{24}FeN_5O$ (relative abundance), 442.1 (100), 443.1 (29.3), 440.1 (6.4); found, 442.1 (100.0), 443.1 (28.7), 440.1 (5.4); [$\{M - MeCN + BF_4\}^-$] calcd for $C_{23}H_{21}B_3F_{12}FeN_5$ (relative abundance), 684.1 (100.0), 683.1 (66.7), 685.1 (26.6), found, 684.0 (100.0), 683.2 (73.4), 685.0 (26.2).

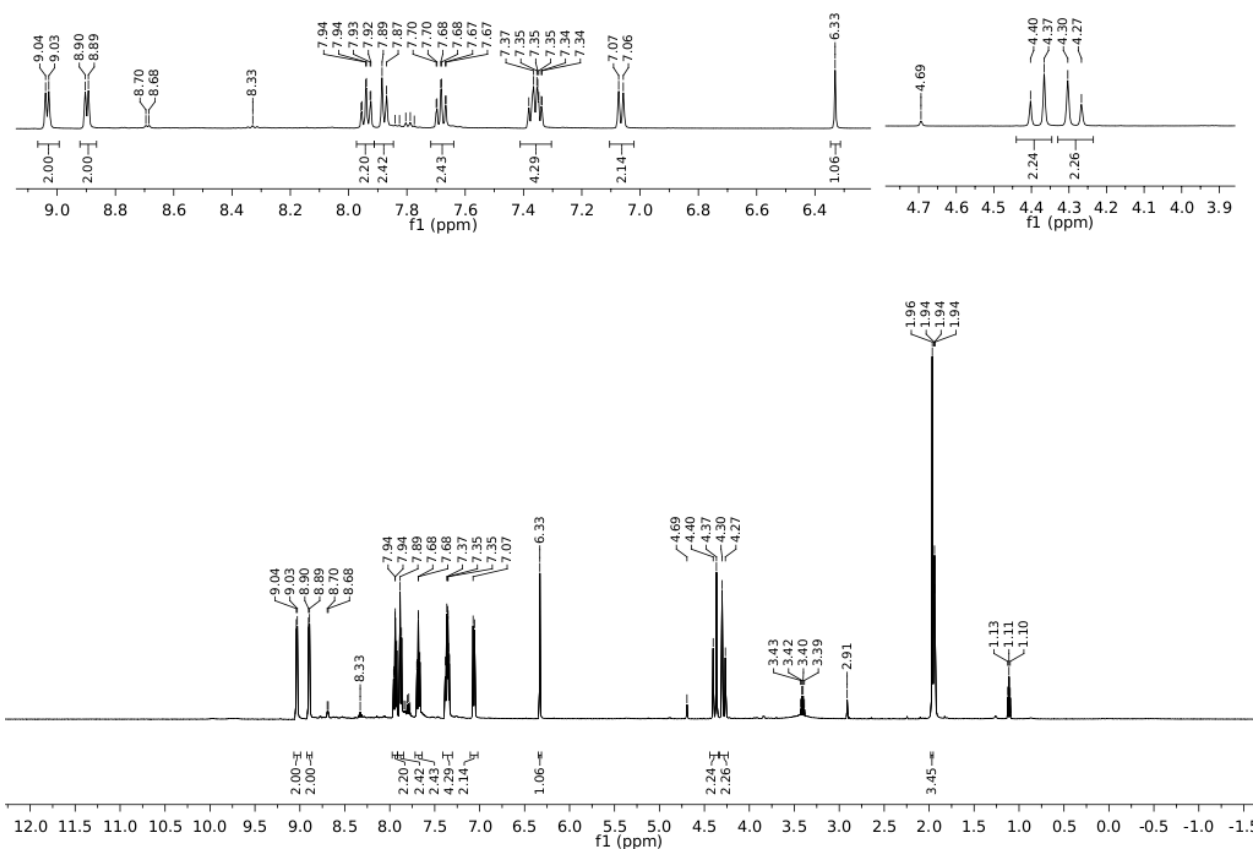


Figure A.23. ^1H NMR of 3BF_4 .

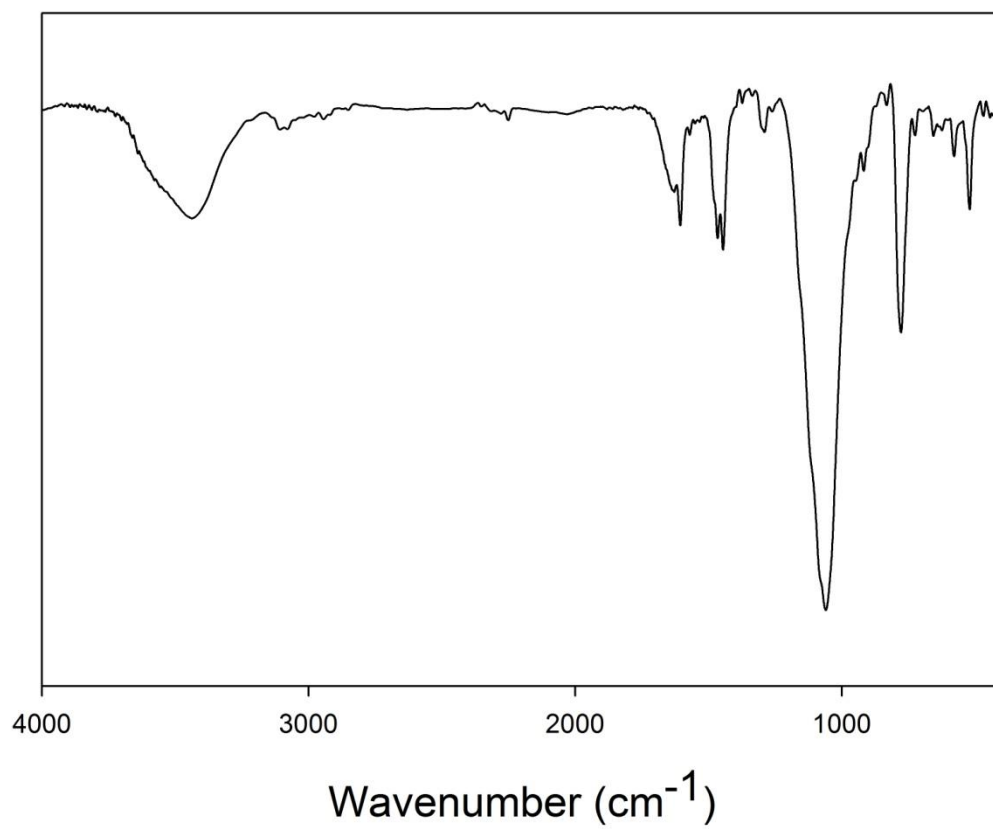


Figure A.24. FTIR (KBr) of 3^{BF_4}



To a 5 mL 3:2 MeCN:MeOH solution containing 0.1150 g (0.1803 mmol) of 3^{BF_4} was added a 1 mL MeOH solution containing 0.617 g (1.803 mmol) of NaBPh₄. The homogeneous solution was stirred an additional 2 h at RT without change. The solvent was then removed from the flask under reduced pressure, and MeOH was added to afford an orange solid. This material was washed with 3 × 5 mL of Et₂O, and dried to afford an orange solid (0.1730 g, 0.1569 mmol, 87%). ¹H NMR (400 MHz, CD₃CN, δ from solvent): 9.00 (d, 2H, *J* = 5 Hz, *HPy*), 8.86 (d, 2H, *J* = 5 Hz, *HPy*), 7.91 (t, 2H, *J* = 10 Hz, *HPy*), 7.82 (d, 2H, *J* = 10 Hz, *HPy*), 7.66 (t, 2H, *J* = 10 Hz, *HPy*), 7.35 (dd, 4H, *J* = 5 Hz, *HPy*), 7.27 (t, br, 18H, *HBPh₄*), 7.03 and 6.99 (overlapping signals 20H, *HPy* and *HBPh₄*), 6.83 (t, 9H, *HBPh₄*), 6.21 (s, 1H, *H₃CN*), 4.31 (d, 2H, *J* = 20 Hz, *CH₂*), 4.23 (d, 4H, *J* = 20 Hz, *CH₂*), 1.96 (s, 3H, coordinated MeCN). ¹H NMR (400 MHz, (CD₃)₂SO, δ from solvent): 97.2 (s), 54.3 (s), 50.33 (s), 49.0 (s), 38.0 (s), 27.1 (s), 26.8 (s), 7.16 (s, *HBPh₄*), 6.90 (s, *HBPh₄*), 6.76 (s, *HBPh₄*), 2.05 (s, *H₃C* free MeCN). FTIR (KBr pellet), *v*_{max} (cm⁻¹): 3448 (w), 3053 (s), 2981 (s), 2915 (w), 1607 (m), 1578 (m), 1478 (m), 1462 (m), 1446 (m), 1425 (m), 1262 (m), 1159 (w), 1084 (w), 1065 (w), 1032 (m), 910 (m), 845 (w), 800 (w), 765 (m), 737 (s), 704 (vs), 624 (w), 613 (s), 466 (w). UV-vis (MeCN, 298 K), *λ*_{max}, nm: 377 and 455). *μ*_{eff} (solution, 293 K): 4.59 BM in (CD₃)₂SO.

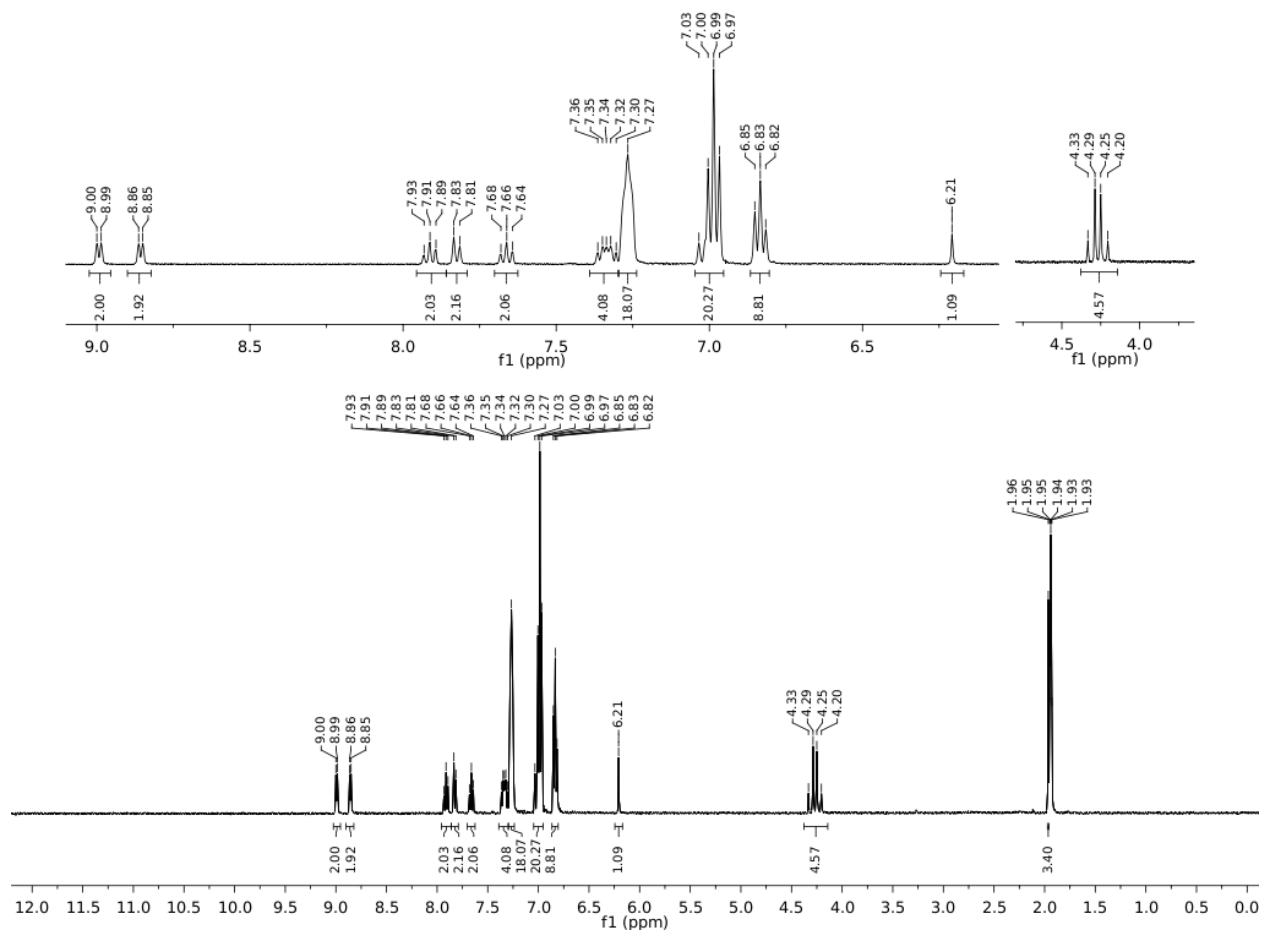


Figure A.25. ^1H NMR of **2** in CD_3CN , RT.

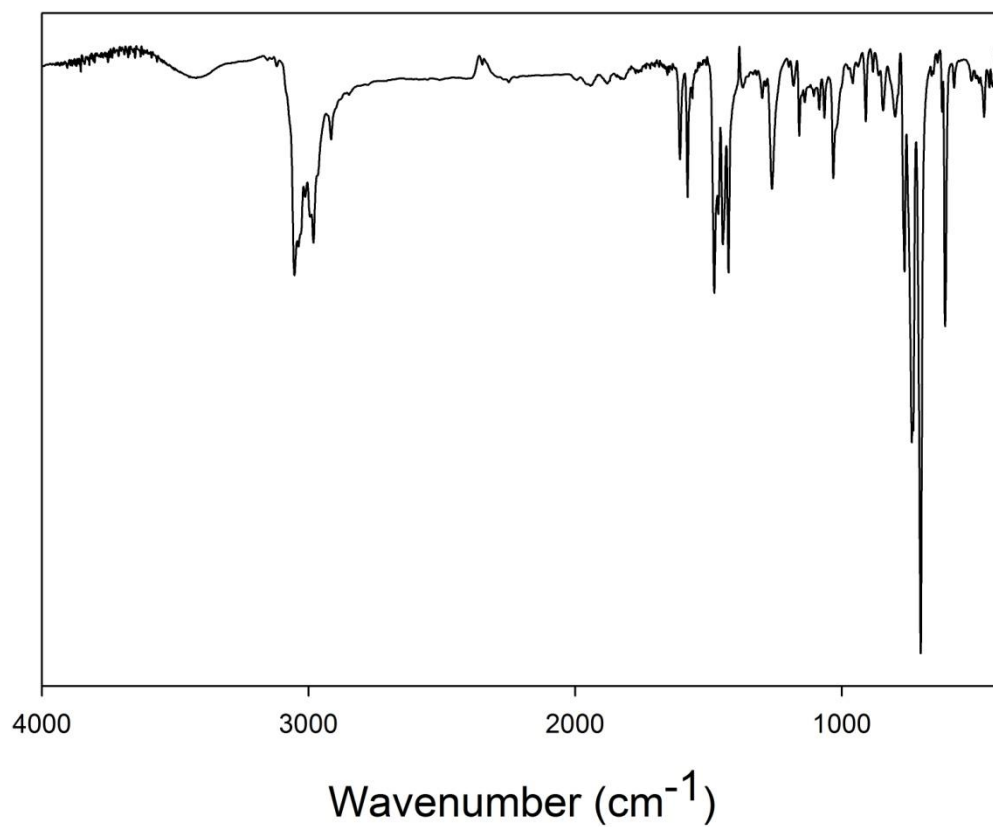


Figure A.26. FTIR (KBr) of 2^{BPh4}.

[Fe(N4Py)NO](BF₄)₂ (3)

The synthesis of this compound has been reported previously.⁹ This procedure was used with the following reagent amounts: **3**^{BF₄} (0.1000 g, 0.1567 mmol) in 1:1 MeCN:MeOH. After NO purge, the solution was placed in a -25 °C to facilitate precipitation of a pale-red solid (0.0500 g, 0.0799 mmol, 51%). FTIR (KBr), ν_{max} (cm⁻¹): 3586 (m), 3236 (w), 3115 (w), 2963 (w), 1678 (vs, ν_{NO}), 1610 (s), 1571 (w), 1488 (m), 1468 (m), 1448 (s), 1319 (w), 1283 (m), 1265 (m), 1167 (m), 1061 (vs), 968 (s), 909 (m), 829 (m), 790 (m), 769 (s), 720 (w), 643 (w), 577 (m), 521 (m), 439 (w).

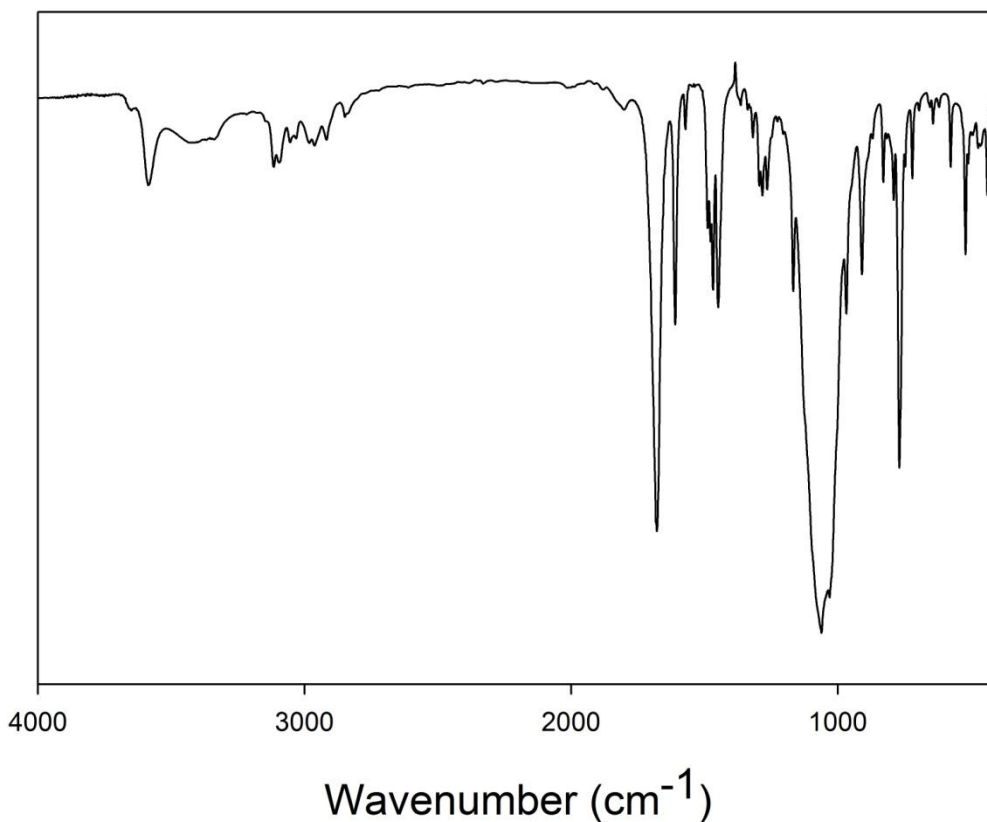


Figure A.27. FTIR (KBr) of **3**.

[Fe(N4Py)NO₂](BPh₄) (4)

To a 3 mL 1:1 MeCN:MeOH solution containing 0.0650 g (0.1019 mmol) of **3**^{BF₄} was added a 0.5 mL MeOH solution containing 0.0182 g (0.2139 mmol) of KNO₂ and 0.0566 g (0.2139 mmol) of 18C6. The solution became more red upon addition. The homogeneous solution was stirred an additional 2 h at RT without change. The solvent was then removed from the flask under reduced pressure, and 3 mL MeOH was added to precipitate a dark orange solid. This material was washed with 3 × 5 mL of Et₂O, and dried to afford an dark orange solid product (0.0691 g, 0.0876 mmol, 86%). FTIR (KBr pellet), ν_{\max} (cm⁻¹): 3395 (m), 3053 (m), 3034 (m), 2963 (w), 2918 (m), 2850 (m), 1606 (m), 1579 (m), 1477 (s), 1444 (s), 1320 (s, ν_{NO_2}), 1284 (s, ν_{NO_2}), 1263 (s), 1182 (w), 1155 (w), 1107 (w), 1094 (w), 1050 (w), 1029 (m), 960 (w), 910 (w), 843 (w), 816 (w), 767 (s), 736 (vs), 706 (vs), 655 (w), 611 (s), 571 (w), 502 (w), 460 (w). UV-vis (MeCN, 298 K), λ_{\max} , nm: 390 and 474. LRMS-ESI (*m/z*): [{M – 2 BPh₄ + NO₂}]⁺ calcd for C₂₃H₂₁FeN₆O₂ (relative abundance), 469.1 (100.), 470.1 (29.7), 467.1 (6.4), found, 469.1 (100.0), 470.1 (27.8), 467.2 (5.9).

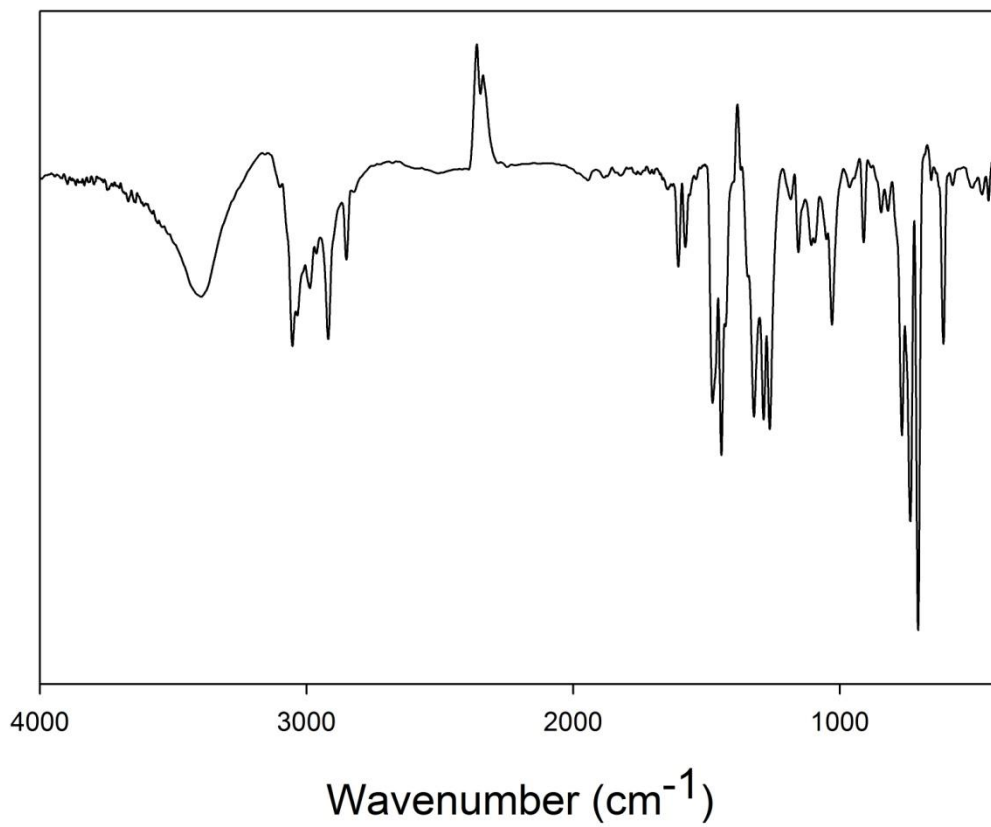


Figure A.28. FTIR (KBr) of **4**.

[Fe(N4Py)NO₂](BPh₄) (4^{15NO₂})

Complex **4^{15NO₂}** was prepared from 0.0200 g (0.0181 mmol) of **2^{BPh₄}** in 1 mL of MeCN by addition of Na¹⁵NO₂ (0.0100 g, 0.1429 mmol) as a 1 mL MeOH aliquot. The solution immediately became more red upon addition and was stirred for 30 min with no further change. The solvent was removed under reduced pressure and 2 mL MeOH was added which left a dark-orange insoluble material. The mixture was placed in a -25 °C freezer to facilitate precipitation. The material was filtered, washed with 3 × 5 mL of cold MeOH and dried to give an orange powder (0.0131 g, 0.0166 mmol, 92%). FTIR (KBr pellet), ν_{\max} of isotope-sensitive peaks (cm⁻¹): 1302 (s, ν_{NO_2} , $\Delta\nu_{\text{NO}_2} = 18 \text{ cm}^{-1}$), 1261 (s, ν_{NO_2} , $\Delta\nu_{\text{NO}_2} = 23 \text{ cm}^{-1}$). LRMS-ESI (m/z): [$\{\text{M} - 2 \text{BPh}_4 + {}^{15}\text{NO}_2\}]^+$ calcd for C₂₃H₂₁Fe¹⁵NN₅O₂ (relative abundance), 470.1 (100.), 471.1 (29.3), 468.1 (6.4), found, 470.2 (100.0), 471.1 (25.1), 468.2 (4.9).

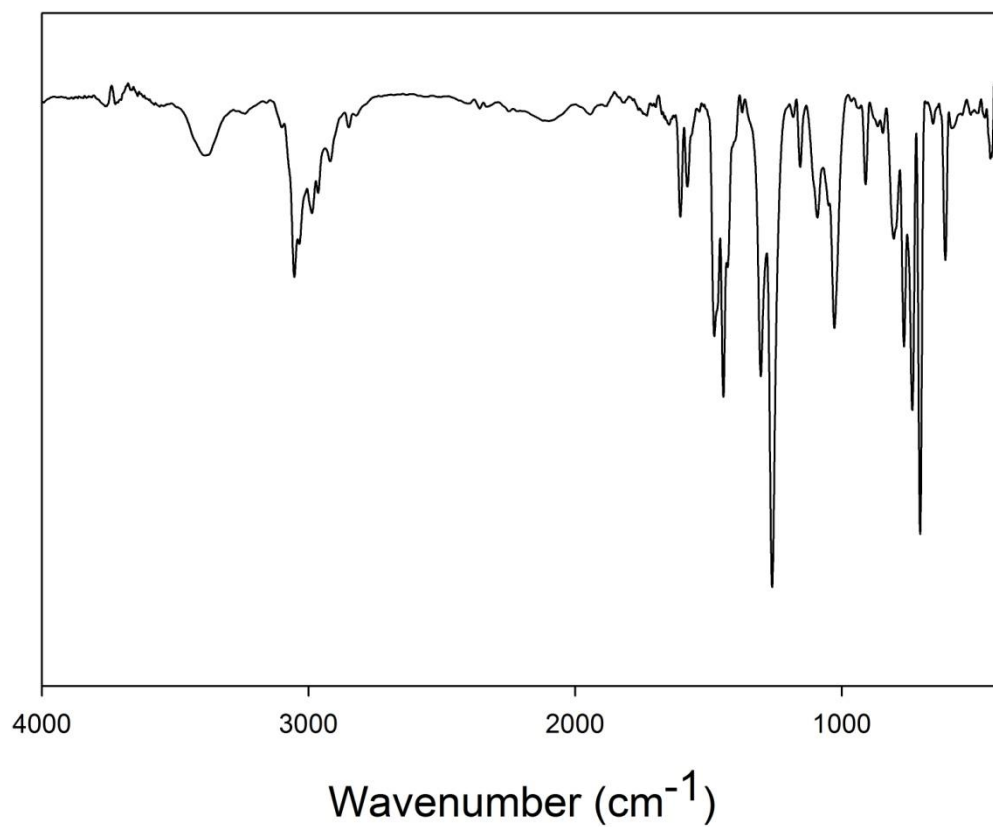


Figure A.29. FTIR (KBr) of 4¹⁵NO₂.

A.7. References

- (1) Lubben, M.; Meetsma, A.; Wilkinson, E. C.; Feringa, B.; Que, L. *Angew. Chem. Int. Ed.* **1995**, *34*, 1512.
- (2) Roelfes, G.; Hage, R.; Que, L.; Feringa, B. L. *J. Inorg. Biochem.* **1999**, *74*, 279.
- (3) Roelfes, G.; Lubben, M.; Chen, K.; Ho, R. Y. N.; Meetsma, A.; Genseberger, S.; Hermant, R. M.; Hage, R.; Mandal, S. K.; Young, V. G.; Zang, Y.; Kooijman, H.; Spek, A. L.; Que, L.; Feringa, B. L. *Inorg. Chem.* **1999**, *38*, 1929.
- (4) Ligtenbarg, A. G. J.; Oosting, P.; Roelfes, G.; La Crois, R. M.; Lutz, M.; Spek, A. L.; Hage, R.; Feringa, B. L. *Chem. Commun.* **2001**, 385.
- (5) Roelfes, G.; Vrajmasu, V.; Chen, K.; Ho, R. Y. N.; Rohde, J. U.; Zondervan, C.; la Crois, R. M.; Schudde, E. P.; Lutz, M.; Spek, A. L.; Hage, R.; Feringa, B. L.; Munck, E.; Que, L. *Inorg. Chem.* **2003**, *42*, 2639.
- (6) van den Berg, T. A.; de Boer, J. W.; Browne, W. R.; Roelfes, G.; Feringa, B. L. *Chem. Commun.* **2004**, 2550.
- (7) Nam, W. *Acc. Chem. Res.* **2007**, *40*, 522.
- (8) Sam, J. W.; Tang, X.-J.; Peisach, J. *J. Am. Chem. Soc.* **1994**, *116*, 5250.
- (9) McQuilken, A. C.; Ha, Y.; Sutherlin, K. D.; Siegler, M. A.; Hodgson, K. O.; Hedman, B.; Solomon, E. I.; Jameson, G. N.; Goldberg, D. P. *J. Am. Chem. Soc.* **2013**, *135*, 14024.
- (10) Chang, J.; Plummer, S.; Berman, E. S. F.; Striplin, D.; Blauch, D. *Inorg. Chem.* **2004**, *43*, 1735.
- (11) Draksharapu, A.; Li, Q.; Logtenberg, H.; van den Berg, T. A.; Meetsma, A.; Killeen, J. S.; Feringa, B. L.; Hage, R.; Roelfes, G.; Browne, W. R. *Inorg. Chem.* **2012**, *51*, 900.
- (12) Sanders, B. C.; Hassan, S. M.; Harrop, T. C. *J. Am. Chem. Soc.* **2014**, *136*, 10230.
- (13) Holm, R. H.; Pinolet, L. H.; Lewis, R. A. *J. Am. Chem. Soc.* **1971**, *93*, 360.
- (14) Wieghardt, K.; Kueppers, H. J.; Weiss, J. *Inorg. Chem.* **1985**, *24*, 3067.
- (15) Widger, L. R.; Davies, C. G.; Yang, T.; Siegler, M. A.; Troepfner, O.; Jameson, G. N. L.; Ivanović-Burmazović, I.; Goldberg, D. P. *J. Am. Chem. Soc.* **2014**, *136*, 2699.

- (16) Seto, M.; Miyamoto, N.; Aikawa, K.; Aramaki, Y.; Kanzaki, N.; Iizawa, Y.; Baba, M.; Shiraishi, M. *Bioorg. Med. Chem.* **2005**, *13*, 363.